Renewable Energy in Cellular Networks: a Survey

Hussein Al Haj Hassan, Loutfi Nuaymi and Alexander Pelov
IMT/Telecom Bretagne/UEB
Department RSM, 2 rue de la Châtaigneraie, 35576 Cesson Sevigné, France
firstname.lastname@telecom-bretagne.eu

***Abstract*—In recent years a lot of research work was dedicated to energy efficiency in cellular networks. An emerging field of interest in that direction is the use of renewable energy sources such as wind and solar – a type of energy that is bound to increase and develop. In this paper we survey the existing works and present the fundamental principles and motivations necessary for a thorough understanding of the usage of renewable energy in cellular networks. Furthermore, we introduce a reference model for renewable energy base station (REBS) and provide analysis of its components. The synthesis of dedicated REBS algorithms, system architectures, deployment strategies and evaluation metrics provides comprehensive overview and helps identify the perspectives in this promising research field.**

***Index Terms*—Cellular Networks; Base Station Reference Model; Renewable Energy; Energy Efficiency; Sustainability.**

I. Introduction

The often cited Gartner report of 2007 [1] states that the information and communication technology (*ICT*) sector is responsible for 2% of CO_2 human footprint. More specifically, mobile communication networks alone consume around 0.5% of the global energy supply [2]. These numbers are bound to increase with the rapid growth of capacity demand, unless significant improvements are brought to networks' efficiency. Hence reducing and optimizing energy consumption is a strategic target for the cellular communication industry [3]. This is not only because it makes business sense, where fuel and energy cost can reach 32.2% of the operational cost as in India [4], but also because mobile operators are more engaged in Corporate Social Responsibility programs with particular focus on sustainability and environmental issues.

Based on the analysis of DOCOMO [5], 75–80% of power consumption is done at the level of Base Station (*BS*) in 3G and LTE networks. Thus reducing the power at this level is essential for the energy efficiency of cellular BS. Several techniques addressing this goal have been proposed, such as cell shaping techniques (switching-off and cell-breathing mechanisms), deployment of small-cells/relays, radio resource allocation algorithms and cognitive radio [6], [7]. Some of the recent works start taking explicitly into account the availability and the specificities of renewable energy (*RE*) sources in the functioning of the cellular network infrastructure. Although a great number of renewable BS has already been deployed in different places such as Japan, China, Austria, Africa, South Asia, South America, Latin America, Caribbean [8], [9] this domain is widely open to research and enhancement.

This survey is aimed at summarizing the state of the art in this nascent direction of cellular network research, understanding the fundamental principles of using RE in powering cellular base stations and introducing possible perspectives to develop this promising domain.

The rest of the paper is organized as follows. In Section II we present the motivation of using renewable energy in cellular networks. We introduce our reference model for renewable energy base station in Section III, along with a survey of the models of its components. The existing work relative to network deployment and global RE cellular system architecture is outlined in Section IV. The recent advances in renewable energy base station management algorithms are then presented in Section V. Finally, Section VI summarizes the metrics used for evaluation across the different studies, before concluding this paper in Section VII.

II. Benefits of using renewable energy in cellular networks

There are many benefits of using renewable energy sources in powering cellular BSs. One of the instinctive and popular justifications regarding renewable energy in general is the desire to render our society more environmentally friendly, e.g. by decreasing the global greenhouse gas (*GHG*) emissions. However, in addition to decreasing the GHG emissions, RE sources can serve as solution to many problems. For example, the authors of [10] propose using RE as a solution in areas where there is no power grid such as islands and deserts. It also solves the problem for places where it is difficult or impossible to get connectivity to the power grid. Until now, the mobile operators rely on diesel generators (*DG*) to run the BSs as a solution for these cases, which is not only expensive due to its price and transportation [11], but also one of the most pollutant sources of energy. A program called "Green Power for Mobile" has been launched by the GSM Association (*GSMA*) to aid the mobile telecommunications industry to deploy various RE sources for powering $640\,000$ new and existing off-grid BSs [9]. This action alone would save about 0.35% of the global diesel consumption. In addition, RE may also be part of the solution in case of a failure in the power grid [12]. In [13], the authors investigate the possible role of RE in reducing the deployment and running costs of the next generation cellular networks. Their study shows that it is economically suitable and environmental friendly to use RE sources in powering micro- and small- cell BSs, and that these resources can serve as basis for new business models. An example of these models would be the introduction of new spectrum regulations for licensing mobile operators capable

978-1-4799-0354-2/13/$31.00 ©2013 IEEE

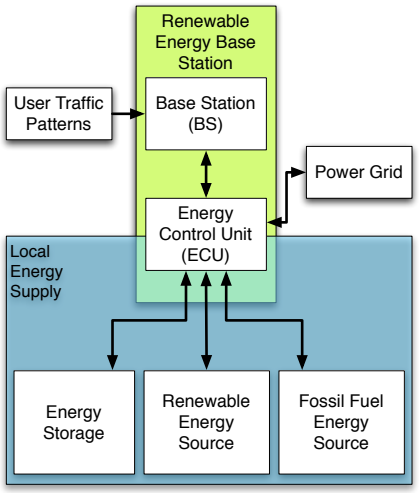

Fig. 1. Reference model of a Renewable Energy Base Station (REBS).

of maintaining low maximum grid power consumption. We can also imagine a combination between Smart Grid functions and RE powered cellular networks, where the network can decrease its consumption in a specific area whenever needed, e.g. in a peak hour. Finally, the RE power can be seen as a source of revenue by the operators, e.g. by selling the excess energy to the grid – a use case particularly well fitted for developed countries with mature energy markets.

Introducing renewable energy to power cellular network base stations makes not only environmental, but – most importantly – economic sense, while at the same time opening opportunities for new business models. It is thus of great importance to study the subject in order to determine the potential gains, applicability scenarios, deployment strategies and new system architectures (among others) which is the focus of the following sections.

III. Renewable Energy Base Station Model (REBS)

There exist multiple factors, which should be modeled in order to correctly analyze a cellular BS powered by RE source. Some of the major parameters and elements include the type of the BS, energy sources (and their models), power control policy and traffic model of the users. The user traffic model is a classical problem in cellular networks with vast amount of dedicated studies and will not be discussed in this paper. In our context, a renewable energy base station (REBS) uses at least one type of non-fuel renewable energy sources such as photovoltaic (*PV*) systems or wind turbines (e.g. bio-fuels are excluded, except when specifically mentioned). Figure 1 presents our REBS reference model, which we are using as basis in this survey.

A. Type of base stations

Several types of cellular BS are found in the literature such as those supporting micro and macro cells. Each type has its specific coverage capability, energy consumption, deployment order and cost [13], [14]. Macro cells are distinguished for their high coverage and can support large number of users. However, this type of BS has a high energy consumption profile, which is in order of thousand of watts. Macro BSs are deployed by the operator and have very high capital and operative expenditure (CapEx and OpEx). Micro cells are known for their shorter range, lower energy consumption profile and lower CapEx and OpEx with respect to their macro counterparts. Operators are capable of deploying them rapidly and for relatively low cost. Small cells (pico- and femto- for example) are characterized by low range and low power. They are typically used to extend coverage and improve capacity. Such kind of BS can be deployed on a limited space and can be installed temporary for special events.

B. Energy consumption model of a base station

Several models of the energy consumption of cellular BSs can be find in the literature [15]. One of the most detailed was developed as a part of the Energy Aware Radio and Network Technologies (EARTH) project [14]. The proposed model can be used for different type of BSs (micro, macro, pico and femto) and takes into account multiple factors. It is summarized by the following equation:

$$P_{in} = N_{Trx}.\frac{\frac{P_{out}}{\eta_{Pa}.(1-\theta_{feed})} + P_{RF} + P_{BB}}{(1-\theta_{DC})(1-\theta_{Ms})(1-\theta_{cool})}$$

where P_{in} is the input power, N_{Trx} is the number of transceivers, P_{out} is the transmitted power, η_{Pa} is the efficiency of power amplifier, P_{RF} is the is the power consumed by the radio frequency chain and P_{BB} is the power consumed by baseband engine. θ_{DC}, θ_{Ms} and θ_{cool} represent the losses incurred due to DC-DC power supply, mains supplies and active cooling respectively. The feeder loss of a macro BS may be mitigated by introducing remote radio head (RRH), where the power amplifier is mounted at the same physical location as the transmition antenna. The relation between RF output power and BS power consumption is nearly linear as shown by [14]. Hence a linear approximation of the BS power model is justified as follows:

$$P_{in} = \begin{cases} N_{Trx}.P_0 + \Delta_P P_{out}, & 0 < P_{out} \leq P_{max} \\ N_{Trx}.P_{sleep}, & P_{out} = 0 \end{cases}$$

where P_0 is the consumed power at the minimum non-zero output power, Δ_P is the slope of the load-dependent power consumption and P_{sleep} is the sleep mode power consumption. The parameters of the power model depend on the BS type, presented in Table I.

C. Energy sources

In a REBS we may have combination of several power sources including a mixture of renewable and non-renewable ones. On one hand, non-renewable sources are known to have reliable and controllable performance, generating known amount of energy. On the other hand, renewable energy sources do not generate stable quantities of energy and are influenced by multiple parameters [8]. For example, solar

panels' performance is determined by the quantity of sunlight, snow fall, cloud coverage, smog, air density, temperature and others. Similarly, wind energy production is affected by many elements such as wind power, altitude, obstructions, air temperature, etc. One of the major approaches to compensate the intermittence of these energy sources is the usage of energy storage.

TABLE I
POWER MODEL PARAMETERS OF DIFFERENT BS TYPES [14].

BS type	N_{Trx}	P_{max} [W]	P_0 [W]	Δ_P	P_{sleep} [W]
Macro	6	20	130	4.7	75
RRH	6	20	84	2.8	56
Micro	2	6.3	56	2.6	39
Pico	2	0.13	6.8	4.0	4.3
Femto	2	0.05	4.8	8.0	2.9

D. Energy storage

There are several ways to ensure the reliability of RE systems [16]. Systems that combine more than one type of RE source have a better chance of being able to supply the load more consistently because they might have different times of low and high generation. However, in some cases it will not be sufficient. Energy storage is introduced in order to maintain the energy balance within the RE sources. It enables energy to be stored when there is an excess of supply, and provides the "missing" energy to the loads to compensate for the deficit of supply. Many types of storage are found depending on the scale they are used for. The most frequently used type is batteries. Batteries form a large part of the CapEx of RE systems and it is important to manage the system to ensure that the maximum lifespan of the battery is achieved by controlling its charging and discharging cycles. In addition, the system must be dimensioned correctly to ensure that the power demand is always met by the supply and to minimize the total cost of the system [13].

E. Renewable energy problematic and model

Dealing with renewable energy sources is not straightforward, due to their inherent intermittence and variance in the performance caused by multiple factors we mentioned in Section III-C. Multiple approaches to modeling the renewable energy generation for REBS can be found. In [17], [18] the harvested energy is modeled as a deterministic discrete process with energy harvests of size E_n arriving at time instances s_n, where E_n and s_n take positive real values. This model is justified by taking the solar energy as an example, where the energy generation can be predictable enough to have a good estimation of the harvested energy at a given time. In [19] the energy harvesting process is modeled as a Discrete-Time Markov Chain with a maximum number of harvested states H. The harvested and stored energy is assumed to be in integer units with a granularity proportional to the total harvested energy. Another model is based on weather statistics and sources' characteristics. This approach is used by [20], where the generated renewable energy is calculated based on the weather conditions (such as wind speed) and the characteristics of the power generator (e.g. cut-in and cut-out speed for wind turbines). As a part of the BS consumption pattern that best suits the weather forecast and backup batteries charging model, the author of [3] decomposes the harvested energy into two parts, the first part being directly used by the system while the second one is stored into the batteries. Each part is represented by a function dependent on the weather forecast and time of generation. However these function have not been explicitly given. In [21] the authors modeled the state of energy storage as G/G/1 queue with arbitrary random processes of energy arrival and departure, characterized by a mean and variance. The values of the means and variances can be estimated by exponentially weighted moving average or other approaches. Diffusion approximation is applied to analyze the energy buffer and depletion probability of a node.

F. Power control unit

Due to the unreliability of RE sources, an energy control unit (ECU) (or alternatively – power control unit) is essential for managing the changes in energy generation and consumption [3]. In case the RE cannot satisfy the energy demand of the BS, the control unit will compensate the needed energy from the back-up storage (or the power grid if such connection exists). In the case of excess RE, the control unit will use it to recharge the batteries. Additionally, we envision several scenarios in which one or more REBS can sell their excess energy back to the grid, even in the cases when their batteries are not fully charged. We also propose to use this unit in order to decrease the energy consumption of the grid in peak hours by using the RE sources and/or batteries. Moreover, the ECU is an essential part for enabling an optimal energy consumption of the system as a whole and/or helping to address the intermittence of some of the RE connected to the power grid. As an illustration, a BS can take into account the source of the energy provided by the grid and change its behavior accordingly, e.g. adjust the available throughput as a function of the locally generated wind energy. We can make a slight distinction between the pure REBS and these types of BSs, which may or may not have their own, local renewable energy sources. We define these BSs as "Renewable Energy-aware Base Stations" (*REaBS*).

IV. SYSTEM ARCHITECTURES AND CELLULAR PLANNING

Adopting RE in cellular systems affects the planning methodology and architecture of cellular networks. In [22], the author proposes several types of RE wireless structure and protocols for different network types, including cellular networks. Off-grid wireless networks powered by isolated RE sources and batteries may suffer from energy unavailability for some time causing the interruption of the services. The Coverage Supply Redundancy Architecture (CSRA) is introduced as a solution. For RE sources, the author proposes using different kinds of generators (solar, wind, ... and batteries) to reduce the possibility of BS outage. The author considers that it is not trivial for neighboring BS to connect to each

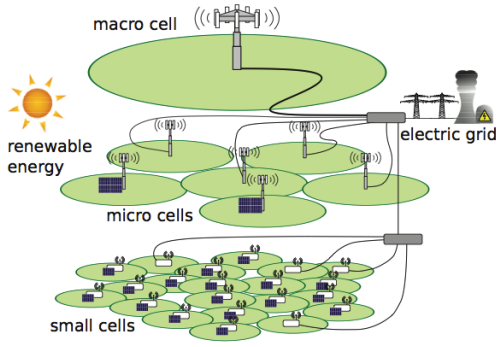

Fig. 2. Renewable HetNet architecture [13].

other through a power line, e.g. for financial reasons. However, it's technically feasible and economic for neighboring BSs to support each other wirelessly, by varying their respective transmission power. To further stabilize the power supply, some CSRA BSs can be augmented with other energy sources such as fuel based or power grid.

An advanced architecture based on the 3GPP HetNet is presented in [13], as illustrated in Figure 2. It defines a multi-tier, self-organized wireless access network composed of several types of BS with different characteristics using the same access technology and spectrum. The architecture consists of a grid-powered macro BSs and overlapped micro- and small- cells powered by RE or grid depending on their conditions (location for example). This architecture keeps the benefits of the fully grid powered HetNets such as long time cost saving, and provides easier deployment for BS difficult to be connected to grid and reduction of carbon emissions. Additionally, it can be beneficial in network roll-out by power operators (licensing to minimum power operator), capacity enhancement by adding RE access networks and cable-less coverage extension (for rural areas). A similar architecture is adopted by [23] where the authors considered the system model as a high power BS powered by grid overlapped by several low power BSs powered by RE sources only. As these architectures are quite general and depend on the state of deployment, it would be of great importance to perform more detailed analysis of their real-world applicability.

In [24], planning of cellular networks equipped with RE sources is investigated. The study takes into account satisfying the users and reducing the CapEx and OpEx. The problem is to select the subset of candidate BSs with minimum cost (sum of CapEx and OpEx), where BSs are connected by dedicated power line connections for energy balancing from other RE sources, a concept introduced in [25]. The problem is shown to be NP-hard, and thus heuristic algorithms are used for cellular planning. The solution consists of two phases, QoS-aware BS deployment and energy balancing connection. In the first phase, the authors assume that there is no power connection between RE sources, and solve the problem based on the QoS constraints. The second phase starts with a fully connected RE sources topology, and then removes the connection with minimum amount of transferred energy until no cost saving is achieved.

A. Deployment experiments and sizing

In 1995 AT&T proposed the usage of RE sources to power cellular networks. As an integrated management approach AT&T proposed to use alternative energy sources to power their products, such as PVs for wireless micro cells [30]. Due to the characteristics of renewable energy and variation of traffic, and thus the needed energy, precise sizing of renewable energy sources and energy storage is essential to avoid any system failure and/or additional cost. Thus, many studies investigated the feasibility of using RE sources and studied equipment sizing of cellular BSs powered by RE. An integrated solution to dynamically decrease the power consumption of wireless BSs and power them with alternative energies is presented in [31]. The authors propose several migration steps towards large deployment of alternative energies in off-grid or poor grid sites. The primary migration step consists of replacing one diesel generator (DG) with a deep-cycle battery bank to provide energy when the generators are switched off. The next step consists of deploying a single alternative energy source to reduce the diesel generators' run time and consumption. The ultimate migration step is to deploy a mixture of alternative energy sources. One pre-existing diesel generator may remain to address the worst-case climatic conditions. This prototype has been tested in Alcatel-Lucent Energy Lab facilities near Paris. In [26], the authors propose another configuration of a standalone PV/wind hybrid energy system with a backup diesel generator for cellular BS site in isolated areas of central India. The methodology used in this feasibility study can be summarized as follows: 1) calculate the power produced by wind/solar sources and 2) measure the data load. The results provide indications as to what should be the requirements to the wind turbines, the solar panels, the battery bank and the backup DG. Finally, the environmental, technical and economical impacts are studied for Bhopal in central India.

As a powerful tool for designing both on and off-grid distributed generation, HOMER can be used in sizing and dimensioning renewable energy and storage of REBS [32]. It can provide a good evaluation of the economic and technical feasibility of a large number of technology options and to account for variations in technology costs and energy resource availability. As an example, the authors of [27] present a feasibility study and analyze the optimal size of a stand-alone hybrid solar/wind powered system of BS in Nepal. The authors used HOMER and mathematical models implemented in MATLAB for performing the feasibility analysis and calculating the optimal configuration for a given load and desired probability of power outage. The model is provided for multiple combinations of PV arrays, wind turbines, batteries, temperatures, reliabilities and system costs. Then based on these parameters, an iterative approach is adopted where all of the combinations are tried and the best one is chosen. Also, the authors of [12] used HOMER to study the feasibility of

TABLE II
SUMMARY OF SOME PAPERS.

Paper	Study	Architecture	Energy sources	Tool/algorithm	Main evaluation metric(s)
[3]	Power management	Single BS	Solar panels	Intelligent energy managing	State of the battery, outage percentage per year, maximum output power
[4]	Reduce the energy expenses	Network of green and normal BSs	RE for green cells, grid for normal cells	Guiding user to REBSs	Throughput degradation in term of ratio of saved non-green power, saved energy in term of traffic load
[12]	Grid failure management	Single BS	Grid, PV, DG	HOMER simulator	Net present cost , cost of electricity
[13]	Heterogeneous network deployment	Multi-tier 3GPP heterogeneous network	Grid, RE (PV plants)	Sizing the system and calculating the cost	Reduced CO_2 emission, cost saving in term of grid cost, amortization period
[17]	Minimizing transmission completion time	Single energy harvesting node	Any RE	Mathematical analysis	–
[18]	Maximizing transferred data	Single link	Any RE	Mathematical analysis, optimal policy	Maximum throughput, cumulative data transmitted
[20]	User satisfaction vs green energy	Macro LTE BS	RE (solar and wind), grid/DG	Weather forecast, power prediction	Percentage of user satisfaction in terms of non-renewable energy
[22]	Architecture designs and protocols	CSRA	RE, grid, backup generator	–	–
[23]	Optimize utilization of green energy	HPBSs overlapped by LPBSs	Grid for HPBS, RE for LPBSs	Cell breathing	Percentage of user outage
[24]	Cellular planning	Network of cellular BSs	RE, grid	Heuristic algorithms	CapEx and OpEx
[25]	Energy cooperation	Network of connected BSs	RE, grid	Linear programming, greedy algorithm	Percentage of saved energy, percentage of lost energy
[26]	Pre-Feasibility	Single GSM BS	RE (solar and wind), DG	Weather forecast, power prediction	Energy type (renewable and non renewable) consumed by the BS
[27]	Feasibility and sizing	Single CDMA BS	RE (solar and wind)	HOMER, iterative algorithm	Excess energy, electricity cost, state of battery
[28]	Optimize cell size for energy saving	Network of cellular BSs	RE, grid	Energy allocation policy, cell breathing	Consumed on-grid and renewable energy
[29]	Reduce the electric bill	Macro LTE BS	RE, grid	Simple price-aware energy management	Cost reduction

implementing RE for an on-grid BS as a solution for power failure and high fuel cost in Bangladesh. The authors present the proposed system, which is composed of PV cells, a battery, a converter, a DG and connection to the power grid. The study showed that the proposed system is more environment-friendly and cost-effective compared to traditional BS, although it requires significant initial investments.

Another approach is proposed by [13], where the authors considered sizing the renewable energy (PV) and storage system of next generation cellular networks envisions adopting the heterogeneous architecture described in [11]. The approach calculates PV land occupation and the storage size. The PV land occupation is calculated based on the BS's power needs and the number of hours of available solar insolation. To size the energy storage system, the amount of energy accumulated through a day is calculated. Then, for macro cells, the storage device nominal power is calculated for two extreme sky conditions, i.e. seven contiguous days of clear sky and seven contiguous days of heavily clouded sky. The two conditions are used to calculate the maximum energy storage and the battery's maximum discharging rate respectively. The number of batteries for a site is calculated based on the average between the two extreme condition nominal powers. The authors assumed that the availability of micro and small cells is not mandatory, thus the storage system rating can be reduced.

V. DEDICATED REBS ALGORITHMS

Recently, the fundamental design criteria of performance metric in green wireless networks have shifted from energy efficiency to energy sustainability [21], i.e. whether the harvested energy can sustain the traffic demands and meet quality of service (*QoS*) requirements of end users in the networks. Applying this concept is essential in any cellular system equipped with renewable energy sources. Moreover, the harvested energy must be utilized in an efficient way. Maximizing the utilization of harvested energy involves at least two aspects [23]. The first aspect is the multistage energy allocation problem that determines how much energy should be used at the current stage and how much must be reserved for future. The second aspect is maximizing the utilization of allocated energy in every stage. These two aspects are shown to be related in [28].

In [4] the authors proposed two detailed approaches, the handover parameter tuning for target cell selection and power control for coverage optimization. In other words, the mobile users are guided to associate with BSs powered by renewable

energy, which will reduce the on-grid energy consumption. They showed that these two approaches can result in a balance between the energy saving and the throughput impact. Another concept is proposed in [3], where the authors present intelligent energy managed service for green BS as a solution. The method predicts the energy generation and energy consumption based on both the weather forecast and the site's power consumption historical data. A hysteresis algorithm, based on the remaining battery load, is used to change the radio transmitted power output for maximum utilization of the harvested energy. A detailed study is done in [18], where a single link continuous time system is assumed to be continuously transmitting with a rate that can be varied at will via power control. The problem of short term maximization of energy harvested node is considered, i.e. maximizing the data transferred under a deadline constraint employing a realistic constraint for the energy battery (finite capacity). This problem is shown to be a shifted optimization problem. Moreover, minimization of the transmission completion time is introduced and shown to be closely related to the former problem. The two problems, are shown to be equivalent given the amount of data. The authors use mathematical analysis and provide formal proof of the necessary conditions for solving both problems and proposing the optimal transmission policy.

In [28] the authors optimize the cell size for energy saving in cellular networks powered by both renewable energy and the grid. The problem of cell optimization is decomposed into two sub-problems: multistage energy allocation (*MEA*) and minimizing energy consumption (*MEC*). A simple algorithm for energy allocation is proposed to allocate the amount of renewable energy used by each BS at each stage based on their demand and the condition of their storage. For the second sub problem, the author propose two step algorithm: 1) minimizing the on-grid energy BSs, 2) maximize the number of BSs that can be switched into sleep mode. Finally, the authors combine the MEA algorithm and the MEC algorithm to solve the cell size optimization. The authors of [23] propose intelligent cell breathing to optimize the utilization of green energy in cellular networks by minimizing the maximal energy depleting rate of BSs powered by RE sources. The authors considered heterogeneous networks with a mixture of high-powered BSs powered by grid and a low-powered base (LBS) stations powered by RE sources. The formulated problem aims at minimizing the maximum power depletion rate of the LBS. An algorithm called "ICE" is proposed as a solution for the min-max problem to achieve low computation complexity. The algorithm finds the energy dependent set and the vector of beacon power level decrements for the LBSs in the set. It then shrinks the coverage of these LBSs by reducing the beacon power levels. The overall power can be increased but the amount of non-green energy consumption is reduced.

The authors of [25] propose a new model for energy cooperation between cellular BSs, where each BS is equipped by RE sources and finite capacity energy storage. These BSs are connected by resistive power line for energy sharing. The authors find the optimal energy cooperation using linear programing in the case where energy and demand profiles are considered deterministic. On the other hand, online greedy algorithm is proposed for the case where energy and demand profiles are stochastic. Moreover, the authors study the effect of availability of energy state information on the gain of the energy cooperation.

In [29] we proposed a comprehensive methodology for REBS deployment and operation optimization of using RE in hybrid base station cellular network. This methodology is detailed by describing the area configuration, summarizing and proposing several objectives and presenting different types of constraints. We applied it for the city of Marseille, France, where we proposed an algorithm aimed at reducing the electric bill. The algorithm is for price-aware energy management and uses the real-time electricity price and the level of charge the battery.

In Table II, we summarize several papers that study RE in cellular networks. The summary includes the study, system architecture, energy sources, tools and main evaluation metrics used in each paper.

VI. Performance metrics

Many metrics are used for evaluating the energy efficiency, as detailed in the survey [6]. However, using RE in cellular networks introduces the need for new metrics to evaluate the performance of the new systems/algorithms. These metrics depend on the perspective of the study. In general we can classify these metrics into the following categories:

1) Economical metrics: The economical point of view is essential for the operators, where economical studies precede the decision of implementing RE in cellular networks. Examples: cost saving, operational cost, investment cost [12], [13], [27].
2) Environmental metrics: In order to evaluate the environmental profit of using RE. The percentage of reduced Carbon emissions is usually used as a reference [13].
3) Technical metrics: The technical states of different components of the system are usually studied to evaluate the performance of the system/algorithm. Special metrics are used for each component such as state of charge of the battery and maximum transmitted power time percentage of the BS [3], [27].
4) Feasibility metrics: These metrics are used to evaluate the applicability of the system, such as reliability as function of RE size and outage percentage in term of storage capacity [27], [3].
5) Quality metric: A wide range of metrics can be used to evaluate the satisfaction of users. Classical metrics can be easily adopted to suit the study of REBS systems. For example degradation of throughput, percentage of users' outage and throughput in terms of RE generation or component size (e.g. battery capacity) [4], [23], [18], [17].
6) Energy metrics: Several metrics can be used to study the utilization of RE, such as saved on-grid energy and

percentage of renewable and non renewable energy used [28], [26], [20].

VII. Conclusion

In this survey we presented the fundamental principles and motivations necessary for a thorough understanding of the usage of renewable energy in cellular networks. Employing RE is not only environment friendly, but has also other benefits with one of the notable points being the shift from energy efficiency to energy sustainability. We introduced a reference Renewable Energy Base Station (*REBS*) model, along with the concept of Renewable Energy-aware Base Stations (*REaBS*). Moreover, we surveyed the existing models for REBS subsystems and the recent advances in specialized algorithms for REBS. On a bigger scale, we presented the system architectures used for REBS-enabled networks along with the cellular planification, dimensioning and sizing approaches. Lastly, we outlined the metrics used for evaluation of the REBS-related research work.

The potential future developments in this domain are promising. Energy efficiency mechanisms can be adjusted in order to adapt to the shift towards energy sustainability. More specifically, we plan to explore the integration of REBS to the power grid and study the theoretical gains from a massive deployment of REaBS.

Acknowledgment

The authors would like to acknowledge the support of the French Ministry of Industry for funding this work under Celtic Opera Net 2 European Project. They also thank Christophe Grangeat for the provided references, and all partners for the fruitful discussions.

References

[1] Gartner, "Green it: The new industry shockwave," in *Presentation at Symposium/ ITXPO conference*, April 2007.

[2] S. Tombaz, A. Vastberg, and J. Zander, "Energy- and cost-effecient ultra-high-capacity wireless access," *IEEE wireless comminications*, October 2011.

[3] D. Valerdi, Q. Zhu, K. Exadaktylos, S. Xia, M. Arranz, R. Liu, and D. Xu, "Intelligent energy managed service for green base stations," in *GLOBECOM Workshops (GC Wkshps), 2010 IEEE*, Dec 2010.

[4] J. Zhou, M. Li, L. Liu, X. She, and L. Chen, "Energy source aware target cell selection and coverage optimization for power saving in cellular networks," in *Green Computing and Communications (GreenCom), 2010 IEEE/ACM Int'l Conference on Int'l Conference on Cyber, Physical and Social Computing (CPSCom)*, Dec 2010.

[5] M. Etoh, T. Ohya, and Y. Nakayama, "Energy consumption issues on mobile network systems," in *Applications and the Internet. SAINT 2008. International Symposium onApplications and the Internet, 2008. SAINT. International Symposium on*, 2008.

[6] L. Suarez, L. Nuaymi, and J.-M. Bonnin, "An overview and classification of research approaches in green wireless networks," *EURASIP Journal on Wireless Communications and Networking*, 2012.

[7] C. Han, T. Harrold, S. Armour, I. Krikidis, S. Videv, P. Grant, H. Haas, J. Thompson, I. Ku, C.-X. Wang, T. A. Le, M. Nakhai, J. Zhang, and L. Hanzo, "Green radio: Radio techniques to enable energy-efficient wireless networks," *Communications Magazine, IEEE*, vol. 49, no. 6, June 2011.

[8] L.-C. Wang and S. Rangapillai, "A survey on green 5g cellular networks," in *Signal Processing and Communications (SPCOM), 2012 International Conference on*, July 2012.

[9] [Online]. Available: http://www.gsmworld.com/our- work/mobile planet/green power for mobile/

[10] A. Fehske, G. Fettweis, J. Malmodin, and G. Biczok, "The global footprint of mobile communications: The ecological and economic perspective," *Communications Magazine, IEEE*, vol. 49, no. 8, August 2011.

[11] Z. Hasan, H. Boostanimehr, and V. K. Bhargava, "Green cellular networks: A survey, some research issues and challenges," *Communications Surveys Tutorials, IEEE*, vol. 13, no. 4, 2011.

[12] S. Moury, M. N. Khandoker, and S. M. Haider, "Feasibility study of solar pv arrays in grid connected cellular bts sites," in *Advances in Power Conversion and Energy Technologies (APCET), 2012 International Conference on*, August 2012.

[13] G. Piro, M. Miozzo, G. Forte, N. Baldo, L. Grieco, G. Boggia, and P. Dini, "Hetnets powered by renewable energy sources: Sustainable next-generation cellular networks," *Internet Computing, IEEE*, vol. 17, no. 1, Jan 2013.

[14] G. Auer, V. Giannini, C. Desset, I. Godor, P. Skillermark, M. Olsson, M. A. Imran, D. Sabella, M. J. Gonzalez, O. Blume, and A. Fehske, "How much energy is needed to run a wireless network?" *Wireless Communications, IEEE*, vol. 18, no. 5, October 2011.

[15] O. Arnold, F. Richter, G. Fettweis, and O. Blume, "Power consumption modeling of different base station types in heterogeneous cellular networks," in *Future Network and Mobile Summit*, 2010.

[16] G. Coppez, S. Chowdhury, and S. Chowdhury, "South african renewable energy hybrid power system storage needs, challenges and opportunities," in *Power and Energy Society General Meeting, IEEE*, July 2011.

[17] J. Yang and S. Ulukus, "Transmission completion time minimization in an energy harvesting system," in *Information Sciences and Systems (CISS), 2010 44th Annual Conference on*, March 2010.

[18] K. Tutuncuoglu and A. Yener, "optimum transmission policies for battery limited energy harvesting nodes," *Wireless Communications, IEEE Transactions on*, vol. 11, no. 3, March 2012.

[19] R. Raghuvir and D. Rajan, "Delay bounded rate and power control in energy harvesting wireless networks," in *Wireless Communications and Networking Conference (WCNC), 2011 IEEE*, March 2011.

[20] M. Carreno and L. Nuaymi, "Renewable energy use in cellular networks," in *accepted to VTC spring*, 2013.

[21] L. Cai, H. Poor, Y. Liu, T. Luan, X. Shen, and J. Mark, "Dimensioning network deployment and resource management in green mesh networks," *Wireless Communications, IEEE*, vol. 18, no. 5, October 2011.

[22] S. Yeh, "Green 4g communications: Renewable-energy-based architectures and protocols," in *Mobile Congress (GMC), 2010 Global*, Oct 2010.

[23] T. Han and N. Ansari, "Ice: Intelligent cell breathing to optimize the utilization of green energy," *IEEE communication letters*, vol. 16, no. 6, June 2012.

[24] M. Zheng, P. Pawełczak, S. Stańczak, and H. Yu, "Planning of cellular networks enhanced by energy harvesting," in *accepted to IEEE Communications Letters*, 2013.

[25] Y.-K. Chia, S. Sun, and R. Zhang, "Energy cooperation in cellular networks with renewable powered base stations," in *accepted to IEEE WCNC 2013*, 2013.

[26] P. Nema, S. Rangnekar, and R. Nema, "Pre-feasibility study of pv-solar / wind hybrid energy system for gsm type mobile telephony base station in central india," in *Computer and Automation Engineering (ICCAE), 2010 The 2nd International Conference on*, vol. 5, Feb 2010.

[27] S. Paudel, J. Shrestha, F. Neto, J. Ferreira, and M. Adhikari, "Optimization of hybrid pv/wind power system for remote telecom station," in *Power and Energy Systems (ICPS), 2011 International Conference on*, Dec 2011.

[28] T. Han and N. Ansary, "Optimizing cell size for energy saving in cellular networks with hybrid energy supplies." in *IEEE Globecom 2012*, 2012.

[29] H. Al Haj Hassan, L. Nuaymi, and A. Pelov, "Classification of renewable energy scenarios and objectives for cellular networks," in *PIMRC 2013 : IEEE 24th annual international symposium on personal, indoor and mobile radio communications*, 2013.

[30] T. A. Okrasunski, C. C. Onori, and J. M. Morabito, "Energy management and the enviroment," *AT'&'T Technical journal*, November 1995.

[31] C. Grangeat, G. Grandamy, and F. Wauquiez, "A solution to dynamically decrease power consumption of wireless base stations and power them with alternative energies," in *Telecommunications Energy Conference (INTELEC), 32nd International*, June 2010.

[32] "Homer simulator project web page, http://homerenergy.com/."

Power Control in Opportunistic and Efficient Resource Block Allocation Algorithms for Green LTE Uplink Networks

Fatima Zohra Kaddour [1,2], Emmanuelle Vivier [2], Mylene Pischella [3], Lina Mroueh [2], Philippe Martins [1]
[1] Telecom ParisTech, 46 rue Barrault, Paris, France
[2] ISEP, 28 rue N-D des Champs, Paris, France
[3] CNAM, 292 rue Saint-Martin, Paris, France

***Abstract*—The energy efficiency in wireless networks is currently a central concern of research. We propose in this paper a new energy efficiency scheme which allocates the mobile's transmission power in function of the allocated Resource Blocks (RB) and the channel conditions of the user on the allocated RBs. We focus on the energy efficiency of the Opportunistic and Efficient Resource Block Allocation (OEA) algorithm and its variant adapted to the Quality of Service (QoS) of the traffics: the QoS based OEA for LTE uplink networks. The OEA and the QoS based OEA allocate the RBs to UEs efficiently and with respect to the SC-FDMA constraints, such that, for one user, contiguous RBs are allocated, and the same Modulation and Coding Scheme (MCS) is used over the whole allocated RBs. Once RBs are allocated to UEs, power control is then applied to the mobile's transmission power considering the MCS used and the channel conditions. This energy efficiency allows users to achieve the same throughput than before the power control and does not affect the MCS selection established at the RB allocation step. This new scheme allows the transmission of a high number of bits per Joule.**

Keywords: Energy Efficiency, Power control, Resource Block allocation, SC-FDMA, LTE.

I. Introduction

Nowadays, in current and next generation of mobile's networks, the telecommunication and information communities are facing an increasing challenges to satisfy the quality of service required by the smart terminal enhanced functionalities. Then the energy consumption of wireless communication networks and the relevant global CO_2 emission show continuous growth for several years. In [1], it has been emphasized that actually the information and communication technology infrastructures consume about 3% of the world-wild energy which causes about 2% of the world-wild CO_2 emissions. Energy costs to the mobile's operators a half of the operating expenses [2]. Moreover, improving the energy efficiency as the resource efficiency is not only beneficial for the global environment, but also makes commercial sense for telecommunication operators supporting sustainable and profitable business.

Within the framework of green communications, a number of technical approaches are investigated in the literature. We focus on the energy efficient wireless transmission techniques on uplink 3rd Generation Partner Project (3GPP) Long Term Evolution (LTE) networks. The 3GPP standard adopted, for the LTE networks, the Orthogonal Frequency Division Multiple Access (OFDMA) and the Single Carrier Frequency Division Multiple Access (SC-FDMA) for both downlink and uplink respectively. The relevance of the SC-FDMA on the uplink is that in addition to the OFDMA advantages, the SC-FDMA generates a low Peak to Average Power Ration (PAPR), by considering the whole allocated Resource Blocks (RB) as a single carrier. The reduction of the PAPR can be more than 25% compared to the OFDMA technique [3]. This advantage not only leads to the decrease of the equalizer complexity and the cost of the mobile terminal by the same way, but also to the decrease of the mobile energy consumption. Using the SC-FDMA technique on the uplink is an encouraging start but it can not increase much the mobile battery life. Therefore, saving the battery life of the mobile's terminal becomes the central concern of the researchers. Works on this scope focus on: (i) maximizing the available energy and (ii) minimizing the energy consumption. The available energy can be increased by (a) the battery capacity improvement which is, unfortunately, not sufficient and is limited due to design aspect, and (b) using the surrounding energy sources, such as kinetic, thermal, and solar energy [4]. The mobile's energy consumption can be minimized by first, optimizing the hardware energy consumption, such as choosing power efficient components and applying power management like performing sleep modes for inactive hardware [5] or the Discontinuous Reception (DRX) in idle mode [6]. The second solution to minimize the mobile's energy consumption is the adjustment of the mobile's parameters, like the brightness display and the processor speed for some applications. In the uplink radio access network, the power consumption reduction is performed by reducing the mobile's transmission power with a power control. In [7], the authors propose to decrease or increase the UE transmission power by 1 dB if needed. A power control depending on the bandwidth frequency was proposed in [8]. This method is usually known as a Soft Frequency Reuse (SFR). It combines a frequency planning and a power control, where a power level is allocated for each portion of the frequency bandwidth. Many combination schemes are proposed, while the main idea is to allocate three different power levels at each third portion of the bandwidth. However, reduction on the mobile transmission power could lead to

978-1-4799-0354-2/13/$31.00 ©2013 IEEE

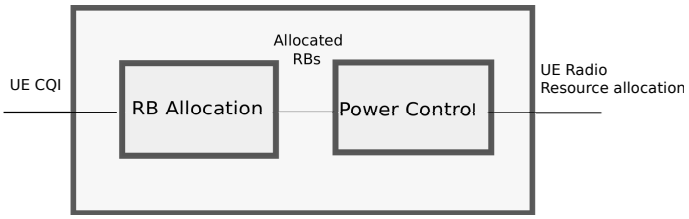

Fig. 1. Energy efficiency scheme

low user's Signal to Interference plus Noise Ratio (SINR) and a low individual throughput. Therefore, the power control should take into account the channel conditions experienced by the User Equipment (UE) and the required SINR which allows the UE to use the same Modulation and Coding Scheme (MCS) and reach the same throughput as before power control application. This study focuses on the energy efficiency of the terminals performed by a power control of the UE's transmission power considering the Resource Block (RB) allocation policy and the MCS used by each UE. We study the energy efficiency according to the Opportunistic and Efficient RB Allocation (OEA) algorithm and the Quality of Service (QoS) based OEA algorithm which is adapted to the QoS traffic, proposed in our previous work [9].
The paper is organized as follows. Section II presents the system model. In Section III, we define the proposed energy efficiency scheme including the RB and the power allocation methods. Simulation parameters are summarized in Section IV. Section V shows the numerical results and a comparison in terms of energy efficiency with other reference RB allocation algorithms. Finally, Section VI concludes the paper.

II. System Model

We consider an uplink LTE network composed of 19 hexagonal cells. Each cell is provided with a tri-sectored eNodeB (eNB). We allocate at each sector a different bandwidth B (i.e. we adopt a $1\times3\times1$ frequency reuse pattern), corresponding to N_{RB} available RBs. The proposed energy efficiency scheme is divided into two entities: (i) the RB allocation, and (ii) the power control, as shown in Figure 1. The RB allocation entity allocates the RBs to the UEs in function of their Channel Quality Identifier (CQI). One RB consists of 84 Resource Elements (REs) corresponding to $N_{sc}^{RB} = 12$ subcarriers of 15 kHz bandwidth each and $N_{symb}^{RB} = 7$ SC-FDMA symbols in the normal prefix cyclic case [10]. On the uplink, the CQI is evaluated by the dint of the Reference Signals (RS) which are sent at each time slot in the 4th SC-FDMA symbol [11]. The RS use 14% of the total number of REs. Then, the number of REs used for data transmission in one RB is equal to 72 and the real throughput (i.e. considering the MCS selection) that can be achieved by each user k can be computed as:

$$R_k = \sum_{c\in\mathcal{A}_k} \frac{72}{T_s}\,\mathrm{BRE}_k \mid \mathcal{A}_k \mid \tag{1}$$

where, T_s is the time slot duration equivalent to 0.5 ms, BRE_k denote the number of bits per RE allowed for UE k by the used MCS and $\mathcal{A}_k$ is the set of RBs allocated to UE k by the RB allocation entity, with $\mid \mathcal{A}_k \mid$ its cardinal. The MCS selection is based on the channel conditions (i.e. the SINR level experienced by each user in each RB c). The specificity of the SC-FDMA technique is that each UE should use the same MCS over the whole allocated RBs. Thus, the MCS selection is based on the minimum signal to interference plus noise ratio experienced by the concerned UE on the whole allocated RBs (i.e. $\forall c \in \mathcal{A}_k$).

In case of frequency and time correlated fast fading and for a given RB, the SINR level of each UE is computed at each RE (i,j) (with $1 \le i \le N_{symb}^{RB}$ and $1 \le j \le N_{sc}^{RB}$), as:

$$\mathrm{SINR}_k^{(i,j)} = \frac{P_{k_{Tx}}^{(i,j)}\; G_t\; G_r(\theta_k)\Lambda}{N + I^{(i,j)}} \tag{2}$$

where Λ is the total channel gain, expressed as:

$$\Lambda = G_c(r_k)\;\mid A_f^{(i,j)} \mid^2 A_s^{(i,j)} \tag{3}$$

$G_c(r_k)$ is the path loss depending of r_k, the distance between the user k and the eNB. $A_s^{(i,j)}$ is the random shadowing over one RE which follows a log-normal distribution with parameter σ_s and $A_f^{(i,j)}$ is the time-frequency correlated coefficients fast fading.

$P_{k_{Tx}}^{(i,j)}$ is the transmission power of user k over one resource element. Since the power is equally divided over all the resource elements of one RB, $P_{k_{Tx}}^{(i,j)}$ can be expressed as:

$$P_{k_{Tx}}^{(i,j)} = \frac{P_{k_{Tx}}}{N_{sc}^{RB} \mid \mathcal{A}_k \mid} \tag{4}$$

with $P_{k_{Tx}}$ the mobile's transmission power, set at its maximum before the power control (i.e. $P_{k_{Tx}}$ equal to P_{max}). The mobile's transmission antenna gain and the eNB antenna reception gain are denoted respectively as G_t and G_r. The eNB antenna reception gain G_r depends on θ_k, angle between UE k and eNB antenna boresight. N is the thermal noise in the considered subcarrier and $I^{(i,j)}$ is the ICI level at each resource element (i,j) obtained by Monte Carlo simulations.

The signal to interference plus noise ratio over one RB c for user k is computed using the mean instantaneous capacity method defined in [12]. It is denoted the effective SINR ($\mathrm{SINR}_{\mathrm{eff}_k}$) and is computed as follows:

$$\mathrm{SINR}_{\mathrm{eff}_k}^{c} = 2^{C_k / N_{symb}^{UL}} - 1 \tag{5}$$

with C_k the theoretical Shannon capacity over the whole RB, computed as:

$$C_k = \frac{1}{N_{sc}^{RB}} \sum_{i=1}^{N_{symb}^{UL}} \sum_{j=1}^{N_{sc}^{RB}} \log_2\left(1 + \mathrm{SINR}_k^{(i,j)}\right) \tag{6}$$

The effective signal to interference plus noise ratio computed for each user k and over each RB c ($\mathrm{SINR}_{\mathrm{eff}_k}^{c}$) will be used as a metric for the RB allocation algorithm detailed in the next section.

III. Energy efficiency scheme

The LTE uplink radio resource management includes the RBs and the power allocation, which can be performed: (i) conjointly, or (ii) separately. The conjoint manner is proposed in [13], where the Binary Integer Programming (BIP) is used to optimally minimize the total power expenditure subject to the rate constraints. The authors consider the contiguity constraint directed by the SC-FDMA technique but compute the total mobile throughput using the theoretical upper bound (i.e. the Shannon capacity). The BIP is commonly proposed as an optimal solution for resource allocation in wireless network, but this method is NP hard. Since the radio resource management occurs at each transmission time interval (which is equal to 1 ms), using the optimal method becomes irrelevant and would cost a lot in terms of computational complexity in the context of green communications, which motivated us to use a heuristic in allocating the RBs and the mobile's transmission power.

The proposed energy efficiency method allocates the mobile's transmission power after the RB allocation. The power control applied to the mobile's transmission power on the allocated RBs ensures the throughput maximization while minimizing the mobile's power consumption without disrupting the RB allocation, the QoS nor the MCS selected. The two steps: (i) RB allocation and (ii) the power control, are described as follows:

A. RB allocation step

For RBs allocation, we use the Opportunistic and Efficient RB Allocation algorithm. We consider that there are N_{UE} users able to transmit their data. Thus, we define $\mathcal{K}$ the set of users able to be scheduled $\mathcal{K} = \{1, \cdots, k, \cdots, N_{UE}\}$ and $\mathcal{C}$ the set of free RBs $\mathcal{C} = \{1, \cdots, c, \cdots, N_{RB}\}$. The OEA algorithm aims to maximize the aggregate throughput of the network by allocating efficiently the resource blocks.

$$\max \sum_{k=1}^{N_{UE}} R_k \tag{7}$$

where R_k is the total individual throughput of user k over the whole allocated RBs, and is computed using Equation 1. The maximization problem is subject to:

1) the exclusivity of the allocated RBs:

$$\sum_{k=1}^{N_{UE}} x_k^c = 1 \quad \forall c \in \mathcal{C} \tag{8}$$

2) the contiguity constraints:

$$x_k^j = 0 \ \forall j > c+2 \text{ if } x_k^c = 1 \text{ and } x_k^{c+1} = 0 \tag{9}$$

3) the MCS robustness:

$$\mathrm{BRE}_k = \min_{c \in A_k} \mathrm{BRE}_k^c \tag{10}$$

where, x_k^c is equal to 1 if the RB c is allocated to UE k, and equal to 0 otherwise and BRE_k^c is the number of bit per RE allowed for UE k on each allocated RB c.

Actually, the algorithm respects the SC-FDMA constraints. It allocates exclusively adjacent RBs to the same UE (by Formulas 8 and 9) and ensures the MCS robustness (by Formula 10). To maximize the aggregate throughput, the algorithm uses as a metric the effective SINR experienced by each user over each RB. It searches first the pair (UE-RB) which maximizes the metric, then extends the allocation to the adjacent RBs. The RBs expansion allocation is done if and only if the individual throughput of the UE increases. To adapt the OEA algorithm to the QoS required by users, we fix a maximum number of allocated RBs per UE which satisfies its QoS requirements. The RBs allocation expansion is performed as long as this maximum number of allocated RBs per UE is not reached. More important step, which is often neglected in the literature, is the update of the metric before each RBs allocation expansion. The update of the metric considering the update of the mobile's transmission power per RB (using Equation 4), allows us to recursively compute the correct value of individual throughput, the parameter which is based on the expansion decision of the RB allocation.

B. Power control step

Since each mobile user k has its set of allocated RBs $\mathcal{A}_k$, the second step determines the appropriate transmission power. It allows the user to use the same MCS as before the power control and to reach the same throughput. To use a given MCS, the UE must experience in the whole allocated RBs a SINR level higher than the minimum SINR range of the used MCS ($\mathrm{SINR}_{MCS,k}$) expressed in dB. To ensure user k to use the same MCS as the one used before the power allocation, we define an SINR target (SINR_{Tg}) expressed in dB as:

$$\mathrm{SINR}_{Tg} = \mathrm{SINR}_{MCS,k} + \Delta_{\mathrm{SINR}} \tag{11}$$

where, Δ_{SINR} is an SINR margin (in dB). The new mobile's transmission power per RB P_{e_k} allocated to UE k and which allows it to reach the target SINR and achieve the same throughput than the one achieved before the power control, is expressed as:

$$P_{e,k} = \frac{P_{k_{T_x}}}{\mid \mathcal{A}_k \mid} \frac{\mathrm{SINR}_{Tg}}{\mathrm{SINR}_{\mathrm{eff}_k,min}} \tag{12}$$

where, $\mathrm{SINR}_{\mathrm{eff}_k,min}$ is the minimum effective SINR experienced by the UE k on the whole allocated RBs:

$$\mathrm{SINR}_{\mathrm{eff}_k,min} = \min_{c \in \mathcal{A}_k} \mathrm{SINR}_{\mathrm{eff}_k}^c \tag{13}$$

The MCS robustness is guaranteed by the $\mathrm{SINR}_{\mathrm{eff}_k,min}$ based power control.

IV. Simulation parameters

To evaluate the performance of the proposed resource allocation algorithm, we evaluate the mobile's energy consumption saving obtained thanks to power control. Our study focuses on the RB and power allocation to one sector of the central cell users. We compare the OEA

algorithm performance with the literature reference's RB allocation algorithms, such as: the Heuristic Localized Gradient Algorithm (HLGA), the Frequency Domain Packet Scheduling - Largest Metric value First algorithm (FDPS-LMF) and the Recursive Maximum Expansion algorithm (RME) proposed respectively in [14], [15] and [16].

The simulations have been run on MATLAB, by considering the LTE standard's parameters. The performance evaluation is studied in low and high loaded network. Then, the total number of pedestrian users per sector varies between 5 to 80 UEs per sector while a bandwidth B $= 5$ MHz is allocated to each sector. This correspond to $N_{RB} = 25$ available RBs per sector. We consider an infinite backlogged traffic, in which, for each user, there is always available data for transmission. The target Bit Error Rate (BER) is equal to 10^{-6} and the throughput is computed using the MCS lookup table taken from [17], restrictted to the MCS listed in Table I, and respecting the MCS robustness. The path loss is modeled by the Okumura Hata model [18] where the carrier frequency is set to 2.6 GHz, the eNB height is at 40 m and the UE height at 1.5 m. The remaining simulation parameters are summarized in Table I.

Cellular layout	Hexagonal grid,19 tri-sector cells.
Max/ Min UE-BS distance	1000 m/30 m
Carrier frequency	2.6 GHz
System bandwidth	$B = 5$ MHz per sector $\Rightarrow N_{RB} = 25$
FFT size	512
Subcarrier spacing	15kHz
Time slot duration	$T_s = 0.5\ ms$
Target Throughput	300 kbps
SINR margin Δ_{SINR}	0.3 dB
Radio channel gain	Okumura Hata for urban areas: $G_c(r_{jc}) = 10^{-a/10} * r_{jc}^{-b/10}$ $a = 136.7$ and $b = 34.4$
BS antenna pattern	$G_r(\theta_{jc}) = -min[12 * (\frac{\theta_{jc}}{\theta_{3dB}})^2, \beta]$ $\theta_{3dB} = 70°$, $\beta = 20$ dB
User power class	$P_{max} = 21$ dBm (125 mW)
User antenna gain	$G_t = 0$ dBi
Rayleigh fading	coef corr $= 0.5$, UE velocity $= 3$ km/h
Log-normal shadowing	$\sigma_s = 5$ dB
MCS setting	QPSK $1/2, 2/3, 3/4$ 16 QAM $1/2, 2/3, 3/4$ 64 QAM $1/2, 2/3, 3/4$

TABLE I
SIMULATION PARAMETERS

V. PERFORMANCE EVALUATION

The objective of the proposed energy efficiency method is to allocate both RBs and the mobile's transmission power efficiently, which allows users to benefit from a higher throughput without wasting RB while radiating at a lower power and increasing the mobile's battery life. Figure 2 shows the aggregate throughput of the central cell while varying the network's load (i.e. varying the number of UE from 5 to 80, which corresponds to a number of UE per number of RBs ratio of 20% to 320%). Since the number

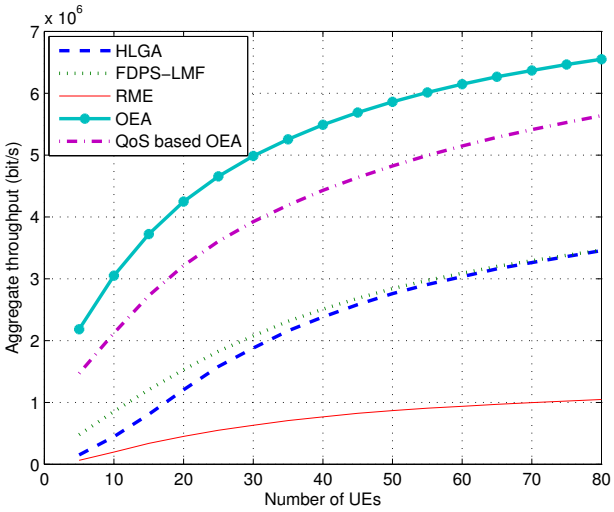

Fig. 2. Aggregate throughput (bits/s)

of UEs per sector and the number of served UEs increase, the aggregate throughput per sector increases whatever the used RB allocation algorithms. We notice that the OEA algorithm reaches its objective and maximizes the aggregate throughput. Its achieves more than 2 Mbps at low loaded network (when there are only 5 UEs per sector) and 6.5 Mbps at highly loaded network (80 UE per sector). The QoS based OEA algorithm achieves a lower aggregate throughput than OEA algorithm, due to the low target throughput fixed at 300 kbps. Then, the QoS based OEA algorithm allocates an adequate number of RBs to UEs which allows them to achieve the target throughput unlike the OEA algorithm, where an UE can be allocated all the RBs that maximize its individual throughput depending on its channel conditions even if it takes all the available RBs allocated to the sector N_{RB}. The HLGA and the FDPS-LMF algorithms achieve a lower aggregate throughput than QoS based OEA algorithm one. Since the RB allocation policy of the HLGA and the FDPS-LMF algorithms is similar, except for the allocation of the remaining RBs, we note a small difference between their total aggregate throughput. The aggregate throughput gap between HLGA and FDPS-LMF is notable at low load because there are more remaining RBs and the HLGA, by allocating the remaining RBs to users which satisfy the contiguity constraints whatever their SINR level, decreases the aggregate throughput. The lower aggregate throughput is given by the RME since it allocates a lot of RBs per UE without any SINR update before the end of the RB allocation. The resulting SINR value computed at the end of the process, is often even too low to unsure the minimum MCS. The HLGA, FDPS and RME also achieve a lower aggregate throughput than the OEA and the QoS based OEA algorithms due to their negligence of the metric update at each RB allocation expansion and the MCS robustness constraints.

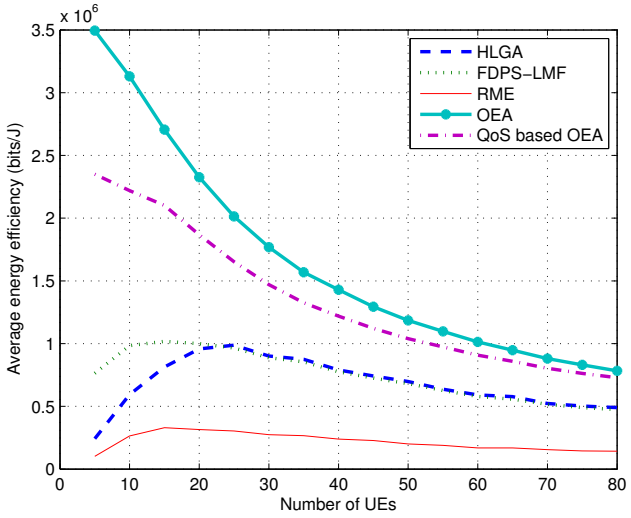

Fig. 3. Average energy efficiency before power control (bits/J)

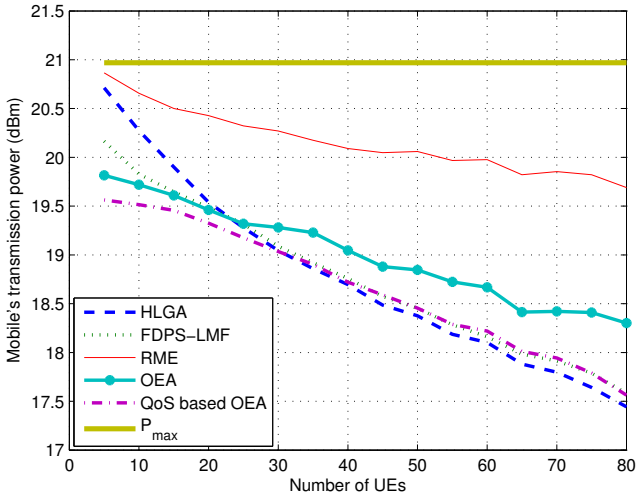

Fig. 5. Average mobile's transmission power per UE (dBm)

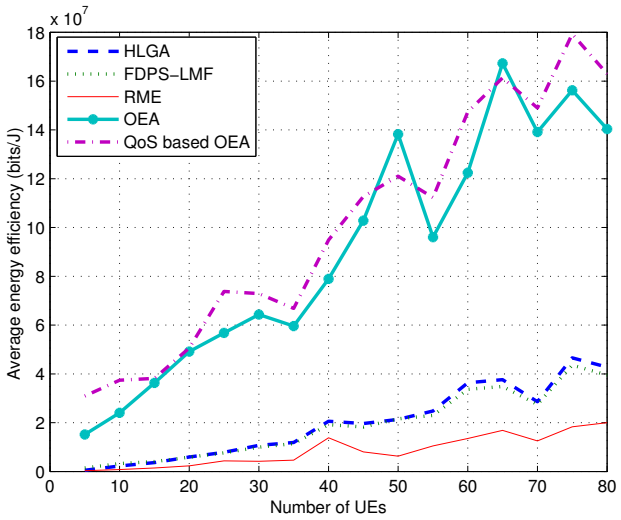

Fig. 4. Average energy efficiency after power control (bits/J)

Figure 3 and 4 represent respectively, the energy efficiency of the transmitted data before and after the power control. The energy efficiency of the transmitted data in bits per Joule is defined by the ratio between the number of data transmitted in one second and the necessary consumed energy for transmission in one second. Before the power control, all the mobiles transmit at their maximum power P_{max}. Since the OEA and the QoS based OEA algorithms achieve a higher throughput, then they achieve a higher energy efficiency. They reach respectively 3.5 10^6 and 2.4 10^6 bits/J at low load, while the RME, FDPS-LMF and the HLGA do not exceed 8 10^5 bits/J. In highly loaded networks, the energy efficiency decreases for the five algorithms to reach 7.5 10^5 bits/J for the OEA algorithm and 7 10^5 bits/J for the QoS based OEA algorithm, 5 10^5 bits/J for both HLGA and FDPS-LMF algorithms and 2 10^5 bits/J for the RME algorithm.

Unlike the maximum transmission power case, the energy efficiency curves increase when the network load increases after applying power control. In case of highly loaded networks the number of allocated RBs to each UE is low, due to the high number of UEs, which makes the power control more efficient. The number of bits transmitted per one Joule achieves 180 Mbits and 170 Mbits for the QoS based OEA and the OEA respectively. The curves are not smoothed as before the power control curves, because the power allocation depends on the minimum SINR range of the used MCS which is not linear.

Figure 5 shows the average mobile's transmission power in dBm. The thick line corresponds to the mobile's maximum transmission power set to 21 dBm (i.e. 125 mW). The minimum observed mobile's transmission power is about 17 dBm, which is higher than the lower bound of the transmission power equal to -48 dBm allowed by the 3GPP standard [10]. We notice that the RME does not decrease a lot the mobile's transmission power still due to the high number of allocated RBs. The algorithms which allow a lowest mobile's transmission power are the HLGA, the FDPS-LMF and the QoS based OEA. This large power reduction is explained by the number of RBs allocated to each UE. Actually if $\mid \mathcal{A}_k \mid$ is low, $P_{k_{Tx}}$ is high and the power control according to the $SINR_{Tg}$ is more efficient. In Figure 6, we represent the ratio of saved energy after the power control. The RME algorithm saves only from 2% to 25% of the mobile's transmission power depending to the network load, where the QoS based OEA algorithm saves from 28% to 65% of the mobile's transmission power, which allows it to increase even more the mobile's battery life.

The computational complexity evaluation of all the RB allocation algorithm entities was detailed in our previous work [9]. The Computational complexity of power control entity is given with $\mathcal{O}(2N_{RB}+1)$ which include the number of

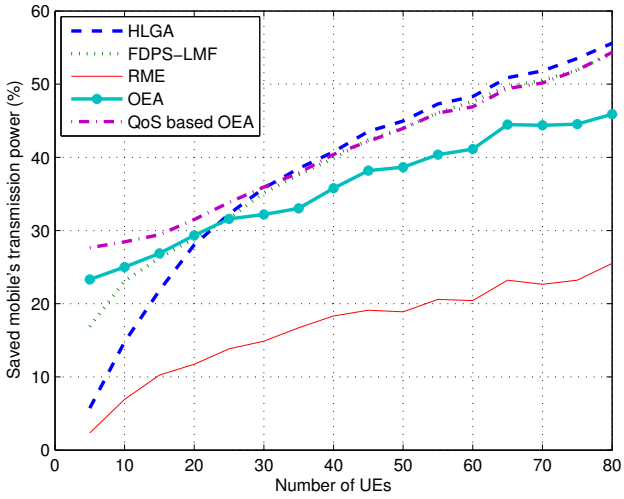

Fig. 6. Saved power

allocated RBs counting and the search of minimum effective SINR experienced by each UE overs its whole allocated RBs. Then, the computational complexity of the proposed radio resource allocation scheme, using OEA and QoS based OEA algorithms, is given with:

$$\mathcal{C}_{RRM} = \mathcal{O}\big(\tfrac{1}{2}N_{\mathrm{UE}}^3 + \tfrac{1}{2}(1-3N_{\mathrm{RB}})N_{\mathrm{UE}}^2 + (2N_{\mathrm{RB}}^2 - \tfrac{3}{2}N_{\mathrm{RB}})N_{\mathrm{UE}}\big) + \mathcal{O}(2.N_{RB}+1) \quad \forall N_{UE} \geq N_{RB} \tag{14}$$

and

$$\mathcal{C}_{RRM} = \mathcal{O}\big(\tfrac{1}{2}N_{\mathrm{RB}}^3 + \tfrac{1}{2}(N_{\mathrm{UE}}-1)N_{\mathrm{RB}}^2 - \tfrac{1}{2}N_{\mathrm{UE}}N_{\mathrm{RB}}\big) \mathcal{O}(2.N_{RB}+1) \quad \forall\ N_{UE} \leq N_{RB} \tag{15}$$

The computational complexity, whatever the number of UE is polynomial, which makes is possible to be implemented in LTE hardware equipments.

VI. Conclusion

In this paper, we investigate the energy consumption problem of the wireless network and more specifically the energy efficiency on the LTE uplink network, which leads to an increase of the LTE mobile's battery's life. We propose a new energy efficiency scheme which depends on the resource block allocation algorithms. The proposed radio resource allocation algorithm allocates first the resource blocks to the UEs, using the Opportunistic and Efficient RB Allocation algorithm and the QoS based Opportunistic and Efficient RB Allocation algorithm, to allocate the RBs to the active users. The RBs are first allocated to UEs according to their channel conditions and respecting the SC-FDMA constraints; then we apply a power control to the mobile's transmission power which reduces the mobile's radiated power without affecting the MCS selection and the individually reached throughput. To evaluate the performances of the proposed energy efficiency scheme obtained by the OEA and the QoS based OEA, we compare the saved energy after power control when the RME, FDPS-LMF and the HLGA algorithms are used for the RB allocation. The numerical results show that the OEA algorithms achieve the higher number of bits per Joule and in case of QoS traffic, the QoS based OEA allows to save more than half of the mobile's energy. The low computational complexity of the proposed radio resource allocation scheme makes it more attractive to be implemented in LTE hardware equipments. In future work, we will compare the proposed energy efficiency scheme with the optimal one, using the binary integer programming method.

References

[1] e Mobility European Technology Platform, *1st International Workshop on Green Wireless 2008 (W-GREEN)*, September 2008. [Online]. Available: http://www.cwc.oulu.fi/workshops/W-Green2008.pdf

[2] Ericsson, *Ericsson Press Release*, June 2008. [Online]. Available: http://www.ericsson.com/ericsson/press

[3] H. G. Myung, "Single Carrier Orthogonal Multiple Access Technique for Broadband Wireless Communications," Ph.D. dissertation, Polytechnic university, 2007.

[4] A. Joseph, "Energy harvesting projects," *Pervasive Computing, IEEE*, vol. 4, no. 1, pp. 69–71, 2005.

[5] A. Lioumpas and A. Alexiou, "Uplink scheduling for Machine-to-Machine communications in LTE-based cellular systems," in *GLOBECOM Workshops (GC Wkshps), 2011 IEEE*, 2011, pp. 353–357.

[6] S. Fowler, "Study on power saving based on radio frame in LTE wireless communication system using DRX," in *GLOBECOM Workshops (GC Wkshps), 2011 IEEE*, 2011, pp. 1062–1066.

[7] F. Calabrese, M. Anas, C. Rosa, P. Mogensen, and K. Pedersen, "Performance of a radio resource allocation algorithm for utran lte uplink," in *IEEE 65th Vehicular Technology Conference (VTC2007-Spring)*, April 2007, pp. 2895–2899.

[8] Nortel, "Adaptive fractional frequency reuse," 2006.

[9] F. Z. Kaddour, M. Pischella, P. Martins, E. Vivier, and L. Mroueh, "Opportunistic and Efficient Resource Block Allocation Algorithms for LTE Uplink Networks," in *Wireless Communications and Networking Conference - WCNC, IEEE*, 2013.

[10] *Evolved Universal Terrestrial Radio Access (E-UTRA); User Equipment (UE) radio transmission and reception*, 3GPP TS 36.101 , V10.3.0 Std., June 2011.

[11] Y.-H. Nam, Y. Akimoto, Y. Kim, M. il Lee, K. Bhattad, and A. Ekpenyong, "Evolution of reference signals for LTE-advanced systems," *Communications Magazine, IEEE*, vol. 50, no. 2, pp. 132–138, 2012.

[12] K. Ramadas and R. Jain, "Wimax system evaluation methodology," *Technical report*, January 2007.

[13] F. I. Sokmen and T. Girici, "Uplink Resource Allocation Algorithms for Single-Carrier FDMA Systems," in *European Wireless Conference*, Lucca, Tuscany, Italy, April 2010.

[14] M. Al-Rawi, R. Jantti, J. Torsner, and M. S. gfors, "Opportunistic Uplink Scheduling for 3G LTE Systems," in *Innovations in Information Technology*, Dubai, UEA, November 2007.

[15] S.-B. Lee, L. Pefkianakis, A. Meyerson, S. Xu, and S. Lu, "Proportional Fair Frequency-Domain Packet Scheduling for 3GPP LTE Uplink," in *INFOCOM*, April 2009, pp. 2611 – 2615.

[16] L. Á. M. R. de Temiño, G. Berardinelli, S. Frattasi, and P. E. Mogensen, "Channel-aware scheduling algorithms for sc-fdma in lte uplink," in *IEEE International Symposium on Personal, Indoor and Mobile Radio Communications, PIMRC*, September 2008.

[17] M. Jar and G. Fettweis, "Throughput Maximization for LTE Uplink via Resource Allocation," in *The Ninth International Symposium on Wireless Communication Systems, ISWCS*, August 2012.

[18] Y. Okumura, E. Ohmori, and K. Fukuda, "Field Strength and its Variability in VHF and UHF Land-Mobile Radio Service," *Review of the Electrical communication Laboratory*, pp. 825–873, 1968.

Energy-efficient and accurate fingerprinting-based localization system for Smartphones

Gianluca Aloi, Giuseppe Caliciuri, Valeria Loscrí, Pasquale Pace
DIMES - Department of Informatics, Modeling, Electronics and System Engineering
University of Calabria, Rende, ITALY
Email: {aloi, gcaliciuri, vloscri, ppace}@dimes.unical.it

***Abstract*—New location-aware smartphones applications making use of positioning information, are recently gaining an increasing diffusion although the same accuracy provided by those classical solutions, based on the well known GPS technology, is progressively reached by adopting new or revised less power-hungry communication technologies. Starting from this general framework and taking into account the novel *green communication paradigm*, the paper a cost-effective and energy-efficient localization architecture based on the improvement of classical cell-tower schemes coupled with a dynamic fingerprinting update phase in order to face the natural changes in the radio environments. The proposed system architecture has been implemented and tested in a real scenario to measure the performances in terms of accuracy and energy saving that will make it preferable to the traditional GPS-based systems in the next future. The obtained results show the effectiveness of the considered approach that makes possible to estimate the current position of a mobile user with a very small error ($\approx 20m$) also achieving an energy consumption reduction of about 38% respect to the classical GPS solutions.**

***Index Terms*—Localization Techniques, Positioning, Fingerprinting, Smartphones.**

I. Introduction

Mass diffusion of personal devices with location capabilities, such as smartphones and tablets, is fostering the development of an increasing number of new intelligent applications and location-aware services. Users' position information are continuously logged and location search queries [1], [2] are frequently used to provide context-aware responses. Due to the limited battery life of mobile devices, the energy efficiency of positioning systems (i.e. GPS based, Wi-Fi based and Cell-ID based) coupled with the necessary precision, is one of the most critical issues in the development of location aware services. For example, it is well known that the high localization accuracy guaranteed by GPS location services has to be paid in terms of battery life, since the GPS power consuming is particularly high [7]. On the other side, standard power saving approaches such as the classical Cell-ID positioning, can only provide an approximate localization that can span from hundreds of meters to a few kilometers; in addition, Wi-Fi based localization techniques could represent a good compromise between accuracy and energy efficiency but, unfortunately, this kind of method can be adopted only in presence of an high density of access points (i.e. indoor or urban areas).

Starting from these consideration, and with the aim of obtaining an energy-efficient and accurate positioning system, we propose a new localization method that improves the accuracy of the classical Cell-ID technique by integrating received signal strengths (RSS) measurements and a cost-effective fingerprinting method. The proposed localization technique was tested in different realistic scenarios to fully validates the presented study. Obtained results demonstrate the goodness of the work in terms of accuracy, simplicity, power saving, costs and feasibility.

The rest of the paper is organized as follow: section II motivates the work by introducing the main objectives to be reached and by discussing related works to this topic; section III presents the proposed localization technique from a theoretical point of view; section IV describes the overall system architecture to support the localization strategy; section V shows the testbed implementation and the obtained results and, finally, conclusions and future research directions have been drawn in section VI.

II. Related works and Motivations

To motivate the work we introduce the main goals to be reached by the proposed localization system and we compare it with existing solutions.

Localization techniques based on GPS [6], as well as recent evolutions consisting in a combination of GPS and Cell-ID sequence matching techniques [8] or into a wise rate-adaptive GPS-based positioning by periodically duty-cycle GPS at a fixed interval, are extremely power-hungry [7]. Our proposed localization system is Cell-ID based and it does not use the GPS signal. The absence of a GPS receiver determines a significant benefit in terms of energy consumption.

Many studies have demonstrated that a fingerprinting method needs a continuous war-driving effort to provide precise localization and positioning services [3]. Since signal strength keeps on fluctuating, due to changes in physical environment, the fingerprinting map/database has to be constantly updated. Nowadays a growing number of insurance companies ask their customers to install a black-box [4], [5] in vehicles to detect the mileage, potential road accidents and other information of interest. The black-box is typically equipped with a GSM/GPRS module that is used to log the GPS position tracking of the vehicle in a remote storage server. Our localization system is based on the hypothesis that, if the measured GPS positions is sent together with the Cell-ID(s) and the associated RSS (Received Signal Strengths), the

978-1-4799-0354-2/13/$31.00 ©2013 IEEE

fingerprinting map/database will be obtained, and periodically updated, almost for free. The main weakness of this approach is the need of a high number of circulating vehicles/black-box to obtain an adequate fingerprint data density and accuracy. However, since it is reasonable to assume that, in a short time, the black-box will become a basic equipment of each vehicle, this weakness should disappear.

The position estimation is performed in few steps. A mobile device detect the current couple (Cell-ID, RSS) for each base station within its coverage area. This set of couples is sent to a Service Center. At the Service Center is performed a fingerprint database search that will returns the position estimation of the mobile device. To improve the accuracy, the position estimation algorithm takes into account also any further information of previously estimate positions. The proposed technique outperforms other similar approaches [10], mainly suited for non-Smartphones devices, in terms of localization accuracy by reaching performances comparable with GPS. As it is reasonable to expect, due to the method of construction of the fingerprint map, the maximum location accuracy is reached near the roads and progressively decreases moving away from them.

Since the proposed architecture requires the exchange of sensitive information only with a trusted service center, it does not require any particular security mechanism to protect the confidentiality or avoid malicious intrusions. In contrast, some other similar approaches have serious security issues because, as discussed in [9], they are based on collaborative or opportunistic strategy that requires the exchange of information between unknown users.

According to the presented motivations, we believe that the proposed positioning and localization system provides an accurate and reliable service and it could become very attractive for mobile devices without GPS antenna or with limited battery life.

III. Localization technique

A. Surveying Phase

The first phase of fingerprinting is called surveying or training phase, where given a set of GSM traces the algorithm builds a model of an environment, which it later uses for predicting device's location. In practice, the main purpose of this phase is the creation of a database that associates the geographical positions of points considered important in a given area with the received signal strengths. This phase is usually carried out by measuring the RSS from a certain number of base stations (typically the 6 strongest cells plus the serving cell). The training phase requires an amount of efforts to the extent area, where the positioning has to be realized. For this reason, planning tools based on refined propagation models are used in order to determine approximate values of powers in areas too large or too difficult to be measured on the field. In general, from a theoretical point of view, at each of the N points $\mathbf{x}^{(i)}$ belonging to a 2D map, the decreasing ordered set of the seven strongest values of measured powers, $\mathbf{p}^{(i)} = (p_j^{(i)}), j = 1, \ldots, 7$, and the identifiers (Cell-ID or Base Station Identity Code) of the corresponding cells, $\mathbf{C}^{(i)} = (C_j^{(i)}), j = 1, \ldots, 7$, are associated in a specific database as in the following tuple $T^{(i)}$:

$$T^{(i)} = (\mathbf{x}^{(i)}, \mathbf{p}^{(i)}, \mathbf{C}^{(i)}), \qquad i = 1, \ldots, N \tag{1}$$

It is worth to recall that the classical Surveying Phase of every localization system, namely to populate the database, could usually be very heavy in terms of resources consumption (*i.e.* time and costs), but we propose to overcome this limitation by relying on the automatic fingerprinting update phase described in section II.

B. Localization Phase

Generally, during the positioning phase, mobile terminals perform some kind of measurements which will be used by an appropriate algorithm for determining the location in the map with the likeliest characteristics. In GSM, every 480 ms the mobile stations send the values of measured powers to the serving base stations on the Slow Associated Control Channel (SACCH). Hence this information is available at the terminals and, when the localization is required, it can be sent to the localization engine through a dedicated data channel. Specifically the mobile station sends a pair $(\mathbf{q}, S)$, consisting of a decreasing sorted vector, $\mathbf{q} = (q_j), j = 1, \ldots, 7$, of measured power values and the Cell-ID of the serving base stations, S. Also the Cell-IDs are available at the terminal because they are broadcasted by the base stations on the Broadcast Control Channel (BCCH). The localization algorithm receives these vectors as inputs and looks for the point in the map with the most similar characteristics, in terms of the metric:

$$L^{(i)}(\mathbf{q}) = (\sum_{j=1}^{7} p_j^{(i)} - q_j)^{\alpha}, \qquad i = 1, \ldots, N. \tag{2}$$

The value of α determines the kind of norm. Specifically, we choose $\alpha = 2$, that is the *Euclidean* norm. The resulting position, $\mathbf{x}^{(k)}$, will have index in the database given by:

$$s_j = \arg \min_{1 \le i \le N} L^{(i)}(\mathbf{q}) \tag{3}$$

The main problem in the research of the best matching is that the algorithm should calculate the function $L^{(i)}$ for each of the N points of the map. In order to shrink the set of candidates we propose some techniques that, by using additional information, incrementally improve the accuracy of localization. In particular, in our work we consider as additional information on the previous estimated position (PP).

IV. System architecture

The proposed system architecture is based on an *Open Source* software platform in order to test the accuracy of the positioning system in real environments by using quite common and cheap smartphones mobile devices such as the LG Optimus One P500. The whole system is composed of the following components:

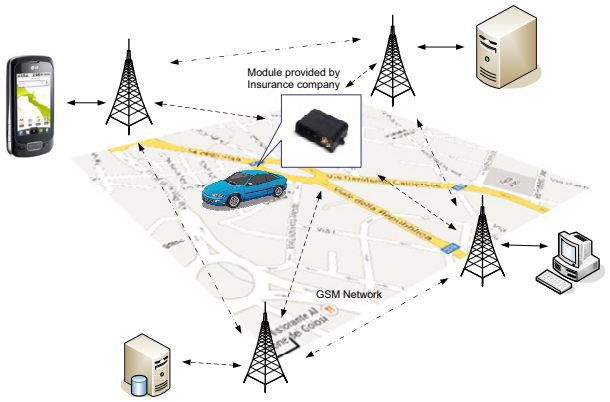

Fig. 1. System architecture.

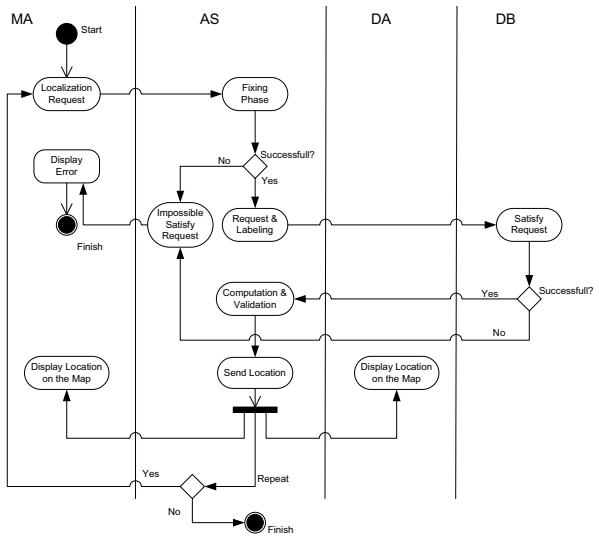

Fig. 2. Messages exchange between different entities of the system.

- A *Mobile Application (MA)* well suited for Android Operating Systems in order to be installed on a large set of different smartphones and mobile devices (MD).
- An *Application Server (AS)* able to receive the localization requests coming from the MDs and to execute the localization algorithm discussed in section III. In particular, the AS has a specific data structure specially designed to store the identification of each user asking for the localization, the exact timestamp, the computed position and the previous computed position used to improve the localization accuracy as described in the next section.
- A *Desktop Application (DA)* able to receive the output of the localization procedure executed by the SA and to show on a GEO refereed map, all the localized devices.
- A *DataBase (DB)* containing all the measurements carried out during the fingerprinting phase and constantly updated with new data coming from the fleet of vehicles equipped with a specific communication module provided by the insurance companies as explained in section II.

A complete scheme of the implemented localization architecture is shown in figure 1 while the detailed timing of messages exchange between the different components of the system is displayed in figure 2.

A. Localization algorithm: Practical implementation

Moving from the theoretic formulation of the localization problem discussed in section III to a feasible implementation, we decided to consider only the 2 strongest cells plus the serving cell sorted by decreasing power values. This choice has been motivated by the fact that, in real environments, the other cells cannot be correctly detected by the MDs most of the time; therefore their use unduly complicating the system without increasing the precision. Moreover, we split the problem in the following three phases:

1) *Fixing* - According to the chosen name, this phase emulates the fixing phase used by the GPS where the first position is shown only when the amount of information is enough to guarantee a sufficient accuracy. In fact, by using real MDs in real environments, we verified that the measurements recorded by the MDs can be affected by errors and few times the identification of some of the cells cannot be correctly acquired by the MD. For this reason, the output of this first phase is reached only when the AS receives a localization request containing admissible power and Cell-ID values. This condition represents the starting point for the localization and tracking phases.
2) *Computation* - In this phase, the localization algorithm compares the measurement made by the MD with the data set stored in the DB by minimizing the euclidean distance with the aim of finding the closest value. Even in this phase we have to face the same anomalies, already described in the fixing phase, mostly due to the use of real MDs in real environments. We have overcome these issues by providing the implemented software with a labeling mechanism consisting into the use of different codes to identify and discard the wrong Cell-ID, consequently reducing the accuracy of the localization process if one did not consider the previous position as implemented in this work (see section V). Table I summarizes the different codes used for labeling the localization requests.
3) *Validation* - In this phase, the localization algorithm validates the computed position of the MD by comparing it with the previous one. This comparison is need to improve the precision accuracy; in fact, since the localization request is performed by the MD every 5 seconds, if the actual position is very far from the one previously computed, this difference is surely due to anomalies in the measurements made by the MD; thus the algorithm behaves returning the already know

previous location of the MD or the nearest location to the previous position. In particular, the position obtained by the localization algorithm is considered to be "*far*" from the previous position by using a specific tuning parameter δ representing the radius of the surroundings which has as its center the previous valid position. Of course the accuracy of the localization strongly depends on this parameter; therefore, we tested different values obtaining very good results by setting $\delta = 30m$.

Tuple (Cell-ID, Power)	Code	Meaning
(C_1,P_1) (C_2,P_2) (C_3,P_3)	1	Exact Request
(C_1,P_1) $(65535\|0,P_2)$ (C_3,P_3)	2	Wrong Cell-ID 2
(C_1,P_1) (C_2,P_2) $(65535\|0,P_3)$	3	Wrong Cell-ID 3
(C_1,P_1) $(65535\|0,P_2)$ $(65535\|0,P_3)$	4	Wrong Cell-ID 2-3

TABLE I
CODES FOR LABELING THE LOCALIZATION REQUESTS.

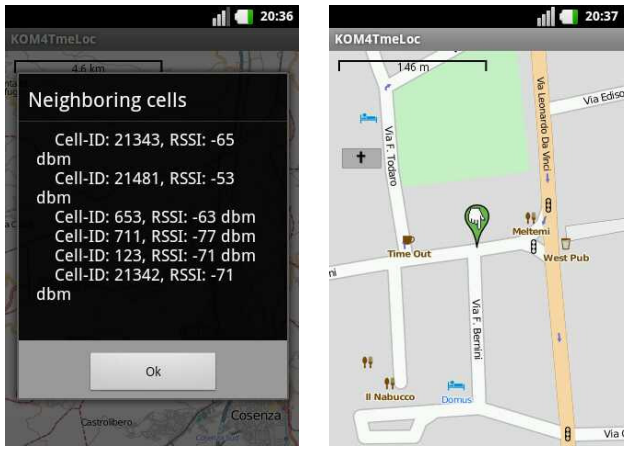

(a) (b)

Fig. 3. a) Neighboring cells discovering - b) Localization & Position showing.

B. Improving accuracy by using Previous Position

In [11] authors showed, from a simulation point of view, the impact of considering additional information to estimate the current position of an user. Based on these results we implemented, in our application server, an updated version of the localization fingerprinting technique where the algorithm takes into consideration the previous estimated position. This improvement was mainly motivated by the fact that, in many cases we have verified the uncertainty in the acquisition of the power levels of the cells during the *Surveying Phase* as explained in the previous subsection, This uncertainty turns into a partial information storage of power levels of the cells within the database of the system with the consequent accuracy reduction of the *Localization Phase*.

This kind of uncertainty can be effectively overcome by exploiting the previous position information as we will show in the next section.

V. TESTBED IMPLEMENTATION AND PERFORMANCE EVALUATION

In order to measure and evaluate the performance of the proposed localization technique, we implemented a real testbed taking into account all the components described in section IV. The software framework we developed is mainly based on Java language; specifically, we considered *Android Eclipse IDE* for the mobile application (MA) and *Java NetBeans IDE* for both server and desktop applications. Data retrieving is based on a MySQL DBMS and finally, we used *OpenStreetMap*[1] to show the localization results on very well known and reliable maps.

A. Mobile application design and supported features

We implemented a communication interface between the mobile application to be installed on every smartphone and the AS running the localization algorithm by using a classical socket communication paradigm throughout the standard 2G/3G network. Each time a mobile user sends a localization request, the mobile application performs a position measurement of the serving cell and the neighbour cells coupled with the related power measurements (see figure 3.a) and then it sends this request to the AS that will elaborate data information and request by returning the position that will be shown on the smartphone (see figure 3.b) and the DA. In particular, if the specific request of the user is a tracking request, the mobile application will automatically send a localization request to the server every 5 seconds; in addition, the developed application is also able to exploit a *Geocoding* service.

B. Testbed scenarios and performances

With the aim of conducting a robust test analysis of the implemented system architecture, we chose to measure the system performance in terms of localization accuracy in two different driving scenarios mainly related to dissimilar road typologies: *Urban* and *Highway* as shown in figure 4.a and 4.b respectively. Obviously these scenarios are affected by the intrinsic characteristics of speed limit ($\approx 50km/h$ in urban areas and $\approx 120km/h$ on the highway) and congestion in different day times. By observing results obtained in Figure 5, we are able to lead two different types of analysis: 1) the first one based on the impact of the scenario on the localization technique performance and 2) the beneficial effect of the previous position information stored by the AS for each user asking for a tracking request. Concerning the impact of the specific scenario, meant as type of road with different speed limitations, etc., we can observe that, without considering any additional information, the localization error increases in the case of high dynamicity of the specific scenario (*i.e.* Highways). In practice, the higher is the average speed, the smaller is the capability of the localization technique to be accurate without using previous position information. This behavior is also strictly related to the database population representing the reference fingerprinting for the localization. In fact, we verified that the number of rows automatically inserted

[1] http://www.openstreetmap.org/

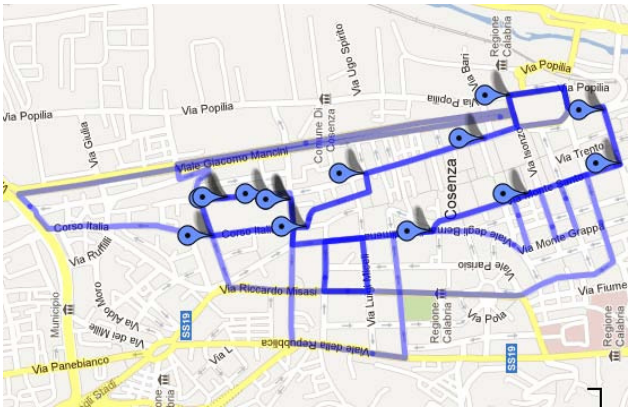

(a)

(b)

Fig. 4. a) Urban scenario - 13Km [http://goo.gl/maps/OD8VG] - b) Higway scenario 36km [http://goo.gl/maps/u0IvA].

into the database and coming from the devices installed on the vehicles from the insurance companies, present a big percentage of wrong cells identifier (labeled with code equal to 2, 3 or 4) if they have been acquired by driving on high speed road such as highways respect to the urban roads with lower speeds. This issue can be effectively overcome by taking into account the information on user' previous position (PP). We verified that this simple and quite small information has a very important impact on the performance of the localization technique and, as we can observe in Figure 5, this additional information makes the algorithm more robust in respect of the different conditions in which the localization is applied. Better performance are mostly related to the "*corrective*" capability of the previous position knowledge on the unidentified information in the database. This is the reason that allows us to reach, for the Highway scenario, the same performance of the urban scenario in terms of localization error.

C. Energy saving measures

In order to effectively demonstrate how the implemented system architecture presents a reduced energy cost, few measurement tests have been carried out by considering a digital multimeter (Fluke 45) directly connected to the smartphone with the aim of acquiring data on the instantaneous energy consumption as shown in figure 6. As it is possible to note by looking the figure 7, the average smartphone energy consumption due to the GPRS (2.5G) connection used to support the proposed localization architecture, is about $194mAh$ in standby condition keeping the screen always on; in contrast, by

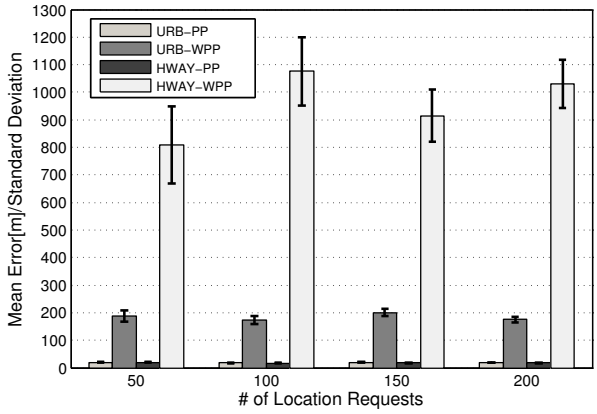

Fig. 5. Localization error in Urban and Highway scenarios by considering previous estimated position (PP) and without previous position (WPP).

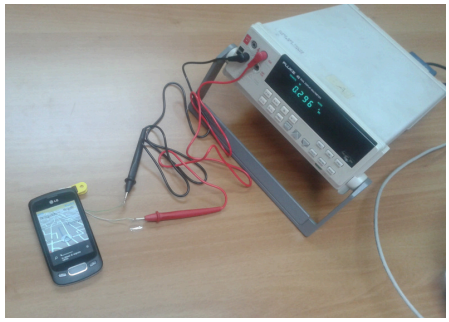

Fig. 6. Energy measurement scheme: Fluke 45 multimeter connected to the smartphone LG Optimus One P500.

activating the GPS interface throughout a common navigation software such as *Sygic*[2], the energy consumption increases reaching an average value of $314mAh$. From a careful analysis of the data collected in one hour test (*i.e.*, figure 7 only shows the results of the first 200 seconds), it is possible to achieve an overall energy saving of 38%. This analysis validates further the goodness of the presented system architecture in terms of energy saving since the use of the GPS implies a great deal of energy as also intensively involves the CPU to perform complex calculations. On the contrary, by adopting the proposed system, the calculations are completely delegated to the server side while, the application on the client side, only receives the computed coordinates of a specific location and display it on the map by greatly extending the smartphone operating time.

For sake of completeness, it is worthy to note that the energy consumption due to the Wi-Fi interface appears to be the lowest and it can be considered as a lower bound even if this kind of communication technology is not well suited for localization and tracking applications in outdoor or sparsely populated areas as explained in the introduction section. On

[2]http://www.sygic.com/en

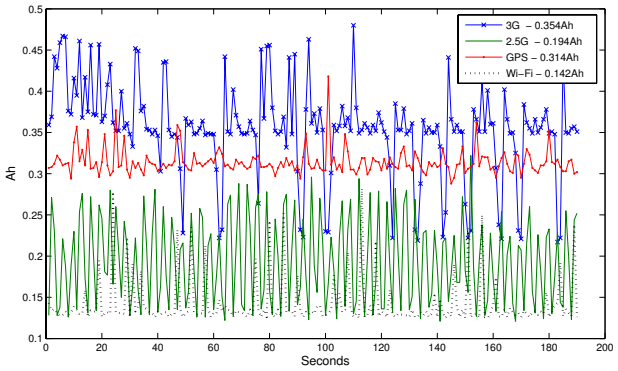

Fig. 7. Energy consumption using GPS, 2.5G, 3G and Wi-Fi radio interfaces.

the contrary, the energy consumption due to the 3G interface is always higher compared to the GPS even if the localization algorithm only needs a small information to be exchanged between the client and the server side of the proposed network architecture.
The latter consideration leads us to conclude that the most suitable transmission technology to support the presented energy-efficient localization system is the 2.5G which can also be used for receiving standard infotainment services.

VI. Conclusion

In this work the practical implementation of an energy effective localization and tracking technique based on an automatic fingerprinting construction and update, has been presented by developing a real testbed on quite common smartphones. We designed a first localization version, where no additional information is considered and an enhanced version where the information about the previous position, is taken into account. Furthermore, we tested the proposed system in two different traffic scenarios with different limitation speeds and traffic patterns by demonstrating that the use of the previous position information is very effective in highly dynamic environment such as the highways. The obtained results confirm that the proposed localization system presents a very low energy consumption with zero-impact in terms of additional hardware, from both the device and the network side.

Acknowledgment

This work has been carried out under the framework of KOM4Tme, Project #B21C11000450005, financed by the European Community and the Italian Ministry of University and Research.

References

[1] H.Y Noh *et al.* "Exploiting indoor location and mobile information for context-awareness service," *Information Processing & Management*, Vol. 48 Issue 1, pp. 1-12, January 2012.

[2] A. Kushwaha, V. Kushwaha, "Location Based Services using Android Mobile Operating System," *International Journal of Advances in Engineering & Technology*, Vol. 1, Issue 1, pp.14-20, March 2011.

[3] M. Y. Chen *et al.*, "Practical metropolitan-scale positioning for gsm phones," Proceedings of the International Conference on Ubiquitous Computing - UbiComp, Vol. 4206, pp. 225-242, 2006.

[4] C. Troncoso, G. Danezis, E. Kosta, J. Balasch, B. Preneel, "PriPAYD: Privacy-Friendly Pay-As-You-Drive Insurance," *IEEE Transactions on Dependable and Secure Computing*, Vol. 8, Issue 5, October 2011, pp. 742-755.

[5] Automotive-InfoBox. Web site: http://www.infomobility.it/ - Accessed on line, 30th March 2013.

[6] P. Pace, G. Aloi, A. Palmacci, "A Multi-Technology Location-Aware Wireless System for Interactive Fruition of Multimedia Contents," *IEEE Transactions on Consumer Electronics*, Vol. 55, Issue 2, May 2009, pp. 342-350.

[7] J. Paek, J. Kim, R. Govindan, "Energy-efficient rate-adaptive GPS-based positioning for smartphones," Proceedings of the 8th international conference on Mobile systems, applications, and services - MobiSys, San Francisco, California, USA, pp. 299-314, 2010.

[8] J. Paek, J. Kim, J. P. Singh, R. Govindan, "Energy-efficient positioning for smartphones using Cell-ID sequence matching," Proceedings of the 9th international conference on Mobile systems, applications, and services - MobiSys, Bethesda, Maryland, USA, pp. 293-306, 2011.

[9] K. Dhondge, H. Park, B Choi, S. Song, "ECOPS: Energy-Efficient Collaborative Opportunistic Positioning for Heterogeneous Mobile Devices," *Journal of Computer Networks and Communications*, Article ID 136213, 13 pages, 2013. doi:10.1155/2013/136213

[10] K. Yadav, V. Naik, A. Singh, P. Singh, U. Chandra, "Low Energy and Sufficiently Accurate Localization for non-Smartphones," IEEE International Conference on Mobile Data Management - (MDM), pp. 212-221, 23-26 July 2012.

[11] V. Loscrí, E. Natalizio, E. Viterbo, D. Mauro, G. D'Aquila, G. Brasili, "Carrier independent localization techniques for GSM terminals", IEEE 19th International Symposium on Personal, Indoor and Mobile Radio Communications, 3–12 March, 2008.

Achilles and the Tortoise: Power Consumption in IEEE 802.11n and IEEE 802.11g Networks

Karina Gomez, Tinku Rasheed, Roberto Riggio and Daniele Miorandi
CREATE-NET, Trento, Italy
name.surname@create-net.org

Cigdem Sengul
Oxford Brookes University, Oxford, United Kingdom
csengul@brookes.ac.uk

Nico Bayer
Telekom Innovation Laboratories, Darmstadt, Germany
nico.bayer@telekom.de

***Abstract*—Cloud computing is currently emerging as the de facto standard for Internet service provisioning. This uptake is motivated, among other aspects, by the significant reduction in energy consumption that can be achieved by centralizing, consolidating and optimizing large IT infrastructures. At the same time, however, users expect to access cloud services via wireless access networks using smartphones and tablets. Several studies already show that wireless technologies such as WiFi and 4G are becoming the dominant access to cloud services. However, while energy efficiency is accounted for the end-user devices and data-centers, the actual energy consumption of wireless access networks is typically overlooked, even though it is expected to account for about 90% of the entire wireless cloud energy footprint. In this paper, we use real–world measurements to present a complete analysis of the power consumption and performance of IEEE 802.11n. We also compare IEEE 802.11n with its predecessor, the widely deployed IEEE 802.11g standard, and confirm that 802.11n (2x2 MIMO) performs $\sim$ 4.5 times better than 802.11g in terms of maximum network throughput as expected while at the same time reducing the required energy per bit by $\sim$ 50%.**

***Index Terms*—Green networks, Energy efficiency, Measurements, Power meters, Testbed, IEEE 802.11, Energino**

I. Introduction

The modern society is becoming more and more dependent on strong and efficient communication networks, as several daily activities are carried out using Internet-based services and systems. Social networks, such as Facebook and twitter, and the Internet in general are the most attractive and instantaneous medium individuals can tap into in order to express feelings, dispatch news, share pictures/files and access hundreds of applications and services. As smartphones and tablets become the most common access devices, this leads to a consistent trend in the increase of data flowing over wireless. According to recent studies, the amount of traffic in wireless networks is increasing at a compound annual growth rate estimated in the range between 300% and 700% [1]. While the current uptake of cloud computing is allowing large IT providers to significantly reduce their energy consumption by consolidating and optimizing centralized computing resources, the users typically expect to access these new services via wireless access networks. These networks are inherently energy inefficient and according to [2], by 2015 will account for up to the 90% of the entire wireless cloud computing energy footprint.

Wireless local area networks (WLANs) are expected to play a significant role in the wireless cloud computing scenario, as IEEE 802.11 family of standards has become the most popular wireless access technology deployed in cities, universities and enterprises. The recently IEEE 802.11n [3] standard significantly improves the throughput over the previous ones – 802.11a/g – with an increase in the maximum data rate from 54 Mb/s to 600 Mb/s. Future extensions such as IEEE 802.11ac and IEEE 802.11ad will deliver performance beyond 1 Gb/s. Currently, practically all smartphones, tablets and laptops are compliant with the IEEE 802.11n standard, which delivers higher capacity than wide area networks (i.e. 3G, LTE, and WiMAX) enabling a better quality of service (QoS) and consequently, a better quality of experience for users.

Given its widespread use, understanding the energy consumption characteristics of the 802.11n technology represents an imperative step in order to design solutions for reducing the impact to the overall CO_2 footprint of wireless networks [4], [5]. In our previous work [6], we analyzed and experimentally measured the energy consumption of several 802.11g-compliant WiFi Access Points (APs) and WiMAX Base Stations (BS). Here, we use a similar methodology to experimentally measure, analyze and compare the energy consumption patterns of 802.11g and 802.11n devices. In particular, our experiments aim at answering how, where and when the power is consumed in WiFi networks. We investigate whether there is any penalty, in terms of energy consumption, when migrating from old to new technologies and the advantages or disadvantages of such migration. The main contributions of the paper are the following:

- We present an empirical analysis of energy consumption associated to data transmission in 802.11n devices, and perform an experimental comparison 802.11g and 802.11n standards in terms of (i) the amount of traffic sent/received by the AP, (ii) the size of the session level data units, and (iii) the transmission power levels.
- We numerically demonstrate that most of the energy consumed by 802.11 AP – $\sim$ 67%-82% – is hardware dependent and that the IEEE 802.11n standard is more energy efficient than the IEEE 802.11g standard.

The remainder of this paper is organized as follows. A brief analysis of the related work is presented in Section II.

978-1-4799-0354-2/13/$31.00 ©2013 IEEE

In Section III we present the experimental settings and the methodology used. The results on power consumption of 802.11n APs are reported and discussed in Section IV, while the comparison between the 802.11g and the 802.11n standards in terms of energy consumption and network throughput is presented in Section V. Finally, Section. VI provides some concluding remarks and discusses directions for future work.

II. Related Work

Energy consumption measurements of 802.11n technologies have been performed for mobile phones [7] and Network Interface Cards (NICs) [8]. In [8], power consumption statistics of an 802.11n NIC across a broad set of operating states (channel width, transmit power, rates, antennas, Multiple–Input/Multiple–Output (MIMO) streams, sleep, and active modes) are reported. The testbed used for the power consumption measurements was composed of two nodes placed close to each other. The NIC used in the experiments is available in a mini-PCI Express form factor. To measure the power consumption, the authors placed an extra circuit and used National Instruments 6218 Data Acquisition Module (NIDAM) for logging the voltage and current consumed by the NIC. In order to inject traffic in the experimental testbed, packets of 1500 bytes large are generated. The main conclusions of this work are that (i) for optimizing energy consumption, it is imperative to use the fastest single-stream rate possible, especially for short packets and (ii) the optimal device settings will also depend on channel conditions and workload. The authors also observed that transmit power levels have very little effect on the power consumed by the interface. In contrast to our work, the authors experimental focus is based only on the power consumption of the single 802.11n NIC rather than of the system as a whole, ignoring the energy expenditures related to other functions, such as operations for packet forwarding and reception, fragmentation and reassembling. Additionally, in this work, we also present a comparison between the different 802.11 standards supported by the devices.

In [7], the authors ran a large number of automated tests using Google Android G1, Magic, Hero and Nexus handsets and present results for the average energy consumption of connection and data transmission over 802.11 wireless networks. The phone's power consumption is measured by inserting a high-precision 0.02Ω measurement resistor in series between a battery terminal and its connector on the phone. A National Instruments PCI-MIO-16E-4 sampling board is used in order to measure the voltage across the phone battery and also the voltage drop across the measurement resistor at 250 kHz. Power consumption measurements for cellular phones are also presented in [9]. Here, the authors compare the performance of LTE, 3G and WiFi by local experiments on mobile devices. Specifically for the WiFi measurements, the data network radio interface is turned off and the mobile device is connected to a wireless 802.11g router in channel 2.437 GHz. For cellular measurements, the WiFi interface is turned off and the mobile device is connected to the 4G network. Finally when 4G is disabled, the device connects to the 3G network. The Monsoon power monitor [10] is used as power input for the mobile device measuring power traces at the same time. The main conclusions of this work are that LTE is as much as 23 times less power efficient compared to WiFi, and even less power efficient than 3G, based on the user traces, and the long high power tail is found to be a key contributor to this behaviour. The results reported by the authors in [7], [9] provides us with insights on the power consumption of the client-side rather than of AP-side, which is addressed in this work.

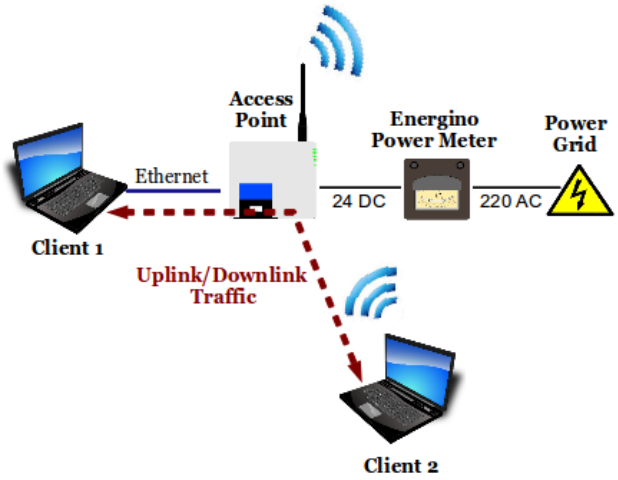

Fig. 1: Network scenario used for the measurement campaign.

III. Evaluation Methodology

In this section the network set-up and the methodology used to investigate and compare the power consumption of 802.11g and 802.11n APs are described.

A. Network set-up

The network set-up used in the indoor scenario is sketched in Fig. 1. The network is composed of a custom 802.11g/n AP and two notebooks. The notebooks, *client 1* and *client 2* in the figure, are regular Fujiitsu SIEMENS and DELL Latitude 6420 respectively, equipped with an Intel PRO/Wireless 3945AB wireless adapter and running Ubuntu 10.04. The first notebook acting as wired *client 1*, which is connected to the AP through Ethernet interface. While the second notebook acting as static wireless *client 2*, which is associated to the AP using the wireless interface (see Fig. 1). The WiFi 802.11g/n AP is part of the Berlin Open Wireless Lab (BOWL) [11] testbed deployed at Telekom Innovation Laboratories in Berlin, Germany. The AP is built around a PCEngines ALIX 3D2 (500MHzx86 CPU, 256MB of RAM) processor board equipped with one 802.11n wireless interface. The AP runs the OpenWRT 10.3.01-rc1 as the operating system. The ath9k [12] Wireless NIC driver has been used during the measurements campaign. The driver is configured to disable RTC/CTS exchange. The AP's operating frequency was set to 2.24 GHz (Channel 11).

B. Power Consumption Monitoring

The power consumption statistics are collected at the AP using *Energino* [13] with a granularity of 10 mW and a sampling period of 100 ms. It is important to remark that

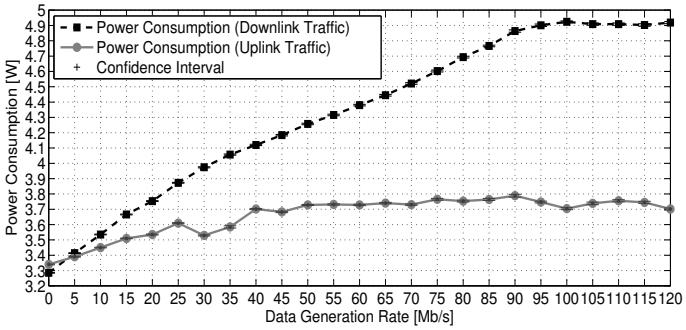

(a) Average Power Consumption (AP)

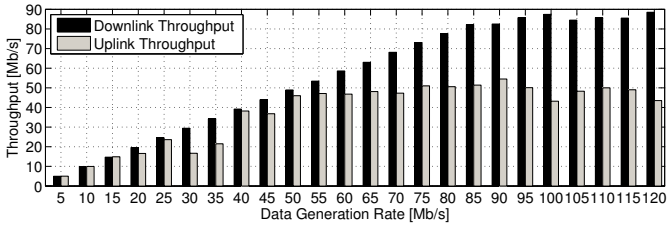

(b) Throughput

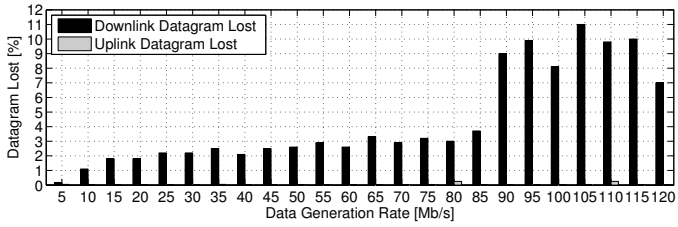

(c) Datagram loss

Fig. 2: Average power consumption and network performance at the 802.11n AP as a function of different traffic generation rates for a constant datagram size of 1280 bytes.

the power consumption is monitored for the whole device. Therefore, the results reported in this paper account for both the power consumed by the processing board for handling the incoming and outgoing traffic (e.g., for segmentation and reassembly, computing checksums, etc.) as well as for the power consumed to deliver the actual frame over the wireless link (e.g., for power amplifiers, modulator/demodulator, etc.).

C. Experiment Methodology

The measurement campaign accounted in this paper aimed at assessing the power consumed by IEEE 802.11gn APs under different workloads. Client and AP are deployed close to each other ($\approx$ 4 m) in order to have good link quality and thus to exploit the high throughput modulation and coding schemes. Synthetic traffic is generated using the Iperf [14] and injected as a single UDP flow. In order to measured the network performance and power consumption statistics of the AP, downlink traffic is generated in the *client 1* toward the *client 2* while uplink traffic is generated in the *client 2* toward the*client 3* as show in Fig. 1. Results reported in this section are the average of measurements collected during 600 seconds and with 95% confidence interval. We considered the following scenarios:

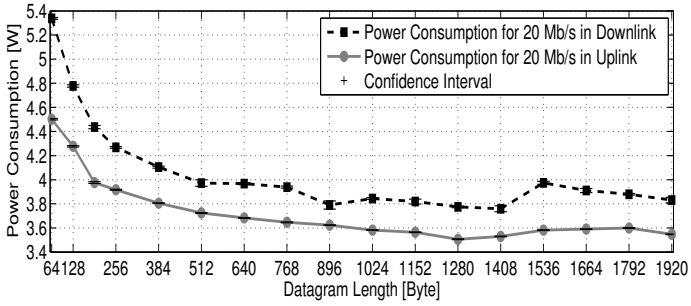

(a) Average Power Consumption (AP)

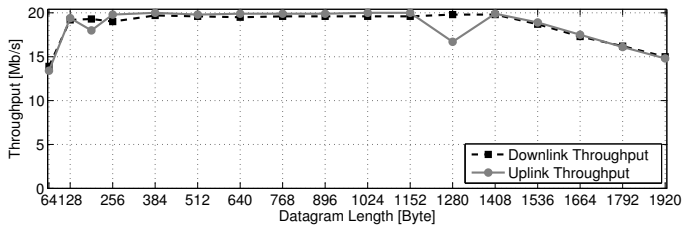

(b) Throughput

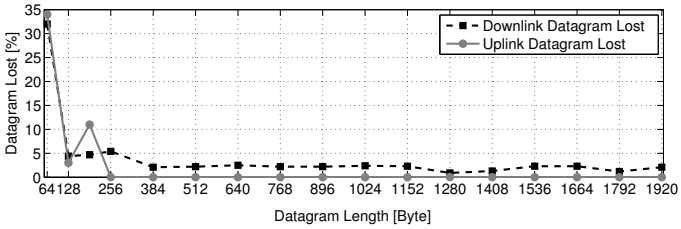

(c) Datagram loss

Fig. 3: Average power consumption and network performance at the 802.11n AP as a function of the datagram size for a constant traffic generation rate of 20 Mb/s.

1) **Variable traffic with fixed datagram length:** In this experiment, the datagram size is kept constant at 1280 bytes, while the traffic generation rate is progressively increased from 5 Mb/s up to (i) 55 Mb/s for 802.11g and (ii) 120 Mb/s for 802.11n in steps of 5 Mb/s for both.
2) **Constant traffic with variable datagram length:** In this experiment, the traffic generation rate is kept constant at 20 Mb/s while the datagram size is progressively increased from 64 to 1920 bytes in steps of 128 bytes.
3) **Variable traffic with variable transmission power level:** In this experiment, the traffic generation rate is progressively increased from 5Mb/s up to 120 Mb/s in steps of 5 Mb/s. The transmission power level is set manually, using the command line interface, to 12 dBm for first experiment and 19 dBm for second experiment.

It is important to note that, unless otherwise specified, the rate adaptation algorithm has been set to auto and the transmission power has been left to its default value equal to 19 dBm for all the experiments.

IV. Measurements and Analysis of the IEEE 802.11n Access Point

In this section, we present the results from the measurements campaign described in the previous section.

A. Variable traffic with fixed datagram length

Fig. 2 summarizes the power consumption and network performance results obtained for the 802.11n AP acting as either a transmitter or a receiver. We observe that:

i) The power consumption behavior is similar for both cases (Fig. 2a). The power consumption is monotonically increasing with the traffic load until it reaches a saturation point. *Saturation* here means that the data generation rate is higher than the physical link data–rate, so the transmitter is constantly backlogged.

ii) The saturation point is different for the two cases (Fig. 2b). Note that the saturation point is determined by the device that is transmitting since it depends on the efficiency of the rate adaptation algorithm. An efficient rate adaptation algorithm should adapt giving priority to higher modulation and coding schemes as much as possible. We observed that, when the AP is acting as a transmitter, the rate adaptation algorithm uses the highest modulation and coding schemes most of the time. Instead, when the *client 2* is acting as a transmitter we observed that it does not use the higher modulation and coding schemes, which consequently means *client 2* saturates earlier than the AP.

iii) When the AP is acting as a transmitter and it reaches the saturation point, the datagram loss increases (Fig. 2c). This is expected since when the transmission buffer is full, new frames are dropped. Instead, when the AP is acting as a receiver the datagram loss is lower than 1%. In this case, the transmitter is the notebook *client 2* and it has enough memory resources for buffering the frames when the wireless interface is saturated.

B. Constant traffic with variable datagram length

The Fig. 3 reports the power consumption and network performance of the 802.11n AP as a function of the datagram size for a constant traffic of 20 Mb/s. We observe that:

i) When the datagram size becomes extremely small, the AP consumes significantly more power than for large datagram sizes under the same traffic conditions (Fig. 3a). The power expenditure includes (a) the overhead related to the MAC header and (b) the internal operations for generating and buffering the small datagrams.

ii) When fragmentation takes place, i.e., when the AP receives a protocol data unit larger than the receiver's maximum transmission unit, the throughput utilization decreases and the power consumption increases. The power expenditure includes (a) the internal operations for packet fragmentation and reassembly, (b) the internal buffering of packets, (c) the overhead related to the additional frame in terms of MAC header and medium access. As it can be seen from Fig. 3a packet fragmentation is more energy consuming than packet reassembly.

iii) The throughput decreases when (i) large datagrams are transmitted/received due to the fragmentation and (ii) small datagrams are transmitted/received due to the associated protocol overhead which tends to saturate the wireless interface (Fig. 3b).

iv) The datagram loss increases when the AP is transmitting small datagrams (see Fig. 3c) since the protocol overhead generated by small datagrams saturates the transmission buffer resulting in a severe datagram loss.

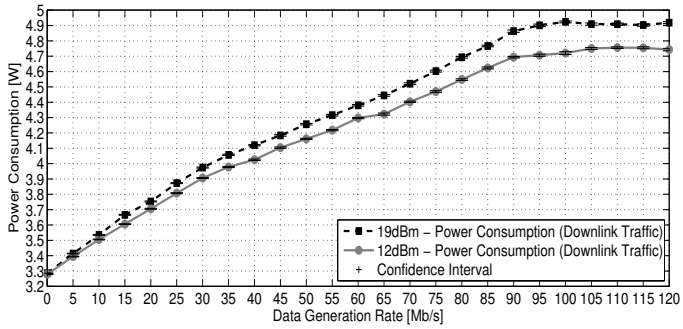

(a) Average Power Consumption (AP)

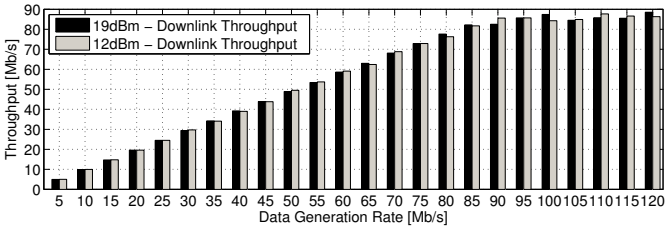

(b) Throughput

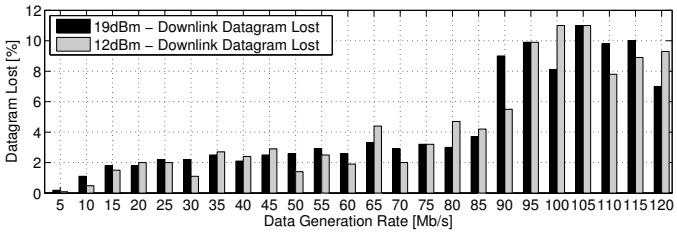

(c) Datagram loss

Fig. 4: Average power consumption and network performance at the 802.11n AP as a function of different traffic generation rates for different transmission power levels rates for a constant datagram size of 1280 bytes.

C. Variable traffic with variable transmission power level

Fig. 4 summarizes the results when the 802.11n AP is acting as either transmitter or receiver using different transmission power levels. We considered two different power levels: 12 dBm and 19 dBm (19 dBm is the maximum transmission power supported by the AP). We observe that:

i) Different transmitter power levels present different power consumption in the saturation regime. The advantage of decreasing the transmission power can be clearly observed in the Fig. 4a.

ii) The network performance does not change much due to the particular set-up used in our deployment, in which the AP and the client are just 4 meters apart. The results for throughput and datagram loss are shown in Fig. 4b and Fig. 4c respectively.

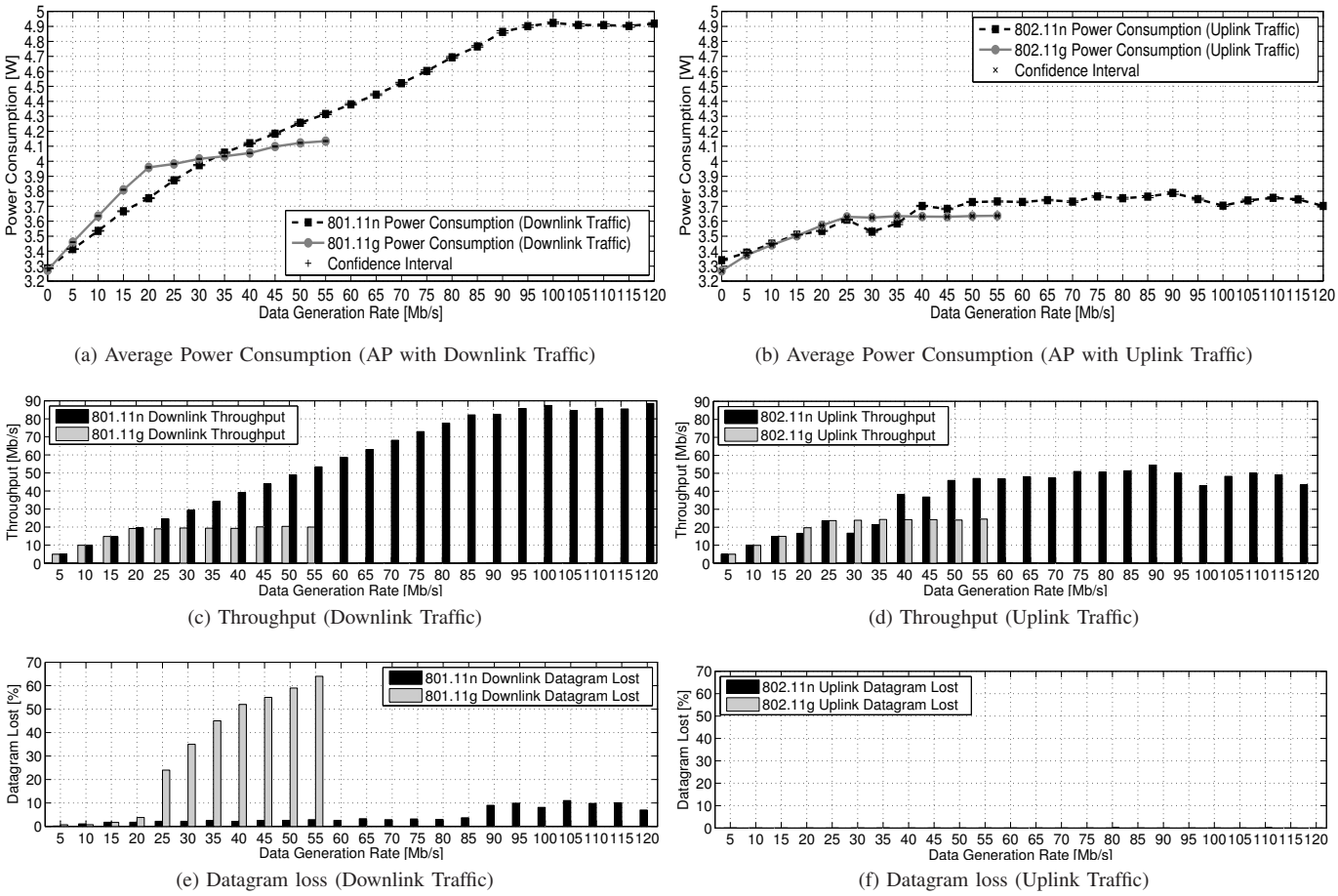

(a) Average Power Consumption (AP with Downlink Traffic)

(b) Average Power Consumption (AP with Uplink Traffic)

(c) Throughput (Downlink Traffic)

(d) Throughput (Uplink Traffic)

(e) Datagram loss (Downlink Traffic)

(f) Datagram loss (Uplink Traffic)

Fig. 5: Comparison of the average power consumption and network performance for the 802.11g AP and 802.11n AP as a function of different traffic generation rates for a constant datagram size of 1280 bytes. AP acting as a transmitter or receiver.

iii) These observations also hold when the AP is acting as a receiver (for more details, see [15]).

V. Power Consumption Comparison between IEEE 802.11g and 802.11n

Fig. 5 compares the power consumption of 802.11g and 802.11n APs. We observe that:

i) The average power consumption of an idle AP is 3.3 W and it is the same for both technologies (see Fig. 5a and Fig. 5b). The power consumption behavior is similar, however, the power consumption at the saturation point is different.

ii) The power consumption for the AP acting as a transmitter at the saturation point is around 4.9 W for 802.11n and 4 W for 802.11g. The power consumption for the AP acting as a receiver is around 3.75 W for 802.11n and 3.63 W for 802.11g.

iii) The energy spent for transmitting or receiving one bit is quantified as $\approx 0.01487\ \mu J/b$ and $\approx 0.009217\ \mu J/b$ respectively in 802.11n case, and $\approx 0.03447\ \mu J/b$ and $\approx 0.01403\ \mu J/b$, respectively in 802.11g case. Therefore, the 802.11n AP is more energy efficient than the 802.11g AP. Note that the energy per bit is computed excluding the measurements of the saturation region.

iv) When the AP reaches the saturation point, the maximum throughput and the power consumption remains constant. The throughput results are shown in Fig. 5c and Fig. 5d. The saturation point for the AP acting as a transmitter is around 90 Mb/s for 802.11n and 20 Mb/s for 802.11g, while for the AP acting as a receiver, it is around 45 Mb/s for 802.11n and 23 Mb/s for 802.11g.

v) The datagram loss performance is shown in Fig. 5e and Fig. 5f. We observe a significant difference in terms of datagram loss between the two technologies, especially when the AP is acting as a transmitter. The reason can be traced back to the higher capacity of 802.11n, which prevents frames from being dropped due to buffer overflows.

Fig. 6 depicts the average energy per bit and network performance at the 802.11g and 802.11n AP as a function of the datagram size for a constant traffic generation rate of 20 Mb/s. We observe that:

i) When the datagram size is extremely small, 802.11n is significantly more energy efficient than 802.11g (see the Fig. 6a and Fig. 6b). The difference in energy efficiency decreases as the datagram size increases.

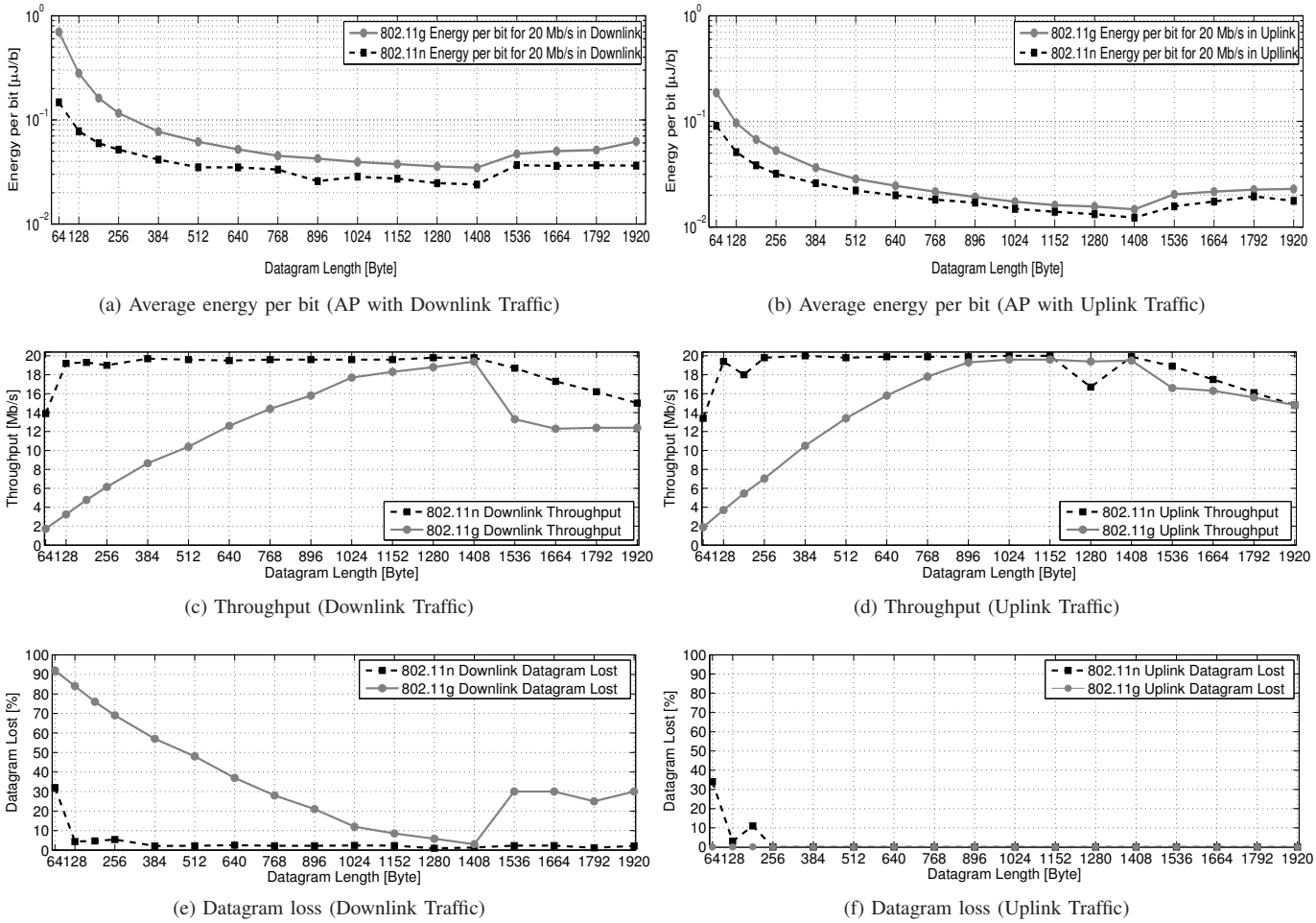

(a) Average energy per bit (AP with Downlink Traffic)

(b) Average energy per bit (AP with Uplink Traffic)

(c) Throughput (Downlink Traffic)

(d) Throughput (Uplink Traffic)

(e) Datagram loss (Downlink Traffic)

(f) Datagram loss (Uplink Traffic)

Fig. 6: Comparison of the average power consumption and network performance at the 802.11g AP and 802.11n AP as a function of the datagram size for a constant traffic generation rate of 20 Mb/s. AP acting as a transmitter or receiver.

ii) The throughput decreases for small datagram sizes for both technologies. However, this is more evident in 802.11g, which is affected for datagram sizes 64-1204 bytes, while for 802.11n, the negative effect is observed 64-128 bytes (see the Fig. 6c and Fig. 6d).

iii) When the AP is acting as a transmitter, the results show that the datagram loss increases for the large datagrams only with 802.11g (see the Fig. 6e), while the datagram loss increases for small datagrams using both technologies. Again, while this occurs for 64-1024 bytes in 802.11g, in 802.11n only 64-128 bytes datagrams incur loss.

iv) When the AP is acting as a receiver, the results show that the datagram loss increases for small datagrams only for 802.11n (see the Fig. 6f). This behavior is related to the memory resources of the device as explained previously.

A. How, where and when the power is consumed in WiFi 802.11g/n AP?

The power consumption of an AP can be divided into two parts for both technologies. The first part is fixed and is related to the power consumption of the circuit plus the basic operation of the AP. The second part is variable and it is related to whether the AP is 802.11n or 802.11g, as well as the operating conditions, including the transmission power level, the datagram size, the modulation and coding schemes and in particular, the traffic load. We also observe that i) large packets use energy more efficiently than small ones, ii) highest modulation and coding schemes are more energy efficient, and ii) the transmit power levels have very little effect on the power consumed by the APs. Additionally, our results indicate that a significant fraction of the energy consumed by AP is not traffic or software dependent in both the 802.11g and 802.11n cases. More specifically, we found that the energy consumed when there are no users in the network, i.e., the energy consumed by hardware and regular signalling, constituted $\sim 67\%$ of the total energy necessary to support highest throughput in the 802.11n case. This percentage is $\sim 82\%$ in the 802.11g case.

B. What is the penalty to pay, in terms of energy, to migrate from old to new technologies?

Based on the results, we can observe that the key innovations of 802.11n standard positively impacts its performance [3]. Such innovations refer to:

- Support of MIMO techniques for increasing the maximum data rate and the transmission range (the 802.11n allows up to 4 x 4 MIMO configuration).
- Inclusion of pre-coding and post-coding techniques for improving the received signal quality.
- Addition of coding rate (5/6) for increasing the data rates achieved by each modulation.
- Doubling of the bandwidth per channel from 20 MHz to 40 MHz (doubling the data rate).
- Support of frame aggregation for packing multiple MAC protocol data units together (reducing the overheads).

Due to these additional features, 802.11n transmits and receives faster than 802.11g. Thus 802.11n offers greater performance than 802.11g in terms of both energy efficiency as well as key network performance metrics (i.e. throughput and datagram loss). We can conclude that 802.11n APs provide higher network throughput than 802.11g APs *without* penalty in terms of energy consumed. Rather, this migration is expected to improve energy efficiency. More specifically, we observe that using 802.11n devices the energy cost for transmitting and receiving one bit from/to session layer is reduced to $\sim$ 50% and $\sim$ 30% with respect to 802.11g, respectively. Our measurements also confirm that 802.11n (2x2 MIMO) performs $\sim$ 4.5 times better than 802.11g in terms of maximum network throughput. Therefore, the migration from old to new technology and the reduction of hardware-dependent energy consumed by the new devices enable more sustainable wireless access.

C. What are the advantages and disadvantages of that migration?

There are several advantages in the migration from old to new technologies from both (i) the improvement of the network throughput and (ii) the reduction of the energy cost related to data transmission. In the case of IEEE 802.11 standard, the migration from old to new standard implies software and (minor) hardware updates. However, this is not the case for several 3G technologies, in which the migration implicates high costs and efforts. On the other hand, when the migration requires a complete replacement of the hardware, the cost to decommission the old equipment must be carefully taken into account. Therefore, the energy efficiency of the devices should be improved in the total life-cycle:

i) During the production of the device, through cleaner manufacturing and use of less materials and energy.
ii) During operation by using less energy and extending lifetime (energy efficiency protocols and algorithms).
iii) In end-of-use by recycling materials and refurbishing for reuse.

VI. Conclusions and Future Work

In this paper, we investigated and compared the power consumption behaviour of 802.11n and 802.11g APs. We observed a similar power consumption pattern for both technologies, namely a linear behavior until the AP reaches a saturation point. However, there are relevant differences in the amount of (i) the power consumed for transmitting and receiving data and (ii) the traffic rate at which the AP saturates. The measurements presented in this paper can be used as input for technology designers and vendors for understanding and improving the energy efficiency of their network devices, paving the way to more efficient hardware and software solutions. More specifically we envision the use of energy efficiency assessment methodology similar to the ones presented in this work across an entire product lifecycle. We also argue in favor of policies and standards accounting for energy efficiency rating for wireless networking equipments.

In terms of future research directions, we plan to investigate deeply how the different MIMO configurations and modulation/coding schemes affect the power consumption behaviour of 802.11n APs. Additionally we are also planning to investigate the trade-off, in terms of network performance and energy consumption, when the link quality between AP and client varies over time.

Acknowledgments

The research leading to these results has been partially supported by the EC Seventh Framework Programme (FP7-2011-8) under the Grant Agreement FP7-ICT-318632.

References

[1] G. Micallef, P. Mogensen, and H. O. Scheck, "Cell size breathing and possibilities to introduce cell sleep mode," in *Proc. of IEEE EWC*, Lucca, Italy, April 2010, pp. 111–115.
[2] CEET, "The Power of Wireless Cloud: An analysis of the energy consumption of wireless cloud," Centre for Energy-Efficient Telecommunications, Tech. Rep., April 2013, online: http://www.ceet.unimelb.edu.au/pdfs/ceet_white_paper_wireless_cloud.pdf.
[3] "802.11n-2009: Enhancements for higher throughput, IEEE," available at: http://standards.ieee.org/findstds/standard/802.11n-2009.html.
[4] Y. Al-Hazmi, H. De Meer, K. A. Hummel, H. Meyer, M. Meo, and D. Remondo, "Energy-efficient wireless mesh infrastructures," *IEEE Network Magazine*, vol. 25, pp. 32–36, March-April 2011.
[5] H.-O. Scheck, "ICT & Wireless Networks and their Impact on Global Warming," in *Proc. of IEEE EWC*, Lucca, Italy, 2010, pp. 911–915.
[6] K. Gomez, D. Boru, R. Riggio, T. Rasheed, D. Miorandi, and F. Granelli, "Measurement–based modelling of power consumption at wireless access network gateways," *Computer Networks Mag.*, vol. 56, July 2012.
[7] A. Rice and S. Hay, "Measuring mobile phone energy consumption for 802.11 wireless networking," *Pervasive Mobile Computing.*, vol. 6, no. 6, pp. 593–606, Dec. 2010.
[8] D. Halperin, B. Greenstein, A. Sheth, and D. Wetherall, "Demystifying 802.11n power consumption," in *Proc. of Power Aware Computing and Systems*, Berkeley, CA, USA, 2010, pp. 1–5.
[9] J. Huang, F. Qian, A. Gerber, Z. M. Mao, S. Sen, and O. Spatscheck, "A close examination of performance and power characteristics of 4g lte networks," in *Proc. of the Mobile systems, applications, and services*. New York, NY, USA: ACM, 2012, pp. 225–238.
[10] "Monsoon power monitor solution," available at: http://www.msoon.com/LabEquipment/PowerMonitor/.
[11] T. Fischer, T. Hühn, R. Kuck, R. Merz, J. Schulz-Zander, and C. Sengul, "Experiences with bowl: managing an outdoor wifi network (or how to keep both internet users and researchers happy?)," in *Large Installation System Administration*, Berkeley, CA, USA, 2011, pp. 24–24.
[12] "Ath9k," available at: http://linuxwireless.org/.
[13] K. Gomez, R. Riggio, T. Rasheed, D. Miorandi, and F. Granelli, "Energino: an hardware and software solution for energy consumption monitoring," in *Proc. of IEEE Winmee*, vol. 56, May 2012.
[14] "Iperf traffic generator," available at: http://iperf.sourceforge.net/.
[15] K. Gomez, "Energy efficiency in wireless access networks: Measurements, models and algorithms," *PhD. Thesis, University of Trento [http://eprints-phd.biblio.unitn.it/]*, April 2013.

Total Energy Efficiency of Cellular Large Scale Antenna System Multiple Access Mobile Networks

Hong Yang, Thomas L. Marzetta
Bell Labs, Alcatel-Lucent, Murray Hill, NJ 07974 USA
Email: {h.yang, tlm}@research.bell-labs.com

***Abstract*—Energy efficiency and spectral efficiency of a Large Scale Antenna System in both dense urban and suburban multi-macro-cellular scenarios are quantified using a new total energy efficiency model, which consists of a rigorous capacity lower bound and a power model accounting for RF generation, LSAS critical computing and a per antenna internal power consumption for other analog electronics and A/D and D/A converters that are associated with each LSAS service antenna. Based on our model, in dense urban, an LSAS with sixty-four 0dB gain service antennas per cell, each service antenna consuming an internal power of 128 mW above the power required for RF generation and for LSAS critical computing, can simultaneously serve 15 users with a total energy efficiency almost 1000 times greater than that of a typical LTE base station and at the same time more than quadruple the aggregate spectral efficiency.**

Keywords*—*energy efficiency; LSAS; Massive MIMO; spectral efficiency; multiple cells; multiple access; power control.

I. Introduction

To meet the ever increasing throughput demand, all current wireless cellular access networks are optimized for spectral efficiency with little attention devoted to their energy efficiency due to the steep cost and scarcity of the spectrum. To achieve any worthwhile improvement in energy efficiency, a new wireless technology is needed. Large-Scale Antenna System (LSAS) is one such technology. It can deliver at least an order of magnitude greater spectral efficiency over current wireless technologies and provide improvements in radiated energy efficiency proportional to the number of service antennas so meaningful trade-offs between spectral efficiency and total energy efficiency become viable for the first time.

LSAS is a form of multi-user MIMO wireless system in which a large antenna array communicates with a multiplicity of typically single-antenna terminals [1], [2], [3] [4], [5], [6], [7]. The array acquires its all-important knowledge of the forward link and reverse link channel state information (CSI) through a combination of reverse link pilots and TDD reciprocity. The large excess of service antennas over terminals confers great spectral efficiency and energy efficiency. It makes the simplest conjugate beam-forming multiplexing pre-coding and matched filter de-coding nearly optimal, it replaces expensive ulta-linear 40-Watt power amplifiers with many cheaper low-power units, and it simplifies power control and resource allocation.

Most studies of LSAS have emphasized its spectacular spectral efficiency and radiated energy-efficiency, however *total* energy efficiency is receiving some attention as evinced by the GreenTouch Consortium [8]. The focus of this paper is the design of macro-cellular LSAS with the sole objective of maximizing total forward link energy efficiency as measured in units of bits per Joule. We include both dense urban and suburban deployments, we arbitrarily restrict the LSAS arrays to either 64 or 128 antennas, and we adopt system parameters consistent with typical LTE practice. The free design parameters - whose values we choose to maximize the system energy efficiency - are the number of terminals simultaneously served and the total radiated power.

The energy efficiency is the ratio of net throughput (bits/second) divided by total expended power (Watts). To evaluate throughput we use an extension to multiple cells of the single-cell capacity lower bound in [4]. Our extended model accounts for receiver noise, channel estimation error and the overhead in acquiring it, the imperfections of the conjugate beam-forming linear pre-coding that is employed, power control, and inter-cellular interference. Interference from the other cells is of two types: non-coherent which can always be overcome by employing more service antennas, and coherent (also called *pilot contamination* [2]) that results from using the same pilot sequences by more than one user terminal in the coverage area and which grows with the number of service antennas at the same rate as the desired signal. We account for three types of power expenditure: RF power generation, power required for LSAS critical computations, and finally an assumed per-antenna internal power consumption for other analog electronics and A/D and D/A converters that are associated with each LSAS service antenna.

The paper is organized as follows. We review the operation of LSAS in Section II including a capacity lower bound. Section III presents our power model. Section IV discusses our choice of LSAS parameters and deployment scenarios. Section V outlines the simulations and presents numerical results. Conclusions are drawn in Section VI.

Notation:

$\triangleq$: an equal sign used to define a new mathematical notation.

J: the number of LSAS cells.

$\mathcal{J} \triangleq \{1, \cdots, J\}$.

K_j: number of users supported by the jth cell, $j \in \mathcal{J}$.

$L_0 \triangleq 0$, $L_j \triangleq \sum_{i=1}^{j} K_i$, $j \in \mathcal{J}$. Thus L_J is the total number of users simultaneously supported by the J LSAS cells.

$\mathcal{L}_j \triangleq (L_{j-1}, L_j] \cap \mathbb{N}$, where $\mathbb{N}$ denotes the set of natural numbers. Thus $\mathcal{L}_j$ is the set of indices for users served by the jth cell, $j \in \mathcal{J}$.

M_j: the number of LSAS service antennas in the jth cell.

978-1-4799-0354-2/13/$31.00 ©2013 IEEE

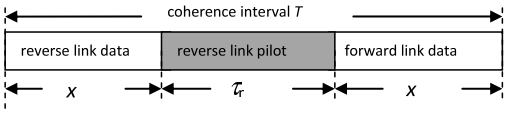

Fig. 1. Structure of an LSAS slot

TABLE I. DEFINITIONS OF VARIOUS TIME INTERVALS

T_{slot}: slot length, which depends on the speed of the mobile
T_{s}: OFDM symbol interval $= 1/14$ ms
T_{g}: OFDM guard interval $T_{\text{s}}/15 = 1/210$ ms
$T_{\text{u}} = T_{\text{s}} - T_{\text{g}}$: OFDM usable interval $= 1/15$ ms

ρ_{f}: total forward link transmit power divided by the noise power at the user terminal receiver.

$\rho_{\text{r},k}$: the reverse-link transmit power of the kth user divided by the noise power at the base-station receiver.

τ_{r}: reverse link pilot sequence, in number of symbols.

$\beta_{k:j}$: the radio-frequency (RF) propagation channel gain between the kth user and the jth cell LSAS antenna array.

$[l]$: the set of indices of user terminals which use the same reverse link pilot sequence as the lth user.

(i): the index of the cell by which the ith user is served.

λ_k: fraction of total forward link RF power in the (k)th cell allocated for the kth user.

II. REVIEW OF LSAS OPERATION

An LSAS cell comprises an array of M antennas that serve K single-antenna terminals over the same time-frequency resources. We assume TDD wide band OFDM operation. All action occurs in a slot (*coherence interval*) of duration such that nobody moves more than 1/4 wavelength. The slot structure is illustrated in Fig. 1.

The channels are substantially constant over the Nyquist frequency interval, equal to the reciprocal of the channel delay-spread [2], which in turn is assumed equal to the OFDM guard interval. The number of tones in the Nyquist interval (14 for the parameters of Table I), times the number of OFDM symbols in the slot, is equal to the non-dimensional sample-duration of the slot

$$T = \frac{T_{\text{u}} T_{\text{slot}}}{T_{\text{g}} T_{\text{s}}},$$

i.e., the number of channel uses that exist in the slot over each interval of frequency such that the channels are approximately constant.

The acquisition of CSI through reverse link pilots is critical for LSAS. Within each frequency Nyquist interval each of the K terminals transmits an assigned orthogonal frequency-time pilot sequence whose sample duration, τ_{r}, is equal to the Nyquist interval (in tones) times the number of OFDM symbols dedicated to pilot transmission. Of necessity $K \leq \tau_{\text{r}} \leq T$. One runs out of orthogonal pilot sequences quickly as K increases so in a multiple cell system some pilot re-use is required. Our analysis is based on a pilot re-use factor of seven as illustrated in Fig. 2, in which reverse link pilot sequences are re-used in cells with the same color. Note that both forward and reverse link date transmissions are done with frequency re-use of one. Other aspects of the cluster in Fig. 2 related to simulation details are explained in Section V-A.

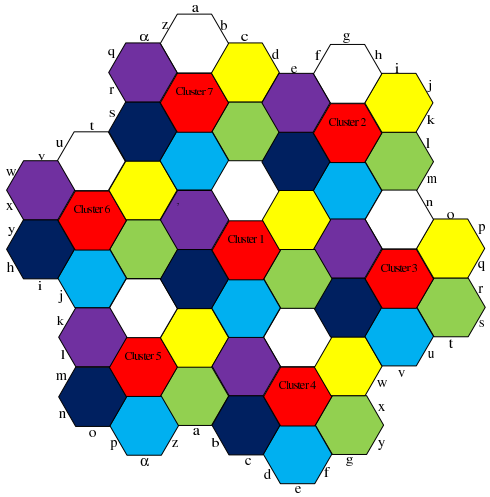

Fig. 2. Wrap-around 49-cell cluster with pilot re-use seven. Each color is associated with a set of pilot sequences that are mutually orthogonal from color to color.

We model the channel frequency response between a particular terminal and a particular service antenna as $g = \sqrt{\beta} h$ where β is a *slow fading* coefficient that embodies geometric attenuation resulting from the random location of the terminal and log-normal shadow fading, and h is a *fast fading* coefficient that we model as independent over service antennas and terminals and zero-mean complex Gaussian. The slow fading coefficients are substantially constant with respect to frequency and within the antenna array, they are constant over many coherence intervals, and they can be readily estimated; we assume that the slow fading coefficients are perfectly known. The fast fading has to be estimated entirely from the received pilot signals. Each service antenna correlates its received pilot signal with each of the K pilot sequences, and then applies Bayesian weights based on the known slow fading to obtain the minimum mean square error (MMSE) estimates for the $\{g\}$.

This paper concentrates solely on forward link data transmission and in particular on conjugate beam-forming. The QAM symbols intended for the K terminals are weighted by power control coefficients and the weighted vector is multiplied by the complex conjugate of the $M \times K$ channel estimate to produce the signals that are transmitted by the M antennas. In what follows the power control coefficients are adjusted so that equal power is spent on the transmission associated with each terminal. In multiple cell operation each base station array concentrates entirely on its own terminals, and there is no coordinated transmission among cells.

A particular terminal receives the QAM symbol intended for it times an unknown gain (as the terminal knows neither the channel nor the base station's channel estimate), plus receiver noise, plus interference from the transmissions intended for all other terminals. Again taking a Bayes approach utilizing the universal knowledge of the slow fading, the correlation between the channel and the channel estimate is known to the terminal, and the received signal can therefore be re-

written as a known gain times the intended QAM symbol, plus uncorrelated effective noise that comprises everything else. The entropy of the effective noise is upper bounded by pretending that it is Gaussian distributed. This leads directly to a rigorous lower bound on the capacity to the terminal in terms of the slow fading coefficients. The other sources of randomness - receiver noise, channel estimates, channel estimation error - are treated ergodically so their instantiations do not appear in the bound. Refer to the notation introduced at the end of Section I, we have [9]

Theorem 2.1: The forward link to the kth user terminal of a multicell LSAS access network with conjugate beam-forming pre-coding has the capacity lower bound

$$\chi_{\mathrm{f},k} = B\frac{(1-\varphi)}{2}\log_2(1+\varrho_k) \tag{1}$$

where B is the carrier bandwidth, $\varphi = \tau_{\mathrm{r}}/T$ is the reverse link pilot overhead percentage, and ϱ_k is the effective forward link signal to interference plus noise ratio (SINR) for the kth user,

$$\varrho_k = \frac{\rho_{\mathrm{f}}\tau_{\mathrm{r}}\rho_{\mathrm{r},k}E_{k:(k)}}{1+\rho_{\mathrm{f}}\left(\sum_{j\in\mathcal{J}}\beta_{k:j}\sum_{l\in\mathcal{L}_j}\lambda_l + \tau_{\mathrm{r}}\rho_{\mathrm{r},k}\sum_{l\in[k]\setminus\{k\}}E_{k:(l)}\right)}. \tag{2}$$

where $E_{k:(l)} \triangleq \frac{M_{(l)}\lambda_l\beta^2_{k:(l)}}{1+\tau_{\mathrm{r}}\sum_{i\in[l]}\rho_{\mathrm{r},i}\beta_{i:(l)}}$ for $l \in [k]$. ∎

Remark 2.2: The slot structure is such that equal amounts of time are spent on forward link and reverse link data transmission, the burden of pilot transmission is assumed to be shared equally between reverse link and forward link, hence the factor of 1/2 in (1). ∎

Remark 2.3: The effects of pilot contamination on SINR is taken into account in Theorem 2.1. It affects both signal and interference calculations. In the SINR expression (2), the signal degradation is reflected in the term E_k in the numerator and the interference is increased with the term $\tau_{\mathrm{r}}\rho_{\mathrm{r},k}\sum_{l\in[k]\setminus\{k\}}E_l$ in the denominator. ∎

III. Power Modeling and Energy Efficiency

In this section, we shall introduce a new power model for the LSAS base station energy efficiency. An LSAS base station expends power in two ways: generation of RF power, and all other internal electronic activities. The total energy efficiency (bits/Joule) of the jth base station is its net aggregate forward link throughput divided by its total expended power, both averaged over the duration of the slot,

$$\eta_j = \frac{\sum_{k\in\mathcal{L}_j}\chi_{\mathrm{f},k}}{P_{\mathrm{RF},j}(1-\tau_{\mathrm{r}}/T)/2 + P_{\mathrm{int},j}}. \tag{3}$$

Remark 3.1: In (3), the RF power is weighted by $(1-\tau_{\mathrm{r}}/T)/2$ because forward link activities occupy only half of the slot as we noted in Remark 2.2, and within the half slot forward link data transmission occupies only the fraction $(1-\tau_{\mathrm{r}}/T)$ during which base station expends RF power for data transmission. The energy spent for reverse link pilot transmissions is provided by the mobiles. ∎

The generation of RF power is assumed to have an efficiency of ε_{P}. i.e.,

$$P_{\mathrm{rad},j} = \varepsilon_{\mathrm{P}}P_{\mathrm{RF},j}, \tag{4}$$

where $P_{\mathrm{rad},j}$ is the radiated power.

The non-RF internal power $P_{\mathrm{int},j}$ is expended on LSAS critical computations and on all other activities such as analog electronics and A/D and D/A conversions. We have

$$P_{\mathrm{int},j} = 2R_{\mathrm{flops},j}/a + Mb, \tag{5}$$

where $R_{\mathrm{flops},j}$ is the total computational rate in flops (floating-point operations per second) required for LSAS critical computations, a is the power-efficiency of computing measured in flops/Watt, the factor-of-two for $R_{\mathrm{flops},j}$ is intended to account for power required for read/write operations, and b is the internal non-RF power consumption associated with each service-antenna.

The LSAS critical computations include FFTs and IFFTs, correlation of the received pilot signals with each pilot sequence, and performing linear pre-coding. We have [4],

$$R_{\mathrm{flops},j} = \frac{M_jB}{2}\left[\frac{T_{\mathrm{u}}}{T_{\mathrm{s}}}\log_2(T_uB) + \frac{T_{\mathrm{g}}\tau_{\mathrm{r}}}{T_{\mathrm{slot}}}\log_2(\tau_{\mathrm{r}}) + \frac{K_jT_{\mathrm{g}}}{T_{\mathrm{slot}}}(T-\tau_{\mathrm{r}})\right] \tag{6}$$

where K_j is the number of users simultaneously served by the jth cell, M_j is the number of LSAS service antennas in the jth base station, and $T_{\mathrm{u}}, T_{\mathrm{s}}, T_{\mathrm{g}}$ and T_{slot} are defined in Table I.

IV. LSAS Parameters and Scenarios

To compare the total energy efficiency performance of an LSAS with that of a typical LTE network, we shall adopt system parameters that are consistent with current LTE deployments.

For the reference LTE system we assume a typical LTE macro-cellular network employing FDD with a 10MHz spectral bandwidth in each direction. Correspondingly, the LSAS, operating in the PCS band ($\sim$ 1.9GHz), uses a spectral bandwidth $B = 20$MHz which is equal to the combined reverse link/forward link spectral bandwidth of the reference system. Contrary to a typical LTE base station antennas with 18dBi antenna gain in the PCS band, we assume a gain of 0dB for the LSAS base station antennas reflecting our aim of using cheaper small-form-factor $\lambda/2 \times \lambda/2$ antennas. The number of service antennas, M, is assumed to be the same for every cell. The number of terminals in each cell, K_j can vary somewhat for different $j \in \mathcal{J}$ as explained in Section V-A and the average number of terminals, $\bar{K}$, is to be determined by energy efficiency optimization. We assume receiver noise figures of 9 dB in contrast to the typical 3 dB to 4 dB in LTE base station receivers, which also reflects our intention of using low-power cheaper base station receivers. Consistent with current industry standard, the radiated power of each user terminal is assumed to be 200mW. The user terminal radiated power matters in our study due to the relevance of reverse link pilot channel performance. The base station total radiated power P_{rad} is assumed to be the same for each base station. $\bar{K}$ and P_{rad} are to be determined jointly by total energy efficiency optimization.

Our scenarios are dense urban and suburban. The dense urban LSAS cell has a radius of 500 meters and utilizes a slot duration of $T_{\mathrm{slot}} = 2$ ms which, adopting the 1/4 wavelength

rule-of-thumb, permits mobility of 71 km/h. The suburban LSAS cell has a radius of 2 km and a slot duration of $T_{\text{slot}} = 1$ ms which permits a mobility of 142 km/h.

We employ the Hata-COST231 propagation model (see for example, [12]) to model the range-dependent attenuation that figures in the slow fading coefficients β. Note that the nominal applicable range for the Hata-COST231 model is from 1 km to 20 km, we have however used the same formula for ranges less than 1 km as it is usually done in RF prediction tools. The log-normal shadow fading has 0dB mean and 8dB standard deviation. The base station antenna height is 30 meters and the mobile antenna height is 1.5 meters for data terminals.

We assume a power amplifier efficiency $\varepsilon_{\text{P}} = 25\%$ and following [11], we assume a computational energy efficiency of $a = 12.8$Gflops/Watt. There is considerable uncertainty as to how much additional internal power consumption can be reduced; therefore in our numerical work we assume a wide range of values for b:

$$b \text{ (in mW)} = 32, 64, 128, 256, 512, 1024, 2048, 4096.$$

V. LSAS Simulations and Numerical Results

Our energy performance formula (3) gives the energy efficiency entirely in terms of the slow fading coefficients, which themselves are random because of the random location of the terminals and the log-normal shadow fading. It is therefore necessary to perform multi-cell simulations to generate a multiplicity of realizations of the slow fading in order to characterize the statistical performance of LSAS.

A. Simulations

Our LSAS simulations are based on 49 hexagonal cells shown in Fig. 2 which are "wrapped around", i.e.. the cluster is replicated periodically by topologically identifying the edges with the same lower-case letters in the figure so that no cell is in a more advantageous position than another. Thus each cell is surrounded by 48 other cells. We have a pilot re-use factor of seven so that each cell (the "home cell") is surrounded by two rings of cells whose pilots are orthogonal to those used in the home cell. Re-use of the home cell's pilots only occurs in the six cells with the same color, which are two rings away from the home cell. This provides effective mitigation of pilot contamination at the cost of a seven-fold increase in the sample duration of the pilot sequences. The pilot contamination effects on the effective interference are quantified in Remark 5.1 in Section V-A1.

Each hexagonal cell is of the same size and K users are randomly distributed within the circle that circumscribes the hexagon.

1) Estimation of RF Condition per Terminal: Because of the vagaries of shadow fading, a particular terminal may not be best served by the cell in which it is geographically located. Consequently we assign each of the $49\bar{K}$ terminals to the base station to which it has the greatest RF channel gain β. Specifically, the kth mobile is served by the (k)th cell where

$$(k) = j^\star = \arg\left(\max_j \{\beta_{k:j}\}\right). \tag{7}$$

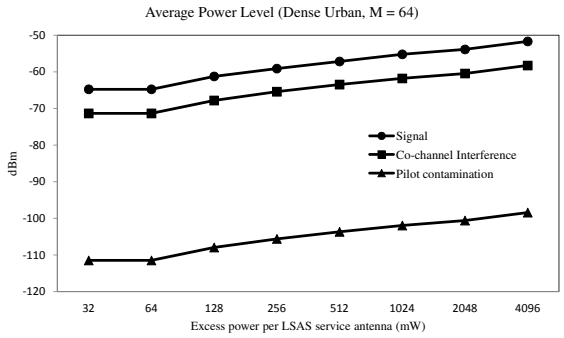

Fig. 3. Signal and interference power levels

As with all wireless networks, a small percentage of users are dropped from service due to possible severe RF conditions caused by shadow fading. Consistent with the coverage performance requirements of tier-1 wireless service providers, we assume 95% coverage probability, i.e., 5% of the users in the worst RF conditions are dropped from service. Ideally, the users with the lowest SINRs should be dropped. However, the SINR for each user, as shown in (2), are interdependent, a simple means to estimate the RF condition for each user independently is needed. For this purpose we define the *co-channel SINR* for the kth user as

$$\text{ccSINR}_k \triangleq \beta_{k:(k)} \Big/ \sum_{j \in \mathcal{J}} \beta_{k:j} \tag{8}$$

and the users with the lowest co-channel SINR are dropped from service. Thus $49\bar{K} \times 5\%$ of the mobiles with the smallest ccSINR are dropped from the service and the remaining $49\bar{K} \times 95\%$ of mobiles are served by the 49 LSAS cells.

Remark 5.1: Note that the definition of co-channel SINR depends only on the RF channel gain of the kth user. It does not depend on forward link power, nor does it depend on the channel gain of other users. Thus it is a very convenient way to estimate the RF condition of each user independently. However, the effective interference for each user consists of not only co-channel interference, but also pilot contamination and thermal noise, using the co-channel SINR as the criterion for excluding mobiles from service makes sense only when co-channel interference is the dominant interference source. With reverse link pilot reuse factor 7, this is indeed the case. Fig. 3 compares the signal power, co-channel interference power, and the pilot contamination power as functions of b for the dense urban deployment and $M = 64$. For all scenarios we see that the pilot contamination power is more than 40 dB lower than the co-channel interference power; the pilot re-use factor of seven has effectively mitigated pilot contamination to a negligible level. We also note that for all scenarios the noise power is more than 20 dB lower than the co-channel interference power. ∎

2) Required Pilot Sequence Length: To obtain the desired pilot re-use factor of seven it is necessary to use pilot sequences of sample duration $\tau_{\text{r}} \approx 7\bar{K}$. The exact required value of τ_{r} has to reflect the varying number of terminals served by the cells. The 49-cell system logically divides into seven disjoint groups with each group using the same set of orthogonal pilot sequences. Let $K_{\max,i}$ be the maximum number of terminals served by an LSAS cell in the ith group.

Then the choice of

$$\tau_{\text{r}} = \sum_{i=1}^{7} K_{\max,i} \tag{9}$$

ensures that every group of seven cells can assign each of its terminals an orthogonal pilot sequence.

3) Maximization of Total Energy Efficiency: The two free design parameters are the forward link radiated power per cell, P_{rad}, (the same for every cell) and the average number of terminals that is served by each cell, $\bar{K}$. The simulation proceeds as follows. First we generate the random positions of the terminals and the log-normal shadow fading which together determine the slow fading coefficients, i.e., β's. We then assign each terminal to a cell according to (7), drop 5% of the users with the lowest co-channel SINRs which are calculated using (8), and determine the required number of pilot sequences using (9). For a given pair $(P_{\text{rad}}, \bar{K})$, the total energy efficiency of the 49-cell cluster is evaluated as $\eta_{\text{cluster}} = \frac{1}{49}\sum_{j=1}^{49} \eta_j$. The above procedure is repeated 100 times and the average of the total energy efficiency is calculated and denoted as $\bar{\eta}_{\text{LSAS}}$, which is a function of $(P_{\text{rad}}, \bar{K})$.

Finally we choose the pair of total radiated power per cell and the average number of terminals per cell $(P_{\text{rad}}, \bar{K})$ to jointly maximize $\bar{\eta}_{\text{LSAS}}$,

$$(P^{\star}_{\text{rad}}, \bar{K}^{\star}) = \arg\max \{\bar{\eta}_{\text{LSAS}}\}.$$

Note that the averaging on the total energy efficiency is taken over $100 \times 49 = 4900$ embedded cells.

B. Numerical Results

Our numerical simulations reveal several important implications which we shall discuss in some detail in the following.

1) Comparison with LTE: A typical 3-sector LTE base station is equipped with a total of 120Watts of radiated power for which a total of 3000 Watts [10] is expended by the base station. It delivers a net aggregate forward link throughput of 40Mb/s per cell, i.e., 4b/s/Hz spectral efficiency, and therefore the total forward link energy efficiency $\eta_{\text{LTE}} \approx 13.3$ Kb/J.

Fig. 4 displays both the expected total energy efficiency of LSAS relative to that of LTE, $\bar{\eta}_{\text{LSAS}}/\eta_{\text{LTE}}$, and the expected aggregate spectral efficiency of LSAS as functions of b for the two deployment scenarios and for $M = 64$ and 128. Relative to LTE, LSAS delivers energy efficiency improvements from 20 to more than 2000 fold, and it delivers spectral efficiency between 8.7 and 25 b/s/Hz compared with LTE's 4b/s/Hz.

For each value of b, the total radiated power per cell P_{rad} and the average number of simultaneous users per cell $\bar{K}$ have been chosen to maximize $\bar{\eta}_{\text{LSAS}}$. In a real world deployment, however, P_{rad} and $\bar{K}$ are subject to variations so they may deviate from the optimal settings somewhat. The effects of the deviations on the total energy efficiency are investigated in Sections V-B2 and V-B3 below.

2) Optimal Total Radiated Power per Cell: Fig. 5 shows total energy efficiency as a function of the total radiated power per cell P_{rad} for $M = 64$ service antennas and for $\bar{K} = 15$ terminals per cell. Each curve is associated with a different assumed value for the excess power per antenna, b.

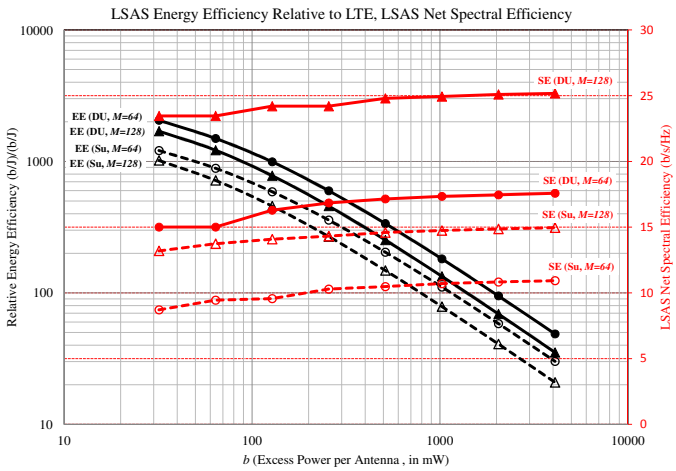

Fig. 4. Energy efficiency as a function of excess power per service antenna

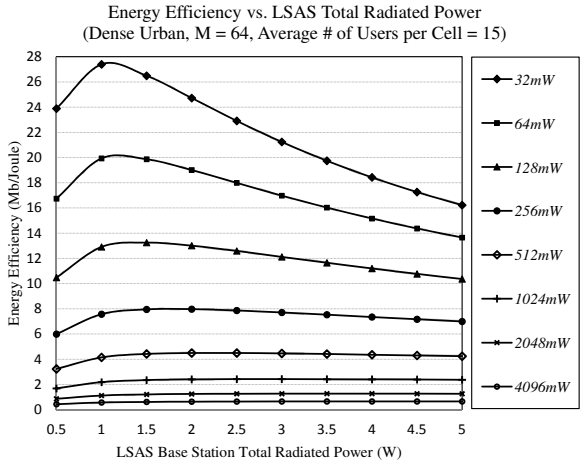

Fig. 5. Energy efficiency as a function of total radiated power

The deployment is dense urban. We observe that in general, the total energy efficiency is not sensitive to perturbations in P_{rad} and as b increases the energy efficiency becomes less sensitive to radiated power. Similar behavior is observed for $M = 128$ and for the suburban deployment, with the maxima of the curves occurring at somewhat higher radiated powers for $M = 128$. Compared with the 120W required by LTE to attain a considerably inferior throughput performance, the optimized total forward radiated powers per cell are remarkably small, ranging from 1 W to 5.5 W for dense urban and from 1.5 W to 8.5 W for suburban, depending on the values of b and M. Note that in general, a dense urban deployment tends to be more interference limited than a suburban deployment because of the four-fold decrease in cell radius such that the mean path loss at the cell edges decreases from 135 dB to 129 dB. Thus the optimized total forward radiated powers are smaller for dense urban deployment.

The optimal total forward radiated power per cell $P^{\star}_{\text{rad}}$ is an increasing function for both b and M due to the fixed power cost b per LSAS service antenna. As b and/or M increases, to maximize the total energy efficiency, the radiated power must also increase to achieve a higher spectral efficiency to compensate for the total power consumption increase.

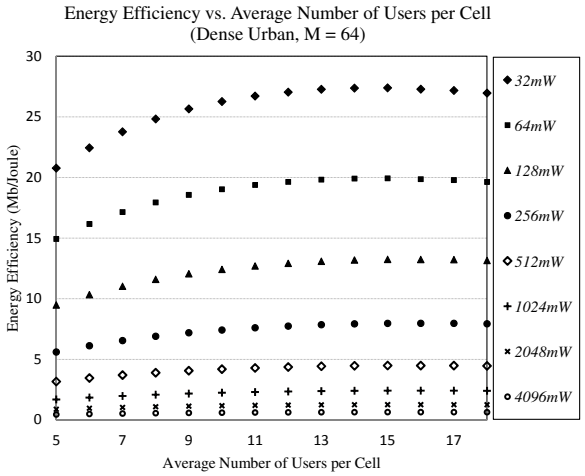

Fig. 6. Energy efficiency as a function of average number of users per cell

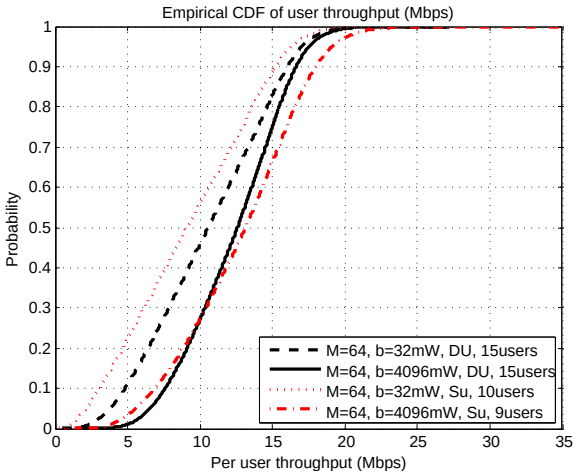

Fig. 7. CDF of per user throughput

3) Optimal Average Number of Simultaneous Users per Cell: More users provide higher spatial multiplexing gain, but longer reverse link pilots must be used, resulting in a larger overhead. These two competing factors guarantee a finite optimal number of users per cell. Due to users random position and random shadow fading, the number of users served by each cell varies. However, the optimal average number of user per cell that maximizes the expected total energy efficiency $\bar{\eta}_{\text{LSAS}}$ can be obtained. As shown in Fig. 6 for dense urban deployment with $M = 64$ antennas, the energy efficiency is insensitive with respect to $\bar{K}$, and for all values of b the optimal $\bar{K}$ is either 15 or 16. Other scenarios exhibit similar behavior. For dense urban with $M = 128$, the optimal $\bar{K}$ is around 18 while for suburban, for all values of b the optimal $\bar{K}$ decreases to either 9 or 10 for both $M = 64$ and $M = 128$. The 2ms dense urban slot permits more terminals to be serviced than does the 1ms suburban slot for the same pilot overhead.

4) Per User Throughput Performance: Fig. 7 shows the cumulative distribution function of the per-terminal throughput for an LSAS with optimized total energy efficiency. Median throughputs per terminal range from 9 to 13 Mb/s, and the 95% likely throughputs range from 3 to 7.5 Mb/s. The powerful beam-forming capability of LSAS makes it far better able than LTE to provide reliable service to terminals at the cell edges.

VI. Conclusions

From energy efficiency and spectral efficiency view points, our results make a compelling case for replacing LTE macro-cells with LSAS macro-cells. With LSAS a service provider is able to not only deliver the vastly greater throughput that the customers demand, but also be "green" at the same time. The exact energy efficiency improvements that can be obtained from LSAS depend heavily on the per antenna power consumption beyond RF generation and LSAS computing. The development of electronics required for low-cost low-power implementations of LSAS are urgently needed to bring this game changing wireless technology to reality.

Our analyses have been concentrated solely on the physical layer performance assuming a regular hexagonal cellular cluster. Further investigations must include the performance of upper layers of the wireless network as pointed out by [13] and [14]. For a real-world deployment, similar analyses can be carried out using the actual cell layout.

References

[1] T. L. Marzetta, "How much training is required for multiuser MIMO," *Proc. 40th Asilomar Conference on Signals, Systems and Computers*, Pacific Grove, CA, pp. 359-363, Oct. 2006.

[2] T. L. Marzetta, "Noncooperative cellular wireless with unlimited numbers of base station antennas," *IEEE Trans. Wireless Commun.*, 9(11):3590-3600, 2010.

[3] F. Rusek, D. Persson, B. K. Lau, E. G. Larsson, T. L. Marzetta, O. Edfors, and F. Tufvesson, "Scaling up MIMO: Opportunities and challengers with very large arrays," *IEEE Signal Processing Magazine*, 30(1):40-60, 2013.

[4] H. Yang and T. L. Marzetta, "Performance of conjugate and zero-forcing beamforming in large-scale antenna systems," *IEEE J. Sel. Areas Commun.*, 31(2):172-179, 2013.

[5] H. Q. Ngo, E. G. Larsson and T. L. Marzetta, "Energy and spectral efficiency of very large multiuser MIMO systems", *IEEE Trans. Commun.* 61(4):1436-1449, 2013.

[6] H. Hoon, G. Caire, H. C. Papadopoulos, and S. A. Ramprashad, "Achieving "Massive MIMO" spectral efficiency with a not-so-large number of antennas", *IEEE Trans. Wireless Commun.*, 11(9):3226-3239, 2012.

[7] J. Hoydis, S. ten Brink, M. Debbah, "Massive MIMO in the UL/DL of cellular networks: How many antennas do we need?", *IEEE J. Sel. Areas Commun.*, 31(2):160-171, 2013.

[8] `http://www.greentouch.org/index.php?page=about-us`

[9] H. Yang and T. L. Marzetta, "Capacity performance of multicell large-scale antenna systems," *Proc. 51st Allerton Conference on Communication, Control, and Computing*, Oct. 2013.

[10] A. Conte, "Power consumption of base stations," *TREND plenary meeting*, Ghent, Feb. 2012.

[11] D. Schneider, "Could supercomputing turn to signal processors (again)?, *IEEE Spectrum*, pp. 13-14, Oct. 2012.

[12] ETSI TR 143 030, "Digital cellular telecommunications systems (Phase 2+); Radio network planning aspects", 3GPP TR 43.030 version 9.0.0 Release 9, 2010.

[13] T. T. Tesfay, R. Khalili, J. Le Boudec, F. Richter, A. J. Fehske, "Energy saving and capacity gain of micro sites in regular LTE networks: downlink traffic layer analysis", *Proc. 6th ACM workshop on Performance monitoring and measurement of heterogeneous wireless and wired networks*, pp. 83-92, Oct. 2011.

[14] T. Bonald, N. Negde, "Capacity gains of some frequency reuse schemes in OFDMA networks", *IEEE GLOBECOM*, 2009.

A Select-Channel Approach to Power-Efficient OFDM Transmission

George Thomas
The William Hansen Hall Department of Electrical and Computer Engineering
The University of Louisiana at Lafayette
Lafayette, LA 70504-3890, USA
gt@ieee.org

***Abstract*—A novel approach involving selective channel signaling is proposed to achieve significant reductions in power requirements in OFDM. It is shown that by using only a subset of the available channels, savings in power can be achieved without sacrificing channel capacity.**

Keywords—OFDM, power efficiency, channel selection.

I. INTRODUCTION

Low-power wireless networks have recently been the focus of much research and a growing array of applications [1, 2]. Most of the applications are in a power-limited environment where the transmitters must minimize power consumption to survive under the twin constraints of limited battery power and infrequent human intervention. Orthogonal frequency division multiplexing (OFDM) has emerged as the preeminent solution to multipath fading and inter-symbol interference in wireless channels and has been adopted as an integral part of most of the recent wireless standards [3]. In this paper we propose an OFDM transmission scheme for wireless networks that need to reduce their power consumption. The basic approach is to limit transmission to only a subset of the available channels at a given time, thus obviously reducing power drain. It may however appear that the use of a reduced number of channels leads to reduced capacity. We present a technique whereby the full capacity can be retained despite the reduced number of channels.

II. BASIC CONCEPT – THE NOISELESS CASE

A. The Generic OFDM

Consider a generic OFDM system which uses n parallel orthogonal channels. Assume that binary signaling is adopted, specifically BPSK, to operate satisfactorily at low power levels and/or to simplify modem design. Assume there is no noise and that any multipath fading effects are well mitigated by the use of OFDM. Each channel delivers a BPSK symbol with energy E_b sufficient to guarantee reliable, error-free reception. In the absence of noise, this minimal but non-zero symbol energy is dictated by receiver sensitivity as well as the distance-dependent attenuation in the channel. In this scenario, we set the *energy cost of transmission* as E_b joules per bit.

B. The Selective-Channel OFDM

Now consider the case where only $m < n$ channels are to be used. We define $\rho = m/n$ as the *channel fill fraction*. The m channels deliver m bits of information (with zero error probability). However we can choose a different set of m channels out of n for each transmission. We can build a codebook that assigns each group of m channels to a unique data vector. The choice of a specific set of m active channels can carry an extra k bits of information, $k = \log_2 \binom{n}{m}$, in addition to the m bits carried by the m chosen channels. (It is assumed that k is an integer, with appropriate round-off when necessary.) Thus the reduction in data throughput (from n to m bits) seems to be at least partially offset by this scheme of encoding the selection of channel sets. The tantalizing question is whether it can fully restore the lost capacity, i.e. can it be that $k \geq n - m$. The answer surprisingly turns out to be in the affirmative.

The selective channel OFDM transmission works as follows. We transmit binary data in blocks of length $N = m + k$. At each transmission instance, we use the k bits to select one of the 2^k sets of m channels. This mode of transmission of k bits of information via channel selection will be referred to as *transmission mode* 1. Next we transmit the remaining m bits in parallel on the selected m channels using BPSK. This more conventional transmission mode will be referred to as *transmission mode* 2.

At the receiver, all n channels are sensed for RF energy. Since there is no noise in the channels, the m active channels are identified correctly. Note that E_b was assumed sufficient to enable this error-free identification of active channels despite attenuation losses and minimum sensitivity thresholds for the receivers. This stage of the receiver operation, which identifies the specific set of channels used, yields k bits error-free. Next, the receiver carries out noise-free detection of the BPSK symbols in each of the m channels that were identified as active, thereby gaining the remaining m bits. Thus $m + k$ bits are transmitted correctly by activating only m channels.

978-1-4799-0354-2/13/$31.00 ©2013 IEEE

C. Capacity Calculation

The total number of bits transmitted is,

$$I_{tot} = m + \log_2\binom{n}{m} = n\big(\rho + h(\rho)\big) \text{ bits} \qquad \text{---(1)}$$

where

$$h(\rho) = -\rho\log_2(\rho) - (1-\rho)\log_2(1-\rho) \qquad \text{--- (2)}$$

is the binary entropy function, and we have used a well-known approximation (see, e.g. Appendix A in [4]) for the binomial coefficient for large n. The total energy spent is

$$E_{tot} = mE_b \text{joules.} \qquad \text{--- (3)}$$

The energy cost per bit averaged over all n channels is now

$$E_{av} = \frac{E_{tot}}{I_{tot}} = \frac{\rho}{\rho + h(\rho)} E_b \le E_b \text{ joules per bit} \qquad \text{--- (4)}$$

for all values of $\rho \in [0,1]$. We define the *average energy fraction* as

$$\alpha = \frac{E_{av}}{E_b} = \frac{\rho}{\rho + h(\rho)} \qquad \text{--- (5)}$$

and the *average information transmitted* per channel as

$$\beta = \frac{I_{tot}}{n} = \rho + h(\rho). \qquad \text{--- (6)}$$

Fig.1 shows a plot of β vs. α.

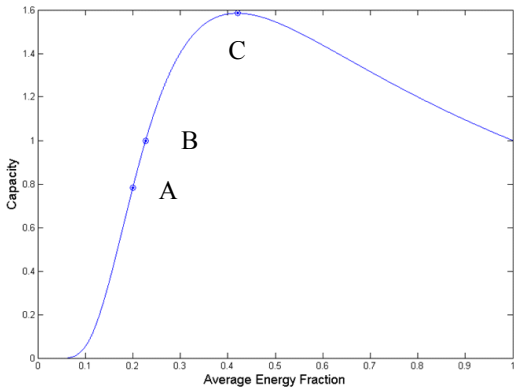

Fig. 1. OFDM information capacity factor β vs. the average energy fraction α.

The plot in fig.1 has the channel fill fraction ρ as a parameter that is zero at the point (0,0) and increases to 1 at the point (1,1). We have marked three specific points along the curve. At the first point A with $\beta \approx 0.8,$, we see that for average energy factor as little as about 20% of the full bit energy, we can achieve almost 80% of the full capacity of all n channels. It must be emphasized that the diminished average energy does not jeopardize accurate detection of the active channels. In each of these active channels we transmit bits at their full energy E_b so that accurate active channel detection is not compromised, but when averaged over all channels including the idle ones, the average energy is attractively low. The fill fraction ρ at point A is just 0.1563 i.e. nearly 85% of the channels are idle.

The second point B, with $\beta = 1$, reveals the surprising fact that for average energy factor at a little over 22%, we can have no loss in capacity (i.e. $\alpha = 1$) even though the channel fill factor is significantly lower than 1. In fact ρ is only 0.2271 at this point. Furthermore, for all higher values of the fill factor, we actually realize even higher average capacity than if we had used all n channels at their full individual capacities, i.e. we realize *excess* capacity.

At the point C at the peak of the plot, this average capacity reaches a maximum of 1.585 bits for $\rho = 0.667$. This can be interpreted as ternary signaling, with a 'null' symbol on idle channels and one of the two binary symbols on the active channels, realizing its maximal capacity $\log_2(3) = 1.585$. And ultimately for $\rho = 1$, we have the conventional system with all channels active, and $\alpha = \beta = 1$.

D. Prospects for Channels with Noise

From fig.1 we see that selective loading of a subset of a given set of channels can not only provide service with no loss of quality at significantly reduced average power but also provide extra capacity in excess of what could be achieved by full loading of all channels. It is intriguing to investigate if this excess capacity can be ploughed back into even lower average power requirements for the same capacity as the fully loaded system. A little thought will indicate that in the noiseless case there is nothing to be gained by pumping the saved power into the active channels. As there is no noise to combat, the energy E_b is sufficient for each active channel. But when noise is present, it may make sense to use the saved energy in the idle channels to boost the performance in the active channels. This we explore in the next section.

III. Selective Channel OFDM with Noise

A. Channel Model

In presence of noise in the individual OFDM channels, the accurate determination of the active channels becomes probabilistic at the receiver side. Non-zero probabilities arise for missed detection of active channels as well as false

detection of activity in idle channel. The asymptotic per-channel information rate for transmission mode 1 falls below the previous value $h(\rho)$. Also, *if* the active/idle channel determination is done accurately, the per-channel information transmitted via the active channels in transmission mode 2 falls below the previously seen ideal value ρ. To determine the attainable capacities in presence of noise, we will develop simple channel models for the two transmission modes.

It looks plausible from fig.1 that at operating points where the average capacity per channel exceeds 1 bit, we may be able to cut back on transmitted bit energy E_b and still stay at average capacity of 1 bit while reducing the average energy further. However, as soon as we begin reducing E_b, we run the risk that the active/idle channel detection at the receiver may now exhibit non-negligible error rates that jeopardize the entire scheme. The earlier assumption of error-free detection of active channels is no longer tenable. We will now need error control coding to mitigate these effects.

B. Error-Correction Coding

We propose the use of a binary error correction code as follows. A block of $k < n$ data bits is encoded into an n-symbol binary code word using an appropriate binary (n, k) error correcting code of rate $r = k/n$. This code word is used as a *channel selection vector* (CSV). Let m be the Hamming weight of this CSV. Then an additional block of m data bits is transmitted as follows. For $i = 1$ to n, if the i-th position in the CSV is a 0, the i-th channel is left idle in this transmission. If the i-th position is a 1, then a bit from the block of m data bits is selected sequentially and the corresponding binary symbol (respectively a −1 or a +1) is sent on the i-th channel. If the average Hamming weight of the code words is m, then, as before, $\rho = m/n$ is the average fill fraction.

Let P watts be the total power available for transmission over all channels in the fully loaded case ($\rho = 1$) and let the total bandwidth of all n channels be $B = nW$ Hz. Assuming additive white Gaussian noise (AWGN) with two-sided power spectral density $N_o/2$ watts/Hz, the signal to noise ratio in each channel is $\gamma = P/N_oW$ and the capacity of each of the n parallel binary-input, unquantized-output AWGN channels is (see e.g. [5], p.153),

$$C_o(\gamma) = -\frac{1}{2}\log_e(2\pi e) - \int_{-\infty}^{\infty} g(x)\log_2 g(x)dx \qquad \text{--- (7)}$$

where

$$g(x) = \frac{1}{2\sqrt{2\pi}}\exp\left(-\frac{\left(x-\sqrt{2\gamma}\right)^2}{2}\right) + \frac{1}{2\sqrt{2\pi}}\exp\left(-\frac{\left(x+\sqrt{2\gamma}\right)^2}{2}\right). \qquad \text{--- (8)}$$

In order to deliver these m bits reliably, however, the m active channels must be correctly decoded at the receiver.

The active/idle channel information can be viewed as being conveyed through a (virtual) asymmetric binary channel (BAC) with cross-over probabilities P_M and P_F. An active channel is sensed erroneously as idle at the receiver with a missed detection probability P_M, and an idle channel is sensed as an active one with a false detection probability P_F. To compute these probabilities specifically, we assume BPSK transmission on the active channels. The transmitted signal set is then

$$s(t) = \begin{cases} 0 \\ +A\cos(\omega_c t) \\ -A\cos(\omega_c t) \end{cases} \qquad 0 \le t < T \qquad \text{--- (9)}$$

respectively for the idle channel or for two possible BPSK symbols on an active channel. T denotes the symbol duration. The received signal is $s(t) + w(t)$ where $w(t)$ is zero-mean AWGN with variance $\sigma^2 = N_0/2$. The matched filter outputs are:

$$\frac{1}{T}\int_0^T [s(t)+w(t)]\cos(\omega_c t)dt = \begin{cases} w \\ (A/2)+w \\ -(A/2)+w \end{cases} \qquad \text{--- (10)}$$

where

$$w = \frac{1}{T}\int_0^T w(t)\cos(\omega_c t)dt \qquad \text{--- (11)}$$

We can readily find that $E[w] = 0$ and $E[w^2] = N_0/4T$. The conditional probability densities for the matched filter outputs for the three cases of signal transmission are therefore three identically shaped Gaussian densities of variance $N_0/4T$, centered at 0 and at $\pm A/2$, as in fig.2 below.

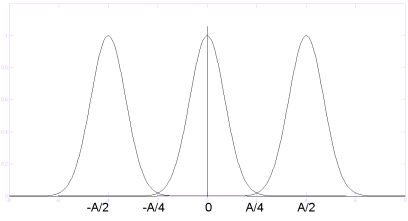

Fig. 2. Channel output conditional probability densities

Thus, underlying the virtual BAC, we really have a ternary physical channel. For deriving the maximum capacity (at the peak point C in figure 1) we should be using all three input symbols equally often. This means that for large n, a third of the channels are idle and the other two thirds carry the two BPSK symbols equally likely, and the three conditional densities are equiprobable. We thus use decision thresholds $\lambda = \pm A/4$ at the intersection points of adjacent densities.

The false detection probability can now be found as

$$P_F = \Pr\{|w| > A/4\} = 2Q\left(\frac{A/4}{\sqrt{N_0/4T}}\right) = 2Q\left(\sqrt{\frac{E_b}{2N_0}}\right) \quad \text{--- (12)}$$

where $E_b/N_o = \gamma$ is the signal-to-noise ratio and $E_b = A^2T/2$ is the symbol energy.

The missed detection probability is

$$P_M = \Pr\{3A/4 \geq w > A/4\} = Q\left(\sqrt{\frac{E_b}{2N_o}}\right) - Q\left(\sqrt{\frac{9E_b}{2N_o}}\right). \quad \text{--- (13)}$$

(Note that if w exceeds $3A/4$ when $-A/2$ is the signal component of the matched filter output, the channel will be correctly determined as active, even though the implied modulation symbol will be incorrect.)

For the BAC defined by the error probabilities P_M and P_F as in (12) and (13), the input symbol probabilities are ρ (for "1": active channel) and $1 - \rho$ (for "0": inactive channel).

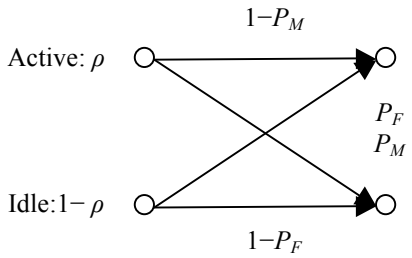

Fig. 3. The Binary asymmetric channel

The mutual information between the channel input and output X and Y is

$$I_o(\rho,\gamma) = H(Y) - H(Y|X) = h(\varepsilon) - \rho h(P_M) - (1-\rho)h(P_F) \quad \text{--- (14)}$$

which is a function of both ρ and γ; and we have used the notation

$$\varepsilon = \rho(1 - P_M) + (1-\rho)P_F \quad \text{--- (15)}$$

for the probability of 'active' channel detection in at the output (i.e. $Y = 1$).

C. Composite Channel Capacity

Thus we have two channels at play here, the signal detection channel with 'capacity' (i.e. mutual information, for a given ρ) equal to I_o as in (14) and the binary-input AWGN channel with capacity C(γ) as in (7) for a given SNR γ. The receiver first carries out active/idle channel determination. This can be done error-free for all code rates $r < I_o$. Thus as a limiting case, nI_o bits are delivered error-free at this stage. With the $n\rho$ active channels correctly determined, the receiver now carries out bipolar signal detection on these channels. These $n\rho$ bits must be coded at rates not exceeding C_o in order for error-free detection which delivers $n\rho C_o$ additional bits of information. The overall information transfer rate per channel is thus

$$C(\rho,\gamma) = I_o(\rho,\gamma) + \rho C_o(\gamma) \quad \text{--- (18)}$$

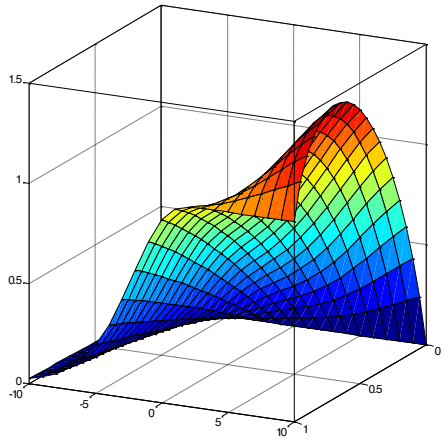

Fig. 4. Capacity vs. E_b/N_o and channel fill fraction ρ

In fig.4 we show a plot of $C(\rho,\gamma)$. For a conventional multi-channel system with full channel loading $\rho = 1$, C increases

with the SNR γ and saturates at 1 bit per channel, as to be expected. For a fractionally loaded system with $\rho < 1$, at high SNR we see per-channel capacities exceeding 1 bit by significant margins, as predicted in (6). The maximum capacity in fig. 4 appears to be a little below 1.5 bits, definitely below the peak of $\log_2(3) = 1.586$ indicated by (6). We attribute this to the restriction imposed by our implementing the ternary channel coding in two stages of binary coding. Given that restriction, the consequent loss of capacity seems to be minimal. We note further that even at somewhat lower SNR values, where the active/idle channel errors (before decoding) are not negligible, the loss of rate due to coding is more than offset by the rate gain from the selective channel signaling and the overall capacity stays well above 1 bit.

It is instructive to view the data in fig.4 as contour plots. These contours shown in fig.5 are for fixed capacity values ranging from 0.05 to 1.45 bits per channel in increments of 0.05. These contours clearly show the tradeoff between energy (E_b/N_o) and channel fill fraction ρ. In particular the contour for $C = 1.0$ is the one that shows how the full *noiseless capacity* of can be maintained *in the presence of noise* and with only fewer than the full set of channels being activated.

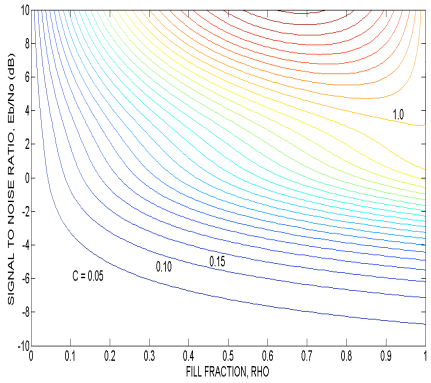

Fig. 5. Tradeoff between E_b/N_o and fill factor for fixed capacities (ranging from 0.05 to 1.45 in increments of 0.05)

Thus it is evident from the foregoing discussion that even in presence of noise that may potentially challenge accurate detection of idle/busy channels at the receiver, it is possible to communicate selectively over only a subset of the available channels and thus safe significantly on energy while keeping the system capacity the same as attainable with all channels activated.

IV. CONCLUSION

In this paper we presented an approach to reducing the power requirement in OFDM systems without sacrificing capacity, by a method of selective channel signaling. It appears well suited for applications to wireless sensor networks and such other low power wireless applications. Our intent here has been to explore the theoretical limits of performance by assuming codes at rates near channel capacity. However, since near-capacity performance has now become practical with the use of turbo-codes and low density parity check codes, this assumption seems to be justified.

OFDM seems to be the preeminent target for application of the selective signaling method presented here but it is by no means the only one. The idea is applicable to any diversity system of parallel and mutually independent transmissions. For example in a time-division multiplex system with n consecutive independent slots, we can select subsets of k slots and thus reduce average transmit power while maintaining the same capacity (or even exceeding it). In optical wavelength-division multiplex (WDM) transmission also the same principle is readily applicable. A recent innovation in wireless transmission, known as spatial multiplexing [6, 7], uses the idea that the identity of a subset of multiple available transmit antennas in a multi-input-multi-output (MIMO) system can be used as an information-bearing symbol. Our proposal can thus be used to reduce power requirements in wireless spatial multiplex systems as well.

REFERENCES

[1] D. Feng, C. Jiang, G. Lim, L. Cimini, G. Feng, and G. Li, "A survey of energy-efficient wireless communications," IEEE Communications Surveys & Tutorials,Vol. 15 , No. 1, pp. 167-178, 2013

[2] G. Li, Z. Xu, C. Xiong, C. Yang, S. Zhang, Y. Chen, and S. Xu, "Energy-efficient wireless communications: tutorial, survey, and open issues," IEEE Wireless Communications, Vol. 18 , No. 6, pp. 28-35, 2011

[3] Y. G. Li and G. L. Stuber, *Orthogonal Frequency Division Multiplexing for Wireless Communications*, Springer, 2006

[4] W.W. Peterson and E.J. Weldon, Jr., Error-Correcting Codes. Cambridge, MA: MIT Press, 1982

[5] A. J. Viterbi and J. K. Omura, Principles of Digital Communication and Coding. New York: McGraw-Hill, 1979.

[6] R. Mesleh, H. Haas, S. Sinanovic, C. W. Ahn, and S. Yun, "Spatial modulation," *IEEE Trans. Veh. Technol.*, vol. 57, no. 4, pp. 2228–2241, July 2008.

[7] J. Jeganathan, A. Ghrayeb, and L. Szczecinski, "Spatial modulation: optimal detection and performance analysis," *IEEE Commun. Lett.*, vol. 12, no. 8, pp. 545–547, Aug. 2008.

Methods to Evaluate the Performance of Multiple Uncooperative Users for Green Cognitive Radio Networks

Xiaohua Li
Department of Electrical and Computer Engineering
State University of New York at Binghamton
Binghamton, NY 13902
Email: xli@binghamton.edu

***Abstract*—In this paper, we propose a method to calculate the throughput of multiple uncooperative cognitive radio users. We use a bank of Markov models to derive the fraction of time that each user spends in successful channel access. The mutual interference among the users is modeled into the transitional probabilities of the Markov models, which makes it tractable to calculate multiple user throughput in large cognitive radio networks (CRN). In addition, to evaluate the level of greenness of the multiple user CRN, we develop a method to optimize the ideal capacity of the fully cooperative CRN. This method relies on solving the sum-of-ratios linear fractional programming for optimization. Simulations are conducted to show the big gap between the uncooperative CRN performance and the ideal performance.**

I. Introduction

With the rapid increase of wireless communication services, wireless spectrum has become a scarce resource. The requirement of high data rate and long lifetime makes power efficiency of the communication system a critical factor. The efficient use of spectrum and energy resources is thus one of the major objectives for green wireless communications. Communication systems with high (or optimal) bandwidth/power efficiency contribute to a green wireless environment with less interference and less "CO_2" emission.

Green communications have attracted great interests during recent years [1]. One of the potential technologies to support green communications is the "cognitive radio network" (CRN) [2][3]. CRN can adapt its use of spectrum and power according to the environment. It can exploit the spectrum white spaces, i.e., spectrum not used by the primary users (PU), without creating detrimental interference to the environment. It can adapt its transmission power according the interference level of the environment. A green CRN is able to realize its communication objectives with less spectrum and power resource consumption.

As a unique feature, CRN conducts spectrum sensing and accesses the spectrum that is not occupied by the PU. It must vacate the spectrum if finding that the PU becomes active. There have been extensive research published in CRN, including areas such as spectrum sensing, transmission/modulation design, theoretical performance/capacity analysis, MAC/Network layer protocols, hardware/testbed development, security, etc. However, there have been very limited study on the greenness analysis, especially for CRN with a large number of uncooperative users. A typical research on CRN may involve developing some spectrum sensing algorithms and spectrum access strategies. But the performance may be evaluated by simulations only due to the complexity of the performance analysis of large distributed CRN [4]-[6].

In this paper, we develop a method to analyze the throughput performance of CRN with multiple uncooperative secondary users. We use an innovative tool, i.e., Markov Model Bank (MMB), to model the operation of multiple CRN users and their mutual interference. Each user has its own sub-Markov model, and the mutual interference among the secondary users is abstracted into the state transition probabilities. This makes it tractable to treat the complex coupling among all the users. Throughput of each user can thus be derived, under various spectrum sensing and spectrum access strategies. To simplify the presentation, we consider a generic spectrum sensing and spectrum access strategy only in this paper. Consideration of multiple strategies in heterogenous CRN will be reported elsewhere, such as [7].

In order to evaluate the level of greenness of the CRN, we need to study how far away the CRN performance (under certain spectrum sensing and spectrum access strategies) is from the ideal (or optimal) performance. More specifically, *the "greenness" in this paper is measured by what throughput the CRN can achieve given the spectrum and energy resource, compared with the ideal case*. For this purpose, we further develop a method to optimize the ideal capacity of the multi-user CRN, under the fully cooperative assumption. We will show that this can be realized by solving the sum-of-ratios linear fractional programming problems. Note that the optimal capacity of CRN has been a challenge, and has been studied for small networks involving a few users only. For example, [8] derived the optimal capacity under some special cases (such as heavy mutual interference).

The organization of this paper is as follows. In Section II, we give the system model. In Section III, we develop the method to derive the throughput of the multiuser CRN. Then in Section IV, we develop the method to calculate the ideal capacity. Simulations are conducted in Section V to compare the throughput of multiuser CRN to its ideal capacity. Conclusions are given in Section VI.

978-1-4799-0354-2/13/$31.00 ©2013 IEEE

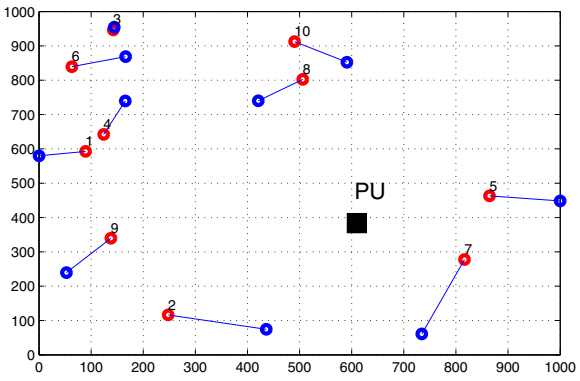

Fig. 1. An example of the CRN with $N = 10$ secondary users and one primary user (PU).

II. System Model

The CRN we consider in this paper consists of a set of N secondary users and some primary users. Each secondary user is a transmitting-receiving pair of nodes, where the transmitting node transmits to the receiving node. The users are uniformly distributed. We assume that the users are either fixed or slowly moving, and conduct communications without the cooperation from other users. While transmitting to the receiving node, the transmitter creates interference to other users as well. An example of the network is shown in Fig. 1.

We assume there are K channels (spectrum resource) available for the N users to choose from. The channels may be occupied by some PU with probability $1 - \theta_k$, where $k = 1, \ldots, K$. Each secondary user conducts spectrum sensing to find all available channels [9], and then selects some available channels randomly to conduct transmission.

For each secondary user, we consider a simplified cognitive radio transmission model that includes three states: spectrum sensing, data transmission and channel switching, as shown in Fig. 2. The working sequence of a cognitive radio always begins with the spectrum sensing. If the spectrum sensing indicates the channel is available for secondary access, then the cognitive radio transmits a data packet, and the model shifts into the data transmission state. If the spectrum sensing indicates the channel is not available (due to either the PU activity or other secondary users activity), then the cognitive radio conducts channel switching, and the model shifts into the channel switching state. In order to simplify the analysis, we assume that the model always shifts back to the spectrum sensing state after the channel switching state or the data transmission state, whether the two operations are successful (without collisions) or not.

We can use a Markov Model Bank (MMB) to model the competitive spectrum access among the N CRN users. The MMB consists of a sub-Markov model for each user, as shown in Fig. 3, where π_{si},π_{di},π_{ci} are the probabilities of the user i staying in the channel sensing, data packet transmission and channel switching modes. The transitional probability q_{si} or q_{sj} denotes the probability that the channel is sensed as available. Although the two users' sub-Markov models look separated from each other, their transitional probabilities

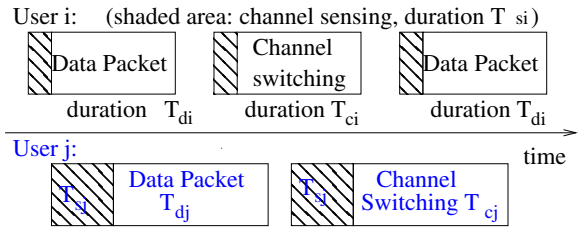

Fig. 2. Illustration of cognitive radio transmissions. Transmission structure with three basic operation modes: channel sensing, data packet transmission, and channel switching for each user i or j.

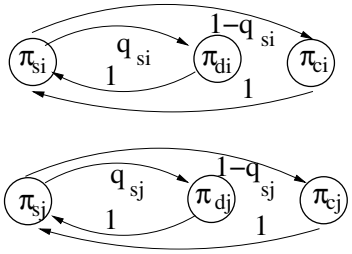

Fig. 3. Markov Model Bank (MMB) for multi-user CRN. MMB consists of a sub-Markov model for each user. Each sub-Markov model has three state probabilities (corresponding to the three basic operation modes), and has channel sensing result q_{si} as transitional probability.

and state probabilities are inter-related due to the mutual interference.

For each user i, let the durations of the spectrum sensing slot, data transmission slot, and channel switching slot be T_{si}, T_{di}, and T_{ci}, respectively. Usually the spectrum sensing duration T_{si} is much smaller than either T_{di} or T_{ci} for high throughput.

In the spectrum sensing slot, we assume that if the signal to noise ratio (SNR) is larger than the detection threshold Γ_s, then the cognitive radio will make a decision that the channel is occupied by primary users or other secondary users, and is thus not available [9]. As long as the interference emitted to the spectrum sensing slot makes the SNR larger than the sensing threshold Γ_s, the cognitive radios must vacate the channel and take the time-consuming channel switching procedure to negotiate a new one. We assume that the cognitive radios do not discriminate whether the interference comes from the primary users or other secondary users.

Let P_i^k be the transmission power of the user i spent in channel k, where $i = 1, \cdots, N$, and $k = 1, \cdots, K$. Assume the user i has maximum overall transmission power $\bar{P}_i$. Then we have

$$0 \leq \sum_{k=1}^{K} P_i^k \leq \bar{P}_i. \tag{1}$$

The signal received by the user i's receiver in the channel k is

$$y_i^k(n) = \sqrt{P_i^k} h_{ii} s_i(n) + \sum_{j=1, j\neq i}^{N} \sqrt{P_j^k} h_{ji} s_j(n) + v_i^k(n) \tag{2}$$

where the $s_i(n)$ is the discrete signal transmitted by the user i, h_{ji} is the complex Gaussian distributed flat fading channel from the user j's transmitter to the user i's receiver, and

$v_i^k(n)$ is the AWGN with zero-mean and power σ_i^{k2}. The instantaneous SNR of the user i in the channel k is thus

$$\gamma_i^k = \frac{P_i^k |h_{ii}|^2}{\sum_{j=1,j\neq i}^{N} P_j^k |h_{ji}|^2 + \sigma_i^{k2}} \tag{3}$$

As the performance metric, we consider the summation of the throughput R_i of all the N secondary users

$$R = \sum_{i=1}^{N} R_i. \tag{4}$$

Each R_i can be calculated from the probabilities of the three states in Fig. 3 and the corresponding slot lengths, as well as the transmission channel capacities based on the SNR, i.e., $\log(1+\gamma_i^k)$. Only the data transmission state is counted toward the throughput. Due to the ideal spectrum sensing assumption, we can omit the data packet collisions in this paper.

III. CRN Throughput analysis

Consider the CRN with a generic spectrum access strategy, i.e., picking randomly only one available channel to access at each time. Then we can skip the channel index k. Note that the spectrum sensing still covers all the K channels. Consider the user i's sub-Markov model in Fig. 3. There is only one unknown state transitional probability q_{si}. According to the steady state property of the Markov model, we can calculate the probabilities of the three states π_{si}, π_{di} and π_{ci} by solving the following equation

$$\begin{bmatrix} -1 & 1 & 1 \\ q_{si} & -1 & 0 \\ 1-q_{si} & 0 & -1 \end{bmatrix} \begin{bmatrix} \pi_{si} \\ \pi_{di} \\ \pi_{ci} \end{bmatrix} = \begin{bmatrix} 0 \\ 0 \\ 0 \end{bmatrix}. \tag{5}$$

This equation has infinitely many solutions. From (5), we can represent π_{di} and π_{ci} by π_{si}, i.e.,

$$\pi_{di} = q_{si}\pi_{si}, \quad \pi_{ci} = (1-q_{si})\pi_{si}. \tag{6}$$

To simplify expressions, without loss of generality, we assume that $T_{di} = T_{ci}$. This is reasonable considering the fact that most of the time the secondary user just needs to wait for one regular data transmission slot before doing channel sensing again. Then the fraction of time that the user i spends in data transmission session has a simple expression $\frac{q_{si}T_{di}}{T_{si}+T_{di}}$, which is also the probability of data packet transmission.

In order to find the state transmission probability q_{si}, we consider the spectrum sensing slot of the secondary user i. For the kth channel, the user i senses the SNR as γ_{si}. The transitional probability

$$q_{si} = P[\gamma_{si} < \Gamma_s]\theta \tag{7}$$

The SNR

$$\gamma_{si} = \frac{I_i}{\sigma_{si}^2} \tag{8}$$

where σ_{si}^2 is the noise power at the user i's sensing receiver (in channel k). The I_i denotes the overall interference received from all other secondary users [10]. Let the set S_i denote all the other secondary users that are using the kth channel simultaneously. Since each secondary user j's probability of being in the data transmission slot is $q_{sj}T_{dj}/(T_{sj}+T_{dj})$, we have

$$I_i = \sum_{j\in S_i} q_{sj}\frac{T_{dj}}{T_{sj}+T_{dj}} P_j |h_{ji}|^2. \tag{9}$$

With the state probabilities, we can define the average throughput of the user i as

$$R_i = \frac{\pi_{di}T_{di}}{\pi_{si}T_{si}+\pi_{di}T_{di}+\pi_{ci}T_{ci}} \log(1+\gamma_i), \tag{10}$$

where γ_i is the data transmission slot SNR, as per (3).

From the probability of the user i staying in the data transmission slot, the throughput (10) can be changed to

$$\begin{aligned} R_i &= q_{si}\frac{T_{di}}{T_{si}+T_{di}} \log(1+\gamma_i) \qquad (11)\\ &= P\left[\sum_{j\in S_i} \frac{q_{sj}T_{dj}}{T_{sj}+T_{dj}} \frac{P_j|h_{ji}|^2}{\sigma_{si}^2} < \Gamma_s\right] \frac{\theta T_{di}\log(1+\gamma_i)}{T_{si}+T_{di}} \end{aligned}$$

In the throughput expression (11), the random variables are the channel coefficients h_{ji}. In order to evaluate the R_i, we define new random variables

$$x_{ji} = q_{sj}\frac{T_{dj}}{T_{sj}+T_{dj}} \frac{P_j}{\sigma_{si}^2} |h_{ji}|^2 \tag{12}$$

Obviously, each variable x_{ji} has exponential distribution with mean

$$E[x_{ji}] = q_{sj}\frac{T_{dj}}{T_{sj}+T_{dj}} \frac{P_j}{\sigma_{si}^2} \tag{13}$$

The summation of the multiple exponential distributions gives a new random variable

$$x_i = \sum_{j\in S_i} x_{ji} \tag{14}$$

which has Hypo-exponential distribution.

According to the cumulative distribution function of the Hypo-exponential random variables [11], we have

$$P[x_i < \Gamma_s] = 1 - \mathbf{a}e^{x_i\mathbf{B}}\mathbf{1}, \tag{15}$$

where $\mathbf{1}$ is a column vector with all elements being 1, $\mathbf{a}$ and $\mathbf{B}$ are vector and matrix whose dimensions are the number of secondary users using the channel k. As a result, we can numerically evaluate the throughput R_i.

To evaluate (15) and (11) is actually to calculate all transitional probabilities q_{si}. From (7), Obviously q_{si} is a function of all other q_{sj}, $j = 1, \cdots, N$. Many non-linear numerical algorithms can be used to find some solutions to q_{si}. Note that it is not necessary to find all the solutions or the globally optimal solutions.

As an example, let us consider a simple case with two secondary users only, i.e., $N = 2$. In this case, the complex Hypo-exponential distribution will be reduced to the simple exponential distribution, which gives us more clear idea of the throughput calculation.

Consider the user i, where $i = 1$ or 2. We use $j = 3 - i$ to denote the other secondary user. The transitional probability is

$$\begin{aligned} q_{si} &= P[\gamma_{si} < \Gamma_s]\theta \\ &= P[q_{sj}\frac{T_{dj}}{T_{sj}+T_{dj}}\frac{P_j}{\sigma_{si}^2}|h_{ji}|^2 < \Gamma_s]\theta \\ &= P[|h_{ji}|^2 < \frac{\Gamma_s\sigma_{si}^2}{q_{sj}P_j}\frac{T_{sj}+T_{dj}}{T_{dj}}]\theta \\ &= [1 - e^{-\frac{\Gamma_s\sigma_{si}^2}{q_{sj}P_j}\frac{T_{sj}+T_{dj}}{T_{dj}}}]\theta \end{aligned} \quad (16)$$

Note that we have used the fact that $|h_{ji}|^2$ is an exponential random variable. For the two secondary users, we have the following equation array to solve their transitional probabilities

$$\begin{cases} q_{si} = (1 - e^{-a_j/q_{sj}})\theta \\ q_{sj} = (1 - e^{-a_i/q_{si}})\theta \end{cases} \quad (17)$$

where $a_i = \frac{\Gamma_s\sigma_{si}^2}{P_j}\frac{T_{sj}+T_{dj}}{T_{dj}}$ and similarly for a_j. Therefore, the values of the two state transitional probabilities can be evaluated numerically. As a matter of fact, our simulation shows that we can simply solve them iteratively based on the form of (17).

In summary, the MMB model we developed in this paper simplifies the mutual interference among all the N users into the set of transitional probabilities. By increasing the complexity of the transitional probabilities, the complexity of the Markov model is much reduced, which makes it feasible to deal with large CRN with many users.

IV. Ideal fully-cooperative capacity analysis

The derivation in the Section III is based on the assumption that the secondary users do not cooperative with each other for channel scheduling, which may degrade the throughput severely. In order to find how far away it is from the best possible results, in this section we derive the optimized throughput of the secondary users in the ideal fully-cooperative CRN.

From the system model in Section II, recall the definition of P_i^k as the transmission power of the user i in the channel k, where $i = 1, \cdots, N$, and $k = 1, \cdots, K$. Recall also that θ_k is the probability that the channel k is not occupied by the PU. Considering the PU activity, not all channels are available simultaneously.

Since each user may use multiple available channels simultaneously, we need to consider a set of any L_m channels

$$C_m = \{k_1, \cdots, k_{L_m}\}. \quad (18)$$

The probability that only channels in C_m are available is

$$P[C_m] = \prod_{\ell=1}^{L_m}\theta_{k_\ell}\prod_{k=1,k\notin C_m}^{K}(1-\theta_k). \quad (19)$$

We have altogether 2^K such sets, i.e., $m = 1, \cdots, 2^K$. Therefore, for optimal throughput evaluation, we need to consider all possible sets, and find the average capacity.

For the ideal (optimized) throughput in each set C_m, we can choose appropriate transmission power P_i^k to maximize the sum of the SNRs of all the N users, i.e.,

$$\begin{aligned} f(C_m) &= \max_{\{P_i^k\}}\sum_{i=1}^{N}\sum_{\ell=1}^{L_m}\gamma_i^{k_\ell} \\ &\text{s.t.} \quad \sum_{\ell=1}^{L_m}P_i^{k_\ell} \le \bar{P}_i, \;\; P_i^{k_\ell} \ge 0, \;\; 1 \le i \le N \end{aligned} \quad (20)$$

Note that $P_i^k = 0$ for all $k \notin C_m$.

Define the transmission power vector

$$\mathbf{z}_m = \left[\frac{P_1^{k_1}}{\bar{P}_1}, \frac{P_1^{k_2}}{\bar{P}_1}, \cdots, \frac{P_N^{k_{L_m}}}{\bar{P}_N}\right]^T. \quad (21)$$

We can rewrite (20) into

$$\begin{aligned} f(C_m) = \;& \max_{\mathbf{z}_m} \sum_{i=1}^{N}\sum_{\ell=1}^{L_m}\frac{\mathbf{a}_{i\ell}^T\mathbf{z}_m}{\mathbf{b}_{i\ell}^T\mathbf{z}_m + 1} \\ & \text{s.t.} \quad \mathbf{A}\mathbf{z}_m \le \mathbf{1}, \;\; \mathbf{z}_m \ge \mathbf{0}. \end{aligned} \quad (22)$$

The vectors

$$\mathbf{a}_{i\ell} = [\cdots\cdots, |h_{ii}|^2, \cdots\cdots]^T\frac{\bar{P}_i}{\sigma_{si}^2}, \quad (23)$$

has the channel coefficients $|h_{ii}|^2$ in a position corresponding to the transmission power $P_i^{k_\ell}/\bar{P}_i$ in $\mathbf{z}_m$. The vector

$$\mathbf{b}_{i\ell} = [\cdots\cdots, \frac{|h_{ji}|^2\bar{P}_j}{\sigma_{si}^2}, \cdots\cdots] \quad (24)$$

consists of channel gains of the interference items. The $N \times NL_m$ matrix $\mathbf{A}$ has the structure

$$\mathbf{A} = \begin{bmatrix} \mathbf{1}^T & & \\ & \ddots & \\ & & \mathbf{1}^T \end{bmatrix}. \quad (25)$$

where $\mathbf{1}$ is the L_m dimensional vector with all entries as 1.

After obtaining the optimal transmission powers and the optimal SNRs by solving (22), we can then calculate the ideal capacity of the CRN. Specifically, for each available channel set C_m, the user i gains capacity

$$R_i(C_m) = \sum_{\ell=1}^{L_m}R_i^{k_\ell}, \quad (26)$$

where

$$R_i^{k_\ell} = \log(1 + \gamma_i^{k_\ell}). \quad (27)$$

The overall capacity of the user i is thus

$$R_i = \sum_{m=1}^{2^K}R_i(C_m)P[C_m]. \quad (28)$$

By maximizing (22), we can maximize the capacity for all the secondary users. Note that (22) is in the form of sum-of-ratios linear fractional programming (LFP). Sum-of-ratios LFP has been found in many applications, which stimulated decades of research. Although the problem in the general setting (with arbitrarily large number of ratios, number of variables, as well as number of constraints) may still be challenging and deserve more investigation, there are many sophisticated algorithms that can be used to solve the special case in our setting, such as those in [12]-[16].

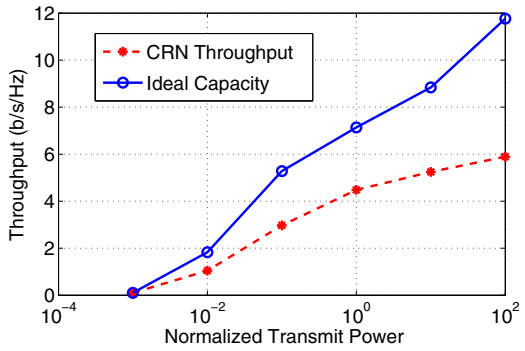

Fig. 4. CRN throughput and the ideal capacity under various (normalized) transmission powers.

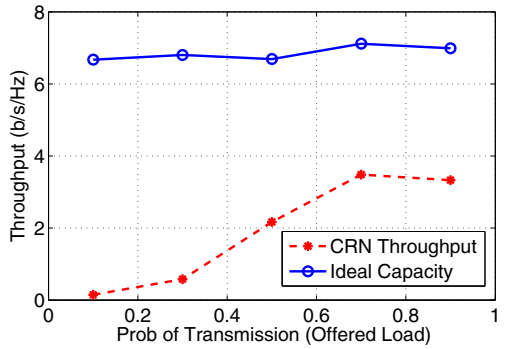

Fig. 5. CRN throughput and the ideal capacity as functions of the offered load (i.e., the probability that each user has data packet to transmit).

V. Simulations

In this section, we report our simulation of the numerical evaluation of the uncooperative CRN throughput as well as the ideal CRN capacity. We simulated a random CRN of $N = 2$ secondary users competing for accessing 1 channel. The nodes' positions were randomly generated within a square of 1000×1000 meters. The edge SNRs were calculated as $10^8 d_{ij}^{-2.6}$ where d_{ij} is the propagation distance.

First, we use the expressions in Section III to calculate the throughput of the uncooperative CRN users and use the expressions in Section IV to optimize the ideal capacity of the CRN users, under various (normalized) secondary user transmission powers $\bar{P}_i$. Simulation results were shown in Fig. 4. It can be clearly seen that the uncooperative CRN can achieve just $1/2$ of the optimized ideal capacity. Therefore, there are still much room to improve the greenness of the CRN.

Then, we calculate the CRN throughput and the ideal capacity under various offered load, where "offered load" refers to the probability that each secondary user has data packet to transmit at any time. Simulation results in Fig. 5 shows that the CRN throughput improves with offered load, until reaching a saturation point (which is because we have assumed almost perfect collision resolution). For green CRN, under light CRN user traffic load, much more users can be allowed to share each channel.

VI. Conclusion

In this paper, we study the greenness of the CRN with a special setting of N uncooperative users. We first develop a method to calculate the throughput of each CRN user. We use a Markov Model Bank (MMB) to model the N users' spectrum sensing, channel access, and channel switching procedure, as well as the mutual interference. Then we develop a method to optimize the ideal capacity under the ideal fully-cooperative assumption. We use the sum-of-ratios linear fractional programming for the optimization. Simulations are then conducted to show that the throughput of the uncooperative CRN is very far away from the ideal capacity.

References

[1] A. Dejonghe et al., "Green reconfigurable radio systems," *IEEE Signal Proc. Mag.*, vol. 24, no. 3, pp. 90101, May 2007.

[2] G. Gur and F. Alagoz, "Green wireless communications via cognitive dimension: An overview," *IEEE Network*, pp. 50-56, March/April 2011.

[3] X. Lian, H. Nikookar, and L. P. Ligthart, "Distributed beamforming with phase-only control for green cognitive radio networks," *Eurasip Journal on Wireless Communications and Networking*, vol. 2012, pp. 1 - 16, Feb. 2012.

[4] B. Wang, Z. Ji, K. J. R. Liu and T. C. Clancy, "Primary-prioritized markov approach for dynamic spectrum allocation," *IEEE Trans. Wirel. Commun.*, vol. 8, no. 4, pp. 1854-1865, Apr. 2009.

[5] J. Huang and X. Chen, "Evolutionarily stable spectrum access," Online material arXiv: 1204.2376v1, Apr. 2012.

[6] J. Hwu, J. Chen and X. Li, "Sum transmission power of multiple cooperative secondary transmitters in dynamic spectrum access networks," *the 42nd Annual Conference on Information Sciences and Systems* (CISS'2008), Princeton University, Mar. 19-21, 2008.

[7] X. Li and C. Xiong, "Performance analysis of coexisting secondary users in heterogeneous cognitive radio network," to appear in the *51st Annual Allerton Conference on Communication, Control and Computing*, Moticello, IL, Oct. 2-4, 2013.

[8] R. Etkin, A. Parekh and D. Tse, "Spectrum sharing for unlicensed bands," *IEEE J. Sel. Areas Commun.*, vol. 25, no. 3, pp. 517-528, March 2007.

[9] A. Mariani,A. Giorgetti and M. Chiani, "Effects of noise power estimation on energy detection for cognitive radio applications," *IEEE Trans. Commun.*, vol. 59, no. 12, pp. 3410-3420, Dec. 2011.

[10] A. Giorgetti and M. Chiani, "Influence of fading on the Gaussian approximation for BPSK and QPSK with asynchronous cochannel interference," *IEEE Trans. Wireless Commun.*, vol. 4, no. 2, pp. 384-389, March 2005.

[11] S. V. Amari and R. B. Misra, "Closed-form expressions for distribution of sum of exponential random variables," *IEEE Trans. Reliab.*, vol. 46, pp. 519522, 1997.

[12] H. P. Benson, "On the global optimization of sums of linear fractional functions over a convex set," *Journal of Optimization Theory and Applications*, vol. 121, no. 1, pp. 19-39, Apr. 2004.

[13] H. P. Benson, "Solving sum of ratios fractional programs via concave minimization," *Journal of Optimization Theory and Applications*, vol. 135, no. 1, pp. 1-17, Oct. 2007.

[14] H. Konno, Y. Yajima, and T. Matsui, "Parametric simplex algorithms for solving a special class of non-convex minimization problems," *Journal of Global Optimization*, no. 1, pp. 65-81, 1991.

[15] H. Konno and N. Abe, "Minimization of the sum of three linear fractional functions," *Journal of Global Optimization*, no. 4, pp. 419-432, 1999.

[16] J. Falk and S. Palocsay, "Optimizing the sum of linear fractional functions," pp. 221-258, in book: *Recent Advances in Global Optimization*, Princeton University Press, Princeton, NJ, USA, 1992.

Parameterized Green Gradient Based Routing (PG^{2}BR) for an Energy Efficient Internet

Julien Mineraud*, Sasitharan Balasubramaniam†, Jussi Kangarsharju‡ and William Donnelly*
*TSSG, Waterford Institute of Technology, Waterford, Ireland. Emails: {jmineraud, wdonnelly}@tssg.org
†Tampere University of Technology, Finland. Email: sasi.bala@tut.fi
‡Department of Computer Science, University of Helsinki, Finland. Email: jakangas@cs.helsinki.fi

***Abstract*—This paper proposes a distributed routing protocol that minimizes the energy consumption of communication networks. The proposed protocol, called PG^{2}BR (Parameterized Green Gradient Based Routing) contains a dual process, which includes i) a two-phase mechanism that gradually powers devices on/off in a decentralized manner, depending on the traffic condition, and ii) a distributed gradient based routing that quickly adapts to topology changes while maximizing resource usage and maintaining QoS requirements. Simulation work on a number of different types of topologies, have shown that PG^{2}BR is highly adaptive to any traffic and network conditions while proposing the best energy savings-QoS trade-off.**

I. Introduction

The growth of the Internet has to led to increase deployments of communication networks in order to maximize connectivity to the end users. The higher reliance to the Internet has also been fueled by more advance and sophisticated services, allowing users to access services from various devices (e.g. multimedia streaming to mobile devices). While this has provided improved connectivity to the end users, this communication infrastructure growth has led to increase energy consumption, which today accounts up to approximately 10% of the world global electricity consumption [1]. This problem is further complicated by the fact that design of communication devices for infrastructure networks (e.g. routers) have not incorporated energy saving capabilities.

Gupta et al. [2] investigated numerous benefits that can lead to a greener Internet by allowing network devices (e.g. line cards in routers) to go to sleep, when under utilized. In particular, the study showed that routers were consuming high quantity of energy, even in idle mode. Chabarek et al. [3] extended the work in [2] to investigate the benefits of energy-awareness while designing networks to save energy. Their study showed that the combination of an energy-aware design and energy-aware routing protocols will lead to tremendous savings of energy.

The solution addressed in this paper focuses on an energy-aware routing protocol that can adapt to varying traffic demand, and minimize energy consumption in the process, without compromising on Quality of Service (QoS). The proposed approach, called PG^{2}BR (Parameterized Green Gradient Based Routing), extends from our original Parameterized Gradient Based Routing (PGBR) [4]. The strength of PG^{2}BR is the ability to adaptively modify the topology without prior knowledge of the traffic demand, by including a new functionality that monitors and powers routers on/off (two-phase mechanism) to adapt to the traffic demand. This provides the capabilities for the network to, (i) maintain sufficient resources required by the traffic demand in order to maintain QoS, and (ii) minimize the energy consumption of the entire network. Furthermore, its fully decentralized two-step mechanism (for uptrend and downtrend traffic demand) enables the savings to be performed at all times and does not require knowledge on traffic pattern or any routing table recalculation to adapt to the topological changes while keeping the impact on QoS extremely low.

We evaluated the PG^{2}BR routing algorithm through a series of simulations, and have compared this with other distributed energy-aware routing protocols. Results from our simulation study, has shown improved performance of the PG^{2}BR routing algorithm for a number of different topologies and traffic traces. As part of our evaluation, we have also conducted extensive sensitivity analysis to determine routing parameters that provide optimum energy savings-QoS trade-off.

The paper is organized as follows: Section II presents the related work. Section III describes our proposed approach, and this is followed by Section IV, which describes the results of our experiments, and finally, Section V concludes the paper.

II. Related Work

Several energy-aware routing protocols have been proposed in recent times to reduce the energy consumption of Autonomous System (AS). These solutions modified existing routing protocols (e.g. OSPF [5], AntNet [6]) to improve the overall energy efficiency.

One example is the work proposed by Cianfrani et al. [7], called Green-OSPF, that modifies the OSPF protocol to save energy of IP networks. To minimize the number of links powered-on in the topology, the authors modified the shortest path calculation of certain routers. In OSPF, each router calculates the Shortest Path Tree (SPT) that defines the shortest routes to all the other nodes. The proposed approach selected a subset of routers, called *importers*, which used SPT of a neighbor router which is called an *exporter*. An *importer* is only connected to a single *exporter*, but an *exporter* could connect to numerous *importers*. Maximizing the number of *importers* reduces the energy consumption of the network considerably. However, the resulting topology may be subject to significant losses of quality. The authors explained their choice by the limited cost of the implementation of their solution, while potentially improving the energy consumption of today's IP networks (e.g. up to 60% of links could potentially be powered-off).

978-1-4799-0354-2/13/$31.00 ©2013 IEEE

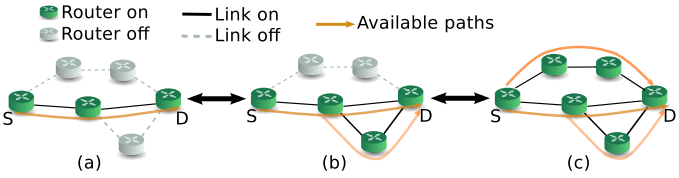

Fig. 1. (a) Core topology, (b) Rising traffic demand, (c) Full topology

From an adaptive routing protocol perspective, Kim et al. [8] proposed AESR, which is adapted from a well-known bio-inspired routing protocol that uses Ant Colony Optimization (AntNet [6]). The algorithm favors routing along highly loaded links, which could possibly lead to powering off lightly loaded links. The authors coupled the pheromone information collected by ants to a traffic centrality factor that redirect ants to highly loaded links. This technique is able to reduce the energy consumption of real networks by up to 60%, using a single parameter β (factor to weight the traffic centrality). Unfortunately, the choice of β might impact negatively on the network QoS performances.

Several energy optimization techniques such as in [1], use either Integer Linear Programming (ILP) or heuristics to solve the multi-commodity flow problems under certain constraints. These constraints may include maintaing a certain level of traffic throughput and minimization of energy consumption of the network. However, as the Internet continues to increase in popularity, this may lead to varying traffic demand. Therefore, requiring pre-knowledge of traffic demand may not be ideal for managing communication networks of the future.

III. Proposed Solution

Our proposed solution extends a fully decentralized flow-based routing protocol with functionalities to save energy. This includes a two-phase mechanism to gradually power devices on or off by reacting to the traffic demand, while ensuring the connectivity of the network's access nodes. In this section, we will present firstly the advantages of using a flow-based routing protocol and secondly the mechanisms that were added to perform energy savings.

A. PGBR

1) Flow-based Routing: A flow-based routing protocol uses routing tables based on flows to forward packets through the network, compared to using only destination information commonly used in current routing protocols. A flow in our solution, is characterized by the 5-tuple (*src*, *dst*, *src port*, *dst port*, *protocol*). Packet differentiation techniques could also be used to separate network traffic into flows, where unique flow id could be selected by the type of service. Therefore, packets from services with similar characteristics (e.g. video) would use the same paths. This is one advantage of flow-based routing, where multiple paths could be set up to satisfy certain service constraints (e.g. delay or capacity). This also enables in-coming new flows to divert traffic to secondary paths in order to avoid certain zones of the network (please note in our solution that on-going traffic paths do not get diverted). In our proposed solution, the avoided zone will be the lightly loaded devices that could be potentially powered-off.

2) Gradient Search for Routes: An implementation of a flow-based routing protocol is PGBR. The original PGBR is a scalable, distributed, gradient based routing algorithm. PGBR uses one-hop information to compute its gradient field, leading packets through the most appropriated route according to the service's requirements. The gradient is calculated using the following equation:

$$G^d_{i\to j} = \alpha l^n_j + \beta l^l_{i\to j} + \gamma h^d_j \quad (1)$$

where $G^d_{i\to j}$ is the gradient of the link $i \to j$ for the destination d, l^n_j is the load of neighbor node j, $l^l_{i\to j}$ is the load of link $i \to j$ and h^d_j is a normalized hop-count value to the destination. The three-tuple (α, β, γ) enables the gradient field to support various service types. The strength of the algorithm is its ability to adapt to varying traffic demand, and at the same time maximizing the use of underlying network resources.

In order to maintain the sanity of their routing table, each router periodically checks flow routing table entries to delete outdated entries. A flow routing table entry is outdated when no packets have been processed over a certain period. In our solution, the protocol will consider switching-off interfaces when the flow routing table does not contain any entry for that interface (in or out) for a period of time. More details on the implementation of PGBR can be found in [9]. The next section introduces the extension made to PGBR to incorporate energy-efficiency awareness.

B. PG^{2}BR

The PG^{2}BR, extends PGBR, by incorporating energy efficiency capability. This extension leads to dual processes, which includes : (i) a two-phase mechanism that gradually power-on devices as the traffic demand increases, and power-off as the traffic demand decreases, and (ii) the PGBR routing algorithm that routes and adapts to the changing network topology resulting from (i). In the case of (i), routers monitor their loads using only information collected by the original PGBR, and power on/off devices to adapt to changing traffic conditions. The following sections, as well as Fig. 2, will describe the details of these mechanisms.

1) Core Topology: While our proposed solution enables a dynamic topology to be formed with respect to the current state of the traffic demand, a minimum guarantee is required to ensure that certain nodes are available to support small amount of traffic during off-peak periods. We define this minimal topology as the core topology, and an example of this is illustrated in Fig. 1a. The core topology guarantees that all access nodes are connected at all times, and devices in this topology are never powered-off. Furthermore, the core topology is designed to have minimum energy requirements (this also sets the minimum energy boundary that the network is consuming).

2) Uptrend Traffic Demand: The decision to switch on/off devices in our proposed approach, is based on a distributed signaling process used in the original PGBR algorithm. In the original PGBR routing algorithm, each node passes its load information to its neighbor, where this information is used to calculate the gradient path (e.g. Fig. 2). The PG^{2}BR uses this information to analyze its current load to decide when a power on/off operation can be performed. In other words, each router

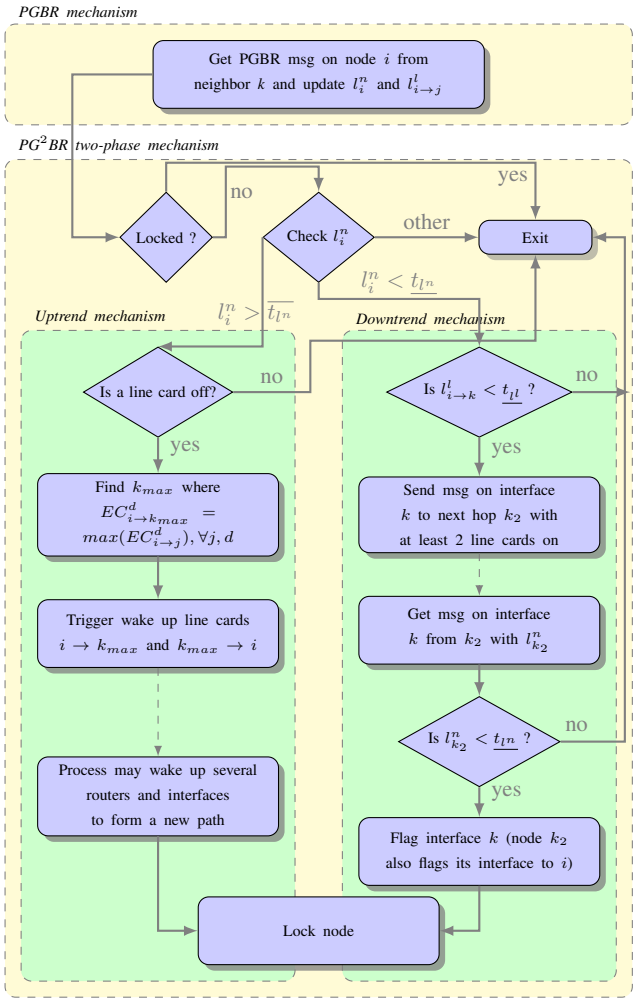

Fig. 2. PG^{2}BR two-phase mechanism

keeps the load information of all its neighbors (node loads) and the loads of the links to the neighbors (link loads). The node load being the average value of all link loads. Another feature has been added to enable the underlying routing protocol to redistribute the traffic: once the configuration changes at a node (power on/off), a lock[1] is applied to the router that forbid any further power on/off operation for a period of time.

The action to power-on a line card is initiated when the node load is over a threshold $\overline{t_{l^n}}$, and the node has at least one interface off and no lock applied. The overall process is depicted in the "uptrend mechanism" box of Fig. 2. If the conditions are matched, the node looks for the best possible interface to power-on. During this process, the algorithm favors powering-on a line-card connected to a neighbor which is already awake in order to minimize the number of chassis powered-on. For all candidate line cards that are off, PG^{2}BR will estimate the cost of powering each interface, before a specific line card is selected to be powered-on.

[1]The lock-out period does not provoke any topology oscillations as the PG^{2}BR algorithm does not impact existing flows. The lock-out period is established to ensure PG^{2}BR has sufficient time to balance the new incoming flows into the modified topology. In the worst case scenario, no topological changes would apply.

The estimated cost of powering the interface $i \to j$ on for destination d is:

$$EC_{i\to j}^d = C_{i\to j}/(h_j^d + 1.0) \quad (2)$$

where $C_{i\to j}$ is equal to $2 * LCC$ if the neighbor node j is on, and $CC + 4 * LCC$, otherwise. The $CC(x)$ corresponds to the energy consumption of a router chassis, while $LCC(x)$ corresponds to the energy consumption of a single line card [3]. The choice of $4 * LCC$ when the neighbor router is off comes from the minimal number of line cards that need to be powered-on in order to connect the neighbor router to two distinct routers of the topology. Consequently, a new path will be available to PG^{2}BR to distribute the load.

Therefore, the interface with the minimum cost is selected to be powered-on. The connectivity to the interface of the next router depends on the power state of that router. In the event the neighboring router is on, then the corresponding interface will be switched on. However, if the neighboring router is asleep, the router is first awaken followed by the powering-on of the line card. The neighbor router will also calculates its own $EC_{j\to k}^d$ in order to select the next best line card to connect itself to the network. This action is repeated until the new path is connected to the network at both ends. Once the router powering-on action has been completed, a lock is applied to all the routers in the path to prevent any further actions to be processed. This, in turn, will provide a short duration of time for the PGBR to correctly re-balance the traffic according to the new topology configuration.

3) Downtrend Traffic Demand: When the conditions are not satisfied for powering-on an interface, and no locks are applied, the router will look for the best opportunity to power-off in order to save energy. The simple process, depicted in the "downtrend mechanism" box of Fig. 2, is based on each router observing the current load on its links. If a link load is below the threshold $\underline{t_{l^l}}$, the router will check its own node load as well as the node load of the next router on that path that could potentially redirect new incoming traffic if that path was shut down (their node loads must be below the threshold $\underline{t_{l^n}}$). If the conditions are met, a flag is set to disable the line card of the link in order to minimize traffic loss, thus becoming unavailable for discovery during a period of time.

This will allow current flows going through this interface to terminate without accepting new flows. In addition, a lock is placed on the corresponding node to ensure that the PGBR mechanisms can re-balance the traffic to fit the new topology, as it does during the uptrend traffic demand. In the event that the interface has not been utilized (i.e. existing flows have been terminated), it will be powered-off after a short duration. Once all the interfaces of a router are powered-off, the whole router will be powered-off.

IV. Performance Evaluation

A. Simulation Setup

All the experiments are performed using ns-3.14 [10] on a cluster of 240 Dell PowerEdge M610 nodes. Each cluster node has 2 quad-core CPUs, 32GB memory, and runs Ubuntu SMP with 2.6.32 kernel. We conducted two evaluations of PG^{2}BR, which includes sensitivity analysis as well as comparison to

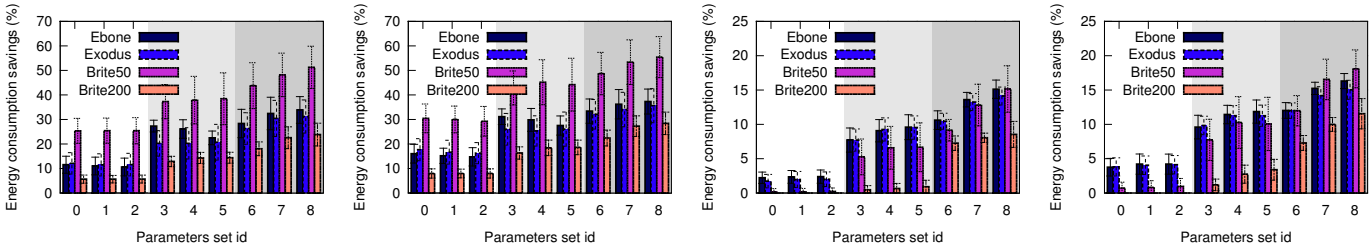

(a) High peak (40%) (b) Low peak (40%) (c) High peak (100%) (d) Low peak (100%)

Fig. 3. Sensitivity analysis of PG^{2}BR parameters for energy savings.

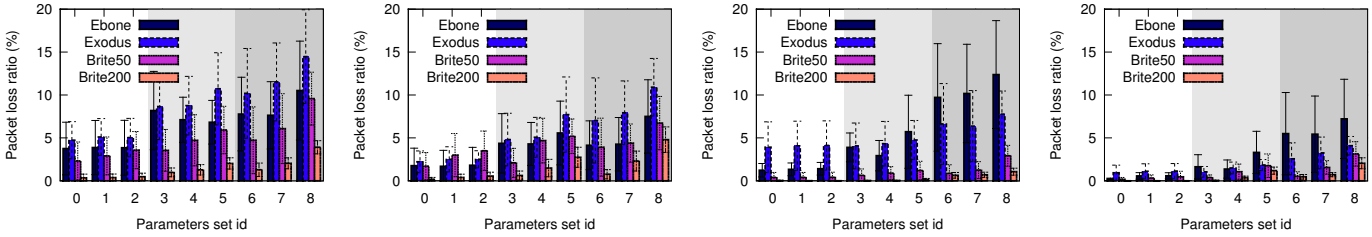

(a) High peak (40%) (b) Low peak (40%) (c) High peak (100%) (d) Low peak (100%)

Fig. 4. Sensitivity analysis of PG^{2}BR parameters for packet loss ratio.

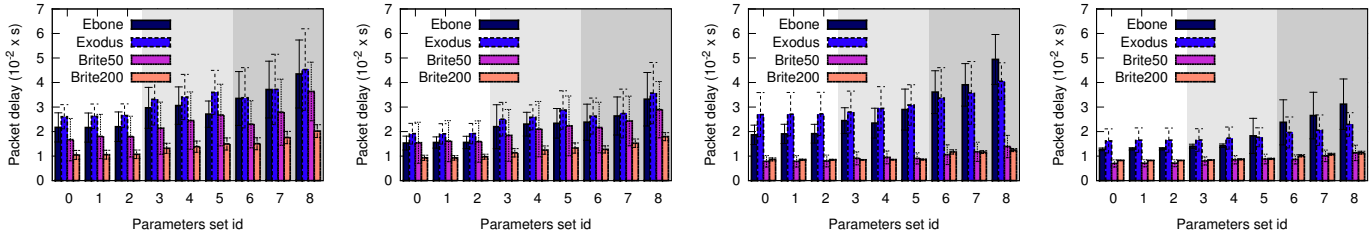

(a) High peak (40%) (b) Low peak (40%) (c) High peak (100%) (d) Low peak (100%)

Fig. 5. Sensitivity analysis of PG^{2}BR parameters for packet delay.

Green-OSPF [7] and AESR [8], which are two state-of-the-art energy-aware routing protocols that do not require prior knowledge of the traffic pattern. All the simulations were tested on four topologies (two real and two random topologies). The two real topologies that were selected are the same topologies used in [8] (Ebone (87 nodes, 161 links) and Exodus (79 nodes, 147 links) from the Rocketfuel project [11]). The two random topologies (Brite50 (50 nodes, 150 links) and Brite200 (200 nodes, 600 links)) were generated using the Brite topology generator [12], utilizing the default parameters of the Waxman model with $n = 3$. For simplicity, we have set all topologies with the same link properties, which includes a link capacity of 10 $Gbps$ and a delay of 2 ms.

For the four topologies, we evaluated two different scenarios: i) only 40% of the nodes are access nodes, and ii) all the nodes are generating traffic. The aim of evaluating two different configurations is to evaluate the adaptability of PG^{2}BR for different environments [2].

In order to achieve realistic traffic patterns, traces from the Totem project [13] were used to generate the traffic matrices at 15 minutes interval, for 24 hours. The resulting 24-hour traffic patterns (one for each source/destination pair) have a diurnal cycle, composed of a low and a high peak zone (e.g. up to 7.6 million flows are generated for a single traffic pattern). The traffic matrices were scaled in order to produce a few congestions when using OSPF alone. This decision was driven by the desire to observe the energy-awareness and its impact on the QoS performance.

The energy consumption of the network devices are identical for all routers and the parameters are set to $CC = 270$ Watts and $LCC = 70$ Watts [3].

B. Sensitivity Analysis of PG^{2}BR

TABLE I. CORRESPONDING NODE AND LINK LOAD THRESHOLDS FOR EACH PARAMETER SETS ID.

		Node load		
		$\underline{t_{ln}} = 0.1$ $\overline{t_{ln}} = 0.2$	$\underline{t_{ln}} = 0.2$ $\overline{t_{ln}} = 0.4$	$\underline{t_{ln}} = 0.3$ $\overline{t_{ln}} = 0.65$
Link load	$\underline{t_{ll}} = 0.1$	0	3	6
	$\underline{t_{ll}} = 0.2$	1	4	7
	$\underline{t_{ll}} = 0.35$	2	5	8

This section presents the sensitivity analysis of PG^{2}BR, by evaluating different combination of parameters and observing the performance in terms of energy savings, packet loss and delay. In total, we evaluated 27 sets of parameters, and each configuration is defined as a parameter id. To improve clarity

[2]In the case when all nodes are generating traffic, none of the protocols are able to switch routers off, thus putting Green-OSPF on an equal footing.

of the results, only the sets with a lock-out period of 7.5 minutes will be presented. Shorter lock-out periods improve the energy savings performances, but this will result in a degradation of the QoS. In this paper, we desire perform energy savings as transparently as possible to the network's users. As summarized in Table. I, the parameter ids numbered from 0 to 2 (e.g. white zone) have "low" node load thresholds ($\underline{t_{l^n}} = 0.1, \overline{t_{l^n}} = 0.2$), parameter ids from 3 to 5 (e.g. light grey zone) have "medium" node load thresholds ($\underline{t_{l^n}} = 0.2, \overline{t_{l^n}} = 0.4$) and parameter ids from 6 to 8 (e.g. dark grey) have "high" node load thresholds ($\underline{t_{l^n}} = 0.3, \overline{t_{l^n}} = 0.65$). Finally, within each group of node load thresholds, the link load thresholds are respectively set to "low" ($\underline{t_{l^l}} = 0.1$), "medium" ($\underline{t_{l^l}} = 0.2$), and "high"($\underline{t_{l^l}} = 0.35$). For instance, set id 4 corresponds to medium node load thresholds, medium link load threshold and a lock-out period of 7.5 minutes. Finally, for each set of parameters, a total of 10 traffic matrices have been evaluated for each topologies (access nodes may differ in the case of 40% access nodes).

Fig. 3, 4 and 5 show the average value of the performance as well as the standard deviation. By analysing the three figures, it is clear that the choice of the node load threshold impact the most on the performances of PG^{2}BR. For instance, Fig. 3b shows the energy consumption savings achieved by each set of parameters, where we can clearly see the three levels of energy savings performances. These levels are not appearing in Fig. 4b and 5b where the impact on QoS increases linearly. Fig. 3, 4 and 5 also shows similar behavior for the four topologies, which reassures the flexibility of using PG^{2}BR for different types of topology to achieve the desired energy savings-QoS trade-off.

The choice of middle range $\underline{t_{l^n}}$ holds a good compromise between high energy savings and network QoS performances. For example, the Ebone topology (Fig. 3a) shows improvement by more than 15% for energy savings for low range thresholds compared to 7% for high range thresholds. The choice of the link load threshold $\underline{t_{l^l}}$ and the lock-out duration influences the performance to a smaller extent. As a consequence, Fig. 3, 4 and 5 shows that the combination of a middle range $\underline{t_{l^l}}$, middle range $\underline{t_{l^n}}$, and a long lock-out duration minimizes impacts on the QoS performances while ensuring good energy savings performances.

C. Comparison of Energy-aware Routing Protocols

This section compares the PG^{2}BR to the Green-OSPF as well as AESR. Firstly, a description and justification on the selected parameters will be presented. The comparison of the three protocols will be evaluated with respect to time, to demonstrate the performance over a 24 hour period. This will be followed by an evaluation on the energy savings and the resulting QoS degradation during the low-peak period for the three energy-aware routing protocols (metrics evaluated include the packet lost ratio and the average packet delay) .

1) Simulation Parameters: The parameters for the routing protocols are as follows: Green-OSPF performs its optimization at 8 am (start of the low-peak period) using 5% (as in [7]) of the routers as exporters. The value of 5% was used because the number of exporters is relatively low in order to maximize

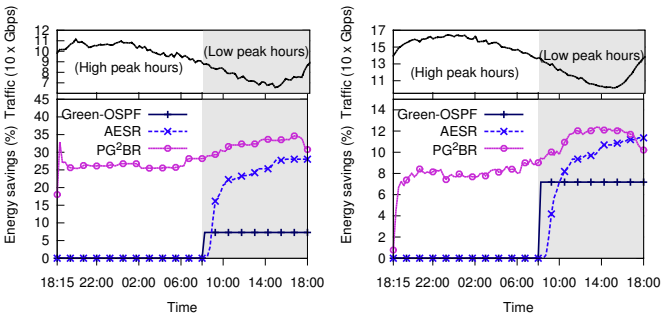

(a) Ebone (40%) (b) Exodus (100%)

Fig. 6. Energy consumption performances with respect to time.

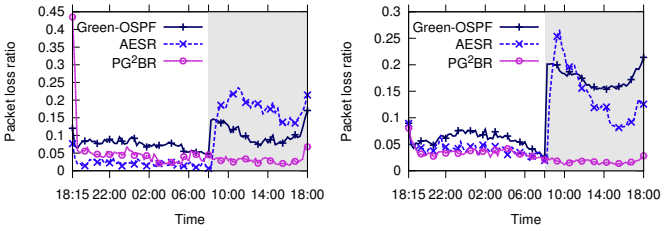

(a) Ebone (40%) (b) Exodus (100%)

Fig. 7. Packet loss performance with respect to time.

the number of links that can potentially be powered-off. This value is also sufficiently high enough to have a relatively low impact on QoS.

AESR produces an ant agent every 0.1 seconds and uses a centrality factor of $\beta = 0.4$ (as in [8]). Similar to Green-OSPF, the protocol also performs its optimization at 8 am. During down trend traffic, the strategy taken by AESR is to power-off lightly loaded interfaces or routers every 15 minutes. Unlike PG^{2}BR and AESR, Green-OSPF algorithm does not allow any routers to be powered-off.

In the case of PG^{2}BR, neighbor messaging are sent every 0.5 seconds and the parameters (α, β, γ) used for the gradient equation 1 are set to $(0.2, 0.2, 1.0)$. These parameters will lead to path discovery that favor shortest paths with little deviations [4] in order to maximize energy savings. PG^{2}BR powers-off the interfaces when they are inactive (e.g. flow routing tables are empty from this interface) for at least 6 minutes. The energy-aware parameters of PG^{2}BR are selected according to the results of the sensitivity analysis, where we chose the values that optimize the trade-off between energy savings and fulfilling QoS requirements of the network. The selected parameters include: $\underline{t_{l^n}} = 0.2$, $\overline{t_{l^n}} = 0.4$, $\underline{t_{l^l}} = 0.2$, and a lock-out period of 7.5 minutes (i.e. this corresponds to parameter set id 4 as shown in Fig. 3, 4 and 5). We used 80 traffic matrices, where all traffic patterns exhibited similar diurnal cycle over a 24 hour period. Our aim is to develop a number of experimental tests, in order to obtain statistical results. All traffic matrices have similar behavior, and are produced from the Totem traces.

2) Evaluation Over 24 Hour Period: The performance of the three routing protocols over a 24 hour period for both the Ebone and the Exodus topologies are shown in Fig. 6, 7 and 8. We focused on Ebone topology with 40% access nodes and Exodus topology with 100% access nodes. Only a single traffic

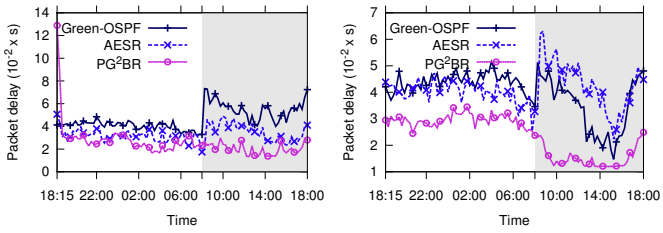

(a) Ebone (40%) (b) Exodus (100%)

Fig. 8. Packet delay performance with respect to time.

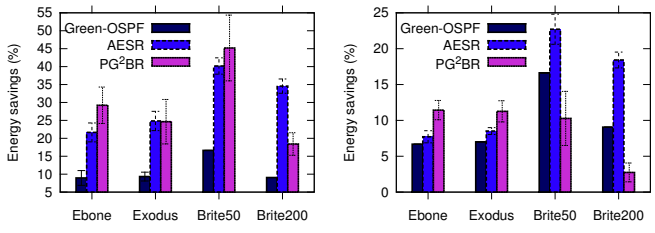

(a) 40% access nodes (b) 100% access nodes

Fig. 9. Comparison of energy savings during the low peak hours.

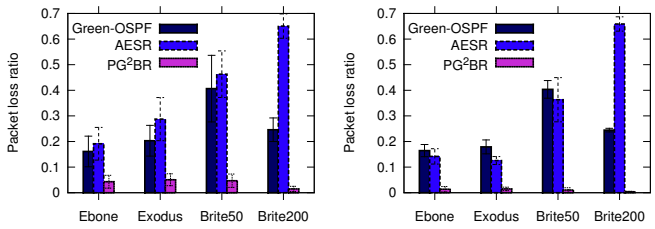

(a) 40% access nodes (b) 100% access nodes

Fig. 10. Comparison of packet loss ratio during the low peak hours.

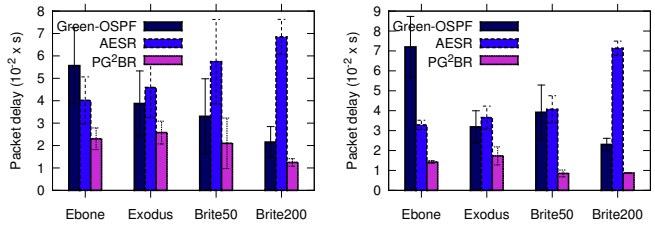

(a) 40% access nodes (b) 100% access nodes

Fig. 11. Comparison of packet delay during the low peak hours.

matrix is shown for each scenario to improve clarity.

As shown in Fig. 6, the traffic demand exhibits two distinct periods; the first period (High peak) lasts 14 hours between 6 pm and 8 am, while the second period (Low peak) represents the remaining 10 hours. For Green-OSPF and AESR, the optimization is executed only during the low peak hours as set out in [7], [8]. However, PG^{2}BR is performing energy savings throughout the entire 24 hour period due to the dual process, which dynamically reacts to traffic pattern changes.

In Fig. 6a, PG^{2}BR is able to dramatically decrease the energy consumption of the network by up to 34.6%. During the day, the protocol reduces the energy consumption by over 25% due to redundant paths in the networks. In the case of Exodus topology with 100% access nodes (Fig. 6b), Green-OSPF removes most of the redundant paths and have similar energy savings as PG^{2}BR (this is during the transitioning period between high to low-peak zones). However, PG^{2}BR can dynamically improve the energy savings by up to an extra 10%. During high peak, PG^{2}BR topological changes are minimal but ensure good performances. The gains obtained by Green-OSPF are the lowest in both 40% and 100% access nodes configurations. However, as shown in Fig. 6b, the difference is reduced as the number of access nodes increases. On the Exodus topology, PG^{2}BR improves the energy savings by up to 5.1%. In Fig. 6a and 6b, AESR is slowly converging to an optimal solution. Regrettably, this shows that AESR is unable to cope with dynamic traffic pattern, thus resulting in degradation of QoS performances. In addition, AESR does not have a two-phase mechanism to switch network devices on when resources are missing. Green-OSPF exhibits simple behaviour with very low dynamics, and is inefficient compared to the other two routing protocols. AESR exhibits higher dynamics but is very slow to converge compared to energy saving performances of PG^{2}BR. However, PG^{2}BR with its dual process is able to dynamically react to traffic pattern changes to save energy, and at the same time maximize available resources. This energy saving process also continues into the high-peak traffic period.

In Fig. 7 and 8, we compare the QoS performances of the three energy-aware routing protocols during the 24 hour period. As previously mentioned, the performances of AESR are the most unreliable. They fluctuates greatly depending on the topology size as well as varying traffic conditions. This is particularly the case for the packet lost ratio (Fig. 7), where the algorithm is not able to adapt to the new traffic conditions resulting in poor packet loss ratio performances. Similar performances are also observed for the packet delay (Fig. 8).

Green-OSPF presents a solution to keep stable QoS performances, which only fluctuates slightly with the traffic pattern. Fig. 7b and 8b shows that this behavior is noticeable when there are 100% access nodes. However, PG^{2}BR demonstrates the best packet loss ratio and delay performance. In comparison to PG^{2}BR, AESR has a lower packet loss ratio and delay only on the Ebone with 40% access nodes during high-peak period. However, this difference in QoS is relatively negligible.

Therefore, the hourly details of Fig. 6, 7 and 8 show that PG^{2}BR is the most stable protocol to maintain QoS requirements, while greatly reducing the total energy consumption of the network. However, the Ebone topology was the only topology to exhibit a small disadvantage for PG^{2}BR during the high-peak hours.

3) Impact of Energy Savings on QoS during Low-Peak Hours: Fig. 9, 10 and 11 show the differences of performance between Green-OSPF, AESR and PG^{2}BR on the four topologies, each evaluated with 10 traffic matrices during the low peak hours. These figures show respectively the average energy savings, packet loss ratio and packet delay and their standard deviations. Fig. 9 shows the energy savings performance of the three energy-aware routing protocols on the four topologies. As shown in the results, PG^{2}BR exhibits the best performance on the three smallest topologies (Ebone, Exodus and Brite50). For instance, with the Brite50 topology, the average energy

savings is 45.2%.

Green-OSPF performs similarly in both configuration because its energy savings does not rely on the traffic but only on the number of exporters. However, the performance of AESR and PG^{2}BR dramatically increase when only 40% of the nodes are generating traffic (e.g. Fig. 9a) as they are able to power-off devices. Fig. 9b shows the possible energy savings that can be obtained when no router can be powered-off (100% access nodes), putting Green-OSPF on an equal footing with other routing protocols. In this configuration, the performance of Green-OSPF improves, but still lower compared to the other two routing protocols. As predicted, the energy savings are much lower when all the routers are powered-on. On the Brite50 topology, the energy savings using PG^{2}BR with 40% access nodes are more than 4 times greater than with 100% access nodes. The energy savings result, as seen in Fig. 9, confirms that AESR has very good energy saving performances due to its capability to also power-off devices. Unfortunately, no mechanism in the protocol have been designed to power-on devices when the resources of the network become limited. As a consequence, AESR does not cope well with QoS requirements when the traffic demand fluctuates. Since the routing algorithm maximizes centralization of the traffic (using parameter β), it leads to high packet loss ratio and delay, especially for the Brite200 topology. Furthermore, the swarming intelligence of ants is lost because insufficient number of ants reaches their destinations on topologies where the average node degree is high (Brite50 and Brite200).

Reducing energy consumption of the network automatically results in the degradation of the QoS performances. Fig. 10 shows the comparison of performances for packet loss ratio. The results also comply with the patterns observed over a 24 hour period (Fig. 7). The results have shown that for Green-OSPF and AESR, the packet loss ratio degradation is proportional to the energy savings. The only exception is for AESR on the Brite200 topology, which does not follow this pattern. However, this is due to slow convergence of the ants in large topologies. On the other hand, PG^{2}BR maintains low average packet loss for all topologies, including 40% and 100% access nodes. The greatest advantage of PG^{2}BR is the adaptability of its underlying protocol PGBR, which aims to maximize the use of network resources. This is also reflected in the delay performances presented in Fig. 8, which shows PG^{2}BR outperforming Green-OSPF and AESR for all topologies and access node configurations.

In summary, PG^{2}BR is able to maintain QoS performance for all topologies in comparison to Green-OSPF and AESR. This is particularly the case for packet loss ratio. At the same time, PG^{2}BR is able to successfully maintain the highest energy savings for all topologies, as well as access node configurations. We can summarize characteristics of each protocols as follows:

Green-OSPF: Simple algorithm but performs poorly in terms of energy savings and QoS delivery because it does not adapt to traffic demand.

AESR: Its overall QoS performances fluctuate severely and it is highly dependent on the topology and access node configuration. A slow convergence time towards high energy savings was observed.

PG^{2}BR: It exhibits good QoS performances for both packet loss and delay, even during high-peak traffic period. The protocol was highly dynamic and adaptable to changing traffic conditions and demonstrated the best energy savings-QoS trade-off.

V. Conclusion

In this paper, we introduced a novel routing protocol that dynamically adapts the network topology to reduce the overall energy consumption. The protocol, called PG^{2}BR, allows each router to autonomously power on/off depending on the traffic demand of the network. The strength of the proposed approach is the ability to eliminate prior knowledge of traffic demand, as the topology changes shapes, while respecting QoS constraints. Through simulations, we show that our protocol outperforms current state-of-the-art energy-aware routing solutions and saves up to 45.2% in electricity consumption, while ensuring good QoS performances.

Acknowledgment

This work has received support from Science Foundation Ireland via the "A Biologically inspired framework supporting network management for the Future Internet" starting investigator award (grant no. 09/SIRG/I1643).

References

[1] L. Chiaraviglio, M. Mellia, and F. Neri, "Minimizing ISP network energy cost : Formulation and solutions," *IEEE/ACM Transactions on Networking*, vol. 20, no. 2, pp. 463–476, April 2012.

[2] M. Gupta and S. Singh, "Greening of the Internet," in *Proceedings of the 2003 conference on Applications, technologies, architectures, and protocols for computer communications - SIGCOMM 2003*. ACM Press, 2003, p. 19.

[3] J. Chabarek, J. Sommers, P. Barford, C. Estan, D. Tsiang, and S. Wright, "Power awareness in network design and routing," in *IEEE INFOCOM 2008 - The 27th Conference on Computer Communications*. IEEE, April 2008, pp. 457–465.

[4] S. Balasubramaniam, J. Mineraud, P. Mcdonagh, P. Perry, L. Murphy, W. Donnelly, and D. Botvich, "An Evaluation of Parameterized Gradient Based Routing With QoE Monitoring for Multiple IPTV Providers," *IEEE Transactions on Broadcasting*, vol. 57, no. 2, pp. 183–194, 2011.

[5] J. Moy, "Ospf version 2," United States, 1998.

[6] G. Di Caro and M. Dorigo, "AntNet : Distributed stigmergetic control for communications networks," *Journal of Artificial Intelligence Research*, vol. 9, pp. 317–365, 1998.

[7] A. Cianfrani, V. Eramo, M. Listanti, M. Marazza, and E. Vittorini, "An energy saving routing algorithm for a green OSPF protocol," in *IEEE INFOCOM 2010 Conference on Computer Communications*. Ieee, March 2010, pp. 1–5.

[8] Y.-m. Kim, E.-j. Lee, and H.-s. Park, "Ant colony optimization based energy saving routing for energy-efficient networks," *IEEE Communications Letters*, vol. 15, no. 7, pp. 779–781, 2011.

[9] J. Mineraud, "An implementation of Parameterised Gradient Based Routing (PGBR) in ns-3," in *IEEE/IFIP 2010 Network Operations and Management Symposium Workshops*. IEEE, 2010, pp. 63–66.

[10] "The ns-3 simulator," http://www.nsnam.org/.

[11] N. Spring, R. Mahajan, and D. Wetherall, "Measuring isp topologies with rocketfuel," *ACM SIGCOMM Computer Communication Review*, vol. 32, no. 4, p. 133, October 2002.

[12] "The brite network topology generator," http://www.cs.bu.edu/brite/, 2001.

[13] S. Uhlig, B. Quoitin, J. Lepropre, and S. Balon, "Providing public intradomain traffic matrices to the research community," *ACM SIGCOMM Computer Communication Review*, vol. 36, no. 1, pp. 83–86, January 2006.

Joint delay and power control in single-server queueing systems

Andrea Bianco, Mario R. Casu, Paolo Giaccone, Marco Ricca
Dipartimento di Elettronica e Telecomunicazioni, Politecnico di Torino, Italy

***Abstract*—Many power-aware resource allocation problems in packet networks can be modeled as single-server queueing systems, in which the power consumption depends on the actual service rate. We consider the scenario in which the queue service rate is controlled to minimize server power consumption. We show that power control methods that tune the service rate by using the queue length or the arrival rate exhibit a non-monotonic curve of delay vs. load. This may lead to malfunctioning in end-to-end flow/congestion control protocols, which are based on the assumption that delays increase with increasing load. We propose a new policy, in which the service rate is changed while keeping almost flat the delay curve, which permits to achieve a close-to-optimal trade-off between power and delay.**

I. Introduction

Reducing the power consumption of telecommunication networks and devices is crucial for a number of reasons: i) the need to increase the battery life in mobile devices, ii) to reduce the energy bill of telecommunication operators and service providers, and iii) to design eco-sustainable products. Furthermore, minimizing power is a key solution to increase hardware performance. Indeed, the higher the processing and switching rates, the higher the power dissipated in chips and their temperature. Thus, reducing power per operation leads to higher switching and processing rates given a finite, and often tight, power and thermal budget.

In packet networks (in a broad sense, including the case of on-chip networks), in which shared resources are modeled as servers accessed via a queueing system that models resource interplay, the speed at which packets are served can be controlled to obtain a target power-performance trade-off. The various techniques proposed to reach this goal, as discussed in Sec. II, share the simple idea of tuning the server speed according to the load: When the load is low, the server slows down its service speed to reduce power consumption at the price of longer delays, and, possibly, lower throughput. When the load is high, the service rate is increased to maximize throughput, thus requiring higher power consumption.

In this paper we focus on the power control of a single-server system, in which arriving packets are enqueued and served in First-In-First-Out (FIFO) order. Albeit simple, this toy system permits to derive general observations that hold also in complex, more realistic scenarios.

We classify the power control methods in two categories, queue-length-based and arrival-rate-based. In the former, when the packets waiting to be served are less/more than a predefined queue occupancy threshold, the server rate is reduced/increased to save power/to reduce delays. Similarly, in the arrival-rate-based method, when the packet arrival rate is smaller/larger than the actual service rate, the server reduces/increases its service rate.

To estimate power consumption we fix our attention on the cubic power-load relation typical of hardware systems that use Dynamic Voltage and Frequency Scaling (DVFS), in which the supply voltage scales jointly with the clock frequency [1], [2]. However, the adopted methodology is general and can be applied to a large family of convex power models.

To the best of our knowledge, for the first time we show that tuning the service rate according to the input traffic load leads to an anomalous behavior in the delay-load curve, which becomes non-monotonic for both queue-length and arrival-rate based methods. This fact may negatively affect the performance of end-to-end flow/congestion control protocols, which often assume that delays increase with increasing network congestion. For example, the congestion avoidance algorithm of some versions of TCP (as TCP Westwood [3]) is based on the estimated instantaneous rate achieved by the flow, which is usually obtained by the number of received packets/ACKs over the Round Trip Time (RTT). Clearly, increasing delays imply a larger RTT; this fact is "seen" by the control algorithm as a congestion indicator and the transmission window will be likely decreased. In the case of non-monotonic delay-load curve, increasing delays could be also due to a smaller load/congestion, which must instead lead to a larger transmission window. As a consequence, the sender might decrease its rate when the congestion decreases, leading to a vicious circle which may stop the sender, at least theoretically.

To remove the non monotonic behavior, we propose a new control method that keeps the delay constant over a large load range, with a minor power penalty with respect to policies that minimize power consumption at the cost of unbounded delays.

II. Related work

The power control problem in systems modeled as single server queues and with control policies based on the queue length and/or the arrival rate was previously investigated, but very rarely with focus on the delay behavior.

A queue-length-based control for DVFS applied to a multicore processor is proposed in [1], in which single-server queues model each core's task queues. An emptying queue means that the core is running fast and is able to absorb its workload; a filling queue indicates that the core is not able to keep up with its assigned workload. The power control

978-1-4799-0354-2/13/$31.00 ©2013 IEEE

is based on a standard Proportional-Integral (PI) feedback controller, which compensates the error between current queue size and target value by accelerating/decelerating the server. This scheme requires careful design and tuning of the control parameters and of the estimation procedures to achieve stability. In the field of Networks-on-Chip, a similar DVFS scheme has been used to control i) the power chip-wide, by using the size of the queues between various voltage domains [4], and ii) to control the power dissipated in on-chip routers using the size of input buffer queues [5]. The model that we present in Sec. IV refers to a version of the PI control, in which the average queue size is exactly equal to the target queue size.

For the power management of electronic systems, the authors of [6] propose a randomized policy for service-rate control based on the knowledge of the Markovian model describing the source behavior (i.e. the workload). As a consequence, the control is arrival-rate-based. The proposed policy achieves a good power-delay trade-off but it requires to solve a large size, nontrivial LP problem.

In a general context of communications between hardware components, the work in [7] focuses on DVFS applied to the interconnections modeled as a network of single-server queues. The authors compare different approaches to estimate the congestion information that feeds the rate algorithm. They also propose an alternative policy that combines arrival-rate-based and queue-length-based schemes and examines queueing delays. By comparing the state of the system with four target values (min/max queue occupancy/arrival rate), the service rate is adapted to minimize power consumption while keeping buffers occupancy small enough. The benefits of such scheme are evaluated through detailed hardware-level simulations, but the authors do not focus on the non-monotonicity of the delay with respect to the arrival rate.

Another example of an hybrid scheme, combining queue-length-based and arrival-rate-based approaches, was studied in [8] for the power management of generic data networks. The scheme takes into account also a setup penalty when changing the rate and a packet deadline (i.e. a maximum delay). Based on [9], which shows that keeping the service rate constant while satisfying a given time deadline is the minimum energy policy when arrival times are known offline, the proposed policy also tries to keep the service rate as constant as possible while meeting a given deadline, which can be violated only with small probability in case of unknown arrival times. The input of the power control are queue size and estimated arrival rate. The main idea is to increase the rate whenever the actual rate does not meet the deadline for the actual backlog, whereas the rate is decreased whenever the queue becomes empty.

A multi-class M/G/1 scenario is considered in [10] in a more theoretical perspective. The power is minimized while satisfying a maximum average delay. The proposed optimal policies are based on the knowledge of the arrival rate and the queueing delay for the packets in the queue.

As a final comment, note that similar approaches have been studied for M/G/1-PS (Processor Sharing) queueing systems, modeling the sharing of server resources. This is a very relevant model for many applications, for which the rate control has been deeply investigated in the past [11].

III. Power and rate control of a single queue

We consider a single server system in which the packet service time S computed by the power controller is defined as

$$S = \alpha T_{pkt} \tag{1}$$

where T_{pkt} is the minimum service time (obtained for maximum service speed) and $\alpha \in [1, \alpha_{\max}]$ is the time *expansion factor*, computed by the power control. Intuitively, α is the level of slow-down with respect to the maximum service rate and can be seen as the "laziness" to serve the packets. For $\alpha = 1$ the server is running at the fastest speed.

We can easily map this model in the DVFS scenario for a single server processor whose clock frequency is inversely proportional to the applied voltage V. Thus, α is the voltage reduction factor with respect to the maximum available voltage $V_{\max}$: $V = V_{\max}/\alpha$. $\alpha_{\max}$ depends on the adopted technology and it usually assumes values in the range 2-3 [12].

We assume that packets arrive according to a stationary Poisson process at rate $\hat{\lambda}_{pkt}$. To be admissible, $\hat{\lambda}_{pkt} < 1/T_{pkt}$. The normalized arrival rate $\lambda \in [0, 1)$ is $\lambda = \hat{\lambda}_{pkt} T_{pkt}$.

We consider the case of *static* policies, in which S is fixed for a given λ. This choice permits to simply build policy models. Static policies provide a bound to the performance of the corresponding *dynamic* policies that react to instantaneous changes in the arrival rate and/or the queue size by dynamically changing S. Indeed, it can be shown that under stationary traffic assumption, keeping S constant is better than changing it while keeping the same average value, both in terms of average delay and power. More precisely, the power for a static policy is lower than the corresponding dynamic policy power due the convexity of the power vs server rate function. This can be formally proved exploiting Jensen inequality (following the same reasoning of the proof of Lemma 1 in [9]). Following standard arguments in queueing theory, it can be also proved that the average delay for a static policy is lower, thanks to the lower (i.e. null) variance in the service rate.

Since the power policy is static, we can consider a fixed S and exploit the Pollaczek–Khinchine formula of M/G/1 for fixed service time (i.e., the corresponding queueing system becomes an M/D/1) to evaluate the average delay W, normalized with respect to T_{pkt}, as:

$$W = \frac{\lambda \alpha^2}{2(1 - \lambda\alpha)} + \alpha \tag{2}$$

To achieve bounded delays and maximize throughput, the power controller cannot reduce the service rate below the arrival rate: $\lambda < 1/\alpha$. If we define the *utilization factor* of the queue as $\rho = \lambda\alpha$, this condition is equivalent to impose $\rho < 1$. This results in the following final constraint:

$$1 \leq \alpha \leq \min\left(\frac{1}{\lambda}, \alpha_{\max}\right) \tag{3}$$

We assume that power consumption can be modeled as

$$P = \frac{\lambda}{\alpha^2} \tag{4}$$

This well-known model is motivated by a DVFS scenario since it captures the dynamic power of CMOS gates powered at voltage $V = V_{\max}/\alpha$, as shown for example in [2]. We omit in (4) all the constant factors so as to normalize $P \in [0, 1]$, as they do not affect the relative behavior of the control policies.

In the following, we discuss three control policies to choose α: (i) one that achieves the minimum power but with large delays/queue length, (ii) one that fixes a given queue utilization, and (iii) one that sets a given queue length. For the sake of comparison, we also define the No-power-Control (NC) policy as the one that always sets $\alpha_{NC} = 1$, for any $\lambda \in [0, 1)$.

A. Minimum Power (MP) policy

The minimum power in (4) is obtained by the maximum value of α subject to (3). This implies that the optimal Minimum Power (MP) policy is

$$\alpha_{MP} = \begin{cases} 1/\lambda & \text{for } \lambda \in [1/\alpha_{\max}, 1) \\ \alpha_{\max} & \text{for } \lambda \in [0, \rho_v/\alpha_{\max}) \end{cases} \tag{5}$$

This policy corresponds to force the queue to run, for any $\lambda \geq 1/\alpha_{\max}$, at an operating point corresponding to $\rho = 1$, for which the average delay and queue size are infinite. By also exploiting (2), it is easy to observe:

Property 1: The average delay is

$$W = \begin{cases} \infty & \text{for } \lambda \in [1/\alpha_{\max}, 1) \\ \dfrac{\lambda \alpha_{\max}^2}{2(1 - \lambda\alpha_{\max})} + \alpha_{\max} & \text{for } \lambda \in [0, 1/\alpha_{\max}) \end{cases} \tag{6}$$

The corresponding power is:

$$P = \begin{cases} \lambda^3 & \text{for } \lambda \in [1/\alpha_{\max}, 1) \\ \dfrac{\lambda}{\alpha_{\max}^2} & \text{for } \lambda \in [0, 1/\alpha_{\max}) \end{cases} \tag{7}$$

B. Fixed Utilization (FU) policy

To avoid infinite delays in (6), we propose to modify the MP policy. Since we must enforce $\rho < 1$ to obtain finite delays, we introduce the parameter $\rho_v \in (0, 1)$, defined as "virtual utilization factor", defining a Fixed Utilization policy, denoted as FU-ρ_v. The policy expansion factor is:

$$\alpha_{FU} = \begin{cases} 1 & \text{for } \lambda \in [\rho_v, 1] \\ \rho_v/\lambda & \text{for } \lambda \in [\rho_v/\alpha_{\max}, \rho_v) \\ \alpha_{\max} & \text{for } \lambda \in [0, \rho_v/\alpha_{\max}) \end{cases} \tag{8}$$

When $\rho_v \to 1$, FU corresponds to the optimal minimum power policy, whereas when $\rho_v \to 0$ FU behaves as NC.

From (8) it is possible to highlight three regimes:

- *high load* (when $\lambda > \rho_v$) in which the service rate is maximum and the power control is not effective;
- *low load* (when $\lambda < 1/\alpha_{\max}$) in which the service rate is the minimum allowed;

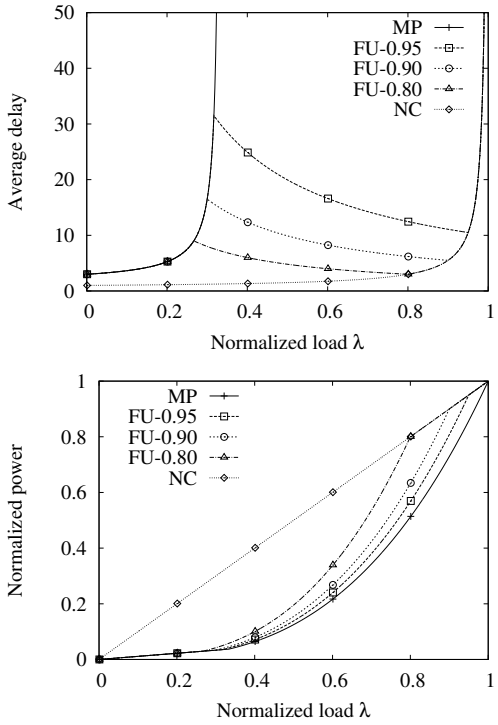

Fig. 1: Performance of FU-ρ_v policy when $\alpha_{\max} = 3$

- *medium load*, in which the service rate is controlled based on the arrival rate λ.

By again exploiting (2), it is easy to show:

Property 2: The FU policy defined via (8) obtains the maximum throughput for any admissible $\lambda \in [0, 1)$, given the finiteness of its average delay:

$$W = \begin{cases} \dfrac{\lambda}{2(1-\lambda)} + 1 & \text{for } \lambda \in [\rho_v, 1) \quad \text{(9a)} \\ \dfrac{\rho_v^2}{2\lambda(1-\rho_v)} + \dfrac{\rho_v}{\lambda} & \text{for } \lambda \in [\frac{\rho_v}{\alpha_{\max}}, \rho_v) \quad \text{(9b)} \\ \dfrac{\lambda \alpha_{\max}^2}{2(1-\lambda\alpha_{\max})} + \alpha_{\max} & \text{for } \lambda \in [0, \frac{\rho_v}{\alpha_{\max}}) \quad \text{(9c)} \end{cases}$$

The corresponding power is:

$$P = \begin{cases} \lambda & \text{for } \lambda \in [\rho_v, 1] \\ \dfrac{\lambda^3}{\rho_v^2} & \text{for } \lambda \in [\rho_v/\alpha_{\max}, \rho_v) \\ \dfrac{\lambda}{\alpha_{\max}^2} & \text{for } \lambda \in [0, \rho_v/\alpha_{\max}) \end{cases}$$

Fig. 1 shows[1] average delay (measured as multiple of T_{pkt}) and normalized power as a function of arrival rate λ, for different values of control parameter ρ_v. For comparison purposes, we also report the results obtained by MP and NC.

As expected, MP delays are unbounded when $\lambda > 1/\alpha_{\max}$, whereas the power is minimum and corresponds to the cubic

[1]All the curves in the following graphs (except the last two ones in the paper) are continuous, points simply help distinguish more easily the curves.

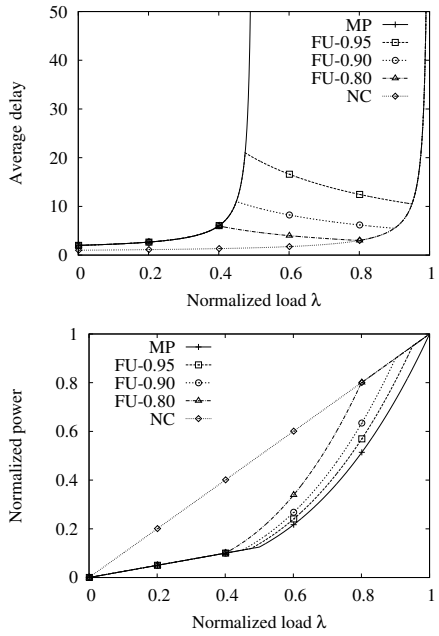

Fig. 2: Performance of FU-ρ_v policy when $\alpha_{\max} = 2$

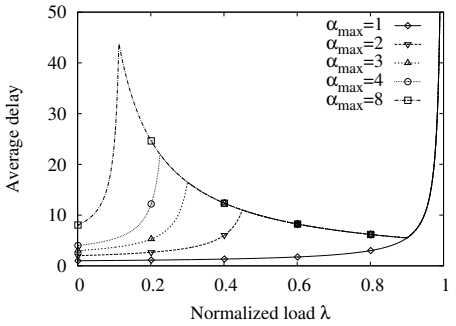

Fig. 3: Delay for FU-0.90 and different values of $\alpha_{\max}$.

function in (7). Conversely, NC delays correspond to those of a standard M/D/1 queue and power grows linearly with λ.

More interestingly, under the FU policy the delays show a non-monotonic behavior as a function of the load, with a local maximum for $\lambda = 1/\alpha_{\max}$. This behavior is due to the fact that, in the medium-load regime, when λ decreases, the service time must increase to keep the same utilization factor ρ_v, since $\lambda\alpha = \rho_v$. Similar results are reported in Fig 2, which refers to the case of $\alpha_{\max} = 2$. Delays start decreasing for a different load value, but the curve shows the same trend.

Fig. 3 shows the effect on delays of different values of $\alpha_{\max}$ for the FU policy. The non-monotonic behavior is more evident for larger values of $\alpha_{\max}$. Note that if α could increase without any bound (i.e., $\alpha_{\max} \to \infty$), then the corresponding delay would tend to infinity for $\lambda \to 0$.

C. Fixed Queue (FQ) policy

Another approach to cope with infinite queue lengths in MP is a power control based on the queue size. For this policy,

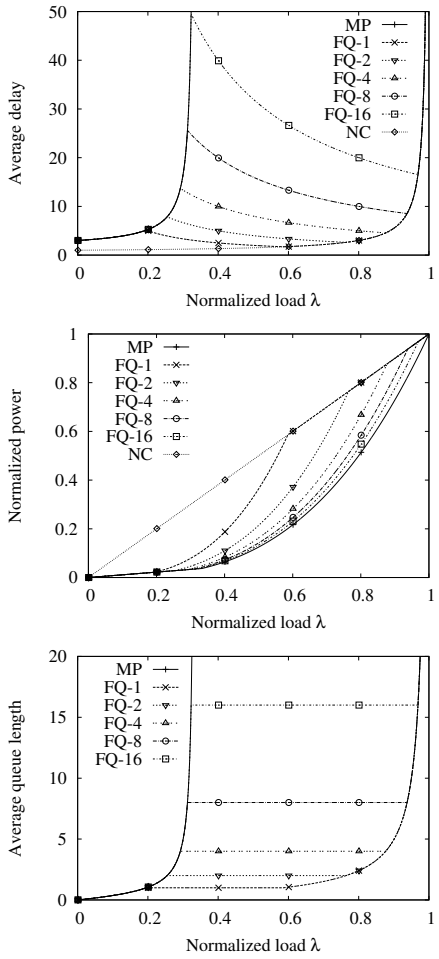

Fig. 4: Performance of FQ-L policies when $\alpha_{\max} = 3$.

FQ, α is chosen so that the average queue size equals a target value L. By using Little's law to express the average queue size, we can set $W(\lambda)\lambda = L$ and, thanks to (2), we have

$$\frac{\lambda^2\alpha^2}{2(1-\lambda\alpha)} + \alpha\lambda = L$$

Solving the above equation and considering the constraints in (3), we can define the FQ policy as follows:

$$\alpha_{FQ} = \begin{cases} 1 & \text{for } \lambda \in [\hat{L}, 1) \\ \hat{L}/\lambda & \text{for } \lambda \in [\hat{L}/\alpha_{\max}, \hat{L}) \\ \alpha_{\max} & \text{for } \lambda \in [0, \hat{L}/\alpha_{\max}) \end{cases} \quad (10)$$

where the new control parameter $\hat{L} = L + 1 - \sqrt{L^2+1}$, and $\hat{L} \in (0, 1)$. Even though this policy targets a fixed queue size L, is still arrival-rate based because it requires to know λ.

In Fig. 4 we show the average delay, power and average queue length for different target queue L and $\alpha_{\max} = 3$. We also report the power achieved by MP and NC, as a reference for the minimum and maximum possible power value, respectively. As expected, the FQ policy is able to guarantee a fixed average queue length under medium load. Furthermore, to achieve small L, the server rate must be

large enough: this translates to small delays but high power consumption. For large L, the server rate can be further lowered. Similar results are observed for other values of $\alpha_{\max}$.

Note that FQ can be seen as the static version of a dynamic policy that varies the service rate using a formal control technique [1]. As noted at the beginning of Sec. III, the static policy outperforms the dynamic one under our assumptions.

It is easy to note a similarity between the (8) and (10), from which stems the equivalence between FU and FQ policies:

Property 3: A FQ-L policy with target queue size L is equivalent to a PM-ρ_v policy with virtual utilization factor ρ_v if any of the following conditions hold:

$$\rho_v = L + 1 - \sqrt{L^2+1} \;\Leftrightarrow\; L = \frac{\rho_v^2}{2(1-\rho_v)} + \rho_v \qquad (11)$$

Indeed, (9b) shows that for the FU policy the average queue size (computed as λW) is also constant for medium load. As a consequence of this equivalence, the same power-delay tradeoff is achieved by the two policies.

IV. Policy with controlled delays

It is possible to avoid the non-monotonic delays behavior by a careful choice of the expansion factor. We propose a new policy, denoted as Fixed Delay (FD), in which we impose that the delay for medium load is fixed. For a fair comparison with the previous policies, we set such fixed value equal to the delay $W'(\rho_v)$ obtained for FU-ρ_v at the specific load $\lambda = \rho_v$:

$$W(\lambda) = W'(\rho_v) \qquad \text{for } \lambda \le \rho_v$$

We can now leverage (2) and the fact that it must be $\alpha = 1$ for $\lambda = \rho_v$, to impose:

$$\frac{\lambda \alpha_{FD}^2}{2(1-\lambda\alpha_{FD})} + \alpha_{FD} = \frac{\rho_v}{2(1-\rho_v)} + 1$$

By solving the equation, we obtain the expansion factor α_{FD} for medium load. Hence, FD policy is defined as follows:

$$\alpha_{FD} = \begin{cases} 1 & \text{for } \lambda \in [\rho_v, 1] \\ \dfrac{-b + \sqrt{b^2 - 4ac}}{2a} & \text{for } \lambda \in [\rho^*, \rho_v) \\ \alpha_{\max} & \text{for } \lambda \in [0, \rho^*) \end{cases} \qquad (12)$$

where $a = -\lambda(1-\rho_v)$, $b = 2(1+\lambda)(1-\rho_v) + \lambda\rho_v$, $c = \rho_v - 2$ and ρ^* can be computed by imposing $\alpha_{FD} = \alpha_{\max}$. Observe that the FD policy is arrival-rate based, as the previous ones.

Fig. 5 shows the performance of the FD policy, for different values of ρ_v. As expected, the average delay is constant for medium load, whereas the power shows the same qualitative behavior of FU (and also FQ). To better highlight the differences, Fig. 6 compares the performance of FU and FD for the same value of ρ_v. By construction, the delay of FD for medium load is the same of FU at load $\lambda = \rho_v$. In the bottom graph, we plot the power ratio between FD and NC, which helps understanding the power reduction with respect to the case without power control. Since $\alpha_{\max} = 3$, the maximum power gain is $\alpha_{\max}^2 = 9$ for low load, corresponding to 11% relative power. For larger loads, the relative power tends to 100% as

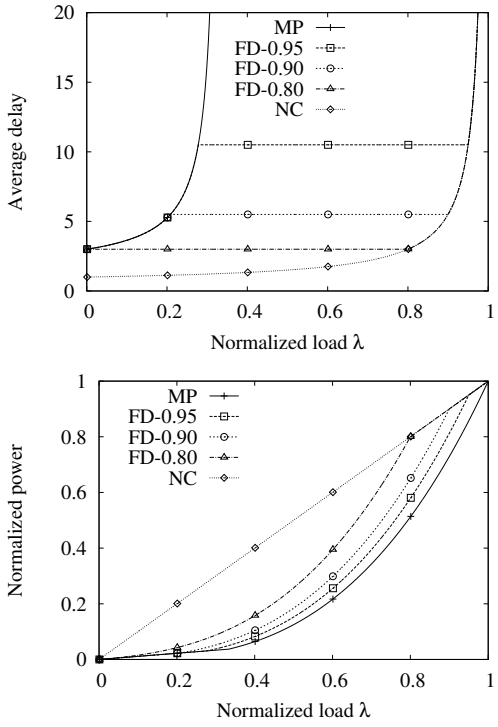

Fig. 5: Performance of FD-ρ_v policy when $\alpha_{\max} = 3$

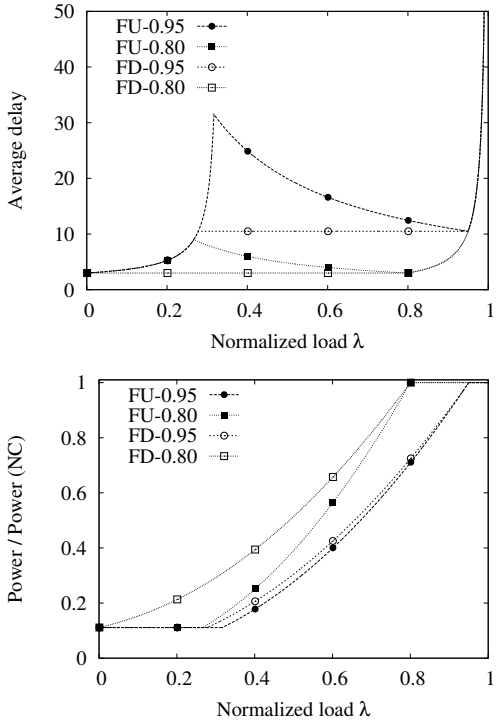

Fig. 6: FU-ρ_v policies vs. FD-ρ_v policies, $\alpha_{\max} = 3$

the power control becomes less and less effective. For medium load, the difference between the two policies for $\rho_v = 0.95$ is small (the power of FD is 15% larger than FD for $\lambda = 0.5$), but FD experiences smaller and monotonic delays (the delay

of FU is 65% larger than FD for $\lambda = 0.5$). Furthermore, for smaller values of ρ_v, the difference becomes larger: e.g., for $\lambda = 0.5$ and $\rho_v = 0.8$, the power of FD is 35% larger than FU, whereas the delay of FU is 60% larger than FD.

A. FD policy for a generic queue

The FD policy requires the knowledge of the analytic formula (2) relating the average delay to the load in the corresponding queueing system. In practical cases, this formula is not available, but this lack can be compensated by the empirical knowledge of $W(\lambda, \alpha)$ that can be obtained by profiling the delay for a large enough set of values of (λ, α).

As an example, we consider a finite M/G/1/K queue, for which $W(\lambda, \alpha)$ can only be numerically computed. To profile queueing delays, we evaluate the average delay $\hat{W}(\lambda, \alpha)$ of the queue with steps $\Delta\lambda = 0.05$ and $\Delta\alpha = 0.01$. Then we set $\hat{W}(\lambda) = \hat{W}(\rho_v)$ as in the original FD policy, and compute the required value of α. To show the feasibility of the approach, we use an ad-hoc C++ queue simulator to simulate the packet arrival process in an M/D/1/K queue and to evaluate delay and power. Graphs[2] in Fig. 7 exhibit the same qualitative behavior of the FD policy adopted for the M/D/1 queue, proving that our approach is feasible also without analytic formulas.

According to the M/D/1/K model, which implies queue finiteness and Poisson arrival process, $\lambda = 1$ is not enough to saturate the queue, and the corresponding average queue size and delay tend to 5, i.e., half the maximum queue size.

V. Conclusions

We considered a single server queueing system in which the server rate is controlled to minimize the power consumption. We showed that the minimum power consumption is obtained only at the cost of unbounded average delays, and that two possible policies that exhibits finite delays while targeting either a fixed utilization (FU) or a fixed length of the queue (FQ) show a non monotonic delay/load curve. To overcome the possible drawbacks of such non-monotonic behavior, we proposed the Fixed-Delay (FD) policy, based on the arrival rate estimation, which achieves a fixed delay for a wide load range, with a slight power penalty if compared to FU and FQ.

As future work, we plan to investigate the interaction between these policies and end-to-end congestion/flow control schemes, in which non-monotonic delays may negatively affect performance. We will also consider the practical case in which arrival rates must be estimated in real time. This study will permit evaluating the performance degradation of dynamic policies with respect to the static policies considered in this work.

Acknowledgments

The research leading to these results has received funding from the European Union Seventh Framework Programme (FP7/2007-2013) under grant agreement n. 257740 (Network of Excellence "TREND").

[2]In these figures only the points shown in the graphs have been simulated.

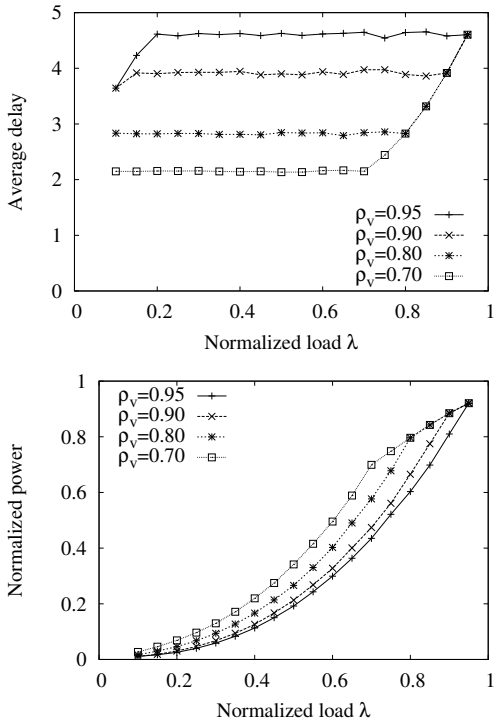

Fig. 7: Performance of FD policy in a simulated M/D/1/K queue with $K = 10$ and $\alpha_{\max} = 3$

References

[1] Q. Wu, P. Juang, M. Martonosi, L.-S. Peh, and D. Clark, "Formal control techniques for power-performance management," *Micro, IEEE*, vol. 25, no. 5, pp. 52–62, 2005.

[2] A. Bianco, P. Giaccone, M. R. Casu, and N. Li, "Exploiting space diversity and dynamic voltage frequency scaling in multiplane network-on-chips," in *Proc. IEEE GLOBECOM*, 2012, pp. 3080–3085.

[3] C. Casetti, M. Gerla, S. Mascolo, M. Sanadidi, and R. Wang, "TCP Westwood: end-to-end congestion control for wired/wireless networks," *Wireless Networks*, vol. 8, no. 5, pp. 467–479, 2002.

[4] U. Ogras, R. Marculescu, D. Marculescu, and E.-G. Jung, "Design and management of voltage-frequency island partitioned networks-on-chip," *IEEE Trans. VLSI Syst.*, vol. 17, no. 3, pp. 330–341, 2009.

[5] M. K. Yadav, M. R. Casu, and M. Zamboni, "A simple DVFS controller for a NoC switch," in *Proc. PRIME*, 2012, pp. 131–134.

[6] L. Benini, A. Bogliolo, and G. De Micheli, "A survey of design techniques for system-level dynamic power management," *IEEE Trans. VLSI Syst.*, vol. 8, no. 3, pp. 299–316, 2000.

[7] L. Shang, L.-S. Peh, and N. K. Jha, "Dynamic voltage scaling with links for power optimization of interconnection networks," in *Proc. HPCA*. IEEE, 2003, pp. 91–102.

[8] S. Nedevschi, L. Popa, G. Iannaccone, S. Ratnasamy, and D. Wetherall, "Reducing network energy consumption via sleeping and rate-adaptation," in *Proc. of USENIX NSDI Symp.*, no. 14, 2008.

[9] M. Lin and Y. Ganjali, "Power-efficient rate scheduling in wireless links using computational geometric algorithms," in *Proc. IWCMC*. ACM, 2006, pp. 1253–1258.

[10] C.-p. Li and M. J. Neely, "Delay and rate-optimal control in a multi-class priority queue with adjustable service rates," in *INFOCOM, 2012 Proceedings IEEE*, 2012, pp. 2976–2980.

[11] T. V. Dinh, L. L. H. Andrew, and Y. Nazarathy, "Architecture and robustness tradeoffs in speed-scaled queues with application to energy management," *International Journal of Systems Science*, pp. 1–12, 2013.

[12] B. Zhai, D. Blaauw, D. Sylvester, and K. Flautner, "Theoretical and practical limits of dynamic voltage scaling," in *Proc. DAC*, 2004, pp. 868–873.

Power Consumption Evaluation of Circuit-Switched Versus Packet-Switched Optical Backbone Networks

Ward Van Heddeghem, Bart Lannoo, Didier Colle and Mario Pickavet
Ghent University-iMinds, Ghent, Belgium
Email: ward.vanheddeghem@intec.ugent.be

Francesco Musumeci and Achille Pattavina
CNIT and Politecnico di Milano, Milan, Italy
Email: fmusumeci@elet.polimi.it

Filip Idzikowski
Technische Universität Berlin, TKN, Berlin, Germany
Email: filip.idzikowski@tu-berlin.de

***Abstract*—While telecommunication networks have historically been dominated by a circuit-switched paradigm, the last decades have seen a clear trend towards packet-switched networks. In this paper we evaluate how both paradigms perform in optical backbone networks from a power consumption point of view, and whether the general agreement of circuit switching being more power-efficient holds. We consider artificially generated topologies of various sizes, mesh degrees and—not yet previously explored in this context—transport linerates. We cross-validate our findings with a number of realistic topologies.**

Our results show that, as a generalization, packet switching can become preferable when the traffic demands are lower than half the transport linerate. We find that an increase in the network node count does not consistently increase the energy savings of circuit switching over packet switching, but is heavily influenced by the mesh degree and (to a minor extent) by the average link length.

I. Introduction

Electricity consumption in telecommunication networks is an important issue — The worldwide electricity consumption of telecommunication networks (which includes operator networks, office network equipment, and customer premises network equipment) has been estimated to be 350 TWh in 2012, accounting for 1.8% of the total worldwide electricity consumption in the same year [1]. While it can be argued that this number in itself is relatively small, it is non-negligible and increasing at a rate of 10% per year. Moreover, its relative contribution to the total worldwide electricity consumption is increasing as well (from 1.3% in 2007 to 1.8% in 2012). As such, the interest to improve the energy-efficiency of telecommunication networks is a hot research topic, and is of importance for economic (reducing the energy cost), technical (reducing the associated heat dissipation) and environmental (reducing the carbon footprint) reasons.

The electricity consumption in backbone networks is expected to rise considerably — The major part of the power consumption in the telecommunication operator networks is currently attributed to the wired aggregation & access network and mobile radio network. The backbone network, in contrast, is estimated to account (in 2012) for only about 8% of the total operator network consumption (which includes the wired aggregation & access, mobile radio and backbone network) [2]. However, the energy consumption in wired access networks is proportional to the number of connected subscribers, while the consumption in the backbone network is proportional to the traffic volume [2]. With the expected increase of traffic volume, high growth rates in the backbone's energy consumption are expected (potentially even overtaking the access network's consumption [3]). For this reason, it is important to react timely to the energy issue of backbone networks.

In this paper we extensively compare the circuit and packet-switched Internet Protocol (IP)-over-Wavelength Division Multiplexing (WDM) networks with respect to their power efficiency. We consider circuit switching in the context of optical circuits, in contrast to the more traditional opto-electronic circuit switching such as in SONET/SDH and OTN.

Earlier work on the power efficiency of circuit vs packet switching — In the last decades, the telecommunication industry has seen a shift from circuit-switched networks to packet-switched networks. We focus on the comparison of circuit switching and packet switching in terms of (inverse) power efficiency, leaving the more complex hybrid solutions aside. There has been some earlier research into the power consumption of circuit switching versus packet switching, identified respectively as bypass and non-bypass architectures in the context of optical networks. In [4] the authors exploited the concept of lightpath-bypass to perform a power-minimized optical network design, based on Integer Linear Programming (ILP) formulations and heuristics. They distinguish non-bypass (packet switching), direct bypass (circuit switching), as well as an intermediate hybrid solution called multi-hop bypass. A similar problem has been faced in our previous work [5], where simulations and an analytical model were used for the power consumption evaluation of bypass and non-bypass scenarios. In the line of these studies, an analytical model based on expectation values has been also developed in [6], where different variations of the optical bypass strategy are evaluated under different mesh degree scenarios, i.e., from a ring up to full-mesh topologies. Capital Expenditure (CapEx) minimized and power minimized networks designed with an ILP and a genetic algorithm have been considered in our previous work [7]. A bypass and non-bypass architectures (differing by traffic grooming, placement of transponders and (non-)existence of Optical Cross-Connects (OXCs)) in IP-over-WDM are distinguished. Finally, in [8], a power consumption evaluation of switching and routing elements is performed to

978-1-4799-0354-2/13/$31.00 ©2013 IEEE

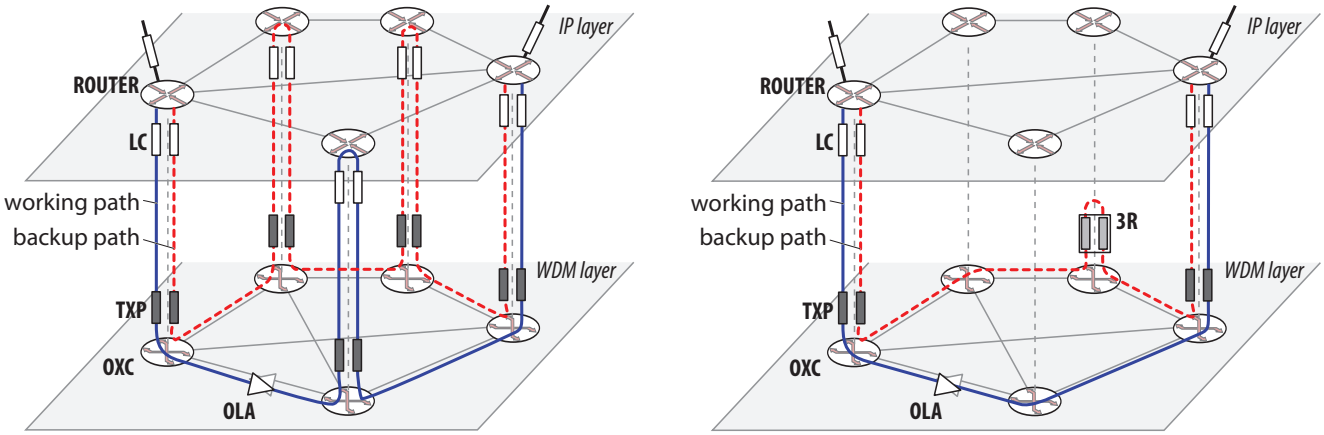

(a) Packet switching

(b) Circuit switching

Fig. 1. The packet-switched and circuit-switched network architectures considered in this paper, showing both the bidirectional working path (solid lines) and backup path (dashed lines) under a 1+1 protection scheme. (LC = line card, TXP = transponder, OXC = Optical Cross-Connect, OLA = Optical Line Amplifier, 3R = 3R regenerator)

compare the circuit and packet switching paradigms, but the analysis is limited to the node level.

The works mentioned above point out the benefits of circuit switching over packet switching in terms of power consumption. These benefits depend however on the investigated network scenario. For example, looking at Fig. 4 of [4], the x-axis depicting "Average of random traffic demand" starts from 20 Gbps/node pair, while the capacity of a single WDM channel is set to 40 Gbps. The missing range 0–20 Gbps/node is expected to show that the packet-switched networks can be less power consuming than the circuit-switched networks, as preliminarily indicated in [5] and [7].

Contributions of this paper — The four key contributions of our paper with respect to the existing research are as follows. (1) In addition to considering the mesh degree and network size (in terms of the number of nodes and average physical link length), we evaluate the influence of the channel linerate on the power efficiency of circuit switching versus packet switching, a parameter which to our knowledge has previously not been assessed. (2) We particularly look at network scenarios where packet switching is preferable from a power consumption point of view. This aspect has to the best of our knowledge not been addressed in the previous literature (as mentioned above, see e.g., lack of the range 0–20 Gbps/node pair of average traffic in the Fig. 4 of [4]). One way in which we do this is by considering the ratio of the average node-to-node demand over the channel linerate. (3) We deeply study the (inverse) power efficiency of both switching paradigms under increasing traffic demand. We show that the power efficiency of packet switching in sparsely-connected networks is almost independent of the traffic demand, whereas for circuit switching the power efficiency improves with increasing traffic. (4) We find that a higher node count does not necessarily make circuit switching more preferable. In highly meshed networks the node count does not influence the relative savings of circuits switching over packet switching at all. Our results show that the mesh degree, the demand/linerate ratio and the physical link length are critical parameters.

All in all, our results provide a better insight into the trade-off of the power efficiency of circuit switching versus packet switching.

Organization of this paper — After outlining the network architecture and power consumption model that we use (Section II), we consider both a set of realistic and artificially generated but regular topologies of different sizes (in terms of nodes), different connectivity degree, and various linerates (Section III). Using the result from our dimensioning tool, we show in Section IV that (a) indeed packet switching can be the preferable option with respect to power consumption below certain traffic demand bitrates, (b) that this crossover point is essentially determined by the ratio of the traffic demand over the linerate, and (c) to a minor extent also by the mesh degree.

II. Network Architecture and Power Consumption Model

A. Network architecture

The general architecture of the network is shown in Fig. 1 on an example of a 5-node topology (IP/Multiprotocol Label Switching (MPLS) and WDM layers). In the *IP/MPLS layer*, a core router is equipped with line cards, providing one or more ports with short reach interfaces. We assume (differently from [8]) that IP routers have to be present in the backbone network under the circuit switching paradigm, since they exchange the IP traffic with other networks (metro, access) attached to them [9]. The buffers located in the router's line cards are used only at the end nodes of the optical circuits. The granularity of the linerates of the interfaces differs: the access or client-side traffic connects to the router using 1-Gbps interfaces, and the core network side interfaces are either 2.5-Gbps, 10-Gbps or 40-Gbps interfaces (which we refer to as 2.5G, 10G and 40G). Note that, depending on the traffic demand bitrate, one or more interfaces can be required per demand.

In the *WDM layer*, long reach transponders with the same capacity as the IP/MPLS layer line cards provide a WDM optical signal, which is switched using an OXC towards the correct physical link. A mux/demux (included in the OXC) aggregates up to 40 channels on a fiber. For each physical link, we assume an unlimited number of fibers to be available. A booster and pre-amplifier (included in the OXC) amplify all channels in a fiber pair respectively upon leaving and entering a node. An Optical Line Amplifier (OLA) is placed every 80 km, and amplifies all channels in a fiber pair. For lightpaths longer than the regenerator span, taken to be 1,500 km, the signal is switched by the OXC to pass through a 3R regenerator.

The way that traffic demands traverse the network is different in packet switching and circuit switching. Under the *packet switching paradigm*, all the traffic in a node—i.e., not only the originating and terminating, but also the transit traffic—is processed at the router in the IP/MPLS layer, as shown by the solid line in Fig. 1(a). This provides the opportunity to groom traffic, that is bundling traffic belonging to demands from different sources that are destined to the same outgoing link. As a result, the transport channels (wavelengths) are filled more efficiently.

Under the *circuit switching paradigm*, traffic demands traverse the network over a single IP hop, since dedicated optical circuits are set up from the source IP/MPLS node to the target node, as shown by the solid line in Fig. 1(b). This allows the transit traffic to remain in the optical domain and thus bypass the IP router. For this reason such architectures are often referred to as *optical-bypass* architectures. However, depending on the ratio between the traffic demand bitrates and the channel capacity (i.e., linerate), lightpaths might not be optimally used. For a given set of demands, this might result in a higher number of channels required compared to packet switching.

In both switching cases, we assume a 1+1 protection scheme at the IP layer. Under this scheme, a backup path (dashed line in Fig. 1) is simultaneously routed over a link-disjoint physical path with respect to the primary one, so that if the working path fails, the traffic can be instantaneously switched over to the backup path.

B. Power consumption model

The power consumption values assumed for each equipment type are listed in Table I. All values are taken from [5], with the exception of the 40G coherent transponder value which is based on [10].

The power-per-port values for the IP router include both the power consumed by the line card and the basic node (i.e., chassis, switch fabric, routing engine, power supply, internal cooling and remaining minor components). We assume the power-per-port value fixed and independent of the load, as the power consumption of present-day IP routers when idle and under full load are very similar [10], [11]. This also implies that the influence on the power consumption of buffering and table look-up associated with packet switching is negligible. The OXC degree d_f is defined as the number of network-side bidirectional fiber ports, assuming that all fiber ports are added/dropped at the tributary side (i.e., towards the IP/MPLS layer). The power consumption value used for the OXC includes mux/demux stages as well as pre- and booster-amplifiers. In addition to the total power consumed by the devices listed in Table I, we assume that an equal amount of overhead power is consumed for site cooling and power supply losses, i.e., the Power Usage Effectiveness is equal to 2.

TABLE I
POWER CONSUMPTION VALUES (SOURCE: [5], [10])

Equipment	Power cons.	Inv. pow. eff.
IP/MPLS 1G-port	10 W	10 W/Gbps
IP/MPLS 2.5G-port	25 W	10 W/Gbps
IP/MPLS 10G-port	100 W	10 W/Gbps
IP/MPLS 40G-port	400 W	10 W/Gbps
OLA (per fiber pair, 80 km span)	110 W	-
Transponder 2.5G	25 W	10 W/Gbps
Transponder 10G	50 W	5 W/Gbps
Transponder 40G (coherent)	167 W	4 W/Gbps
3R regenerator xG	2 · transponder xG	-
OXC, 40 ch., with degree d_f	150 W + d_f· 135 W	-

III. CONSIDERED TOPOLOGIES AND POWER CALCULATION METHODOLOGY

A. Topologies

To understand the influence of the connectivity degree and network size (in terms of number of nodes and average physical link length) on the power consumption, we consider a number of artificially generated topologies, ranging from minimally meshed (ring) up to maximally meshed (full-mesh) networks, see Table II. To be able to cross-validate our results based on artificial topologies, we also consider three realistic networks: the Spanish Telefónica I+D (TID) network model (forecasted potential topology for the year 2020 [12]), the DICONET pan-European Géant network [13], and the well-known U.S. NSF network [5]. They are also listed in Table II. For all of the networks, the IP topology is taken identical to the WDM topology under the packet switching paradigm. All links are bidirectional. For each of these variations we consider networks with the number of nodes N equal to 10, 15, 25, and 33.

Similarly to [6] we define the mesh degree M of a network as the ratio of the average node degree of the network under consideration, $\overline{d}$, and the node degree of a full-mesh network having the same number of nodes as the considered network, i.e., d_{mesh} =N−1, so we get $M = \frac{\overline{d}}{d_{mesh}}$. The half-mesh networks have a mesh degree of $M = 0.5$, so that the average desired node degree is easily calculated as $\overline{d} = \frac{N-1}{2}$. To generate these half-mesh networks we (a) start from a ring network with the required number of nodes N and number of links $L_{ring} = N$, (b) then calculate the number of links to add in order to have the desired[1] average mesh (and node) degree,

[1]Note that, depending on the number of nodes and the requested degree, the theoretical number of links to add might be a fractional number. So we round this value up or down to the closest integer to get a practical (i.e., integral) number of links to add. As a result, the actual degree of the network might differ slightly from the requested one.

TABLE II
TOPOLOGIES CONSIDERED IN THIS STUDY

Topology	Number of nodes N	Number of bidir. links L	Avg. node degree $\overline{d}$	Mesh degree M	Link length (avg) [km]
ring	10	10	2	0.22	255
ring	15	15	2	0.14	166
ring	25	25	2	0.08	100
ring	33	33	2	0.06	75
half-mesh	10	23	4.5	0.50	255
half-mesh	15	53	7	0.50	166
half-mesh	25	150	12	0.50	100
half-mesh	33	264	16	0.50	75
full-mesh	10	45	9	1.00	255
full-mesh	15	105	14	1.00	166
full-mesh	25	300	24	1.00	100
full-mesh	33	528	32	1.00	75
TID	33	53	3.21	0.10	(52.4)
Géant	34	54	3.18	0.10	(753)
NSF	14	21	3.00	0.23	(1083)

and (c) eventually add these links distributed evenly across the ring (connecting the most-distant nodes, based on the hop count, first). Note that the number of links in such a half-mesh network is given by $L = L_{ring} + \left(N \cdot \frac{\overline{d}-2}{2}\right) = N \cdot \frac{N-1}{4}$.

For the physical link lengths, which influence the power consumption of the OLAs and 3R regenerators, we assume that each of the generated networks covers a geographical area with a diameter of 2,500 km (which is comparable to a country-sized network). The physical link lengths are then taken to be 2,500 km divided by the number of links in a ring network. For the half-meshed and full-mesh networks we take all other physical links to have the same length, even if this is topologically unrealistic (Table II).

B. Network dimensioning and power consumption calculation

We calculate and evaluate the power consumption in the above listed networks for both the packet and circuit-switched architectures, using a custom Java-based dimensioning tool. The general steps in calculating the power consumption are as follows. First, for each topology, a traffic matrix is generated with uniform demands (i.e., an identical demand between each node pair). We also vary the demands bitrate values in different runs. Second, each demand is routed across the network. To achieve 1+1 protection at the IP layer (see Fig. 1), the two shortest link-disjoint physical paths between the source and target nodes are calculated using a minimum cost flow algorithm, where we assume the overall path length, expressed in number of hops, as cost. Third, wavelengths (i.e., channels) and fibers to be used are selected in a first-fit fashion. This means that the algorithm finds the first free wavelength/fiber pair that is available on the physical path between source and target nodes. Fourth, from the node port counts we derive the power consumption of IP/MPLS routers, transponders and OXCs. From the link and path lengths we calculate the number of required OLAs and regenerators, and subsequently their power consumption. Because of the dimensioning tool constraints, we generalized on the OXC power consumption and calculate an average OXC power consumption value based on the average node degree of the network.

IV. RESULTS AND OBSERVATIONS

In this section we compare the power consumption of packet switching (PS) and circuit switching (CS) architectures, evaluated over the artificially generated topologies (from ring to full-mesh) and cross-validated with the realistic topologies.

For this evaluation we use three metrics: the absolute power consumption (kW), the inverse power efficiency (W/Gbps), and the relative power consumption savings of CS over PS (%).

A. General observations

Sparser topologies consume more — From Fig. 2(a) and (b) we see that sparser topologies (i.e., more ring-like) consume more power than more meshed topologies. This is due to longer paths needed both in the PS and CS.

Power efficiency improves with increasing demands, except for PS in sparse topologies — Fig. 2(c) and (d) show the inverse power efficiency, i.e., the power (in Watt) required to transport a uniform demand of 1 Gbps. We see that the power efficiency of PS (dashed lines) is almost independent of the traffic demand in ring-like networks, whereas in highly-meshed topologies its efficiency starts off worse but gradually improves with increasing traffic. CS (solid lines) behavior is similar to the latter irrespective of the mesh degree.

Higher demands favor CS — For higher traffic demands the PS architecture consumes more power than the CS architecture. On the other hand, for lower traffic the most power-efficient architecture of the two depends on the mesh degree and channel capacity.

B. Influence of the channel linerate (2.5G, 10G, 40G)

Inefficient usage of capacity for higher linerates in CS — In Fig. 2(a) and (b) it can be seen that the CS architecture exhibits (i) a very minor linear component (e.g., the CS-10G curve is almost flat between 12 Gbps and 20 Gbps), due to the fine granularity of the 1G IP client side ports, and (ii) a much more pronounced stepwise component due to the coarser granularity of the IP network side add/drop ports. The steps occur when the demand bitrate reaches a multiple of the channel linerate (2.5G/10G/40G). Because of the range of the demand bitrate on the x-axis, the stepwise behavior is most prominent for the 10G architecture. The overcapacity for the 40G at such relatively low demands is clear in Fig. 2(b). There is no such stepwise function (or at least, it is much smaller) for PS, because the traffic is groomed, so that the channel capacity (i.e., the linerate) can be used more efficiently even for lower traffic values, and as a result the curve is more linear. As such, the stepwise contribution of CS makes the higher-capacity technology (e.g., 40G) much less convenient at low loads. On the other hand, due to the more linear behavior of PS, higher capacity transport technologies such as 10G and 40G are sooner (i.e., already at low loads) more convenient.

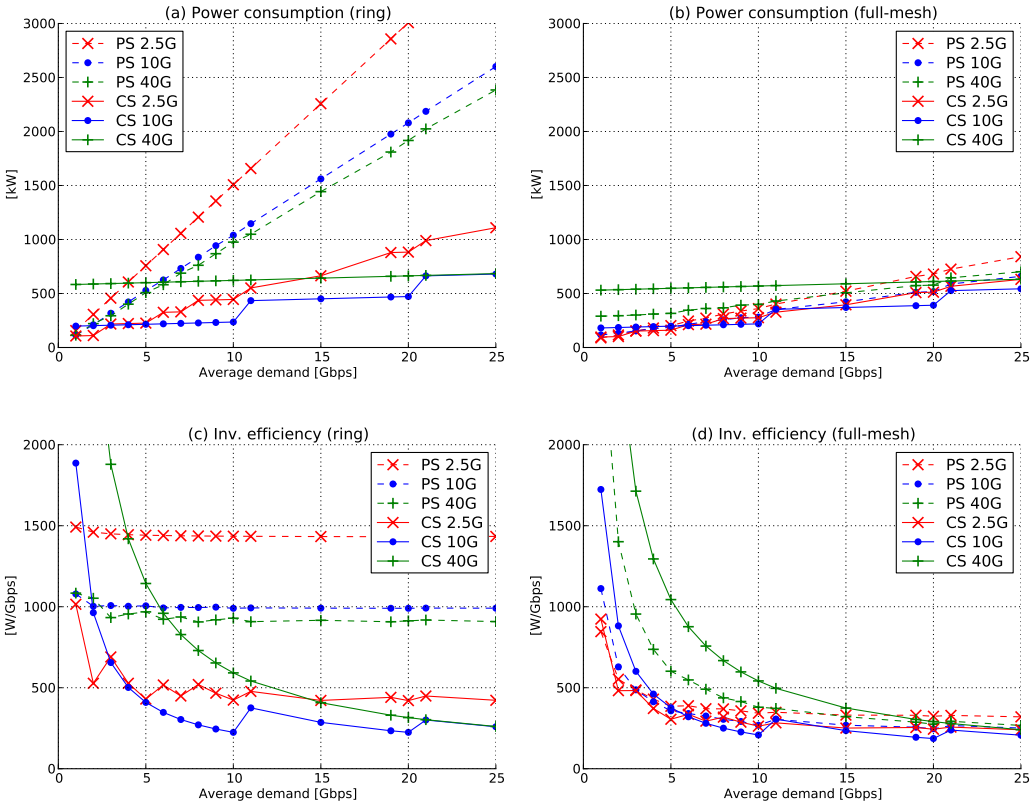

Fig. 2. The total power consumption and inverse power efficiency of a 15-node ring and full-mesh topology with increasing node-to-node traffic demand. The packet-switched (PS) paradigm shows an overall linear behavior, whereas the circuit-switched (CS) paradigm shows a stepwise behavior whenever the traffic demand becomes a multiple of the channel capacity. The power efficiency of PS in sparsely-connected networks is almost independent of the traffic demand, whereas for CS the power efficiency improves with increasing traffic.

Improved power efficiency for higher channel linerates — As shown in Table I, the transponders used for the different transport capacities are gradually more power-efficient per Gbps. This is also clearly visible in Fig. 2(c) where the PS 10G architecture consumes much less power per Gbps than the 2.5G architecture. The difference between the 10G and the 40G architecture is much smaller. The reason for the small increase of power efficiency moving from 10G to 40G is because we assumed a coherent 40G transponder, which comes at an extra power cost.

C. Influence of the demand/linerate ratio

To get a clear understanding of when CS is more power-efficient than PS (or vice versa), we plot in Fig. 3 the power consumption savings of CS over PS. Positive values indicate that CS is preferable, negative values indicate that PS is preferable. For a fair comparison between the different channel linerates, we plot this metric against the ratio of the average demand bitrate over the channel linerate. For a ratio equal to 1, the average demand bitrate is equal to the linerate.

High demand/linerate ratios favor CS, low demand/linerate ratios favor PS — Fig. 3 shows that increasing demand/linerate ratios lead to higher savings of CS over PS. Low demand/linerate ratios always make PS the preferable paradigm. Both Fig. 3(a) and (b) also clearly show the stepwise behavior around integral multiples of this ratio. Note that the sparse granularity of the data points smooths out the behavior, especially for the 2.5G architecture (for example, for 2.5G we have only three data points below the demand/linerate ratio of 1.5 because we consider integer node-to-node demands at 1, 2, 3, ... Gbps). This behavior originates from the stepwise behavior of the power consumption of the CS architecture. The CS savings increase until the demand reaches the channel capacity (as there is an increasing usage of the channel capacity), and then suddenly drops when the demands surpass the channel capacity (thereby requiring an extra WDM channel).

CS is always preferable for demands higher than half the channel linerate — Fig. 3 also indicates that there is a rather narrow transition window of the demand/linerate ratio where CS becomes more preferable than PS. In sparse networks (Fig. 3(a)) PS is the preferable option up to about demands being 1/10 to 1/3 of the channel linerate. In highly connected networks (Fig. 3(b)), the crossover window is much smaller, and PS is the preferable option for demands being up to half the channel linerate, independently of the utilized transmission technology. The reason that the crossover point is at half the channel linerate is because once a node-to-node demand is larger than half of the channel linerate, there is no free capacity left to groom another demand onto the same channel, and a separate channel is required for each demand.

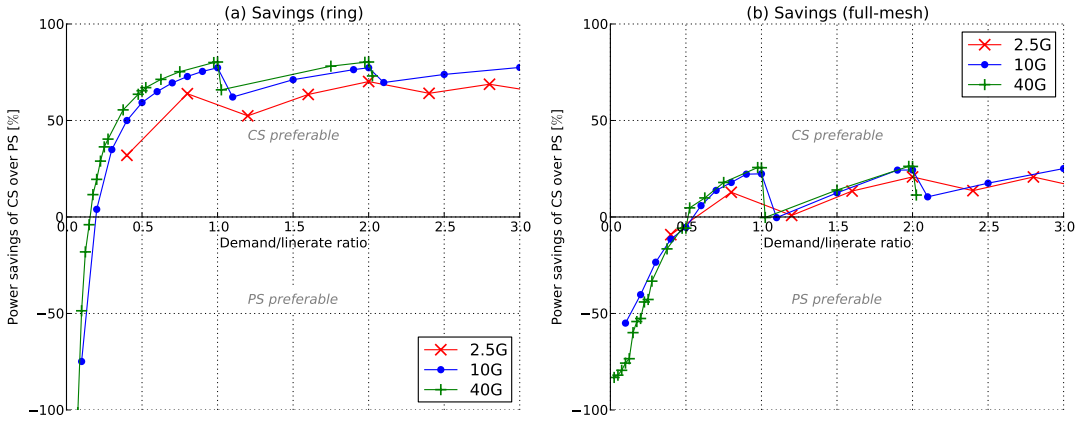

Fig. 3. Power savings of CS over PS mapped to the ratio of the demand bitrate over the channel linerate (15-node topology). The savings show a stepwise behavior around integral multiples of this ratio (i.e, the savings suddenly drop when the node-to-node traffic demands surpass the channel linerate). The ratio's transition window where CS becomes more preferable than PS is relatively small and relatively independent of the channel linerate (especially for highly-meshed networks, where it is fixed at 1/2).

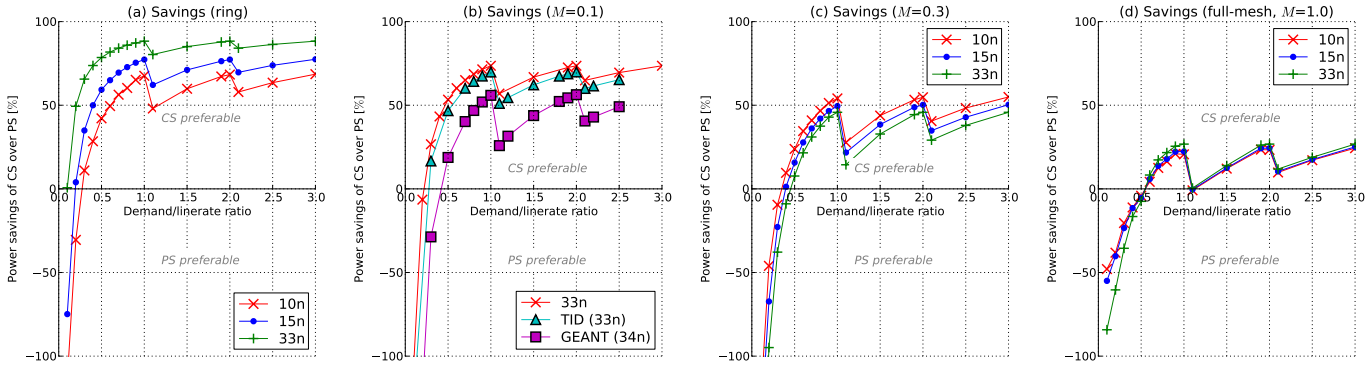

Fig. 4. Influence of the node count on the power savings of CS over PS (for linerate = 10G). Only for sparse topologies (i.e, (a) through (c)) the node count has an influence on the savings. While for a ring topology a higher node count leads to more savings, this is not consistently the case for other sparsely meshed topologies. The apparent deviation of the Géant topology from the general trend is explained in Fig. 5.

D. Influence of the network size (number of nodes and physical link lengths)

Fig. 4 shows the power consumption savings of CS over PS for networks with different number of nodes (the network with N=25 has been omitted for clarity). The subfigures (a) to (d) correspond to an increasing mesh degree. Fig. 4(b) represents a mesh degree M=0.1, and contains in addition two realistic topologies that also have M=0.1 (the lowest mesh degree of the 10-node and 15-node topology is higher than 0.1, see Table II).

In highly meshed network, the number of nodes does not influence the relative savings — When comparing the four subfigures it is clear that for highly meshed networks, the number of nodes does not influence the relative savings (i.e., all curves coincide in Fig. 4(d)). This is because the IP-layer hop count is low regardless of the number of nodes (the hop count is equal to 1 in full-mesh topologies).

Networks with more nodes do not *necessarily result in larger relative savings of CS over PS* — For sparse topologies (Fig. 4(a) through (c)) on the other hand the node count has considerable influence on the relative savings of CS over PS. For the ring topology, a higher node count makes CS more preferable. This is due to the higher hop count in larger ring networks, which implies a much higher IP-layer contribution, which increases the PS power consumption. This is inline with [4]. However, our results indicate that the above rule cannot be applied universally to all sparse topologies. In Fig. 4(c) a higher node count does not consistently correspond to increased CS savings (the savings for 33-node artificial topology are lower than for the 15-node topology). Moreover, while in Fig. 4(b) the realistic TID network (33 nodes) savings seems to be inline with the 33-node artificial topology, the Géant network (34 nodes) is certainly not. There must be another parameter with considerable influence at work.

Higher link lengths result in reduced savings for CS — In order to explore the reason of the above described anomaly, Fig. 5(a) plots, in addition to the 33-node artificial topology (physical link length = 75 km) and the original Géant topology (average physical link length = 753 km), the same Géant topology where all links have been (artificially) set to 75 km. The

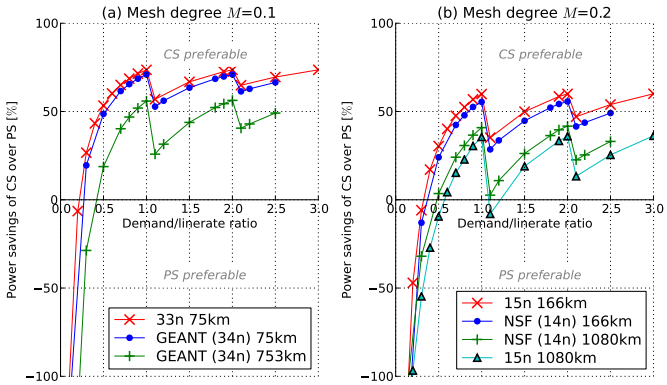

Fig. 5. Influence of the average physical link length on the relative savings of CS over PS (linerate = 10G). Higher link lengths result in lower savings, and explain why the savings profile of topologies such as Géant (average physical link length = 753 km) does not correspond very well with our artificial topology of the same node count but much lower link length.

figure shows that the difference in link length is the reason of the diverging behavior of the original Géant topology from the artificial 33-node topology. The high link length of the original Géant topology increases the number of required OLAs and 3R regenerators and the associated power consumption. As the additional power consumption has a larger relative impact on the CS power consumption, the power consumption savings of CS over PS decrease accordingly. This is also confirmed by Fig. 5(b) where the NSF network (14 nodes, mesh degree M = 0.2, average physical link length = 1080 km) is compared with our artificial 15-node M = 0.2 topology. When the link lengths are adjusted (either from the artificial topology, or from the NSF network), the savings curves become very similar.

E. Influence of the mesh degree

Although we have not focused on the mesh degree yet, it is already clear from the previous figures and discussion that this parameter is of considerable influence on the power savings of CS over PS.

Savings of CS over PS decrease with increasing mesh degree — As shown in Fig. 6, the savings of CS over PS tend to decrease for increasing mesh degree, as adding more edges decreases the hop count and thus more interfaces (i.e., router ports and transponders) can be saved in intermediate nodes of the PS architecture while still performing traffic grooming. On the other hand, for the CS architecture, a higher mesh degree only impacts the OLAs (and eventually, the regenerators) consumption, which constitutes a less relevant contribution in the total consumed power if compared to the power spent by the interfaces.

High channel linerates with low traffic conditions favor PS — An exception to this behavior is obtained for higher channel linerates under low traffic conditions (i.e, low demand/linerate ratios). This is shown in Fig. 7, which plots the savings in function of the mesh degree for different demand/linerate ratios. In this case, passing from ring to half-mesh topologies has, as previously, a higher benefit for the PS than for the CS solution. However, adding further links to the network (i.e., going towards full-mesh topologies), there is lower opportunity for traffic grooming (recall that demands are routed over the two shortest link-disjoint physical paths), so with high channel linerates interfaces are underutilized, thus causing higher relative power consumption.

It is interesting to point out that for the full-mesh case the power consumption of PS and CS are *not* equal (i.e., CS over PS savings are not zero), as one might incorrectly expect. The link disjoint backup paths always require two hops in both switching paradigms, but the intermediate node requires IP ports under the PS paradigm only, leading to CS being more preferable. However, an exception to this is observed for high linerates (e.g., 40G), combined with low demands bitrate (e.g., 5 Gbps per demand). In this case the opportunity to groom traffic in the PS scenario produces higher power benefits in comparison to the high demands bitrate situation, and thus the CS option is outperformed.

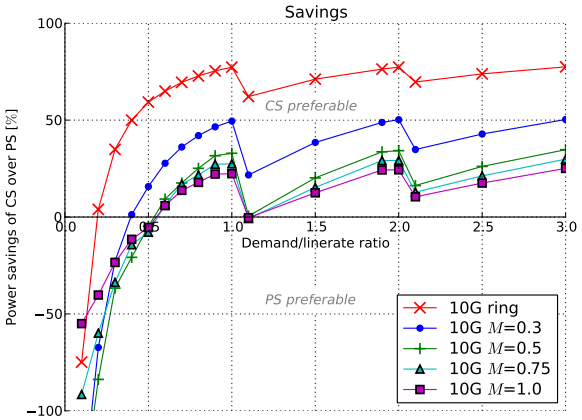

Fig. 6. Influence of the mesh degree on the relative savings of CS over PS (for linerate = 10G, and 15-node topologies). Higher mesh degrees (M) result in lower savings.

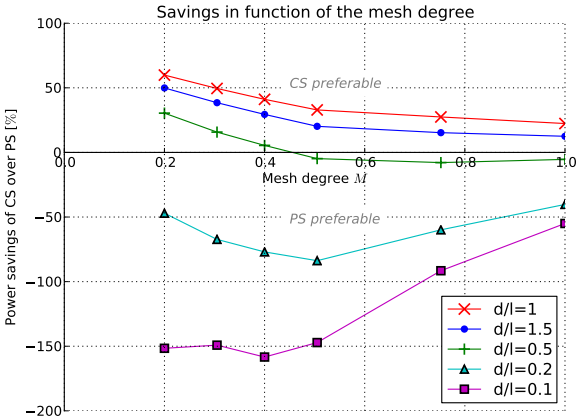

Fig. 7. Influence of the mesh degree and the demand/linerate ratio d/l on the relative savings of CS over PS (for linerate = 10G, and 15-node topologies). For low demand/linerate ratios there is an optimum point where PS is favorable.

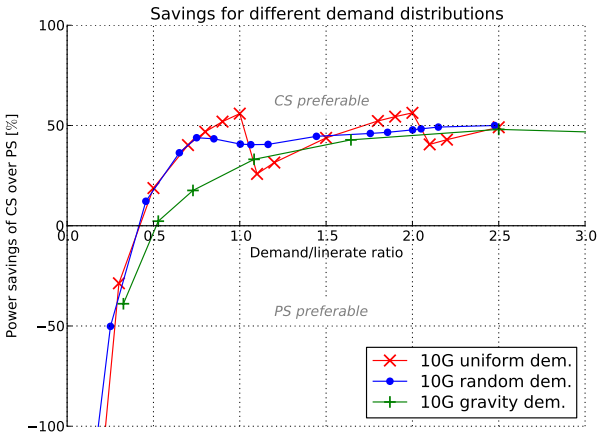

Fig. 8. Influence of different demand types on the savings of CS over PS (Géant topology, linerate=10G). While uniform demands show a distinct step-wise behavior, more realistic demand sets (i.e, random and gravity demands) smooth out this behavior.

F. Sensitivity to non-uniform demands

In all of the above scenarios we assumed fully-meshed uniform demands. To see the effect of non-uniform demands on the power savings of CS over PS, we consider in Fig. 8 two additional demand types: (a) a gravity traffic matrix where nearby nodes have larger demands, thus closer resembling real life demands [13], and (b) a random fully meshed traffic matrix where each demand is evenly distributed between -30% and +30% of the nominal demand.

Realistic traffic has a smoother savings profile — While the uniform demands show the distinct step-wise behavior, the behavior is much smoother for random demands and gravity demands. However, the general trend observed before remains valid: CS is preferable for demands higher than half the channel linerate (on average) also under the gravity and random traffic matrices.

V. Conclusion and Further Work

In this paper we extensively compared the power consumption of circuit and packet switching architectures in optical backbone networks. We evaluated the impact of the channel linerate, the network size (both number of nodes and physical link length), demand/linerate ratio and the network mesh degree to assess under which conditions each switching paradigm represents the most power-efficient solution.

We found that, in general, circuit switching is preferable, as fewer IP router ports and WDM transponders are needed. However we point out on the top of the related work that for relatively low traffic values—i.e., when the demands bitrate is lower than at least half the channel linerate—the packet switching solution is more power-efficient, thanks to the opportunity of exploiting traffic grooming to better utilize network resources.

Our key finding is that an increase in the network node count does not consistently increase the power savings of circuit switching over packet switching, but is heavily influenced by the mesh degree and (to a minor extent) by the average physical link length. Increasing the network mesh degree produces higher energy benefits for packet switching than for circuit switching, as more power can be saved in intermediate nodes in the former case.

While we have performed a sensitivity study with respect to non-uniform traffic demands, useful further work would consist in extending this with traffic demands originating from actual measurements. Furthermore, should the power consumption of future packet switches become more proportional to the load, it is likely that this will influence the outcome of our comparison. Finally, our routing algorithm is in both switching paradigms based on a shortest-path approach. It would be interesting to see if power-optimized routing (e.g., achieved with solving an ILP problem) changes the trends that we have observed.

Acknowledgments

The work described in this paper was carried out with the support of the iMinds-project GreenICT and the European Community's Seventh Framework Programme (FP7/2007-2013) under grant agreement n. 257740 (Network of Excellence TREND).

References

[1] S. Lambert, W. Van Heddeghem, W. Vereecken, B. Lannoo, D. Colle, and M. Pickavet, "Worldwide electricity consumption of communication networks," *Optics Express*, vol. 20, pp. B513–B524, December 2012.

[2] C. Lange, D. Kosiankowski, R. Weidmann, and A. Gladisch, "Energy consumption of telecommunication networks and related improvement options," *Journal of Selected Topics in Quantum Electronics*, vol. 17, no. 2, pp. 285–295, 2011.

[3] J. Baliga, R. Ayre, K. Hinton, W. V. Sorin, and R. S. Tucker, "Energy Consumption in Optical IP Networks," *Journal of Lightwave Technology*, vol. 27, pp. 2391–2403, July 2009.

[4] G. Shen and R. Tucker, "Energy-minimized design for IP over WDM networks," *Journal of Optical Communications and Networking*, vol. 1, pp. 176–186, June 2009.

[5] W. Van Heddeghem, F. Idzikowski, W. Vereecken, D. Colle, M. Pickavet, and P. Demeester, "Power consumption modeling in optical multilayer networks," *Photonic Network Communications*, vol. 24, pp. 86–102, October 2012.

[6] S. Aleksić, W. Van Heddeghem, and M. Pickavet, "Scalability and power consumption of static optical core networks," in *Proc. of Globecom, Anaheim, USA*, December 2012.

[7] A. Bianco, E. Bonetto, F. Musumeci, A. Pattavina, and M. Tornatore, "CapEx/OpEx evaluation of circuit vs packet switched optical networks," in *Proc. of ONDM, Brest, France*, April 2013.

[8] S. Aleksić, "Analysis of Power Consumption in Future High-Capacity Network Nodes," *Journal of Optical Communications and Networking*, vol. 1, pp. 245–258, August 2009.

[9] X. Dong, T. El-Gorashi, and J. Elmirghani, "On the energy efficiency of physical topology design for IP over WDM networks," *Journal of Lightwave Technology*, vol. 30, pp. 1931–1942, June 2012.

[10] W. Van Heddeghem, F. Idzikowski, E. Le Rouzic, J. Mazeas, H. Poignant, S. Salaun, B. Lannoo, and D. Colle, "Evaluation of power rating of core network equipment in practical deployments," in *Proc. of GreenCom, online*, September 2012.

[11] A. Vishwanath, J. Zhu, K. Hinton, R. Ayre, and R. S. Tucker, "Estimating the Energy Consumption for Packet Processing, Storage and Switching in Optical-IP Routers," in *Optical Fiber Communication Conference*, 2013.

[12] F. Idzikowski *et al.*, "Final report for the IRA "Energy-efficient use of network core resources," Deliverable D3.3, TREND Project, 2012.

[13] D. Staessens *et al.*, "Value analysis report on the use of the network planning tool," Deliverable D7.3, DICONET, European ICT-research project, 2010.

Reliability Differentiation in Energy Efficient Optical Networks with Shared Path Protection

Ajmal Muhammad[⋆], Paolo Monti[◦], Isabella Cerutti[▷], Lena Wosinska[◦], Piero Castoldi[▷]
[⋆] Linköping University, Linköping, Sweden, Email: ajmal@isy.liu.se
[◦] KTH Royal Institute of Technology, Stockholm, Sweden, Email: {pmonti,wosinska}@kth.se
[▷] Scuola Superiore Sant'Anna, Pisa, Italy, Email: {i.cerutti,p.castoldi}@sssup.it

***Abstract*—Energy and resource efficiency are two contrasting objectives to optimize in dynamic and survivable optical networks. Known solutions for improving the energy efficiency include the use of the shared path-protection (SPP) mechanism and of a low power consuming mode (i.e., sleep) for protection resources. On the other hand, resource efficiency can be improved by introducing the concept of Differentiated Reliability (DiR) which can be combined with SPP in order to match the level of provisioned protection resources to the reliability requirements for each specific demand.**

This paper assesses the energy efficiency of the DiR concept combined with SPP and sleep mode support. A multi-objective optimization algorithm is proposed with the intent of jointly optimizing the energy and resource efficiency when dynamically establishing lightpaths with specific reliability levels. Simulation results show that when the proposed multi-objective cost function is properly tuned, not only the SPP-based DiR approach reduces the blocking probability but it is also able to save power for any network load. By enabling sleep mode additional power savings can be achieved at low loads, leading to an overall saving of up to 25%.

I. Introduction

Energy saving is gaining importance in WDM networks as a way to reduce the capital expenditures of network operators. Strategies for reducing the power drained by the optical layer of survivable WDM networks mainly resort to techniques for turning off the unused devices and for sharing the devices as much as possible. The former technique can be enabled by the introduction of a *sleep mode* option in the equipment. Since the devices deployed for protection are unused most of the time (e.g., in absence of failures), they can be set to sleep and promptly re-activated when the recovery is triggered. Sleep mode for protection was proposed in [1]–[3] and is able to save significant amount of power especially at low loads, when the planning [1], [4] and the dynamic management [5] of survivable WDM networks with path protection is properly optimized. The path protection technique concerns the possibility to share protection resources among different connections, i.e., by using *shared path protection* (SPP) mechanism. Energy-efficient planning of static networks with SPP have been addressed in [6], [7]. Both techniques (i.e., sleep mode and SPP) can been exploited together [8], [9] for enhanced power saving.

When applying such energy-saving techniques in dynamic WDM networks, the drawback is a possible degradation of the network performance in terms of blocking probability [10]. This is due to the fact that the minimization of power consumption and the minimization of resource utilization are conflicting objectives, which need to be balanced so that power saving can be achieved without compromising the other network performance. For instance, the routing of the protection path for a lightpath may span on a large number of links which are shared and used only for protection, leading to a low power consumption but to a poor resource utilization in the long run.

To overcome this issue, this paper considers the concept of *Differentiated Reliability* (DiR) [11], which enables connections to have different reliability levels. In DiR the protection path need not be always available for any possible link failure scenario, resulting in a significant reduction of the resource utilization and thus blocking probability [12]. However, the impact of DiR on the power consumption of the network is still unclear. Initial finding [13] indicates that power saving up to about 20% are achievable when a static WDM network is planned in an energy-efficient way with DiR support compared to the conventional dedicated path-protection scheme. However, to the best of authors' knowledge, the tradeoff between energy efficiency and blocking probability in the presence of DiR has not been addressed yet.

The objective of this paper is two-fold. First of all, the DiR concept is applied to a dynamic WDM network with the objective of jointly optimizing energy efficiency, resource utilization, and offered reliability performance beyond the requested level (referred to as reliability excess). This requires the search for the best compromise between these contradictory objectives. In addition, the DiR technique is combined with SPP mechanism and sleep mode support, for enhanced power saving. The impact of the different energy saving techniques are assessed to offer insights on the most suitable solutions for energy saving and performance.

For this purpose, an algorithm is proposed for the dynamic selection of the working and protection paths with corresponding wavelengths, while ensuring the requested reliability level for each connection demand. Such algorithm is based on a multi-objective cost function, which accounts for these different optimization objectives in a flexible way. Moreover, a comprehensive comparison of the energy-saving techniques (e.g., DiR, SPP, and sleep mode) is carried out to assess their power saving and blocking probability, under different tuning of the multi-objective cost function.

978-1-4799-0354-2/13/$31.00 ©2013 IEEE

II. System Model and DiR Concept

This section presents the assumptions used to model the wavelength division multiplexing (WDM) network under exam, and then it provides a detailed description of the DiR concept. This work considers a generic WDM network with a mesh topology, where wavelength conversion is not available. It is assumed that only single-link failures may occur in the network, i.e., the probability that two or more links are down at the same time is considered to be negligible [14]. It is also assumed that a link failure disrupts demands in both directions of propagation.[1] The WDM network is modelled as a graph $\mathcal{G}(\mathcal{V}, \mathcal{E})$, where $\mathcal{V}$ represents the set of nodes and $\mathcal{E}$ the set of unidirectional links. Each link $(m, n) \in \mathcal{E}$ is characterized by two parameters: the set of wavelengths Λ and the value of the link failure probability ($P_f(m, n)$). For example, assuming single link failures and a uniform distribution of faults among all the links, the link failure probability is: $P_f(m, n) = |\mathcal{E}|^{-1}, \forall (m, n) \in \mathcal{E}$, where $\sum_{(m,n)\in\mathcal{E}} P_f(m, n) = 1$.

Demands are assumed to arrive randomly at the network nodes and they must be served as they are received. Each demand consists of one lightpath that needs to be provisioned between two nodes, with a given level of reliability. A demand is blocked when the network does not have enough resources for setting up the lightpath with the requested level of reliability. The reliability level is modelled in terms of *Maximum Conditional Failure Probability* (MCFP). The MCFP level represents the maximum acceptable probability that, upon a link failure, the connection will not survive. The protection scheme must satisfy this value for each demand. The possibility of assigning a MCFP value different from zero to each specific demand allows a differentiation of the provisioned level of reliability, known as the DiR concept [12].

In this work, shared path protection (SPP) is considered for protecting lightpaths affected by a single link failure. With SPP, protection resources (i.e., wavelengths) can be shared among different working lightpaths provided that they are link-disjoint. When demand d requests a reliability level $MCFP^{(d)} = 0$, the demand is provisioned with shared resources along a link-disjoint path to be 100% survivable against any single fault. For a less stringent level of MCFP (i.e., $0 < MCFP^{(d)} \leq 1$), protection need not be available for every possible link failure scenario.

Notice that, thanks to the DiR concept, two working paths having a link in common can also share protection resources if the shared link belongs to the set of unprotected links of either one of the two working paths. Similarly, it is also possible to have a working path completely unprotected provided that its path failure probability satisfies the requested MCFP level.

Fig. 1 illustrates an example of SPP-based DiR or SPP-DiR. In the figure, the links in the network are bidirectional and can accommodate two wavelengths for each direction of propagation. Assume a uniform link failure distribution, i.e., $P_f(m, n) = \frac{1}{7}\ \forall (m, n) \in \mathcal{E}$. Three demands need to be provisioned at different time instants. Demand d_1 arrives first and requires $MCFP^{(d_1)} = 0$. The selected working path is $C-B$. The protection path is $C-E-B$. Then, demand d_2 arrives with $MCFP^{(d_2)} = 0$. The selected working path is $D-E-A$. The protection path is therefore $D-C-B-A$. Finally, demand d_3 arrives and requires $MCFP^{(d_3)} = \frac{1}{7}$. This MCFP level allows demand d_3 to be protected on any link but one. Taking advantage of this possibility, it is possible to route the working path along $D-E-B$ and set link $D-E$ as unprotected. The protection path for d_3 is $D-C-B$ and is used only in the case of the failure of link (E, B). As shown in the example, protection resources on link (C, B) are shared between demands d_2 and d_3 even though their working paths are not link-disjoint. Notice that if demand d_3 would have required a higher reliability level, i.e., $MCFP^{(d_3)} < \frac{1}{7}$, such demand would have been blocked due to the lack of available wavelengths in the network.

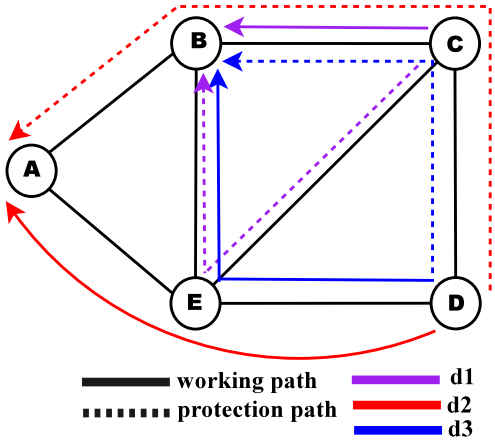

Figure 1. An example of a SPP-based protection scheme with DiR.

The SPP-DiR problem is a variation of the SPP problem, which is known to be NP-hard [15]. For this reason an energy aware SPP-DiR heuristic for routing the working and protection paths and for the selection of the protection wavelengths is proposed.

III. Energy-Aware SPP-based DiR

The Energy-Aware SPP-DiR algorithm aims at finding for each demand d a pair of working and protection paths $(w^{(d)}, b^{(d)})$ able to satisfy the wavelength continuity constraint and the $MCFP^{(d)}$ requirement while keeping both the number of used resources and the energy consumption at a minimum.

Let $\lambda_w^{(d)}, \lambda_b^{(d)} \in \Lambda$ be the wavelengths that are chosen for the working and protection paths of d, respectively. Let $H_w^{(d)}$ be the set of links that are in the working path of d. Let $H_b^{(d)}$ be the set of links that are in the protection path assigned to d. Let $H_u^{(d)} \subseteq H_w^{(d)}$ be the set of working links of d that are unprotected, i.e., upon the failure of a link in $H_u^{(d)}$ demand d is permanently disrupted. Let $MCFP^{(d)}$ be the minimum reliability degree requested by d. Let D be the set of demands that are already established in the network. Let $\hat{d}$ be an arriving

[1] This work can be extended to account for node failures, by ensuring node disjointness.

demand. Demand $\hat{d}$ is accepted and inserted in D if all the following constraints are satisfied:

- *link-disjointness*: i.e., the working and the protection path must be link-disjoint, i.e.,

$$H_w^{(\hat{d})} \cap H_b^{(\hat{d})} = \{\emptyset\}; \tag{1}$$

- *protection sharing*: a protection wavelength cannot be shared by multiple demands if they share the same (protected) working link, i.e.,

$$\forall d \in D, d \neq \hat{d}: \begin{cases} (H_w^{(d)} \setminus H_u^{(d)}) \cap (H_w^{(\hat{d})} \setminus H_u^{(\hat{d})}) \neq \{\emptyset\} \\ H_b^{(d)} \cap H_b^{(\hat{d})} = \{\emptyset\} \ \vee \ \lambda_b^{(d)} \neq \lambda_b^{(\hat{d})}; \end{cases} \tag{2}$$

- *MCFP requirement*: the conditional failure probability guaranteed to demand $\hat{d}$ does not exceed the $MCFP^{(\hat{d})}$ required by $\hat{d}$, i.e.,

$$P_f^{(\hat{d})} = \sum_{(m,n) \in H_u^{(\hat{d})}} P_f(m,n) \leq MCFP^{(\hat{d})}. \tag{3}$$

If any of the above constraints cannot be satisfied, demand $\hat{d}$ is blocked. Notice that the protection paths of demands $\hat{d}$ and $d \in D$ are allowed to share a wavelength $\lambda_b^{(\hat{d})} = \lambda_b^{(d)}$, i.e., only if the following constraint is satisfied:

$$(H_w^{(\hat{d})} \cap H_w^{(d)}) \subseteq (H_u^{(\hat{d})} \cup H_u^{(d)}). \tag{4}$$

The selection of the routing and wavelength for $\hat{d}$ (i.e., $w_i^{(\hat{d})}$, $b_j^{(\hat{d})}$ and $\lambda_{b_j}^{(\hat{d})}$) is jointly optimized for the number of resources used, the power consumption, and the excess of reliability[2]. The cost function, $C_{i,j,k}^{(\hat{d})}$, is a linear combination of these three quantities weighted with coefficient γ for the resource cost, coefficient η for the power consumption, and a unitary coefficient for the excess of reliability.

$$C_{i,j,k}^{(\hat{d})} = \gamma \cdot \left(|H_{w_i}^{(\hat{d})}| + |H_{b_j}^{(\hat{d})}| - |H_{s_{(i,j,k)}}^{(\hat{d})}| \right) + \eta \cdot \left(P_{w_i} + P_{b_{(j,k)}} \right) + \left(MCFP^{(\hat{d})} - P_{f_{(i,j,k)}}^{(\hat{d})} \right). \tag{5}$$

The first term in (5) gives an estimation of the resources (that is number of links on which wavelengths are to be reserved) needed to provision $\hat{d}$ on $w_i^{(\hat{d})}$ and $b_j^{(\hat{d})}$ using wavelength $\lambda_{b_j}^{(\hat{d})} = \lambda_k$ for $b_j^{(\hat{d})}$. Shared resources are accounted by subtracting the number of protection links in which the protection wavelength is shared, i.e., $|H_s^{(\hat{d})}|$, with $H_s^{(\hat{d})} \subseteq H_b^{(\hat{d})}$. The second term accounts for both the power consumption of $w_i^{(\hat{d})}$ and $b_j^{(\hat{d})}$, i.e., P_{w_i} and P_{b_j} (see Sec. IV). Finally, the third term includes the excess of reliability defined as the difference between the required $MCFP^{(\hat{d})}$ level and the value of $P_{f_{(i,j,k)}}^{(\hat{d})}$ computed as in (3) for the specific triplet $w_i^{(\hat{d})}$, $b_j^{(\hat{d})}$, and $\lambda_{b_j}^{(\hat{d})} = \lambda_k$.

[2]Note that the choice of for the wavelength of the working path has no impact on the cost function.

Algorithm 1 Energy-Aware SPP-based DiR

1: $\mathcal{G}(\mathcal{V}, \mathcal{E})$: network topology;
2: $\hat{d}$: lightpath demand;
3: $W^{(\hat{d})}$: set working paths for $\hat{d}$ sorted for hop length;
4: $B^{(\hat{d})}$: set protection paths for $\hat{d}$ sorted for hop length for path $w_i^{(\hat{d})}$;
5: Initialization: $\widetilde{C} = -1$;
6: **for** each path $w_i^{(\hat{d})} \in W^{(\hat{d})}$ **do**
7: Let $\Lambda_{w_i}^{(\hat{d})}$ be set of continuous wavelengths for $w_i^{(\hat{d})}$;
8: **if** $\Lambda_{w_i}^{(\hat{d})} \neq \emptyset$ **then**
9: **for** each $b_j^{(\hat{d})} \in B^{(\hat{d})}$: $H_w^{(\hat{d})} \cap H_b^{(\hat{d})} = \{\emptyset\}$ (Eq. (1)) **do**
10: Let $\Lambda_{b_i}^{(\hat{d})}$ be the set of continuous wavelengths for $b_j^{(\hat{d})}$;
11: **if** $\Lambda_{b_i}^{(\hat{d})} \neq \{\emptyset\}$ **then**
12: **for** each $\lambda_k \in \Lambda_{b_i}^{(\hat{d})}$ **do**
13: **if** $w_i^{(\hat{d})}, b_j^{(\hat{d})}, \lambda_k$ satisfy Eqs. (2) and (3) **then**
14: Compute cost $C_{i,j,k}^{(\hat{d})}$ (Eq. (5));
15: **end if**
16: **end for**
17: **end if**
18: **end for**
19: **end if**
20: **end for**
21: Select $w_i^{(\hat{d})}$, $b_j^{(\hat{d})}$ and λ_k : $\widetilde{C} = \min_{i,j,k}\{C_{i,j,k}^{(\hat{d})}\}$;
22: **if** $\widetilde{C} \neq -1$ **then**
23: Return $w_i^{(\hat{d})}$, $b_j^{(\hat{d})}$, λ_k, $\Lambda_{w_i}^{(\hat{d})}$;
24: **else**
25: Block $\hat{d}$;
26: **end if**

Algorithm 1 aims at computing the routing of both the working and protection paths, and at selecting the protection resources for each arriving demand $\hat{d}$. The route of the working path (i.e., $w^{(\hat{d})}$) is selected within a set of pre-computed candidates $W^{(\hat{d})}$. For path $w^{(\hat{d})}$, the route of the protection path (i.e., $b^{(\hat{d})}$) is selected among a number of pre-computed candidates $B^{(\hat{d})}$. First, the algorithm checks the wavelength availability for the working path by starting from the first path in $W^{(\hat{d})}$, $w_1^{(\hat{d})}$. If the same wavelength is not available on all the links of $w_1^{(\hat{d})}$, the path is discarded and the next path in $W^{(\hat{d})}$ is considered. Otherwise a link-disjoint protection paths in $B^{(\hat{d})}$ is considered (i.e., satisfying the link disjoint constraint in Eq. (1)). For each link-disjoint path in $B^{(\hat{d})}$, $b_j^{(\hat{d})}$, the resource availability is checked. First the set of available continuous wavelengths ($\Lambda_{b_i}^{(\hat{d})}$) is computed, then each $\lambda_k \in \Lambda_{b_i}^{(\hat{d})}$ is checked. If λ_k is already used for protection purposes by other protection paths the protection sharing constraint (Eq. (2)) is checked. If satisfied and if the MCFP requirement (Eq. (3)) is met, then the triplet w_i, b_j, and λ_k is a feasible solution

and the value of $C_{i,j,k}^{(\hat{d})}$ is computed (Eq. (5)). Among all the feasible solutions, the one at minimum cost $C_{i,j,k}^{(\hat{d})}$ is selected. If a feasible solution is not found, then the lightpath demand $\hat{d}$ is blocked. Finally, the wavelength for the working path $\lambda_w^{(\hat{d})}$ is selected within the set of available wavelengths $\Lambda_{w_i}^{(\hat{d})}$ using the first-fit strategy. The computational complexity of Algorithm 1 is $O[|W^{(\hat{d})}||B^{(\hat{d})}||D||\Lambda||\mathcal{V}|^3]$. The number of provisioning demands, $|D|$, can be upper bounded by $O[|\mathcal{E}||\Lambda|]$, leading to an overall complexity of $O[|W^{(\hat{d})}||B^{(\hat{d})}||\mathcal{E}||\Lambda|^2|\mathcal{V}|^3]$.

IV. Sleep Mode and Power Model

For higher energy efficiency, sleep (i.e., idle) mode can be enabled at the optical layer. The optical devices that are unused are turned off and disconnected from the WDM and the electrical network. Optical devices used only for protection purposes are set in idle state and they consume a (possibly) low amount of power to ensure that they can be promptly activated at any moment.

For a WDM network operating at 40 Gb/s, the optical devices draining power are: OXC controllers (150 W at each node) [16], in-line amplifiers (155 W + 55 W $\times$ 80 km) [17], transmitters and receivers. A transmitter and receiver include drivers (2×9 W), laser (6.6 W), photodiode and transimpedence amplifier (2×0.4 W), ADC (2×2 W), and management (20% of the overall power) [3]. When supporting sleep mode, the drivers and the ADC of the transmitter for the protection can be set to idle, leading to a saving of 26.92 W. Similarly, if sleep mode is enabled and a link is supporting only protection paths, the in-line amplifiers along the links are set to idle, leading to a negligible amount of power.

In the cost function $C_{i,j,k}^{(\hat{d})}$ in Eq. (5), the total power consumed by a working (P_w) and a protection (P_b) path is the sum of the power drained by the devices traversed by each path (i.e., transmitters and receivers, OXC controllers, and amplifiers) according to the operational state (active vs. idle vs. off) that would be enabled after the connection is established.

V. Numerical Results

The performance of the proposed energy-aware SPP-based DiR algorithm is assessed with a custom-built event-driven simulator. The evaluation is carried out on the Pan-European topology (COST 239) [18], which consists of 11 nodes and 52 unidirectional links with 16 wavelengths per link.

The link failure probability is derived using a uniform distribution of failures, that is $P_f(m,n) = \frac{1}{52}\ \forall (m,n) \in \mathcal{E}$. Demands are assumed to arrive in the network following a Poisson process. Established lightpaths are assumed to have an exponentially distributed duration, whose average value is set to 1. It is also assumed that detailed link status information is promptly disseminated throughout the network so that each node controller can execute the proposed algorithm with updated information. Also, the latency for reserving the network resources is considered negligible.

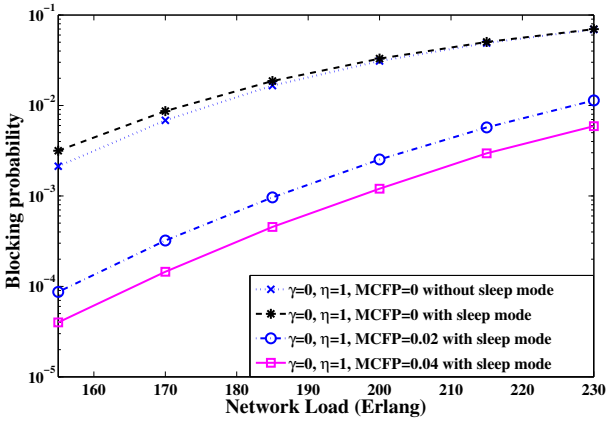

Figure 2. Blocking probability versus offered network load when minimizing power consumption.

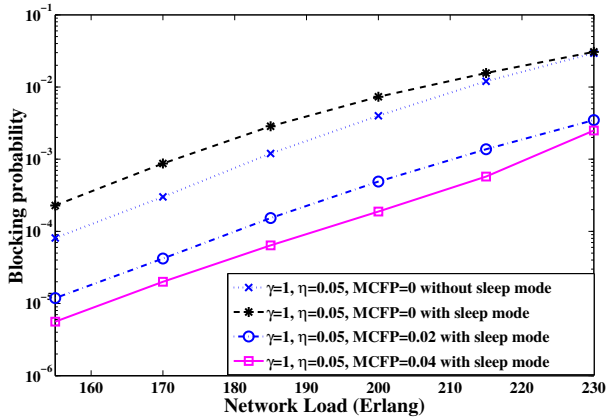

Figure 3. Blocking probability versus offered network load when minimizing power consumption and then resource utilization.

Demands are uniformly distributed among all node pairs. Unless otherwise specified, each demand is assigned the same reliability requirement $MCFP = MCFP^{(d)} = 0.02,\ \forall d$. With this value and in the network topology under consideration, each demand may be able to have up one working link that is unprotected ($|H_u^{(d)}| = 1,\ \forall d$). The number of candidate routes for each working path and for each protection path of a given candidate working path is set to 5 ($|W^{(d)}| = |B^{(d)}| = 5,\ \forall d$), which are computed using K shortest path routing [19]. Simulation results are collected to achieve a confidence interval of 6% or better with 90% confidence level. The performance of enabling DiR and sleep mode is assessed in terms of average blocking probability and time-averaged power per established lightpath.

The average blocking probability as a function of the load is evaluated in Figs. 2-4. In Fig. 2, the cost function is tuned for minimizing the power consumption, i.e., $\gamma = 0,\ \eta = 1$. The impact of the MCFP level and sleep mode is assessed. Two insights can be gained. First, the blocking probability slightly increased when enabling sleep mode. The reason is that, for the working lightpaths, in the presence of sleep mode the cost function forces the selection of longer paths (i.e., to set as much as possible resources in sleep mode) rather than shorter ones but without sleeping links. In turn, this leads to a higher resource utilization and thus higher blocking. Second,

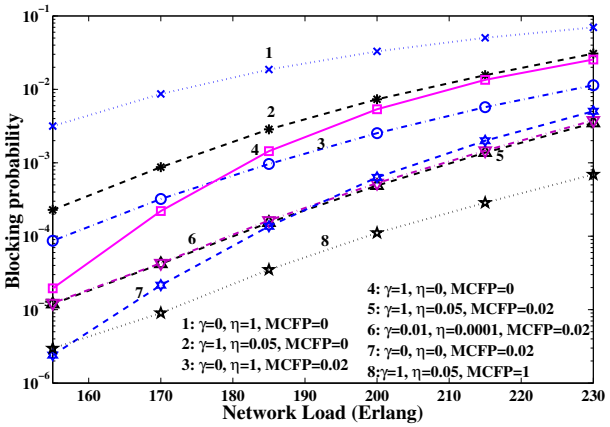

Figure 4. Blocking probability versus offered network load for different combinations of the cost coefficients.

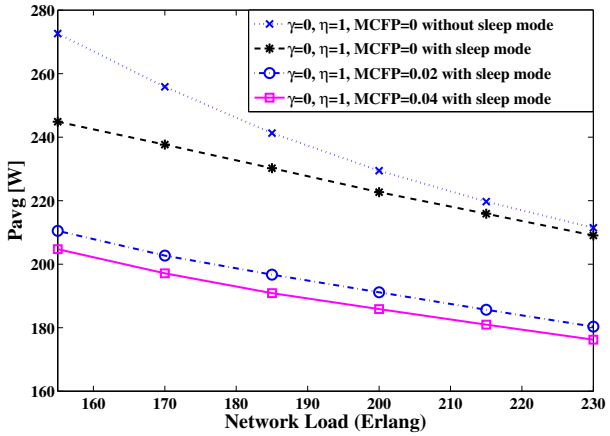

Figure 5. Avg. power per established lightpath versus offered network load when minimizing the power consumption.

an improvement of more than one order of magnitude in blocking probability can be achieved when a lower reliability level is requested ($MCFP = 0.02$). However, if the reliability level is further decreased (e.g., $MCFP = 0.04$), the marginal improvement reduces.

Fig. 3 shows the value of the blocking probability when the cost function aims at minimizing the power consumption as primary objective and the resource utilization as a secondary objective. By accounting also for the resource utilization, the blocking probability is reduced by more than one order of magnitude with respect to the results for power optimization only (Fig. 2), for all the different scenarios.

Fig. 4 considers different optimization functions. When the primary objective is the resource minimization, the blocking probability slightly improves with respect to the case of minimizing also the power consumption (Fig. 3) but only at low loads. For $MCFP = 0.02$, the difference of blocking probability is modest when changing the cost coefficient γ and η so that resource minimization becomes the primary objective (curves 5 and 6). However, when minimizing the excess of reliability (i.e., $\gamma = 0$, $\eta = 0$), sharing of resources is not incentivized leading to lower blocking probability when the load is low, but higher blocking probability when the load is high.

The average power consumption (per established lightpath)

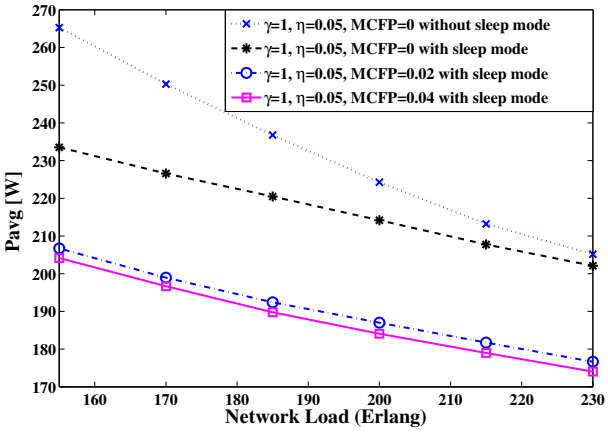

Figure 6. Avg. power per established lightpath versus offered network load when minimizing the power consumption and then the resource utilization.

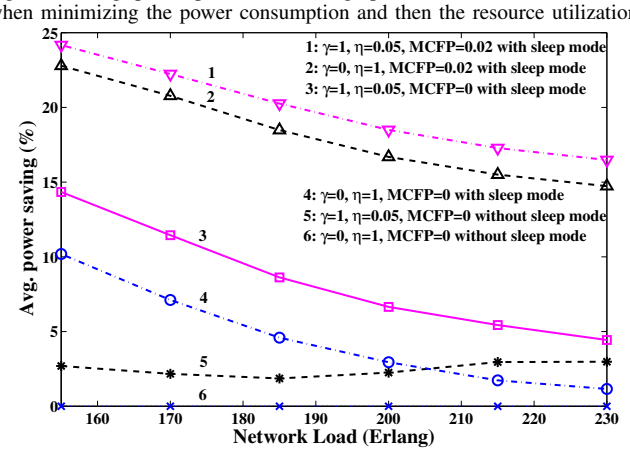

Figure 7. Average power saving versus offered network load.

as a function of the load is evaluated in Figs. 5-8. In Fig. 5, the cost function is tuned for minimizing the power consumption, i.e., $\gamma = 0$, $\eta = 1$. The power consumption per lightpath decreases with the offered network load. The main reason is that the power consumption of load-independent devices (e.g., power consumption of in-line amplifiers, which can be considered independent of the number of amplified working lightpaths) can be shared among a larger number of lightpaths. By introducing the sleep mode, the slope of the curve is reduced, meaning that less power is wasted at low loads for powering scarcely used resources. This results in a power saving of about 10% at low loads. By closely matching the connection reliability level ($MCFP = 0.02$), the power saving can be further improved by 13%. However, there is no significant advantage in further increasing MCFP (e.g., $MCFP = 0.04$). This limitation is mainly due to the network topology, which is highly connected. Indeed the network connectivity leads to paths with short hop lengths, making it difficult to find protection paths in which more than one link can be unprotected.

Fig. 6 shows the average power consumption per lightpath when the cost function aims at minimizing the power consumption as primary objective and the resource utilization as secondary objective. The curves experience the same trend as in Fig. 5. However, by incorporating the resource cost factor (i.e., setting $\gamma = 1$) in the optimization function, the power

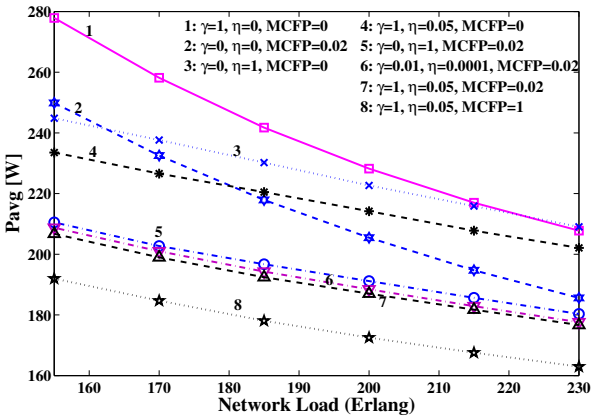

Figure 8. Avg. power per established lightpath versus offered network load, for different combinations of the cost coefficient.

consumption reduces compared to Fig. 5. This unexpected result can be explained by the fact that among the different solutions at minimum power the one using less resources is selected. This at the end ensures that each provisioned demand uses overall less resources, leading to an overall energy saving.

The average power savings of the different cases with respect to the conventional energy-aware SPP (i.e., $\gamma = 0$, $\eta = 1$ and $MCFP = 0$) with sleep mode disabled is assessed in Fig. 7. Sleep mode enables savings up to 10% at low loads, but these benefits rapidly decrease at high loads. A more significant power saving, almost independent of the load, is achievable by introducing DiR. The highest power saving, up to 25%, is achieved by jointly optimizing power consumption and resource utilization ($\gamma = 1$, $\eta = 0.05$, $MCFP = 0.02$) while enabling DiR and sleep mode.

The impact of the selected optimization function on the power consumption is further analyzed in Fig. 8. For $MCFP = 0.02$, minimal differences in terms of power consumption are observed when the coefficient γ and η are varied to minimize either the network power or the wavelength resources used (curves 5, 6, and 7). However, when minimizing the reliability excess (i.e., $\gamma = 0$, $\eta = 0$ and $MCFP = 0.02$) the average power consumption of the lightpath demands is exacerbated compared to other combinations of the cost coefficient. This is because the strategy ignores the sharing of resources and active devices, and thus it selects the paths that match the MCFP level regardless of their hop length and power consumption.

VI. Conclusion

In this paper, the DiR concept has been combined with SPP and sleep mode to enable an energy-efficient utilization of resource in dynamic WDM network, while guaranteeing the required reliability level for each connection. An algorithm for routing working and protection paths, for selecting the corresponding wavelength, and for ensuring the requested maximum conditional failure probability is proposed, which aims at optimizing the weighted combination of power consumption, resource utilization, and reliability excess.

Simulation results show that the energy aware SPP-based DiR is able to improve not only the blocking probability [11] but also the power consumption. Both benefits are achievable when the multi-objective function is tuned to minimize both the power consumption and the resource utilization, which favors the sharing of protection and the minimization of the used resources.

On the other hand, sleep mode enables power saving at low loads but leads to higher blocking probability. However, when sleep mode is combined with the energy aware SPP-based DiR, up to 25% of power is saved while the blocking probability is reduced by up to one order of magnitude even at 98% reliability levels, with respect to the conventional SPP without sleep mode.

Acknowledgment

This work has been carried out with the partial support of ARNO-T3 project funded by Tuscany region (Italy) under PAR FAR 2007-2013 and by the FP7/2007-2013 program under grant agreement no 318137 (ICT-DISCUS).

References

[1] A. Muhammad and et al., "Energy-efficient WDM network planning with dedicated protection resources in sleep mode," in *GLOBECOM proc.*, 2010.

[2] F. Musumeci and et al., "Energy-efficiency of protected IP-over-WDM networks with sleep-mode devices," *J. High Speed Networks*, vol. 19, no. 1, pp. 19–32, 2013.

[3] A. Morea and et al., "Power management of optoelectronic interfaces for dynamic optical networks," in *ECOC proc.* IEEE, 2011, pp. 1–3.

[4] P. Monti and et al., "Energy-efficient lightpath provisioning in a static WDM network with dedicated path protection," in *ICTON proc.*, 2011.

[5] A. Jirattigalachote and et al., "Dynamic provisioning strategies for energy efficient WDM networks with dedicated path protection," *Optical Switching and Networking*, vol. 8, no. 3, pp. 201–213, 2011.

[6] C. Cavdar and et al., "Energy-efficient design of survivable WDM networks with shared backup," in *GLOBECOM*, 2010.

[7] S. S. Jalalinia and et al., "Survivable green optical backbone networks with shared path protection," in *OFC proc.*, 2012.

[8] N.-H. Bao and et al., "Power-aware provisioning strategy with shared path protection in optical WDM networks," *Optical Fiber Technology*, vol. 18, no. 2, pp. 81–87, 2012.

[9] R. He and et al., "Dynamic power-aware shared path protection algorithms in WDM mesh networks," *J. of Comm.*, vol. 8, no. 1, pp. 55–65, 2013.

[10] P. Wiatr and et al., "Power savings versus network performance in dynamically provisioned wdm networks," *IEEE Communication Magazine*, vol. 50, no. 54, pp. 48–55, May 2012.

[11] A. Fumagalli and et al., "Differentiated reliability (DiR) in WDM rings without wavelength converters," in *ICC proc.*, 2001.

[12] P. Monti and et al., "Resource-efficient path-protection schemes and online selection of routes in reliable WDM networks," *J. Opt. Netw.*, vol. 3, no. 4, pp. 188–203, Apr 2004.

[13] J. L. Vizcaino and et al., "Differentiated quality of protection to improve energy efficiency of survivable optical transport networks," in *OFC proc.*, 2013.

[14] S. Ramamurthy and et al., "Survivable WDM mesh networks, Part I - Protection," in *INFOCOM proc.*, 1999, pp. 21–25.

[15] C. Ou and et al., "New and improved approaches for shared-path protection in wdm mesh networks," *Lightwave Technology, Journal of*, vol. 22, no. 5, pp. 1223–1232, 2004.

[16] S. Aleksic, "Analysis of power consumption in future high-capacity network nodes," *IEEE/OSA JOCN*, vol. 1, no. 3, 2009.

[17] W. Van Heddeghem and et al., "Power consumption modeling in optical multilayer networks," *Photonic Network Comm.*, vol. 24, no. 2, pp. 1–17, 2012.

[18] P. Batchelor and et al., "Study on the implementation of optical transparent transport networks in the european environment results of the research project cost 239," *Photonic Network Communications*, vol. 2, no. 1, pp. 15–32, 2000.

[19] V. Jimenez and et al., "Computing the k shortest paths: A new algorithm and an experimental comparison," *Springer*, vol. 1668, pp. 15–29, 1999.

Dynamic Energy Management Employing Renewable Energy Sources in IP over DWDM Networks

Xin Chen, Chris Phillips
EECS
Queen Mary,University of London
Mile End Road, London, United Kingdom, E1 4NS
Email: {xin.chen,chris.phillips}@eecs.qmul.ac.uk

Jiayuan Wang, Sarah Reupp
FOTONIK
Technical University of Denmark
Kgs. Lyngby, Denmark 2800
Email: {jwan,srru}@fotonik.dtu.dk

***Abstract*—The continued growth of energy consumption has been one of the main constraints for the development of the Internet. The increasing emissions of greenhouse gases associated with electricity generation also raise public concern for the environment. In this paper, we propose a dynamic energy management framework employing renewable energy sources in IP over DWDM core networks. The main concept is to combine infrastructure sleeping and virtual router migration to improve the network energy efficiency. By using the energy source information provided by the smart grid, the nodes that are powered by a renewable energy source are selected, where possible, for hosting virtual routers during off-peak hours. Therefore, the energy consumption and CO_2 emissions are both reduced. A heuristic algorithm based on a multi-objective evolutionary algorithm is proposed to select appropriate physical platforms to host the virtual routers.**

I. Introduction

Telecommunications infrastructure consumes about 1% of the world's total electricity [1]. The growing traffic demand gives rise to rapidly increasing energy consumption. In the next 10 years, it is predicted that the traffic will increase by 1200%, which corresponds to a 150% increase of energy consumption [2]. If no effective way to improve the energy efficiency is found, the energy consumption issue is likely to become one of the main constraints for the future development of the Internet [3]. The increasing greenhouse gas emissions, mainly CO_2, associated with electricity generation have also been a threat to the environment and climate. It is a worldwide goal to reduce the energy consumption and CO_2 emissions. With the development of smart grid networks, network operators will have the possibility to choose their energy supply from a variety of energy sources. There are large differences between CO_2 emissions among different energy sources. For example, for generating the same amount of electricity, the CO_2 emission of traditional energy sources (e.g. coal and fossil fuel) is around 30 times larger than that of green energy sources (e.g. solar and wind) [4]. This makes greener energy sources an attractive proposition when considering reducing CO_2 emissions. In this paper, we propose a dynamic energy management framework for the IP over DWDM core networks exploiting renewable energy sources for reducing the energy consumption and CO_2 emissions. The actual network is considered to be two conceptually separated networks: a substrate network and a virtualization network. In the substrate network, each node is a physical platform (PP) providing the hardware support for one or more virtual router instances. A virtualization network exists above the substrate network, which is composed of a set of virtual routers (VRs). The virtual network manages, configures and monitors the routing functionalities. The research goal is to move VRs onto fewer PPs and place the unused PPs in a sleep mode to save energy during the off-peak hours. The sleeping PPs are awakened again during busy periods. The approach is considered together with energy source information, i.e. when consolidating the VRs onto fewer PPs, the nodes employing renewable energy sources are preferred in order to further reduce the CO_2 emissions.

The rest of this paper is organized as follows. The related work is described in Section II and the energy model and CO_2 emissions model are introduced in Section III. In Section IV, the operating procedure of the novel dynamic energy management framework is described. Section V provides an introduction to the heuristic algorithm used for selecting the appropriate destination PPs. This is followed by a description of the simulation modelling in section VI. Simulation results and a discussion are presented in Section VII. Finally, Section VIII concludes the paper.

II. Related Work

Currently, the majority of energy usage is associated with the access networks of the overall Internet. Since the access networks (often Passive Optical Network (PON) systems) can scale to higher access rates with only minor power consumption increases, the power consumption of PONs will probably remain relatively constant [1]. Conversely, the power consumption of backbone network (switches and routers) may become the dominant consumer in future and research into energy efficient core networks is ongoing [5].

978-1-4799-0354-2/13/$31.00 ©2013 IEEE

There are various types of energy efficient solutions. Some work focuses on static mechanisms which aim to design (i.e. plan) the network system in an energy-efficient manner. With known traffic demands, the problem is considered in a global fashion for minimizing the network energy consumption whilst maintaining the quality of service. For example, some work uses Integrated Linear Programming (ILP)/Mixed Integrated linear Programming (MILP) to plan power-aware networks [6]. Some studies consider dynamic adaptation [7], which modulate the capacities of the network resources according to current traffic loads and service requirements. These include approaches such as rate adaption and infrastructure sleeping. Infrastructure sleeping enables equipment to be switched off during the off-peak hours. The traffic demand in a core network typically has a regular diurnal pattern based on the activity of the users, which is high during working hours and much lower during hours normally associated with sleep [8] [9]. Sergui et al [10] discussed and evaluated several simple sleeping schemes by testing them with real-world traffic workloads and topologies. However, the major disadvantage of infrastructure sleeping is that when a router is switched off, the router loses the ability to exchange routing protocol signaling messages. In other words, the logical IP-layer topology changes when a node disappears. As a consequence, it triggers a reconvergence event that can cause network discontinuities and disruption. Therefore, the virtual router migration (VRM) approach is used [10] [11]for concealing changes in the substrate network configuration form the IP-layer topology whist effectively turning off physical platforms. Because employing the renewable energy sources can lower CO_2 emissions, it have been considered for improving the energy efficiency in wireless communication networks [13], data centers [14] and core networks [15].

III. Energy and CO_2 Emission Model

For estimating the energy consumption and CO_2 emissions of a network employing dynamic energy management, separate energy and CO_2 emission models are proposed. The CO_2 emission model is derived from the energy model. For the energy model, the following components are included in the energy consumption considerations:

1.Physical Platform (PP). The energy consumption of a PP is made up of static and dynamic sections. The static section represents the base system (including chassis, switch fabric and route processor). The dynamic section covers line card power consumption which is traffic dependent, based on whether the card is active or asleep. In our scenario, a PP also has active and sleep states. When a PP enters the sleep state, the base system and the line cards stop working except for a management module which is maintained for receiving the signaling messages. Thus, a sleeping PP consumes a small fraction of the active base system power. In addition, line card(s) can be turned off individually depending on the VR requirements that the PP is hosting.

2.Reconfigurable Optical Add Drop Multiplexer (ROADM). The ROADM provides a flexible way of adding, dropping or switching any wavelength to any node. All ROADMs remain active in order to support the traffic transmission in the optical layer.

3.Optical Amplifier (OA). We assume that the energy consumption of OAs is not depending on the traffic and OA amplifies the entire C-band.

The power consumption of a working PP P_{ppw} can thus be represented as:

$$P_{ppw} = P_{base} + \kappa \cdot P_{lc} \tag{1}$$

where P_{base} denotes the PP base system power consumption. κ is the number of active line cards on the PP. And it is dynamic depending upon the VR requirements that the PP is hosting. P_{lc} represents the power consumption of a line card.

The power consumption of a sleeping PP P_{pps} is thus:

$$P_{pps} = \theta \cdot P_{base} \tag{2}$$

where θ is a fraction of a sleeping PP of the base system power consumption.

The OA power consumption P_{OA} in a network with N nodes is:

$$P_{OA} = \sum_{i,j=1;i\neq j}^{N} \left\lceil \frac{d_{i,j}}{\delta_{OA}} \right\rceil \cdot e_{OA} \tag{3}$$

where $d_{i,j}$ stands for the physical link length between node i and node j. e_{OA} is the power consumption of an optical amplifier, δ_{OA} is the maximum allowed link length without need of amplifying.

The ROADM is assumed to be always on and a PP connects with a ROADM. The total power consumption P_{total} is:

$$P_{total} = \alpha \cdot P_{ppw} + (N-\alpha) \cdot P_{pps} + N \cdot P_{roadm} + P_{OA} \tag{4}$$

where α is the number of active PPs and N is the number of ROADMs in the network. Combining from Eq.(1) to Eq.(4), P_{total} can be expressed as:

$$P_{total} = \alpha \cdot P_{base} + \sum_{i=1}^{\alpha} \kappa_i \cdot P_{lc} + \theta \cdot (N-\alpha) \cdot P_{base} + N \cdot P_{roadm} + \sum_{i,j=1;i\neq j}^{N} \left\lceil \frac{d_{i,j}}{\delta_{OA}} \right\rceil \cdot e_{OA} \tag{5}$$

For the CO_2 emissions, all nodes are assumed to initially use a dirty energy sources (i.e. coal) until the energy source changing time. The energy source of each node changes every h period with a random selection shown in Table I. The total CO_2 emissions, CE, in a network with N nodes is expressed as:

$$CE = \sum_{i=1}^{N} \sum_{j=1}^{\left\lfloor \frac{T-t_s^{i,1}}{h} \right\rfloor + 2} S_{i,j} \cdot E_{i,j} \tag{6}$$

where T is the total simulation time and $t_s^{i,1}$ is the first energy source changing time of node i. $\left\lfloor \frac{T-t_s^{i,1}}{h} \right\rfloor + 2$ stands for

TABLE I
SUMMARY OF LIFECYCLE CO2 EMISSION INTENSITY. [4]

Energy Source	CO_2 $(Tonnes/GWh)$
Coal	888
Oil	733
Natural Gas	499
Solar	85
Biomass	45
Nuclear	29
Hydroelectric	26
Wind	26

the times of energy source changes. $S_{i,j}$ represents the CO_2 emission intensity of the jth period of node i and $E_{i,j}$ is the energy consumption of the jth period of node i.

When a virtual router migration(VRM) happens, the network power consumption may vary. In the jth period of node i, $M_{i,j}$ times of VRM happen, and then $E_{i,j}$ is:

$$E_{i,j} = \left(t_m^1 - t_m^0\right) \cdot P_{i,j}^1 + \sum_{k=2}^{M_{i,j}} \left(t_m^k - t_m^{k-1}\right) \cdot P_{i,j}^k + \left(t_m^n - t_m^{M_{i,j}}\right) \cdot P_{i,j}^n \quad (7)$$

where t_m^1 is the first VRM happening time and t_m^k is the kth VRM happening time in the jth period of node i. t_m^0 is the start time and t_m^n is the end time of a period. $P_{i,j}^1$ represents the first power consumption before the first VRM. $P_{i,j}^k$ is the power consumption after the kth VRM happening time and $P_{i,j}^n$ is the power consumption after $M_{i,j}$th VRM to the end of jth period.

IV. DYNAMIC ENERGY MANAGEMENT PROCEDURE

In this section, the operating procedure of the novel dynamic energy management framework with renewable energy sources is described. The flowchart is shown in Fig. 1. Initially, all nodes use coal based energy sources and all PPs are working. The energy source of each node is changed periodically (e.g. every 3h, 6h and so forth). Typically the network information is monitored at 5 minute intervals. The information includes the network traffic load, the PP state, the energy sources being used and the optical resources. A PP has three operating modes whilst it is active: **Quiet, Normal and Busy**. Thresholds are defined to distinguish between the Quiet, Normal and Busy modes. A PP is lightly loaded if the PP's utilization is lower than the Quiet threshold. A PP is Busy if its utilization is higher than the Busy threshold. The collected information is used for determining whether the network state matches the conditions suitable for migration. There are either of two conditions needed to trigger Virtual Router Migration(VRM). The first condition is that some PPs enter their Quiet mode. The VRs can then potentially be consolidated onto fewer PPs and the PPs which do not accommodate any VRs can be placed in their sleep state. The second condition is that some PPs enter their Busy mode. In this case, some VRs are moved away from the busy PPs. For selecting the appropriate destination PPs for VRs, VRM_CO2 algorithm (described in Section V) is invoked. After obtaining a viable solution for possible VR destinations, new optical connections are established for redirecting the traffic to these remotely relocated VRs. Finally, after the VR(s) are moved to their appropriate destination PP(s) based on the identified solution, the corresponding PPs are put to sleep (or reawakened).

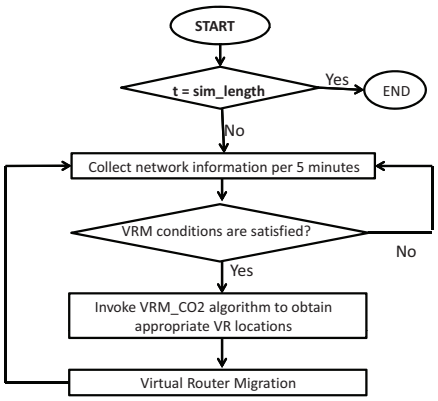

Fig. 1. The Framework Flowchart

V. HEURISTIC ALGORITHM

A heuristic algorithm called VRM_CO2 based on Multi-Objective Evolutionary Algorithms (MOEAs) is developed to select the appropriate locations for VRs. MOEAs use evolutionary methodologies to solve the problems involving multiple conflicting objectives and an intractably large and highly complex search space. The goal of MOEAs is to find a group of trade-off solutions called a Pareto-optimal solution set and then a preferred solution can be chosen based on user-defined criteria. A flowchart for the heuristic algorithm is shown in Fig.2. MOEAs work on a set of candidate solutions called a population. By employing two basic principles: selection and reproduction, the population is modified generation after generation. During the selection process, the fittest individuals have a greater chance of survival and are put into the mating pool. In reproduction step, the solutions in the mating pool are used to create new solutions by mutation and crossover. When the terminal condition is reached, such as reaching a given number of iterations the simulation stops and a group of good solutions are obtained. More detail of MOEAs can be found in our previous work [16], which contains a two-objective evolutionary algorithm. In this work, the following three objectives are considered in VRM_CO2:

1) **Power Consumption.** The power consumption of a solution can be calculated from Eq.(5). The objective is to minimize the number of active PPs without detrimentally impacting on performance of any VRs.
2) **VRM Cost.** The VRM cost for a moved VR contains two parts. The first part depends on hop count between default PP to destination PP locations. Each VR has a default PP. Traffic that enters from the access network is always processed by a particular VR. If the VR moves

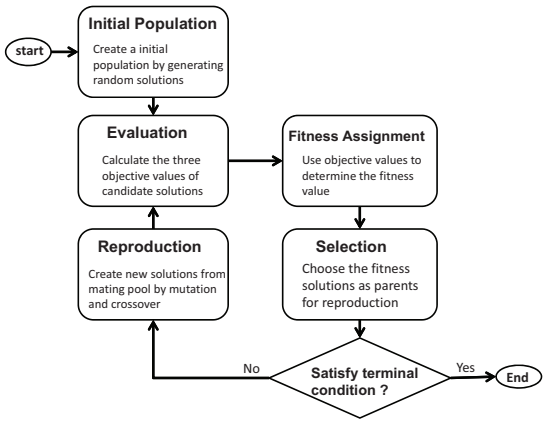

Fig. 2. Heuristic Algorithm Flowchart

away from its default PP, some additional optical connections are needed for redirecting the data traffic from its default point of entry to the remotely located VR. The second part is the hop count from the current PP to destination PP locations. If current PP and destination PP is far away from each other, it will use a longer optical channel to transmit the VR instance.

3) **Energy Source.** The energy source information of each node is known from the smart grid. When choosing the appropriate destination PPs, the nodes employing renewable energy sources are preferred.

VI. Simulation Modelling

Two network topologies are used in our simulation: a simple 6-node 8-links network (6N8L) and NSFNET (14N21L) [17]. The traffic load changes according to a sinusoidal function [18] with added noise:

$$t^{sd}(t) = t^{sd} \cdot \left[\frac{1-\gamma}{2} \left(1 + sin\left(2\pi \cdot f_0 \cdot t\right)\right) + \gamma \right] + \epsilon \quad (8)$$

where t^{sd} is the average amount of traffic going from source node s = 1,...,N to destination node d = 1,...,N. A similar daily traffic pattern is used for each VR source-destination pair. f_0 is a time related parameter. γ is a parameter to control the off-peak time traffic percentage. For example, if the off-peak traffic is equal to 30% of the peak traffic, the value of γ is 0.3. We set the off-peak period traffic to be 20% of the peak load. ϵ is a random noise variable. The time index in the simulation does not correspond with hours in a natural day. The traffic is generated based on a sinusoidal wave function with added noise. Therefore, the peak period is from around hours 4 to 10 and the off-peak period is from hours 16 to 22. All the PPs are homogeneous. PPs have 1 $Tbps$ switch fabric capacity and support a maximum of 16 active line cards. The threshold for the Quiet mode is 30% and Busy threshold is 80%. Initially, each VR runs on its default PP. The fiber is unidirectional and each fiber contains 40 $\times$ 40Gps channels. The first fit algorithm is used for allocating the channels.

TABLE II
Power Consumption of Network Architecture [19], [20], [21]

Name	Power Consumption (W)
PP Base System	5800
Line Card	550
ROADM	350
OA	10

After a channel is established, we assume it lasts for 6 hours. The network information is collected every 5 minutes and the energy source changing interval is 6 hours. In the heuristic algorithm, the population size is 50 in the 6N8L network and 100 in the 14N21L network. The crossover rate is 0.9 and mutation rate is 0.1. The number of generations of the 6N8L network is 2000 and is 20000 for the 14N21L network. When the generation count reaches the maximum, the algorithm stops and a group of potentially viable solutions is obtained. The simulated duration with the 6N8L network is 30 days and 10 days for the 14N21L network. The power consumption data are taken from the existing commercial products. Table II shows the power consumption of the equipment employed.

VII. Simulation Results and Discussion

In order to assess the performance of our dynamic energy management framework, four schemes are examined:

- Scheme 1: No VRM, No change of energy source
- Scheme 2: No VRM, changing energy sources
- Scheme 3: VRM, No change of energy source
- Scheme 4: VRM, changing energy sources

Two activities are considered with these different schemes: VRM and energy source variations. Scheme 1 is a baseline scenario which has no VRM and no energy source change. Scheme 2 provides CO_2 emission reduction if renewable energy sources are used. Scheme 3 uses VRM without changing the energy sources. In Scheme 3, CO_2 emissions are not taken into account in the VRM_CO2 algorithm. When choosing the possible destination PP, only the power consumption and VRM cost values are considered. A VR may choose a relatively close PP to move to for lowering the VRM cost. In Scheme 4, the new dynamic energy management framework with renewable energy sources is employed. Three objectives are taken into account in the VRM_CO2 algorithm and the nodes employing green energy are preferred.

The energy consumption each hour in the 14N21L network is shown in Fig.3. The energy consumption values have been normalized to the values obtained with Scheme 1. Since there is no VRM in Scheme 1 and 2, the energy consumption each hour is the same for the whole day. The energy consumption fluctuates with the traffic load in Scheme 3 and 4. During off-peak hours, e.g. hour 16-22, the energy saving achieved with Scheme 3 and 4 is around 50%. The CO_2 emission values each hour are shown in Fig.4. The values have been normalized to the values obtained with Scheme 1. There is no energy change in Scheme 1, the CO_2 emissions stay the same throughout the day. The emissions during off-peak hours

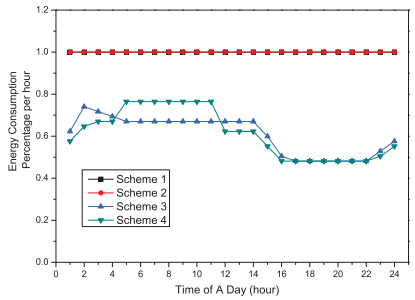

Fig. 3. Energy Consumption in the 14N21L Network

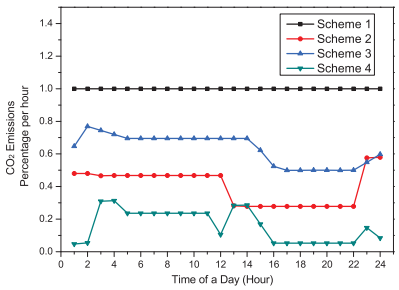

Fig. 4. CO_2 Emissions in the 14N21L Network

(e.g. hour 16-22) is lower than that of peak hours (e.g. 6:00-12:00) in the remaining three schemes. Scheme 2 saves around 20% CO_2 emissions since it still uses coal energy sources and the saving comes from the resource consolidation. When renewable energy sources are available in the network, the average saving with Scheme 3 is 65%. Scheme 4 achieves the highest saving around 85%. It implies that by using the new energy management framework, CO_2 emissions can be further reduced approximately by 20%. Fig. 5 shows the number of occupied optical channels with the four schemes. We record the number of occupied optical channels every 5 minutes throughout the day. Scheme 1 and 2 give the same results because No VRM is used. With Scheme 3, power consumption and VRM cost are considered when choosing the destination PPs. The VR is moved to a relatively close PP for lowering the VRM cost. More optical channels are used in Scheme 3 for redirecting the traffic to remotely located VRs. Compared with Scheme 3, one additional CO_2 emission objective is evaluated for selecting the destination PP in Scheme 4. The nodes powered by renewable energy sources are preferred. However, there may be no available green nodes around the VR. This may cause the VRs to be moved further away to nodes with green energy sources resulting in a longer optical path. Thus, the number of occupied optical channels in Scheme 4 is higher than that for Scheme 3.

We also observe the impact of the traffic load on the energy consumption and CO_2 emissions in Figs. 6-9 with two networks. For simplicity, the energy consumption and CO_2

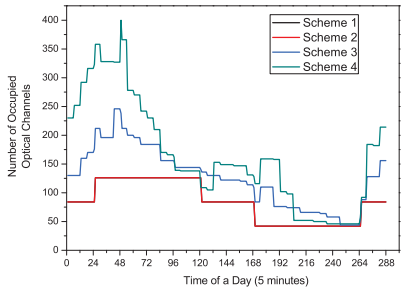

Fig. 5. Number of Occupied Optical Channels in the 14N21L Network

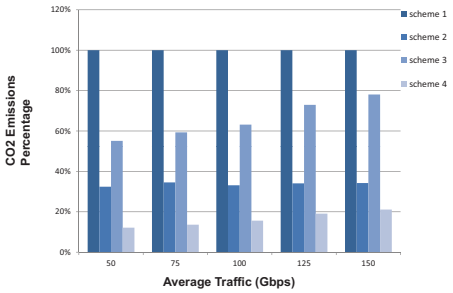

Fig. 6. Average Traffic and CO_2 Emissions in the 6N8L network

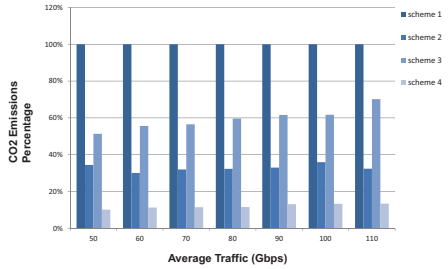

Fig. 7. Average Traffic and CO_2 Emissions in the 14N21L network

emissions are normalized to the values obtained in Scheme 1. In Figs. 6 and 7, the CO_2 emission increase with traffic load for Scheme 3 and 4. It is clear from Figs. 8 and 9 that the energy consumption increases with increasing traffic load for Scheme 3 and 4. It implies that in a busier network, it is more difficult to obtain energy and CO_2 savings using our framework.

In Fig. 10, we observe how the average hop count changes in response to changes in the average traffic load. By applying the VRM scheme, the layer 3 topology remains unchanged whilst the optical layer is adjusted to allow the traffic to be forwarded appropriately to the current VR locations. When the traffic goes through a ROADM, the hop count is incremented by one. Scheme 1 and 2 have same hop count since there is no VRM and the hop count is equal to the shortest path hop count. When VRM is employed in Scheme 3, around 1 more hop is

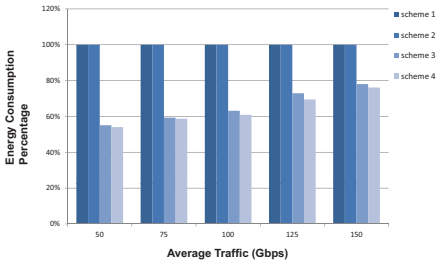

Fig. 8. Average Traffic and Energy Consumption in the 6N8L network

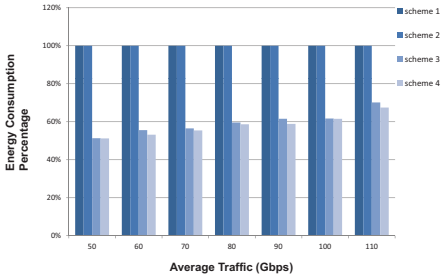

Fig. 9. Average Traffic and Energy Consumption in the 14N21L network

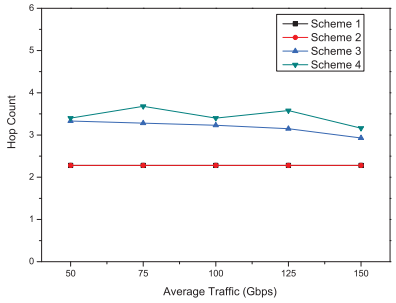

Fig. 10. Hop Count in the 6N8L Network

needed for redirecting traffic to the remote VRs. Compared with Scheme 3, Scheme 4 takes CO_2 emissions into account. Thus, Scheme 4 requires approximately 0.3 hops more than for Scheme 3 because it may take longer path to reach the green nodes.

VIII. Conclusion

In this paper, we propose a new dynamic energy management framework that favours the used of renewable energy sources for IP over DWDM core networks. Infrastructure sleeping and virtual router migration are combined to reduce the overall network energy consumption during the off-peak periods. VRM is used to conceal changes in the substrate network configuration from the IP-layer topology to avoid routing discontinuities and service disruption when PPs enter or leave their sleep state.

We also develop an evolutionary based heuristic algorithm to solve the destination physical platform selection problem. The paper provides details of the dynamic energy management framework and the simulation models that we constructed. Simulation results show that energy savings of around 35% are possible with the 6N8L network and 40% in NSFNET. When energy sources are employed in a network without virtual router migration, CO_2 emissions are reduced around 60%. Approximately a further 20% reduction in CO_2 emissions is achievable when the new energy management framework is used at the expense of an increased number of occupied optical channels and marginally longer path for the traffic.

References

[1] Tucker, et al., *Energy consumption in telecommunications*, 2012 IEEE Optical Interconnects Conference, pp.1,2, 20-23 May 2012

[2] Lange, C., et al., *Energy consumption of telecommunication networks*, 35th European Conference on Optical Communication, ECOC, Sept. 2009

[3] Caria, M., et al., *To switch on or off: A simple case study on energy efficiency in IP-over-WDM networks*, 2011 IEEE 12th International Conference on High Performance Switching and Routing (HPSR), July 2011

[4] *Comparison of Lifecycle Greenhouse Gas Emissions of Various Electricity Genertation Sources*, World Nuclear Association Report, online: http:/www.world-nuclear.org/uploadedFiles/org/WNA/Publications/Working_Group_Reports/comparison_of_lifecycle.pdf

[5] Bolla, R., et al., *Enabling backbone networks to sleep* IEEE Network, vol.25, no.2, pp.26-31, March-April 2011

[6] Wang, L., et al., *Energy Efficient Design for Multi-shelf IP over WDM Networks*, 2011 IEEE Conference on Computer Communications Workshops (INFOCOM WKSHPS), April 2011

[7] Bolla, R., et al., *Energy Efficiency in the Future Internet: A Survey of Existing Approaches and Trends in Energy-Aware Fixed Network Infrastructures*, Communications Surveys & Tutorials, IEEE, 2011

[8] Uhlig, S., et al., *Providing public intradomain traffic matrices to the research community*, SIGCOMM Comput. Commun. January 2006

[9] *Abilene Network Traffic Statistics.* Online available: http://www.abilene.iu.edu/

[10] Nedevschi, S., et al., *Reducing network energy consumption via sleeping and rate-adaptation*, in Proc. 5th USENIX Symposium on Networked Systems Design and Implementation, 2008

[11] Agrawal, M., et al., *RouterFarm: Towards a dynamic, manageable network edge*, In Proc. SIGCOMM workshop, 2006

[12] Wang, Y., et al., *Virtual routers on the move: live router migration as a network-management primitive*, In Proc.SIGCOMM', October 2008

[13] Kumar, A., et al., *Energy optimization in wireless communication network through renewable energy sources (RES)*, 2012 IEEE 5th India International Conference on Power Electronics (IICPE), Dec. 2012

[14] Xiaowen Dong, et al., *Energy optimization in wireless communication network through renewable energy sources (RES)*, Global Telecommunications Conference (GLOBECOM 2011), 2011 IEEE, Dec. 2011

[15] Xiaowen Dong, et al., *IP Over WDM Networks Employing Renewable Energy Sources*, Journal of Lightwave Technology, Jan.1, 2011

[16] Xin Chen; Phillips, C.,*An Evolutionary Based Dynamic Energy Management Framework for IP-over-DWDM Core Networks*,COST IC0804 European Conference, EE-LSDS 2013, Vienna, April, 2013

[17] Xin Chen; Phillips, C., *Virtual router migration and infrastructure sleeping for energy management of IP over WDM networks*, International Conference on Telecommunications and Multimedia, pp.31,36, July 2012

[18] Chiaraviglio, L., et al.,*Reducing Power Consumption in Backbone Networks*, IEEE International Conference on Communications. ICC '09, pp.1,6, 14-18 June 2009

[19] Coiro, A., et al., *Reducing Power Consumption in Wavelength Routed Networks by Selective Switch Off of Optical Links*, IEEE Journal of Selected Topics in Quantum Electronics, vol.17, no.2, pp.428,436, March-April 2011

[20] Cisco data sheet, *Cisco CRS-1 16-Slot Single-Shelf System*, online: http://www.cisco.com/en/US/prod/collateral/routers/ps5763/ps5862/product_data_sheet09186a008022d5f3.pdf.

[21] Ciena data sheet, *CN 4200 ROADM*, online: http://www.ciena.com/products/4200-ROADM/

What do we need to do to "green" data-center networks? A fundamental perspective

Pulkit Grover
Carnegie Mellon University
pulkit@cmu.edu

***Abstract*— While traditional information theory has driven the choice of communication strategies for most of today's communication systems, it focuses almost exclusively on minimizing the transmit power of the system. In modern short-distance applications, including high-speed data-center networks, the energy consumed in the circuitry to enable reliable between servers can dominate the transmit energy across the links. Recent theoretical results and empirical observations show that in such situations, operating close to the traditional information-theoretic limits can be highly inefficient from a system-level energy-perspective. In this position paper, we use these results to propose a way forward for obtaining energy-efficient strategies for future Ethernet, including the NGBASE Ethernet which is currently being standardized.**

We also introduce our Total Energy Minimization platform, *TotEM*, that will collect information to enable communication system designers to make the most energy-efficient choices.

I. Introduction: Data-center network energy consumption

Information and Communication Technologies (ICTs) today consume about 8% of the world's generated electricity, and are slated to consume upwards of 15% of the world energy by 2020 [1]. Data-centers themselves consume about 2% of the world electricity, larger than the total electrical energy consumption of most countries. Within a data-center, 15-20% of power (and, in some cases, even up to 50% [2]) is consumed in networking [3]. Thus, even from a world-energy standpoint, networking in data-centers is a non-negligible fraction of the total electrical energy consumption.

While this fact in itself may not motivate the industry to adopt energy-efficient networking strategies, the economics of energy-efficient data-centers very well could. Gunaratne *et al.* observe in [4] that "ethernet network interface controllers (NICs) in the US alone consume hundreds of millions of US dollars in electricity per year." The imminent saturation of Moore's law especially in the context of energy [5][1] and the advent of the BigData era [6] has forced massive parallelization which requires extreme-speed movement of massive amounts of data. As networking starts bearing more and more burden for faster computing, energy consumed in networking is increasing, and networking speeds are becoming the bottleneck in faster computing. As Bryant *et al.* point out in [6], analogous to Moore's law for circuits, "We need a "Moore's Law" technology for networking, where declining costs for networking infrastructure combine with increasing bandwidth" to keep pace with the massive amounts of data being generated. Thus, sheer market forces are driving extensive exploration of energy-efficient networking strategies [2], [7]–[9].

Towards reducing energy consumption of ethernet links, it was observed that these links consume significant amounts of energy even when unutilized, or underutilized. This observation led to a serious effort for developing is called the "Energy-Efficient Ethernet" [10] where link energy is proportional to the link utilization.

In this position paper, we argue that there are significant inefficiencies also in the low-level physical layer. For instance, the standards allow little flexibility in the design of the PHY layer in response to the changing conditions, thereby consuming almost the same power regardless of the communication distance (see Fig. 2). We believe that this energy can be reduced by appropriate choice of communication strategies that *adapt* their energy and complexity based on the communication distance. Further, while some of these adaptations can be introduced at the design time, some need to be introduced in the standardization process itself.

Reducing networking energy is conceptually a difficult problem because even a single data-center communication link is a complex system. Multiple components, such as transmission, decoding, equalization, etc. consume comparable amounts of power (see, for example, [11]–[13]). Thus in order to minimize system-level power, one needs to understand and exploit the inherent tradeoffs between these power sinks, such as the ADC power, equalization power, the encoding/decoding power, etc. We survey recent results that make progress in this direction, indicate a gap in this understanding, and chart out a path towards improving data-center energy-efficiency from this physical-layer perspective.

II. A core conceptual difficulty: a legacy of traditional information theory?

A. A potential shortcoming of the current theory

From the fundamental perspective that we adopt in this position paper, what is the difficulty in reducing networking energy? Energy/power required in communication has been

[1]Moore's law continues unabated for the number of transistors per unit area, but has essentially saturated for power consumed in processing.

978-1-4799-0354-2/13/$31.00 ©2013 IEEE

a central problem in traditional information theory for a long time, sometimes implicitly in the form of reducing Signal-to-Noise ratio (SNR) [14], [15], and sometimes explicitly in reducing transmit energy consumed per bit [16]. The main insight is illustrated using what are called "waterfall" curves (see Fig. 1) that show that unboundedly low target error probabilities can be obtained with bounded transmit power: the key is to choose a sufficiently long and sophisticated error-correcting code. This surprising and extremely powerful insight has driven the design of error-correcting codes for many decades, and the resulting codes are used in many systems today [17]–[19], including in data-center networks [12], [20].

Focusing on the problem of choosing an error correcting code, isn't traditional information theory sufficient for today's networks? When information theory was first developed (starting in 1948 with Shannon's seminal paper), the primary applications of interest were long-distance (e.g. deep-space) communications. At such large distances, the transmit power dominated all other powers in the system [11]. These fundamental limits and strategies could afford to ignore the power consumed in processing circuitry. However, many communication systems today — including those in today's data-centers — are short-distance communication systems where power consumed in circuitry at the transmitter and receiver often dominates the transmit power [12], [13], [20]. Further, there is a tradeoff between transmit and encoding/decoding power [11], [21], which has sometimes been used as a motivation to do away with use of an error correcting code altogether [22]. Our experimental results [23] strongly suggest that that a more graceful reduction in code complexity with the change in communication distance is the energy-optimal approach. Similar suggestions for analog circuit components (though, crucially, not for the code/encoder/decoder) have been made in the presentations for NGBASE-T standardization [24]–[26].

From a fundamental perspective, this raises an interesting question: is this rethinking of designing short-distance communication systems really fundamental? Or is it simply an issue of improvements in circuit designs? Even just taking into account the energy consumed in circuit logic, or just the energy consumed in wiring, our work over the past six years (e.g. [11], [27]–[38]) show that — in contrast with Shannon's waterfall curves — the required total (transmit + circuit) energy/power for communication must diverge to infinity as the error probability is driven to zero. Further, in this limit, the error-correcting code must operate farther and farther away from the Shannon limit [11]. The energy consumed in wires is an aspect that has hitherto been ignored in much of theory (including Andrew Yao's communication complexity [39] and CS-theoretic circuit complexity [40]). This brings out the importance of measuring complexity of encoding/decoding for different code constructions not only in terms of the required blocklength, or the required number of operations, but also in the required wire-lengths.

Thus, the traditional models and the traditional theory, that do not explicitly account for power consumed in processing, are not the most relevant for reducing energy in data-center networks. We need models of implementations, just as we have models of channels. More precisely, we need models for encoding/decoding circuitry that walk a fine line: they should be precise enough to enable good estimates of energy, and yet abstract enough that they can be analyzed theoretically.

Often when the possible choices for component design are not too large, these power models are easier to obtain. For instance, fairly precise models of power consumption in analog-to-digital converters (ADCs) are available (e.g. [41]). Equalizers [34], mixers, beamformers, and other analog circuit components can be modeled to within reasonable accuracy as well.

What about encoding and decoding? There is an abstraction that is used as a proxy for power consumed in here: the Turing machine model [42] that, roughly speaking, counts the number of elementary operations. While lowering Turing-complexity has (justifiably and successfully) motivated design of many new families of codes [19], [43], the Turing-complexity for all modern codes based on sparse-graphs is linear in the length of the code [19]. Thus, does it really matter which code you choose?

In practice, it does: the energy consumed by an encoder/decoder can depend strongly on code construction. In [44], we chose two sparse-graph codes of the same blocklength and node degrees, but different code-girths and edge connections (in the Tanner graph representation of the code [19]). Increasing code-girth, while it reduces error-probability, is accompanied with an increase in *wiring length* [38], an aspect that is ignored by the Turing machine model. The paper [44] computes the increase in power requirements that arise from this increase in wire length. While reducing wiring length with proper code-design has been investigated in the literature (e.g. [45], [46] use optimization approaches, and [38] takes a fundamental-limits-based approach), the understanding is still very limited. Indeed, the fundamental limits [31], [38] and the achievable strategies have a gap in the order sense.

B. The current practice: the one-size-fits-all approach of current data-center networking standard

Does the current communication standard in data-centers suffer from the inefficiencies indicated above? Indeed, and the evidence is there in the publicly available documents that record the development process[2] for the "10 GBASE-T" standard [48], the IEEE standard for Ethernet over twisted-pair copper cables transferring multi-giga-bits-per-second. Most of the copper-cable routers and switches used today in data-centers operate on this standard.

Fig. 1 provides the key evidence of how traditional information theory (that ignores power consumed in circuitry at transmitter/receiver) guided the design of the 10 GBASE-T

[2]The entire documentation is available for public access here: http://www.ieee802.org/3/10GBT/public/index.html.

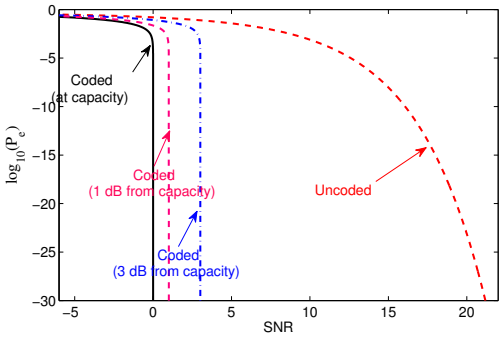

A Shannon-theoretic view of code-performance focuses on just the transmit power

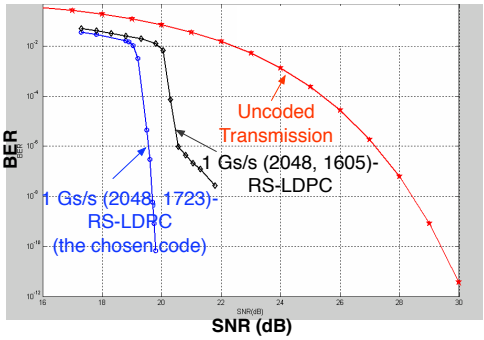

This figure, taken from presentations used in 10 Gbase-T standardization [Rao et al.], shows that the code-choice was guided by principles in traditional information theory.

Fig. 1. The figure shows how traditional transmit-power-focused Shannon-theoretic view was used in code-choice in 10 GBASE-T standardization. The figure on the top is the famous Shannon "waterfall" curve [11], and the one on the bottom is from [47]. Our work has shown that this view can be misleading when choosing codes that minimize transmit + encoding/decoding/processing power [11]. The message is: ECC-choice must depend on, or adapt to, the communication distance.

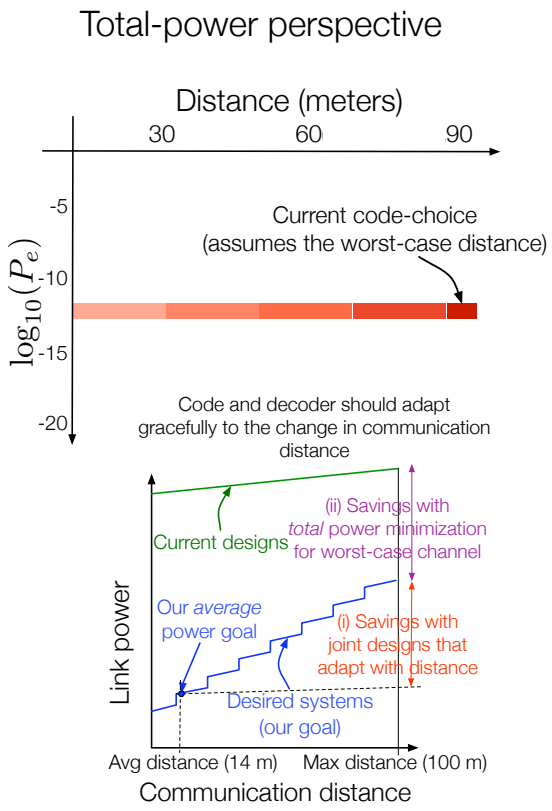

Fig. 2. Energy/power consumed in communicating to a given distance must scale approximately linearly with the communication distance. However, the current systems overbudget by aiming for the worst-case communication distance, thereby introducing significant inefficiency in communication energy/power.

standard. While this figure in itself does not establish the inefficiency, a closer look at the documentation for 10 GBASE-T does: the choice of the error-correcting code (ECC) was driven by the worst-case distance of communication of 100 meters. The average distance is a much shorter 14 meters! It is our contention that at shorter distances, a different choice of ECC would reduce power consumed in correcting errors at the receiving end significantly. Fig. 2 illustrates how a proper choice of the code can make energy consumption increase almost linearly with the communication distance.

Our argument thus far relies on thinking of point-to-point communication across a single link. However, a data-center has a complex network of links. Our proposal to increase transmit power in lieu or reducing encoding/decoding power and thereby reducing the total link power raises the following natural question.

C. Wouldn't increased transmit power result in larger interference/cross-talk?

If increasing transmit power reduces the requirements on decoding power, it also increases "cross-talk" interference between wires in the same cable, or different cables (also referred to as "ANEXT," or Alien Near-End Cross Talk"). Our study [11] shows that under the simplification where interference is ignored as noise, when higher density of link is needed in the same geographical area, the total power optimal code choice approaches capacity. At low link density, however, one can use codes that operate far from capacity.

Even when density of links cannot be controlled (for instance, the number of wires in a cable is fixed), there is an interesting possibility to boost the SNR at the decoder input *without increasing the transmit power*: improving the quality of analog components and/or equalizer. Our analysis of tradeoffs between equalization power and transmission power [34] shows that the link capacity can be raised by increasing the equalization power, which effectively raises the numerator of the SNR. Improved beamforming or a higher precision ADC would have a similar effect. Thus tradeoffs between all of these components can be understood in this energy-setting, providing pareto optimal constructions.

This study needs to be complemented by analyzing situations where sophisticated signal processing techniques, such as interference alignment [49] or successive interference cancelation, can be used to boost the SNR at the receiver.

D. Does the "analog part" of the circuitry consume most of the power?

With technology scaling for CMOS circuits, the energy/power consumption in digital power has gone down tremendously in the past three decades. This has led to the speculation that the power consumed in analog back-end/front-end of a transmitter/receiver will dominate (see, for example, [50]). We believe that this is far from conclusive for the following reasons:

1) There is a tradeoff between the complexity and power consumption of the analog and digital parts;
2) The digital part (that includes the decoder, and sometimes the equalizer as well) can be made more complex, thereby reducing the power requirements on the analog part;
3) While CMOS device size scaling still seems to be following Moore's law, the scaling in power consumption seems to be stalling; and finally
4) In many indoor wireless systems (e.g. see [22]), an error correcting code is *not* used because typical error correcting techniques (that are actually meant for long-distance communication) consume significantly more power than the analog front/back ends.

Consider the following example: an 8-bit ADC and a 40 tap analog equalizer provide a certain effective SNR going into the decoder. However, if we were to use instead a 2-bit ADC and perform a 20 tap digital equalizer, but use a more complex code that operates closer to the Shannon limit, we lower the requirements on the effective SNR. This analysis was performed for understanding tradeoffs between an analog/mixed-signal equalizer and a decoder in [34].

In the context of NGBASE-T implementations, if the decoder consumes significantly less power than the analog components, then the code complexity can be increased in order to offset power consumed in analog components. Thus, we believe that the observation that CMOS power scaling could lower digital power consumption (if, optimistically, it continues) should spur an even deeper understanding and development of coding strategies.

E. In summary, why are current networks energy inefficient?

The current data-center networks are inefficient for the following reasons:

(i) Inspired by traditional information theory, *the physical-layer is designed for the worst-case distance*: The *average* cable-length for communication inside a data-center is 14 meters [51], while the physical layer is designed for *worst-case* cable-length of 100 meters [25], [26]!

(ii) *Even the worst-case design is not optimized for total-power*: The current code (an "RS-LDPC" code [12], [13], [47]) was chosen by how closely it approaches capacity (as evidenced in [47]), *not* by a total-system-power criterion.

(iii) *The physical-layer is designed for significant crosstalk interference*: Improved shielding can reduce crosstalk significantly [52], and is not terribly expensive[3]. Even without improved shielding, crosstalk varies widely across a data-center [53], especially after implementation of "Energy-Efficient Ethernet" [10] that reduces link power at low-data-rates. However, the physical-layer in 10-Gbase-T does not adapt to interference-level or to the available shielding [53]. Designing systems for worst-case crosstalk is overly conservative and energy-inefficient.

In summary, the data-center physical layer is designed for the worst-case distance, worst-case interference, almost-worst-case shielding, and even for this worst-case, is guided by traditional information theory that is focused at minimizing just the transmit power.

III. How do we proceed towards a solution?

A. Trial and error, or sound models and theory?

Can one approach the problem without modeling different codes and encoding/decoding algorithms and estimating the required total power? After all, modeling power consumption of encoder/decoders is a laborious process.

However, a trial and error approach could be highly inefficient. The number of codes is impossibly large for us to test them all experimentally (super-exponential in the block-length). For a fixed code, the number of encoding/decoding algorithms is many, and for each encoding/decoding algorithm, there are many possible implementation architectures. Further, implementation technologies continue to evolve, and multiple technologies are in use today. In absence of any models and fundamental results, it is impossible to tell how close the chosen code/encoder/decoder architecture is to the unavoidable limit on total power.

Thus the relevant question is not *whether* we should model encoder/decoder implementations, and circuits in general, but *how* we can model them. It is a difficult problem, but as we have argued (see, for example, [23]), not an insurmountable one. It is clear to us that within reasonable limits, approximate models would be significantly more useful than the current approach, which is essentially relies on no implementation models at all.

What could help is a publicly available database that models and posits energy/power requirements for the encoder/decoder of a given code, with realistic upper and lower bounds, to minimize the system-level power. Any research results that contribute to either the upper or the lower bound should be added to this database, thereby enriching the tradeoff space.

B. TotEM: a platform for total energy minimization in communication systems

This strongly suggests that practically, we need **extensive, if crude, models of power consumed in encoding/decoding**

[3]Cabling costs are only 2-3% of the total hardware cost, and less than 0.5% of the total data-center IT cost [52].

circuits (see e.g. [23], etc.) through circuit simulations and ASIC and FPGA implementations (e.g. [12], [20]). These models need to be incorporated in code search and analysis in order to obtain system-level power-efficient codes and encoding/decoding algorithms and implementations. Towards obtaining these models, we are currently creating the "*TotEM*" (Total Energy Minimization) platform, available at http://www.ece.cmu.edu/~pgrover/totem.html, where we are collecting links to publications that:

1) Provide data-points for energy and power requirements for encoding/decoding of different code constructions
2) Provide models for encoding/decoding power, including wiring lengths of encoders/decoders.
3) Obtain fundamental limits on total power consumption, including the power consumed in transmission (*i.e.*, the power amplifier), encoding, decoding, ADC, equalizer, mixer, low-noise amplifier, etc.
4) Obtain code constructions that have the potential to lower encoding/decoding power significantly.

Improvements at the bottom level (circuit technology) and at the top-level energy management (e.g. [2], [8], [9]) could continue to keep energy consumption under control, at least for a few more years. However, to improve speeds by a factor of 10 or more will require a fundamental re-thinking of system-design that integrates all levels of the system hierarchy. *TotEM* is one step towards such an integrated approach.

IV. Conclusions: What steps are needed to reduce data-center networking energy

We believe that the following steps are required:

1) Joint design of energy-efficient error-correcting codes, decoder circuitry, the equalizer, the ADC, etc. to minimize the system-level power consumption. In particular, focus should be on minimizing *total* system power.
2) Theoretical results should be used to guide the choice of code families, and intuition into circuit architecture design. For both fundamental results and code designs, complexity of encoding and decoding must be computed not only in required blocklength and/or number of operations, but also in required wiring lengths.
3) Effects of interference or cross-talk should be re-examined in this setting where transmit power can be increased in order to reduce encoding/decoding power.

This problem is of large and broad importance (even in energy-consumption at world-scale), and yet, as we argue above, it we lack sufficient understanding at a theoretical as well as a practical level. Interactions between different communities, namely, networking/computer scientists, information theorists, coding theorists, circuit designers, etc., should be encouraged in order to obtain improved models and to identify and reduce crosslayer inefficiencies. Some platforms, such as the GreenTouch initiative[4], and ICT footprint initiative[5], exist, and these should be used to enhance such interactions.

[4]See http://www.greentouch.org/.

Acknowledgments

We thank Hugh Barrass, Bruce Nordman and Pedro Reviriego Vasallo for most useful discussions and pointers to NGBASE references.

We acknowledge the generous support of NSF-ECCS-1343324, seed grants from the NSF Center for Science of Information NSF-CCF-0939370, and a startup grant from Carnegie Mellon University.

References

[1] M. Pickavet, W. Vereecken, S. Demeyer, P. Audenaert, B. Vermeulen, C. Develder, D. Colle, B. Dhoedt, and P. Demeester, "Worldwide energy needs for ict: The rise of power-aware networking," in *2nd International Symposium on Advanced Networks and Telecommunication Systems (ANTS)*, 2008, pp. 1–3.

[2] B. Heller, S. Seetharaman, P. Mahadevan, Y. Yiakoumis, P. Sharma, S. Banerjee, and N. McKeown, "Elastictree: Saving energy in data center networks." in *NSDI*, vol. 3, 2010, pp. 19–21.

[3] A. Greenberg, J. Hamilton, D. A. Maltz, and P. Patel, "The cost of a cloud: research problems in data center networks," *ACM SIGCOMM Computer Communication Review*, vol. 39, no. 1, pp. 68–73, 2008.

[4] C. Gunaratne, K. Christensen, B. Nordman, and S. Suen, "Reducing the energy consumption of Ethernet with adaptive link rate (ALR)," *IEEE Transactions on Computers*, vol. 57, no. 4, pp. 448–461, 2008.

[5] L. Kish, "Moore's law and the energy requirement of computing versus performance," in *IEE Proceedings on Circuits, Devices and Systems*, vol. 151, no. 2, 2004, pp. 190–194.

[6] R. Bryant, R. H. Katz, and E. D. Lazowska, "Big-data computing: Creating revolutionary breakthroughs in commerce, science and society," 2008. [Online]. Available: http://www.cra.org/ccc/files/docs/init/Big_Data.pdf

[7] K. Christensen, P. Reviriego, B. Nordman, M. Bennett, M. Mostowfi, and J. A. Maestro, "Ieee 802.3 az: the road to energy efficient ethernet," *Communications Magazine, IEEE*, vol. 48, no. 11, pp. 50–56, 2010.

[8] D. Abts, M. R. Marty, P. M. Wells, P. Klausler, and H. Liu, "Energy proportional datacenter networks," in *ACM SIGARCH Computer Architecture News*, vol. 38, no. 3. ACM, 2010, pp. 338–347.

[9] Y. Shang, D. Li, and M. Xu, "Energy-aware routing in data center network," in *Proceedings of the first ACM SIGCOMM workshop on Green networking*. ACM, 2010, pp. 1–8.

[10] Wikipedia, "Energy-efficient ethernet." [Online]. Available: http://en.wikipedia.org/wiki/Energy-Efficient_Ethernet

[11] P. Grover, K. Woyach, and A. Sahai, "Towards a communication-theoretic understanding of system-level power consumption," *IEEE Journal on Selected Areas in Communication*, Sep. 2011.

[12] Z. Zhang, V. Anantharam, M. Wainwright, and B. Nikolic, "An efficient 10 GBASE-T ethernet LDPC decoder design with low error floors," *IEEE Journal of Solid-State Circuits*, vol. 45, no. 4, pp. 843–855, Apr. 2010.

[13] Z. Zhang, "Design of LDPC decoders for improved low error rate performance," Ph.D. dissertation, UC Berkeley, Berkeley, CA, 2009.

[14] C. E. Shannon, "A mathematical theory of communication," *Bell System Technical Journal*, vol. 27, pp. 379–423, 623–656, Jul./Oct. 1948.

[15] A. E. Gamal and Y.-H. Kim, "Lecture notes on network information theory," Mar. 2010. [Online]. Available: http://arxiv.org/abs/1001.3404

[16] S. Verdu, "On channel capacity per unit cost," *IEEE Trans. Inf. Theory*, vol. 36, pp. 1019–1030, 1990.

[17] R. J. McEliece, *Are there turbo-codes on Mars?*, Chicago, IL, Jun. 2004.

[18] The DVB-S2 standard. [Online]. Available: http://en.wikipedia.org/wiki/DVB-S2

[5]See http://www.ict-footprint.com/

[19] T. Richardson and R. Urbanke, *Modern Coding Theory*. Cambridge University Press, 2007.

[20] A. Darabiha, A. Carusone, and F. Kschischang, "Power reduction techniques for LDPC decoders," *IEEE J. Solid-State Circuits*, vol. 43, no. 8, pp. 1835 –1845, Aug. 2008.

[21] S. L. Howard, C. Schlegel, and K. Iniewski, "Error control coding in low-power wireless sensor networks: when is ECC energy-efficient?" *EURASIP Journal on Wireless Communications and Networking*, pp. 1–14, 2006.

[22] C. Marcu, D. Chowdhury, C. Thakkar, J.-D. Park, L.-K. Kong, M. Tabesh, Y. Wang, B. Afshar, A. Gupta, A.Arbabian, S. Gambini, R. Zamani, E. Alon, and A. Niknejad, "A 90 nm CMOS low-power 60 GHz transceiver with integrated baseband circuitry," *IEEE Journal of Solid-State Circuits*, vol. 44, no. 12, pp. 3434 – 3447, 2009.

[23] K. Ganesan, Y. Wen, P. Grover, A. Goldsmith, and J. Rabaey, "Choosing "green" codes by simulation-based modeling of implementations," in *IEEE Globecom*, Dec 2012.

[24] D. Dove, "NGBASE-T SR: A Scalable BASE-T Approach," Sep. 2012, http://www.ieee802.org/3/NGBASET/public/sep12/dove_01b_0912.pdf.

[25] P. Wu, G. Parnaby, and W. Lo, "NGBASE-T Requirements: Learning from 10GBASE-T," Jan. 2013, http://www.ieee802.org/3/NGBASET/public/jan13/WuParnaby_01a_0113_NGBT.pdf.

[26] M. Bennett and P. Reviriego, "Reach and Energy Efficiency in NG-BASE-T," Nov. 2012, http://www.ieee802.org/3/NGBASET/public/nov12/bennett_01_1112_ngbt.pdf.

[27] P. Grover, "Bounds on the tradeoff between rate and complexity for sparse-graph codes," in *IEEE Inf. Theory Workshop (ITW)*, Lake Tahoe, 2007.

[28] P. Grover and A. Sahai, "Green codes: Energy-efficient short-range communication," in *Proceedings of the 2008 IEEE Symposium on Information Theory*, Toronto, Canada, Jul. 2008.

[29] ——, "Time-division multiplexing for green broadcasting," in *Proc. IEEE Symposium on Information Theory (ISIT)*, Seoul, Jul. 2009.

[30] P. Grover, H. Palaiyanur, and A. Sahai, "Information-theoretic tradeoffs on throughput and chip power consumption for decoding error-correcting codes," in *Proceedings of the 2010 IEEE Symposium on Information Theory*, Austin, TX, USA, Jun. 2010.

[31] P. Grover, A. Goldsmith, and A. Sahai, "Fundamental limits on the power consumption of encoding and decoding," in *Proc. IEEE International Symposium on Information Theory (ISIT)*, Jul. 2012.

[32] P. Grover, ""Information-friction" and its impact on minimum energy per communicated bit," in *IEEE International Symposium on Information Theory (ISIT)*, Istanbul, Turkey, Jul. 2013.

[33] ——, "Fundamental limits on the power consumption for lossless signal recovery," in *IEEE Inf. Theory Workshop (ITW)*, Sep. 2012.

[34] P. Grover, A. Sahai, and J.-H. Park, "Simple models for power optimization across transmission, equalization and decoding," in *Proceedings of the 19th European Signal Processing Conference (EUSIPCO)*, Barcelona, Spain, Aug. 2011.

[35] P. Grover, K. Woyach, H. Palaiyanur, and A. Sahai, "An interference-aware perspective on decoding power," in *6th International symposium on turbo codes and iterative information processing*, Brest, France, Sep. 2010.

[36] K. Ganesan, P. Grover, and A. Goldsmith, "How far are ldpc codes from fundamental limits on total power consumption?" in *Proceedings of the Allerton Conference on Communication, Control, and Computing*, Monticello, IL, Oct. 2012.

[37] P. Grover, A. Goldsmith, A. Sahai, and J. Rabaey, "Information theory meets circuit design: Why capacity-approaching codes require more circuit area and power," in *Proceedings of the Allerton Conference on Communication, Control, and Computing*, Monticello, IL, Sep. 2011.

[38] P. Grover and A. Sahai, "Fundamental bounds on the interconnect complexity of decoder implementations," in *Conference on Information Sciences and Systems (CISS)*, Baltimore, MD, Mar. 2011.

[39] A. C.-C. Yao, "Some complexity questions related to distributive computing (preliminary report)," in *ACM symposium on Theory of computing (STOC)*, New York, NY, USA, 1979, pp. 209–213.

[40] I. Wegener, "The complexity of boolean functions," 1987.

[41] B. Murmann, "ADC performance survey 1997-2012." [Online]. Available: http://www.stanford.edu/m̃urmann/adcsurvey.html

[42] M. Sipser, *Introduction to the theory of computation*. PWS Pub Co, 1996.

[43] E. Arikan, "Channel polarization: A method for constructing capacity-achieving codes for symmetric binary-input memoryless channels," *IEEE Trans. Inf. Theory*, vol. 55, no. 7, pp. 3051 –3073, july 2009.

[44] K. Ganesan, P. Grover, and J. M. Rabaey, "The power cost of overdesigning codes," in *IEEE Workshop on Signal Processing Systems (SiPS)*, Oct. 2011.

[45] V. Nagarajan, S. Laendner, O. Jaykumar, O. Milenkovic, and S. Khatri, "High-throughput VLSI implementations of iterative decoders and related code construction problems," *The Journal of VLSI Signal Processing*, vol. 49, no. 1, pp. 185 –206, 2007.

[46] M. Mohiyuddin, A. Prakash, A. Aziz, and W. Wolf, "Synthesizing interconnect-efficient low density parity check codes," in *Proceedings of the 41st annual Design Automation Conference*, ser. DAC '04, New York, NY, USA, 2004, pp. 488–491.

[47] S. Rao, R. Hormis, and E. Krouk, "The 4D-PAM8 Proposal for 10GBASE-T," Nov. 2003, P802.3 Task Force Meeting, http://www.ieee802.org/3/10GBT/public/nov03/rao_1_1103.pdf.

[48] *IEEE Std. 802.3an-2006: "Physical Layer and Management Parameters for 10 Gb/s Operation, Type 10GBASE-T," amendment to IEEE Std. 802.3-2005*. IEEE, Sept. 2006.

[49] V. Cadambe and S. Jafar, "Interference alignment and degrees of freedom of the K-user interference channel," *IEEE Trans. Inf. Theory*, vol. 54, no. 8, p. 3425, 2008.

[50] Y. Li, B. Bakkaloglu, and C. Chakrabarti, "A system level energy model and energy-quality evaluation for integrated transceiver front-ends," *IEEE Transactions on Very Large Scale Integration (VLSI) Systems*, vol. 15, no. 1, pp. 90–103, 2007.

[51] A. Flatman, "Data Centre Link Lengths," Mar. 2011, http://tinyurl.com/FaltmanCablingSurvey.

[52] V. Maguire and T. Harpel, "40 Gbps over twisted-pair cabling: Planning for a new ethernet application." [Online]. Available: http://tinyurl.com/cat7acabling

[53] H. Barrass, M. Bennett, B. Booth, C. DiMinico, P. Kish, D. Law, S. Muller, B. Tolley, and G. Zimmerman, "10gbase-t: 10 gigabit ethernet over twisted-pair copper," Ethernet Alliance, Cambridge, MA, Aug. 2007.

Energy-Aware Data Center Management in Cross-Domain Content Delivery Networks

Chang Ge, Ning Wang, Zhili Sun
Centre for Communication Systems Research
University of Surrey, Guildford, UK
Email: {C.Ge, N.Wang, Z.Sun}@surrey.ac.uk

***Abstract*—A content delivery network (CDN) typically consists of geographically-distributed data centers, each containing servers that cache and deliver web contents close to end-users for localized content access purpose. In recent years, optimization of CDN data center energy consumption has attracted increasing research efforts. The key technical challenge is the tradeoff between CDN energy consumption and the content service capability at both the server and the network sides. In this article, we introduce a data center management scheme that effectively reduces the energy consumption of cross-domain CDNs through dynamically provisioning servers and coordinating content delivery operations with respect to dynamic server and network load. The proposed scheme focuses on optimizing the energy-performance tradeoff in two aspects. On one hand, servers in CDN data centers are put to the sleep mode during off-peak hours to save energy. On the other hand, CDN Quality-of-Service (QoS) performance is assured through honoring constraints on servers and network link loads, especially through restricting inter-domain content traffic volume. As a result, the proposed scheme is able to reduce CDN data center energy consumption without compromising its end-to-end QoS performance. According to our experiments based on realistic CDN scenarios, the proposed scheme is able to reduce data center energy consumption by up to 45.9% while achieving desired QoS performance.**

I. Introduction

In a content delivery network (CDN), multiple data centers (DC) containing content servers are strategically established within proximity of Point-of-Presence (PoP) nodes to serve end-users' content requests [1]. As web content objects (such as webpages and videos) are normally replicated and cached at the DCs, they are efficiently delivered to end-users in a more scalable and efficient manner thanks to localized content access. In general, each content request is resolved to either a local (preferred) or a remote DC. The contents are effectively delivered through the virtual path from the DC to the PoP where the user is attached, and the determination of the virtual overlay links' mapping to ISP physical networks are based on the underlying intra- and inter-domain routing configurations. In order to support end-to-end Quality-of-Service (QoS) assurance in content delivery operations, the CDN operator may "rent" bandwidth resources along the virtual links in the overlay across PoP nodes through establishing service level agreements (SLA) with underlying ISPs. In this way, a certain proportion of bandwidth resources in the ISP network is reserved for dedicated use by the CDN infrastructure. Such bandwidth reservation is typically achieved via virtualization techniques [2].

In recent years, energy efficiency in the information communication technologies (ICT) sector has attracted more and more interests from both the research community and the industry, which is especially the case for DCs and CDNs. In the literature, most relevant research works have focused on *standalone* DCs, which involves power management, performance management or both [3]. Meanwhile, there have been research works on reducing CDN energy consumption in recent years, which aim to optimize CDN energy consumption from either a theoretical perspective [4] or a practical perspective [5][6]. However, the scenario of energy saving in large-scale CDN infrastructures that typically cover *multiple inter-connected* ISP domains has not been well addressed.

For the CDN operators, it is crucial to meet end-users' QoS requirements through delivering the requested content objects with short end-to-end delay and assured bandwidth support. Therefore, in order to accommodate the uncertainty in user activities, CDN operators typically keep all DCs and their servers constantly up and running, even during off-peak hours when many servers are idle due to low content request volume. As a result, it is observed in [7] that most modern DC servers are utilized by only around 10% to 50% in average, which are rarely fully utilized during daily workloads. Moreover, a distinct observation is that a server consumes at least 60% of its peak power (around 100$\sim$300 Watts) when it is active, even without serving any content request. In contrast, this figure drops to only 5 Watts when it is configured into the sleep mode [7]. Therefore, it can be inferred that modern DCs suffer from poor energy efficiency due to under-utilized servers, and it is desired for the CDN operators to put some servers to the sleep mode when incoming content request volume is low, for instance during off-peak hours. However, although this technique has been widely applied to *standalone* DCs, this is not a trivial task in the cross-domain CDN scenario where multiple DCs are deployed in a geographically-distributed manner. This is because the decision on servers' sleep mode reconfiguration needs to consider not only the DC servers' service capabilities, but also network resource availability to support end-to-end content deliveries and assure QoS performance in terms of end-to-end delay.

In this article, we propose an energy management scheme that is specifically developed for cross-domain CDN infrastructures. The fundamental idea is to strategically reconfigure DC servers to the sleep mode without deteriorating the service

978-1-4799-0354-2/13/$31.00 ©2013 IEEE

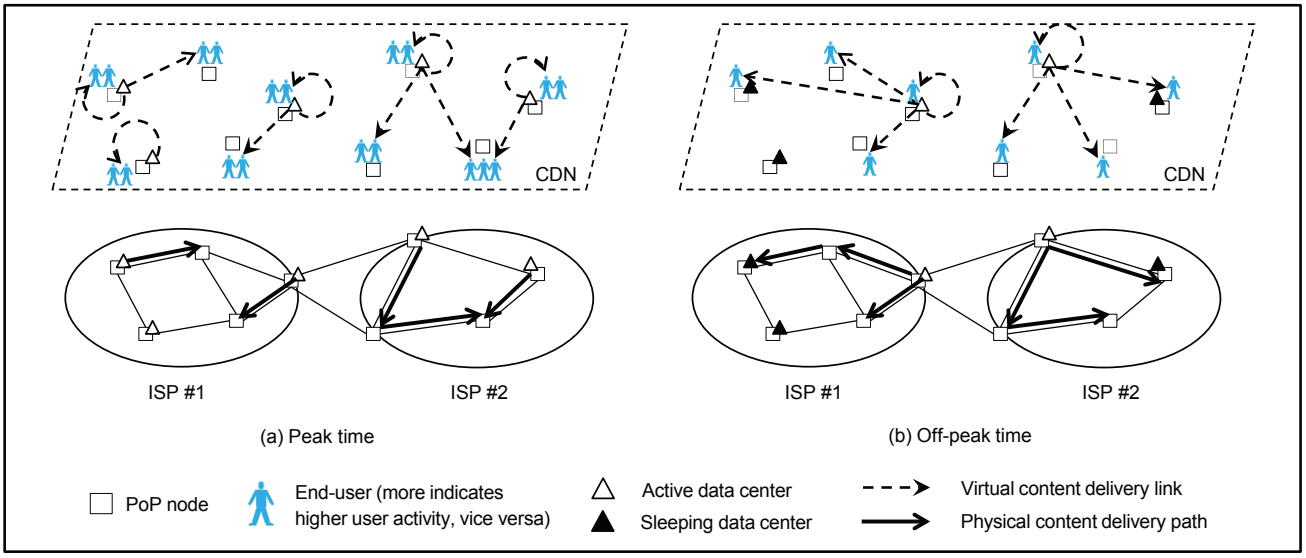

Fig. 1. Energy management scheme illustration: a) Peak time, when all DCs are active and serving user requests; and b) Off-peak time, when some DCs are in the sleep mode and requests are resolved to fewer active DCs.

capabilities on both the DC side and the network side. It is observed that user activities in a CDN typically follow a dynamic but relatively regular daily pattern [8], which implies that during off-peak hours, only a subset of all servers is needed to serve the requests. Therefore, in our scheme, content servers are dynamically provisioned with respect to the present content request volume instead of being kept active all the time. However, the realization of such an operation needs careful consideration on the tradeoff between the DC energy consumption and the CDN QoS performance. On one hand, the proposed scheme tries to put as many servers as possible to the sleep mode, as long as the remaining servers are capable of handling the present content requests. On the other hand, the server status reconfigurations also lead to changes in bandwidth utilization of the underlying ISP networks, as some end-users need to fetch content objects from more remote DCs. Intuitively, such request redirections will incur increased bandwidth consumption due to the growth of inter-PoP content traffic. In order to cope with such energy-performance tradeoff, specific constraints, which keep both DC servers and virtual links under their load capacities, need to be taken into account to avoid QoS deterioration in content consumption sessions with reduced content serving capability.

Moreover, there are some practical issues that are considered by our proposed scheme while performing on/off state reconfigurations on CDN servers. Firstly, during the server state reconfigurations, some ongoing or new content requests may need to be redirected to alternative DCs that are located at different PoP nodes. In a cross-domain CDN, this implies the possibility that the new DC might even be located within a different ISP domain. In this case, it can be inferred that the volume of inter-domain content traffic will be unnecessarily increased. Such a situation is effectively prevented in our proposed scheme which is still locality aware. Secondly, the reliability and lifetime of the server hardware will be affected if servers are turned on or off frequently [5]. In order to avoid such a situation, our scheme not only limits the number of on/off state transitions performed on servers, but also ensures that a server stays asleep for a sufficiently long period of time before it is activated.

II. Energy Management Scheme Overview

We consider large-scale CDN infrastructures that cover multiple autonomous ISP domains. In each domain, there exist a set of PoP nodes where local end-users initiate requests for web content objects. Each incoming content request is resolved to distinct DCs with specific policies. By default, a request is resolved to a local or nearby DC for improved QoS in terms of end-to-end delay [9]. Furthermore, within the specified DC, the request is assigned to a content server according to some load balancing policies (such as round-robin) to prevent servers from being overloaded [5]. These techniques are typically enforced via an overlay control plane in a centralized manner by the CDN operator [1]. In the proposed scheme, we focus on managing the PoP-to-DC request resolution policy across a CDN infrastructure, but it can be easily employed together with other DC-to-server request mapping policies to pursue further energy saving.

We first illustrate our main idea for energy saving in CDNs in Fig. 1. The conventional request mapping operation is shown in Fig. 1(a), in which five DCs are established to serve content requests from nine PoP nodes within two ISP domains. We can see that since the DCs are attached to five of the PoP nodes, requests from these nodes can be resolved locally without incurring inter-PoP bandwidth consumptions. For the other four PoP nodes, their requests are resolved to the DCs that are the closest to them, which is the common practice in real CDN environments to minimize user-experienced latency

[9].

At present, the CDN operators normally keep all DCs and servers up and running, so that end-users could experience optimized latency when requesting web contents [10]. Although this is necessary at peak hours as illustrated in Fig. 1(a), such a practice may lead to significant waste of CDN energy during off-peak hours. The main reasons are discussed as follows:

- From a single PoP node's perspective, the local end-users' request volume varies over different time periods within a single day, which is usually very low at midnight and early morning. Such a pattern has been observed in [8], which reflects the relatively-steady characteristic of CDN request volume at individual PoP nodes.
- From a CDN's perspective, content requests originate from geographically-distributed PoP nodes that are attached with end-users. Considering the difference in the global time zones among the PoP nodes or ISP domains, as well as the daily fluctuating pattern in end-user activities described above, it is unlikely that all domains experience high request volume simultaneously if we consider cross-continental ISPs (which is the case in typical large-scale CDNs).

Based on the two reasons above, it can be inferred that during off-peak hours, only a subset of servers is sufficient to serve all requests due to the low content request volume from local end-users. In this case, the remaining servers can be safely reconfigured to the sleep mode without introducing negative impact on the CDN performance, which will lead to considerable gains in energy saving of CDN data centers. Such a scenario is illustrated in Fig. 1(b), which shows that the servers in three DCs are put to the sleep mode during off-peak time in order to save energy. Meanwhile, all requests are served by the remaining two active DCs.

While considering energy savings, we also aim to assure the CDN performance in terms of end-to-end QoS. Such an objective is achieved by considering the following two aspects.

Firstly, basic performance assurance is provided through preventing DC servers and virtual content delivery links from reaching their full load capacities. As servers are responsible for handling user requests and delivering content objects, their response time degrades rapidly as they approach load capacities, which in turn affects the CDN QoS performance. Regarding CDN virtual links, as illustrated in Fig. 1, they are used to establish mappings between DCs and PoP nodes that are attached with end-users. Furthermore, network traffic incurred by content delivery will be mapped to underlying ISP networks for the actual delivery. Therefore, limiting traffic over virtual links reduces the risk of congestion in ISP networks, which has implications to end-to-end QoS performance.

Secondly, the CDN performance is further assured through avoiding the generation of unnecessary inter-domain content traffic. This is based on the following considerations. As DC servers are being put to the sleep mode, some requests will have to be redirected to an alternative DC, which could be located in another ISP domain. This should be avoided because a) inter-domain content delivery incurs significantly longer network distance, which increases end-to-end delay; and b) since inter-domain links are more critical compared to intra-domain links, they are more vulnerable to traffic congestions. Therefore, in order to reduce risk of congestion and assure user-experienced latency, inter-domain content delivery is avoided in our scheme when saving CDN energy. Such a scenario is illustrated in Fig. 1(b), in which content delivery sessions are restricted within each domain as three of the five DCs are put to sleep.

III. Energy Management Framework and Policies

In this section, we present the framework of our energy management scheme with relevant policies and show how it is embedded in a typical CDN platform. We also discuss some practical considerations that need to be taken into account when applying the scheme in real CDN environments. For the sake of clarity but without losing generality, we base our discussions on the scenario of Akamai networks [1], which is one of the largest CDN operators in the world.

A. Centralized Energy-Aware CDN Management

Since a CDN is a virtual overlay network built on top of physical ISP networks, it is essentially an application layer infrastructure over the Internet. In Fig. 2, we illustrate the functional blocks of a typical CDN platform with energy-awareness, which involves the following key components:

- **Monitoring Agents (MA)**. In a CDN, it is necessary to continuously monitor the conditions of DCs, servers and virtual links, since it is important that such information is up-to-date so that other components are able to make appropriate decisions on CDN management. The MA units keep reporting necessary context information above to data collection and analysis units and real-time mapping units, so that responses can be immediately made to cope with the events occurred in the CDN.
- **Data Collection and Analysis (DCA)**. The DCA unit is responsible for collecting data for general routine purposes such as logging, analyzing and billing.
- **Mapping Scoring (MS)**. The MS unit is part of the request mapping system in a CDN, and its responsibility includes creating an up-to-date Internet topology map including network connectivity, latency and loss information. The map is continuously refreshed by the MS unit.
- **Real-Time Mapping (RTM)**. The RTM unit is the other part of the CDN request mapping system. It creates a map with only DCs, servers and end-users, so that content requests are resolved to the best DC and server. It is responsible for request resolutions at both PoP-to-DC and DC-to-server levels, which are based on real-time information received from the MS and MA units. The RTM unit then instructs the DNS (domain name system) to resolve individual requests to their designated DCs and servers.
- **Communications and Control System (CCS)**. CCS is the channel for disseminating management information

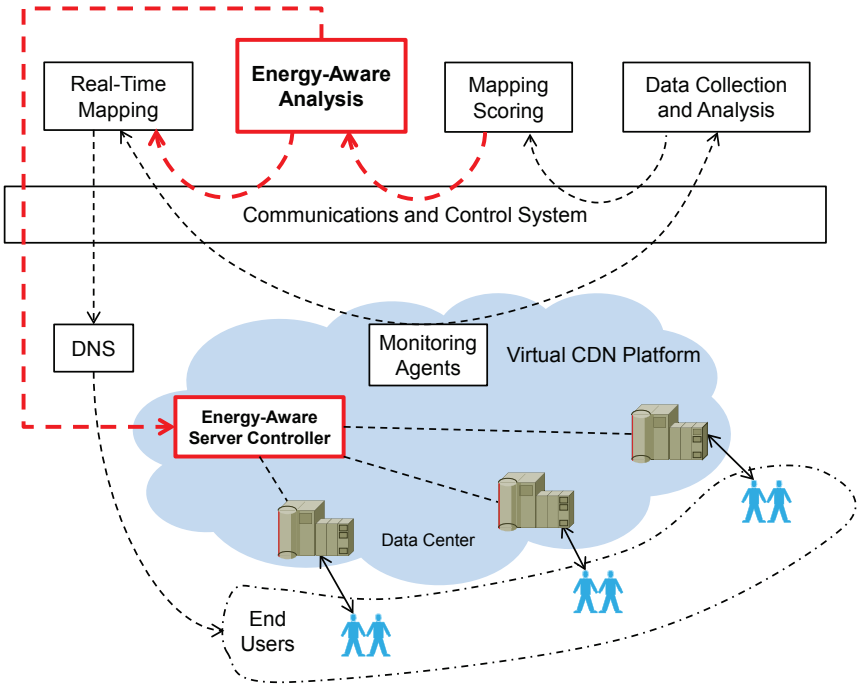

Fig. 2. Functional block diagram of proposed energy-aware CDN data center management system, based on [1]

such as control messages and status updates. As shown in Fig. 2, all management instructions between the functional units need to go through CCS.

So far we have described the basic functional components in a typical CDN platform. The question is - how can our proposed scheme be embedded in such an infrastructure? In Fig. 2, we also illustrate two additional management units that enable our scheme to be deployed in a CDN.

- **Energy-Aware Analysis (EAA)**. The EAA unit is the key component that is needed in our scheme, which is used to determine which specific servers need to be turned on or put to sleep. In order to make such a decision, it takes real-time CDN information as an input from the MS unit. With this information, The EAA unit is able to determine *how many* servers need to be turned on or off. Next, the CDN operator specifies a request-mapping policy to EAA, which is then used to determine mappings from user PoPs to DCs and servers to achieve optimized energy consumption and assured CDN QoS performance. Two examples of such request-mapping policies will be described in the next subsection. Afterwards, the EAA unit sends the mapping instructions to the RTM unit, which in turn instructs DNS to resolve the user requests.
- **Energy-Aware Server Controller (EASC)**. As a controller unit, EASC is built on top of the CDN platform to establish control over DCs and servers. As EASC receives instructions from the EAA unit on state reconfiguration of servers, it sends instruction signals to the specified servers for on/off status change. Such a technique is readily available in modern CDN platforms [1].

With the illustration of Fig. 2, we have shown that our energy-saving scheme is able to be embedded in modern CDN infrastructure in the form of functional blocks. By coordinating with other management components, our scheme is capable of utilizing real-time CDN information to make decisions to optimize the CDN energy consumption with assured QoS performance.

B. Request Mapping Policies

In the EAA unit, the CDN operator is able to specify different request-mapping policies that are suitable for CDNs with different characteristics and requirements. In this subsection, we show two examples of such policies, *i.e.,* Min-Energy-Dist and Min-Energy-DC.

- **Min-Energy-Dist**: This policy simultaneously optimizes DC energy consumption and network distances traversed by content delivery sessions. In other words, as the number of servers that are actively serving requests is minimal, requests are resolved to local or nearby DCs to optimize network distance and end-to-end delay. Under this policy, user requests are resolved in a distributed manner, and it is likely that every DC in the CDN will have some servers running to serve requests.
- **Min-Energy-DC**: While minimizing DC energy consumption, this policy aims to consolidate active servers into as few DCs as possible. In other words, content requests are resolved to the fewest possible number of active DCs, and the remaining DCs will have no active server running within them. This policy corresponds to the scenario illustrated in Fig. 1(b).

These two policies both have their own advantages and disadvantages. Regarding Min-Energy-Dist, since every DC has a subset of servers running, servers in each DC are provisioned in a more flexible way. For example, if the request volume suddenly increases in a specific area, the DCs in that area will have the flexibility to activate their own sleeping servers to handle the spike in local demand. However, since every DC has some servers running, the overall DC operational costs (*e.g.,* cooling system energy consumption) will be kept at relatively high levels. Regarding Min-Energy-DC, consolidating active servers to fewer DCs leads to easier DC and server management from a centralized point of view. Furthermore, if all servers in a DC are not needed for a certain period of time, then the entire DC could be scheduled for maintenance or sleeping for a given period of time, which introduces possibility of further saving in DC operational costs. However, the CDN becomes more prone to sharply-increased request volumes as entire DCs are being scheduled for sleeping mode reconfigurations. Therefore, Min-Energy-Dist is more suitable for CDNs with more dynamic user demands, where optimizing CDN QoS is prioritized over saving energy consumption. On the other hand, Min-Energy-DC is better for CDNs with regular user activity patterns, where DCs can be safely reconfigured to the sleep mode during off-peak hours without the need to worry about sudden increase in request volumes.

C. Working as a Whole System

After presenting the detailed information on the functional components and relevant operational policies, we now briefly describe how they work together as an energy-aware CDN management system. As MA and DCA continuously report up-to-date condition information on CDN network, DCs and servers to MS, the management system is always aware of the current CDN condition. Hence, MS forwards updated information to EAA, which is the key component of our scheme for decision-making purpose. EAA has two main responsibilities. Firstly, as EAA takes input from MS (as illustrated in Fig. 2), it makes decisions on which specific DC that each content request is resolved to, and send corresponding request mapping instructions to RTM. RTM then instructs DNS to resolve individual content requests to their designated DCs. Secondly, after EAA makes decisions on request mapping, it is able to determine which specific servers are safe to be turned on or off. It then instructs EASC to remotely configure the specified servers to on or off status. Such a management process repeats as MA and DCA keep refreshing CDN condition information in the system. As a result, the CDN energy consumption is optimized by EAA's instructions to RTM and EASC on request mapping and server on/off reconfigurations respectively. Meanwhile, the CDN QoS performance is assured during EAA's decision-making process by considering server and network load conditions.

It is worth noting that during the decision-making process above, EAA also aims to limit the number of on/off state transitions of the servers, so that wear-and-tear effect on server hardware is minimized. Such an objective is achieved via the following approaches. Firstly, as EAA is aware of the current status of servers, it tries to maximize the continuity in server on/off status during reconfigurations. In other words, on/off state reconfiguration will not be performed on a server unless the current request mapping policy requires so. Secondly, EAA also ensures that after a server has entered the sleeping mode, it will stay asleep for a sufficiently long period of time before it is powered on (unless the request volume suddenly increases and requires the server to be activated). Henceforth, the reliability and lifetime of CDN hardware are optimized by EAA while it saves energy consumption.

D. Content Delivery Session Redirection

At the moment when server on/off state reconfigurations take place, some ongoing content consumption sessions may need to be redirected on the fly to alternative servers as their originally-designated servers are affected. Generally, there are two different options for such session redirections:

- The session is redirected to another server located in the same DC. In this case, the redirection is seamlessly achieved through instructing the new server to deliver the content on behalf of the previous one. This is similar to the fast local server fault-recovery mechanism used by Akamai networks, and normally no human-perceived disruption to the ongoing content consumption sessions will take place.
- The session is redirected to another server located in a different DC. Normally, the ongoing content consumption sessions will firstly be disrupted while being switched to another DC. Furthermore, after the session is established between end-user and the new DC, QoS degradation may also occur due to increased network distance. In order to avoid a sudden and dramatic QoS deterioration for ongoing content consumption sessions in the above process, it would be better to "suspend" the server through letting it finish all the ongoing content delivery sessions, but not mapping any more new request to it until the server has finished all these ongoing sessions and hence is able to go to sleep. In this way, no ongoing session will be disrupted. Such a suspension mechanism has also been used by Akamai networks to fix servers with partial hardware faults.

Both options could take place in the two request mapping policies we have described, *i.e.,* Min-Energy-Dist and Min-Energy-DC. In Min-Energy-Dist, since all requests are

TABLE I
REPRESENTATIVE USER ACTIVITY SCENARIOS

#	**USA (GMT-8 to GMT-5)**		**EU (GMT to GMT+2)**	
	Time	User Activity	Time	User Activity
#1	[20:00, 23:00]	Medium	[04:00, 06:00]	Off-Peak
#2	[04:00, 07:00]	Off-Peak	[12:00, 14:00]	Peak
#3	[16:00, 19:00]	Peak	[00:00, 02:00]	Medium

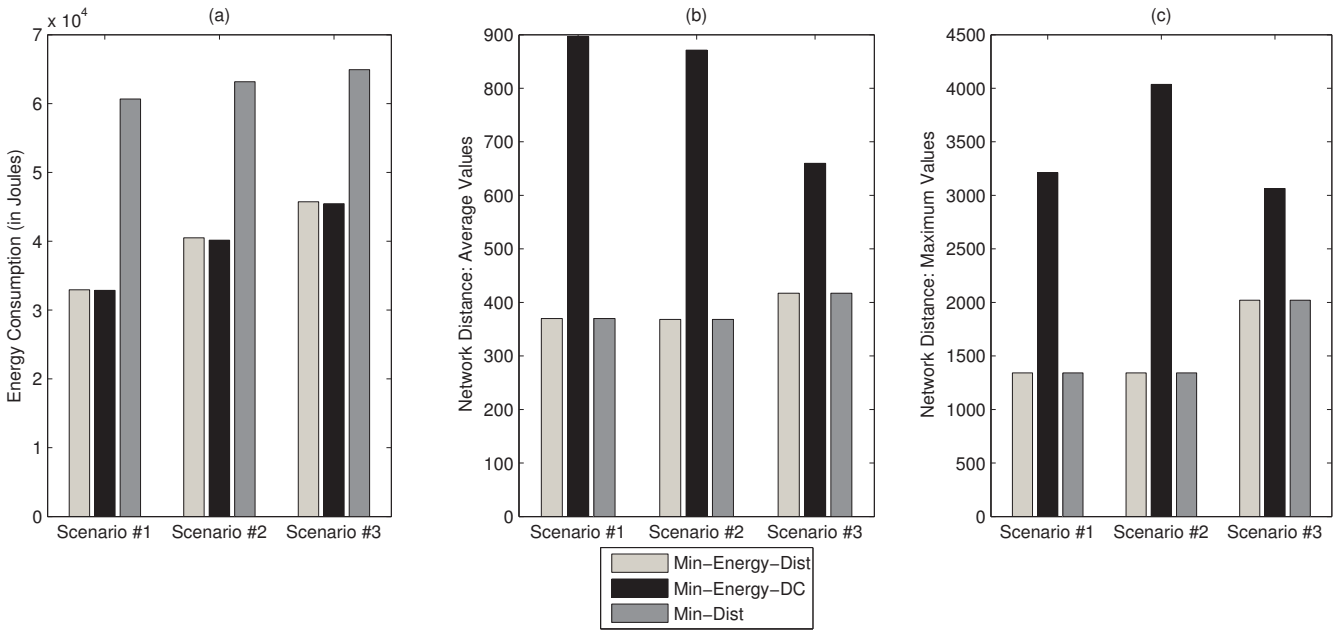

Fig. 3. Performance comparison among schemes with respect to different user activity scenarios: a) energy consumption; b) average network distance; and c) maximum network distance

resolved locally, the policy will firstly try to identify an alternative server in the same DC for seamless diversion, and an ongoing session will only be diverted to another DC if a local alternative server is not available. In Min-Energy-DC, it is more likely that ongoing sessions will be diverted to alternative DCs as active servers are consolidated to fewer DCs. However, under either policy or scenario, ongoing content consumption sessions will not be disrupted based on the techniques we have used.

IV. Experimental Results

In order to evaluate the performance of the proposed scheme, we use the real topologies from GEANT [11] and Internet2 networks [12], which are two interconnected autonomous domains in Europe and US respectively. Altogether, there are 34 PoP nodes that are distributed over Europe (25 nodes) and US (9 nodes), as well as 55 (bi-directional) network links interconnecting them (including 5 inter-domain links). We set 9 DCs to be deployed in the network (5 in GEANT and 4 in Internet2) and assume a 1:1 over-subscription ratio, which means the DC servers have *just* enough capabilities to serve all users in the network *simultaneously*. With respect to the conventional DC deployment strategy in a CDN [9], these 9 DCs are deployed to the 9 PoP nodes whose associated cities have the highest local populations.

We use the content request and traffic traces from the ClarkNet WWW server (an ISP covering Washington DC metro area) which is publicly available at the Internet Traffic Archive [13], and apply them to all PoP nodes according to the following approach. Firstly, we assume that end-users at all PoP nodes initiate content requests by following the same *pattern* as shown in the trace. Thereafter, the exact number of requests at each PoP node is approximated by applying a specific scaling factor to the request volume in the trace, which is proportional to the PoP's local population. This is necessary as the population associated to each PoP can vary substantially in reality.

As previously described, the proposed scheme takes into account time zone differences among PoP nodes in the CDN. Therefore, in the experiments, we identify three representative snapshots that reflect the changes in the CDN request volume within a single day while considering the geographical factor. For each snapshot, we calculate the overall request volume over one-minute period. These snapshots are listed in Table I, where they are referred to as scenarios #1, #2 and #3.

With the inputs specified above, we compare the performances of the following schemes.

Firstly, with the objective of minimizing DC energy consumption, we compare the request mapping policies of **Min-Energy-Dist** and **Min-Energy-DC**, which have been described in the previous section. Meanwhile, we also consider a reference scheme as a benchmark comparison:

Min-Dist: The scheme, as described in [14], optimizes content delivery efficiency through mapping requests locally or nearby. However, no energy awareness was considered and all servers are kept active regardless of the current request volume, which matches the common practice in DCs [10].

The experimental results are shown in Fig. 3, in which the following two metrics are compared in each of the three user activity scenarios:

- **Energy consumption** (in Joules): the amount of energy consumed by each scheme over the one-minute period,

TABLE II
DATA CENTER LOAD PERFORMANCE DETAILS

Data Center ID		GEANT (Europe)					Internet2 (US)			
		DC #1	DC #2	DC #3	DC #4	DC #5	DC #6	DC #7	DC #8	DC #9
Scenario #1	Min-Energy-Dist	66.7%	58.9%	93.3%	45.6%	73.3%	51.1%	37.8%	25.6%	13.3%
	Min-Energy-DC	100%	100%	100%	0%	34.4%	0%	34.4%	0%	92.2%
Scenario #2	Min-Energy-Dist	30.0%	18.9%	30.0%	15.6%	25.6%	100%	63.3%	62.2%	23.3%
	Min-Energy-DC	0%	18.9%	0%	100%	0%	68.9%	0%	100%	80.0%
Scenario #3	Min-Energy-Dist	16.7%	36.7%	55.6%	25.6%	37.8%	100%	100%	100%	60.0%
	Min-Energy-DC	0%	0%	100%	0%	68.9%	87.8%	73.3%	98.9%	100%

which is used to evaluate *energy-saving performance*.

- **Network distance**: the network distances traversed by content objects in each scheme while they are being delivered from DCs to end-users. This is calculated through aggregating the weights of links along the content delivery paths, which are proportional to real end-to-end delay according to the settings of GEANT and Internet2 networks [11][12]. Both *mean* and *maximum* values are investigated to reflect both average and worst cases in end-to-end delay, which are used to evaluate the CDN QoS performance.

It can be immediately observed from Fig. 3(a) that the proposed scheme can substantially reduce energy consumption of the servers in CDN data centers. In the three user activity scenarios, energy consumption has been reduced by 45.9%, 36.4% and 30.0% respectively. Generally speaking, the higher the content request volumes are, the less energy consumption can be saved as more active servers are needed to serve the requests.

From Fig. 3(b) and (c), it can be seen that regarding the average and maximum network distances traversed by content requests, Min-Energy-Dist and Min-Dist have achieved the same results. This shows that the Min-Energy-Dist policy is capable of significantly reducing DC energy consumption without compromising the CDN QoS performance. Compared with these two policies, Min-Energy-DC has increased network distances while achieving the same amount of energy saving as Min-Energy-Dist. This is because requests are mapped to fewer DCs instead of being resolved locally, and some requests need to travel among PoP nodes in order to be served.

In order to further indicate how Min-Energy-Dist and Min-Energy-DC perform, we show how the DC loads (in percentage) differ in these two policies under the three user activity scenarios in Table II. It can be observed that in Min-Energy-Dist, the requests tend to be distributed evenly among the DCs. This is because the DCs are deployed in a distributed fashion among all PoP nodes, and all requests are resolved to either a local or the nearest DC to optimize network distance. In contrast, it is shown in Table II that Min-Energy-DC tries to resolve requests to fewer DCs while pushing them toward their load capacities but without overloading them. Under such a policy, some DCs in the areas with medium or low user activity will not have any running server in them.

Based on Fig. 3 and Table II, it is shown that Min-Energy-Dist optimizes CDN energy consumption with respect to locality-based policy, which introduces some flexibility to the CDN server provisioning as every DC is active with a subset of servers running. On the other hand, Min-Energy-DC also optimizes CDN energy consumption, but through resolving requests to fewer DCs. Although it causes tradeoff in network distances, it introduces easier DC and server management as well as possibility of further saving in DC operational costs. Overall speaking, these two policies are able to save the same amount of energy under the same scenario, and it is up to the CDN operators to determine which one is more suitable with respect to their specific CDN requirements.

V. SUMMARY

In this article, we have introduced a novel energy management scheme that is able to effectively reduce CDN energy consumption. Based on the present request volume in the CDN, our scheme provisions the minimal number of active servers to serve content requests and reconfigures the rest to the sleep mode for energy saving purposes when the content demand is low. The CDN QoS is assured through honoring constraints on load capacities of servers and virtual links in the CDN, as well as restricting inter-domain content traffic to avoid increased end-to-end delay. Meanwhile, reliability and lifetime of CDN hardware is assured through avoiding frequent on/off state transitions of servers. From a practical perspective, the proposed scheme can be built as functional blocks and be embedded in modern CDN management platforms. Our experiments, which are based on realistic CDN scenarios and traffic traces, have demonstrated that the proposed scheme can achieve the energy reduction of up to 45.9% without compromising the CDN performance in terms of end-to-end delay.

ACKNOWLEDGEMENT

This work was partially funded by EU FP7 EVANS Project (PIRSES-GA-2010-269323).

REFERENCES

[1] E. Nygren, R. K. Sitaraman, and J. Sun, "The Akamai network: a platform for high-performance internet applications," *SIGOPS Oper. Syst. Rev.*, vol. 44, pp. 2–19, August 2010.

[2] N. Feamster, L. Gao, and J. Rexford, "How to lease the internet in your spare time," *SIGCOMM Comput. Commun. Rev.*, vol. 37, pp. 61–64, January 2007.

[3] C. Ge, Z. Sun, and N. Wang, "A survey of power-saving techniques on data centers and content delivery networks," *IEEE Communications Surveys & Tutorials*, vol. PP, no. 99, pp. 1 –21, 2012.
[4] L. Chiaraviglio and I. Matta, "Greencoop: cooperative green routing with energy-efficient servers," in *Proc. ACM e-Energy'10*. New York, NY: ACM, 2010, pp. 191–194.
[5] V. Mathew, R. K. Sitaraman, and P. Shenoy, "Energy-aware load balancing in content delivery networks," in *Proc. IEEE INFOCOM'12*. Florida, OL: IEEE, March 2012, pp. 954–962.
[6] P. X. Gao, A. R. Curtis, B. Wong, and S. Keshav, "It's not easy being green," in *Proc. ACM SIGCOMM'12*. New York, NY, USA: ACM, 2012, pp. 211–222.
[7] L. A. Barroso and U. Holzle, "The case for energy-proportional computing," *Computer*, vol. 40, no. 12, pp. 33–37, 2007.
[8] P. Gill, M. Arlitt, Z. Li, and A. Mahanti, "Youtube traffic characterization: a view from the edge," in *Proc. ACM IMC'07*. New York, NY, USA: ACM, 2007, pp. 15–28.
[9] R. Krishnan, H. V. Madhyastha, S. Srinivasan, S. Jain, A. Krishnamurthy, T. Anderson, and J. Gao, "Moving beyond end-to-end path information to optimize cdn performance," in *Proc. ACM IMC'09*. New York, NY, USA: ACM, 2009, pp. 190–201.
[10] C. Ge, N. Wang, and Z. Sun, "Optimizing server power consumption in cross-domain content distribution infrastructures," in *Proc. IEEE ICC'12*, June 2012, pp. 2628 –2633.
[11] Geant project home. [Online]. Available: www.geant.net
[12] The internet2 network. [Online]. Available: www.internet2.edu/network/
[13] Traces in the internet traffic archive. [Online]. Available: http://ita.ee.lbl.gov/html/traces.html
[14] J. M. Almeida, D. L. Eager, M. K. Vernon, and S. J. Wright, "Minimizing delivery cost in scalable streaming content distribution systems," *IEEE Trans. on Multimedia*, vol. 6, no. 2, pp. 356–365, 2004.

Underfloor Air Containment

Mikko Pervilä and Jussi Kangasharju
Department of Computer Science
University of Helsinki
PL 68, FI-00014 Helsingin yliopisto
Email: {pervila,jakangas}@cs.helsinki.fi

***Abstract*—This paper presents Underfloor Air Containment (UAC), a straightforward extension to Cold Aisle Containment (CAC). Both techniques aim to eliminate air stream mixing and thus reduce the volume of supply air needed for cooling. In UAC the underfloor air supply plenum of a data center is mechanically restricted to the floor sections containing the perforated tiles. We have implemented UAC in our department's 110 kW, 74 m^2 data center. Through experimental evaluation and per-tile air velocity measurements, we show that UAC improves the air velocities passing through the perforated tiles in the CAC by 9%. Our solution is light-weight, very low cost, and rapidly installable in other data centers.**

I. Introduction

In 2007 a popular analysis by Gartner [1] estimated that the combined greenhouse gas (GHG) emissions caused by all fields of ICT amounted to 2% of the man-made total. Combining that data with the SMART 2020 report [2] we can see that the GHG emissions from ICT are growing much faster than the overall GHG emissions. This strongly implies that the share of ICT today is considerably larger than the often-quoted 2% and probably nearer to 3%. There has been no indication that the growth rate would have yet substantially diminished.

Thus, urgent action is required to cut down emissions from all fields of ICT. If we are to avoid a climate catastrophe, directly applicable techniques must be adapted both at the edges of the network and its core. As small changes repeated often enough can yield large savings globally, it is less important to concentrate only on the largest consumers. Even smaller reductions should be installed if their capital costs are relatively small or insignificant compared with the savings.

When 41% of data centers (DCs) are formed by small-scale installations [3] and they are often operated by companies whose expertise is not in DC operation [4], it is hardly surprising that these DCs can become very inefficient through gradual evolution. In order to reduce the energy requirements of these DCs, we need techniques that can be applied retroactively. And to remain attractive for the DC maintainers, these techniques must have small capital expenses, short installation times, and require little expert knowledge to install. Our previous work fits neatly into this category of *data center energy retrofits*.

Most DCs employ computer room air conditioning (CRAC) units that supply cold air for the servers. The air can be supplied either directly or through a raised floor called an underfloor plenum. Regardless of the method, without air stream separation server exhaust air can easily mix with the supply air flow, mitigating its cooling effectiveness. Earlier, we have verified the effectiveness of an air stream separation technique called cold aisle containment (CAC) [5], [6]. We have shown that an effective CAC setup can be built using very low cost plastics, in a short time span, and using very limited knowledge. This makes our solutions applicable to a wide range of existing data centers.

This article presents a complimentary technique that further optimizes the cooling air flow for DCs using an underfloor supply plenum. The idea is rather straightforward: we extend the air stream containment into the plenum under the server racks. By doing so we effectively diminish the volume of space where cooling is supplied by the CRAC units. This in turn leads to less turbulence caused by underfloor blockages, smaller leakage of air through gaps in the raised floor structure, and a larger air flow rate where cooling is needed.

A. Related Work

The key issues of using an underfloor plenum are air flow blockages and leakages [7]–[10]. Blockages are relatively well understood and often caused by power and network cabling, floor support structures, extinguishing systems, and other accumulated materials in the plenum. Air flow leackages are often caused by cable cutouts inadequately sealed by grommets, but also by other gaps in the the raised floor.

Despite the well known issues regarding the plenum, relatively few solutions to improve the air flow through the raised floor have appeared. Zhou et al. [11] recently proposed adaptive vent tiles (AVT), which are a motorized version of the standard perforated types. Using AVTs and an elegant optimization algorithm, they were able to reduce the cooling power usage by 10–14 kW in a DC employing a 300 kW IT load. At least one company specializing in DC environments offers products designed for plenum air flow control [12]. Unfortunately, they do not provide any public data about the efficiency gains of using their product. Finally, VanGilder and Schmidt [8] evaluated raised floor air uniformity, but exluded underfloor blockages from their CFD simulations.

To our knowledge, this article is the first academic study on the benefits of using UAC in a DC. We present two main experiments involving the combination of UAC and the low-tech CAC [5] we built earlier, and then UAC combined with a much more expensive, improved CAC we have only recently completed. An in-depth examination of perforated floor tile air velocities shows that the aggregate improvement of UAC is about 9% over the whole CAC.

This paper is structured as follows. Section II describes our data center and the UAC setup that we evaluate. Section III presents our measurements and results. In Section IV we discuss the limitations and wider applicability of our UAC solution. Finally, Section V concludes the paper.

978-1-4799-0354-2/13/$31.00 ©2013 IEEE

II. Data Center Layout

Our experimental DC is named the Exactum DC after the building housing it. For brevity, we reiterate only the key attributes here. For further details, see our previous studies [5], [6]. A floor plan of the DC is shown in Fig. 1. The raised floor is constructed using $60 * 60$ cm tiles, some of which are perforated to allow for air flow. The width of the DC is 11 tiles and the length 19 tiles, yielding a floor area of just over 74 m^2, excluding some unusable space wasted by the architecture.

The floor is raised by approximately 60 cm and consists of three types of tiles and their accompanying support structures, as pictured in Fig. 2. The tiles are raised from the actual floor below using support pedestals, which are adjustable to ensure a completely level floor plan. Pedestals are distributed so that they support the tiles from their corners, meaning that most pedestals support four tiles each. Pedestals closer to the walls of the room may support either one or two tiles, also by their corners.

Most of the tiles in the DC are solid and demonstrated by the white color in Fig. 1. In addition, there are two types of perforated tiles which differ in their air flow rate due to the fraction of perforated to solid area. Perforated tiles with a smaller flow rate are depicted by a light gray color and designated the identifiers $1, 7, 9, 19, 21, 23$. The larger flow rate tiles are marked by a dark gray color and designated $2, 4, 5, 6, 8, 17, 20, 22, 24, 25$. Note that #25 is located outside of the CAC. This perforated tile was installed by our administrators in order to make sure that the network devices located in the rack next to it would receive adequate air flow. These devices incorporate reverse air flow, meaning that they draw their supply air from the back of the rack.

A. Gaps in the Floor

In addition to the perforated tiles mentioned previously, air flows through the raised floor through gaps between the tiles and cable cutouts made intentionally. Gaps between the tiles occur when the tiles are handled due to maintenance. The tiles can now easily switch orientation, meaning that they no longer rest exactly as intended on the pedestals. This can even lead to visible gaps forming between the tiles. Also, as the tiles are worn down by use, smaller leakages occur near the edges where the tiles meet.

Cable cutouts are made in the floor near the rears of many racks to allow electrical or network cabling to be installed in the underfloor plenum. Cutouts should always be sealed with grommets. Grommets typically use either flaps or brush-like structures to reduce air flow around the cables. The quality and age of the grommets dictates how well they handle their intended purpose, but the overall result is that some air always leaks through.

B. Air Velocity Measurements

Since the Exactum DC is a live production environment for many research groups, its current layout has evolved somewhat piecemeal. This includes a cooperation effort of no less than four different university departments responsible for the servers, network, power cabling, and cooling respectively. Due to the weight of history, some installation details have become lost. Unfortunately, this includes the manufacturers and models of the perforated tiles, meaning that we do not currently know what the tiles' perforated areas are.

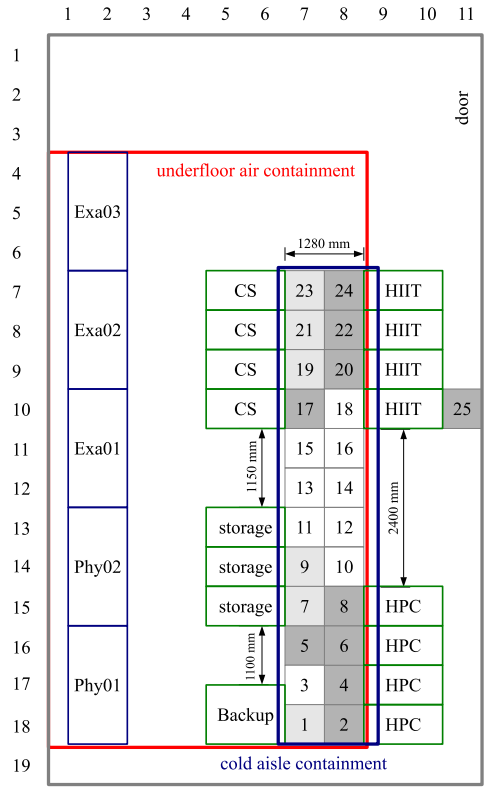

Fig. 1. Exactum DC layout and perforated tile numbering

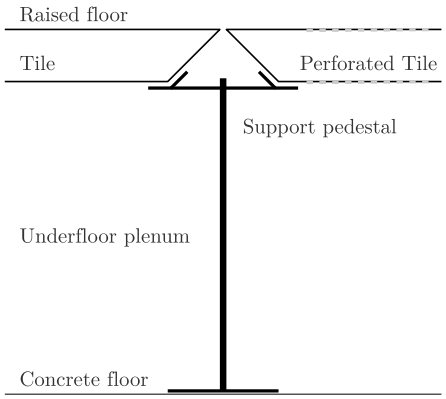

Fig. 2. Underfloor plenum, tiles and support structure

This implies a small problem to solve concerning measurement units. Air flow in DCs is usually measured in volumetric flow rates, meaning that the results are reported in ft^3/min, l/s, or m^3/s. Since the perforated areas are currently unknown, instead of using volumetric flow rates, we have chosen to report air velocities in m/s. While volumetric air flows are calculated assuming a uniform flow through a duct or a perforated tile, air velocities are spotwise measurements. Avoiding the assumption of uniform air flow proves useful in Sect. III-C, where we measure the tiles per quadrant and confirm that significant differences do occur per tile.

For our measurements, we used a TSI VelociCalc 5725 rotating vane anemometer. The meter is calibrated to an error rate of < 0.1 m/s, and it is able to record air velocity, volumetric flow rate, and temperature. Though the volumetric flow rate measurements as such are useless without the correct perforated areas of the tiles, this combination of data points means that we can later reconstruct the real volumetric flow rates per tile. Detailed specifications regarding the meter are available on the web site[1].

C. Underfloor Air Containment

The installation of the UAC itself was relatively simple. Our construction material was polyethylene sheets reinforced by nylon wire mesh. The mesh made the material not only heavier and more durable, but also simplified attaching the sheet to the support pedestals (see Fig. 2) using cable ties. The material costs for the installation amounted to 39.77 €.

In order to minimize leakages, we affixed the UAC curtain so that its top edge was wedged between the raised floor tiles. Conversely, the bottom edge was weighted down on the concrete floor using steel bars. As the plastic sheet was relatively heavyweight to begin with, installation was quite simple and completed in one hour by the first author working alone, i.e., one hour of work effort for one person.

The UAC curtain is depicted in Fig. 1 by the rectangle colored in red. The topmost edge runs between rows 3 and 4 from the CRAC side of the room to between columns 8 and 9. Then, the UAC extends rearwards towards the section between rows 18 and 19. From here, the UAC turns again towards the CRACs and continues to the wall just next to the CRAC designated "Phy01" [5].

The primary effect of the UAC is to reduce the volume of the underfloor plenum used for supplying cold air for the servers in the CAC. By installing UAC, we have reduced the cooled floor area by $(209 - 120)/209 \approx 42.6\%$. Note that while floor tile leakage may be roughly uniform throughout the raised floor, the cable grommets are not evenly distributed. Thus, our UAC can be expected to remove roughly half of the leakage due to the grommets, as the other half are still in the pathway of the supply air, i.e., in front of the CRACs.

We opted for a rectangular shape for the UAC for ease of construction and did not attempt to fully minimize the area to be cooled. An obvious optimization would be to have the top edge go diagonally from the CRAC "Exa03" towards tiles #23 and #24. However, we do not believe this to yield significant additional benefits and the ease of construction was a more important factor in our case.

D. Existing and New CAC

As outlined in our article [5], our CAC setup was installed using low-cost plastics. This means that the construction materials consisted mostly of transparent polyethylene plastic sheets and duct tape. The wall materials were later upgraded to polypropylene sheets for easier access through sliding doorways. This incurred some additional costs, for a total of 373.40 €. Some leakages have later on appeared near the roof of the CAC, caused by degrading duct tape.

[1]http://www.tsi.com/VELOCICALC-Rotating-Vane-Anemometer-5725/

Though the leakages could have easily been reinforced with more duct tape, we had other incentives to improve the outlook of the CAC. Thus, we set out to not only install UAC, but also improve the CAC with a much more advanced (and high-cost) setup. For further details regarding material and construction choices, please visit our web site[2]. We return to the costs of the improved CAC in Section IV and its effects in Section III-A. Without spoiling too much in advance, the improvements provided by the much improved materials where almost completely visual and not quantitative.

E. Measurement Methodology

In order to separate the effects of the two different changes, we set out to do our measurements in phases as follows.

1) 8 h period representing situation before any changes
2) 8 h period representing UAC + existing CAC
3) 8 h period representing UAC + improved CAC
4) 8 h period representing no UAC + improved CAC

In order to yield meaningful before/after type measurements we set all four operational[3] CRAC units to a fixed blower speed. This setting is temporary and the units will be returned to a variable speed after our measurements have been completed.

The rationale between the different measurements is as follows. First, the situation before any changes was undertaken to verify that the air velocity, and thus, flow rate, through either kind of tile was reasonably stable throughout the CAC. Any larger variations would have been indicative of dynamic turbulence effects in the underfloor plenum, or possibly malfunctioning blower units in the CRACs. In all measurements, the readings were extremely stable no matter how long the measurement intervals were.

Second, the measurement taken with UAC and our previous CAC indicates whether UAC could improve our less than ideal CAC setup. If the UAC could improve air flow in the CAC enough to eliminate exhaust recirculation caused by leakages, other DCs could avoid costly CAC improvements altogether.

Third, the measurements completed with the improved CAC represent the "ideal" situation attainable using a DIY installation. The fourth measurements were completed to attain the per tile and per quadrant readings, which we will discuss in the next section.

III. Measurement Data

All measurements were done with the rotating vane resting on top of the measured tile, and each position was carefully marked for repeatability. The measurement interval was 60 s and each sample was taken over a 10 s average. We did experiment with other mesurement and sampling intervals, but the differences remained below the measurement error. Whenever not explicitly stated otherwise, we have reported the average results over all samples taken.

Initially, we verified the flow rates of only three tiles in the CAC. These tiles are numbered in Fig. 1 as tiles #6,

[2]http://wiki.helsinki.fi/display/ExactumDC/Third+CAC

[3]Even though the DC has five units, one has been taken offline following the efficiency improvements caused by our CAC setup [5].

#20, and #25 respectively. Tiles #6 and #20 correspond to the CAC temperature measurement sensor positions further detailed earlier [6]. This allowed us to compare the effects of changing air velocities with our CAC temperatures.

We had only one anemometer at our disposal. The 8 h measurement periods were completed by interleaving 2 h measurements from tiles #6 and #20, swapping the vane position at each interval. Measurements at tile #25 were done after the 8 h periods and were considerably shorter, since we had already verified that the readings remained stable despite the measurement period.

A. Three Tiles Only

In phase 1 of our measurements, we recorded the air velocities with all CRACs set to fixed blower speeds, no UAC, and with the previous CAC still installed. Air velocity through tile #6 was 2.61 m/s (stdev 0.0164) while tile #20 showed 3.1 m/s (stdev 0.0149). Within our measurement error, tile #25 maintained the same flow at 2.99 m/s (stdev 0.0468).

Subsequently, we constructed the first version of the UAC and measured phase 2. The air velocity measured at tile #25 dropped to 1.88 m/s (stdev 0.0506) and conversely, tile #20 arose to 3.34 m/s (stdev 0.0204). We also verified that the temperature delta from the floor of the CAC to its roof measured at tile #6 was reduced from approx. 1.7°C to zero. This strongly suggested that more air was flowing into the CAC and, consequently, less outside of it. Hence, UAC seemed to be improving our previous CAC, which indicates that even the low-cost version remains sufficient for many DCs.

Despite the encouraging results, our first problem was the air velocity measured at tile #6, as it had now dropped to 2.19 m/s (stdev 0.0248) – a reduction of approx. 0.3 m/s. After repeating our measurements and improving the UAC with rubber (polyurethane) foam seals near the CRAC walls, we were able to further reduce the velocity at tile #25 to 1.47 m/s (stdev 0.0111). Yet, this did not improve air flow at tile #6. At this point, we constructed the improved version of the CAC and verified our measurements (not shown). There were no visible changes in either the air velocities or the temperature measurements.

B. Each Tile

After negotiations with multiple colleagues with extensive backgrounds in computational fluid dynamics (CFD) modelling, we set out to measure a much more holistic picture of the perforated tiles in the CAC. Using 30-minute intervals we recorded the air velocity at each of the 16 perforated tiles.

Table I records the latest measurements. First, note that the reduction of tile #25 is by design, since it is left on the other side of the UAC. Second, it seems that our initial selection of tiles was extremely lucky, since #6 was only the other of the two tiles in the CAC with reduced air velocities. If we had not chosen this measurement point, parts of the picture would have remained unseen to us.

By calculating the changes in air velocities at each tile, we can now estimate the aggregate change caused by UAC. For the comparison to be fair, we include tile #25 in the aggregate "before UAC", since the perforated tile was installed on purpose. In other words, we exclude it from being part of the unintentional leakage of the raised floor. Conversely, we disregard the negative change of tile #25 in the aggregate "after UAC". Whatever air flows through the tile now is part of the raised floor leakage, though we can not measure all of it.

TABLE I. AIR VELOCITIES IN M/S, MEASURED PER TILE

Tile #	Before UAC	After UAC	Change
1	1.19	1.4	0.21
2	2.49	2.58	0.09
4	2.24	2.12	-0.12
5	2.46	2.58	0.12
6	2.63	2.24	-0.39
7	1.54	1.59	0.05
8	2.39	3.4	1.01
9	1.47	1.62	0.15
17	3.47	3.9	0.43
19	1.46	1.64	0.18
20	2.9	3.45	0.55
21	1.55	1.72	0.17
22	2.72	3.09	0.37
23	1.59	1.74	0.15
24	3.35	3.73	0.38
25	3.3	1.38	-1.92
total	36.75	38.18	1.43

TABLE II. AIR VELOCITIES IN M/S, MEASURED PER TILE QUADRANT

	Before UAC		After UAC		Change	
Tile #	avg	stdev	avg	stdev	avg	stdev
1	1.33	0.056	1.29	0.120	-0.0375	0.065
2	2.94	0.505	2.90	0.521	-0.0375	0.016
4	2.72	0.538	2.93	0.761	0.205	0.223
5	2.17	0.240	2.40	0.269	0.235	0.029
6	2.93	0.726	3.28	0.731	0.3525	0.005
7	1.38	0.234	1.51	0.206	0.1275	-0.028
8	3.06	0.332	3.51	0.284	0.455	-0.048
9	1.44	0.117	1.59	0.137	0.15	0.019
17	3.27	0.275	3.87	0.179	0.6	-0.096
19	1.40	0.062	1.58	0.087	0.18	0.025
20	3.06	0.258	3.60	0.206	0.535	-0.052
21	1.48	0.128	1.61	0.144	0.13	0.016
22	3.21	0.280	3.37	0.329	0.155	0.049
23	1.56	0.064	1.71	0.075	0.1475	0.012
24	3.42	0.172	3.68	0.178	0.26	0.006
25	3.25	0.165	1.38	0.346	-1.87	0.181
total	38.60	4.15	40.19	4.57	1.5875	0.421

Therefore, the effect of UAC can be calculated simply as $(1.43+1.92)/36.75 \approx 0.091$ or roughly 9%. In order to verify this number we then decided to increase our granularity, and measure each tile at four different positions.

C. Each Quadrant

Next, we verified our measuments by examining each tile more closely. We divided each tile clockwise into four quadrants so that using the orientation of Fig. 1, the top right quadrant of each tile is titled Q1, the bottom right Q2, and so on. The additional measurements revealed that the underfloor air flow was very nonuniform indeed.

We will discuss some of the more surprising readings and then present the average results both in Table II and Fig. 3.

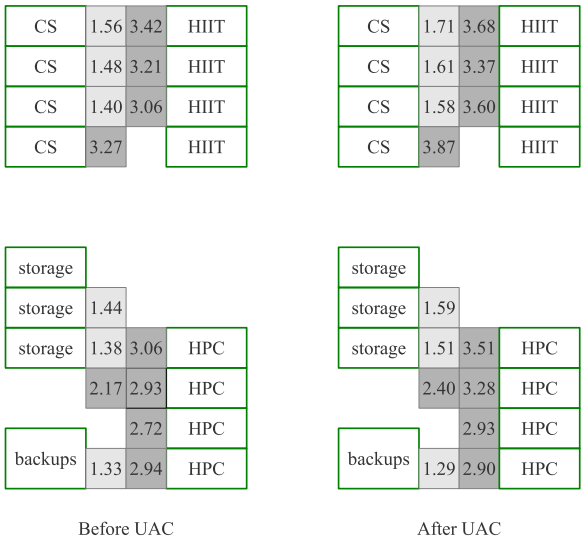

Fig. 3. Per tile air velocities in m/s, calculated as averages of the per quadrant measurements

Most notably, the tiles which exhibit reductions in air velocity are no longer the same as in the per tile measurements. When the air velocities are calculated as the averages of the four per quadrant measurements, the negative changes are now found in tiles #1 and #2. Their negative changes are also much smaller.

In addition, there are quite significant differences per quadrant for some of the tiles. For example, in our readings taken without UAC, the largest intra-tile reduction occurred at tile #6. Its Q2 indicated an air velocity of 3.6 m/s while Q4 measured only 2.08 m/s. In other words, a reduction of almost 50% in less than 30 cm. With UAC, the situation changed somewhat, but large differences in the tile quadrants could still be seen. The largest change occurred at tile #4 when its Q1 showed 3.57 m/s and Q3 only 1.94 m/s. All in all, the sum of stdevs increased very slightly from 4.15 before UAC to 4.57 after UAC.

We can also calculate the aggregate changes between the different halves of the CAC, as represented by tiles 1–9 and 17–24. By doing this, we notice that UAC seems to benefit the door-side half of the CAC more, as its aggregate increases by 2 m/s, while the rear half's increases by only 1.45 m/s.

Despite these changes, the overall effects of installing UAC remained the same even when the air velocity measurements were completed per quadrant. Including #25 in the situation before UAC and omitting it from after UAC yields us a calculation of $(1.5875 + 1.87)/38.60 \approx 0.09$ or, again, very close to 9%.

D. Measurement Errors

For future studies, it is useful to provide some estimates for the measurement errors between the readings taken per quadrant and per tile. By calculating the average air velocity for each tile from the four per quadrant calculations and choosing this average as the tile's "true" reading, we get the differences to the per-tile measurements as presented in Table III.

TABLE III. MEASUREMENT DIFFERENCES IN M/S PER QUADRANT AND PER TILE

	Before UAC	After UAC
Tile #	**error**	**error**
1	-0.1375	0.11
2	-0.45	-0.3225
4	-0.4825	-0.8075
5	0.2925	0.1775
6	-0.2975	-1.04
7	0.1625	0.085
8	-0.665	-0.11
9	0.035	0.035
17	0.2	0.03
19	0.065	0.065
20	-0.16	-0.145
21	0.07	0.11
22	-0.4925	-0.2775
23	0.0325	0.035
24	-0.0725	0.0475
25	0.0525	0.0025
total	-1.8475	-2.005

From these numbers we can notice that the measurements per tile seem to undercount the aggregate changes somewhat. The aggregate error is -1.8475 m/s without UAC and -2.005 m/s with UAC. Interestingly, the errors are very unbalanced when measured separately for the CAC halves. Without UAC, the aggregate error for the door-side half (tiles 1–9) of the CAC is -1.543 m/s, while the rear half's error is only -0.305 m/s. With UAC, the aggregate errors both rise and lower to -1.873 and -0.133 m/s respectively.

Although UAC works, it can not homogenize the air velocities, and thus not the air flow rates through the tiles. While the key result of a 9% gain was achieved through both the per tile and per quadrant measurements, the first-mentioned do hide some parts of the overall flow heterogeneity. This seems to be an effect of extremely complex air flow changes in the plenum under the perforated tile, making CFD modelling of the effects we have measured difficult indeed [8].

IV. DISCUSSION

First, the costs of our improved CAC operation were an order of magnitude higher, raising from the 373.40 € mentioned in Section II-D to 2,338.25 € for the new material costs. In addition, the installation took much longer. The previous CAC was installed in 6 man-hours, while the new installation took six and a half man-*days* to complete. While we completed the more professional CAC in order to verify the efficiency of the previous low cost solution [5], it is no surprise that our IT operators were much more pleased with the end result, despite the additional costs they paid. The goodwill generated is of importance while negotiating future experiments in our DC, although other operators can make do with the low-cost version just as well.

In theory, the main drawback of installing CAC or UAC is the reduction of supply air volume in the DC [13]. This means that in case of a power supply failure, there is a smaller reservoir of cold air in the DC. This flaw must carefully be balanced against the benefits of CAC. The main benefit is that CAC can much more easily be retrofit into an existing DC.

By comparison, a hot aisle containment (HAC) setup requires considerably more complete air ducts for the exhaust or return flow. As neither HAC or CAC can entirely avoid overheating scenarios, it is our recommendation that the shutdown temperatures of servers should not be disabled. Fortunately, in most commercial servers this remains impossible.

Another drawback is that UAC may not be applicable in all DC environments. If the CRAC units are distributed evenly along all of the walls of a DC, there may not exist suitable floor areas for installing UAC. This is an unavoidable problem of some DC environments. However, for global energy reductions to occur, it is enough that UAC is employed in those cases where it remains applicable.

Finally, UAC is not able to remove or even diminish turbulence caused by underfloor blockages. Despite this drawback, it presents a sizeable improvement in air velocity through the perforated tiles in the CAC. A 9% improvement in CRAC blower speed means that more servers can be installed in the DC. In addition, we have earlier shown that in the same conditions, CAC yielded an improvement of 20%. As both CAC and UAC can be installed very cheaply, their combined enhancement of almost 30% CRAC blower power makes the payback time very attractive[4]. CAC is by now a very much standard DC technique for improving air flow. It is our hope that UAC will also catch on.

V. Conclusion

In this paper we have presented our Underfloor Air Containment solution for optimizing air flow under a data center raised plenum. Our solution complements existing cold air containment techniques and allows for a more efficient control of the cooling supplied by CRACs. We have implemented UAC in our department's 110 kW, 74 m^2 data center and our extensive measurements show that UAC has improved the aggregate air velocity by 9% within the CAC. UAC is readily adoptable in other data centers with minimal installation cost and effort required. UAC also combines well with CAC.

In addition to the benefits of UAC, we have demonstrated how underfloor blockages can yield very nonuniform air velocities, and thus flow rates, through the perforated tiles in a CAC. While UAC is unable to homogenize the air flow, there are direct benefits of increasing the aggregate air flow in the CAC. Simultaneously, these effects imply that the measurements attained by prototype testing would have been extremely difficult to attain through computational fluid dynamics modelling only. Finally, installing UAC reduces the needs for high-quality cable cutouts or grommets. The savings attained through reduced energy and purchase costs yield an almost immediate payback time for the materials involved.

Acknowledgment

The authors would like to thank Timo Ojanen for repeatedly lending his construction skills throughout the deployments of our prototypes. Without Timo, not much would have been built. Markus Nuorento was of crucial help during the construction phases and provided not only manual labour, but critical improvements in the construction process. Mikko Rantanen helped out with sealing the UAC and also doing some of the wind speed measurements. Petri Kutvonen and Pekka Tonteri deserve special praise for their open-mindedness in allowing us to experiment with an operational DC. Finally, Sampo Smolander, Pekko Metsä, Tomas Lindén, and Taina Ruuskanen from the Department of Physics were especially helpful in verifying the measurement methodology.

This work has been supported by the Nokia Foundation.

[4]In our case with Finnish electricity prices, the payback times of our combined installation is on the order of a few months. For higher prices, the times would be correspondingly shorter.

References

[1] Gartner, "Gartner Estimates ICT Industry Accounts for 2 Percent of Global CO2 Emissions," p. 1, 2007, http://www.gartner.com/it/page.jsp?id=503867.

[2] M. Webb, "SMART 2020: Enabling the low carbon economy in the information age," pp. 1–87, 2008, http://www.theclimategroup.org/publications/2008/6/19/smart2020-enabling-the-low-carbon-economy-in-the-information-age/.

[3] M. Bramfitt and P. Delforge, "Utility Energy Efficiency Program Design: Server Room Assessments and Retrofits," pp. 1–16, 2012. [Online]. Available: http://docs.nrdc.org/energy/files/ene_12041101a.pdf

[4] J. G. Koomey, "The NYT article on Power, Pollution, and the Internet: My initial comments," 2012. [Online]. Available: http://www.koomey.com/post/32281701993

[5] M. Pervilä and J. Kangasharju, "Cold air containment," in *Proceedings of the 2nd ACM SIGCOMM workshop on Green networking - GreenNets '11*. New York, New York, USA: ACM Press, 2011, pp. 7–12. [Online]. Available: http://dl.acm.org/citation.cfm?doid=2018536.2018539

[6] M. Pervilä, M. Rantanen, and J. Kangasharju, "Implementation and Evaluation of a Wired Data Center Sensor Network," in *Proceedings of the 1st International Workshop on Energy-Efficient Data Centres (E2DC 2012)*, 2012.

[7] R. Schmidt and E. Cruz, "Raised Floor Computer Data Center: Effect on Rack Inlet Temperatures of Chilled Air Exiting both the Hot and Cold Aisles," in *Thermal and Thermomechanical Phenomena in Electronic Systems, 2002. ITHERM 2002. The Eighth Intersociety Conference on*, 2002, pp. 580–594. [Online]. Available: http://ieeexplore.ieee.org/xpls/abs_all.jsp?arnumber=1012507&tag=1

[8] J. W. VanGilder and R. R. Schmidt, "Airflow Uniformity Through Perforated Tiles in a Raised-Floor Data Center," in *Proceedings of IPACK2005*. San Francisco, CA, USA: ASME, 2005, pp. 493–501. [Online]. Available: http://link.aip.org/link/ASMECP/v2005/i42002/p493/s1&Agg=doi

[9] S. Bhopte, B. Sammakia, R. Schmidt, M. Iyengar, and D. Agonafer, "Effect of Under Floor Blockages on Data Center Performance," *Thermal and Thermomechanical Proceedings 10th Intersociety Conference on Phenomena in Electronics Systems, 2006. ITHERM 2006.*, pp. 426–433, 2006. [Online]. Available: http://ieeexplore.ieee.org/lpdocs/epic03/wrapper.htm?arnumber=1645374

[10] P. Hannaford, "Ten cooling solutions to support high-density server deployment," pp. 1–16, 2006. [Online]. Available: http://www.networkworld.com/whitepapers/nww/pdf/WP42.pdf

[11] R. Zhou, C. Bash, Z. Wang, A. Mcreynolds, T. Christian, and T. Cader, "Data Center Cooling Efficiency Improvement through Localized and Optimized Cooling Resources Delivery," in *Proceedings of ASME 2012 International Mechanical Engineering Congress & Exposition (IMECE 2012)*. http://www.hpl.hp.com/techreports/2012/HPL-2012-205.pdf: HP Laboratories, 2012, pp. 1–9. [Online]. Available: http://www.hpl.hp.com/techreports/2012/HPL-2012-205.pdf

[12] E. E. Ltd., "EZIFLUTE Underfloor Airflow Control Panels," 2013. [Online]. Available: http://www.edpeurope.com/en/product/eziblank-blanking-panel-solutions/eziflute-underfloor-airflow-control-panels

[13] J. Niemann, "Hot Aisle vs. Cold Aisle Containment," pp. 1–13, 2008.

Designing a Governor Policy for Energy Saving and Heat Control in Frequency-Scaling Green Routers

Alfio Lombardo, Vincenzo Riccobene, Giovanni Schembra
Dipartimento di Ingegneria Elettrica, Elettronica e Informatica (DIEEI) - University of Catania
{lombardo, vincenzo.riccobene, schembra}@dieei.unict.it

***Abstract*— Energy costs for telecommunications networks are mainly due to the consumption of both devices and cooling facilities. For this reason the target of this paper is to propose an analytical discrete-time Markov model that allows green router designers to both evaluate performance of temperature-constrained green routers and design Governor policies to achieve the best trade-off between quality of service and energy saving in respect of a given target on the working temperature. The proposed model is applied to a case study to show how it can be used to the above purposes.**

Keywords; Green Routers, Heat Dissipation, Power Consumption, Performance Evaluation, Markov model, NetFPGA.

I. INTRODUCTION

Today's most telecommunications networks are often provisioned for worst-case or busy-hour load, and this load typically exceeds their long-term utilization by a wide margin; moreover, as shown in [1], current network nodes have a power consumption that is practically constant and does not depend on the actual traffic load they face. The implication of these factors is that most of the energy consumed in networks today is wasted.

A non-marginal side effect of high-energy dissipation is the increment of the temperature of the places where network devices reside, with a consequent further waste of energy used by cooling machines to maintain the temperature of the local environment constant.

The steadily rising energy cost and the need to reduce the global greenhouse gas emission make this occurrence unsustainable: today, 37% of the total ICT emissions are due to telecommunications companies infrastructures and devices [2]. For this reason, addressing energy efficiency challenges in wireline networks is receiving considerable attention in the literature today [3-4]; moreover many research projects have been started on this topic (see for example [5-7]). Thus, some novel hardware devices, so-called "green routers", are expected in the near future to allow to enter different power states according to the input traffic. A lot of work was done in the past, focusing on the definition of power management techniques [4]. The energy aware technique to be used in a green router depends on a number of factors, including the role of the router in the network, the profile of incoming traffic, the hardware complexity and the related costs with respect to the energy we can potentially save and the QoS we want to guarantee to the users.

Now, let us note that the introduction of green management techniques to make network routers green has an important consequence on the decrease of working temperature of the hardware device. As known, temperature is one of the major factors which must be considered and addressed in the design and the manufacture of electronic devices, and specifically routers, since operating at higher temperature degrades system reliability, causes performance degradation and leads to higher cooling and packaging costs.

Moreover, "smaller and faster" are the chief demands driving today's electronic design. These issues translate into high power densities, higher operating temperatures and lower circuit reliability. Therefore, greening a router can be considered as a leveraging approach to move towards this direction. In other words, reduction of the average temperature in green routers due to the application of algorithms aimed at reducing energy consumption will allow designers to modify hardware, reducing its size and the size of the passive and active cooling systems, since a package designed for the worst case is excessive. However, the above hardware modifications can make again router circuits heat beyond their designed thermal limits. For this reason, the working range of temperature becomes again an important issue in green router design.

With all this in mind, the paper target is to extend the router governor policy and the analytical model of a green router introduced in [8] with given requirements in terms of temperature, QoS and energy consumption. Such a governor is in charge to set the current clock frequency. Besides, the analytical model allows the designer to determine in advance if the device will operate within recommended thermal ranges when the green router governor uses a given energy saving policy. In addition, the same model can be used to evaluate the achieved amount of energy saving.

The proposed model is a multi-dimensional discrete-time Markov model. More specifically, in this work we extend the router governor policy introduced in [8] in order to support a generic number of frequencies (in [8] only two frequencies are considered), and consequently we propose a new model to capture it.

The paper is structured as follows. Section II describes the considered green router and introduces the proposed policy. Section III describes the Markov model of the considered system. Section IV shows the case study of a NetFPGA reference router in order to demonstrate the applicability of the model. Section V shows all the results of our analysis. Finally, Section VI ends the paper with some authors' conclusions and future directions.

978-1-4799-0354-2/13/$31.00 ©2013 IEEE

II. REFERENCE ARCHITECTURE AND PROPOSED POLICY

In this paper we consider a router that implements frequency scaling capabilities to save energy when the input traffic load is low. Frequency scaling, a capability implemented by many routers today, is the possibility of changing the core clock frequency in a set of different values to dynamically scale the energy consumption of the device. The base problem of this approach is that, if on the one hand the device power consumption can be reduced using lower clock frequencies with respect to the higher one, on the other hand such a decision can deteriorate the router performance. For example, in the NetFPGA Reference Router [8] we consider here as a reference platform, clock frequency switches cause a block interval of 2 ms, and therefore all the incoming packets during this interval are lost. Other routers, although with different hardware architecture and implementation, behave at the same way: at each clock frequency variation they present a QoS degradation, in terms of either loss probability, delay and energy consumption peaks. From this perspective, the approach proposed in this paper, which aims at finding the best trade-off between energy efficiency and QoS, is very general since it can be used to minimize such a cost by only changing the particular target parameter.

In order to manage frequency switches maintaining QoS acceptable while decreasing energy consumption, we introduced a Router Governor, that is an entity, which decides the router policy to be adopted to change the router clock frequency. In the following, QoS is defined by the following parameters:

- Probability of packet loss during frequency switching intervals;
- Energy saving gain;
- Mean temperature on the CPU surface.

Energy saving gain is defined as follows:

$$\rho = \frac{P_{MAX} - P_{MEAN}}{P_{MAX}} \cdot 100\% \qquad (1)$$

where P_{MAX} is the power consumed if no saving policy is applied, while P_{MEAN} is the mean value of the consumed power when the Router Governor works to save energy. Let us note that other traditional QoS parameters characterizing the router, like for example loss probability and queueing delay, are not considered here because they are not altered by the presence of our Router Governor. More specifically, the Router Governor has the following tasks:

1. Avoiding that the probability of packet loss during clock frequency switches exceeds a given threshold;
2. Maximizing the energy saving percentage while respecting the previous item.
3. Monitoring the mean temperature on the CPU surface.

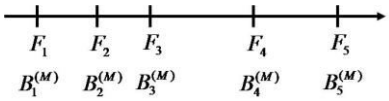

Fig. 1. Set of clock frequencies implemented by the Router, and relative maximum supported bitrates.

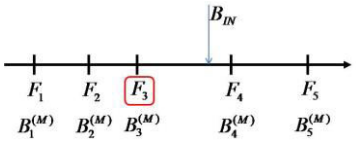

(a) Example for rule 1.

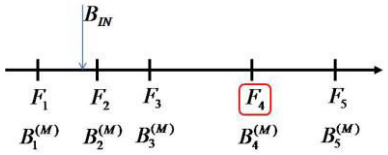

(b) Example for rule 2.

Fig. 2. Set of clock frequency implemented by the Router, and relative maximum supported bitrates.

Let Φ be the set of clock frequencies supported by the router CPU, and F_i the i-th clock frequency, sorted in such a way that $F_i < F_{i+1}$. Let us indicate the maximum bitrate that can be supported with no loss when the CPU is working at the frequency F_i as $B_i^{(M)}$. These values are sketched in Fig. 1. Let us now define the Router Governor policy:

- **RULE 1**: if the clock frequency was previously set to F_i (see Fig. 2a, where $i = 3$) and the current input bit rate B_{IN} is greater than $B_i^{(M)}$ ($B_3^{(M)}$ in Fig. 2a), then the clock frequency is switched to the minimum clock frequency belonging to Φ that does not cause losses (F_4 in Fig. 2a);
- **RULE 2**: if the clock frequency was previously set to F_i (see Fig. 2b where $i = 4$) and the current input bit rate B_{IN} is lower than $B_{i-1}^{(M)}$ (lower than $B_3^{(M)}$ in Fig. 2b), then the clock frequency can be switched down to a value F_k less than F_i, but not less than the minimum clock frequency belonging to Φ that does not cause losses (i.e. F_2 in Fig. 2b). However, since a frequency switch causes a QoS deterioration, this is done with a probability $p_G(B_{IN}, i, k)$ which is adaptive to the current input bit rate B_{IN}: the greater the distance between B_{IN} and the maximum bit rate that can be supported by the new clock frequency, the lower the risk of a new frequency switch necessity. To this purpose, referring to the example illustrated in Fig. 2b, the switching probability is defined as follows:
  - the new clock frequency is set to F_2 with a probability: $p_G(B_{IN}, 4, 2) = \delta \frac{B_2^{(M)} - B_{IN}}{B_4^{(M)} - B_{IN}}$;

- if the result of the previous draw was negative, and so the clock frequency was not set to F_2, the new clock frequency is set to F_3 with a probability: $p_G(B_{IN},4,3)=\delta\dfrac{B_3^{(M)}-B_{IN}}{B_4^{(M)}-B_{IN}}$;
- if the clock frequency is not set to F_3, the clock frequency remains F_4.

Generally speaking, if the current clock frequency is F_i and the input bit rate B_{IN} is lower than $B_{i-1}^{(M)}$, the clock frequency can be changed in the set $\{F_j,\ldots,F_i\}$, where F_j is the minimum clock frequency not causing loss. More specifically, the clock frequency is set to F_k, with $k\in[j,i]$, with a probability:

$$p_G(B_{IN},i,k)= =\left[\prod_{h=j}^{k-1}\left(1-\delta\frac{B_h^{(M)}-B_{IN}}{B_i^{(M)}-B_{IN}}\right)\right]\cdot\begin{cases}\delta\dfrac{B_k^{(M)}-B_{IN}}{B_i^{(M)}-B_{IN}} & \text{if } k<i\\ 1 & \text{if } k=i\end{cases} \quad (2)$$

The term $\delta\in[0,1]$ allows the designer to make clock frequency switches more rare. It is easy to argue that its value plays a very important role in the router performance in terms of loss probability and energy saving. A side but important effect of the Router Governor policy is on the router CPU surface temperature that should not exceed a given threshold. The design of the parameter δ will be assisted by the analytical model that will be described in Section III.

III. MARKOV MODEL

In this section we define a discrete-time model of the system described so far, in order to capture the behavior of both the frequency clock process and the surface temperature of the CPU residing on the considered router. Since it depends on the input traffic bit rate, we define the Markov model state as $S^{(\Sigma)}(n)=\left(S^{(C)}(n),S^{(I)}(n),S^{(T)}(n),S^{(S)}(n)\right)$, where:

- $S^{(C)}(n)\in\Im^{(C)}$ is the clock frequency process at the generic slot *n*;
- $S^{(I)}(n)\in\Im^{(I)}$ represents the quantized input traffic bit rate at the generic slot *n*;
- $S^{(T)}(n)\in\Im^{(T)}$ is the temperature at the generic slot *n*;
- $S^{(S)}(n)\in\Im^{(S)}=\{0,1\}$ is the indicator variable of a switch at the generic slot *n*: $S^{(S)}(n)=1$ if, in the slot *n*, the router is switching its clock frequency.

The set $\Im^{(T)}$ contains the considered quantized input traffic values. The set $\Im^{(T)}$ is constituted by a set of quantized values the temperature can assume when the router works.

Now, in order to define the system model, we have to decide the slot duration and the time diagram of each slot. As far as the slot duration is concerned, we use the interval between two consecutive observations of the input bit rate, and we will indicate it as Δ. In our case we will set $\Delta=2$ μs. In order to define the model time diagram, we consider two generic states: $s_{\Sigma 1}=(s_{C1},s_{I1},s_{T1},s_{S1})$ in the slot *n*, and $s_{\Sigma 2}=(s_{C2},s_{I2},s_{T2},s_{S2})$ in the slot $n+1$. We assume the following event sequence:

1. The first action at the beginning of the slot $n+1$ is the evaluation of the new value of the input traffic bit rate. This value is obtained sampling the bit rate values smoothed with an EWMA filter with a time constant equal to the time slot.
2. Then, according to the new value of the input traffic bit rate, the Governor decides the clock frequency for the new slot. As said so far, a clock frequency modification determines that the router will remain frozen for a number of slots to make the clock frequency switch. All these slots will be characterized by the state variable $S^{(S)}(n)=1$. Let $\overline{T}_F$ be the duration of this period.
3. Then, at the end of the slot $n+1$, the system state variables are observed.

Now we can define the generic element of the state transition probability matrix as follows:

$$Q^{(\Sigma)}_{[s_{\Sigma 1},s_{\Sigma 2}]}=\text{Prob}\left\{S^{(\Sigma)}(n+1)=s_{\Sigma 2}\middle|S^{(\Sigma)}(n)=s_{\Sigma 1}\right\}= =Q^{(I)}_{[s_{I1},s_{I2}]}\cdot\eta^{(C)}_{[s_{C1},s_{C2}]}(s_{I2})\cdot Q^{(T)}_{[s_{T1},s_{T2}]}(s_{C2},s_{I2})\cdot Q^{(S)}_{[s1,s_{S2}]}(s_{C1},s_{C2}) \quad (3)$$

where:

- $Q^{(S)}_{[s_{S1},s_{S2}]}(s_{C1},s_{C2})$ is the transition probability of the clock switch indicator variable. It is defined as follows:

$$Q^{(S)}_{[s_{S1},s_{S2}]}(s_{C1},s_{C2})= =\begin{cases}1 & \text{if } (s_{C2}\neq s_{C1},\ s_{S1}=0,\ s_{S2}=1)\\ 1 & \text{if } (s_{C2}=s_{C1},\ s_{S1}=0,\ s_{S2}=0)\\ \Delta/\overline{T}_F & \text{if } (s_{S1}=1,\ s_{S2}=0)\\ 1-\Delta/\overline{T}_F & \text{if } (s_{S1}=1,\ s_{S2}=1)\\ 0 & \text{otherwise}\end{cases} \quad (4)$$

  where $\overline{T}_F$ is the mean duration of the clock frequency switching period. Thus the term $\Delta/\overline{T}_F$ is the probability that the router leaves the switching period.
- $\eta^{(C)}_{[s_{C1},s_{C2}]}(s_{I2})$ gives the probability of a clock frequency switch depending on the clock frequency switching law used by the Governor to decide the clock according to the input traffic bit rate. It is set to 0 when it is not possible that the Governor sets the value of s_{C2} according to the input traffic value s_{I2} and the current clock frequency s_{C1}. According to the Governor policy illustrated in Section II, it is defined as follows:

$$\eta^{(C)}_{[s_{C1},s_{C2}]}(s_{I2})=\begin{cases}1 & \text{if } \phi(s_{I2})>s_{C1}\\ & \quad\text{and } s_{C2}=\phi(s_{I2})\\ 1 & \text{if } s_{C1}=s_{C2}=\phi(s_{I2})\\ p_G(s_{I2},s_{C1},s_{C2}) & \text{if } \phi(s_{I2})<s_{C1}\\ & \quad\text{and } \phi(s_{I2})\le s_{C2}\le s_{C1}\\ 0 & \text{otherwise}\end{cases} \quad (5)$$

The term $p_G(s_{I2}, s_{C1}, s_{C2})$ is the frequency clock switching probability defined in (2). As said in Section II, it is adaptive with the current value of the input bit rate. The design of this function will be discussed in Section V.

- $Q^{(I)}$ is the state transition probability matrix for the quantized input traffic. It is an input of the problem, because it characterizes the traffic crossing the router;
- $Q^{(T)}(s_{C2}, s_{I2})$ is the state transition probability of the temperature. It will be calculated below.

Let us indicate the derivative of the time-variant temperature behavior when the system state is $s_{\Sigma 1}$ as $\gamma(s_{C2}, s_{I2}, s_{T1})$. Therefore the temperature value in the slot $n+1$ is calculated from the value in the slot n as follows:

$$T_2 = s_{T1} + \gamma(s_{C2}, s_{I2}, s_{T1}) \cdot \Delta \tag{6}$$

Since T_2 may not belong to the set $\Im^{(T)}$, the new state of the temperature, s_{T2}, will be one of the two most adjacent states to T_2 belonging to this set. Let us indicate the most adjacent state with a temperature greater than T_2 as $\lceil T_2 \rceil$, and the most adjacent state with a temperature lower than T_2 as $\lfloor T_2 \rfloor$. The new temperature state s_{T2} will be either $s_{T2} = \lceil T_2 \rceil$ or $s_{T2} = \lfloor T_2 \rfloor$ with a probability dependent on the distance between the real temperature calculated as in (6) and the temperature associated to the adjacent states $\lceil T_2 \rceil$ and $\lfloor T_2 \rfloor$. More specifically:

$$S^{(T)}(n+1) = \begin{cases} \lceil T_2 \rceil & \text{with prob: } (T_2 - \lfloor T_2 \rfloor)/(\lceil T_2 \rceil - \lfloor T_2 \rfloor) \\ \lfloor T_2 \rfloor & \text{with prob: } (\lceil T_2 \rceil - T_2)/(\lceil T_2 \rceil - \lfloor T_2 \rfloor) \end{cases} \tag{7}$$

Now, from the matrix $Q^{(\Sigma)}$ we can derive the system steady-state probability array $\underline{\pi}^{(\Sigma)}$ by solving the following system:

$$\begin{cases} \pi^{(\Sigma)} Q^{(\Sigma)} = \pi^{(\Sigma)} \\ \pi^{(\Sigma)} \cdot \underline{1}^T = 1 \end{cases} \tag{8}$$

where $\underline{1}^T$ is a column array with all the elements equal to one. Its generic element, $\pi^{(\Sigma)}_{[s_\Sigma]}$, is the steady-state probability of the state $\underline{s}_\Sigma = (s_C, s_I, s_T, s_S)$.

Now we derive the main important QoS parameters, with the aim of both evaluating router performance and supporting Router Governor design.

First let us calculate the probability of loss occurring during the switching periods. It is defined as:

$$P^{(Loss)} = \lim_{m \to +\infty} \frac{L(m)}{V(m)} = \frac{\overline{L}}{\overline{V}} \tag{9}$$

where $L(m)$ and $V(m)$ are the cumulative number of lost bits and arrived bits in *m* consecutive slots. The term $\overline{V}$ is the mean value of arrived bits per slot, and can be calculated from the input bit rate traffic statistics as follows:

$$\overline{V} = \sum_{s_\Sigma \in \Im^{(\Sigma)}} s_I \pi^{(\Sigma)}_{[s_\Sigma]} \tag{10}$$

The term $\overline{L}$ represents the mean value of bits lost per slot. Since in our case bits are lost only during clock frequency switches, we have:

$$\overline{L} = \sum_{s_C \in \Im^{(C)}} \sum_{s_I \in \Im^{(I)}} \sum_{s_T \in \Im^{(T)}} s_I \pi^{(\Sigma)}_{[s_C, s_I, s_T, 1]} \tag{11}$$

The power saving percentage during periods when the router can reduce its clock frequency can be calculated as in (1), where P_{MEAN} is the mean value of the consumed power when the input bit rate is less than or equal to 2 Gbit/s. It can be calculated as follows:

$$P_{MEAN}(s_I) = \sum_{\forall s_C \in \Im^{(C)}} \Psi(s_C, s_I) \cdot \sum_{\forall s_T \in \Im^{(T)}} \sum_{\forall s_S \in \Im^{(S)}} \pi^{(\Sigma)}_{[s_C, s_I, s_T, s_S]} \tag{12}$$

The term $\Psi(s_C, s_I)$ is a model input, and represents the power consumed when the router is loaded with an input traffic bit rate of s_I and the clock frequency is s_C.

Let us now derive the marginal steady-state probability array for the temperature process when the input bit rate is $B_{IN} = s_I$:

$$\pi^{(T|s_I)}_{[s_T]} = \frac{\sum_{\forall s_C \in \Im^{(C)}} \sum_{\forall s_S \in \Im^{(S)}} \pi^{(\Sigma)}_{[s_C, s_I, s_T, s_S]}}{\sum_{\forall s_C \in \Im^{(C)}} \sum_{\forall s_T \in \Im^{(T)}} \sum_{\forall s_S \in \Im^{(S)}} \pi^{(\Sigma)}_{[s_C, s_I, s_T, s_S]}} \tag{13}$$

Finally, from the probability array in (13) we can calculate the mean temperature value:

$$E\{T \mid s_I\} = \sum_{\forall s_T \in \Im^{(T)}} s_T \cdot \pi^{(T|s_I)}_{[s_T]} \tag{14}$$

IV. CASE STUDY

In this section we will provide a case study for our model. In particular, starting from a set of measurements achieved for a NetFPGA platform in a previous work of the same authors [8], we extended them in order to provide a complete case study of a device with a higher number of clock frequencies.

More specifically, as regards the consumed power, we use the model that allows us to calculate the power consumed when the router works at a clock frequency f_C and is loaded by an input traffic bit rate B_{IN}:

$$\Psi(f_C, B_{IN}) = P_C(f_C) + K P_E(f_C) + N_I(B_{IN}) \cdot E_p(f_C) + \\ + R_I(B_{IN}) \cdot E_r(f_C) + R_O E_t(f_C) \tag{15}$$

The term $P_C(f_C)$ is the constant baseline power consumption of the NetFPGA card (without any Ethernet ports connected); $P_E(f_C)$ is the power consumed by each Ethernet port (without any traffic flowing); $E_p(f_C)$ is the energy required to process each packet (parsing, routing lookup, etc.); $E_r(f_C)$ is the energy required to receive, process and store a byte on the ingress Ethernet interface; $E_t(f_C)$ is the energy required to store, process and send a byte on the egress Ethernet interface; *K* is the number of Ethernet ports connected (1 to 4); $N_I(B_{IN})$ is the input traffic bitrate to the NetFPGA card in packets-per-second (pps); $R_I(B_{IN})$ is the input rate to the NetFPGA card

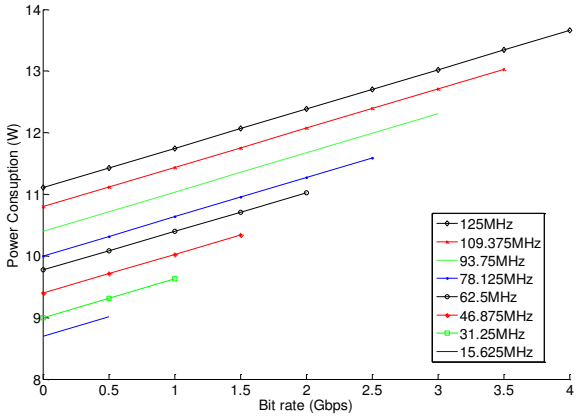

Fig. 3. Power consumption model for a router with 8 clock frequencies.

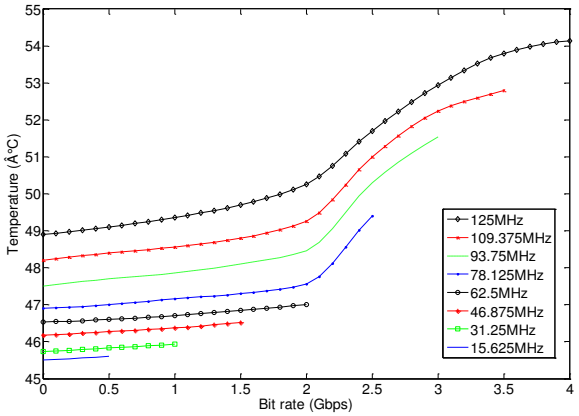

Fig. 4. Temperature model for a generic router with 8 clock frequencies.

in bytes-per-second; $R_O(B_{IN})$ is the output rate from the NetFPGA card in bytes-per-second.

We have extended the set of measurements presented in [8] considering a router supporting eight different clock frequencies (125 MHz, 109.375 MHz, 93.75 MHz, 78.125 MHz, 62.5 MHz, 46.875 MHz, 31.25 MHz, 15.625 MHz) . Results achieved by the power model in (15) are shown in Fig. 3.

As far as the CPU surface temperature data are concerned, we extended measurements results presented in [8] with the curves shown in Fig. 4, showing the steady-state values of the temperature when the router CPU works at a clock frequency f_C and is loaded by an input traffic bit rate B_{IN}. Each curve in Figs. 3 and 4 covers only the supported bit rate for each specific CPU clock frequency (i.e. the maximum supported input bit rate without incurring in any packet loss when the system works at 15.652 MHZ is 0.5 Gbps, etc …).

The derivative of the time-variant temperature behavior when the current temperature is T_{curr}, $\gamma(s_{C2}, s_{I2}, s_{T1})$, are a large set of data and are available at [9].

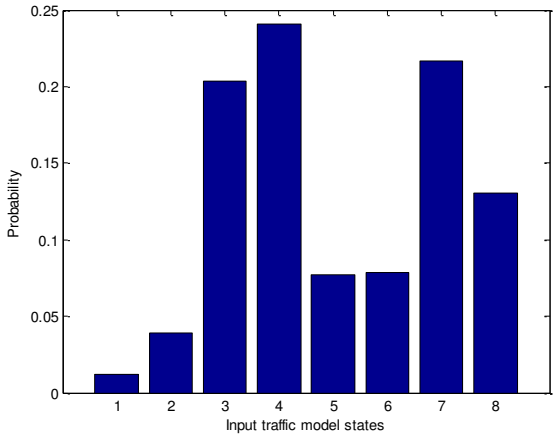

(a) Probability density function.

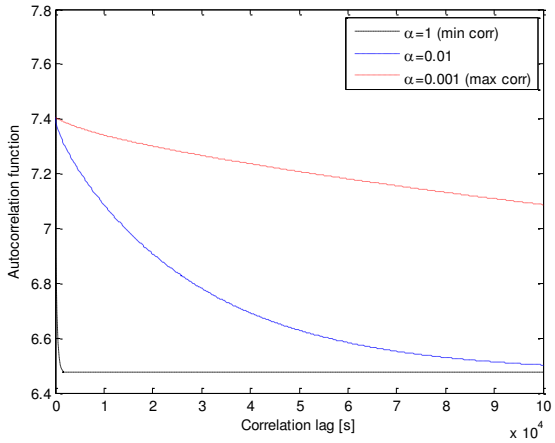

(b) Autocorrelation function.

Fig. 5. Input traffic first- and second-order statistics.

INFERIOR PSEUDO-DIAGONAL		MAIN DIAGONAL		SUPERIOR PSEUDO-DIAGONAL	
Pos	**Value**	**Pos**	**Value**	**Pos**	**Value**
		(1,1)	9.9990e-001	(1,2)	1.0000e-004
(2,1)	3.1569e-005	(2,2)	9.9993e-001	(2,3)	3.5098e-005
(3,2)	6.7811e-006	(3,3)	9.9994e-001	(3,4)	4.8774e-005
(4,3)	4.1255e-005	(4,4)	9.9995e-001	(4,5)	6.3636e-006
(5,4)	1.9848e-005	(5,5)	9.9994e-001	(5,6)	3.8975e-005
(6,5)	3.8314e-005	(6,6)	9.9992e-001	(6,7)	3.8609e-005
(7,6)	1.3970e-005	(7,7)	9.9990e-001	(7,8)	8.6030e-005
(8,7)	1.4286e-004	(8,8)	9.9986e-001		

Table I. Non-null elements of the Input traffic transition probability matrix.

V. MODEL APPLICATION

In this section we apply the model described so far to both evaluate performance of a router with a Router Governor implementing the proposed green clock frequency management policy, and design the δ parameter used in the switching probability $p_G(s_{I2}, s_{C1}, s_{C2})$ by the Governor to

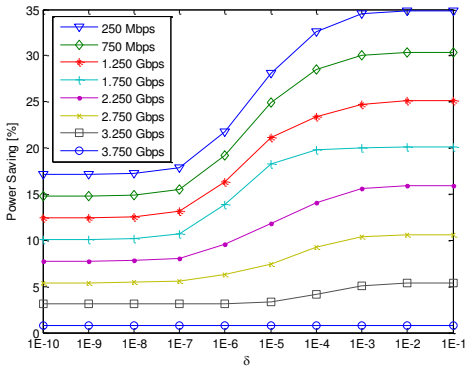

Fig. 6. Power saving for different values of input bit rates.

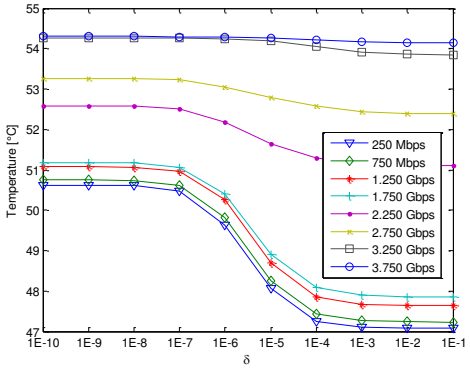

Fig. 7. Mean temperature for different values of input bit rates.

decide whether to switch clock frequency or not according to the current bit rate, B_{IN}.

Quantizing the traffic in eight different bit rate levels, ranging from 0.4 Gbit/s to 3.9 Gbit/s with steps of 0.5 Gbit/s, we measured its first- and second-order statistics in terms of probability density function (pdf) and autocorrelation function (acf), which are represented in Fig. 5. More specifically, the measured autocorrelation function is the one labeled with $\alpha = 1$. Then, solving an inverse eigenvalue problem [10], we derived the input traffic Markov model characterized by the transition probability matrix $Q^{(1)}$, which is a tri-diagonal matrix whose non-null elements are listed in Table I. The considered traffic has a mean value of 2.54 Gbit/s and a standard deviation of 0.965 Gbit/s. Moreover, in order to analyze the impact of the traffic correlation on the achieved performance, we considered two more cases of input traffic, characterized by transition probability matrices derived from the one listed in Table I by multiplying the terms of the pseudo-diagonals by a coefficient $\alpha = 10^{-2}$ and $\alpha = 10^{-3}$. The terms of the main diagonals are then calculated such that the sum of each row is equal to one. In this way first-order statistics remained unchanged, while traffic becomes more correlated for decreasing values of α. The autocorrelation functions evaluated for the two new cases are shown in the same Fig. 5b.

Fig. 6 shows the power saving gain achieved during periods with different values of input bit rates ranging between 250 Mbit/s and 3.750 Gbit/s. The plots are calculated through (12) against the switching parameter δ. The reader can notice that, as expected, for higher values of δ, the power saving gain increases because δ influences the clock frequency switching probability. Moreover, in the case of low input bit rate the power saving gain of the system is more sensitive to the value of δ used into the policy, while it is insensitive in the opposite case. This behavior is due to the fact that when δ takes high values the clock frequency strictly follows the traffic and the CPU is set to lower frequency more often.

Fig. 7 shows the mean temperature for different values of input bit rates; it is possible to notice that the higher the value of δ the lower the heat dissipation of the CPU surface. Also in that figure, we can notice that in the case of low input bit rate the temperature of the system is more influenced by the selected value of δ.

Fig. 8 shows the loss probability for the three different considered cases of traffic correlations, obtained with three different values of α. It is clear that the higher the correlation of the input traffic $(\alpha = 0.001)$ the lower the loss probability. This is due to the fact that high-correlated traffic requires less clock frequency switches.

Figs. 9 and 10 respectively show the power saving gain and the temperature against the loss probability. They have been obtained by calculating the three above performance parameters as functions of δ, and then putting them together by associating the values achieved for the same value of δ. From these figures it is possible to see that lower values of loss probability correspond to low power saving gain and, at the same time, to high temperature. Moreover, Figs. 6-10 allow the designer to choose the more suitable value of δ. Moreover, these figures can be used to support the design of the system. For example, we can derive the maximum power saving that can be obtained for the presented case study when we accept a given loss probability (Fig. 9) and the corresponding mean temperature (Fig. 10). The higher the required power saving gain, or the lower the required mean temperature, the higher the loss probability we have to accept.

VI. CONCLUSIONS

In this paper we have proposed a new governor policy for green routers using frequency scaling to save energy. The policy allows to limit the performance worsening due to frequent clock frequency switches. In order to design the frequency switching probability, we have defined an analytical discrete-time Markov model. This model can also be used by green router designers to control the statistics of the temperature on the CPU surface, for given input traffic first- and second-order statistics. Moreover, the model allows the manufacturers to evaluate the energy saving gain which is possible to obtain. In the case study we have shown how the model can be used to design the Router Governor parameters to achieve the target of maintaining the mean temperature below a given threshold and achieve a certain amount of power saving gain for a given threshold on the loss probability. The future directions that we will pursue are related to an extension of the

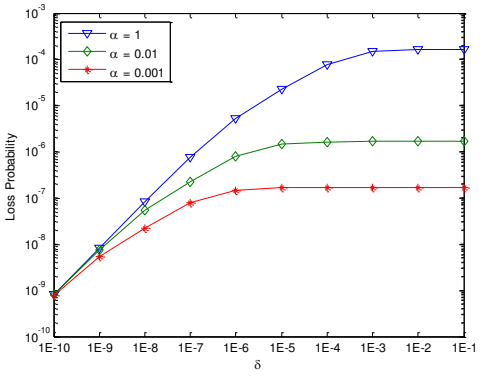

Fig. 8. Loss probability for different input traffic correlation.

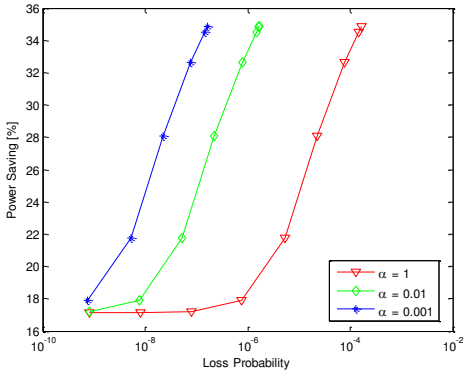

Fig. 9. Power saving gain vs. loss probability.

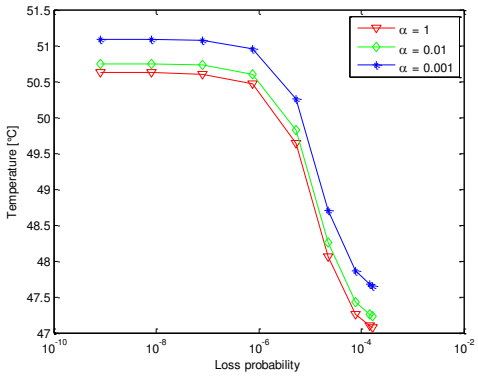

Fig. 10. Temperature vs. loss probability.

model to capture both the dependence of the power on the environmental temperature, and a Governor policy based on the behavior of input and output queues. Moreover, we will apply the model to find the most appropriate number of clock frequencies, as the best tradeoff between the QoS deterioration caused by an increasing of the number of possible clock frequencies, and the energy saving gain improvement given by a router whose clock frequency is able to closely follow the traffic behavior.

ACKNOWLEDGMENT

The research leading to these results has received funding from the European Union Seventh Framework Programme (FP7/2007-2013) under grant agreement n. 257740 (Network of Excellence "TREND").

REFERENCES

[1] P. Barford, J. Chabarek, C. Estan, J. Sommers, D. Tsiang, and S. Wright, "Power awareness in network design and routing," in Proc. of IEEE INFOCOM 2008, Phoenix, USA, April 2008, 2008.

[2] The Climate Group, "The climate group: Global e-sustainability initiativereport, smart 2020 enabling low carbon economy in the informationage, http://www.smart2020.org/publications/," 2008.

[3] M. Gupta and S. Singh, "Greening of the Internet," in Proc.of the 2003 conference on Applications, technologies, architectures,and protocols for computer communications, SIGCOMM '03, New York, NY, USA:

[4] S. Nedevschi, et al., "Reducing network energy consumption via sleeping and rateadaptation," in Proc. of the 5th USENIX Symposium on Networked Systems Design and Implementation, 2008.

[5] Econet, "http://www.econet-project.eu/," 2010.

[6] Trend, "http://www.fp7-trend.eu/," 2010.

[7] Greentouch, "http://www.greentouch.org/," 2011.

[8] A. Lombardo, D. Reforgiato, V. Riccobene, G. Schembra, "A Markov model to control heat dissipation in Open Multi-Frequency Green Routers", in Proc. of SustainIT 2012, 4-5 October 2012, Pisa, Italy.

[9] www.diit.unict.it/arti/TR/TR6.zip

[10] ''SMAQ: A measurement-based tool for traffic modeling andqueuinganalysis Part II: Network applications,'' IEEE Commun. Mag.,vol. 36, p. 66, Aug. 1998

Energy-Efficient Resource Allocation for Orthogonal Multi-antenna Multi-carrier Channel

Fabien Héliot, Muhammad Ali Imran, and Rahim Tafazolli
Centre for Communication Systems Research (CCSR), Faculty of Electronics & Physical Sciences,
University of Surrey, Guildford GU2 7XH, UK. Email: F.Heliot@surrey.ac.uk

***Abstract*—Energy efficiency (EE) is growing in importance as a key performance indicator for designing the next generation of communication systems. Equally, resource allocation is an effective approach for improving the performance of communication systems. In this paper, we propose a low-complexity energy-efficient resource allocation method for the orthogonal multi-antenna multi-carrier channel. We derive explicit formulations of the optimal rate and energy-per-bit consumption for the per-antenna transmit power constrained and per-antenna rate constrained EE optimization problems as well as provide a low-complexity algorithm for optimally allocating resources over the orthogonal multi-antenna multi-carrier channel. We then compare our approach against a classic optimization tool in terms of energy efficiency as well as complexity, and results indicate the optimality and low-complexity of our approach. Comparing EE-optimal with spectral efficiency and power optimal allocation approaches over the orthogonal multi-antenna multi-carrier channel indicates that the former provides a good trade-off between power consumption and sum-rate performances.**

***Index Terms*—Energy efficiency, resource allocation, MIMO, multi-carrier, realistic power model.**

I. Introduction

Network operators not only require the next generation of communication systems to be more spectrally efficient, as with all the previous generations, but to also be more energy-efficient for ensuring both the economical and environmental sustainability of their activity. Thus, energy efficiency (EE) is growing in importance as a key performance indicator such that it has lately attracted a lot of research interests [1]–[9].

Given that resource allocation and link adaptation are effective techniques for improving the performance of communication systems, these techniques have been thoroughly investigated in the past but mainly from a spectral efficiency (SE) or peak rate performance perspective. With the growing importance of EE in communication systems, resource allocation based on the EE criterion is becoming a popular research topic [3]–[9]. For instance, the work in [4] proposed an iterative gradient search algorithm for obtaining the EE-optimal resource allocation in the uplink of an orthogonal single-antenna multi-carrier/user channel. This work was then revisited in [6] by considering a more realistic power model for the user equipment (UE). Whereas, an EE-optimal resource allocation scheme for single-antenna orthogonal frequency multiplexing (OFDM) system was derived in [5]. More recently, we have proposed low-complexity energy-efficient resource allocation algorithms for the single-antenna broadcast channel, orthogonal single-antenna multi-carrier/user channel and single-antenna multi-user multi-cell system in [7], [8] and [9], respectively.

Contrary to the previous EE-based resource allocation works in [3]–[9], we here assume that the base station (BS) as well as UE(s) have multiple antennas and propose a low-complexity energy-efficient method for optimally allocating resources in the orthogonal multi-input multi-output (MIMO) multi-carrier/user channel. More specifically, we extend our work of [8] for the MIMO scenario by considering a realistic multi-antenna power consumption model and derive explicit formulations of the optimal rate and energy-per-bit consumption for the per-antenna transmit power constrained and per-antenna rate constrained EE optimization problems. In Section II, we first recall the per-subchannel rate and power formulations over the orthogonal MIMO multi-carrier/user channel, detail the power consumption models for both the BS and UE(s), and formulate the energy-per-bit consumption. In Section III, we first introduce the two optimization problems that are solved in this paper, i.e. minimizing the energy consumption over the orthogonal MIMO multi-carrier/user channel when considering a per-antenna power or rate constraint, and solve them by means of closed-form expressions. Based on these expressions, we provide a low-complexity algorithm for optimally allocating the power and rate in an energy efficient manner. In Section IV, we numerically show the optimality and low-complexity of our method in comparison with a traditional convex optimization method. As an application, we compare the EE-optimal, SE-optimal and power-optimal allocation methods and our results indicate that the former provides a good trade-off between power consumption and sum-rate performances. Conclusions are drawn in Section V.

II. System and Power Consumption Models

A. System Model

We consider the orthogonal MIMO multi-carrier/user channel, where NK independent subchannels are used for transmitting data between a BS and one or several users. Moreover, we assume that each orthogonal subchannel is affected by block fading and that perfect channel state information is available at both the transmitter and receiver ends such that the achievable rate of the (n,k)-th parallel subchannel can be expressed as

$$\mathcal{C}_{n,k} = \log_2\left(1 + \frac{g_{n,k}p_{n,k}}{\Gamma\sigma^2}\right), \quad (1)$$

which corresponds to the (n,k)-th rate of a MIMO-OFDM system with N spatial and K frequency flat subchannels [10]

978-1-4799-0354-2/13/$31.00 ©2013 IEEE

as well as of a K-user $N \times N$ MIMO-OFDMA transmission over a frequency-selective and block faded channel. In equation (1), $g_{n,k}$ is the channel gain over the (n,k)-th subchannel, σ^2 is the noise power, and Γ represents the signal-to-noise ratio gap between the theoretical achievable rate and a practical coding and modulation scheme as in [4]. Conversely, the transmit power related to the (n,k)-th subchannel, $p_{n,k}$, can be expressed as

$$p_{n,k} = \Gamma\sigma^2 \left(2^{\mathcal{C}_{n,k}} - 1\right) g_{n,k}^{-1}, \tag{2}$$

according to (1), such that the total transmit power can then be given by

$$P(\boldsymbol{\mathcal{C}}) = \sum_{n=1}^{N}\sum_{k=1}^{K} a_{n,k}^{-1}\left(2^{\mathcal{C}_{n,k}} - 1\right), \tag{3}$$

where $\boldsymbol{\mathcal{C}} = [\mathcal{C}_{1,1}, \ldots, \mathcal{C}_{1,K}, \mathcal{C}_{2,1}, \ldots, \mathcal{C}_{N,K}] \succeq 0$ and $a_{n,k} \triangleq (\Gamma\sigma^2)^{-1} g_{n,k}$.

B. Power consumption model and EE-SE trade-off formulation

Even though BSs and UEs are different in their architectures and components, it has been shown in [2] and [4], respectively, that their power consumptions can be modelled as $P_{\text{in}} = \Delta P + P^{Ci}$, i.e. a linear relation between the consumed and transmit powers. Given that each antenna has its own RF chain [2], this model has been refined for the MIMO setting in [11] as

$$P_{\text{in}} = t(\Delta P + P^{CipA}) + P^{Ci}, \tag{4}$$

where Δ is the radio frequency (RF) dependent slope of the power model, P^{CipA} is the per antenna circuit power, t is the number of transmit antennas and P^{Ci} is the circuit power that is not dependent on t. In addition, the transmit power, P, is such that $P \in [0, P_n^{\max}]$ with $P_n^{\max}$ being the per-antenna maximum transmit power. Consequently, the total consumed power in the downlink or uplink of a multi-antenna multi-carrier/user system can be linearly abstracted as

$$P_{\Sigma}(\boldsymbol{\mathcal{C}}) = P_{\text{c}} + \Delta P(\boldsymbol{\mathcal{C}}), \tag{5}$$

when assuming the power model in (4) for the BS and UE(s), and where $P_{\text{c}} = tP_{\text{BS}}^{CipA} + P_{\text{BS}}^{Ci} + \varsigma\kappa(rP_{\text{UE}}^{CipA} + P_{\text{UE}}^{Ci})$ or $P_{\text{c}} = \kappa(tP_{\text{UE}}^{CipA} + P_{\text{UE}}^{Ci}) + \varsigma(rP_{\text{BS}}^{CipA} + P_{\text{BS}}^{Ci})$ in the downlink or uplink scenario, respectively. Moreover, r is the number of receive antennas, $\kappa = 1$ and K in the OFDM and OFDMA settings, respectively; whereas ς characterizes the ratio between transmission and reception overhead powers with $0 \leq \varsigma \leq 1$. Intuitively, less overhead power is necessary for receiving than for transmitting signals. Note that $N = \min\{t, r\}$.

According to [12], the energy consumption, E_b, or EE, $1/E_b$, can simply be defined as a ratio between the total consumed power and the sum-rate such that the EE-SE trade-off of MIMO multi-carrier/user systems with full channel state information can be expressed according to (1), (3) and (5) as

$$E_b(\boldsymbol{\mathcal{C}}) \triangleq \frac{P_{\Sigma}(\boldsymbol{\mathcal{C}})}{W\sum_{n=1}^{N}\sum_{k=1}^{K}\mathcal{C}_{n,k}} = \frac{P_c + \Delta\sum_{n=1}^{N} P_n(\boldsymbol{\mathcal{C}})}{\sum_{n=1}^{N} R_n(\boldsymbol{\mathcal{C}})}, \tag{6}$$

where $P_n(\boldsymbol{\mathcal{C}}) = \sum_{k=1}^{K} a_{n,k}^{-1}\left(2^{\mathcal{C}_{n,k}} - 1\right)$, $R_n(\boldsymbol{\mathcal{C}}) = W\sum_{k=1}^{K}\mathcal{C}_{n,k}$, and W is the channel bandwidth.

III. EE Optimization over the orthogonal MIMO multi-carrier channel

We have recently solved in [8] the following EE-based problems over the orthogonal single-antenna multi-carrier channel:

$$\min_{\boldsymbol{\mathcal{C}}} E_b(\boldsymbol{\mathcal{C}}), \text{s.t. } \boldsymbol{\mathcal{C}} \succeq 0 \text{ and} \tag{7a}$$

$$\min_{\boldsymbol{\mathcal{C}}} E_b(\boldsymbol{\mathcal{C}}), \text{s.t. } \boldsymbol{\mathcal{C}} \succeq 0, \sum_{n=1}^{N} P_n(\boldsymbol{\mathcal{C}}) \leq P^{\max}. \tag{7b}$$

However, given that in a realistic BS each antenna has its own RF chain and, hence, power constraint, per-antenna power constraint is more relevant than sum-power constraint from an EE point of view. Thus, we here extend our work of [8] and aim at minimizing the energy consumption when considering a per-antenna power or rate constraint by solving

$$\min_{\boldsymbol{\mathcal{C}}} E_b(\boldsymbol{\mathcal{C}}), \text{s.t. } \boldsymbol{\mathcal{C}} \succeq 0, P_n(\boldsymbol{\mathcal{C}}) \leq P_n^{\max} \text{ or} \tag{8a}$$

$$\min_{\boldsymbol{\mathcal{C}}} E_b(\boldsymbol{\mathcal{C}}), \text{s.t. } \boldsymbol{\mathcal{C}} \succeq 0, R_n(\boldsymbol{\mathcal{C}}) \geq R_n^{\min}, \tag{8b}$$

respectively, for any $n \in \mathcal{N} = \{1, \ldots, N\}$.

We have proved in [8] that $E_b(\boldsymbol{\mathcal{C}})$ is a convex function when $P_c \geq \Delta\sum_{m\in\mathcal{M}^\bullet} a_m^{-1}$ and $|\mathcal{M}^\bullet| \geq 1$, where $m = (n-1)K + k$, $n \in \mathcal{N}$, $\mathcal{M}^\bullet = \{m \in \{1, \ldots, NK\} | \mathcal{C}_m^\bullet > 0\}$ is the optimal set of allocated subchannel indices and $\mathcal{C}_m^\bullet$ is the optimal value of $\mathcal{C}_m$ in the unconstrained problem of (7a). As long as each antenna does not transmit at full power $P_n^{\max}$ or achieve its minimum rate requirement $R_n^{\min}$, the problems in (8) revert to the unconstrained problem in (7a). Given that E_b in (6) is convex, it has a unique global minimum $E_b^\bullet$ which is obtained for $\boldsymbol{\mathcal{C}} = \boldsymbol{\mathcal{C}}^\bullet$, where $\boldsymbol{\mathcal{C}}^\bullet$ is the EE-optimal unconstrained achievable rate vector.

A. Power constrained EE optimization

Let us define $\overline{\mathcal{N}} = \{n \in \mathcal{N} | P_n(\boldsymbol{\mathcal{C}}^\bullet) \geq P_n^{\max}\}$ and $\underline{\mathcal{N}} = \{n \in \mathcal{N} | P_n(\boldsymbol{\mathcal{C}}^\bullet) < P_n^{\max}\}$ are the index sets of antenna which are power constrained and power unconstrained, respectively, when $\boldsymbol{\mathcal{C}} = \boldsymbol{\mathcal{C}}^\bullet$.

Proposition 1: In the case that at least one antenna transmits at full power when $\boldsymbol{\mathcal{C}} = \boldsymbol{\mathcal{C}}^\bullet$, the EE-optimal achievable rate of the k-th subchannel served by any power constrained antenna n (i.e. $n \in \overline{\mathcal{N}}$) can be given in closed-form by

$$\mathcal{C}_{n,k}^\star = \log_2\left(\frac{P_n^{\max} + \sum_{i\in\mathcal{K}_n^\star} a_{n,i}^{-1}}{K_n^\star a_{n,k}^{-1}}\right), \tag{9}$$

for $k \in \mathcal{K}_n^\star$, where $\mathcal{K}_n^\star = \{k \in \mathcal{K} = \{1, \ldots, K\} | \mathcal{C}_{n,k}^\star > 0\}$ is the optimal set of allocated subchannel index for antenna n in the power constrained case, and $K_n^\star = |\mathcal{K}_n^\star|$ is the number of elements in $\mathcal{K}_n^\star$. Note that $\mathcal{C}_{n,k}^\star = 0$ for $k \in \mathcal{K} \setminus \mathcal{K}_n^\star$. See proof in Section A of the Appendix.

Remark 1: Equation (9) indicates that the rate allocation of each power constrained antenna can be performed independently by means of a simple binary search on $K_n^\star$. In addition, it ensures that any power constrained antenna n (i.e. $n \in \overline{\mathcal{N}}$) transmits over at least one subchannel, the one with the best channel gain, such that $1 \leq K_n^\star \leq K$.

function pAPC($K, n, P_n^{\max}, [a_{n,1}, \ldots, a_{n,K}]$)
  Set $U = K$;
  while $P_n^{\max} + \sum_{i=1}^{U} a_{n,i}^{-1} \leq U a_{n,U}^{-1}$ **do**
    Set $\mathcal{C}_{n,U}^{\star} = 0$;
    Set $U = U - 1$;
  end while
  Set $\mathcal{K}_n^{\star} = \{1, \ldots, U\}$ and $K_n^{\star} = U$;
  Compute $\mathcal{C}_{n,k}^{\star}$ for any $k \in \mathcal{K}_n^{\star}$ by using (9);
return $\mathcal{C}_{n,k}^{\star}$;
end function

Proposition 2: In the case that at least one antenna transmits at full power when $\boldsymbol{\mathcal{C}} = \boldsymbol{\mathcal{C}}^{\bullet}$, the EE-optimal achievable rate of the k-th subchannel served by any unconstrained antenna n (i.e. $n \in \underline{\mathcal{N}}$) can be expressed in closed-form as

$$\mathcal{C}_{n,k}^{\star} = \log_2 \left(a_{n,k} \frac{P_c^{\star}}{K^{\star}} \left[W_0 \left(\frac{P_c^{\star}}{K^{\star}} e^{\frac{\ln(2) R_c^{\star}}{K^{\star}} - 1} \right) \right]^{-1} \right), \quad (10)$$

for $k \in \mathcal{K}_n^{\star}$, where W_0 denotes the real branch of the Lambert function [13], $K^{\star} = \sum_{i \in \underline{\mathcal{N}}} K_i^{\star}$,

$$P_c^{\star} = \frac{P_c}{\Delta} + \sum_{i \in \overline{\mathcal{N}}} P_i^{\max} - \sum_{i \in \underline{\mathcal{N}}} \sum_{j=1}^{K_i^{\star}} a_{i,j}^{-1} \text{ and} \quad (11a)$$

$$R_c^{\star} = \sum_{i \in \overline{\mathcal{N}}} \sum_{j=1}^{K} \mathcal{C}_{i,j}^{\star} + \sum_{i \in \underline{\mathcal{N}}} \sum_{j=1}^{K_i^{\star}} \log_2(a_{i,j}). \quad (11b)$$

Note that $\mathcal{C}_{n,k}^{\star} = 0$ for $k \in \mathcal{K} \setminus \mathcal{K}_n^{\star}$. See proof in Section B of the Appendix.

Remark 2: It can be remarked in (10) and (11) that the unconstrained part of the optimization is dependent on the result of the constrained part, such that the per-antenna power constrained EE optimization must be performed in two stages.

Based on equation (9), we propose the function "pAPC" for optimally allocating the power and rate in an energy efficient and low-complexity manner over the MIMO multi-carrier/user channel in the per-antenna power constrained scenario.

B. Rate constrained EE optimization

Similarly to the power constrained scenario, let use define $\overline{\mathcal{N}} = \{n \in \mathcal{N} | R_n(\boldsymbol{\mathcal{C}}^{\bullet}) < R_n^{\min}\}$ and $\underline{\mathcal{N}} = \{n \in \mathcal{N} | R_n(\boldsymbol{\mathcal{C}}^{\bullet}) \geq R_n^{\min}\}$ are the index sets of antenna which are rate constrained and rate unconstrained, respectively, when $\boldsymbol{\mathcal{C}} = \boldsymbol{\mathcal{C}}^{\bullet}$.

Proposition 3: In the case that at least one antenna transmits below its target rate when $\boldsymbol{\mathcal{C}} = \boldsymbol{\mathcal{C}}^{\bullet}$, the EE-optimal achievable rate of the k-th user served by any rate constrained antenna n (i.e. $n \in \overline{\mathcal{N}}$) can be given in closed-form by

$$\mathcal{C}_{n,k}^{\star} = \log_2(a_{n,k}) + \frac{1}{K_n^{\star}} \left(\frac{R_n^{\min}}{W} - \sum_{i \in \mathcal{K}_n^{\star}} \log_2(a_{n,i}) \right), \quad (12)$$

for $k \in \mathcal{K}_n^{\star}$, where $\mathcal{K}_n^{\star}$ is the optimal set of allocated user index for antenna n in the rate constrained case. Note that $\mathcal{C}_{n,k}^{\star} = 0$ for $k \in \mathcal{K} \setminus \mathcal{K}_n^{\star}$. Moreover, the EE-optimal achievable rate

function pARC($K, n, W, R_n^{\min}, [a_{n,1}, \ldots, a_{n,K}]$)
  Set $U = K$;
  while $R_n^{\min}/W - \sum_{i=1}^{U} \log_2(a_{n,i}) \leq U \log_2\left(a_{n,U}^{-1}\right)$ **do**
    Set $\mathcal{C}_{n,U}^{\star} = 0$;
    Set $U = U - 1$;
  end while
  Set $\mathcal{K}_n^{\star} = \{1, \ldots, U\}$ and $K_n^{\star} = U$;
  Compute $\mathcal{C}_{n,k}^{\star}$ for any $k \in \mathcal{K}_n^{\star}$ by using (12);
return $\mathcal{C}_{n,k}^{\star}$;
end function

function Unc($K, \boldsymbol{\omega}, \widehat{\mathbf{a}}, P_c^{\star}, R_c^{\star}$)
  Sort $\widehat{\mathbf{a}}$ in descending order and obtain the index set $\boldsymbol{\pi}$;
  Set U =length($\widehat{\mathbf{a}}$), $\eta = 1$;
  while $\left\{ \widehat{a}_{\pi_U} e^{\left(1 + \frac{P_c^{\star} \widehat{a}_{\pi_U}}{U}\right)} < 2^{\frac{R_c^{\star}}{U}} \right\}$ &$\{\eta == 1\}$ **do**
    Set $P_c^{\star} = P_c^{\star} + \widehat{a}_{\pi_U}^{-1}$ and $R_c^{\star} = R_c^{\star} + \log_2\left(\widehat{a}_{\pi_U}^{-1}\right)$;
    Set $\mathcal{C}_{\omega_j,k}^{\star} = 0$ for $j = \lfloor (\pi_U - 1)/K \rfloor + 1$ and $k = (\pi_U - 1) \mod \{K\} + 1$;
    Set $U = U - 1$;
    if $U == 0$ **then**
      Set $\eta = 0$ and $U = 1$;
    end if
  end while
  if $\eta == 1$ **then**
    Compute $\mathcal{C}_{\omega_j,k}^{\star}$ for $j = \lfloor (\pi_i - 1)/K \rfloor + 1$, $k = (\pi_i - 1) \mod \{K\} + 1$ and any $i \in \{1, \ldots, U\}$ by using (10) with $K^{\star} = U$;
  end if
return $\mathcal{C}_{\omega_j,k}^{\star}$;
end function

of the k-th user served by any unconstrained antenna n (i.e. $n \in \underline{\mathcal{N}}$) can be expressed in closed-form as in (10), but where

$$P_c^{\star} = \frac{P_c}{\Delta} + \sum_{i \in \overline{\mathcal{N}}} \sum_{j=1}^{K} a_{i,j}^{-1} \left(2^{\mathcal{C}_{i,j}^{\star}} - 1 \right) - \sum_{i \in \underline{\mathcal{N}}} \sum_{j=1}^{K_i^{\star}} a_{i,j}^{-1} \text{ and} \quad (13a)$$

$$R_c^{\star} = \sum_{i \in \overline{\mathcal{N}}} \frac{R_i^{\min}}{W} + \sum_{i \in \underline{\mathcal{N}}} \sum_{j=1}^{K_i^{\star}} \log_2(a_{i,j}). \quad (13b)$$

Based on equation (12), we propose the function "pARC" for optimally allocating the power and rate in an energy efficient and low-complexity manner over the MIMO multi-carrier/user channel in the per-antenna rate constrained scenario.

C. EE optimization algorithm

Since E_b in (6) is convex, it has a unique global minimum, which is obviously the best operation point in terms of EE. Consequently, our algorithm must first search for this optimal unconstrained energy-efficient point, i.e. $\boldsymbol{\mathcal{C}} = \boldsymbol{\mathcal{C}}^{\bullet}$ by using the "Unc" function, which is defined above. However, if this $\boldsymbol{\mathcal{C}}^{\bullet}$ fails to meet the per-antenna rate or power constraint, then the allocation must be refined by using the "pARC" or "pAPC" functions, respectively, such that the optimal constrained energy-efficient point becomes $\boldsymbol{\mathcal{C}}^{\star}$. The results of the "pARC" and "pAPC" functions must then be plugged back into the "Unc" function for further refining the optimization until no more antennas are constrained or all the antennas are constrained, as it is indicated in Algorithm 1.

Algorithm 1 Fast Algorithm for Minimizing the total E_b over the orthogonal multi-antenna multi-carrier channel (FAME-OMMC)

1: ***Inputs:*** $N, K, W, P_c, \Delta, P_n^{\max}, R_n^{\min}$ and $a_{n,k}, \forall n \in \mathcal{N}, k \in \mathcal{K}$;
2: Set $\widehat{\mathbf{a}} = [a_{1,1}, \ldots, a_{1,K}, a_{2,1}, \ldots, a_{N,K}]$;
3: Set $P_c^\star = \frac{P_c}{\Delta} - \sum_{i=1}^{NK} \widehat{a}_i^{-1}$ and $R_c^\star = -\sum_{i=1}^{NK} \log_2\left(\widehat{a}_i^{-1}\right)$;
4: Set $\boldsymbol{\omega} = [1, \ldots, N], \widehat{\boldsymbol{\omega}} = [\varnothing]$;
5: **while** $\{\boldsymbol{\omega} \neq \varnothing\} \& \{\boldsymbol{\omega} \neq \widehat{\boldsymbol{\omega}}\}$ **do**
6: Compute $\mathcal{C}_{\omega_j,k}^\star$ for any $\omega_j \in \boldsymbol{\omega}$ and $k \in \mathcal{K}$ by using "Unc";
7: Set $\widehat{\boldsymbol{\omega}} = \boldsymbol{\omega}, \boldsymbol{\omega} = [\varnothing]$ and $\widehat{\mathbf{a}} = [\varnothing]$;
8: **for** $n = \widehat{\boldsymbol{\omega}}$ **do**
9: **if** $\left\{R_n(\boldsymbol{\mathcal{C}}^\star) \leq R_n^{\min}\right\} \| \left\{P_n(\boldsymbol{\mathcal{C}}^\star) \geq P_n^{\max}\right\}$ **then** ▷ **Constrained Optimization**
10: Set $P_c^\star = P_c^\star + \sum_{i=1}^{K} a_{n,i}^{-1}, R_c^\star = R_c^\star + \sum_{i=1}^{K} \log_2\left(a_{n,i}^{-1}\right)$;
11: **if** $R_n(\boldsymbol{\mathcal{C}}^\star) \leq R_n^{\min}$ **then** ▷ **Rate Constrained**
12: Compute $\mathcal{C}_{n,k}^\star$ for any $k \in \mathcal{K}$ by using "pARC";
13: Set $P_c^\star = P_c^\star + \sum_{i=1}^{K} a_{n,i}^{-1}\left(2^{\mathcal{C}_{n,i}^\star} - 1\right)$;
14: Set $R_c^\star = R_c^\star + R_n^{\min}/W$;
15: **end if**
16: **if** $P_n(\boldsymbol{\mathcal{C}}^\star) \geq P_n^{\max}$ **then** ▷ **Power Constrained**
17: Compute $\mathcal{C}_{n,k}^\star$ for any $k \in \mathcal{K}$ by using "pAPC";
18: Set $P_c^\star = P_c^\star + P_n^{\max}$ and $R_c^\star = R_c^\star + \sum_{i=1}^{K} \mathcal{C}_{n,i}^\star$;
19: **end if**
20: **else**
21: Set $\boldsymbol{\omega} = [\boldsymbol{\omega} \;\; n\;]$ and $\widehat{\mathbf{a}} = [\widehat{\mathbf{a}} \;\; [a_{n,1}, \ldots, a_{n,K}]\;]$;
22: **end if**
23: **end for**
24: **end while**
25: **return** $\boldsymbol{\mathcal{C}}^\star$.

Our low-complexity algorithm in Algorithm 1 clearly reflects this two-stage procedure, where the unconstrained search is performed at line 6 and the rate and/or power constrained updates are performed at lines 12 and 18, respectively. As in the water-filling algorithm, our algorithm in Algorithm 1 is based on closed-form expressions and unidimensional searches, which makes its computational complexity low. However, it has an iterative structure (while loop in line 5) for ensuring optimality; it requires on average 2.5 iterations to converge. We assume here that the channel gains $a_{n,k}$ are sorted in descending order for each antenna prior to using our algorithm, such that $a_{n,1} \geq a_{n,2} \geq \ldots \geq a_{n,K}$ for any $n \in \mathcal{N}$. In addition, $\lfloor . \rfloor$ and mod stand for the "floor" and modulo operators in lines 6 and 13 of the "Unc" function.

IV. Numerical Results and Discussions

In order to demonstrate the reliability of our algorithm for optimally allocating power and rate over the orthogonal MIMO multi-carrier/user channel in an energy-efficient manner, we compare in Figs. 1 and 2 the results, averaged over 1000 runs, of our FAME-OMMC algorithm against the Matlab "fmincon" function in terms of energy-per-bit performance (upper graph) as well as relative computational complexity (lower graph). We define the relative computational complexity between these two methods as the ratio of the "fmincon" execution time to our algorithm execution time. Given that (6) is a convex function, the minimization problems in (8a) and (8b) can be optimally solved via traditional convex optimization tools such as the Matlab "fmincon" function and, hence, we use the latter as a benchmark. Figure 1 depicts the EE-optimal per-antenna power constrained results of both our Algorithm and "fmincon" as a function of noise power for $P_n^{\max} = 20$ W and $R_n^{\min} = 0$ bit/s, $\forall n \in \mathcal{N}$, as well as various values of N and K when considering the power parameter values of Table I, $W = 1$ and $\varsigma = 1/2$. Whereas, Fig. 2 shows the EE-optimal per-antenna rate constrained results of both our Algorithm and "fmincon" for $P_n^{\max} = 10^6$ W, $R_n^{\min} = 20$ bit/s, $\forall n \in \mathcal{N}$, and the same other parameters as in Fig. 1.

TABLE I: Power parameter values

Parameters	Δ	P^{CipA} (W)	P^{Ci} (W)	$P_n^{\max}$ (W)
BS	4.7 [2]	100	180	20 [2]
UE	–	0.03	0.07	–

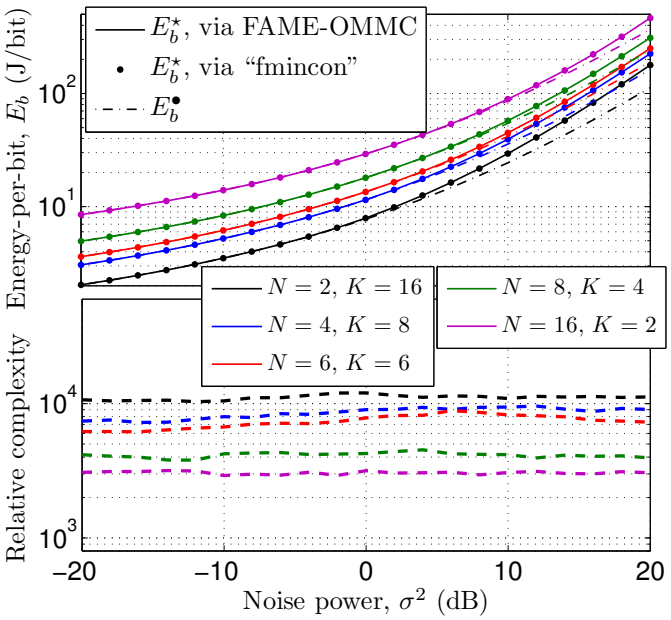

Fig. 1: Comparison of our FAME-OMMC algorithm with "fmincon" in terms of E_b and complexity for various values of N and K with $P_n^{\max} = 20$ W, $R_n^{\min} = 0$ bit/s, $\forall n \in \mathcal{N}$.

Both Figs. 1 and 2 clearly indicate the tight match between our FAME-OMMC algorithm results and the "fmincon" function, which, in turn, graphically confirms the great accuracy and reliability of our energy-efficient resource allocation algorithm. Comparing the EE-optimal unconstrained results $E_b^\bullet$, i.e. for $P_n^{\max} = 10^6$ W and $R_n^{\min} = 0$ bit/s, $\forall n \in \mathcal{N}$, with the constrained results indicates that the EE-based resource allocation becomes constrained when the channel quality degrades, i.e. when the noise power increases; indeed, we know from [14] that over the MIMO channel the EE-optimal power increases with the noise power. Whereas, the relative computational complexity results in the lower part of Figs. 1 and 2 graphically show the low-complexity of our algorithm in comparison with a conventional gradient-search algorithm; indeed, our algorithm can reduce the computational complexity by at least three orders of magnitude, i.e. > 2000 times, in every presented settings.

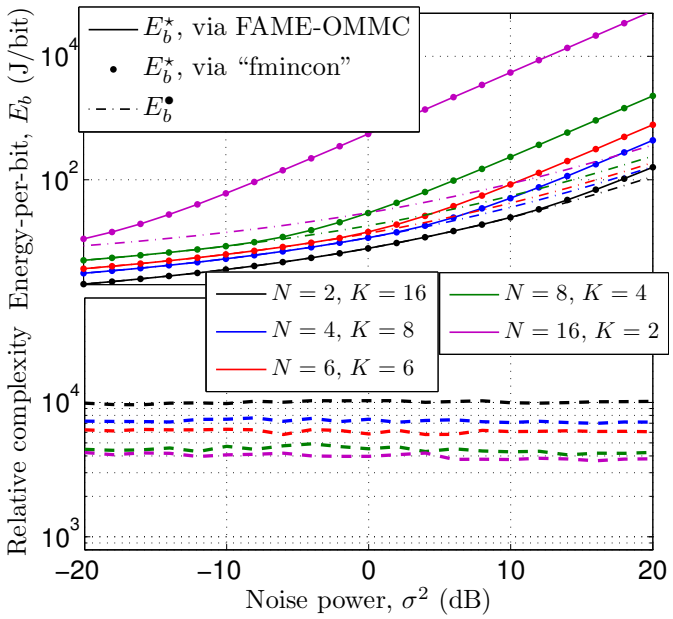

Fig. 2: Comparison of our FAME-OMMC algorithm with "fmincon" in terms of E_b and complexity for various values of N and K with $P_n^{\max} = 10^6$ W, $R_n^{\min} = 20$ bit/s, $\forall n \in \mathcal{N}$.

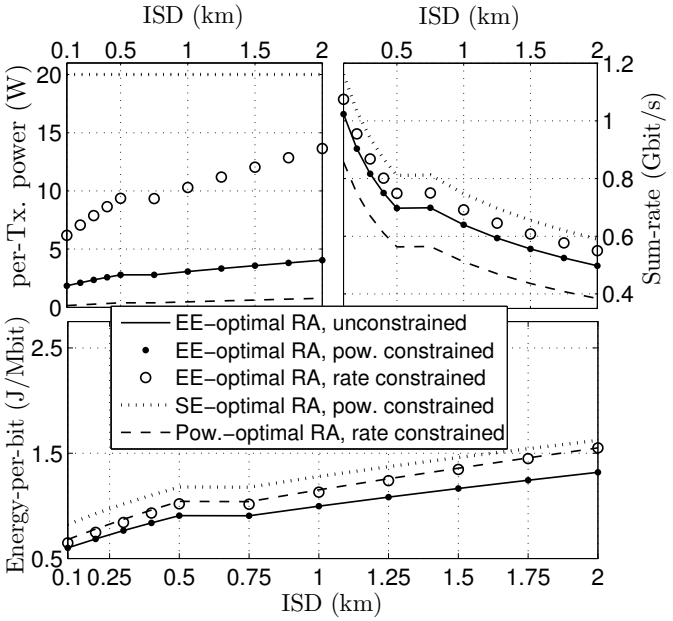

Fig. 3: Performance comparison of the EE-optimal, SE-optimal and power-optimal resource allocations as a function of the ISD for $N = 4$ and $K = 256$ users.

TABLE II: System parameter values

System parameters [15]	f_c	2.1 GHz
	W	10 MHz
	N_0	-165.2 dBm/Hz
	G_{TxRx}	14 dBi
	h_{BS}	25 or 35m if ISD $\leq$ or $>$ d_{BP}
	h_{av}	20 or 5m if ISD $\leq$ or $>$ d_{BP}
	W_{St}	20m
	h_{UT}	1.5m

As an application, we study the trade-off between power, energy and rate in Fig. 3 by comparing our FAME-OMMC algorithm with rate adaptation, i.e. SE-optimal resource allocation subject to a per-antenna power constraint, and margin adaptation, i.e. power-optimal resource allocation subject to a per-antenna rate constraint, when considering a realistic downlink setting with both path-loss and small scale fading. We utilize the following pathloss model such that the pathloss between the BS and the k-th user is given by

$$\rho_k = 10^{(G_{\text{TxRx}} - \text{PL}(d_k))/10}, \tag{14}$$

where G_{TxRx} is the antenna gain of the transmission and $\text{PL}(d) = \text{Pb}_{\text{LOS}}(d)\text{PL}_{\text{LOS}}(d) + (1 - \text{Pb}_{\text{LOS}})\text{PL}_{\text{NLOS}}(d)$ is the distance dependent path-loss function. In addition, Pb_{LOS} is the line-of-sight (LOS) probability, $\text{PL}_{\text{LOS}}(d)$ and $\text{PL}_{\text{NLOS}}(d)$ are the LOS and non-LOS (NLOS) path-loss functions, whose values can be found in Table 27 of [15]. Note that we considered here the urban macro (UMa) setting in Table 27 of [15] for the parameter values given in Table II, where d_{BP} is the breakpoint distance [15].

Relying on this pathloss model, the power parameter values of Table I, and the system parameter values of Table II with $\sigma^2 = N_0 W$, we plot the EE-optimal unconstrained, power and rate per-antenna constrained as well as SE-optimal per-antenna power constrained and power-optimal per-antenna rate constrained resource allocation performances in terms of per-antenna transmit power, sum-rate and energy consumption for $N = 4$ and $K = 256$ uniformly distributed users with one user per subcarrier. In the power-optimal rate constrained resource allocation, we set $R_n^{min} = 0.9 \min_k\{R_k(\boldsymbol{\mathcal{C}}^\bullet)\}$, $\forall n \in \mathcal{N}$, and in EE-optimal rate constrained resource allocation, we set $R_n^{min} = \max_k\{R_k(\boldsymbol{\mathcal{C}}^\bullet)\}$, $\forall n \in \mathcal{N}$. The results indicate that our EE-optimal resource allocation provides the lowest energy-per-bit consumption in comparison with the power and SE-optimal allocations. Our method reduces the energy-per-bit consumption by reducing the transmit power by more than 80% in comparison with the SE-optimal allocation. The power-optimal allocation provides an even larger reduction in transmit power but at the expense of a lower sum-rate, which results in a higher energy-per-bit consumption. Moreover, in this particular setting, the EE-optimal unconstrained and power constrained allocations are the same since none of the antennas have to transmit at full power for minimizing the energy consumption.

V. Conclusion

In this paper, a low-complexity energy-efficient resource allocation methods for the orthogonal MIMO multi-carrier/user channel has been proposed when considering a realistic multi-antenna power model. We have derived explicit formulations of the optimal rate and energy-per-bit consumption for the

per-antenna transmit power constrained and per-antenna rate constrained EE optimization problems. Based on these formulations, we have designed a low-complexity EE-optimal algorithm for allocating resources over the orthogonal MIMO multi-carrier/user channel. Simulations have demonstrated that our method is both accurate and low-complexity when compared to a traditional convex optimization method. Our results have also showed that EE-based allocation can significantly reduce the consumed power and provide a good trade-off between power consumption and sum-rate performance.

APPENDIX

A. Proof for Proposition 1

Proof: In the case that at least one antenna transmits at full power when $\boldsymbol{\mathcal{C}} = \boldsymbol{\mathcal{C}}^{\bullet}$, the Lagrangian associated to the problem in (8a) is equivalent to

$$\mathcal{L}(\boldsymbol{\mathcal{C}}, \widehat{\boldsymbol{\mu}}) = \left[P_c + \Delta \left(\sum_{n \in \overline{\mathcal{N}}} P_n^{\max} + \sum_{n \in \underline{\mathcal{N}}} P_n(\boldsymbol{\mathcal{C}}) \right) \right] \times \left(\sum_{n=1}^{N} R_n(\boldsymbol{\mathcal{C}}) \right)^{-1} + \sum_{n \in \overline{\mathcal{N}}} \widehat{\mu}_n \left(P_n(\boldsymbol{\mathcal{C}}) - P_n^{\max} \right), \tag{15}$$

where $\widehat{\mu}_n$ is a slack variable and $\widehat{\boldsymbol{\mu}} = [\widehat{\mu}_1, \ldots, \widehat{\mu}_N]$. According to (15), solving $\nabla \mathcal{L}(\boldsymbol{\mathcal{C}}^{\star}, \widehat{\boldsymbol{\mu}}^{\star}) = \mathbf{0}$ yields

$$E_b(\boldsymbol{\mathcal{C}}^{\star}) = \begin{cases} \mu_n^{\star} \Delta \dfrac{\partial P_n(\boldsymbol{\mathcal{C}}^{\star})}{\partial \mathcal{C}_{n,k}} \left[\dfrac{\partial R_n(\boldsymbol{\mathcal{C}}^{\star})}{\partial \mathcal{C}_{n,k}} \right]^{-1}, \text{if } n \in \overline{\mathcal{N}} \text{ or} & \text{(16a)} \\ \Delta \dfrac{\partial P_n(\boldsymbol{\mathcal{C}}^{\star})}{\partial \mathcal{C}_{n,k}} \left[\dfrac{\partial R_n(\boldsymbol{\mathcal{C}}^{\star})}{\partial \mathcal{C}_{n,k}} \right]^{-1}, \text{if } n \in \underline{\mathcal{N}}, & \text{(16b)} \end{cases}$$

where $\mu_n^{\star} = \widehat{\mu}_n^{\star} \sum_{n=1}^{N} R_n(\boldsymbol{\mathcal{C}}^{\star})$ with $R_n(\boldsymbol{\mathcal{C}}^{\star})$ being a constant scalar value. Given that $\frac{\partial P_n(\boldsymbol{\mathcal{C}}^{\star})}{\partial \mathcal{C}_{n,k}} = \ln(2) a_{n,k}^{-1} 2^{\mathcal{C}_{n,k}^{\star}}$ and $\frac{\partial R_n(\boldsymbol{\mathcal{C}}^{\star})}{\partial \mathcal{C}_{n,k}} = W$, equation (16) implies that

$$a_{n,i}^{-1} 2^{\mathcal{C}_{n,i}^{\star}} = a_{n,k}^{-1} 2^{\mathcal{C}_{n,k}^{\star}} \tag{17}$$

for any $n \in \mathcal{N}$ and $i, k \in \mathcal{K}_n^{\star}$. Since $P_n(\boldsymbol{\mathcal{C}}^{\star}) = P_n^{\max}$ for $n \in \overline{\mathcal{N}}$, it implies with $P_n(\boldsymbol{\mathcal{C}}) = \sum_{i=1}^{K} a_{n,i}^{-1} \left(2^{\mathcal{C}_{n,i}} - 1 \right)$ and (17) that

$$P_n^{\max} = K_n^{\star} a_{n,k}^{-1} 2^{\mathcal{C}_{n,k}^{\star}} - \sum_{i \in \mathcal{K}_n^{\star}} a_{n,i}^{-1} \tag{18}$$

for any $n \in \overline{\mathcal{N}}$ when $\boldsymbol{\mathcal{C}} = \boldsymbol{\mathcal{C}}^{\star}$. Equation (9) is then a simple reformulation of (18). ■

B. Proof for Proposition 2

Proof: Equation (16) also implies that

$$a_{i,j}^{-1} 2^{\mathcal{C}_{i,j}^{\star}} = \mu_n^{\star} a_{n,k}^{-1} 2^{\mathcal{C}_{n,k}^{\star}} \tag{19}$$

for any $i \in \underline{\mathcal{N}}$, $n \in \overline{\mathcal{N}}$, $j \in \mathcal{K}_i^{\star}$ and $k \in \mathcal{K}_n^{\star}$. By using (19), i.e. substituting $a_{i,j}^{-1} 2^{\mathcal{C}_{i,j}^{\star}}$ with $\mu_n^{\star} a_{n,k}^{-1} 2^{\mathcal{C}_{n,k}^{\star}}$, into (6), the latter can be reformulated as

$$E_b(\boldsymbol{\mathcal{C}}^{\star}) = \frac{\Delta \left[P_c^{\star} + \left(\sum_{i \in \underline{\mathcal{N}}} K_i^{\star} \right) \mu_n^{\star} a_{n,k}^{-1} 2^{\mathcal{C}_{n,k}^{\star}} \right]}{W \left[R_c^{\star} + \left(\sum_{i \in \underline{\mathcal{N}}} K_i^{\star} \right) \left(\mathcal{C}_{n,k}^{\star} + \log_2(\mu_n^{\star} a_{n,k}^{-1}) \right) \right]}, \tag{20}$$

where $P_c^{\star}$ and $R_c^{\star}$ are given in (11a) and (11b), respectively. Moreover we know from (16a) that

$$E_b(\boldsymbol{\mathcal{C}}^{\star}) = \ln(2) \Delta \mu_n^{\star} W^{-1} a_{n,k}^{-1} 2^{\mathcal{C}_{n,k}^{\star}}. \tag{21}$$

By inserting (21) into (20), we obtain an equality solely in terms of the unknown variable $\mu_n^{\star}$ that yields after some simplifications

$$\mu_n^{\star} = \frac{P_c^{\star}}{K^{\star} a_{n,k}^{-1} 2^{\mathcal{C}_{n,k}^{\star}}} \left[W_0 \left(\frac{P_c^{\star}}{K^{\star}} e^{\frac{\ln(2) R_c^{\star}}{K^{\star}} - 1} \right) \right]^{-1}. \tag{22}$$

We finally obtain (10) by inserting (22) into (19). ■

ACKNOWLEDGMENT

The research leading to these results has received funding from the European Commission's Seventh Framework Programme FP7/2007-2013 under grant agreement n°318273-project LEXNET.

REFERENCES

[1] H. Zhang et al., "Energy efficiency in communications," *IEEE Commun. Mag.*, vol. 48, no. 11, pp. 48–79, Nov. 2010.

[2] G. Auer et al., "How Much Energy is Needed to Run a Wireless Network ?" *IEEE Wireless Commun.*, vol. 18, no. 5, pp. 40–49, Oct. 2011.

[3] F. Meshkati, H. V. Poor, S. C. Schwartz, and N. B. Mandayam, "An Energy-Efficient Approach to Power Control and Receiver Design in Wireless Networks," *IEEE Trans. Commun.*, vol. 5, no. 1, pp. 3306–3315, Nov. 2006.

[4] G. Miao, N. Himayat, and G. Y. Li, "Energy-Efficient Link Adaptation in Frequency-Selective Channels," *IEEE Trans. Commun.*, vol. 58, no. 2, pp. 545–554, Feb. 2010.

[5] R. S. Prabhu and B. Daneshrad, "An Energy-efficient Water-filling Algorithm for OFDM Systems," in *Proc. IEEE ICC'10*, Dresden, Germany, Jun. 2010.

[6] C. Isheden and G. P. Fettweis, "Energy-Efficient Multi-Carrier Link Adaptation with Sum Rate-Dependent Circuit Power," in *Proc. IEEE Globecom*, Miami, USA, Dec. 2010.

[7] F. Héliot, M. A. Imran, and R. Tafazolli, "Energy-efficiency based resource allocation for the scalar broadcast channel," in *Proc. IEEE WCNC*, Paris, France, Apr. 2012.

[8] ——, "Energy-efficiency based resource allocation for the orthogonal multi-user channel," in *Proc. IEEE VTC-Fall*, Québec city, Canada, Sep. 2012.

[9] ——, "Low-complexity energy-efficient coordinated resource allocation in cellular systems," *IEEE Trans. Commun.*, vol. 61, no. 6, pp. 2271–2281, Jun. 2013.

[10] H. Bölcskei, D. Gesbert, and A. J. Paulraj, "On the Capacity of OFDM-Based Spatial Multiplexing Systems," *IEEE Trans. Commun.*, vol. 50, no. 2, pp. 225–234, Feb. 2002.

[11] F. Héliot, M. A. Imran, and R. Tafazolli, "On the energy efficiency-spectral efficiency trade-off over the MIMO Rayleigh fading channel," *IEEE Trans. Commun.*, vol. 60, no. 5, pp. 1345–1356, May 2012.

[12] S. Verdu, "Spectral Efficiency in the Wideband Regime," *IEEE Trans. Inf. Theory*, vol. 48, no. 6, pp. 1319–1343, Jun. 2002.

[13] R. M. Corless, G. H. Gonnet, D. E. G. Hare, D. J. Jeffrey, and D. E. Knuth, "On the LambertW Function," *Adv. Comput. Math.*, vol. 5, pp. 329–359, 1996.

[14] F. Héliot, M. A. Imran, and R. Tafazolli, "Energy-efficient power allocation for point-to-point MIMO systems over the Rayleigh fading channel," *IEEE Wireless Commun. Lett.*, vol. 1, no. 4, pp. 304–307, Aug. 2012.

[15] A. Ambrosy et al., "D2.2: Definition and Parameterization of Reference Systems and Scenarios," INFSO-ICT-247733 EARTH (Energy Aware Radio and NeTwork TecHnologies), Tech. Rep., Jun. 2010.

Joint Information and Energy Transfer in the Spatial Domain with Channel Estimation Error

Stelios Timotheou and Ioannis Krikidis
Department of Electrical and Computer Engineering,
University of Cyprus, Cyprus
E-mail: {timotheou.stelios, krikidis}@ucy.ac.cy

***Abstract*—In this paper, we investigate a new technique for simultaneous information and energy transfer in multiple-input multiple-output (MIMO) networks with radio frequency (RF) energy harvesting (EH) capabilities. The proposed technique exploits the spatial decomposition of the MIMO channel and uses the eigenchannels either to convey information or to transfer energy. In order to generalize our study, we consider channel estimation error in the decomposition process and we model the interference between the eigenchannels. An optimization problem that minimizes the total transmitted power subject to information and energy constraints is formulated as a mixed-integer nonlinear program and solved to optimality by a polynomial complexity algorithm developed by exploiting the special characteristics of the problem. Numerical results show that the imperfect channel estimation is beneficial from RF-EH standpoint and is characterized by an optimal (non-zero) value.**

***Index Terms*—RF energy transfer, MIMO channel, single-value decomposition, channel estimation error, optimization.**

I. Introduction

The integration of renewable energy sources into communication networks is a hot research topic. It provides significant energy gains and is an efficient green communication solution for the expected future data traffic increase. Traditional renewable energy sources such as solar energy and wind depend on the weather conditions and are characterized by a high instability; the integration of these energy sources requires a fundamental re-design of communications systems in all levels of protocol stack in order to ensure robustness and reliability [1]. On the other hand, recently there is a lot of interest to use electromagnetic radiation as a potential renewable energy resource. The key idea of this concept is that electromagnetic waves convey energy, which can be converted to DC energy by using some specific rectenna circuits. This approach achieves a wireless energy transfer, recycling the transmitted RF radiation and is introduced as a fully controlled and continuous renewable energy resource; these characteristics motivate the development of new green wireless applications and services.

Most of the work on RF energy transfer concerns the design of rectenna circuits in different frequency bands, which is a fundamental aspect towards the development of this technology [2]–[4]. From an information theoretic standpoint, evaluating the channel capacity for different network configurations, when RF energy harvesting requirements characterize the receiver nodes, is a challenging problem. The work in [5] discusses the joint transfer of information and energy for a single-input single-output (SISO) channel and is extended in [6] for a set of parallel point-to-point channels; the authors in [7] study the capacity for two baseline multi-user systems with RF energy constraints, namely multiple access and multihop channels. However, information theoretic studies assume that the receivers are able to decode information and harvest energy from the same RF signal without limitations. Although this assumption provides some useful theoretical bounds it cannot be supported by the current practical implementations.

In order to satisfy the above practical limitation, the work in [8] deals with the beamforming design for a basic broadcast MIMO channel, where the source conveys information to one receiver while transfers energy to the other one. In that work, the authors introduce two main practical techniques for simultaneous information/energy transfer: a) "time switching" (TS), where the receiver switches between decoding information and harvesting energy and b) "power splitting" (PS), where the receiver splits the received signal in two parts for decoding information and harvesting energy, respectively. The works in [9]–[11] focus on the TS technique for different network topologies. Specifically, in [9] the authors investigate the optimal switching strategy for a SISO channel in order to achieve various trade-offs between wireless information transfer and energy harvesting with/without CSI knowledge at the transmitter. The work in [10] presents a TDMA-based multiuser broadcast channel where the downlink (broadcast channel) is used for energy harvesting while the uplink for conveying information from the users to the access point. In [11], the authors apply the TS technique for a basic relay channel and investigate the optimal switching rule. On the other hand, in [12] the authors study the performance of a cooperative system, where the relay is powered by employing a PS technique on the received signal. The work in [13] studies the optimal transmitted power for a MISO interference channel with PS where the destinations have both information/energy constraints.

In this work, we propose a simultaneous information and energy transfer in the spatial domain for a basic point-to-point multiple-input multiple-output (MIMO) channel. Based on the single-value decomposition (SVD) of the MIMO channel, the communication link is transformed to parallel channels that can convey either information data or energy; this binary allocation is in respect to the current practical limitations. In order to make our analysis more general (and practical), we

978-1-4799-0354-2/13/$31.00 ©2013 IEEE

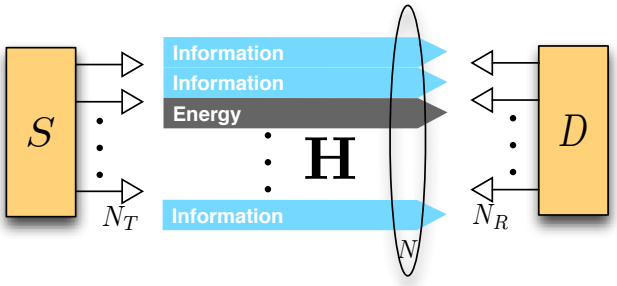

Fig. 1. The system model.

assume an imperfect channel estimation that affects the orthogonality of the eigenchannels (the imperfect channel knowledge generates an interference to the eigenchannels). We study the minimization of the transmitted power when the receiver is characterized by both information rate and energy transfer constraints. The optimization problem requires the assignment of each eigenchannel to information/energy transfer and is solved by using tools from Lagrange optimization theory. An interesting result is that imperfect channel estimation is beneficial for the energy transfer and is characterized by an optimal (non-zero) value.

Notation: Upper case and lower case bold symbols denote matrices and vectors, respectively. $\mathrm{diag}(\mathbf{x})$ represents a diagonal matrix with the vector $\mathbf{x}$ in the main diagonal, $\det(\cdot)$ denotes determinant, $\mathbf{I}_n$ is the identity matrix of order n, $\log(\cdot)$ denotes the logarithm of base 2, $\mathbb{E}[\cdot]$ represents the expectation operator and the superscript H denotes the Hermitian transpose operation.

The rest of this paper is organized as follows. In Section II, we present the system model and introduce the spatial domain energy harvesting as well as the associated optimization problem. In Section III, we deal with the solution of the optimization problem considered. Section IV provides simulation results to evaluate the performance of the proposed technique. Finally, Section V concludes the paper.

II. System Model & Problem Formulation

We assume a simple point-to-point MIMO model consisting of one source S with N_T transmit antennas and one destination with N_R receive antennas. The source is connected to a constant power supply while the destination has RF transfer capabilities and can harvest energy from the received electromagnetic radiation. We consider flat fading spatially uncorrelated Rayleigh MIMO channel where $\mathbf{H} \in \mathbb{C}^{N_R \times N_T}$ denotes the channel matrix. The channel remains constant during a transmission time and changes independently from one transmission to the other one. The entries of $\mathbf{H}$ are assumed to be independent, zero-mean circularly symmetric complex Gaussian (ZMCSCG) random variables with unit variance (which ensures $\mathrm{rank}(\mathbf{H}) = N = \min\{N_T, N_R\}$). The received signal is described by

$$\mathbf{y} = \mathbf{H}\mathbf{x} + \mathbf{n}, \tag{1}$$

where $\mathbf{x} \in \mathbb{C}^{N_T \times 1}$ denotes the transmitted signal with $\mathbb{E}[\mathbf{x}\mathbf{x}^H] = \mathbf{Q}$ and $\mathbf{n} \in \mathbb{C}^{N_R \times 1}$ represents the noise vector having ZMCSCG entries of unit variance. We assume that the channel matrix is subject to a channel estimation error and therefore is *imperfectly* known at both the transmitter and the receiver with a MMSE estimation error $\mathbf{E} \triangleq \mathbf{H} - \widehat{\mathbf{H}}$, where the entries of $\mathbf{E}$ are ZMCSCG with variance σ_ϵ^2 and the entries of $\widehat{\mathbf{H}}$ are also i.i.d. ZMCSCG with variance $1-\sigma_\epsilon^2$ [14]. The channel estimation is performed at the destination via a downlink pilot/training sequence and is communicated to the source by using an uplink feedback channel; the channel estimation process is beyond the scope of this paper. Based on the estimated channel knowledge $\widehat{\mathbf{H}}$, a lower bound of the instantaneous mutual information is given by [14]

$$I(\mathbf{x};\mathbf{y}) = \log\det\left(\mathbf{I}_M + \frac{1}{1+\sigma_\epsilon^2 P}\widehat{\mathbf{H}}\widehat{\mathbf{H}}^{\mathbf{H}}\mathbf{Q}\right). \tag{2}$$

It is worth noting that for $\sigma_\epsilon^2 = 0$ (perfect channel knowledge), the above expression gives the exact mutual information of the MIMO channel. By using the SVD of the $\widehat{\mathbf{H}}$ channel, it has been proven in [14] that the lower bound of the mutual information[1] is maximized when $\mathbf{Q} = \mathrm{diag}(P_1, \ldots, P_N)$ and takes the form

$$I(\mathbf{x};\mathbf{y}) = \sum_{i=1}^{N} \log\left(1 + \frac{P_i\lambda_i}{1+\sigma_\epsilon^2 P}\right), \tag{3}$$

where λ_i is the i-th eigenvalue of i-th eigenvalue of $\widehat{\mathbf{H}}\widehat{\mathbf{H}}^H$, P_i is the power allocated to the i-th eigenchannel and $P = \sum_i P_i$. The expression in (3) shows that the imperfect channel estimation generates an interference to the N parallel single-input single-output channels (eigenchannels). We assume that the destination is characterized by both information rate and RF energy harvesting requirements; this means that for each transmission the destination requires an instantaneous information rate C_I and an energy C_{EH} as an input to its rectenna circuits (the amount of energy that can be stored depends on the energy conversion efficiency of the specific implementation).

A. Simultaneous information/energy transfer: optimization problem

The proposed scheme exploits the SVD structure of the MIMO channel and achieves simultaneous information and energy transfer in the spatial domain. More specifically, the transformation of the MIMO channel to N parallel SISO channels allows the simultaneous transfer of data traffic and RF energy by using an eigenchannel either to convey information or energy. An eigenchannel cannot be used to convey both information and energy; this limitation refers to practical constraints and is inline with the other approaches proposed in the literature (i.e. power splitting). The proposed technique sacrifices some degrees of freedom in order to satisfy the RF energy harvesting constraint. The receiver can achieve

[1]This bound can be achieved based on the SVD of the estimated channel matrix and by appropriate precoding and receiver shaping at the source and the destination, respectively.

simultaneous information and energy transfer by having two different circuits at each antenna, one for information decoding and one for energy harvesting. During each transmission an appropriate optimization problem is solved which determines the usage of each antenna and a switching mechanism selects the appropriate circuits.

In this paper, we focus on the minimization of the transmitted power given that both information and energy constraints are satisfied. Based on the notation considered, the proposed technique introduces the following optimization problem

$$\begin{aligned} & \min \sum_{i=1}^{N} P_i \\ \text{subject to } & \sum_{i=1}^{N} \pi_i \log\left(1+\frac{P_i\lambda_i}{1+\sigma_\epsilon^2 P}\right) \geq C_I \\ & \sum_{i=1}^{N} (1-\pi_i)\left(P_i\lambda_i+\sigma_\epsilon^2 P\right) \geq C_{EH} \\ & P_i \geq 0 \\ & \pi_i \in \{0,1\}, \end{aligned} \tag{4}$$

where the binary variable π_i defines if the i-th eigenchannel is used for information transfer ($\pi_i = 1$) or energy transfer ($\pi_i = 0$). This mathematical program involves binary and continuous variables, as well as nonlinear functions; hence it belongs to the class of mixed-integer nonlinear optimization problems, which are very hard to solve in the general case.

We note that the energy harvested due to the receiver noise is negligible. The optimization problem can be solved in the source node and then flag bits can be used in each eigenchannel in order to inform the receiver about their "content". Fig. 1 schematically presents the system model and the transformation of the MIMO channel to N eigenchannels for potential transfer of information/energy.

III. Optimal Solution

In this section, we deal with the solution of the above optimization problem. We start by finding the optimal power allocation to problem (4) for a given channel assignment towards the satisfaction of the information and energy constraints. We also show that we can obtain the optimal assignment by examining a polynomial number of combinations and develop an algorithm that solves problem (4) optimally.

Assume that a given assignment of channels is made such that $\pi_{i_1} = 1$, $i_1 \in \mathcal{I}$ and $\pi_{i_2} = 0$, $i_2 \in \mathcal{E}$. Due to this assignment, problem (4) can be written as:

$$\begin{aligned} \min \quad & P = \sum_{i=1}^{N} P_i \\ \text{subject to} \quad & \sum_{i_1\in\mathcal{I}} \log\left(1+\frac{P_{i_1}\lambda_{i_1}}{1+\sigma_\epsilon^2 P}\right) \geq C_I \\ & \sum_{i_2\in\mathcal{E}} \left(P_{i_2}\lambda_{i_2}+\sigma_\epsilon^2 P\right) \geq C_{EH} \\ & P_i \geq 0,\ i \in \{\mathcal{I}\cup\mathcal{E}\} \end{aligned} \tag{5}$$

Because there is no imposed upper bound on the transmitted power in each channel, only one channel with non-zero value will be assigned for EH purposes. If a set of channels $\mathcal{E}$ are assigned to satisfy the EH constraint, then only at most one channel will have non-zero value; that will be the channel with the largest eigenvalue in the set of energy channels, λ_e, $e \in \mathcal{E}$. Despite the fact that the power assigned to other channels in $\mathcal{E}$ is zero, they still contribute towards the satisfaction of the EH constraint due to the presence of the term $\sigma_\epsilon^2 P$ in the EH constraint. Another important observation is that channels with $P_i = 0$ can only be the channels with the overall smallest eigenvalues as "better" channels can contribute towards the satisfaction of the information rate and EH constraints. Regarding the set of information channels $\mathcal{I}$, it is easy to see that in the optimal solution, no information channel should have zero power. This is because channels with zero power contribute to the EH constraint but not to the information constraint. The above analysis implies that in order to find the optimal assignment we need two different indices. The first index e indicates the energy channel with a possibly non-zero value, while the second indicates the channel with the largest eigenvalue with $P_{i_2} = 0$, $i_2 \in \mathcal{E}$ - $\{e\}$. Based on the above observations, we can conclude that in order to find the optimal assignment, we only need to examine $O(N^2)$ different assignment combinations.

Next we show that given a fixed assignment $\mathcal{I}$, $\mathcal{E}$ we can obtain the optimal required total power in closed form without explicitly solving the problem. This is a very important result, as it illustrates that to obtain the optimal value of problem (4) one can find the objective for different assignments inexpensively and only solve the problem for the assignment that provides the best objective value. The problem is comprised of two subproblem associated with the satisfaction of the information and EH constraints.

Let us first examine the energy subproblem. Assuming a given power allocation for the information channels we have that:

$$\begin{aligned} \min \quad & P_e \\ \text{subject to} \quad & P_e\lambda_e + |\mathcal{E}|\sigma_\epsilon^2 P \geq C_{EH} \\ & P_e \geq 0, \end{aligned} \tag{6}$$

It is easy to see that the optimal solution to the above problem is $P_e = \max\{0,\ (C_{EH} - |\mathcal{E}|\sigma_\epsilon^2 \sum_{i\in\mathcal{I}} P_i)/(\lambda_e + |\mathcal{E}|\sigma_\epsilon^2)\}$. Note that the EH constraint is always binding when $P_e > 0$, as a non-binding solution is not beneficial neither for the objective nor for the information constraint in problem (5).

The information subproblem can be written as:

$$\begin{aligned} \min \quad & \sum_{i\in\mathcal{I}} P_i \\ \text{subject to} \quad & \sum_{i\in\mathcal{I}} \ln\left(1+\frac{P_i\lambda_i}{1+\sigma_\epsilon^2 P}\right) \geq \ln(2)\cdot C_I \\ & P_i \geq 0,\ i \in \mathcal{I}. \end{aligned} \tag{7}$$

Applying Lagrange multipliers to the above problem yields:

$$\min_{\boldsymbol{\nu}\geq\mathbf{0},\mu_1\geq 0}\mathcal{L}(\mathbf{P},\boldsymbol{\nu},\mu_1)=\sum_{i\in\mathcal{I}}P_i$$
$$+\mu_1\left[\ln(2)\cdot C_I-\sum_{i\in\mathcal{I}}\ln\left(1+\frac{P_i\lambda_i}{1+\sigma_\epsilon^2 P}\right)\right]-\sum_{i\in\mathcal{I}}P_i\nu_i.$$

The optimal value for this problem can be obtained by setting the derivatives of the Lagrange function with respect to P_i, $i\in\mathcal{I}$, equal to zero.

$$\frac{\partial\mathcal{L}(\mathbf{P},\boldsymbol{\nu},\mu_1)}{\partial P_i}=1-\mu_1\left[\frac{\lambda_i-\sigma_\epsilon^2}{\left(1+\sigma_\epsilon^2 P\right)^2}\cdot\left(1+\frac{P_i\lambda_i}{1+\sigma_\epsilon^2 P}\right)^{-1}\right.$$
$$\left.+\sum_{j\in\mathcal{I}\setminus\{i\}}\frac{-\sigma_\epsilon^2}{\left(1+\sigma_\epsilon^2 P\right)^2}\cdot\left(1+\frac{P_i\lambda_i}{1+\sigma_\epsilon^2 P}\right)^{-1}\right]-\nu_i=0,\ \ i\in\mathcal{I}. \tag{8}$$

Note that the derivation of the above formula is a result of the fact that the total power P is also a function of P_i. Straightforward algebraic manipulation of the above formula gives:

$$\frac{\lambda_i}{(y+P_i\lambda_i)}=-\frac{\nu_i y}{\mu_1}+\frac{y}{\mu_1}+\sum_{i\in\mathcal{I}}\frac{y\sigma_\epsilon^2}{\left(1+\sigma_\epsilon^2 P\right)^2}$$
$$\times\left(1+\frac{P_i\lambda_i}{1+\sigma_\epsilon^2 P}\right)^{-1},\ \ i\in\mathcal{I}, \tag{9}$$

where $y=1+\sigma_\epsilon^2 P$. Note that the second and third terms of the right hand side of Eq. (9) are always constant while the first term is constant when $\nu_i=0$, which is true when $P_i>0$. Nonetheless, we have already explained that this situation occurs for the optimal assignment. Hence we have that:

$$\frac{\lambda_i}{(y+P_i\lambda_i)}=\frac{1}{K}\Leftrightarrow\frac{y}{\lambda_i}+P_i=K,\ \ i\in\mathcal{I} \tag{10}$$

Substituting Eqs. (10) into the information constraint, we obtain:

$$\sum_{i\in\mathcal{I}}\log_2\left(\frac{K\lambda_i}{y}\right)=\log_2\prod_{i\in\mathcal{I}}\left(\frac{K\lambda_i}{y}\right)=C_I\Rightarrow K=y\beta, \tag{11}$$

where

$$\beta=\left(2^{C_I}/\prod_{i\in\mathcal{I}}\lambda_i\right)^{\frac{1}{|\mathcal{I}|}} \tag{12}$$

Substitution of Eq. (11) into (10) yields

$$P_i=y(\beta-1/\lambda_i)>0\Rightarrow(\beta-1/\lambda_i)>0, i\in\mathcal{I}.$$

We have already shown that all information channels must have non-zero power; this implies that the above condition is necessary for optimality. Hence, any given assignments that do not satisfy the particular condition can be rejected without any further consideration.

Apart from Eq. (11), we can obtain a second formula that combines variables y and K by summing Eqs. (10) for $i\in\mathcal{I}$:

$$y\sum_{i\in\mathcal{I}}\frac{1}{\lambda_i}+\sum_{i\in\mathcal{I}}P_i=|\mathcal{I}|K=|\mathcal{I}|\beta y.$$

Substituting in the above expression the fact that $y=1+\sigma_\epsilon^2\left(P_e+\sum_{i\in\mathcal{I}}P_i\right)$ yields the following expression for y:

$$y=\frac{P_e+\sigma_\epsilon^{-2}}{\sum_{i\in\mathcal{I}}\frac{1}{\lambda_i}+\sigma_\epsilon^{-2}-|\mathcal{I}|\beta}. \tag{13}$$

Based on the above analysis, to obtain the optimal power P for a fixed assignment, $\{\mathcal{I},\mathcal{E}\}$, we need to examine two cases: (a) $P_e=0$, and (b) $P_e>0$. In order to examine if the first case holds, we compute y from Eq. (13) with $P_e=0$ and check if the solution provides a feasible EH constraint. If this is the case then the value obtained for y is optimal for the particular channel assignment; otherwise the second case is examined.

To eliminate P_e from Eq. (13) and obtain the optimal value of y in the second case, we rewrite the binding EH constraint as a function of y

$$P_e=\frac{C_{EH}-(y-1)|\mathcal{E}|}{\lambda_e}, \tag{14}$$

and substitute it into Eq. (13) to obtain:

$$y=\frac{\frac{C_{EH}}{\lambda_e}+\frac{1}{\sigma_\epsilon^2}+\frac{|\mathcal{E}|}{\lambda_e}}{\sum_{i\in\mathcal{I}}\frac{1}{\lambda_i}+\frac{1}{\sigma_\epsilon^2}+\frac{|\mathcal{E}|}{\lambda_e}-|\mathcal{I}|\beta}. \tag{15}$$

To check for infeasible solutions, we further need to ensure that the obtained solution for y yields a positive value for P_e according to Eq. (14). As y is a monotonically increasing function of P, by finding the best feasible value for y among all feasible assignments, y_{opt}, we can derive the optimal allocation of power into channels, as outlined in Alg. 1.

It should be emphasized that Alg. 1 has two very attractive characteristics: (a) it solves a nonlinear combinatorial optimization problem involving binary variables, in polynomial time, as it requires the examination of a polynomial number of fixed assignments (approximately $N^2/2$), and (b) the optimal power allocation needs to be derived only for the optimal assignment $\mathcal{I}_{opt}$, e_{opt}, and not for all examined fixed assignments which reduces the execution time of the algorithm. Although each assignment appears to be of computational complexity $O(N)$ due to the presence of $\sum_{i\in\mathcal{I}}\frac{1}{\lambda_i}$ and $\prod_{i\in\mathcal{I}}\lambda_i$, we can reduce the computational complexity to $O(1)$. This can be achieved by storing the sum and product terms for fixed EH assignment, e, and updating their values for an increasing number of information channels $i=e+1,...,N$. Hence, the total complexity of Alg. 1 is $O(N^2)$.

IV. Numerical results

Computer simulations are carried-out in order to evaluate the performance of the proposed RF-EH technique. In order to simplify the demonstration of the results, we assume a MIMO channel with eigenvalues drawn from the uniform distribution in the range $[0,N]$; the simulation setup consists of $N=8$

Algorithm 1 : Optimal solution to problem (5)

Initialization: $y_{opt} = \infty$, $\mathcal{I}_{opt} = \varnothing$, and $e_{opt} = \varnothing$. Eigenvalues sorted in descending value.
for $e = 1$ to N **do**
  for $i = e + 1$ to N **do**
    1. Initialise fixed assignment: $\mathcal{I}$= $\{1, ..., i-1\}/e$.
    if ($|\mathcal{I}| > 0$) **then**
      2. Compute β according to (12).
      //The condition below must be true at the optimal solution; otherwise examine another assignment.
      if ($\beta - 1/\lambda_j > 0$, $j = \max\{\mathcal{I}\}$) **then**
        3. Compute the value of y according to Eq. (13) and set $P_e = 0$.
        if ($|\mathcal{E}|(y-1) < C_{EH}$) **then**
          4. Compute the values of y and $P_e > 0$ according to Eqs. (15) and (14) respectively.
        end if
        if (($y_{opt} > y$) AND ($y \geq 1$) AND ($P_e \geq 0$)) **then**
          5. Store the optimal solution found so far: $y_{opt} = y$, $\mathcal{I}_{opt} = \mathcal{I}$, and $e_{opt} = e$.
        end if
      end if
    end if
  end for
end for
if ($1 \leq y < \infty$) **then**
  6. Having found optimal assignment $\mathcal{I}_{opt}$, $e_{opt} = e$ and y_{opt} compute power allocation as follows:
  Compute $P_{opt} = (y_{opt} - 1)\sigma_\epsilon^{-2}$, β_{opt}, $K_{opt} = \beta_{opt} y_{opt}$, and finally $P_i, i \in \mathcal{I}_{opt}$ according to Eq. (10).
else
  7. Deem problem infeasible.
end if

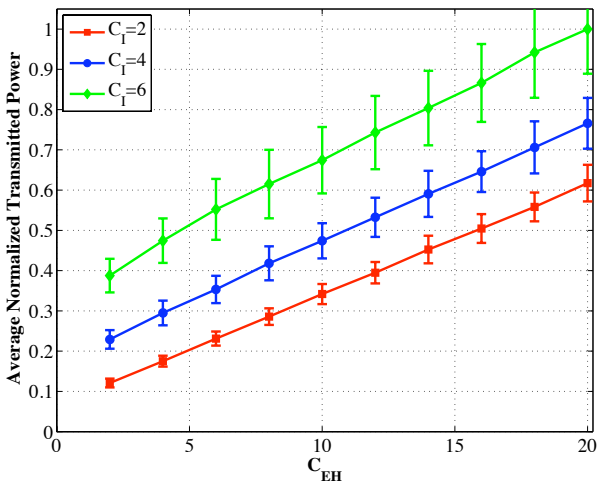

Fig. 2. Average normalized transmitted power versus EH threshold; $\sigma_\epsilon^2 = 0.1$ and $N = 8$.

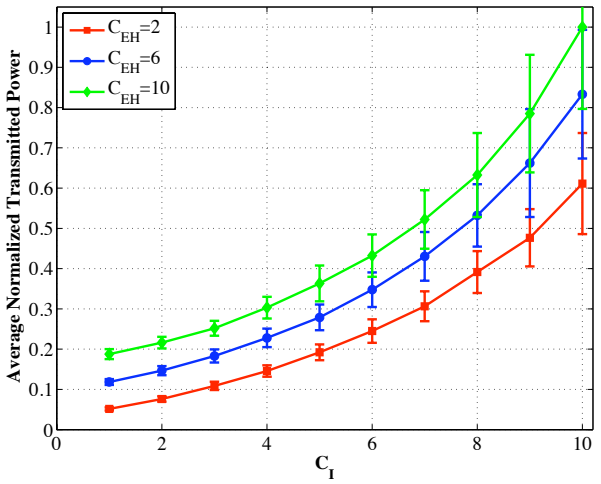

Fig. 3. Average normalized transmitted power versus the information threshold; $\sigma_\epsilon^2 = 0.1$ and $N = 8$.

and $\sigma_\epsilon^2 = 0.1$, while we run 1000 problem instances for each set of parameters. In Fig. 2, we plot the average normalized transmitted power versus the RF-EH constraint (C_{EH}) for $C_I = \{2, 4, 6\}$. It can be seen the required transmitted power is increased as the information and the RF-EH constraints increase. An interesting observation is that the transmitted power increases linearly in order to give a linear increase in the C_{EH} threshold. On the other hand, Fig. 3 plots the average normalized transmitted power versus the information threshold (C_I) for $C_{EH} = \{2, 6, 10\}$. The main observations are inline with the the previous figure and thus the transmitted power increases as C_I and C_{EH} increase. It is worth noting that the increase is not linear since the information constraint is characterized by the logarithmic function.

Fig. 4 shows the impact of the variance of the channel estimation error σ_ϵ^2 on the required transmitted power for different RF-EH thresholds $C_{EH} = \{0.1, 0.3, 0.5, 0.7, 0.9, 1.1\}$. As it can be seen that σ_ϵ^2 significantly affects the total power consumption; the main remark is that this imperfection seems to be beneficial for the total transmitted power. More specifically, a perfect channel estimation results in higher power consumption while a non-zero σ_ϵ^2 improves the energy consumption of the system. In addition, we can see that an optimal value for the σ_ϵ^2 exists that minimizes the total power consumption. The main reason for this behavior is that σ_ϵ^2 affects the orthogonality of the eigenchannels and results in an interference between them, which is useful for the satisfaction of the RF-EH constraint. This result shows that although the imperfect channel estimation degrades the performance in conventional systems, it becomes useful for the proposed spatial domain information/energy transfer. Therefore, the proposed technique is not sensitive to the variance of the channel estimation error; this attribute is attractive to practical implementations. Fig. 5 shows the impact of σ_ϵ^2 for different information rate thresholds. The main results are similar to Fig. 4 and confirm our conclusions.

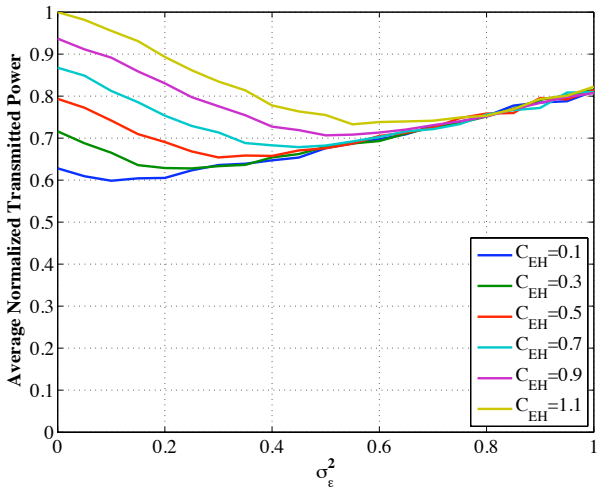

Fig. 4. Average normalized transmitted power versus the variance of the estimation error for various values of C_{EH}; $C_I = 2$ and $N = 8$.

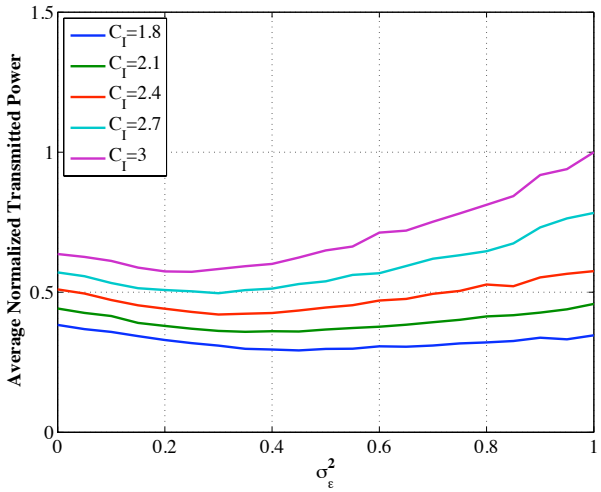

Fig. 5. Average normalized transmitted power versus the variance of the estimation error for various values of C_I; $C_{EH} = 0.6$ and $N = 8$.

V. Conclusion

We have investigated the simultaneous information and energy transfer in the spatial domain for a MIMO channel with RF-EH capabilities. By using the SVD decomposition of the wireless channel under an imperfect channel knowledge, the proposed technique uses the eigenchannels for conveying either information or energy. To minimize the transmitted power subject to some well-defined information and energy constraints, the problem is formulated as a mixed-integer nonlinear optimization program. A polynomial complexity algorithm that produces the optimal solution to the considered problem is developed with the use of Lagrange multipliers.

References

[1] S. Sudevalayam and P. Kulkarni, "Energy harvesting sensor nodes: survey and implications," *IEEE Commun. Surveys Tuts.*, vol. 13, no. 3, pp. 443–461, 2011.

[2] A. Dolgov, R. Zane, and Z. Popovic, "Power management system for online low power RF energy harvesting optimization," *IEEE Trans. Circ. Syst.*, vol. 57, pp. 1802–1811, July 2010.

[3] H. Sun, Y. -X. Guo, M. He, and Z. Zhong, "Design of a high-efficiency 2.45-GHz rectenna for low-input-power energy harvesting," *IEEE Ant. Wireless Propag. Lett.*, vol. 11, pp. 929–932, 2012.

[4] P. Nintanavongsa, U. Muncuk, D. R. Lewis, and K. R. Chowdhury, "Design optimization and implementation for RF energy harvesting circuits," *IEEE J. Emerg. Selec. Topics Circ. Syst.*, vol. 2, pp. 24–33, March 2012.

[5] L. R. Varshney, "Transporting information and energy simultaneously," in *Proc. IEEE Int. Symp. Inform. Theory*, Toronto, Canada, Jul. 2008, pp. 1612- 1616.

[6] L. R. Varshney, "On energy/information cross-layer architectures," in *Proc. IEEE Int. Symp. Inform. Theory*, Cambridge, MA, Jul. 2012.

[7] A. M. Fouladgar and O. Simeone, "On the transfer of information and energy in multi-user systems," *IEEE Commun. Lett.*, vol. 16, pp. 1733–1736, Nov. 2012.

[8] R. Zhang and C. K. Ho, "MIMO broadcasting for simultaneous wireless information and power transfer," *IEEE Trans. Wireless Commun.*, accepted for publication, 2013.

[9] L. Liu, R. Zhang, and K. -C. Chua, "Wireless information transfer with opportunistic energy harvesting," *IEEE Trans. Wireless Commun.*, vol. 12, pp. 288–300, Jan. 2013.

[10] H. Ju and R. Zhang, "Throughput maximization for wireless powered communications networks," *IEEE Trans. Wireless Commun.*, submitted for publication, April 2013. [Online:] http://arxiv.org/pdf/1304.7886v1.pdf

[11] I. Krikidis, S. Timotheou, and S. Sasaki, "RF energy transfer for cooperative networks: data relaying or energy harvesting?," *IEEE Commun. Lett.*, vol. 16, pp. 1772–1775, Nov. 2012.

[12] A. A. Nasir, X. Zhou, S. Durrani, and R. A. Kennedy, "Relaying protocols for wireless energy harvesting and information processing," *IEEE Trans. Wireless Commun.*, vol. 12, pp. 3622-3636, July 2013.

[13] S. Timotheou, I. Krikidis, and B. Ottersten, "MISO interference channel with QoS and RF energy harvesting constraints," in *Proc. Int. Conf. Commun.*, Budapest, Hungary, June 2013.

[14] T. Yoo and A. Goldsmith, "Capacity and power allocation for fading MIMO channels with channel estimation error," *IEEE Trans. Inf. Theory*, vol. 52, pp. 2203–2214, May 2006.

How much energy can be saved by energy-delay tradeoff in radio access network?

M. M. Aftab Hossain, Konstantinos Koufos and Riku Jäntti
Department of Communications and Networking
Aalto University, Finland
{mm.hossain, konstantinos.koufos, riku.jantti}@aalto.fi

***Abstract*—The energy-delay tradeoff is one of the fundamental tradeoffs when looking for energy efficient wireless access networks. The potential to save energy at the base station (BS) by introducing delay in the downlink is constrained by both the non-ideal efficiency characteristics of power amplifier (PA) and the energy cost suffered by the mobile terminals (MT) due to the longer reception time. One possible way to control energy consumption at the MT is to introduce transmission delay in the uplink too. In this paper, we study the potential for energy saving by introducing transmission delay both in the uplink and in the downlink of a wireless network. We show that the energy saving potential depends on the network load (both uplink and downlink) and the PA efficiency (employed at the BS and the MT). Energy can be saved for most of the load combinations in uplink and downlink without draining out the battery of MT. One exception is the case with very low uplink load and very high downlink load. In that case, energy can be still saved at the cost of small excess energy consumption at the MT.**

Keywords*—Energy Efficiency; Power Amplifier Efficiency; Energy-delay tradeoff

I. Introduction

An exponential growth of capacity demand is making energy consumption as well as CO_2 emission by wireless networks a critical issue. More than 50 billion nodes are expected to be connected by 2020 [1]. At the same time, more and more data is going to be transferred over wireless networks. Energy cost is already a huge contributor to the total operational cost. As a result, energy efficiency of radio technologies is an important and urgent issue.

The operation of cellular networks is mostly served by macro base stations (BSs) where the traditional power amplifier (TPA) consumes around $55\%-70\%$ of total energy [2], [3]. TPA:s reach maximum efficiency near their compression region, where they rarely operate due to the high peak to average power ratio (PAPR) of non-constant envelope signals e.g. code division multiple access (CDMA) and orthogonal frequency-division multiplexing (OFDM) signals. Deployment of more efficient PA:s is a means to reduce energy consumption. For instance, envelope tracking power amplifier (ET-PA) achieves better efficiency by tracking the RF signal and regulating the supply voltage accordingly. Though the energy consumption in the BS dominates the total consumption in the radio access, energy efficiency in the mobile terminal(MT) is also very important from the user's perspective in order to prolong battery lifetime.

From Shannon's capacity formula, it is known that the required energy to transmit a certain amount of data decreases by increasing the transmission time. This energy-delay trade-off is one of the fundamental trade-offs that could be used to regulate the energy consumption in the radio access part [4]. With an ideal power amplifier (PA), energy can be saved up to infinite delay. For realistic PA:s, energy consumption starts increasing after prolonging the transmission time beyond a certain limit. In a recent paper, we studied the energy-delay trade-off incorporating realistic PA efficiency characteristics in a multi-cell/multi-user cellular downlink scenario in the presence of slow fading [5]. We showed that there is a significant potential for energy saving at the cost of additional flow level delay.

Besides [5], the energy-delay trade-off has been studied in [6] for the downlink, in [7] for the uplink and in [8]–[12] for either downlink or uplink. In this paper, we take a holistic approach and formulate the energy minimization problem by taking into account both the uplink and downlink energy consumption. Also, none of the previous studies considers the impact of introducing transmission delay on the energy consumption at the receiving end. Introducing delay in the downlink of a BS requires the MT to stay at receiving mode for longer time and consequently increases their energy consumption. As a result, the energy saving potential in the downlink is also constrained by the excess energy consumption at the MT. It is possible to introduce additional delay in the uplink to compensate that excess energy consumption. Note that the PA at the MT side consumes a low share of the total energy as the maximum transmission power is only around 200 mW while the power needed for data processing is much higher. Even though the potential for energy saving by introducing delay in the uplink is less significant, we show that energy saved by a small additional delay in the uplink surpluses the excess energy required due to delay in the downlink for all load combinations except when the uplink load is very low.

In the current technologies e.g. LTE and 3G, a BS keeps transmitting round the clock. A large amount of energy is wasted as the daily maximum loads are 2-10 times higher than the daily minimums whereas the energy consumed by a BS with no real load is around half of the energy required to serve maximum load [2]. In our analysis, we show that the percentage for energy saving using energy-delay tradeoff increases drastically if the idle power consumption could be reduced. Also at the MT side, energy consumption is dominated by the so-called 'tail energy' which is consumed after each transmission as the MT stays at high energy state to reduce the overhead associated with switching ON in case another transmission follows [13]. Using proxy at the BS to

978-1-4799-0354-2/13/$31.00 ©2013 IEEE

accumulate and bundle data before transferring it to the MT is a means to reduce the number of tails and reduce energy wastage [14].

II. System model

We consider a network of macro BSs. Each BS site consist of 3 hexagonal-shaped sectors. Each sector is served by a BS equipped with its own PA and directional antenna. The BSs for a site is co-located at the center of the site. Hereafter, a sector is referred as a cell. In our analysis, a BS has been modeled as a single-server queue that serves the users in one-by-one fashion. We use the flow level delay as performance metric which is appropriate for elastic type of traffic. The flow level delay can be considered as the inverse of the flow level throughput [17]. For proportional fair scheduling the flow level throughput of a user at location u in the coverage area of a cell $\mathcal{C}$, $u \in \mathcal{C}$, ρ_u, can be related to the transmission rate r_u as [17], [18]

$$\rho_u = \left(1 - \sum_{u \in \mathcal{C}} \frac{\lambda_u S_u}{r_u}\right) r_u \tag{1}$$

where λ_u is the packets per second generated in a flow and S_u is the packet size for the location u. In order to study energy-delay tradeoff we use simple models for the PA efficiency, transmission rate and aggregate interference, as detailed in [5].

A. Power amplifier

We consider two types of PA:s with different efficiency characteristics. The TPA is characterized by high efficiency only close to its compression region. The required input power for mean transmit power level equal to $p \leq p_{max}$ is

$$P_{PA}^{(TPA)}(p) = \frac{1}{\eta_{max}} \sqrt{p \cdot p_{max,A}} \tag{2}$$

η_{max} denotes the maximum PA efficiency and $p_{max,A}$ is the maximum output power of the PA.

In case of ET-PA the total power consumption is approximately linear function of the actual transmit power

$$P_{PA}^{(ETPA)}(p) = \frac{1}{(1+\alpha)\eta_{max}} (p + \alpha p_{max,A}) \tag{3}$$

where $\alpha = 0.0082$ is a PA dependent parameter [16].

B. Transmission rate

For modeling the transmission rate we consider that the users can adapt their modulation and coding scheme so that they can reach the Shannon capacity bound. In that case, the transmission rate at location u is

$$r_u = W \cdot \log_2(1 + \gamma_u) \tag{4}$$

where W is the positive signal bandwidth and γ_u is the SINR at location u.

C. Aggregate interference model

In order to model the aggregate interference level in a slow fading environment we employ the Fenton-Wilkinson approximation method as in [19]. In the downlink, the locations of the interfering BS are fixed. The mean and variance of the aggregate interference received by a MT at a location can be found at [5, Eq. (29), Eq. (30)].

In the uplink, the interferers are the MT:s which can be situated at any place in a sector. In order to calculate the uplink generated interference at the k-th BS we need to compute the generated interference from all the cells $i = 1, \ldots, K : i \neq k$. The generated interference from the i-th cell can be found by averaging over the path-loss values from all the locations u inside the i-th cell. This is motivated from the fact that all MTs in a cell are served with equal probability as we considered proportional fair scheduling. By following similar approach as in [5], the mean and variance of the aggregate interference can be read as

$$\mathrm{E}\{I\} = e^{\frac{\sigma^2}{2\xi^2}} \sum_i \bar{q}_i |\mathcal{C}_i|^{-1} \sum_{u \in \mathcal{C}_i} e^{\frac{\mu_{i,u}}{\xi}} \tag{5}$$

$$\mathrm{var}\{I\} = e^{\frac{\sigma^2}{\xi^2}} \sum_i \left(\bar{q}_i e^{\frac{\sigma^2}{\xi^2}} - \bar{q}_i^2\right) |\mathcal{C}_i|^{-1} \sum_{u \in \mathcal{C}_i} e^{\frac{2\mu_{i,u}}{\xi}}. \tag{6}$$

where σ in dB stands for the slow fading standard deviation due to each interfering MT, $\bar{q}_i$ is the mean activity in the uplink of the i-th cell, $\xi = 10/\log 10$ is a scaling constant, $|\cdot|$ denotes set cardinality and $\mu_{i,u}$ in dB is the distance-based pathloss from the location u of the i-th cell to the interfered BS at the k-th cell.

III. Problem Formulation

The total energy consumption at the radio access part for a wireless system can be written as

$$\begin{aligned} E_{total} &= E_{dl} + E_{ul} + E_{other} \\ &= E_{tx}^{BS} + E_{rx}^{MT} + E_{tx}^{MT} + E_{rx}^{BS} + E_{other} \end{aligned} \tag{7}$$

where the downlink energy consumption, E_{dl}, consists of energy required for the BS to transmit data, E_{tx}^{BS}, and the energy required for the mobile station to receive that data E_{rx}^{MT}. Similarly for the uplink, E_{tx}^{MT} is the energy consumed at the MT for transmission and E_{rx}^{BS} is the energy consumed at the BS for reception. Finally, E_{other} may refer to cooling, DC-DC conversion loss in the BS, etc.

The total energy consumption to transmit and receive a packet of size S_u bits in the downlink at location u of the k-th cell $u \in \mathcal{C}_k$ is

$$\begin{aligned} e_{dl}(p_u, \mathbf{p}_{-k}) &= (P_{PA}^{BS}(p_u) + P_C^{BS} + P_{rx}^{MT}) x_u(p_u, I_u(\mathbf{p}_{-k})) \\ &= S_u \frac{P_{PA}^{BS}(p_u) + P_C^{BS} + P_{rx}^{MT}}{r_u(p_u, I_u(\mathbf{p}_{-k}))}. \end{aligned} \tag{8}$$

where x_u is the transmission time and $I_u(\mathbf{p}_{-k})$ is the generated interference expressed as a function of the transmit power of interfering BSs. The vector, $(\mathbf{p}_{-k})$, contains the transmit power values used in other cells that generate interference at the k-th cell, P_C^{BS} represents the constant power consumption during transmission and P_{rx}^{MT} represents the ectronic energy consumed by the MT during reception.

If we ignore the energy cost associated with switching the PA on and off, the mean total energy consumption for serving a user is obtained by averaging the energy consumption over

all the locations $u \in \mathcal{C}_k$

$$\begin{aligned}\bar{e}_{dl,k}(\mathbf{p}_k, \mathbf{p}_{-k}) &= \mathrm{E}_u\{\lambda_u e_{dl}(p_u, \mathbf{p}_{-k})\} \\ &\quad + \Big(1 - \sum_{u\in\mathcal{C}} \lambda_u x_u(p_u, I_u(\mathbf{p}_{-k}))\Big) \frac{P^{BS}_{idle}}{|\mathcal{C}_k|} \\ &= \frac{1}{|\mathcal{C}_k|}\Big(\sum_{u\in\mathcal{C}} \lambda_u S_u \frac{P^{BS}_{PA}(p_u) + P^{BS}_{C} - P^{BS}_{idle} + P^{MT}_{rx}}{r_u(p_u, I_u(\mathbf{p}_{-k}))} \\ &\quad + P^{BS}_{idle}\Big) \end{aligned} \tag{9}$$

where $\mathbf{p}_k$ is the power allocation vector for the k-th BS with elements $p_u : u \in \mathcal{C}_k$ and P^{BS}_{idle} is consumed when the BS does not transfer any signal.

Similarly for the uplink, the mean energy consumption can be written as

$$\begin{aligned}\bar{e}_{ul,k}(\mathbf{p}_k, \mathbf{p}_{-k}) &= \frac{1}{|\mathcal{C}_k|}\Big(\sum_{u\in\mathcal{C}} \lambda_u S_u \frac{P^{MT}_{PA}(p_u) + P^{MT}_{C} - P^{MT}_{idle} + P^{BS}_{rx}}{r_u(p_u, I_u(\mathbf{p}_{-k}))} \\ &\quad + P^{MT}_{idle}\Big) \end{aligned} \tag{10}$$

where $\mathbf{p}_k$ is the power allocation vector for the MT in the k-th cell with elements $p_u : u \in \mathcal{C}_k$ and $\mathbf{p}_{-k}$ contains the transmit power values used by the MTs from the interfering cells. Hereafter, we use superscript e.g. $\mathbf{p}^y_k, y \in \{BS, MT\}$ to differentiate power vectors for BS and MT.

Let us consider a reference scenario for downlink transmission with transmit power levels equal to p^{BS}_{max} for all locations inside the cells. The corresponding flow throughput at the location u of a cell, $\rho_{ref,u}$, can be computed after evaluating the transmission rates using the maximum transmit power level in equation (4) and substituting them into equation (1). The inverse of the reference throughput is used as the reference transmission delay. Increasing the transmission delay in the downlink by a factor of $1/\Delta^{BS}$ decreases the flow throughput by a factor of Δ^{BS}. Let us assume that the maximum allowable reduction is Δ^{BS}_{max} and thus, $\Delta^{BS} \geq \Delta^{BS}_{max}$. In order to ensure the flow throughput target at location u, the transmit power level should be higher than $p^{BS}_{min,u}$ and thus, $p^{BS}_{min,u} \leq p^{BS}_{u} \leq p^{BS}_{max}$. The details for the computation of the required transmit power level, $p_{min,u}$, to ensure a target flow throughput can be found in [5].

Energy saving in the BS by introducing delay in the downlink increases energy consumption in the MT due to prolonged reception time. In order to compensate this excess energy, delay can be introduced in the uplink too. In the uplink, the reference flow throughput is computed with fractional power control i.e path loss is compensated partially for the MTs. Δ^{MT}_{max} is defined as the maximum allowable reduction of the flow throughput in the uplink. The required uplink transmit power to ensure the target flow throughput is denoted by $p^{MT}_{min,u} : p^{MT}_{min,u} \leq p^{MT}_{u} \leq p^{MT}_{max,u}$.

In this paper we investigate the potential for energy saving in uplink and downlink without draining out significant battery life of the MT. We assume that the total energy consumption (downlink and uplink) in the MT should not increase beyond $\alpha\%$ with respect to the reference scenario, i.e. downlink transmit power equal to p_{max} and fractional power control in the uplink. Taking into consideration all the constraints, the energy minimization problem can be formulated as

$$\underset{\Delta^y, \mathbf{p}^y_k \forall k}{\text{Minimize}} : \sum_{k\in\mathcal{K}} \bar{e}_{dl,k}(\mathbf{p}^{BS}_k, \mathbf{p}^{BS}_{-k}) + \sum_{k\in\mathcal{K}} \bar{e}_{ul,k}(\mathbf{p}^{MT}_k, \mathbf{p}^{MT}_{-k}) \tag{11i}$$

$$\text{Subject to: } \Delta^y > \Delta^y_{max} \forall y, \tag{11ii}$$

$$\frac{\triangle E^{MT}_k}{E^{MT}_k} \leq \alpha \ \forall k \tag{11iii}$$

where $y \in \{BS, MT\}$, E^{MT}_k refers to the energy consumption of the MT:s in the reference scenario and $\triangle E^{MT}_k$ is the difference between energy consumption using energy-delay trade-off and reference scenario.

A. Optimization algorithm

In order to solve the optimization problem (11) we discretize the delays in uplink and downlink: $\Delta^{MT} \in [\Delta^{MT}_{max}, 1]$ and $\Delta^{BS} \in [\Delta^{BS}_{max}, 1]$ respectively, and construct the Cartesian product of the delay vectors. For given delay pair the minimum required power levels for uplink and downlink, $p^{BS}_{min,u}, p^{MT}_{min,u}, \forall u$, can be evaluated and the optimization problem can be read as

$$\underset{\mathbf{p}^y_k, \forall k}{\text{Minimize}} : \sum_{k\in\mathcal{K}} \bar{e}_{dl,k}(\mathbf{p}^{BS}_k, \mathbf{p}^{BS}_{-k}) + \sum_{k\in\mathcal{K}} \bar{e}_{ul,k}(\mathbf{p}^{MT}_k, \mathbf{p}^{MT}_{-k}) \tag{12i}$$

$$\text{Subject to: } \mathbf{p}^y_{min,k} \prec \mathbf{p}^y_k \prec \mathbf{p}^y_{max,k} \ \forall k, y \in \{BS, MT\} \tag{12ii}$$

$$\frac{\triangle E^{MT}_k}{E^{MT}_k} \leq \alpha \ \forall k. \tag{12iii}$$

In order to solve the optimization problem (12) we decompose it into two independent problems, one for the uplink and one for the downlink, without taking into account the constraint (12iii). For instance, the optimization problem for the uplink is

$$\underset{\mathbf{p}^{MT}_k, \forall k}{\text{Minimize}} : \sum_{k\in\mathcal{K}} \bar{e}_{ul,k}(\mathbf{p}^{MT}_k, \mathbf{p}^{MT}_{-k}) \tag{13i}$$

$$\text{Subject to: } \mathbf{p}^{MT}_{min,k} \prec \mathbf{p}^{MT}_k \prec \mathbf{p}^{MT}_{max,k} \ \forall k. \tag{13ii}$$

The power allocation vector, $\mathbf{p}^{MT}_k$, is identified using best response iteration algorithm (BRIA). The optimality of the BRIA is proved in [5]. The optimization problem for the downlink is also solved in a similar way. Note that the pair of power allocation vectors $\mathbf{p}^{BS}_k, \mathbf{p}^{MT}_k$ must be discarded if it does not satisfy the optimization constraint (12iii). The optimization process is repeated over all delay pairs and the pair minimizing the objective function in equation (12i) is finally selected.

IV. Numerical results

In this paper, we take a holistic approach to study the potential for energy saving in both uplink and downlink using the energy-delay trade-off. The potential for saving energy mostly lies in the downlink as the power consumed for downlink transmission is manifold higher than the power consumed in the uplink during reception [15]. The total energy consumed in the uplink is not that significant in comparison with downlink, whereas MT energy efficiency is very important from the user's perspective. As a result, saving energy in the BS during uplink at the cost of excess energy consumption in the MT is undesirable. Considering the practicalities explained above, we

maximize the energy saving potential in the BS downlink and emphasize the energy saving in the MT. In order to do that, in the uplink, we maximize energy saving only in the MT i.e. we ignore E_{rx}^{BS} while minimizing the uplink power consumption, $\bar{e}_{ul,k}(\mathbf{p}_k, \mathbf{p}_{-k})$. In this way we allow for maximum energy saving in the MT uplink by energy-delay tradeoff and use this saving to compensate excess energy consumed in the MT due to the delay in the BS downlink. We try to maximize energy saving in the BS downlink even at the cost of excess energy consumption in the MT. However, we constrain the excess energy consumption of the mobile terminal to 2%.

A. Parameter Setting

We consider a cellular network consisting of 19 BS, each having 3 regular hexagonal-shaped sectors. A grid of 64 points emulating the possible locations of the users is generated inside each cell. The parameter settings are summarized in the Table I. Unless explicitly expressed, we assume that all cells are offered the same load. In order to ignore the border effects i.e. to maintain same interference conditions for all cells, wrap around technique has been employed. Idle power consumption, P_{idle}^{BS}, for the base stations employing TPA and ET-PA has been calculated to be 53.6 W and 45.4 W using the equation suggested in Earth project [2]. For simplicity, we ignore the power needed for packet processing at the BS which is also very small. In that case, the constant part of the energy consumed by the BS during transmission and idle power consumption becomes similar, $P_C^{BS} \approx P_{idle}^{BS}$. At the terminal side, we consider power consumption during reception, $P_{rx}^{MT} = 1200$ mW, static power consumption during transmission $P_C^{MT} = 1200$ mW along with maximum transmission power equal to 200 mW. We ignore the rate dependency of the processing power for both reception and transmission in the MT. Note that the energy consumption during idle state at the MT is very small, $P_{idle}^{MT} \approx 0$. The maximum additional delay, $1/\Delta_{max}^{y}, y \in \{BS, MT\}$ considered in this analysis is 5%. In [5], we showed that energy saving potential by

TABLE I: simulation Parameters

Reference parameters	
Parameter	*Value*
Number of sectors/BS	57
Grid size inside each sector	64 points
Cell radius	1 km
BS PA maximum output power	53 dBm
MT PA maximum output power	27 dBm
maximum BS transmit power	46 dBm
maximum MT transmit power	23 dBm
maximum PA efficiency	80%
Path loss exponent	3
Shadow fading standard deviation	5.5 dB
Bandwidth	20 MHz
Noise level	-106 dBm
Target outage	10%

introducing energy-delay tradeoff in a multi-cellular network is highly dependent on the network load and the efficiency characteristics of the PA. The percentage of energy saving is high for low network loads while it is not that significant when the network operates with a high load. Note that energy-delay trade-off is only possible in the dynamic part i.e. energy consumed by the PA.

B. Downlink Energy consumption

The energy consumption at the BS dominates the total energy consumption in the downlink. In Fig. 1, we show the energy saving percentage at the BS by employing energy-delay tradeoff in the downlink. A high percentage of the dynamic part of the energy can be saved at low load. However, at low load, the idle energy consumption dominates and the overall saving percentage becomes pretty low. At a high load, the saving potential by energy-delay tradeoff decreases in the dynamic part. As a result, overall saving potential is peaked at medium network loads.

If the idle power consumption is ignored, we can see that energy saving potential by energy-delay trade-off appears more significant. In Fig. 2, we show that energy saving percentage jumps manifold if energy is not wasted when their is no data transmission i.e. the idle power consumption is ignored. Introduction of deep DTX/DRX i.e. sending more and more components into sleep mode during low to medium load is a must for future generation of network design. In that case, the energy saving potential by energy-delay trade-off is much more promising.

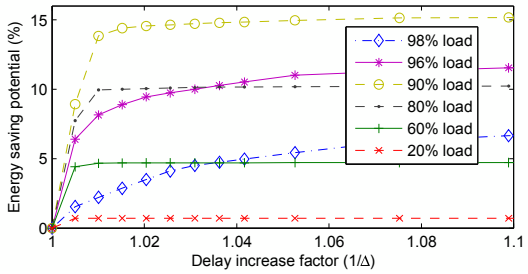

Fig. 1: Energy saving percentage at the BS with ET-PA.

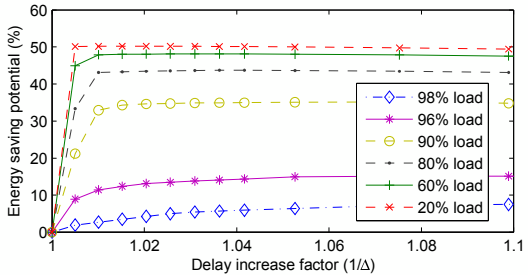

Fig. 2: Energy saving percentage at the BS in the dynamic part, $P_{idle}^{BS} = 0$, with ET-PA.

BS involving TPA can benefit from energy-delay tradeoff up to moderate load only, see Fig. 3 and Fig. 4. If the network load is higher than 60%, the energy saving potential becomes insignificant. The efficiency of TPA keeps falling drastically when the BS reduces its output transmit power making it

more beneficial to transmit at maximum power. As a result, the window accommodated for energy-delay trade-off to take place is very small. Both the idle power consumption as well as overall power consumption is much higher for BS utilizing TPA when compared to ET-PA. This behavior emphasizes the need to upgrade network components with more energy efficient PA:s in order to reduce energy consumption.

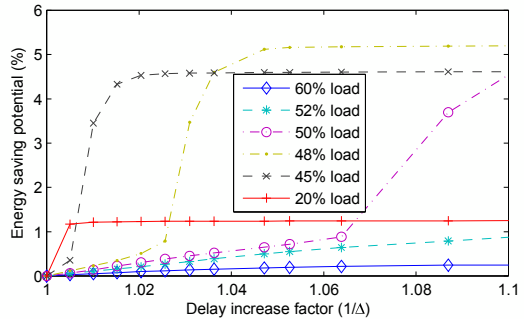

Fig. 3: Energy saving percentage at the BS with TPA.

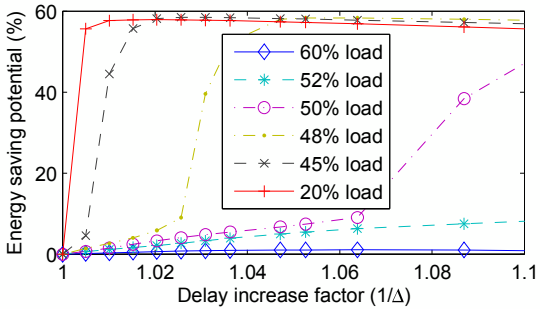

Fig. 4: Energy saving percentage at the BS in the dynamic part, $P_{idle}^{BS} = 0$, with TPA.

C. Impact of energy-delay tradeoff on MT

While the saving in the uplink is not significant for overall energy saving, the energy consumption in the MT is important and necessitates careful consideration. Fig. 5 depicts the energy saving percentage at the MT for different load combinations in the uplink and downlink. We denote the downlink load by λ_B and uplink load by λ_T. No delay is considered in the downlink to study the maximum saving potential at the MT. One can see that energy saving potential is highest for moderate high uplink network load. The percentage of saving decreases with increased downlink load as the overall energy consumption increases.

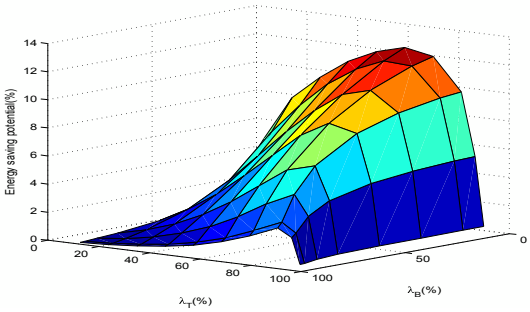

Fig. 5: Maximum energy saving percentage at the MT at different load combinations.

Next, we allow for energy-delay tradeoff both in uplink and downlink. In Fig. 6 and Fig. 7, we show the relation between energy saving in the downlink and its impact on the MT. We restrict the excess energy consumption in the MT to $\alpha = 2\%$. One can see that there is room to save energy both for the BS and the MT for a range of combinations of uplink and downlink loads. However, when the load in the downlink is high and the uplink load is low, the saving in the uplink is not enough to compensate the excess energy consumed at the MT due to delay in the downlink.

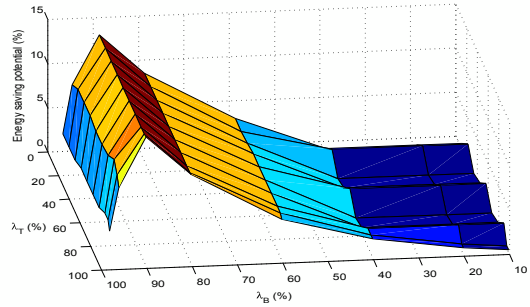

Fig. 6: Maximum energy saving percentage at the BS when maximum 2% loss at the MT is allowed.

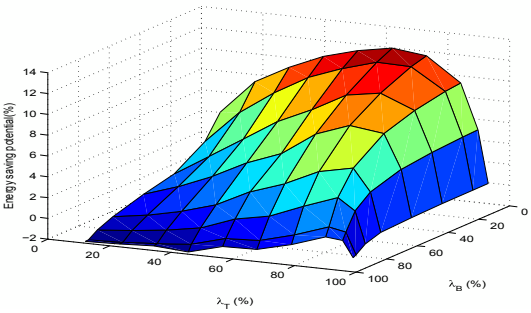

Fig. 7: Energy saving at the MT during maximum energy saving at the BS.

In these analyses we considered both the static power during transmission and the processing power during reception

to be equal, i.e. 1200 mW. However, these power consumptions are different for different technologies e.g. LTE, 3G [20], [21]. Also, for any technology, the processing power during reception and the processing power during transmission is neither same to each other nor remains constant at different network loads. We do not consider the load dependency of the processing power and also ignore the difference between static power consumption during transmission and the processing power during reception. However, we repeat the calculations for different processing power e.g. {600, 900, 1200, 1500}mW and found the corresponding best best case save in the MT {21.59, 16.03, 12.75, 10.60}% respectively. Similarly, for worst case i.e. very high downlink load and very light uplink load, the excess energy consumption in the MT for both 600mW and 900mW case is less than 1%. For 1500mW case, we relax the 2% constraint in order to keep the same downlink saving and find that the maximum excess energy consumption becomes 2.5%.

However, in our analysis, we do not consider the fact that energy consumption in the MT is dominated by so called 'tail energy' which is wasted in the high power state after the completion of each transfer. In the current generation of radio technologies e.g. 3G and LTE, the terminal stays in the high power state for around 12 seconds and tail energy contributes around 60% of total energy consumption. Energy-delay tradeoff does not increase this part of the energy consumption in the MT. If the tail energy is included, even for the worst case scenario when uplink load is very low, the excess energy consumption will be around 1% of the actual total energy consumption, hence negligible. Using proxy in the BS to accumulate, bundle data before transferring to MT is a very good remedy for tail energy wastage. However, that does not affect the energy saving potential by the energy-delay tradeoff as this proxy reduces the number of tails only.

V. Conclusions

A considerable amount of energy at macro BS can be saved by introducing transmission delay in the downlink. The prolonged transmission time at the BS increases the reception time at the MT and subsequently its energy consumption which is critical from the user's perspective. Fortunately, there is an opportunity to compensate the excess energy consumption at the MT by introducing delay in the uplink too. The uplink and downlink delays that minimize the overall energy consumption depend on the network load and the PA efficiency characteristics. For moderate to high network loads, small delays are sufficient to reduce the total energy consumption at the BS by as much as 15%. At the same time, MT consumption increases slightly for very high download and very low uplink load. For other load combinations, MT also saves energy. This saving potential becomes less significant in case of smaller BS (e.g. micro, femto BS) as their energy consumption breakdown is less dominated by the share of PA. Note that in the existing cellular networks, a significant amount of energy is wasted because the energy consumption of macro BS does not scale down accordingly with the reduction of load. It is urgent to devise appropriate mechanism (e.g. aggressive DTX/DRX, switching off a part of the network) for future energy efficient cellular networks in order to reduce energy consumption while serving low or no load. Introduction of energy-delay tradeoff along with such schemes will result in a very energy efficient network.

References

[1] "Deployment strategies for Heterogeneous Networks," whitepaper by NSN, May 2012. Available online: http://www.ericsson.com/res/docs/whitepapers/wp-50-billions.pdf

[2] INFSO-ICT-247733 Earth Deliverable D2.3, 2010. Available online: https://bscw.ict-earth.eu/pub/bscw.cgi/d71252/EARTH_WP2_D2.3_v2.pdf

[3] H. Karl, "An overview of energy-efficiency techniques for mobile communication systems," Telecommunication Networks Group, Technical University Berlin, Tech. Rep. TKN-03-XXX, Sept. 2003.

[4] Y. Chen *et al.* , "Fundamental trade-offs on green wireless networks," in *IEEE Commun. Mag.*, vol. 49, no. 6, pp. 30-37, Jun. 2011.

[5] M. M. A. Hossain *et al.*, "Minimum energy power and rate control for fair scheduling in the cellular downlink under flow level delay constraint," in *IEEE Trans. Wir. Commun.* vol .12, issue 7, 2013.

[6] M. J. Neely, "Optimal Energy and Delay Tradeoffs for Multiuser Wireless Downlinks," *IEEE Trans. on Inf. Theory*, vol. 53, no. 9, pp. 3095-3113, Sept. 2007.

[7] K. Han *et al.*, "Power amplifier characteristic-aware energy-efficient transmission strategy," in *Proc. of 6th Int. IFIP-TC6 Conf. on Ad Hoc and Sensor Networks, Wireless Networks, Next Generation Internet*, 2007.

[8] B. Prabhakar *et al.*, "Energy-efficient transmission over a wireless link via lazy packet scheduling," in *Proc. IEEE INFOCOM*, pp. 386-394, 2001.

[9] E. Uysal-Biyikoglu *et al.*, "Energy-efficient packet transmission over a wireless link," *IEEE/ACM Trans. on Netw.*, pp. 487-499, 2002.

[10] R. A. Berry, and R.G. Gallager, "Communication over fading channels with delay constraints," *IEEE Trans. on Inf. Theory*, vol. 48, no. 5, pp. 1135-1149, May 2002.

[11] W. Chen *et al.*, "Energy-Efficient Scheduling with Individual Delay Constraints over a Fading Channel," *in Symp. of Modeling and Optimization in Mobile, WiOpt*, pp. 1-10, 2007.

[12] A. E. Gamal *et al.*, "Throughput-delay trade-off in energy constrained wireless networks," in Symp. on *Inform. Theory*, pp. 439, 2004.

[13] N. Balasubramanian *et al.*, "Energy consumption in mobile phones: a measurement study and implications for network applications", in the Proceedings of the 9th ACM SIGCOMM conference on Internet measurement conference, November 04-06, 2009, Chicago, Illinois, USA

[14] L. Wang *et al.*, "Proxies for energy-efficient web access revisited," in the proceeding of the 2nd Int. Conf. on Energy-Efficient Computing and networking pp. 55-58.

[15] C. Desset et al., "Flexible power modeling of LTE base stations," Wireless Communications and Networking Conference (WCNC), 2012 IEEE, pp. 2858-2862, 2012.

[16] M. M. A. Hossain and R. Jäntti, " Impact of efficient power amplifiers in wireless access," *Online Conference on Green Communications* pp.36-40, Sept. 2011.

[17] T. Bonald, "Throughput Performance in Networks with Linear Capacity Constraints, in the *Proc. of Annu. Conf. on Inform. Sci. and Syst.*, pp. 644-649, 2006.

[18] T. Bonald *et al.*, "A queuing analysis of max-min fairness, proportional fairness and balanced fairness," *Queue. Syst.*, vol. 53, pp. 65-84, 2006.

[19] K. Ruttik, K. Koufos, R. Jäntti, "Modeling of the Secondary System's Generated Interference and Studying of its Impact on the Secondary System Design," *J. Radioengineering*, Dec. 2010.

[20] N. Balasubramanian *et al.*, "Energy Consumption in Mobile Phones: A Measurement Study and Implications for Network Applications", Proceedings of the 9th ACM SIGCOMM conference on Internet measurement conference, Chicago, Illinois, USA, pp. 280-293 2009.

[21] Huang J. *et al.*, "A close examination of performance and power characteristics of 4G LTE networks", Proceedings of the 10th international conference on Mobile systems, applications, and services, Low Wood Bay, Lake District, UK, pp. 225-238, 2012

Joint Benefits of Fractional Frequency Reuse and Relays in LTE Networks

Marthala Vishnu Vardhan Reddy [1], Emmanuelle Vivier [3], Fatima Zohra Kaddour [2,3]
[1] Vellore Institute of Technology, Vellore, India
[2] Telecom ParisTech, 46 rue Barrault, Paris, France
[3] ISEP, 28 rue N-D des Champs, Paris, France

***Abstract*—This paper provides a joint implementation of Fractional Frequency Reuse (FFR) and relays in the downlink of multi-cellular networks like Long Term Evolution (LTE) networks. The forecasted benefits concern inter-cell interference (ICI) mitigation in each cell. Based on this network architecture and related improvements, individual user throughputs and signal to interference plus noise ratio (SINR) are calculated for all the users and compared to the classical $1 \times 3 \times 3$ frequency reuse scheme. System level simulation results show that our presented scheme can achieve significant improvements in terms of individual user throughput and spectrum efficiency.**

Keywords: OFDMA, Fractional Frequency Reuse, fixed relay, Inter-Cell Interference.

I. Introduction

The Orthogonal Frequency Division Multiple Access (OFDMA) technique is a very promising radio access technique due to its inherent robustness against frequency selective fading and its capacity for achieving high spectral efficiency [1]. It has been adopted for downlink air interfaces of 3rd Generation Partnership Project (3GPP) Long Term Evolution (LTE). The OFDMA is based on the Orthogonal Frequency Division Multiplex (OFDM) coding method. Hence, it supports intra-cell orthogonality which leads to an intra-cell interference cancelation. However, there still exist Inter-Cell Interference (ICI) caused by the power radiated by the base stations of the neighboring cells using the same frequency band. Since the users are uniformly distributed in the cells network, the more affected by the ICI are the users which are located at the edge of the cell because of the near-far problem. To provide all the subscribers with a high quality of service, we have to mitigate the inter-cell interference.
The ICI mitigation can be achieved by adapting the frequency planning and the power allocation. When the same frequency bandwidth is used by all the networks cells (i.e. a frequency reuse factor of 1), the spectrum utilization is efficient, but at the expense of a high ICI level in fully loaded networks. In this case, the authors of [2] [3] propose an adapted resource allocation scheme which needs the cooperation of the base stations and allocates the unitary radio resources, known as Resource Blocks (RBs) in LTE, to users in function of their Channel State Information (CSI). The inconvenience in this method is the highest level of signalization information transmitted between the base stations. A Soft Frequency Reuse (SFR) was proposed by [4]. This method aims to allocate different transmission power levels in different bandwidths. Then it allocates bandwidth with low transmission power to the users near the base station and the bandwidth with higher transmission power level to users at the edge of the cell. This method does not solve much the problem for the edge users, since it allocates them the highest transmission power levels and the resulting radiated power will cause more ICI to the users at the neighboring cells' edge. To address this problem we can: (i) use a low transmission power at the edge of the cells and use relays to overcome the pathloss effect [5] or (ii) allocate different bandwidth to the neighboring cells (i.e. a frequency reuse factor ≥ 3). A Fractional Frequency Reuse (FFR) was also proposed for the LTE uplink in [6], where the users are classified in: (i) Cell Central Users (CCUs), and (ii) Cell Edge Users (CEUs); and different bandwidths are allocated to the two users classes. Therefore, the interference level of the CCUs is reduced, which helps them to achieve a higher throughput.

In this paper, a fractional frequency reuse planning is jointly proposed with the deployment of relays for the cell edge users as it is proposed in [7] and an adapted power allocation and frame structure are proposed for downlink transmission in LTE networks. This frequency and power planning allow us to achieve a high spectrum efficiency and to mitigate the inter-cell interference, which results in an aggregate throughput improvement, and gains in radio power consumption, which is favorable in the topic of green communications.

The remainder of this paper is organized as follows. Section II presents the proposed joint implementation of the FFR and the relays planning. Inter-cell interference analysis is provided in Section III. The performances of the proposed planning scheme are given in Section IV. Finally, we conclude the paper in Section V.

II. Joint FFR and Relays Planning implementation scheme

The objective of the joint fractional frequency reuse and relays implementation is to allocate efficiently the frequency bandwidths and the transmission powers of the base stations and relay stations in order to mitigate the inter-cell interference and to improve, by the same way, the aggregate throughput in the network and the spectrum efficiency.

978-1-4799-0354-2/13/$31.00 ©2013 IEEE

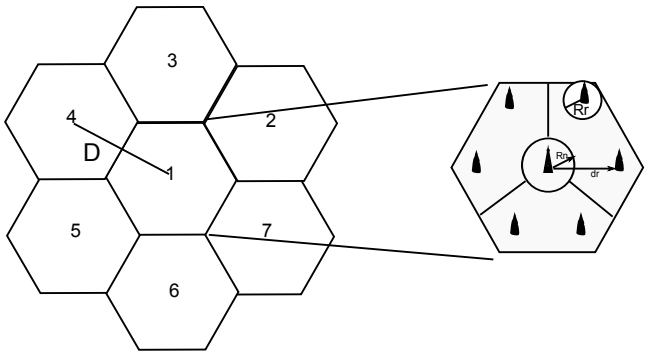

Fig. 1. Relays localization

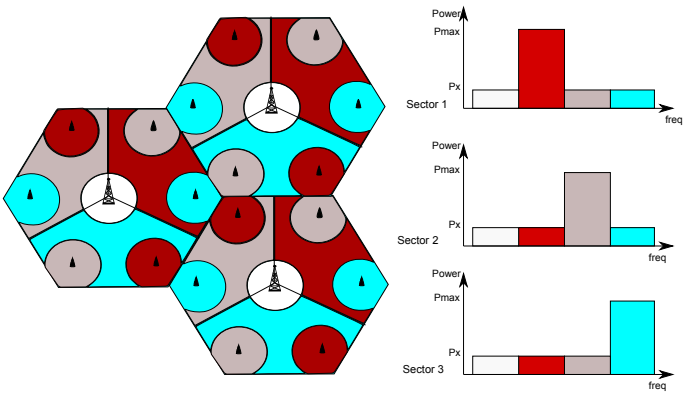

Fig. 2. Joint FFR and relays proposed frequency planning

A. Fractional Frequency Reuse with Relays

We consider an hexagonal grid of 7 cells (i.e. one central cell and one ring of interfering cells), each cell being equipped with a tri-sectored base station (BS) located at the center of the cell. In each sector, two Relay Stations (RS) are placed on the above rooftop: at a distance d_r equal to $\frac{3}{8}$ of D between the RS and the BS, where D is the inter-BS distance, and an angle of 26 degrees with regards to the sector antenna boresight direction [11] as shown in Figure 1. We classify each user in function of its localization in a sector: CCU when the user is located in the inner region (a circle centered at the center of the cell with radius Rn), RRU when the user falls under the relay region (i.e. the circular region of radius Rr around the RS) and CEU when the user is in the remaining region of the cell. CCUs and CEUs are served directly by the BS. RRUs are served by the RS, they involve BS-RS and RS-MS links for the entire downlink transmission.

The frequency planning requires four bandwidths and is as follows: first we allocate the same frequency bandwidth for the inner region of each cell (i.e. a frequency reuse factor equal to 1). An omnidirectional antenna is used for transmission in this central part of the cell. Then, to cancel the inter-sector interference, three bandwidths are necessary for the three cells edge regions. Consequently, for these edge regions, the transmission is ensured by tri-sectored antennas. Finally, in order to efficiently use the frequency bandwidths, we reuse on the relays regions the frequency bandwidths that are allocated to the neighboring sectors. For these relays regions, omnidirectional antennas are used.

B. Transmission power allocation

We propose an efficient energy allocation which aims (i) to provide to the users an acceptable received power and (ii) to reduce the ICI levels. To obtain a high channel quality for CEU, the power allocated to the base station antenna is high and fixed at its maximum P_{max}. The RS and BS transmission powers are reduced and set to P_x due to the proximity of the served users. This power reduction mitigates the interference between the sectors and the relays using the same frequency bandwidth.

The joint fractional frequency reuse and relays cells configuration, and the power allocation scheme proposed, are given in Figure 2. In LTE, the smallest radio resource that can be allocated to a user is one RB which is consisting of $N^{RB} = 12$ subcarriers of 15 kHz each. Therefore, the RB bandwidth is equal to 180 kHz [9]. Considering that each user is allocated one RB and applying the proposed frequency and power planning, the Signal to Interference plus Noise Ratio $SINR_k^c$ of each user k on RB c can be computed as follows:

$$SINR_k^c = \frac{P_{Tx} Pl(r_k) G_e(\theta_k) G_{rk} \alpha_{sh} \alpha_{fd}}{I + N} \quad (1)$$

where P_{Tx} is the antenna power transmission equal to P_{max} or P_x depending on the BS/RS power allocation, $Pl(r_k)$ is the radio channel path loss depending on r_k the distance between the user k and the transmitter. $Pl(r_k)$ is computed as follows:

$$Pl(r_k) = 1^{\frac{-a}{10}} r_k^{\frac{-b}{10}} \quad (2)$$

considering a carrier frequency of 2.6 GHz, the users, BS and RS antennas heights, and the coefficients a and b given in Table I computed using the Okumura Hata propagation model [10]. The antenna transmission gain $G_e(\theta_k)$ depends on the angle $\theta_k \in [-180°, 180°]$ between user k and the boresight of the serving antenna. In case of CEUs, the antenna transmission gain is set to:

$$G_e(\theta_k) = -\min\left[12\left(\frac{\theta_k}{\theta_{3dB}}\right)^2, A_m\right] \quad (3)$$

with θ_{3dB} being the 3 dB beam width, set to 70° and $A_m = 20$ dB being the maximum attenuation [8]. Omnidirectional antennas serve CCUs and RRUs and their transmission gain $G_e = G_{Om}$ is constant. The reception gain of the mobile antenna G_{r_k} is equal to 1. Finally, α_{sh} is a correlated log-normal shadowing coefficient with standard deviation σ_{sh} and is obtained using the formulas in [8], α_{fd} is the Rayleigh fast fading coefficient, of standard deviation σ_{fd} and I is the total ICI caused by the neighboring cells. The value for I can be computed as:

$$I = \sum_{i=1}^{n} P_{x_i} Pl(r_i) G_e(\theta_i) G_r \alpha_{sh} \alpha_{fd} \quad (4)$$

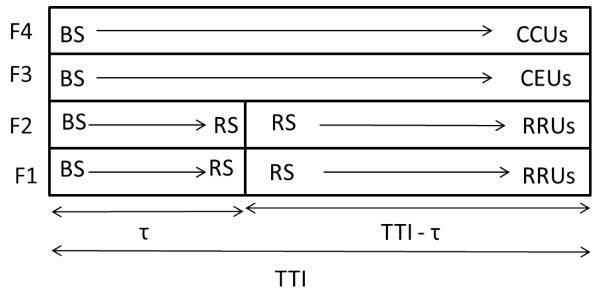

Fig. 3. Downlink TTI Frame (1st sector)

where P_{x_i} is the i^{th} interfering transmitters transmission power, $Pl(r_i)$ is the path loss depending on r_i the distance between the i^{th} interfering transmitter and the served user, $G_e(\theta_i)$ the interfering antenna transmission gain depending on θ_i the angle between the antenna and the served user, and n is the number of interfering antennas using the same frequency band.

C. Frame Structure

In downlink transmission of 3GPP/LTE neworks, each frame is composed of 14 OFDM symbols and is known as Transmission Time Interval (TTI). The duration of each TTI is 1ms. In the downlink TTI frame proposed on Figure 3, the total frequency bandwidth is divided into four bands F1, F2, F3 and F4. On F3 (respectively F4) band, the transmitter is the BS during all the TTI duration, at maximum transmission power P_{max} (respectively P_x). On F1 and F2 bands, the transmitters are: first the BS at P_{max}, during τ TTI, and then the RS at P_x, during $(1-\tau)$ TTI. The value for τ is the one adopted in [12]: 23%, considering a SINR on the BS-RS links higher than 15 dB, which corresponds to at least a $\frac{3}{4}$ coded 64-QAM transmission.

III. Interference Analysis

The main purpose of using joint FFR and relays is to mitigate ICI. As we know, interference will come from the transmitters using the same frequency band. Moreover, CEUs are served by directional antennas, so all the users who are in the boresight of interfering antenna will suffer more intereferences. Interference from omnidirectional antennas on CCUs and RRUs is less compared to directional antennas because of lower transmission powers. In this section we are going to analyze the interferences of the joint scheme of FFR and relays for the users in the three regions of the cell.

Let us consider the first sector of a cell and the link for CCUs, i.e. users served directly by the power controlled BS using the frequency band F4. Six interfering BS using the same frequency band (colored in blue on Figure 4(a)) are considered, and the resulting interference I can be calculated by using (4) with n=6.

For the CEUs of the same sector, i.e. users served directly by the maximum powered BS using the frequency band F3, the interferences from other transmitters are as shown in blue on Figure 4(b). They come from both BS and RS and the value for I can also be calculated using (4) with n_{BS} = 6 and n_{RS} = 14.

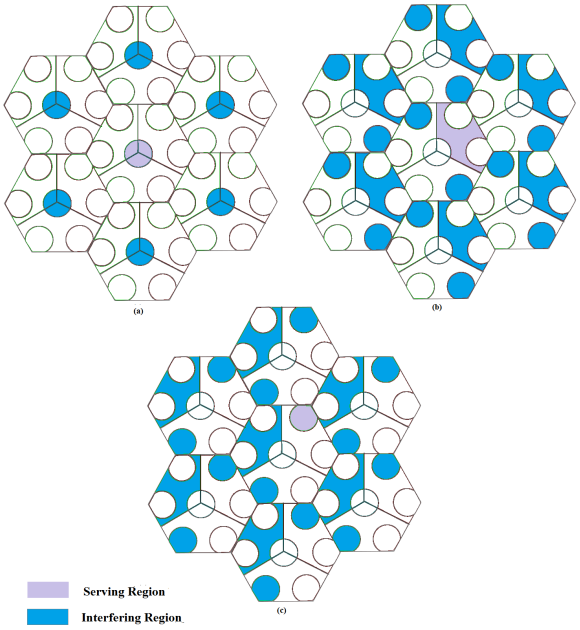

Fig. 4. Interference for users depending on their position in the sector

Finally, for the RRUs of the same sector, i.e. users served by the RS using the frequency band F1 or F2, interferences come from one RS or one BS per sector, as illustrated on Figure 4(c). The resulting value for I can still be calculated using (4) with n_{BS} = 7 and n_{RS} = 13. Whereas the number of interfering transmitters is the same as for CEUs, the aggregate level of interferences is lower because of limited coverage area due to RS low transmission powers.

IV. Simulation parameters and results

We consider a system with a 20 MHz LTE bandwidth. The bandwidth has been divided equally into four different subbands, each one having a bandwidth of 5 MHz, i.e. 25 RBs. The total bandwidth is totally used in each sector, each region having a given bandwidth. The inter site distance D is set to 1732 m. The radius of the RS and central BS areas is chosen as equal to 290 m in order to have equal surface areas for each region.

We consider in our downlink transmission a fully loaded system where each user is allocated one RB at each TTI and we evaluate the performances of the joint FFR and RS network deployement in terms of ICI, SINR, throughput and energy consumption, and compare them to the ones obtained in a classical $1 \times 3 \times 3$ classical frequency reuse network (i.e the same frequency planning as in our proposed scheme, but without RS). The main simulation parameters are given in Table I.

Figure 5 shows the ICI Cumulative Distribution Function (CDF) of the proposed scheme of joint implementation of FFR and RS, compared to the same distribution issued from a

Parameter	Values
System bandwidth	20 MHz
Inter-site distance (D)	1732 m
Carrier frequency	2.6 GHz
BS antenna height	35 m
RS antenna height	15 m
UE antenna height	1.5 m
Okumura Hata propagation model parameters	$a = -136.7$ $b = -34.4$
Thermal Noise density	-174 dBm/Hz
Antenna beam pattern $G_e(\theta_k)$, where θ_k is the angle MS subtends with antenna boresight	$G_r(\theta_{jc}) = -\min[12 * (\frac{\theta_{jc}}{\theta_{3dB}})^2, A_m]$ $\theta_{3dB} = 70°$, $\beta = 20$ dB
Directional antenna gain (boresight) G_{max}	17 dBi
Front-to-back power ration A_m	20 dB
3-dB beamwidth θ_{3dB}	70°,
G_{Om} Omnidirectional antenna gain	13 dB
P_{max}	43 dBm
P_x	30 dBm
σ_{sh}	8 dB
σ_{fd}	1
Radius of inner cell region R_n	290 m
Radius of relay region R_r	290 m

TABLE I
LIST OF SIMULATION PARAMETERS

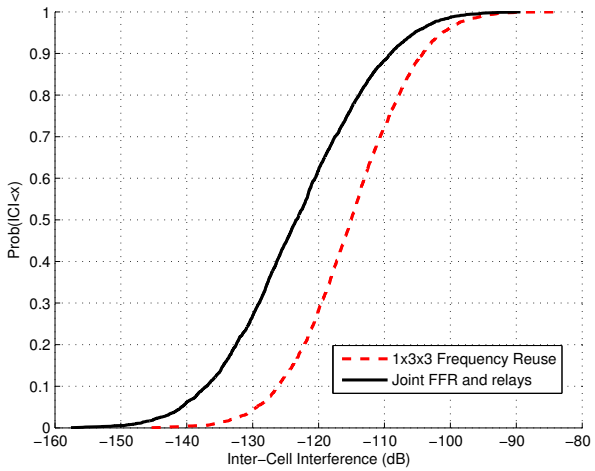

Fig. 5. Inter-Cell Interference CDF in a sector

classical $1 \times 3 \times 3$ classical frequency reuse. It is observed that our joint scheme mitigates ICI by around 10 dB and is especially very advantageous for users that already benefit from low ICI, i.e CCUs. This mitigation is due to the power control that decreases the transmission power in CCU and RRU regions and is illustrated on Figure 6. Actually, despite the RRUs are far away from the BS, they suffered from about 5 dB less interferences than CCUs because of our scheme placing them in a region that suffers interferences from far away power controlled RS and mostly backside of the nearest directional BS. This improvement over ICI control benefit the overall SINR and following system performances. The SINR

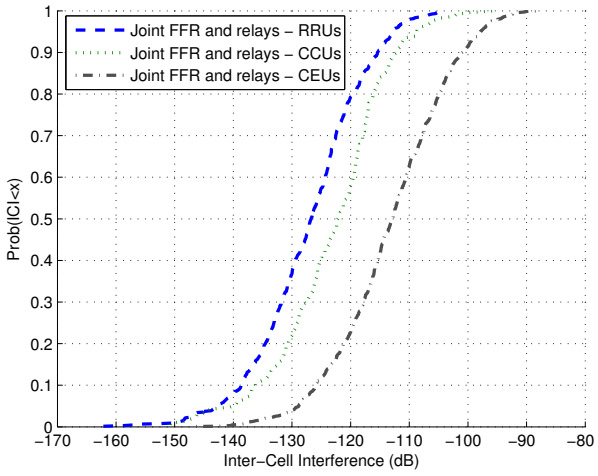

Fig. 6. Inter-Cell Interference CDF for CCUs, CEUs and RRUs in a sector

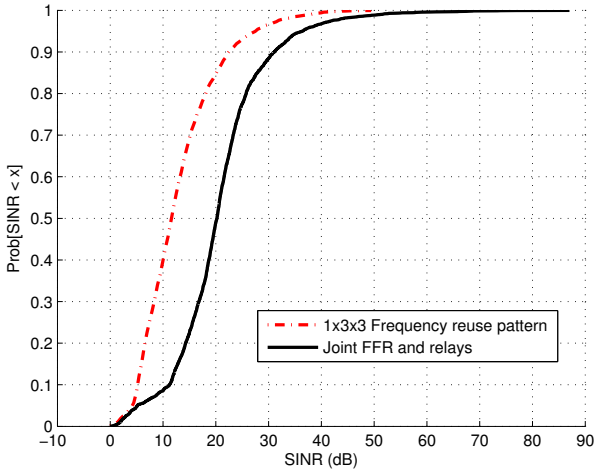

Fig. 7. CDF of SINR received by all users in a sector

is depicted on Figure 7 that compares the CDF for all the users in the sector for both network configurations: joint FFR and RS, and classical $1 \times 3 \times 3$ frequency reuse network. It can be observed that SINR is improved by the joint scheme by almost 9 dB.

As a consequence of a better SINR, the overall individual user throughput is higher and its CDF is given on Figure 8. The associated LTE throughputs have been calculated using Table II values issued from [13]. Clearly it can be seen that the individual throughputs has been enhanced, and even doubled, in the joint FFR and RS deployment scheme. Consequently, this deployement scheme also enhances the aggregate throughput that defines the sector's capacity; actually, it reaches 75 Mbits/s instead of 27 Mbits/s with Monte-Carlo simulations that considered 33 users uniformly distributed in the whole sector area for the classical $1 \times 3 \times 3$ frequency reuse scheme, and 8 users (respectively 25 and 25 users) uniformly

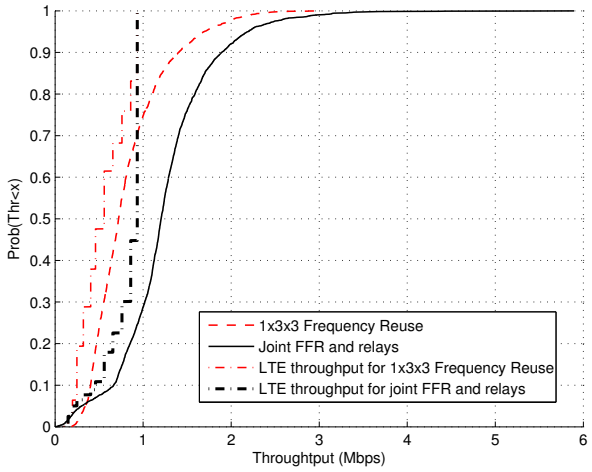

Fig. 8. CDF of individual throughput offered to all the users in a sector

distributed in the CCU region (respectively in the CEU region and in each RRU region) of the sector for the joint FFR and RS deployment scheme. Finally, we compute the power spectral density (W/Hz) of both network configurations, thanks to the users location in the cell and the BS and RS transmission powers given in Table III. The $1 \times 3 \times 3$ frequency reuse scheme results in a 3.2 W/Hz, whereas, for our joint scheme it is 1.35 W/Hz. It means that the joint scheme has reduced by around 68% the radio total transmission power.

SINR range (dB)	Modulation	Code rate	Throughput (kbps)
$-7 < SINR \leq -5$	QPSK	0.07	26
$-5 < SINR \leq -3$	QPSK	0.11	39
$-3 < SINR \leq -1$	QPSK	0.18	63
$-1 < SINR \leq 1$	QPSK	0.30	101
$1 < SINR \leq 3$	QPSK	0.43	147
$3 < SINR \leq 5$	QPSK	0.58	197
$5 < SINR \leq 7$	16QAM	0.36	248
$7 < SINR \leq 8.5$	16QAM	0.47	320
$8.5 < SINR \leq 10$	16QAM	0.60	400
$10 < SINR \leq 11.5$	64QAM	0.45	458
$11.5 < SINR \leq 13.5$	64QAM	0.55	558
$13.5 < SINR \leq 15$	64QAM	0.65	655
$15 < SINR \leq 17$	64QAM	0.75	760
$17 < SINR \leq 19.5$	64QAM	0.85	860
$SINR \geq 19.5$	64QAM	0.92	933

TABLE II
SINR TO CODE RATE MAPPING AND LTE THROUGHPUT [13]

		Transmission power (dBm)	
		Classical $1 \times 3 \times 3$ frequency reuse scheme	Joint FFR and RS scheme
Users	CCUs	43	30
	CEUs	43	43
	RRUs	43	30

TABLE III
TRANSMISSION POWER TOWARDS ALL THE USERS IN THE SECTOR

V. CONCLUSION

In this paper, we have implemented a joint FFR and RS scheme for downlink transmission in LTE networks. We have provided analysis of the inter-cell interference suffered by all the users and we compared the obtained results with a classical $1 \times 3 \times 3$ frequency reuse scheme. Our simulation results showed that, as a result of the inter-cell interference power decrease, the SINR per user is improved by about 9 dB, and that the individual and average aggregate throughputs have more than been doubled. We have also reduced the transmitters power and therefore the radio energy consumption. However, it is still possible to improve the ICI control by adopting coordinated multi-point transmission. In future work, we will consider a new RB allocation algorithm and study the the influence of allocating more RBs to a user on the inter-cell interference level.

REFERENCES

[1] M. Liang et al, "A Novel Frequency Reuse Scheme for OFDMA Based Relay Enhanced Cellular Networks," in *IEEE 69th Vehicular Technology Conference, VTC Spring 2009*, Spain, April 2009

[2] Alcatel, OFDMA with interference control for improved HSDPA coverage, in *3GPP, TSG-RAN WGP N37 R1-040572*, May 2004.

[3] D. Gang, Z.Ting, X.Ning, Z.Ping, "A downlink radio resource allocation algorithm based on inter-cell interference mitigation for multi-cell OFDMA system," in *Communication and Networking in China, 2006. ChinaCom06*, China, october. 2006.

[4] H. Lei, X. Zhang, D. Yang, "A new frequency reuse scheme for multicell OFDMA systems," in *IEEE Vehicular Technology Conference, VTC 07-Fall*, USA, September 2007.

[5] 3rd Generation Partnership Project; Technical Specification Group Radio Access Network; Evolved Universal Terrestrial Radio Access (E-UTRA); Further advancements for E-UTRA physical layer aspects (Release 9), 3GPP TR 36.814, V9.0.0, March 2010.

[6] J. Heyman, Intercell interference management in an ofdm-based downlink, Ph.D. thesis, Department of Electrical Engineering Linkopings University SE-581 83 Linkoping, Sweden, 2006.

[7] Z. Zhao, X. Fang, Y. Zhu, Y. Long, "Two Frequency Reuse Schemes in OFDMA-TDD Based Two-hop Relay Networks," in *IEEE Wireless Communications & Networking Conference*, Australia, April 2010.

[8] R. Srinivasan, J. Zhuang, L.Jalloul, R.Novak, J.Park. IEEE 802.16m evaluation methodology document(EMD).2008-11-26.

[9] Evolved Universal Terrestrial Radio Access (E-UTRA); User Equipment (UE) radio transmission and reception, 3GPP TS 36.101, v10.3.0, June 2011.

[10] Y. Okumura, E. Ohmori, and K. Fukuda, "Field Strength and its Variability in VHF and UHF Land-Mobile Radio Service," Review of the Electrical communication Laboratory, pp. 825-873, 1968.

[11] M. Minelli, M. Coupechoux, J.-M. Kelif, M. Ma and Ph. Godlewski, "Relays-Enhanced LTE-Advanced Networks Performance Studies," *IEEE Sarnoff Symposium*,USA, May 2011.

[12] L. Mroueh and E. Vivier, "Efficient Green Relaying PHY-MAC Strategy for LTE-Advanced Networks," in *IEEE International Symposium of Wireless Communication System (ISWCS)*, France, August, 2012.

[13] M. Jar and G. Fettweis, "Throughput maximization for LTE uplink via resource allocation," in *IEEE International Symposium of Wireless Communication System (ISWCS)*, France, August. 2012.

A Weighted Fair Queuing Algorithm for Charging Electric Vehicles on a Smart Grid

Yingjie Zhou[*,††,†], Nicholas Maxemchuk[†,#], *Fellow, IEEE*, Xiangying Qian[†], and Yasser Mohammed[†]
[*]College of Computer Science, Sichuan University
[††]School of Communication and Information Engineering, University of Electronic Science and Technology of China (UESTC)
[†]Department of Electrical Engineering, Columbia University
[#]Institute IMDEA Networks
Email: yjzhou09@gmail.com,nick@ee.columbia.edu,{xq2120,ym2364}@columbia.edu

***Abstract*—We are concerned with charging electric vehicles at home. The energy demand from electric vehicles can increase more rapidly than our ability to increase the generating capacity or the distribution facilities in the electric network. Our objective is to use a smart power distribution algorithm to reduce the inconvenience to electric vehicle owners. When there isn't sufficient capacity to charge all of the vehicles simultaneously, we will select different subsets of vehicles to charge in each 5 minute interval. The smart grid will control a switch on each charger. The order in which we charge the vehicles has a significant effect on the number of vehicles that are delayed when they would like to leave the charging station, and the amount of time that they are delayed. By reducing these measures, electric vehicles can be deployed more rapidly.**

We compare a weighted fair queuing algorithm for selecting the charging order and compare it with a first-come-first-served algorithm and a round robin charging rule. The weights are selected based on the battery level when vehicles arrive at their charging stations. We assume that there is a correlation between day-to-day driving distances, and charge vehicles that require more charge more rapidly.

The three charging rules are evaluated using measured data on the power usage, commuting characteristics, and the distribution of commuting times.

Keywords—weighted fair queuing, electric vehicle charging, smart grid

I. INTRODUCTION

Electric vehicles are a key green technology. The use of electric vehicles is being encouraged to reduce the carbon emissions created by internal combustion engines. As the number of electric vehicles increases rapidly, the power that they consume is increasing more rapidly than we can add additional generating capacity to the power grid or distribution facilities to different parts of the network. In order to allow the use of electric vehicles to grow as quickly as possible, we must guarantee that electric vehicle owners experience as little inconvenience as possible until additional generating capacity or distribution facilities can be constructed.

The specific problem that we are addressing is charging electric vehicles at home on a standard 120 volt, 15 amp circuit. During peak electric use, the number of vehicles that are being charged may exceed the available capacity. In order to prevent brown outs or rolling blackouts, we must control the number of vehicles that are being charged below specific bottlenecks, based on the available capacity. Several techniques have been proposed to shift the demand for charging to non-peak consumption periods [1,2,3] including pricing mechanisms that reduce the cost of electricity during non-peak hours [4,5,6]. These mechanisms are based on the average demand, and lack the fine grained control that is needed to use all of the available power, including the power that is available during the peak use hours.

Our approach is to use the smart grid to control charging by activating switches on the chargers for 5 minute intervals. In each interval we measure the power that is consumed by other loads and calculate the number of vehicles that can be charged with the available power. The available power changes over the course of the day, as shown in Figure 1. When there isn't sufficient power to charge all of the vehicles simultaneously, we select a subset to charge in each 5 minute interval. Our objective is to reduce the inconvenience that vehicle owners will experience if their vehicles do not have sufficient charge when they want to depart.

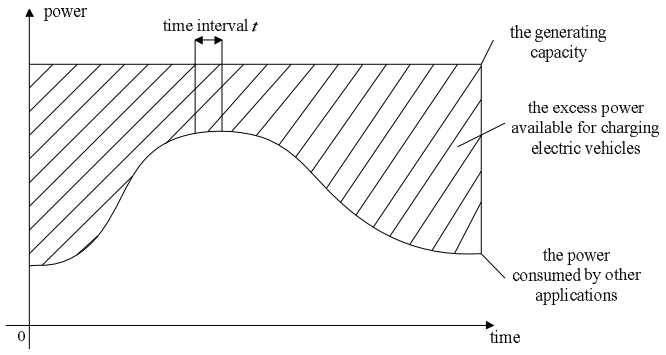

Fig.1. The excess power available for charging electric vehicles.

In a previous paper [7] we investigated charging strategies based upon information that users provided on their expected departure time and their expected driving distances. The objective was to provide sufficient charge to reach their destination, and to treat the users fairly, in that we did not

978-1-4799-0354-2/13/$31.00 ©2013 IEEE

decrease the delay of one user at the expense of a user with a larger delay. These techniques were compared with first-come-first-served and round robin selection strategies. The strategies provide exceptionally good reductions in the fraction of users who are delayed and the amount of time that they are delayed. However, other techniques, such as pricing, are required to discourage users from obtaining more charge more quickly, by indicating earlier departure time or longer expected driving distances.

In this paper, we investigate a selection procedure that does not require information from a user. We predict a users driving distance, based upon the amount of charge in the battery when the user arrives. We assume that there is a correlation between driving distances on successive days. We do not estimate the users' departure time. Our objective is to charge all of the batteries to full capacity, but to charge those batteries that arrive with less charge more quickly. The algorithm that we use is a weighted fair queuing algorithm, similar to algorithms that have been used in ATM networks, but with a twist. There are multiple servers, corresponding to the number of vehicles that can be charged simultaneously, rather than a single server, and the number of servers changes continuously. The algorithm is described in Section 3.

II. BACKGROUND

In this section, we formulate the problem of allocating the power available for charging, in Section 2.1, and describe the real world data that we use for evaluating the proposed algorithm, in Section 2.2.

A. Problem Formulation

We assume that there is sufficient power, over the course of the day to charge all of the electric vehicles. When the vehicles require more power than the power company can provide over the course of the day, the delays to charge the vehicles are unbounded. When the number of vehicles that are charging is less than the number that the power company can charge at a particular time, they all receive charge. When the number of charging vehicles require more power than is available, a subset of the vehicles is selected.

The selection is implemented by a controllable on/off switch on the vehicle's charging station. To avoid the switch changing too frequently, time is divided into five minute intervals, and during each interval the power company selects the subset of the vehicles that will receive charge. The switches for this subset of vehicles are turned on. This strategy is straightforward to implement and should operate with any battery charging system.

We evaluate the selection rules based upon the fraction of the vehicles that are forced to leave late in order to acquire sufficient charge (F_D), and the average time that those vehicles are delayed (D_{FD}). We compare the rules as a function of the supply and demand ratio (*SDR*) of the power available to charge electric vehicles.

SDR is defined as the ratio of (the total power available for charging electric vehicles over the course of a day) divided by (the total power required to charge all of the electric vehicles that are charged during a day to a full battery). The power that is available to charge electric vehicles is the power that can be generated for the day minus the power that is required for other applications (*POA*). The *POA* is based on available statistics [18]. The generating capacity is assumed to be constant for each day, but will be set to different value according to the maximum amount of *POA*. In the simulation of this paper, the generating capacity is set to be 125% of the maximum amount of *POA*.

We investigate the improvement that the proposed algorithm achieves when $1 \le SDR \le 2.5$. When $SDR < 1$, no distribution mechanism is useful, since the power company cannot generate sufficient power and the delays to charge the vehicles are unbounded. When $SDR > 2.5$, all of the distribution mechanisms work reasonably well. And when $1 \le SDR \le 2.5$, different distribution mechanisms perform significantly differently.

B. Real World Data

We use the real world data to evaluate our algorithm. We assume that the vehicles arrive for charging according to a Poisson distribution whose arrival rate λ changes as a function of the time of day. The Poisson distribution is a reasonable assumption because the vehicles operate independently. We use the departure time distribution for commuters from 2009's American Commuter Survey [8]. We approximate the distribution of when vehicles arrive at their charger by shifting the commuter distribution by 10 hours. For instance, the arrival rate for vehicles arriving at home at 6 PM is the arrival rate for vehicles leaving on their commute at 8 AM.

The total number of vehicles in our simulations is scaled to about 3,000. This is appropriate for a medium-sized city based on President Obama's goal of putting one million electric vehicles on the road in the U.S by 2015 [9]. This number is calculated by assuming 80 large cities with 5000 vehicles each, and 200 medium-sized cities.

We assume the amount of time that a vehicle is plugged into its charger satisfies a Normal distribution. The mean of the distribution is 14 hours and the standard deviation is 4 hours. The charging time is lower bounded at 6 hours and upper bounded at 22 hours, which occur with a probability of 4.55% . We use the Normal distribution because the desired plug-in time for each vehicle is an independent and identically distributed event, so that the sum of a large number of these random variable is a normal distribution.

We assume that all vehicles are charging at home and the electric vehicles are plugged into a 120 volt, 15 amp circuit, the common circuit in most houses. We surveyed current electrical vehicles, including the Nissan LEAF[10], FORD 2012 Focus Electric[11], BMW Mini E[12], THINK City[13], Mitsuibishi iMeiv[14] and SMART[15]. We set the full battery

at 28kwh and the range of a fully charged battery as 100 miles, which requires 186.7 units of 5-minute charging intervals. It takes about 15.5 hours to fully charge an electric vehicle with an empty battery, while our average charging time is 14 hours. Current electric vehicles can travel only 6 miles for each hour that they are connected to a charger. The slow charging rate makes it unreasonable to push all charging to non-peak hours during the night. There are not enough non-peak hours. The constraint is because electric vehicle are being sold with the claim that they only require a standard electric outlets. We suspect that most electric vehicle owners, who commute longer distances, will have 240 volt, 30 amp circuits, similar to those for a clothes dryer, installed in their garage, so that they can drive 24 miles for each hour that they receive charge.

The one way distance that a vehicle is expected to commute is based on the Department of Transportation's Omnibus Household Survey [16]. We fitted their data with an exponential distribution with λ =1, and truncated the two way commuting distances for electric vehicle owners to 70 miles, to allow 20 miles for other purposes and 10 miles for emergencies.

III. ALGORITHM

The inspiration for our scheduling is the weighted fair queuing (WFQ) algorithm that was used in ATM networks, as described in [17]. In ATM networks, different flows were given different rates by placing them in queues that are served with different frequencies. When a flow is served it obtains a fixed size slot. In our problem we want to provide vehicles with a five minute charging slot. We would like to provide some vehicles with more charging slots than others by placing them in queues that are served more frequently.

The difference between our algorithm and those used in ATM is the number of servers. Most ATM algorithms were designed for a single server. Our algorithm is designed for a larger number of servers. The number of servers is the number of vehicles that can be charged simultaneously in the five minute interval. In addition, the number of servers is likely to change during the time a vehicle is connected to its charging station.

WFQ does not guarantee an ATM circuit a rate, but a rate relative to the other circuits that are being served at the time. If there are N active queues, with priorities P_i, and the sum of the priorities is S, then in a cycle with S transmissions, each queue receives P_i slots during the S transmissions. With a single server we can give each of the queues its number of slots before servicing the next queue, or we can spread out the slots assigned to a single queue, by creating sub-cycles within the cycle S. For instance, if the number of sub-cycles equals the number of priority levels, and in sub-cycle i we service all queues with priority P_i or greater, then after the completion of the sub-cycles, each queue with priority P_i has received P_i slots. As ATM queues become active or inactive, S changes.

Scheduling in a multi-server environment is more difficult. We assume that a customer, a vehicle rather than a queue in our problem, can only be served by one server in a slot. It would not make sense to say that we can charge two vehicles in a slot and that we elect to provide one vehicle twice the charge. Rather than determining a precise schedule, we hypothesize that we can space the slots assigned to a vehicle equally, then select the vehicles based upon the order of their next occurring slots.

Another problem with multiple servers is that we may not be able to keep all of the servers active and still maintain the relative rates. As a simple example, consider a system with two servers, and two customers with priorities 1 and 2. The second customer deserves twice the service rate of the first. The second customer receives service in every interval. If the first customer receives service every other interval, then ¼ of the service opportunities are lost and cannot be recovered. Instead we will allow the first customer to be served in every slot. He will build up a surplus, that will be indicated by his next scheduled slot occurring further into the future. If later there are new customers, he will allow them to be served while he pays down his surplus.

We implement the algorithm in the vehicle charging application as follows: When a vehicle arrives at its charging station it receives a priority, that determines how often it should be served relative to the other vehicles. As a straightforward implementation for WFQ, we assign vehicle i a priority between 1 and 11 as

$$P_i = \left(\frac{\max(|\,Required\ battery - Current\ battery\,|, 0)}{Full\ battery}\right) * 10 + 1$$

The "*Required battery*" is the amount of energy that we predict that the vehicle needs for its next day's commute. It is estimated from the difference in battery levels when departing the charging station and when returning to the charging station in the recent past. Without history information, we can estimate the *Required Battery* as (*Full Battery – Current Battery*), which assumes that we left the station with a full battery and will require the same amount of energy tomorrow as today. The priority is 1 when we predict that the vehicle has arrived with sufficient power for the next day's commute, it still receives a minimum charging rate. A vehicle receives a priority 11 when it arrives with an empty battery and we believe that it requires a full battery for the next day's commute.

Weighted fair queuing is implemented by assigning each vehicle a service number S_i, that determines its next service interval in a system in which it receives equally spaced service intervals. The vehicles with the smaller service numbers receive service first, and their service number is incremented by Z/P_i, where $Z=\sum_j P_j$, whenever they receive service.

We start our simulation with the next service number at 0, calculate the P_i for each of the initial set of vehicles and schedule each of these vehicles at S_i. The S_i are placed in increasing order in list, L. This is the initial waiting list. The size of the waiting list is M_W.

The number, M_C, of electric vehicles that can be served in the next 5 minute cycle is calculated based on the generating capacity and the current load on the network. If $M_W<M_C$, all of

the vehicles in the list are charged in the next cycle. Otherwise, the first M_C vehicles in the list are selected for charging.

When V_i is charged, its next charging period is calculated as $S_i=S_{i,old}+Z/P_i$ and it is placed in the ordered list L.

Vehicles are removed from the charging list when their battery is at full capacity, or if their driver decides to depart with a partially charged battery. Their priority is subtracted from Z. When a new vehicle arrives at a charger, its priority is added to Z. The vehicle's value of S_i set to the average value of the M vehicles served in the last interval plus its interval between service:

$$S_i = \frac{\sum_j S_j}{M} + \frac{Z}{P_i}$$

IV. EVALUATION

In this section, we describe the simulation and then evaluate the performance of our proposed distribution algorithm using the model and real-world data specified in Section 2. Finally, we compare the measurement results with two other schemes: Round Robin and First Come First Serve and demonstrate the improvements of WFQ.

A. Simulation

The smart grid based electric vehicles charging management system is simulated in MATLAB R2011a with two input parameters: supply and demand ratio (*SDR*) and number of days (n). The simulation compares the WFQ distribution algorithm with a round-robin system, and a first-come-first-served (FCFS) algorithm, that charges the vehicles in the order that they arrive. The improvements are measured in terms of two metrics: the fraction of delayed vehicles and the average delay of the delayed vehicles.

For each simulation, n is 15, and *SDR* ranges from 1 to 2.5 (in steps of 0.1 from 1 to 1.2; in steps of 0.2 from 1.2 to 2; in steps of 0.25 from 2 to 2.5). To avoid initial effects and to guarantee that all electric vehicles included in the measurements have departed by the end of the simulation, the measurements start on the 4th day and end on the (n-2)nd day.

One case should be noted explicitly. Some electric vehicles require more energy than they can possibly receive in the interval that they are connected to their chargers. These vehicles are forced to leave late in order to acquire sufficient charge, even if they are charged continuously. We call this an inevitable delay. To remove the inevitable delay from the measurements of all charging schemes, we replace their requested departure time by the earliest time the electric vehicle can leave if it charges continuously.

B. Analysis

Fig.2 shows the Fraction of Delayed Electric Vehicles (F_D) for the three charging schemes (Round Robin, FCFS, WFQ) with respect to a range of *SDR* values. The WFQ scheme always results in the smallest fraction of delayed vehicles. When the *SDR*=1, over 7% of electric vehicles cannot leave on time with Round Robin or FCFS. However, WFQ results in an F_D of 5%. In order to achieve an F_D of less than 2%, Weighted Fair Queuing requires an *SDR*≥1.8, compared to FCFS which requires an *SDR*≥2.0 and Round Robin which requires an *SDR*≥2.5. In addition, none of the vehicles are delayed in WFQ when *SDR*≥2.5.

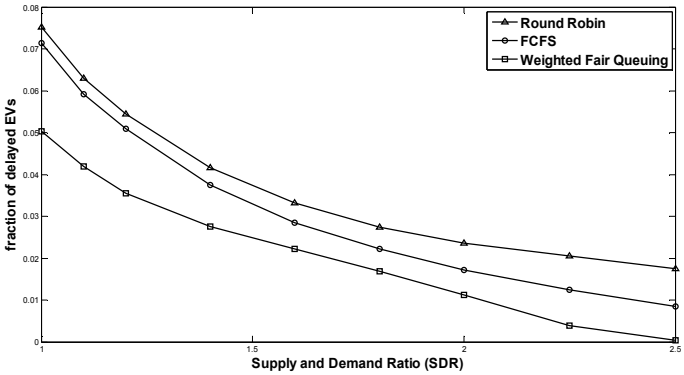

Fig.2. Fraction of delayed vehicles using different charging schemes.

Fig.3 shows the Average Delay of Electric Vehicles that are delayed, D_{FD}. In comparison with a Round Robin based charging scheme, WFQ decreases the average delay by more than 40 minutes over the entire range of *SDR* (2.5≥*SDR*≥1).; And, in comparison with FCFS, the average delay decreases by more than an hour over the entire range of *SDR*. Moreover, when *SDR*=1.8, WFQ has an average of 22 minutes, while Round Robin has an average delay of 63 minutes, and FCFS has an average delay of 94 minutes. When *SDR*≥2, D_{FD} for WFQ is less than 10 minutes; while FCFS and Round Robin have delays between half an hour and one hour.

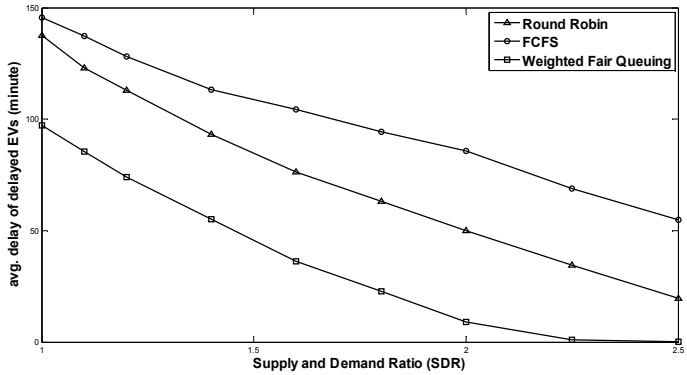

Fig.3. The average delay of the delayed vehicles using different charging schemes.

V. CONCLUSION

WFQ can make the rapid deployment of electric vehicles more acceptable. In the long term there will be sufficient electric power for electric vehicles. However, there will be growing pains while our electric generation and delivery infrastructure catches up with the new demand. How well we deal with the transition will determine how quickly electric vehicles are deployed.

WFQ, at an *SDR* of 2, delays 2% of the vehicles by an average of less than 10 minutes. If once every two months your neighbor who owns an electric vehicle is delayed by 10 minutes, he is unlikely to complain, and you would probably still buy the vehicle. If however, one of the other selection processes are used, and once a month your neighbor is delayed about an hour, you are likely to hear about it, and decide to wait until the bugs are worked out.

What would be worse still, is not using a smart distribution network to control the charging of these vehicles. In that situation rolling blackouts, or brownouts will probably be necessary to handle over loads, and there will be mornings when entire neighborhoods will wake up to find that they cannot go to work that day. People are likely to buy gas generators as a backup to charge their electric vehicle, and those who have not converted to electric vehicles are likely to remain with their gas cars.

REFERENCES

[1] E. Sortomme, M. M. Hindi, S. D. J. MacPherson and S. S. Venkata, "Coordinated Charging of Plug-In Hybrid Electric Vehicles to Minimize Distribution System Losses", IEEE Transactions on Smart Grid, pp.198-205, Vol. 2, No. 1, Mar. 2011

[2] S. Deilami, A. S. Masoum, P. S. Moses and M. A. S. Masoum, "Real-Time Coordination of Plug-In Electric Vehicle Charging in Smart Grids to Minimize Power Losses and Improve Voltage Profile", IEEE Transactions on Smart Grid, pp.456-467, Vol. 2, No. 3, Sept. 2011

[3] O. Sundström and C. Binding, "Flexible Charging Optimization for Electric Vehicles Considering Distribution Grid Constraints", IEEE Transactions on Smart Grid, pp.26-37, Vol. 3, No. 1, March 2012

[4] Z. Fan, "A Distributed Demand Response Algorithm and Its Application to PHEV Charging in Smart Grids", IEEE Transactions on Smart Grid, pp.1280-1290, Vol. 3, No. 3, Sept. 2012

[5] N. Rotering and M. Ilic "Optimal charge control of plug-in hybrid electric vehicles in deregulated electricity markets", IEEE Trans. Power Syst., pp.1021 -1029, Vol. 26, No. 3, 2011

[6] R. A. Verzijlbergh, M. O. W. Grond, Z. Lukszo, J. G. Slootweg, and M. D. Ilić, "Network Impacts and Cost Savings of Controlled EV Charging", IEEE TRANSACTIONS ON SMART GRID, pp.1203 -1212, Vol. 3, No. 3, Sept 2012

[7] Y. Zhou, X. Qian, C. Wang and N. Maxemchuk, "Distributing Power to Electric Vehicles on a Smart Grid", Submitted, 2012 http://www.ee.columbia.edu/~nick/ref.2935.pdf

[8] B. McKenzie and M. Rapino, "Commuting in the United States: 2009", American Community Survey Reports, Sep.2011.

[9] http://www1.eere.energy.gov/vehiclesandfuels/pdfs/1_million_electric_vehicles_rpt.pdf

[10] http://www.nissanusa.com/leaf-electric-car/index#/leaf-electric-car/tags/show/360

[11] http://www.ford.com/electric/focuselectric/2012/

[12] http://www.miniusa.com/minie-usa/

[13] http://www.thinkev-usa.com/why-think-city/faq/

[14] http://www.mitsubishi-motors.com/special/ev/whatis/index.html

[15] http://www.smartusa.com/models/electric-drive/technology.aspx

[16] www.bts.gov/publications/omnistats/volume_03_issue_04/html/figure_02.html

[17] Leon-Garcia, I. Widjaja "Communication Networks: Fundamental Concepts and Key Architectures," McGraw-Hill, 2000.

[18] www1.eere.energy.gov/cleancities/toolbox/pdfs/driving_san_diego.pdf

[19] I. Sharma, C. A. Cañizares, and K. Bhattacharya. "Modeling and impacts of smart charging PEVs in residential distribution systems", IEEE Power and Energy Society General Meeting, 2012

[20] O. Ardakanian, C. Rosenberg, and S. Keshav. "Real Time Distributed Congestion Control for Electrical Vehicle Charging", ACM SIGMETRICS Greenmetrics Workshop, 2012

A Power Scheduling Game for Reducing the Peak Demand of Residential Users

Antimo Barbato*, Antonio Capone †, Lin Chen ‡, Fabio Martignon ‡¶ and Stefano Paris §
* DIIMM, University of Bergamo, antimo.barbato@unibg.it
† DEIB, Politecnico di Milano, capone@elet.polimi.it
‡ LRI, Paris-Sud University, {lin.chen,fabio.martignon}@lri.fr
¶ IUF, Institut Universitaire de France
§ LIPADE, Paris-Descartes University, stefano.paris@parisdescartes.fr

***Abstract*—Smart Grids have recently gained increasing attention as a means to efficiently manage the houses energy consumption in order to reduce their peak absorption, thus improving the performance of power generation and distribution systems. In this paper, we propose a fully distributed Demand Management System especially tailored to reduce the peak demand of a group of residential users. We model such system using a game theoretical approach; in particular, we propose a dynamic pricing strategy, where energy tariffs are function of the overall power demand of customers. In such scenario, multiple selfish users select the cheapest time slots (minimizing their daily bill) while satisfying their energy requests.**

We theoretically show that our game is potential, and propose a simple yet effective best response strategy that converges to a Pure Nash Equilibrium, thus proving the robustness of the power scheduling plan obtained without any central coordination of the operator. Numerical results, obtained using real energy consumption traces, show that the system-wide peak absorption achieved in a completely distributed fashion can be reduced up to 20%, thus decreasing the CAPEX necessary to meet the growing energy demand.

***Index Terms*—Demand Management System, Power Scheduling, Game Theory, Potential Games.**

I. Introduction

The electricity generation, distribution and consumption are in the throes of change due to significant regulatory, societal and environmental developments, as well as technological progress. For these reasons, recent years have witnessed the redefinition of the power grid in order to tackle the new challenges that have emerged in electric systems. One of the most relevant challenges associated with the current power grid is represented by the *peaks* in the power demand due to the high correlation among energy demands of customers. Since electricity grids have little capacity to store energy, power demand and supply must balance at all times; as a consequence, energy plants capacity has to be sized to match the total demand peaks, driving a major increase of the infrastructure cost, which remains underutilized during off-peak hours. High energy peaks are mostly due to residential users, which cover a relevant portion of the worldwide energy demands [1], but are inelastic with respect to the grid requirements as they usually run their home appliances only depending on their own requirements. For this reason, residential users can play a key role in addressing the peak demand problem. Time Of Usage (TOU) tariffs represent a clear attempt to drive users to shift their energy loads out of the peak hours [2].

The most promising solutions to tackle the peak demand challenge, such as other issues related to the electric grid, is represented by the Smart Grid, in which an intelligent infrastructure based on Information and Communication Technology (ICT) tools is deployed alongside with the distribution network, which can deal with all the decision variables while minimizing the effort required to end-users. All data provided by the grid, such as the consumption of buildings [3] [4], electricity costs and distributed renewable sources data, can be used to optimize its efficiency through *Demand Side Management* (DSM) methods. DSM represents a proactive approach to manage the household electric devices by integrating customers' needs and requirements with the retailers' goals [5]. The final objective of DSM is to modify consumers' demand for energy in a proper way by deciding *when* and *how* to execute home appliances, and how to use electricity so as to improve the overall system efficiency while guaranteeing low costs and high comfort to users. Demand side management can be designed for different goals such as to reduce the peak demand by means of shifting loads from peak hours to off-peak hours and to achieve deep penetration of renewable resources by means of adjusting the energy demand to the supply.

In this paper we propose a novel, *fully distributed DSM system* aimed at reducing the peak demand of a group of residential users (e.g., a smart city neighborhood). We model our system using a game theoretical approach, where the players are the end customers, the set of strategies is their daily energy demand, and the objective function the players aim at minimizing is their daily electricity bill. Each customer can modify his daily energy demand by means of scheduling home device activities and deciding when to buy energy from the electricity retailer with the final goal of reducing his daily energy bill. Energy tariffs, in particular, are defined by the retailer as a function of the *total power demand* of customers, based on a dynamic pricing strategy. The proposed game, by means of scheduling energy tasks of residential users to minimize their bills, automatically ensures the reduction of the electricity demand at peak hours because of the dynamic pricing approach.

We demonstrate that our proposed pricing strategy leads to a *potential game*, provided that the pricing is convex with respect to the total demand, c. Moreover, if the pricing is linear

978-1-4799-0354-2/13/$31.00 ©2013 IEEE

in c, we show that the game is exactly potential, the potential function being the total cost paid by all householders, P. Such feature guarantees the existence of at least one pure Nash equilibrium (where no customer has an incentive to deviate unilaterally from the scheduling pattern he decided upon), namely the strategy that minimizes P. Furthermore, in such games, best response dynamics always converges to a Nash equilibrium.

In summary, our paper makes the following contributions:

- The proposition of a novel, fully distributed Demand Side Management (DSM) method able to reduce the peak demand of a group of residential users, which we model and study using a game theoretical framework. In our vision, the energy retailer fixes the energy price dynamically, based on the total power demand of customers; then, end customers automatically schedule their electrical appliances, reaching an efficient Nash equilibrium point.
- Detailed mathematical proofs that our proposed game is potential, and in particular *exactly potential* when the pricing scheme imposed by the energy retailer is linear in the total demand of customers.
- The demonstration of the Finite Improvement Property, according to which any sequence of asynchronous improvement steps (and, in particular, *best response dynamics*) converges to a pure Nash equilibrium.
- The numerical evaluation to show the effectiveness of the proposed game and best response dynamics in several scenarios, with real electric appliances scheduled by householders.

The paper is organized as follows. In Section II we review the most relevant works on demand management mechanisms. Section III, describes the main characteristics of the distributed system we propose to manage the energy consumption of residential users. Section IV presents our proposed game model. The distributed optimization model that we propose to reach stable (equilibrium) solutions, based on a best-response mechanism, is presented in Section V. Numerical results are presented and analyzed in Section VI. Finally, Section VII concludes the paper.

II. Related Work

Demand side management methods have been deeply studied by the scientific community due to the numerous advantages achievable through this kind of mechanism [6]. In [7], a dynamic programming framework is proposed to balance user's comfort level and preferred lifestyle with the goal of minimizing the electricity bill. A similar solution is presented in [8], where an optimization model is proposed which schedules the activities with the aim of minimizing energy costs and maximizing users comfort, taking into account users requirements. Energy costs and users' comfort are also modeled in [9], which proposes a method to manage houses energy consumption with the aim of optimizing a three-term objective function, taking into account the overall energy cost, the schedule deviation with reference to the user preferences and the climate comfort. In this work, houses are assumed to be equipped with photovoltaic (PV) generation and storage resources.

Solutions [7]-[9] are based on a single-user approach in which the energy plans of residential customers are individually and locally optimized. However, in order to obtain relevant results, the energy management problem must not be applied to single users but to *groups* of users (e.g., neighborhood or micro-grids). For this reason, some solutions are proposed in the literature to manage energy resources of groups of customers. In [10], for example, the energy bill minimization problem is applied to a group of cooperative residential users equipped with PV panels and storage devices (i.e., electric vehicle batteries). A global scale optimization method is also proposed in [11], in which an algorithm is defined to control domestic electricity and heat demand, as well as the generation and storage of heat and electricity of a group of houses. These multi-user solutions require some sort of centralized coordination system run by the operator in order to collect all energy requests and find the optimal solution. To this purpose, a large flow of data must be transmitted through the Smart Grid network, hence introducing scalability constraints and requiring the definition of high-performance communication protocols. Furthermore, the collection and transmission of users' metering data can introduce novel threats to customers' security and privacy. Finally, the coordination system should also verify that all customers comply with the optimal task schedule, since the operator has no guarantee that any user can gain, deviating unilaterally from the optimal solution. For these reasons, some *distributed* DSM methods have been proposed in which decisions are taken locally, directly by the end consumer. In this case, Game Theory represents an ideal framework to design DSM solutions. Specifically, in [12] a distributed demand-side energy management system among users is proposed. In this system, the users' energy consumption scheduling problem is formulated as a game, where the players are the users and their strategies are the daily schedules of their household appliances and loads. The goal of the game is to either reduce the peak demand or the energy bill of users. Game theory is also used in [13], in which a distributed load management is defined to control the power demand of users through dynamic pricing strategies. However, in these works, a very simplified mathematical description is used to model houses, which does not correspond to real use cases.

In this paper we propose a DSM method, based on a game theoretical approach, which overcomes the most important limitations of the works proposed in the literature and described above. Our DSM is a fully distributed system, in which no centralized coordination is required, and only a limited amount of data needs to be transmitted through the Smart Grid. For these reasons, scalability, communication, privacy and security issues are greatly mitigated. Moreover, a realistic model of household contexts is provided. Specifically, a mathematical description of home devices is provided. Devices are defined as non-preemptable activities characterized by specific load consumption profiles, determined based on real data, and

are scheduled according to users' preferences defined based on real use-case scenarios. Finally, a parallel analysis between users' and overall electric system performance achieved through the proposed demand management mechanisms is provided.

III. System Model

The power scheduling system here proposed is designed to manage the electric appliances of a group of residential users consisting of $\mathcal{H}$ houses (e.g., a smart city neighborhood). This system is used to schedule the energy plan of the whole group of users over a 24-hour time horizon based on a *fully distributed* approach, with the final goal of improving the efficiency of the whole power grid by reducing the peak demand of electricity, while still complying with users' needs and preferences. More specifically, in our model we represent the daily time as a set $\mathcal{T}$ of time slots. Each householder [1] $h \in \mathcal{H}$ has a set of non-preemptive electric appliances, $\mathcal{A}_h$, that must be executed only once during the day. Specifically, each appliance load profile is modeled as an ordered sequence of phases, $\mathcal{F}$, in which a certain amount of energy is consumed. We assume that the consumption l_{ahf} of a device $a \in \mathcal{A}_h$ belonging to user $h \in \mathcal{H}$ in each phase $f \in \mathcal{F}$ is an average of the real consumption of the device within the time slot's duration (see Figure 1, where 15-minute phases are used).

Each device $a \in \mathcal{A}_h$ of user $h \in \mathcal{H}$ needs to run for d_{ah} *consecutive* slots within a total of $\mathcal{R}_{ah}$ slots delimited by a minimum starting time slot, ST_{ah}, and a maximum ending time slot, ET_{ah} verifying the constrain $ST_{ah} \leq ET_{ah} - d_{ah}$. These two parameters, ST_{ah} and ET_{ah}, represent the users preferences in starting each home device; they can be directly provided by users or automatically obtained through learning algorithms such as the one presented in [14]. In our model, we consider two different kinds of devices:

- *Shiftable* appliances (e.g., washing machine, dishwasher): they are manageable devices that must be scheduled and executed only once during the day. In particular, for each shiftable device $a \in A_h$ of the householder $h \in \mathcal{H}$, the minimum starting time and the maximum ending time verify the constraint $ST_{ah} < ET_{ah} - d_{ah}$, hence their scheduling is a variable of the model.
- *Fixed* appliances (e.g., light, TV): they are not manageable devices that must be executed only once during the day. For each fixed device $a \in \mathcal{A}_h$ of the householder $h \in \mathcal{H}$, the minimum starting time and the maximum ending time verify the constraint $ST_{ah} = ET_{ah} - d_{ah}$, hence their scheduling is not a variable of the model and cannot be optimized.

Devices scheduling is represented by x_{aht}, which are defined for each activity $a \in \mathcal{A}_h$ of each user $h \in \mathcal{H}$, and for each time slot $t \in \mathcal{T}$; they are equal to 1 if the activity a starts in time slot t, 0 otherwise. x_{aht} associated with shiftable appliances are variables of the problem, while

[1] In this paper, we use the terms *householder* and *user* interchangeably.

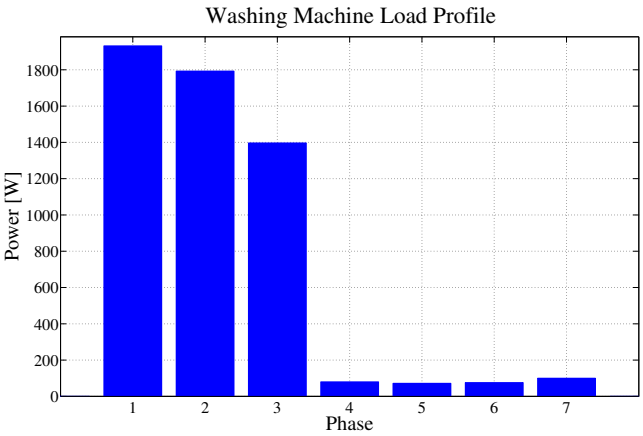

Figure 1: Example of a load profile l_{ahf} of a washing machine.

those associated with fixed appliances are only parameters and cannot be modified. In order to use home appliances, householders can buy energy from the electricity retailer. In particular, the amount of electricity bought by user $h \in \mathcal{H}$ at time $t \in \mathcal{T}$ is denoted by y_{ht}. Let $c_t(\cdot)$ denote the price of electricity at time $t \in \mathcal{T}$. In our model, we suppose that $c_t(\cdot)$ is an increasing function of the total power demand, y_t, of the group of users $\mathcal{H}$ at time t. The objective of the power scheduling system is to minimize the daily bill of each user, by optimally scheduling house appliance activities and managing the power exchange with the network. Intuitively, based on the definition of the electricity price, by reducing the users' bills, the model is able to decrease the corresponding peak demand.

IV. Power Scheduling Game

We now describe the *power scheduling game* used to model the fully distributed DSM system we propose in our paper. In such scenario, each user $h \in \mathcal{H}$ must decide when to use his home appliances (i.e., the x_{aht} values) and, consequently, when to buy energy from the grid (i.e. y_{ht}) in order to minimize his bill. Since the energy price is defined as a function of the total energy demand of the *whole group* of users, the power scheduling problem cannot be solved with a centralized model because of the conflict between users' goals. For this reason, a distributed approach naturally arises, where all decisions are made locally and directly by end consumers. Specifically, in this paper we model the power scheduling problem as a game, since game theory naturally models interactions in distributed decision making processes.

In this regard, let us define the total price, P, paid by all customers to the electricity retailer, as a function of $\mathbf{I} \triangleq \{\mathbf{I_h}\}_{h \in \mathcal{H}}$, where the strategy of user h is $\mathbf{I_h} \triangleq \{x_{aht}\}_{a \in \mathcal{A}_h}$:

$$P(\mathbf{I}) = \sum_{h \in \mathcal{H}} \sum_{t \in \mathcal{T}} y_{ht} \cdot c_t(y_t) \tag{1}$$

where y_{ht} is a function of x_{aht} and c_t is a function of y_t that represents the total power demand of users at time t.

The following Theorem holds:

Theorem 1. *The considered power scheduling game is a potential game if $c_t(y_t)$ is convex with respect to y_t, with $P(\mathbf{I})$ being the potential function. Specifically, if $c_t(y_t)$ is linear w.r.t. y_t, $P(\mathbf{I})$ is the exact potential function, i.e.,*

$$P(\mathbf{I'_h}, \mathbf{I_{-h}}) - P(\mathbf{I_h}, \mathbf{I_{-h}}) = P_h(\mathbf{I'_h}, \mathbf{I_{-h}}) - P_h(\mathbf{I_h}, \mathbf{I_{-h}}) \quad \forall h \in \mathcal{H}, \mathbf{I_h}' \tag{2}$$

where $P_h(\mathbf{I})$ is the price of customer h paid to the operator under the strategy profile $\mathbf{I_h}$. If $c_t(y_t)$ is strictly convex w.r.t. y_t, it holds that

$$P(\mathbf{I'_h}, \mathbf{I_{-h}}) \geq P(\mathbf{I_h}, \mathbf{I_{-h}}) \iff P_h(\mathbf{I'_h}, \mathbf{I_{-h}}) \geq P_h(\mathbf{I_h}, \mathbf{I_{-h}}) \quad \forall h \in \mathcal{H}, \mathbf{I_h}' \tag{3}$$

Due to the page limit, we do not detail the proof. The above theorem readily implies the following corollaries.

Corollary 1 (Efficiency of Equilibrium)**.** *If $c_t(y_t)$ is convex w.r.t. y_t, then the equilibrium also minimizes the total price paid to the operator.*

Corollary 2 (Convergence to Equilibrium)**.** *If $c_t(y_t)$ is convex w.r.t. y_t, then the game has the Finite Improvement Property (FIP). Any sequence of asynchronous improvement steps is finite and converges to a pure equilibrium. Particularly, the sequence of best response update converges to a pure equilibrium.*

Potential games have nice properties, such as existence of at least one pure Nash equilibrium, namely the strategy that minimizes $P(\mathbf{I})$. Furthermore, in such games, best response dynamics always converges to a Nash equilibrium.

Hereafter we describe a simple implementation of best response dynamics, which allows each householder to improve his cost function in the proposed power scheduling game. Such algorithm, detailed in the following, is the best response strategy for a user u minimizing objective function (4), $\sum_{t\in\mathcal{T}}(c_t \cdot y_{ht})$, assuming other users are not changing their strategies.

Specifically, each customer, in an iterative fashion, defines his optimal power scheduling strategy based on electricity tariffs (calculated according to other players' strategies) and broadcasts his energy plan (i.e., his daily power demand profile) to the group $\mathcal{H}$. At every iteration, energy prices are updated according to the last strategy profile and, as a consequence, other users can decide to modify their consumption scheduling by changing their strategy according to the new tariffs. The iterative process is repeated until convergence is reached. Once convergence is reached, householders' power scheduling and energy prices are fixed.

The best response mechanism is executed by solving, in an iterative way, an optimization model. Specifically, at every iteration and based on the energy demands of other users, this model is used to optimally decide the power plan of the user in charge of defining his energy demand at this step of the iterative process, with the goal of minimizing his bill. The optimization model that we have defined for the best response mechanism is described in the following section.

We will show in the Numerical Results section that our proposed algorithm converges, in few iterations, to a Nash equilibrium.

V. Single User Optimization Model

The single-house problem is modeled as a Mixed Integer Nonlinear Programming (MINLP) model which determines, for each residential user u (here called *active user*), his energy plan, i.e., when to buy energy from the grid and when to start the shiftable appliances based on the energy plan of the other householders, with the final aim of minimizing his daily energy bill.

OBJECTIVE FUNCTION

The goal of the problem is to minimize the daily electricity bill of the *active householder* over a 24 hour time horizon divided into $|\mathcal{T}|$ time slots, $\mathcal{T}$ being the set of such time slots. To this end, we define the continuous non-negative variables y_{ut} and c_t representing, respectively, the amount of electricity bought by *active user* u and the price of electricity in each time slot $t \in \mathcal{T}$. The objective function can be modeled as:

$$\min \sum_{t\in\mathcal{T}} (c_t \cdot y_{ut}) \tag{4}$$

CONSTRAINTS

Appliances scheduling: The house appliance activities to be executed by the user u are represented by the set $\mathcal{A}_u$. For each activity $a \in \mathcal{A}_u$, binary variables x_{aut} have to be defined, which are equal to 1 if the activity a starts in time slot t, and 0 otherwise. Such variables must satisfy two sets of constraints:

$$\sum_{t=ST_a}^{ET_a-d_a+1} x_{aut} = 1 \qquad \forall a \in \mathcal{A}_u \tag{5}$$

$$p_{atf} = l_{auf} x_{au(t-f+1)} \qquad \forall a \in \mathcal{A}_u, t \in \mathcal{T}, f \in \mathcal{F} : f \leq t \tag{6}$$

The first set of constraints guarantees that the activity a starts in exactly one time slot and it is carried out in the required interval (ST_{au}, ET_{au}). The second set of constraints forces the power required by each appliance in each time slot, p_{atf}, to be equal to the load profile l_{auf} of the phase carried out in the considered time slot.

Power demand constraints: In every time slot $t \in \mathcal{T}$, the power demand y_{ut} of the *active householder* must meet the total power consumption of home appliances. For this reason we define the following constraints:

$$y_{ut} = \sum_{a\in\mathcal{A}_u} \sum_{f\in\mathcal{F}} p_{atf} \qquad \forall t \in \mathcal{T} \tag{7}$$

Moreover, in every time slot $t \in \mathcal{T}$, the electricity bought from the grid cannot exceed the Peak Power Limit (PPL) defined by the retailer and denoted by π^{PPL}:

$$y_{ut} \leq \pi^{PPL} \qquad \forall t \in \mathcal{T} \tag{8}$$

Electricity price constraints: The price of electricity c_t, in each time slot $t \in \mathcal{T}$, is a linear increasing function of the total power demand of the group of users $\mathcal{H}$. In particular, it is computed according to the following constraints:

$$c_t = c^{MIN} + s(y_{ut} + p_t) \qquad \forall t \in \mathcal{T} \tag{9}$$

where p_t is the total power demand of other householders of the group $\mathcal{H}$, c^{MIN} is the minimum electricity price and s is the slope of the cost function [15].

VI. Numerical Results

This section presents the numerical results that illustrate the validity of our proposed distributed DSM system to reduce the peak demand of a group of residential neighbors.

We first describe the experimental methodology of our simulations, then we analyze and discuss the performance achieved by the proposed mechanism.

A. Experimental Methodology

In our simulations, we consider two typical residential scenarios composed of identical houses with four and five shiftable devices out of eleven realistically-modeled appliances[2], respectively. The basic domestic configuration and the load profile consumption of each appliance have been defined based on literature data relevant to the Italian standard user obtained in the project MICENE carried on at Politecnico di Milano [15]. We vary the number of houses in the range $[1, 5]$ to assess the performance of the proposed DSM system when the competition increases.

In order to evaluate the effect of the scheduling flexibility on users bills and the efficiency of the electrical grid, we consider three different scenarios, where residential users have (1) no flexibility, (2) tight and (3) loose temporal constraints on the execution of shiftable devices. Specifically, for each appliance we fix different bounds both on the starting and ending time (i.e., ST_a and ET_a), thus modeling the interval during which the user is willing to use its shiftable devices. We consider a set $\mathcal{T}$ of 24 time slots of 1 hour each.

Concerning the electricity prices, we fix the minimum electricity price $c^{MIN} = 50 \times 10^{-6}$ € and the slope of the cost function $s = 4 \times 10^{-8}$ €/kWh, according to the data gathered in the project [15].

In order to gauge the performance of the proposed DSM system, we measured the following performance metrics:

- *Social Welfare*: defined as the sum of users utility, $\sum_{h \in \mathcal{H}} u_h$. Note that this value represents the electricity bill of the group of houses.
- *Fairness*: we consider the *Jain's Fairness Index (JFI)* [16], defined according to Equation (10):

$$\text{Jain's Fairness Index} = \frac{(\sum_{h \in \mathcal{H}} u_h)^2}{|\mathcal{H}| \cdot \sum_{h \in \mathcal{H}} {u_h}^2} \tag{10}$$

The *Jain's Fairness Index* measures the spread of the price paid by users, and it varies from $1/|\mathcal{H}|$ (no fairness) to 1 (perfect fairness).

[2]Namely, Refrigerator, Purifier, Lights, Microwave Oven, Oven, TV, Iron, Washing machine, Dishwasher, Boiler, Vacuum Cleaner

B. Performance Evaluation

Figures 2(a) and 2(b) show the Social Welfare achieved by the proposed DSM system as a function of the number of houses participating in the power scheduling game. As illustrated in the figures, users always benefit from higher flexibility. Indeed, long scheduling intervals for shiftable appliances (curves identified by "Long" in the figures) result always in cheaper scheduling plans than those obtained with short and fixed intervals (curves identified by "Short" and "Fix", respectively), since the distributed DSM system can explore a larger solution space.

It can be further observed that increasing the number of shiftable devices (from 4 to 5 out of 11) does not permit to reduce significantly the electricity bill when users have thigh constraints on the starting and ending time of their appliances.

We underline that all houses pay an equal share of the electricity bill illustrated in Figures 2(a) and 2(b). Indeed, the Jain's Fairness Index, which we do not show for the sake of brevity, is always very close to 1. Finally, we observe that, throughout all our tests, convergence to the equilibrium is achieved within 5 iterations in the worst case, and in the large majority of the scenarios within only less than 2.

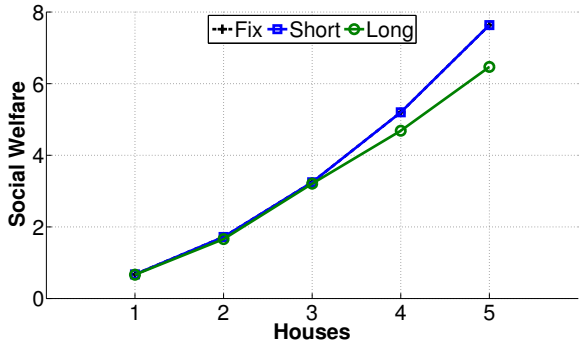

(a) 4 Appliances

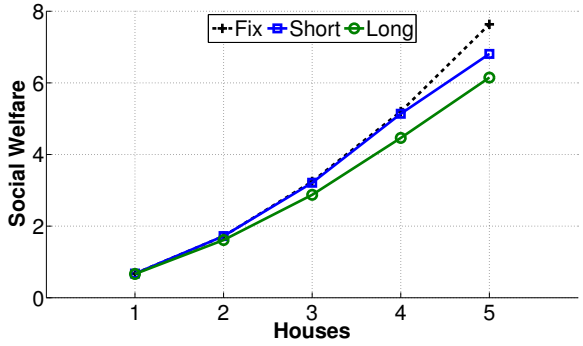

(b) 5 Appliances

Figure 2: Social Welfare considering four (a) and five (b) shiftable appliances for each house.

In Figure 3, the overall electricity demand resulting from the proposed method, in the case of a five-house group, is compared to that of an unmanaged group of residential users. As illustrated in Figure 3(b), in addition to decreasing the

electricity bill, the proposed distributed DSM system reduces the energy demand during peak hours (i.e. high-price hours) up to 20% without any centralized coordination among users. Note, however, that a significant energy peak reduction can be obtained when users have loose temporal constraints on the execution of their devices (i.e., a high degree of flexibility). Indeed, as illustrated in Figure 3(a), when only 4 out of 11 devices are shiftable, the peak reduction is negligible (the curves *Short Flexibility* and *No Flexibility* are overlapped).

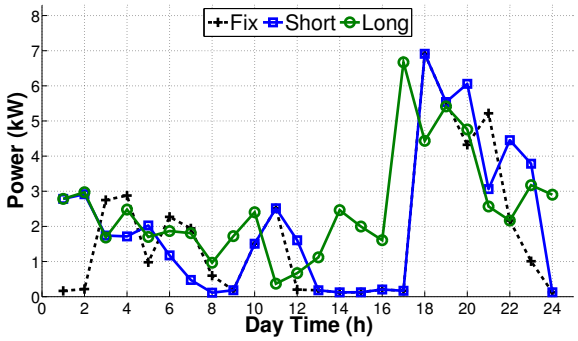

(a) 5 Houses - 4 Appliances

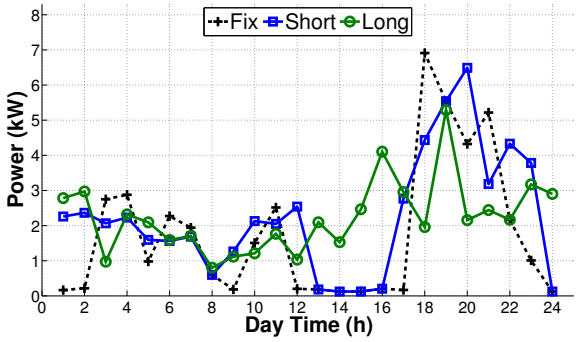

(b) 5 Houses - 5 Appliances

Figure 3: Electricity demand for five houses with four (a) and five (b) shiftable appliances, respectively.

VII. Conclusions

In this paper, we tackled a fundamental problem that has recently emerged in electric systems, namely the *peak absorption* in the power demand, which arises due to the high correlation among energy demands of residential customers. To solve this issue, we proposed a novel, fully distributed Demand Side Management (DSM) system aimed at reducing the peak demand of a group of residential users.

We modeled our system using a game theoretical approach, where the players are the end customers, the set of strategies is their daily energy demand, and the objective function the customers aim at minimizing is their daily electricity bill. We demonstrated that the proposed game is potential, and in particular exactly potential when the pricing scheme imposed by the energy retailer is linear in the total demand of customers. For this reason, we proposed a best response dynamics mechanisms which converges in few steps to efficient Nash equilibrium solutions. Numerical results, obtained using realistic load profiles and appliance models demonstrate that residential users can minimize their electricity bill in a completely distributed fashion and reduce the peak absorption of the entire system.

Acknowledgment

This work was partially supported by Italian MIUR and French ANR in the framework of the PRIN Gatecom and ANR Green-Dyspan projects.

References

[1] European Commission. European Union Energy in figures and fact-sheets, sep 2011. Available on: http://ec.europa.eu/energy/publications/.

[2] Definition of an instrument for the gradual application of prices differentiated by hour bands to domestic customers in protected categories, Resolution ARG/elt 22/10, 2010. Available on: http://www.autorita.energia.it.

[3] Xiaofan Jiang, Stephen Dawson-Haggerty, Prabal Dutta, and David Culler. Design and implementation of a high-fidelity ac metering network. In *Information Processing in Sensor Networks, 2009. IPSN 2009. International Conference on*, pages 253–264. IEEE, 2009.

[4] Nicola Bressan, Leonardo Bazzaco, Nicola Bui, Paolo Casari, Lorenzo Vangelista, and Michele Zorzi. The deployment of a smart monitoring system using wireless sensor and actuator networks. In *Smart Grid Communications (SmartGridComm), 2010 First IEEE International Conference on*, pages 49–54. IEEE, 2010.

[5] Clark W Gellings and John H Chamberlin. Demand-side management: concepts and methods. 1987.

[6] G. Strbac. Demand side management: Benefits and challenges. *Energy Policy*, 36(12):4419–4426, 2008.

[7] D. Livengood and R. Larson. The energy box: Locally automated optimal control of residential electricity usage. *Service Science*, 1(1):1–16, 2009.

[8] M. Jacomino and M.H. Le. Robust energy planning in buildings with energy and comfort costs. *4OR - A Quaterly Journal of Operations Research*, 10(1):81–103, 2012.

[9] A. Agnetis, G. Dellino, P. Detti, G. Innocenti, G. de Pascale, and A. Vicino. Appliance operation scheduling for electricity comsumption optimization. In *IEEE Conference on Decision and Control and European Control Conference, CDC-ECC*, pages 5899–5904, Orlando, Florida, dec 2011.

[10] A Barbato, A Capone, G Carello, M Delfanti, M Merlo, and A Zaminga. House energy demand optimization in single and multi-user scenarios. In *Smart Grid Communications (SmartGridComm), 2011 IEEE International Conference on*, pages 345–350. IEEE, 2011.

[11] Albert Molderink, Vincent Bakker, Maurice GC Bosman, Johann L Hurink, and Gerard JM Smit. Domestic energy management methodology for optimizing efficiency in smart grids. In *PowerTech, 2009 IEEE Bucharest*, pages 1–7. IEEE, 2009.

[12] A Mohsenian-Rad, Vincent WS Wong, Juri Jatskevich, Robert Schober, and Alberto Leon-Garcia. Autonomous demand-side management based on game-theoretic energy consumption scheduling for the future smart grid. *Smart Grid, IEEE Transactions on*, 1(3):320–331, 2010.

[13] C. Ibars, M. Navarro, and L. Giupponi. Distributed demand management in smart grid with a congestion game. In *IEEE, SmartGridComm '10*, pages 495–500, Gaithersburg, USA, oct 2010.

[14] A. Barbato, A. Capone, M. Rodolfi, and D. Tagliaferri. Forecasting the usage of household appliances through power meter sensors for demand management in the smart grid. In *Smart Grid Communications (SmartGridComm), 2011 IEEE International Conference on*, pages 404–409. IEEE, 2011.

[15] Micene project. *Available on-line at http://www.eerg.it/index.php?p=Progetti_-_MICENE*, 2012.

[16] R. Jain. *The Art of Computer Systems Performance Analysis: Techniques for Experimental Design, Measurement, Simulation, and Modeling*. Wiley - Interscience, 1991.

The EDISON Project: Enhanced Energy Saving Solution for Lighting using DC Power Supply

M. Celidonio, D. Di Zenobio, E. Fionda, L. Pulcini, E. Sergio
Fondazione Ugo Bordoni (FUB)
Viale del Policlinico 147, Rome, Italy

Abstract— **The EDISON project[1], funded under the 7th Framework Programme for Research and Technological Development (FP7), has the ambitious goal to demonstrate, through targeted Pilot actions implemented in different European countries, that an innovative ICT-based solution for lighting infrastructure may improve energy efficiency, reduce CO_2 emissions and encourage the use of small-scale renewable energy sources in public buildings. The proposed solution is based on the use of Solid State Lamps (SSLs) combined with a particular method of providing power to them, in order to realize a Smart Energy Platform (SEP) designed to directly contribute to reducing energy losses and consumption in building lighting.**

Keywords— Energy efficiency, smart metering, SSL, PowerLAN, DC power supply, SELV system

I. INTRODUCTION

At present, one of the main challenges for building managers is to identify effective energy saving strategies which take into account efficiency, financial and environmental aspects.

In the last years, the technologies, standards and expertise required to overcome those challenges have matured. As an example, last control and monitoring network architectures are converging towards IP-based solutions and, thanks to this innovative approach, an increasing acceptance and diffusion of these networks are taking place. This results in an extraordinary, compelling set of circumstances. All the advancements in technology development, standardization processes and general expertise are combining to unleash opportunities for facility and ICT managers like never before, improving building and business performance.

In this context, the EDISON (Energy Distribution Infrastructure for SSL Operative Networks) project, funded by the European Commission under the fifth Call of the CIP-ICT PSP projects of the 7th Framework Programme (FP7) in the theme "ICT for a low carbon economy and smart mobility", proposes an innovative ICT-based lighting infrastructure that along with power electronics, customized software tools, wired and wireless capabilities, constitutes an integrated network able to logically coordinate and organize all the data originated in ICT components and systems (e.g. smart metering, sensors, renewable energy sources, etc.), with the opportunity of delivering them where and when they are requested, in order to get both valuable energy savings and workspace productivity enhancements.

The EDISON solution is actually implemented in more than 10 Pilots, in different countries in Europe (Belgium, Italy, Ireland, etc.). All the Pilots are running and the first results, provided in section V, are confirming the high efficiency of the proposed technical approach.

One of the key aspect of the EDISON solution is represented by its capability to be implemented both in energy retrofitting actions, replacing the existing lighting power supply infrastructure with "a 48 VDC Extra Low Voltage Lighting Power Distribution Network", and in new buildings construction, making the corresponding lighting infrastructure "native EDISON" compliant.

According to this peculiar characteristic, in Section II, a brief overview regarding the ELV systems is provided, followed by a detailed description of the system architecture in Section III. Successively, Section IV deals with a functional analysis of the EDISON key components and Section V illustrates an analysis of the benefits available with the EDISON platform, which also includes an example of energy savings estimation. Finally, the paper ends with some concluding remarks.

II. BACKGROUND: ELV SYSTEMS

The International Electrotechnical Commission (IEC) defines a circuit as an "Extra Low Voltage" (ELV) circuit if the electrical potential of any conductor against earth (GND) is not more than either 50 volts for AC, or ripple-free 120 volts for DC under dry conditions, in accordance with IEC 60449 [1], as reported in Table 1.

The IEC also defines three types of extra-low-voltage systems:

[1] EDISON Project: www.project-edison.eu

978-1-4799-0354-2/13/$31.00 ©2013 IEEE

- Separated/Safety Extra Low Voltage (SELV): electrical system in which the voltage cannot exceed ELV under normal conditions, and under single-fault conditions, including earth faults in other circuits [2] (Figure 1);

IEC voltage range	AC	DC	Defining Risk
High voltage (supply system)	> 1000 Vrms	> 1500 V	electrical arcing
Low voltage (supply system)	50 – 1000 Vrms	120 – 1500 V	electrical shock
Extra-low voltage (supply system)	< 50 Vrms	< 120 V	low risk

Table 1: Voltage limit specified in IEC 60449

- Protected Extra Low Voltage (PELV): electrical system in which the voltage cannot exceed ELV under normal conditions, and under single-fault conditions, except earth faults in other circuits (Figure 2);
- Functional Extra Low Voltage (FELV): describes any other extra-low-voltage circuit that does not fulfill the requirements for a SELV or PELV circuit (Figure 3).

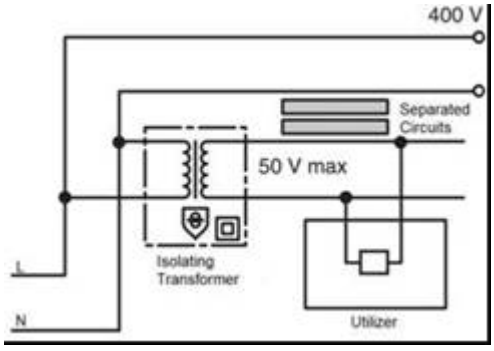

Figure 1:SELV system

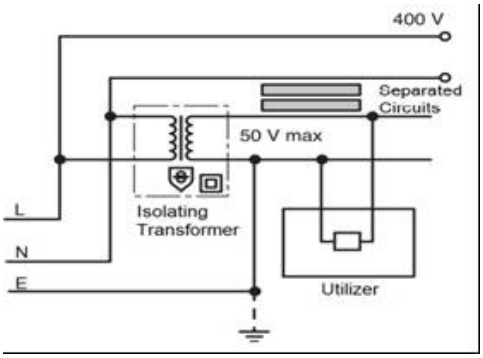

Figure 2:PELV system

In the EDISON solution the existing lighting power supply infrastructure is replaced with "a DC Extra Low Voltage Lighting Power Distribution Network" and specifically a SELV system.

The resulting innovative lighting infrastructure is fed by a low voltage DC pair of wires (Line + Neutral). The third wire (Earth), which is used in the existing lighting power infrastructure, is not necessary and becomes available to be used to form a pair of "DATA" wires, when coupled with the common Neutral wire.

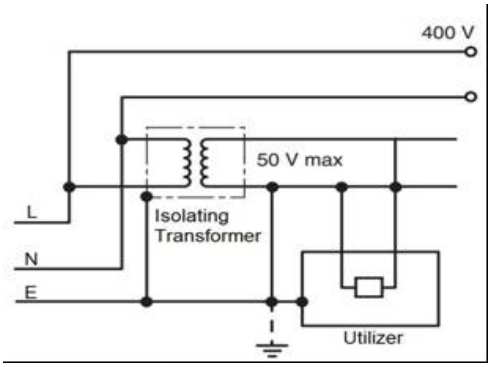

Figure 3:FELV system

III. EDISON LIGHTING NETWORK ARCHITECTURE

The idea that characterizes the EDISON approach is based on the use of Solid State Lamps (SSLs), e.g. LEDs, fed by DC power supply, in order to realize a Smart Energy Platform (SEP).

The SEP accommodates all EDISON components, both hardware and software, and delivers a smart lighting system, powered and controlled through the electrical wires available from the existing infrastructure. It is able to feed the LED lamps by a low voltage DC pair of wires (Line + Neutral), 48 VDC, and permits to exchange data with the field and to interact with lighting dimming modules, sensors and actuators, giving evidence of the energy saving results, efficiency, real time operations, etc. The distributed high-density sensors network included in the SEP, in fact, eliminates the need for time-consuming occupancy/lighting sensor calculations for daylight harvesting, providing more than just advanced lighting management.

More in detail, Figure 4 shows the most general implementation of the EDISON platform where the lighting infrastructure is powered by the utility grid after an opportune AC/DC conversion. Alternatively, it can be powered directly by a renewable energy supply system, reducing significantly the power conversion losses.

Thanks to the ICT EDISON platform (SEP), smart metering data, signals outcoming from monitoring and alarm networks or related to alternative energy sources, particularly PV systems (e.g. indicators of electrical losses, energy conversion metering systems, etc.), can be properly collected and analyzed.

The intelligence of the system is located inside the Central Power Control (CPC) component. Furthermore, when the system is not powered directly by renewable energy sources, also the AC/DC conversion is performed inside the CPC.

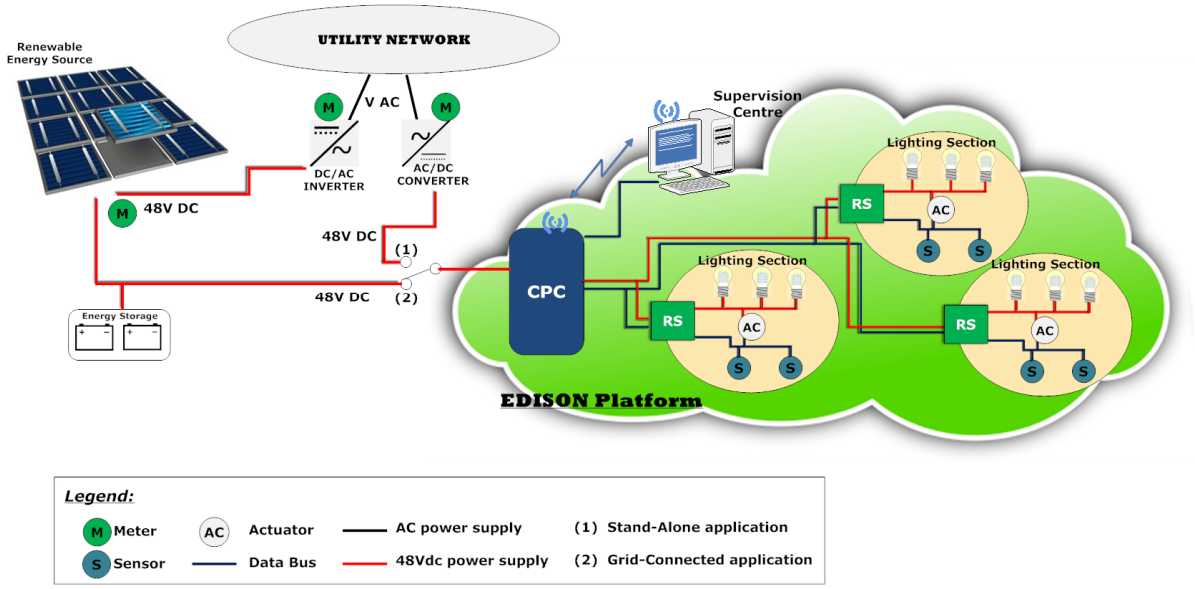

Figure 4:EDISON Architecture

The CPC powers all the linked lighting sections and manages through Remote Stations (RS) the actuators and ICT components present in the same infrastructures.

The resulting wired infrastructure constitutes an integrated power line/digital network or, in brief, a "PowerLAN".

In order to be easily integrated in the existing lighting infrastructures of the building, the EDISON solution has been designed to operate in three different configurations [3]:

- the first reference model addresses plants where the lighting infrastructure is separated from the EMF infrastructure and a single electrical switchboard panel controls the overall electrical network (see Figure 5);

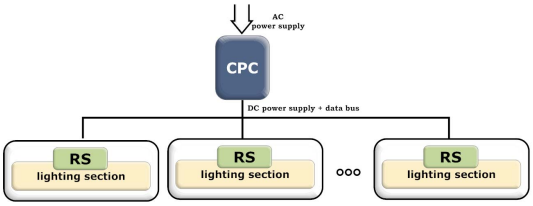

Figure 5: Electrical Network with a single electrical switchboard panel

- the second one addresses plants where the separation of the lighting and EMF infrastructures is not available everywhere but it is performed locally. It means that a master electrical switchboard panel controls local slave panels (see Figure 6);

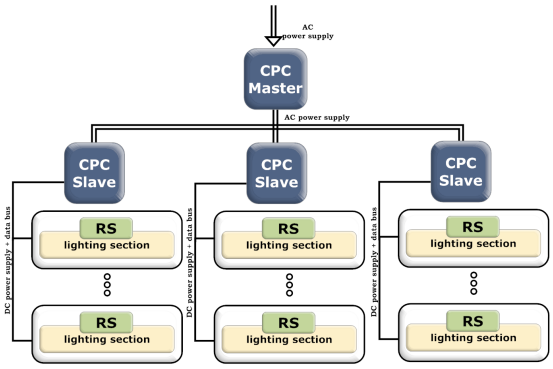

Figure 6: Electrical Network with Master & Slave electrical switchboard panels

- the last reference model addresses plants where the lighting infrastructure operates with a relay system (see Figure 7).

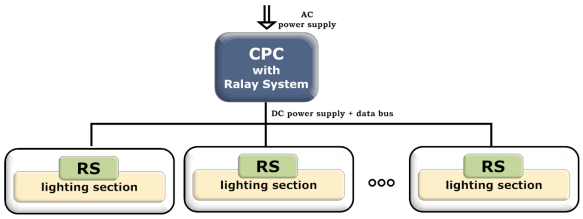

Figure 7: Electrical Network with a relay system

Each of the above mentioned configurations presents the common key features:

- compliance with SELV systems;

- Line + Neutral wires used for the power supply at 48VDC;
- Earth + Neutral wires used as data communication bus in the local network.

In presence of sensors and/or actuators that are not directly connected to the PowerLAN for both data and power supply, the CPC communicates with them via a wireless interface, allowing to cover every hard-to-reach corner of the building. In addition, wireless technology streamlines retrofits and results in faster download times, providing an important route for upgrading the system and to enhance the number and types of devices that may be connected to the CPC.

A supervision centre monitors and records all information related to the lighting network status by means of a dedicated software tool, opportunely developed to operate with EDISON devices, in order to visualize the objects inside the network, to interact with them and to monitor and provide statistics on energy consumptions.

IV. EDISON PLATFORM KEY COMPONENTS

As already illustrated, the basic elements of the EDISON platform are the CPC and the RS. In the following sub-sections a detailed description of these components is provided [3].

A. Central Power Control (CPC)

The Central Power Control is performed according to the existing electrical infrastructure of the building and, on the basis of the above mentioned reference models, it can be developed in three different modes: General, CPC-Master and CPC-Slave.

Depending on the type of work it should perform, the CPC can be able to:

- count the power consumptions, through a Smart Metering System and make the measured data available to the supervision centre;
- feed the whole lighting infrastructure of the building;
- manage several lighting sections by controlling related RS devices via a communication link based on EDISON data communication link (protocol ModBus over LIN PHY interface);
- allow the wired or wireless communication between the CPC-SLAVE and Supervision Centre, using PowerLine modems (PLC) or Wi-Fi devices;
- receive the general information of the lighting section, like the status of sensors, from the RSs and communicates them to the Supervision Centre by wired or wireless link;
- manage the whole lighting infrastructure by controlling the relay switches.

To implement all the above listed functions, the CPC, in its general configuration, consists of (see Figure 8):

- A power system;
- A smart metering system;
- A microcontroller board;
- I/O interfaces;
- Relay switches;
- An Ethernet switch;
- An emergency switch;
- Some switch breakers.

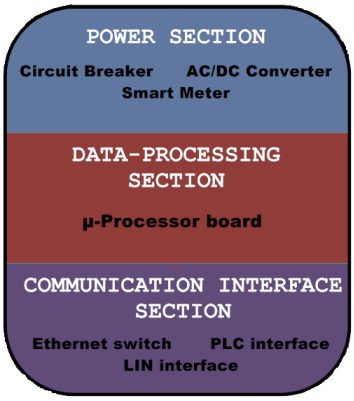

Figure 8: Central Power Control

B. Remote Station (RS)

The Remote Station, represented in Figure 9, aims to control either a single or several lighting sections, e.g. room, group of rooms, large office, museum hall, etc.

It is able to monitoring the status of the sensors, both presence and light, and consequently, to switch on/off the lamps. It communicates with CPC providing the general status of the controlled lighting section (the level of illumination, presence of people, etc.). The RS, according to CPC control signals, manages the ON/OFF power status of the lighting section as well.

The general components in the RS are:

- An Automatic/Manual switch (that could be even a relay Double-Toggle contact);
- A Microprocessor Board;
- I/O Interfaces;
- Led driver;
- AC/DC Converter.

The management of the switching of the LED lamps on/off can be performed in both manually and automatically. In manual mode, anyone is able to turn the lamps on/off by using the common switch box. On the contrary, in automatic mode the switching of the lamps on/off, or dimming, is performed by the RS automatically, depending on the sensors status.

The RS elaborates, records and forwards the received information from sensors to a Supervision Centre, through the Central Power Control (CPC), with the support of dedicated bidirectional communication links.

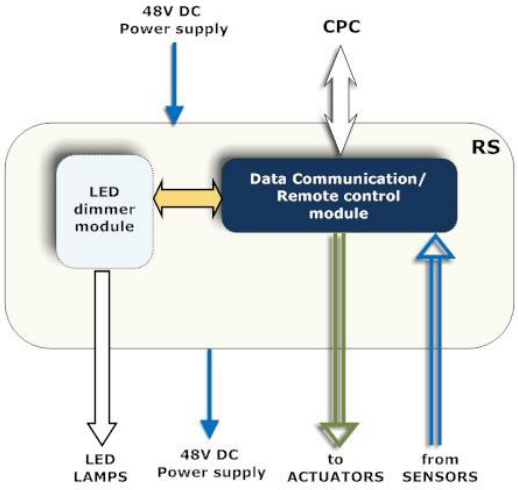

Figure 9: Remote Station

C. *Communication link*

The EDISON platform is developed with a top-down approach, allowing the collection of data, with wired or wireless connections, between:

- CPC and RS's;
- RS and sensors/actuators.

The information exchanged among these elements is referred to:

- Sensors status;
- Peak energy consumption;
- Current energy consumption;
- Switching the Lighting section on or off.

In the specific, data communication between RS and sensors/actuators is performed in analog way, using the DATA wires (Earth+Negative).

Data exchange between CPC and RS is performed through a standard LIN interface [4] [5] or, alternatively, using RS485 or RS232 (customized) protocols depending on the specific arrangement of the devices (CPC, RS's) inside the infrastructure.

Finally the communication between CPC and supervision center is carried out through Power Line modems using Ethernet interface.

V. BENEFITS OF THE EDISON PLATFORM

In the previous sections important benefits that can be achieved thanks to the adoption of EDISON solution have emerged. In the present section these benefits will be analysed more in detail.

A. *DC powered lighting infrastructure*

One of the obstacles that should be taken into account installing LED lamps, despite their otherwise compelling benefits, is that driver circuits for these devices must include power conversion capability to transform alternating-current (AC) branch distribution voltages (typically 240 V AC) to low-voltage direct-current (DC) power. While this process is fairly simple, it requires an extra cost for converters inside the LED lamps and reduces the otherwise extraordinary power to light conversion efficiency of the LEDs themselves.

Even the fluorescent high efficiency lighting systems suffer of an efficiency drop because all electronic ballasts have a front end that converts AC input voltage to DC voltage. Electronic ballasts require DC voltage to efficiently drive fluorescent lamps at high frequency as well as to facilitate dimming, programmed starts and other digitally managed tasks.

The situation is not much different on the power generation side when site-based photovoltaic (PV), wind or other renewable sources are put into play. In fact the native DC power generated by these increasingly efficient sources must be converted and synchronized with the utility-based AC power. This comes at a higher initial investment cost for inverters, isolation, controls and noise filters, and a significant operating efficiency loss. Making matters worse is the sometimes necessary use of a UPS battery-based backup system, which nearly doubles the initial loss, as DC power is converted to AC two times before making contact with the devices. To put this in perspective, because of accumulated conversion losses, a typical device in a building data centre will only see half of the power that was first measured and paid for at the utility power meter.

In that sense, the use of light control modules and lighting fixtures as proposed in the EDISON approach allows to implement a hybrid distribution layer, where the low-voltage power does not replace AC in a building, but complements it.

The goal is to efficiently aggregate or eliminate multiple AC to DC conversions, thereby making devices simpler, safer and more flexible in use. Typical AC to DC conversion efficiencies range is between 85% and 92%, taking into account that the lower values are referred to converters inside lamps.

The more evident effects of such a choice are, consequently:

- Efficiency: both alternative power generation and device consumption becomes more efficient with the consolidation or elimination of poor and highly fractionated power conversion actually installed inside LED lamps.

- Cost reducing: more and more devices, like LED lamps, are DC power native, and therefore it is easier and cheaper to build a lighting infrastructure whose elements are directly connected to DC power.

To these positive aspects, other advantages linked to the use of low-voltage power may be considered, such as:

- Safety: it is allowed the use of greatly simplified and less expensive class-2 wiring and device protection, which greatly reduce spark and fire hazards and eliminate shock/startle hazards.
- Flexibility: it is allowed "hot-swap" plug-and-play connectivity that essentially is embedded into existing building structure and elements, i.e. suspended ceiling grid, modular furniture, etc.

Couple these basic benefits with the enormous capability offered by either digital RF devices or the proposed control modules operating on the PowerLAN by using the Earth wire as DATA wire, and the result is a system with the promise to deliver control capability all around, eliminating the need for battery-powered switches, sensors and controls.

B. Energy savings estimation

According to the targets set out in EU's "Climate and Energy Package" [6], which are:

- +20% renewable energy in final energy consumption,
- - 20% energy consumption vs. projected levels thanks to energy efficiency,
- - 20% greenhouse gas emissions,

the European Union intensified its efforts to favor a more environmentally-sustainable energy policy, demonstrating to be poised to take the lead at global level in the fight against climate change.

In this respect, EDISON solution aims to reduce energy consumption of the public buildings by more than 20% in addition to the savings due to the SSL employment (about 50%). In order to have an idea of possible energy savings, Table 2 compares some specific energy parameters using the traditional lighting systems and the EDISON infrastructure.

The following hypotheses have been taken into account:

- replacement of 500 NEON tubes (36W) with 500 LED tube of about the same luminosity (18W);
- daily use of lighting infrastructure for 10 hours;
- total use of lighting infrastructure: 260 days per year;
- emission factor: 0,75 kg CO2/kWh [7].

	Tube Consumption (W)	Num. of tube	Total Consumpiton (kW)	Use of lighting infrastructure (Hours per day)	Electricity Consumption (kWh per day)	Electricity Consumption (kWh per year)	Total savings (kWh)	CO2 savings (kg)
Traditional Lighting Infrastructure (with NEON tube)	36	500	18	10	180	46800	30420	22815
EDISON lighting infrastructure (with LED tube)	18	500	9	10	90	16380		

Table 2: Example of an estimation of energy savings with EDISON solution

According to these calculations, the estimated annual energy savings is about 30 MW, which means a reduction of about 23 tons of CO_2 gas emitted into the atmosphere. In addition, considering the long lifetime of LED lamps with respect to other lamps technologies, it results also a significant reduction in maintenance costs.

C. Energy efficiency preliminary results

Taking into account that the most attractive aspect of the project, which has convinced the EC to fund it, is its promise to demonstrate that the employment of advanced ICT components and systems compliant with the requirements of the EDISON solution can contribute directly in reducing annual energy consumption in public buildings, a preliminary energy efficiency evaluation based on the first results carried out in the Pilot Action at Vrije Universiteit Brussels (VUB), is provided in this section.

The area interested in this Pilot Action is represented by the student restaurant located inside the University Campus which involves about 100 lighting points (exclusively based on the use of SSL lamps), with a total active power of about 700 W.

The evaluation model adopted in order to have an idea of the energy efficiency level which is possible to achieve through the implementation of the proposed solution is based on a comparison between the electricity consumptions of the lighting system measured when the EDISON Platform is active or inactive (i.e. without ICT components), see Figure 10. Data reported are referred to an observation period of 5 working days in a week (from Monday to Friday), collected in two consecutive weeks.

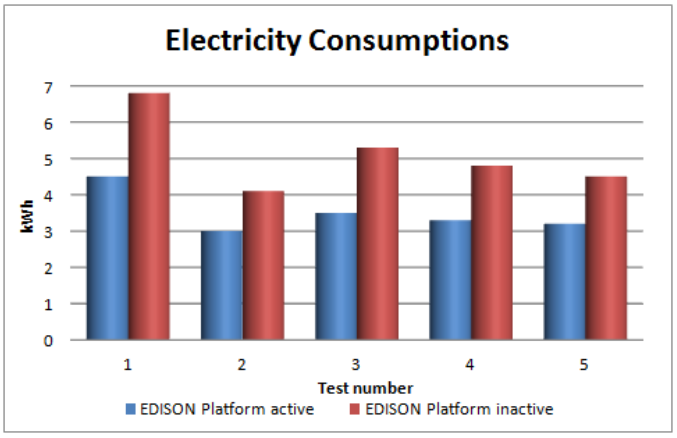

Figure 10: Comparison of electricity consumption when the EDISON platform is active or inactive

The obtained results are emphasized in Table 3, where an efficiency gain of about 30% is witnessed in case the EDISON platform works properly with respect to the mere functioning of a lighting system that only uses the SSL lamps.

In terms of kWh, considering a daily average value of 2 kWh saved for each working day with a maximum duration of 9 hours, as resulting from Table 3, and that the restaurant is open approximately 250 days per year, it is possible to estimate an energy yearly saving of about 500 kWh, corresponding to a

reduction of 110 kg of CO_2 emissions per year, taking into account that about 220 grams of CO_2 are produced in Belgium per kWh [8].

Test number	Test Duration	Electricity Consumptions (kWh)		Efficiency gain (%)
		EDISON Platform active	EDISON Platform inactive	
1	9 h	4,5	6,8	33
2	5 h 30 m	3,0	4,1	27
3	7 h	3,5	5,3	33
4	6 h 25 m	3,3	4,8	31
5	6 h	3,2	4,5	29

Table 3: Comparison of electricity consumption when the EDISON platform is active or inactive

Obviously, this efficiency gain increases up to 75-80% if the electricity consumptions obtained through the use of the EDISON platform are compared with the ones obtained in presence of traditional lighting infrastructure, which uses the fluorescent lamps.

D. Potential value added services

The innovative technological approach of EDISON makes available a local communications network based on electrical wires (power lines communications), that could help in implementing value-added services aimed at solving the most difficult challenges in building management systems.

Some examples of additional services that may be made available using the platform are:

- Monitoring the temperature of indoor areas and control the ON/OFF state of HVAC systems in order to have a good compromise between environmental comfort and energy savings;
- Sensor Access Alarm management to enable security personnel in order to view, acknowledge and respond to alarms, such as a door being forced open, an alarm sensor being triggered or a card reader being used at an unauthorized time;
- Video surveillance service providing real-time monitoring of a facility's environment, people, and assets, inside and outside the buildings.

VI. CONCLUSIONS

On the basis of the analysis illustrated in this paper is evident that the solution proposed by the EDISON Consortium to the EU, in the context of the FP7 CIP-ICT Programme, is a very ambitious challenge in the direction to introduce a new way of thinking lighting networks in buildings, both for retrofitting actions and new constructions.

The EDISON solution gives the possibility to implement different system configurations responding to the constraints and the requirements of the lighting infrastructure to be controlled, and to the degree of flexibility and interoperability requested to the control system.

The architecture and the hardware components used in the solution are not limited to a single service, and could be devoted to services different from lighting, representing in this way an open control platform for building automation and monitoring.

The adoption of EDISON approach allows to take advantage of multiple benefits, like:

- the proposed lighting power supply infrastructure is a DC Extra Low Voltage Lighting Power Distribution Network and specifically a SELV system;
- make quick and safer installation of lighting fixtures and other low voltage devices;
- facilitate the direct connection and efficient use of energy from solar, wind, or other native DC alternative energy sources;
- reduce energy consumption through the usage of LED lamps, sensors and control devices, up to a maximum level of 80%, as demonstrated through the preliminary results collected in the VUB Pilot Action;
- contribute to a more environmentally-sustainable energy policy, reducing CO_2 gas emission and leading to a global level in the fight against climate change.

The intelligent lighting infrastructure resulting from the adoption of the EDISON approach offers, in conclusion, increasing mobility, flexibility, reliability, visibility and opportunities to create comfortable, safe and sustainable environments.

REFERENCES

[1] IEC 60449, “Voltage bands for electrical installations of buildings”, Ed. 1.0, January 1973

[2] Edison Project Report, Deliverable D4.1.1 “EDISON hardware & software implementation and integration”, March 2013

[3] Edison Project Report, Deliverable D3.1.1 “EDISON hardware & software design”, December 2012

[4] LIN Overview. LIN Administration. Retrieved 28 October 2011.

[5] LIN Protocol Implementation Using PICmicro® MCUs, Authors: Dan Butler, Thomas Schmidt, Thorsten Waclawczyk, Microchip Technology Inc., 2002

[6] “20 20 by 2020 Europe's climate change opportunity”, Communication from the Commission to the European Parliament, the Council, the European Economic and Social Committee and the Committee of the Regions, COM(2008) 30 final, Brussels, January, 2008

[7] A. Caliri, L. Panei, “Potenzialità delle tecnologie di cattura e stoccaggio dell’anidride carbonica nell’industria italiana”, ENEA, 2012

[8] International Energy Agency (IEA), “CO2 Emissions from Fuel Combustion – Highlights”, Ed. 2012, November 2012

TAG – We're It

(the IEEE 802.24 Smart Grid TAG)

Tim Godfrey
EPRI
Overland Park, KS, USA
tim.godfrey@ieee.org

Clint Powell
PWC, LLC
Chandler, AZ, USA
cpowell@ieee.org

Benjamin Rolfe
Blind Creek Associates
Los Gatos, CA, USA
ben@blindcreek.com

Shigenobu Sasaki
Niigata University
Niigata, Japan
shinsasaki@ieee.org

***Abstract*—This paper provides an informative overview of the recently formed IEEE 802.24 Smart Grid Technical Advisory Group (TAG) and the role of IEEE 802 communications standards in Smart Grid. Communications are an integral part in the definition of the Smart Grid. Standards and recommendations developed by the IEEE 802 LAN/MAN Standards Committee (LMSC) and its Working Groups are a critical element in data communications for the smart grid.**

Keywords—IEEE 802; smart grid; communications; standards;

I. INTRODUCTION

The IEEE 802.24 Smart Grid TAG was formed to serve as a focal point for standards and information developed by the IEEE 802 LMSC as they pertain to their application in the Smart Grid. The IEEE 802 LMSC develops and maintains networking standards and recommended practices for local, metropolitan, and other area networks. IEEE 802 standards are widely used in many types of data communication networks applications. Included in IEEE 802 work groups active in the Smart Grid standards area are the 802.1, 802.3 Ethernet, 802.11 Wireless LAN, 802.15 Wireless PAN, and 802.16 Broadband Wireless Access, 802.18, 802.19, 802.20, 802.21, and 802.22 working groups.

In this paper we provide an overview of the work done in LMSC related to Smart Grid and grid modernization applications. The purpose and objectives of the 802.24 TAG, and a short overview of how 802 working groups are addressing Smart Grid communication requirements is presented.

II. BACKGROUND OF IEEE 802.24 TAG

The activities of many organizations such as SGIP, and the use of IEEE 802 developed/developing standards in grid modernization have seen rapid growth. In response to this growth IEEE 802 recognized that a focal point was needed between IEEE 802 and the various external entities. This recognition led to the establishment of the 802.24 TAG within the IEEE 802 LMSC.

A. Role/Charter of IEEE 802.24 TAG

The role of the IEEE 802.24 TAG is summarized by its charter, which is to:

- Act as a liaison and point of contact with regulatory agencies, industry organizations, other standards development organizations (SDO's), government agencies, IEEE societies, etc., for questions regarding the use of 802 standards in Smart Grid applications.
- Facilitate coordination and collaboration among 802 groups.
- Provide speakers as needed and available to present on 802 standards in Smart Grid applications.
- Develop white papers, guidelines, presentations and other documents that describe the application of 802 standards to Smart Grid applications.
- Act as a resource for understanding 802 standards for certification efforts by industry bodies.

B. Differences between a TAG and WG

Within the context of IEEE 802 LMSC the TAG assists other working groups within the IEEE 802 LMSC, or the IEEE 802 LMSC (executive committee) directly.

The key difference between a TAG and a Working Group is that a TAG does not develop standards. A TAG has voting members, and follows the rules for voting membership as in the whole of IEEE 802. Votes or ballots may be conducted in a TAG to approve documents and for other procedural matters.

III. CURRENT IEEE 802 STANDARDS RELATED TO SMART GRID

There are several IEEE 802 standards related to Smart Grid. IEEE 802 standards having particular application to the Smart Grid, which will be covered below include: 802.3, 802.11, 802.15, 802.16, and 802.22. Fig. 1 shows how some of these standards apply to the Smart Grid space.

978-1-4799-0354-2/13/$31.00 ©2013 IEEE

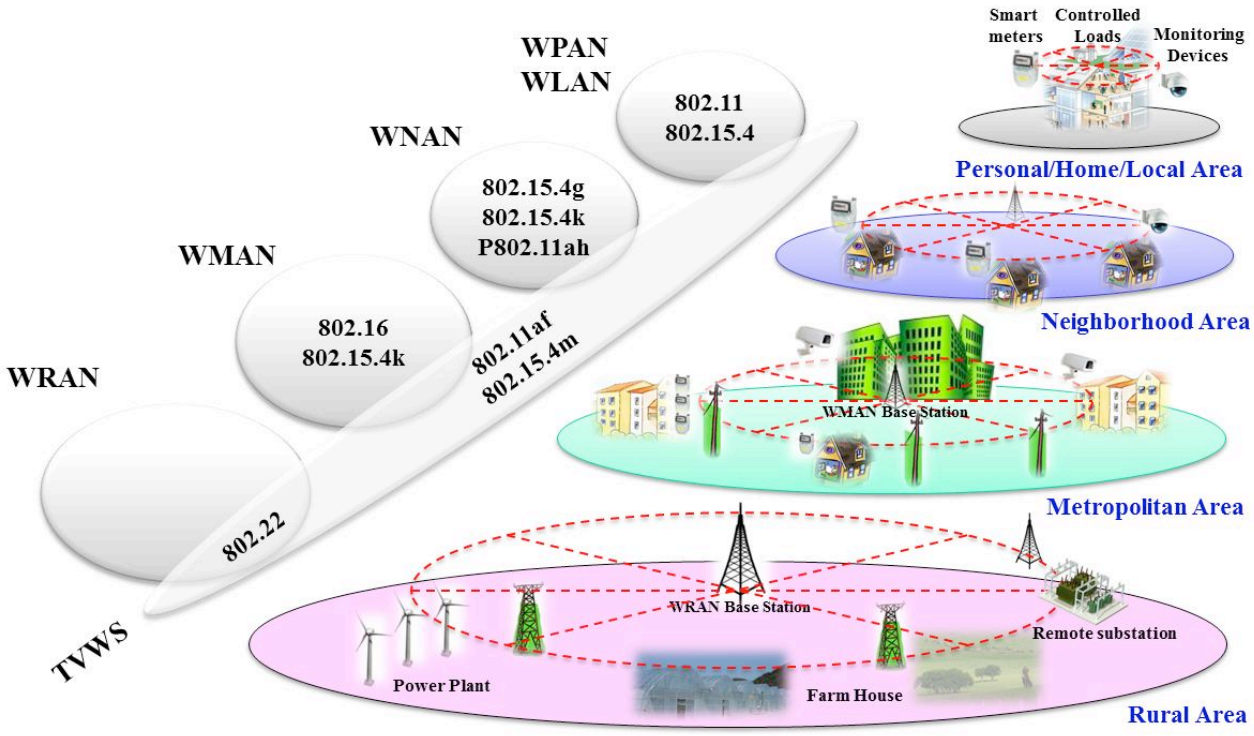

Fig. 1. Example Smart Grid Related IEEE 802 Wireless Standards Activities

A. *IEEE 802.3*

IEEE 802.3 develops standards for Ethernet based wireline networks. This standard defines Ethernet local area, access and metropolitan area networks. Ethernet is specified at selected speeds of operation; and uses a common media access control (MAC) specification and management information base (MIB). The Carrier Sense Multiple Access with Collision Detection (CSMA/CD) MAC protocol specifies shared medium (half duplex) operation, as well as full duplex operation. Speed specific Media Independent Interfaces (MIIs) provide an architectural and optional implementation interface to selected Physical Layer entities (PHY). The Physical Layer encodes frames for transmission and decodes received frames with the modulation specified for the speed of operation, transmission medium, and supported link length. Other specified capabilities include: control and management protocols, and the provision of power over selected twisted pair PHY types.

Ethernet is widely used in the current grid. Ethernet is used in enterprise and home networks for computer, equipment, and server connection. It is used in industrial control, manufacturing, and other special applications. It is pervasive in data centers, widely deployed in metropolitian area networks, and with adaptations in wide area networks. It is a common back haul technology used with wireless communications technologies. It has similar applications in Smart Grid.

IEEE 802.3 is specified independent of its MAC client. Typical implementations use EtherType identified data via an 802.1 MAC client, and TCP/IP for OSI layers 3 and 4.

Interoperability with legacy equipment is evaluated with all enhancements. Some proposals are rejected by the working group to avoid such incompatibility. IEEE 802.1 bridges (switches) allow evolution rather than forklift upgrade of equipment (e.g., with 10 Mb/s through 1000 Mb/s twisted pair port types, an end station may be upgraded independent of the switch)

The Ethernet frame format has remained consistent for decades. Maximum frame size has increased slightly to support the addition of headers and trailers of higher layer protocols. A circa 1985 10BASE5 connected station can be switched onto a 100GBASE- link via 802.1 bridging. Autonegotiation has allowed plug and play between the most common Ethernet port types (10BASE-T, 100BASE-TX and 1000BASE-T).

Ethernet currently defines three frame sizes, the basic 1500 byte information field, slightly larger to allow IEEE Std 802.1Q Virtual LAN (VLAN) tagging, and 2000 bytes to allow other enveloping protocols e.g., (IEEE Std 802.1AE MAC Security). While legacy equipment may not be able to be upgraded to use VLAN or MACSec, it can still interoperate because the basic information size remains 1500 bytes. Because of Ethernet's pervasive use, newer LAN types have been designed to be compatible with Ethernet (Wi-Fi, PLC, etc.) For example IEEE Std 802.11 was specified recognizing Ethernet would be used to interconnect access points. This Ethernet like behavior allows a new LAN type to quickly merge into IEEE Std 802.1 bridged networks. The independence of higher layer protocols like TCP/IP similarly allows interoperability with different network types.

B. *IEEE 802.11*

IEEE 802.11 develops standards for wireless local area networks (Wireless LAN). The scope of this standard is to

define one medium access control (MAC) and several physical layer (PHY) specifications for wireless connectivity for fixed, portable, and moving stations (STAs) within a local area. The PHY and MAC layers developed by IEEE 802.11 serve as the foundation for Wi-Fi. An example Wi-Fi network, in the context of the Smart Grid, is shown in Fig. 2.

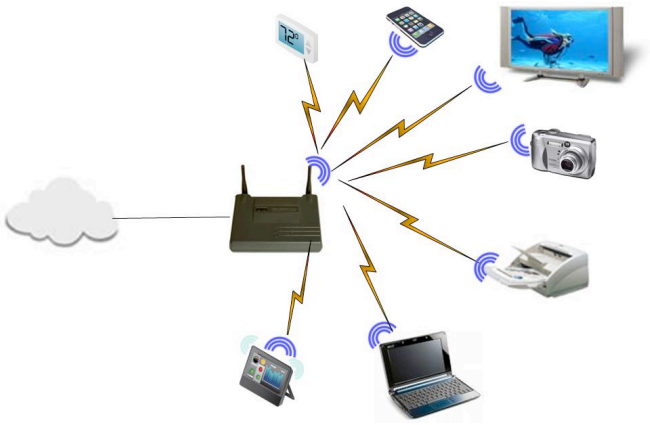

Fig. 2. Example Wi-Fi Network

IEEE 802.11 defines the protocol and compatible interconnection of data communication equipment via radio in a local area network (LAN) using the carrier sense multiple access protocol with collision avoidance (CSMA/CA) medium sharing mechanism. The medium access control (MAC) supports operation under control of an access point as well as between independent stations. The protocol includes authentication, association, and reassociation services, an optional encryption/decryption procedure, power management to reduce power consumption in mobile stations, and a point coordination function for time bounded transfer of data.

The IEEE 802.11af amendment defines 802.11 operation in the TV White Space (TVWS) bands. This amendment includes PHY changes to support the VHF and UHF frequency bands, as well as MAC changes to support the special rules established by the FCC (and other regulatory bodies) for devices operating in these bands. To allow sharing with existing broadcasters and wireless microphone users, 802.11af devices must comply with procedures for geo-location and database access, as well as cognitive radio sharing protocols. These are substantially different from the rules for "traditional" unlicensed bands such as 2.4 GHz.

TVWS bands are interesting to utilities for several reasons. First, there is a shortage of broadband spectrum for utility use. Many utilities own VHF and UHF spectrum, but it is in narrow channels designed for voice communications. TV channels are 6 MHz wide, and can support date rates into the Mbps, as opposed to the low Kbps rates achieved with voice channels. Another positive aspect of TVWS is the excellent propagation of VHF and UHF frequencies, compared to the alternative bands above 2 GHz.

There are also downsides for utility use of TVWS. There are no available TV channels in many metropolitan areas, so TVWS may not be a viable option in many areas. There are also antenna height and power restrictions. Despite the use of cognitive radio techniques, it is still shared spectrum and there is no guarantee of exclusive use of any channel. However, TVWS holds the promise to serve some applications in some locations, as one of many options used for utility wireless networks.

P802.11ah is a current project in 802.11 to modify the PHY and MAC layers to support operation of 802.11 in the sub-GHz licensed exempt bands. The licensed exempt sub-GHz band is widely used for metering and advanced infrastructure applications, providing favorable propagation characteristics in outdoor, non-line of sight environments. With 802.11ah, the range of a single link may be extended above 1km.

Many sub-GHz unlicensed bands provide limited bandwidth. 802.11ah addresses these bands by defining operating modes with narrower bandwidth channelization than current 802.11 OFDM PHYs, occupying from 1 to 16 MHz per channel, with correspondingly lower data rates, reducing the channel bandwidth required. Combined with the capability to bond non-contiguous channels to aggregate capacity, this allows use of spectrum that currently cannot be used by 802.11 systems in a standardized way. The P802.11ah amendment includes MAC enhancements intended to provide efficient use of the limited bandwidth available below 1 GHz and support further range enhancement techniques.

C. IEEE 802.15

IEEE 802.15 comprises a family of wireless standards and recommended practices developed to address a wide variety of applications, from very short range, low power personal area networking, very high data rate short range connectivity, and low rate, low power ubiquitous connectivity.

IEEE 802.15.4 defines the PHY and MAC layer specifications for low-rate wireless connectivity. PHY layer specifications have been developed to address a wide variety of operating environments and applications, including PHY specifications with characteristics developed specifically to address applications in Smart Grid and grid modernization. The 802.15.4 MAC has evolved as a simple core functionality that enables interoperability, and a number of optional feature sets that address more specialized applications. All 802.15.4 standards use the same core 802.15.4 MAC layer and may or may not utilize the optional features.

The MAC architecture supports all network architectures typically applied to Smart Grid (HAN and NAN), including single hop and multi-hop topologies.

IEEE 802.15.4 is used by industry alliances and other SDOs to develop application focused interoperability standards in applications including industrial control, consumer devices, home area networking (HAN), neighborhood area networking (NAN), machine to machine (M2M), RFID, critical infrastructure monitoring and Smart Grid. Examples of industry alliances using 802.15.4 include the ZigBee Alliance, ISA-100, and the Wi-SUN Alliance. Other SDOs that have developed standards based on 802.15.4 include IETF, ETSI and TIA.

IEEE 802.15.4 serves as the foundation for ZigBee (SEP 1 and SEP 2), 6LowPAN and Wi-SUN specifications, which are

widely used in the home area networking (HAN) and neighborhood area networking (NAN) spaces within the Smart Grid space. The ZigBee Smart Energy Profile 1 (SEP1) for HANs, built on top of the IEEE 802.15.4 PHY and MAC, continues to be adopted by utilities around the globe. The ZigBee Smart Energy Profile 2 (SEP2), for HANs, is also built on top of the IEEE 802.15.4 PHY and MAC. The SEP2 profile, also for HANs, completed its development and was ratified in April this year. The main differences between SEP1 and SEP2 are the support of IPv6 and increased security support. As a result of the profile being able to run over IPv6 the Consortium for Smart Energy Profile 2 Interoperability (CSEP) was formed to ensure interoperability of products employing SEP 2. The founding members of CSEP are the ZigBee, Wi-Fi, and HomePlug Alliances. CSEP is working hard towards completing and ratifying an SEP2 test plan, that will be used for certification of devices, within the next few months. In addition to this work is under way in IEEE P2030.5 to adopt SEP2 as an IEEE Standard.

Examples of HAN and NAN networks are shown in Fig. 3 and Fig. 4 respectively.

Fig. 3. Example HAN

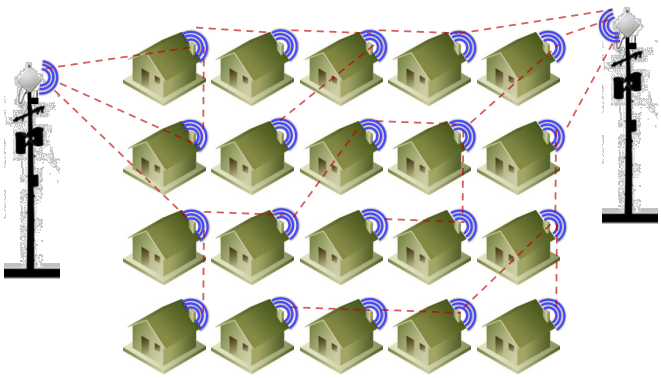

Fig. 4. Example NAN

The recent IEEE 802.15.4g and 802.15.4e amendments define additions to IEEE 802.15.4's PHY and MAC that were specifically developed to address NAN networks used in meter to meter and meter to collection point networks, supporting both mesh and non-mesh topologies. IEEE 802.15.4g defines multiple signaling schemes (modulation and data rates) for use in many bands around the world, both global and regional. This allows for deployments to be tailored to many system parameters such as size of the coverage area, capacity and the terrain/environments. IEEE 802.15.4g defines a common signaling mode (CSM) and also supports backwards compatibility to existing deployed solutions. IEEE 802.15.4g's support of multiple PHYs in tandem with the CSM gives it the ability to addresses varying deployments (size, configuration, etc.), allow for forward migration of existing systems, and enables future growth. IEEE 802.15.4e adds multiple MAC enhancements applicable to low power operation, distributed network architectures, and support of frequency hopping, which when combined with the additions in 802.15.4g enable robust communications in the presence of the interference and propagation impairments that are encountered in the NAN environment.

Due to the flexibility and ability of the standard, from the original 802.15.4 (2003), the 802.15.4 (2006) revision and the 802.15.4 (2009 and 2011) roll ups, 802.15.4 continues to evolve. Currently in development is IEEE 802.15.4m. This standard is defining the use of the TVWS, regionally around the globe for 802.15.4, which can then be utilized in Smart Grid applications such a NAN and field area networks (FAN). The IEEE 802.15.4m amendment is likely to be approved in 2014.

Current and future revision work will enable improved coordination with other SDOs and entities that depend on 802.15.4. Emerging activities in the 802.15 working group which are applicable to Smart Grid include study of potential enhancements for layer 2 routing, and a recommended practice for security key management protocols over 802.15 standards.

D. IEEE 802.16

IEEE 802.16 develops standards for wireless metropolitan area networks (Wireless MAN), typically operating in licensed frequency bands.

The IEEE 802.16 standard is the basis for WiMAX. The 802.16 standard has progressed through a series of amendments since the first standard was completed in 2001. The most recent revisions of the base standard are 802.16-2012, and 802.16.1a-2012. After the completion of the 802.16m amendment in 2011, the new Advanced Air Interface that it defined was split off into a separate standards document, designated 802.16.1. The base standard, 802.16, contains the amendments 802.16d (commonly referred to as fixed WiMAX) and 802.16e (commonly known as mobile WiMAX). Commercial WiMAX products offered for grid applications are generally based on the mobile WiMAX feature set, although some fixed WiMAX products are also available.

IEEE 802.16 networks, as a member of the IEEE 802 family of standards, follow an architecture that is shared by other widely used standards such as IEEE 802.3 (Ethernet) and IEEE 802.11 (Wi-Fi). This architecture makes WiMAX easy to integrate into a utility enterprise IT infrastructure. The flat Layer 2 connectivity of 802.16 supports non-IP protocols such as IEC 61850 GOOSE messages, as well as enabling simultaneous support of IPv6 and IPv4 over the network.

Two amendments recently completed by the IEEE 802.16 working group provide additional support for the specific requirements of the Smart Grid Field Area Network: 802.16n and 802.16.1a (GRIDMAN) and 802.16p and 802.16.1b (M2M). These amendments provide complementary enhancements to 802.16 and 802.16.1. They are designed to address unique requirements of Smart Grid applications running on Field Area Networks. The GRIDMAN amendments (802.16n and 802.16.1a) define new capabilities that enable network devices to dynamically change their mode or role in case of failure or disruption. One common failure scenario is the loss of a base station's backhaul connection as shown in Fig. 5 and Fig. 6.

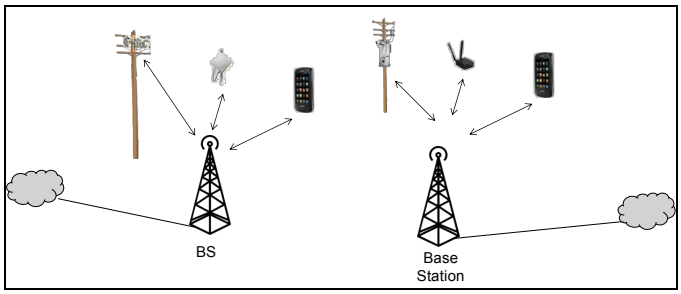

Fig. 5. Normal Operation

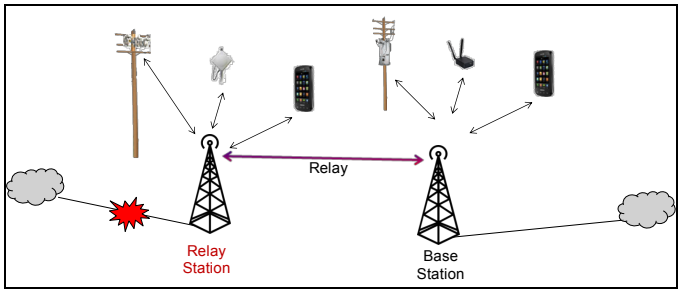

Fig. 6. Backhaul fails - affected Base Station becomes Relay Station

If a base station loses its infrastructure connection (backhaul), it can become a relay, and relay data through another base station. Another use case addressed by the 802.16 GRIDMAN amendments is enabling terminal devices to serve as relays to extend range at cell edge or fill in the coverage hole left by a failed base station. The GRIDMAN amendments also add the ability for the relay node to simultaneously originate and terminate traffic from locally connected devices.

The enabling of dynamic roles for network components provides resilience against failure. In a Smart Grid deployment, not all devices need to implement GRIDMAN enhancements. As part of network design, a subset of devices in specific locations will be identified to provide maximum reliability benefit from the mode-changing capability. Devices supporting HR or High Reliability (802.16n / 802.16.1a) devices can operate on the same network at the same time as standard devices.

The M2M amendments (802.16p and 802.16.1b) provide enhancements to better support Machine to Machine applications. Example applications are smart metering and distribution automation. In an urban area, thousands of meters and other devices could be in the range of a base station. The M2M amendments add support for addressing and managing larger numbers of devices connecting to a single base station. It also provides improvements in low-power longer sleep modes to enable very low duty cycle operation of grid-connected devices, and enable the possibility of battery-operated sensor devices. Further enhancements to network entry support orderly and controlled connection of a large number of devices to the network. Additionally, the MAC protocol is enhanced to better support small burst transmissions with low latency. Finally, the amendment provides optimizations and simplifications due to the expected low mobility of grid connected devices.

The combination of enhanced capabilities provided by the GRIDMAN and M2M amendments, built on the established WiMAX ecosystem, provide additional support to enhance Smart Grid FANs and applications. The new capabilities defined in GRIDMAN and M2M can be added incrementally to operational WiMAX networks. These tailored utility-centric solutions are not yet planned by operators of cellular networks, where the business focus is on the retail mobile phone customer.

E. IEEE 802.22

IEEE 802.22 has developed a cognitive radio based wireless regional area networks (WRAN) standard operating in the VHF/UHF TV broadcast bands between 54 MHz and 862 MHz (a.k.a. TV white space). Due to the primary use, some of these bands may not be utilized at a specific location. The latest revision of the standard is IEEE 802.22-2011. This standard specifies the air interface, including the cognitive medium access control layer (MAC) and physical layer (PHY), of point-to-multipoint wireless regional area networks comprised of a professional fixed base station with fixed and portable user terminals.

IEEE 802.22 provides connectivity in a rural area, which enables wide area situation awareness. 802.22 based networks not only provide spectrum information through sensing, but also radio parameters through the MIBs and management plane interfaces. An example of WRAN is shown in Fig. 7.

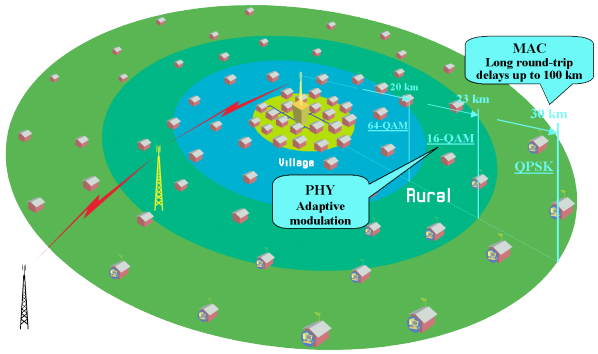

Fig. 7. WRAN Example [4]

Key features of IEEE 802.22 are:

1. Support for data rates up to 22.7 Mbps by using OFDM with 2048 FFT size and coded 64-QAM.

2. OFDMA/TDD frame structure that enables long-range communication up to 30 km distance.

3. Coexistence methods that enable the current standard to operate simultaneously in the same area with other networks. TVWS database, spectrum sensing, self-coexistence and coexistence beacon protocol (CBP) are used for coexistence between other systems and the same 802.22 systems.

The IEEE 802.22 WG is currently working on the P802.22b amendment to the IEEE 802.22-2011 standard, which specifies support for enhanced broadband services and monitoring applications. The standard supports aggregate data rates greater than the maximum data rate supported by the IEEE Std. 802.22-2011. This standard defines new classes of 802.22 devices to address these applications and supports more than 512 devices in a network. This IEEE P802.22b standard will further enhance 802.22 capabilities of cognitive Smart Grid and cognitive machine-to-machine applications. Other potential applications are Regional Area Smart Grid – Metering, Distribution Automation (DA), Volt-VAR management, Conservation Voltage Reduction (CVR), Sensor monitoring, management and control, other transmission control (e.g. synchrophaser), and AMI / AMR backhaul.

IEEE 802.22 covers large regional area and may be used as low cost backhaul to control and monitor hundreds of Smart Grid devices, and IEEE 802.22b further expands the coverage of 802.22 by creating high capability and low capability customer premise equipment (CPE) to allow for communication with thousands of Smart Grid devices. IEEE 802.22b will also provide communications support for demand response signaling. The IEEE 802.22b amendment is likely to be approved in 2014.

IV. Activities of the IEEE 802.24 TAG

A. SGIP Catalog of Standards (CoS) Standards Information Form (SIF) Contributions

The SGIP, as part of its Charter obligations, produces and maintains a "Catalog of Standards" (CoS). The CoS is a compendium of standards and practices considered to be relevant for the development and deployment of a robust and interoperable Smart Grid. In order to be considered for inclusion into the CoS the SGIP has defined criteria that standards, practices, and guides must meet. Included in this is the filling out of the Standards Information Form or Template (SIF), which contains a set of summary attributes of the standard being submitted for consideration.

The SIF is divided into 2 major sections. The 1st section of the SIF covers the Use and Application of the Standard, while the 2nd section of the SIF covers the Functional Description of the Standard. All together there are more than 140 attributes/questions that are used in assessing the standard. The IEEE 802.24 TAG is in process of filling out SIFs for all relevant 802 standards. To date it has helped to complete SIFs for IEEE 802.3, IEEE 802.11, IEEE 802.15, and IEEE 802.22.

B. Inputs to NIST

The IEEE 802.24 TAG is currently working on updates to the 802 portion of the NIST wireless characteristics matrix.

C. OtherActivities

The IEEE 802.24 TAG has appointed liaisons to both IEEE P2030.5 and SGIP, with liaisons to other organizations sure to follow. These individual liaisons will help ensure that the IEEE 802.24 TAG is kept informed of the activities/status of the groups outside of IEEE 802.

In addition to the SGIP and NIST there are smart grid related activities going on in other SDOs with whom IEEE 802 has a collaborative relationship, such as Telecommunication Industry Association (TIA), European Telecommunications Standards Institute (ETSI), Internet Engineering Task Force (IETF), International Telecommunication Union (ITU), and others.

V. Conclusions - Future IEEE 802.24 TAG Efforts

The 802 family of standards supports standards based communication applicable to many elements of the modernized grid. Recent years has seen increased activity in many 802 working groups to address the specific needs of grid modernization and smart grid communications. The successful application of standards depends in part on availability of good information exchange between the SDO and potential users of the standard and the relevant industries.

The IEEE 802.24 TAG has been created to ensure quality information is available to the smart grid industry on 802 standards and how they may be applied and provide pertinent information to the 802 working groups developing standards so that the needs of the industry are better addressed. As such 802.24 provides a focal point both within 802 and between 802 and other organizations to enhance the development and promotion of standards based solutions in the Smart Grid. Work in IEEE 802.24 has only been going on for a few short months and it is already making an impact on the visibility and use of 802 standards in the Smart Grid standards area.

Moving forward, IEEE 802.24 will continue to provide information exchange between 802 and external organizations, providing timely information to help promote and apply 802 standards in grid modernization and support development of relevant standards within 802. The Priority Action Plan group 2 (PAP2) of the SGIP is currently working on the Guidelines for Assessing Wireless Standards for Smart Grid Applications. This is just one example of an area in which IEEE 802.24 will provide input and guidance.

The standards developed within IEEE 802 are only a piece of the entirety of IEEE standards development efforts related to the smart grid. There are many IEEE standards that are being applied to the Smart Grid efforts as shown below in Fig. 8. The Smart Grid efforts around the world are forging ahead by adding communications, networking, and control to the power grid. One thing that is crystal clear in the Smart Grid efforts is that a single technology will not be able to do everything across all domains.

ACKNOWLEDGMENT

The authors would like to thank the IEEE 802 LAN/MAN Standards Committee (Executive Committee) for recognizing the need for and approving the formation of the 802.24 TAG, and their continued support of its activities. The authors would also like to thank the 802 Working Groups for their continued support and contributions to the 802.24 TAG.

REFERENCES

[1] IEEE 802.24 TAG http://ieee802.org/24/.

[2] IEEE 802.24 Tutorial, doc: IEEE 802.24-12-0023-01-0000, Nov. 2012.

[3] IEEE 802 LMSC Policies and Procedures, v13 January 3, 2013. http://standards.ieee.org/about/sasb/audcom/pnp/LMSC.pdf.

[4] IEEE Std. 802.22™-2011, July 2011.

Wide Area Network (WAN)			NAN/FAN			Smart Meters	HAN, BAN, IAN		Technology Standards
Substation	Core/Metro Network/Backhaul Network		Substaion						
	Wireline	Wireless		Wireline	Wireless		Wireline	Wireless	
LAN IEEE 1815/IEC 61850 Several Options	IEEE 802.1 IEEE 802.3	IEEE 802.16d/e IEEE 802.20 IEEE 802.22	LAN IEEE 1815/IEC 61850 Several Options	IEEE 802.1 IEEE 802.3 IEEE 1901	IEEE 802.11 IEEE 802.15.4 IEEE 802.16	IEEE SC31 (1377, 1701, 1703, P1704)	IEEE 802.1 IEEE 802.3 IEEE 1901 IEEE 1901.2 IEEE P1905.1	IEEE 802.11 IEEE 802.15.4	

Fig. 8. Example IEEE Smart Grid Related Standards

A Nested Game-Based Optimization Framework for Electricity Retailers in the Smart Grid with Residential Users and PEVs

Yang Li, Yanzhi Wang, Shahin Nazarian, and Massoud Pedram
University of Southern California
Los Angeles, CA USA
{yli760, yanzhiwa, shahin, pedram}@usc.edu

***Abstract*—In the smart grid, real-time pricing policy is an important mechanism for incentivizing the consumers to dynamically change or shift their electricity consumption, thereby improving the reliability of the grid. Retailers are incorporated to the smart grid with distributed control mechanism in order to reduce the amount of communication overhead associated with the direction interaction between utility companies and consumers. The retailer procures electricity from both traditional and renewable energy sources, and sells it to its consumers. The consumers include residential users that can only consume power, and plug-in electric vehicles (PEVs) that can either consume power or supply power stored in its battery to the grid. In this work, a novel four-stage nested game model is proposed to model the interaction of the electricity retailer, utility companies, and consumers. The objective of the retailer is to maximize its overall profit as well as perform frequency regulation, whereas the goal of each consumer is to maximize a predefined utility function. In the game theoretic framework, the retailer should decide the amounts of electricity purchased from the renewable and traditional energy sources, respectively, as well as the real-time pricing scheme for its consumers. The consumers will react to the pricing mechanism and maximize their utility functions by adjusting the electricity demand. The optimal solution of the nested game is provided through: (i) finding the subgame perfect equilibrium (SPE) of all the consumers, and (ii) optimizing the retailer's action using the backward induction method. Experimental results demonstrate the effectiveness of the proposed game theoretic modeling and optimization framework.**

I. INTRODUCTION

With the increasing demand of energy worldwide, the design of future electricity systems has become a big concern [1]. Traditional power grids are usually utilized to deliver electricity from central generators to a large number of users [2]. In contrast, the recently proposed *smart grid* uses two-way flows of electricity and information to create an automated and distributed energy delivery network [2]. Smart grid takes advantage of the modern communication system to gather information from consumers and suppliers in order to improve efficiency, reliability, and sustainability of the power grid. This outstanding merit makes smart grid an ideal choice to gradually replace the energy inefficient traditional power grid. The improvement of energy efficiency in electricity infrastructure based on smart grid will alleviate the problem of energy deficiency faced by many countries all over the world [1].

Currently, there are many researches working on the modeling and application of smart grid in both industry and academia. Most of them focus on the management of smart grid and demand side optimization to enhance efficiency and reliability. Reference work [3], [4] proposed a centralized control optimization method to achieve the optimal energy efficiency. It provides important insights on how to efficiently match the energy supply of power grid and demand of consumers during peak and off-peak hours without wasting the generated energy. However, it may be difficult to realize the assumptions behind the centralized control method: (i) the smart grid central controller can directly control the energy usage of each consumer, and (ii) each consumer needs to provide their demand information to the energy provider in advance, which is especially difficult for the consumers with high mobility such as plug-in electric vehicles (PEVs). Therefore, a decentralized smart grid control framework is a proper candidate to overcome those shortcomings [5].

Decentralized/distributed control mechanism in the smart grid requires the utility companies to employ *day-ahead pricing* or *real-time pricing schemes* in order to incentivize the consumers to perform *demand side management* (DSM), e.g., shifting their loads from peak hours to off-peak hours. Both utility companies and energy users aim at maximizing their own profits or minimizing costs [5]. When day-ahead pricing is applied, the utility company announces the time-of-use dependent price signal over the next billing period (the next day), and the customers respond to the price signal by adjusting their load demand over the whole billing period [5]. When real-time pricing is applied, the utility company announces the relationship (usually a superlinear function) between the electricity price and the total load demand over the next time slot (typically a few minutes to one hour.) This pricing scheme fits very well for applications such as vehicle-to-grid (V2G) systems (e.g., [6]-[8]). Since the electricity price is dependent on the total load demand of all the users, game theory has been proposed as the analysis tool for the distributed users in the real-time pricing scenario [6], [11]. Consumers are usually modeled as rational players in a non-cooperative game and their actions are the load demand values. The Nash equilibrium among all the consumers is derived from the relationship between electricity price and total load demand.

Retailers are incorporated to the smart grid with distributed control mechanism in order to reduce the amount of computation and communication overheads associated with the direct interaction between utility companies and consumers. A retailer is an intermediary between the utility companies and consumers. In an electricity market, retailers procure electricity

978-1-4799-0354-2/13/$31.00 ©2013 IEEE

from various energy sources, including both renewable and non-renewable ones, and then sell the electricity to its customers [12]. Due to the intermittent nature of the electricity generated from renewable power sources and the fluctuation of power demand, the retailer needs to judiciously determine the amount of electricity they procure from different sources, in order to (i) increase the reliability of power supply, (ii) reduce the cost from purchasing electricity, and (iii) provide frequency regulation for the grid [6]. A Stackelberg game is adopted in [12] to model the interactions between the electricity retailer and consumers. The backward induction method, which is a standard solution method for Stackelberg games [13], is applied to derive the optimal amount of electricity purchased and the electricity price set by the retailer.

In this paper, we consider an extension over [12]. The proposed system model is comprised of both renewable and non-renewable (traditional) energy sources, a retailer, and a set of energy consumers. The retailer buys electricity from both energy sources and applies real-time pricing for the consumers. The consumers can be divided into two categories: residential users that can only consume power and PEVs that can either consume power or supply power stored in its battery to the grid. We present a four-stage nested game model for the interaction of the electricity retailer, utility companies, and consumers. The objective of the retailer is to maximize its overall profit as well as perform frequency regulation. Here the PEVs' battery can serve as regulation unit through charging and discharging process which is auxiliary to the original frequency regulation mechanism built inside retailer's power grid. If the number of PEVs is relatively large, retailer will benefit from this in the sense that it can avoid using high cost frequency regulation facilities such as turbine speed governors. Meanwhile, the goal of each consumer is to maximize a predefined utility function. The retailer is involved in the first three steps of decision making in the nested game. In Step I and II, the retailer decides the amounts of electricity purchased from the renewable power source and the traditional power source, respectively. In Step III, the retailer provides the optimal real-time pricing scheme to its consumers to specify the relationship between energy price and total load demand, based on all the previous decisions. In the last stage (Stage IV), all the consumers will react to the pricing mechanism and maximize their utility functions by adjusting the electricity demand. We propose the optimal solution of the nested game for both the retailer and the consumers. First, we find the subgame perfect equilibrium (SPE) for all the consumers (i.e., residential users and PEVs) in Stage IV. Then we optimize the retailer's action in the first three stages using the backward induction method. We use the dynamic programming method to reduce the computation and storage complexity during backward induction.

The rest of this paper is organized as follows. The proposed system model is described in Section II. The nested game formulation and its analysis are discussed in Section III. Section IV provides the backward induction-based optimization procedure of the nested game. Simulation results are presented in Section V, and we conclude in Section VI.

II. System Model

In this section, we present the system model. Consider a smart grid system with both renewable and non-renewable utility companies, various consumers, and an electricity retailer. The retailer plays an important role in the system. It acquires electricity from the utility companies at certain price levels and supplies its customers (consumers). The retailer provides the real-time pricing signal to specify the relationship between the electricity price and the total load demand over the next time slot. In reality, a two-way communication infrastructure built in the smart grid can help the retailer to announce such real-time information to the consumers. There are two categories of consumers in the smart grid system model. One kind is the residential users that can only consume power. The other kind is PEVs that have a built-in battery as the energy storage. They can not only buy electricity from the retailer to charge the battery but also sell energy to the retailer to get certain amount of profit when they have excessive stored energy. All the consumers will react to the pricing signal and adjust their power demands from the grid.

A. Energy Sources (Utility Companies)

In our model, the retailer has two main sources to purchase electricity through power grid. One is from the renewable power sources such as wind or solar power generation facilities. The other is from the traditional power sources such as coal-fired power stations. From the perspective of cost per unit electricity, the renewable power source is a good choice for the retailer to lower down the cost of purchasing electricity. However, in terms of the reliability of power supply, the traditional power source is better. The reason is that the renewable power (e.g., wind or solar) generations are difficult to maintain a high quaility of continuous and steady power supply since they largely depend on the weather condition and other factors. This creates a reliabity issue when the retailer tries to buy electricity from such energy sources.

In the proposed model, let $P_{\mathbf{R}}$ denote the *reliability factor* of the renewable energy source, i.e., the probability that the renewable power supply purchased by the retailer turns out to be reliable, where the subscript $\mathbf{R}$ represents for "renewable". Let $D^{\mathbf{R}}_{0,buy}$ and $D^{\mathbf{R}}_{0,actual}$ denote the amounts of renewable energy purchased and actually received, respectively, by the retailer. $D^{\mathbf{R}}_{0,actual}$ is a random variable, and we have the following relationship:

$$D^{\mathbf{R}}_{0,actual} = \begin{cases} D^{\mathbf{R}}_{0,buy} & \text{with probability } P_{\mathbf{R}} \\ 0 & \text{with probability } 1 - P_{\mathbf{R}} \end{cases} \quad (1)$$

On the other hand, the amount of purchased (and received) energy from the traditional energy source is denoted by $D^{\mathbf{NR}}_{0,actual}$, where the subscript $\mathbf{NR}$ represents for "non-renewable". Then the total amount of energy D_0 received by the retailer from the power sources is given by:

$$D_0 = D^{\mathbf{R}}_{0,actual} + D^{\mathbf{NR}}_{0,actual} \quad (2)$$

Moreover, let $price^{\mathbf{R}}$ and $price^{\mathbf{NR}}$ denote the unit energy prices from the renewable and traditional power sources, respectively, and obviously $price^{\mathbf{R}} < price^{\mathbf{NR}}$. The total energy cost that the retailer pays for purchasing energy is:

$$price^{\mathbf{R}} \cdot D_{0,buy}^{\mathbf{R}} + price^{\mathbf{NR}} \cdot D_{0,actual}^{\mathbf{NR}} \quad (3)$$

A desirable plan for the retailer is to purchase a portion of electricity from renewable resources and the rest from traditional power plants. With a proper tradeoff of energy cost and reliability, the retailer could enhance its overall profit.

B. Consumer Model and Real-Time Pricing

Let N denote the number of consumers associated with the retailer. Let d_i denote the energy demand of user i in the time slot of interest. If $d_i \geq 0$, the i^{th} user is consuming energy purchased from the retailer. If $d_i < 0$, the i^{th} user is selling energy to the retailer and this negative energy demand only applies to PEVs. Let D represents the total demand of all the users, and then we have:

$$D = \sum_{i=1}^{N} d_i \quad (4)$$

Furthermore, let D_{neg} represent the sum of all the negative energy demands, and we have:

$$D_{neg} = \sum_{i=1}^{N} d_i \, \mathbf{I}[d_i < 0] \quad (5)$$

where $\mathbf{I}[x]$ is an indicator function that equals to 1 if the Boolean variable x is true, and equals to 0 otherwise.

The retailer serves a group of consumers and determines the pricing policy for the consumers to purchase or sell electricity. It should balance the energy demand (from the energy sources) and supply (to the consumers) in order to perform proper frequency regulation [6]. Balancing demand and supply is a difficult task for the retailer because of the fluctuation in load demands, especially for PEVs with high mobility. The real-time pricing policy is adopted by the retailer to achieve this goal. The basic principle is that if there is an increase or decrease in the overall energy consumption with respect to the total amount of energy procured by the retailer, it will adjust the electricity prices to encourage users to use less or more electricity, respectively.

Given these reasons and principles, the real-time pricing policy is described as follows. Let p_c and p_d denote the unit energy prices for the consumer to purchase energy from or sell energy to the retailer, respectively. Then the relationship between the prices p_c, p_d and the total load demand D can be mathematically described as follows:

$$p_c(D) = \beta(D - D_0) + p_B \quad (6)$$

$$p_d(D) = \gamma(D - D_0) + p_B \quad (7)$$

where β and γ are coefficients determined by the retailer. p_B represents the base price for the consumer to purchase and sell electricity when $D = D_0$. As we can see from (6) and (7), if the total load demand D is higher than D_0, p_c will be increased to discourage the users from consuming more energy. Moreover, p_d will also be increased to attract more users (PEVs) to discharge their batteries and contribute to the energy supply of retailer. On the other hand, if the current total demand D is less than D_0, a preferable pricing scheme is to encourage consumers to buy more electricity and sell less. Therefore, the price of buying electricity p_c will be lower and the benefit of selling electricity p_d will also be less.

At the demand side, each residential user cares about two aspects. One is to minimize the cost when the user purchases electricity from the retailer. The other is to maximize its own satisfaction level. As a combination of these two effects, each i^{th} user (if it is a residential user) maximizes a utility function with the following form:

$$UR_i(d_i, p_c) = -a_i d_i^2 + e_i d_i - p_c(d_i, d_{-i}) \cdot d_i \quad (8)$$

where d_{-i} denotes the energy demand profile of the other users than user i. We know that $p_c(d_i, d_{-i})$ is a function of both d_i and d_{-i} because it is an increasing function of the total demand D as shown in (6). Moreover, a_i and e_i in (8) are positive coefficients. a_i and e_i may be different for different residential users. This type of utility function is a concave function and has a most desirable d_i value to get the maximum payoff when d_{-i} is given. The most desirable value of d_i is determined by a_i, e_i and $p_c(d_i, d_{-i})$. Because residential users can only buy electricity from the retailer, $d_i \geq 0$ is a constraint during the utility optimization process of residential users.

For the PEVs with a battery storage bank, they can buy electricity from the retailer at price p_c as well as sell its electricity to the retailer at price p_d to gain some profit. We use the following type of utility functions for the PEVs:

$$UEV_i(d_i, p) = \varepsilon_i \sqrt{S_{ini,i} + d_i} - p \cdot d_i \quad (9)$$

where

$$p = \begin{cases} p_c(d_i, d_{-i}) & (d_i \geq 0) \\ p_d(d_i, d_{-i}) & (d_i < 0) \end{cases} \quad (10)$$

where ε_i ($\varepsilon_i > 0$) is a coefficient for the utility function of the i^{th} user (if it is a PEV.) $S_{ini,i}$ is the amount of energy initially stored in the PEV's battery. Clearly, there are different initial energy levels among all the PEVs. The PEVs want to maintain enough charge in the battery and sell the excessive amount of electricity to the retailer in order to gain some profit. The first term of (9) shows that each PEV intends to maximize its final energy level stored in the battery after charging/discharging, whereas the second term of (9) shows that each PEV also wants to minimize the electricity cost for charging or maximize the revenue from discharging the battery. Each PEV needs to determine whether to buy or sell electricity based on the real-time pricing policy, the initial energy level, and also other users, in order to maximize its own utility.

C. Retailer's Utility Function

For the retailer, the goal is to maximize its overall profit as well as perform frequency regulation through matching the power supply and demand. Therefore, the retailer needs to minimize the cost of buying electricity from power grid and the mismatch between D and D_0, as well as maximize the revenue of selling electricity to its users. According to the above objectives, we formulate its utility (payoff) function as follows:

$$U_{retailer} = \left(D - D_{neg}\right) \cdot p_c(D) + D_{neg} \cdot p_d(D) - D_{0,actual}^{\mathbf{NR}} \cdot price^{\mathbf{NR}} - D_{0,buy}^{\mathbf{R}} \cdot price^{\mathbf{R}} - \theta \cdot (D - D_0)^2 \quad (11)$$

In (11), $\left(D - D_{neg}\right) \cdot p_c(D) + D_{neg} \cdot p_d(D)$ is the sum of the retailer's revenue from selling electricity to the users (and purchasing electricity from some users.) $D_{0,actual}^{\mathbf{NR}} \cdot price^{\mathbf{NR}}$ and $D_{0,buy}^{\mathbf{R}} \cdot price^{\mathbf{R}}$ represent the cost of purchasing electricity from traditional power sources and renewable power sources, respectively. $|D - D_0|$ is the mismatch between total energy demand from all users and the total amount of electricity energy purchased by the retailer. In (11), $\theta \cdot (D - D_0)^2$ is used in the formulation where θ $(\theta > 0)$ is a constant, and the retailer will get a higher payoff by minimizing this term.

III. NESTED GAME FORMULATION AND ANALYSIS

Based on the system model, we present a four-stage nested game based formulation to model the hierarchical decision making process and the interactions between the retailer and various users. The proposed nested game formulation is illustrated in Fig. 1.

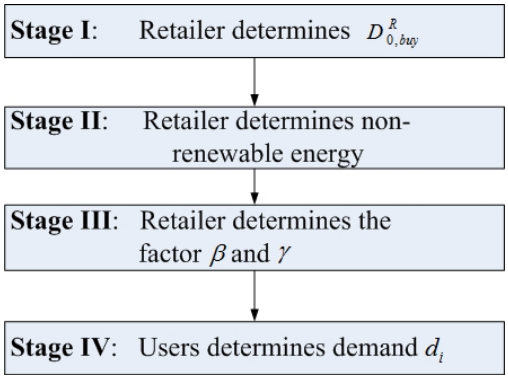

Fig. 1. Four-stage nested game based formulation for the interaction system.

As shown in Fig. 1, we provide an overview of the four-stage nested game as follows:

- Stage I: The retailer determines the amount of electricity to purchase from renewable energy sources, i.e. $D_{0,buy}^{\mathbf{R}}$, based on the reliability factor $P_{\mathbf{R}}$.
- Stage II: The retailer determines the amount of electricity to purchase from traditional energy sources, $D_{0,actual}^{\mathbf{NR}}$, based on the amount of electricity $D_{0,actual}^{\mathbf{R}}$ acquired from the renewable sources in Stage I. The total amount of purchased electricity D_0 is also decided in this stage since $D_0 = D_{0,actual}^{\mathbf{R}} + D_{0,actual}^{\mathbf{NR}}$.
- Stage III: The retailer provides a pricing mechanism by determining the factors β and γ based on D_0. The goal in this stage is to maximize the retailer's profit as well as minimize the mismatch between D_0 and D.
- Stage IV: Based on the pricing mechanism offered by the retailer in Stage III, each user i (residential user or PEV) will maxmize its own utility function by determining its demand d_i with awareness of the pricing mechanism and the other users. This forms a non-cooperative subgame of the nested game. We prove the existence and uniqueness of Nash equilibrium in this game, which is the SPE of the overall nested game.

Backward induction [13] encapsulates the sequential rationality of decision making and is used as a powerful technique to obtain the best strategies for the players in each stage of the nested game (or a sequential game in general.) It reflects the sequential dependencies of decisions in each stage of the nested game. Based on the backward induction principle, we first find the SPE in Stage IV among all the residential users and PEVs given the retailer's pricing mechanism. Then we move backward to analyze and optimize the retailer's strategies in the first three stages. We will discuss the optimization procedure in detail as follow.

A. Game Theoretic Optimization in Stage IV

In this stage, each user will adjust its demand d_i according to the β and γ values (provided by the retailer in Stage III) and the awareness of other users. As a self-interest individual, each i^{th} user wants to maximize its own utility by finding a proper value d_i. The total demand D, which depends on the energy demands of all users, will also affect p_c and p_d through (6) and (7). Hence, the interaction of users forms a normal-form game where all users take action simultaneously. We name this game the *Energy Demand Optimization* (EDO) game. The EDO game is a subgame of the overall four-stage nested game.

The Nash equilibrium of a normal-form game is the optimal strategy profile for all the players in the sense that no player can find a better strategy (i.e., the value of d_i) if he deviates from the current strategy unilaterally. In other words, no player (residential user or PEV) will have incentive to leave this strategy in the Nash equilibrium. Hence, Nash equilibrium is of particular interest to a non-cooperative normal-form game. The Nash equilibrium of the EDO game is the SPE of the four-stage nested game. Next, we prove the existence and uniqueness of the Nash equilibrium in the EDO game if $\beta = \gamma$, i.e., the prices $p_c(D)$ and $p_d(D)$ are equal to each other. The unique Nash equilibrium can be found using standard convex optimization technique [15], as described in Algorithm 1. On the other hand, Algorithm 1 will find the approximate best response for each user in the more general case of $\beta \neq \gamma$.

Theorem I: The Nash equilibrium of the EDO game exists and is unique if $\beta = \gamma$.

Proof: According to the utility function of each consumer in (8) and (9), we are essentially trying to maximize a strictly concave utility function for each player on a closed convex set. Therefore, from the first and third theorem in [14], the existence and uniqueness of the Nash equilibrium is proved. ■

Algorithm 1: Find the SPE solution for the subgame in Stage IV.

Given an initial value for the demand d_i of each user *i*

Do the following procedure iteratively:

For each $1 \le i \le N$:

(1) Perform optimization for consumer *i* to find the optimal d_i value assuming that the power demands of the other users are given. We optimize Eqn. (8) for residential users or Eqn. (9) or PEVs.

(2) Update the d_i value for consumer *i*.

End

Until the solution converges.

Since the factors β and γ are determined by the retailer, for different β and γ values, we can get different SPE solutions in Stage IV by applying Algorithm 1. We define two matrices **Total_Demand** and **Total_Demand_Neg**. Each entry $\mathbf{Total\_Demand}(\beta, \gamma)$ denotes the total demand D of the users obtained from the SPE with given β and γ values provided by the retailer. Similarly $\mathbf{Total\_Demand\_Neg}(\beta, \gamma)$ stores the corresponding D_{neg} value. These matrices are used to reduce the computation complexity in the backward induction process.

B. Optimization for The Retailer's Utility in Stage III

The player in Stage III of the nested game is the retailer. In this stage, we are given the amount of electricity D_0 that the retailer acquires from energy sources. The optimization variables are the β and γ values. Because the $D_{0,actual}^{\mathbf{NR}} \cdot price^{\mathbf{NR}}$ and $D_{0,buy}^{\mathbf{R}} \cdot price^{\mathbf{R}}$ values in the original objective function (11) of the retailer are given in this stage, the retailer maximizes the following objective function:

$$\left(D - D_{neg}\right) \cdot p_c(D) + D_{neg} \cdot p_d(D) - \theta \cdot (D - D_0)^2 \qquad (12)$$

Please note that with given β and γ values, the corresponding D and D_{neg} values obtained from Stage IV are stored in entries $\mathbf{Total\_Demand}(\beta, \gamma)$ and $\mathbf{Total\_Demand\_Neg}(\beta, \gamma)$, respectively. The retailer employs the *ternary search* method, which is an extension of the well-known binary search method, in order to find the optimal β and γ values assuming that objective function (12) is a quasi-concave function of β and γ. In this stage, we define the matrix **Obj_StepIII**, where each entry $\mathbf{Obj\_StepIII}(D_0)$ denotes the value of objective function (12) with given D_0.

C. Optimization for The Retailer's Utility in Stage II

In this stage, the player is also the retailer. We are given the actual renewable energy $D_{0,actual}^{\mathbf{R}}$ obtained from the renewable power sources. The optimization variable is the amount of energy $D_{0,actual}^{\mathbf{NR}}$ for the retailer to purchase from the traditional power plants. Because the $D_{0,buy}^{\mathbf{R}} \cdot price^{\mathbf{R}}$ value in the original objective function (11) of the retailer is given in this stage, the retailer maximizes the following objective function in Stage II:

$$\begin{aligned}\left(D - D_{neg}\right) \cdot p_c(D) + D_{neg} \cdot p_d(D) - \theta \cdot (D - D_0)^2 \\ - D_{0,actual}^{\mathbf{NR}} \cdot price^{\mathbf{NR}}\end{aligned} \qquad (13)$$

where $D_0 = D_{0,actual}^{\mathbf{R}} + D_{0,actual}^{\mathbf{NR}}$. In this stage, we perform a simple search algorithm on $D_{0,actual}^{\mathbf{NR}}$ to find the optimal solution that maximizes objective function (13) based on $D_{0,actual}^{\mathbf{R}}$. Please note that the optimal value of $\left(D - D_{neg}\right) \cdot p_c(D) + D_{neg} \cdot p_d(D) - \theta \cdot (D - D_0)^2$ (i.e., the first line of Eqn. (13)) is stored in matrix entry $\mathbf{Obj\_StepIII}(D_0)$ with given D_0 value.

In this stage, we define the matrix **Obj_StepII** after the optimization procedure. Each entry $\mathbf{Obj\_StepII}\left(D_{0,actual}^{\mathbf{R}}\right)$ stores the value of objective function (13) with given $D_{0,actual}^{\mathbf{R}}$.

D. Optimization for The Retailer's Utility in Stage I

In the first stage, the retailer determines the amount of electricity energy $D_{0,buy}^{\mathbf{R}}$ to purchase from the renewable power sources. The objective function for the retailer is Eqn. (11). Similarly, we perform a simple search algorithm on $D_{0,buy}^{\mathbf{R}}$ to find the optimal solution, based on the matrix **Obj_StepII** and the realization factor $P_{\mathbf{R}}$ value. This optimization step is very critical for the retailer to improve its payoff. If the retailer purchases too much electricity from renewable power sources, the quality of steady power supply cannot be guaranteed due to the reliability issues. In contrast, acquiring electricity from conventional power plant only is not a cost-effective strategy because $price^{\mathbf{NR}} > price^{\mathbf{R}}$.

IV. SIMULATION RESULTS

In this section, we present the experimental results on the proposed nested-game based optimization framework. We have implemented an interactive simulation system of smart grid, including electricity retailer, PEVs and other electricity consumers. The effectiveness of the proposed optimization framework is demonstrated through comparison results.

In our simulation system we consider a user group of 20 consumers. Among all the consumers, 10 of them are residential users and the rest are PEVs. As is shown in residential user's utility function (8), a_i is set to 2.5 for all the residential users and d_i is set to a randomized value between 175 and 225. For PEV's utility function (9), ε_i is set to a randomized value between 10 and 600 and $S_{ini,i}$ is uniformly distributed between 35 and 200 since each PEV has different storage of charge (SOC). We change the factor β and γ in real-time pricing Eqn. (6) and (7) between 0.05 and 0.3, and D_0 from 50 to 180 to get the corresponding D through algorithm 1 under different circumstances. And the base price p_B is set to 8. In Stage I and II, $price^{\mathbf{NR}}$ is set to 15 and $price^{\mathbf{R}}$ is set to 4 and θ equals to 2.

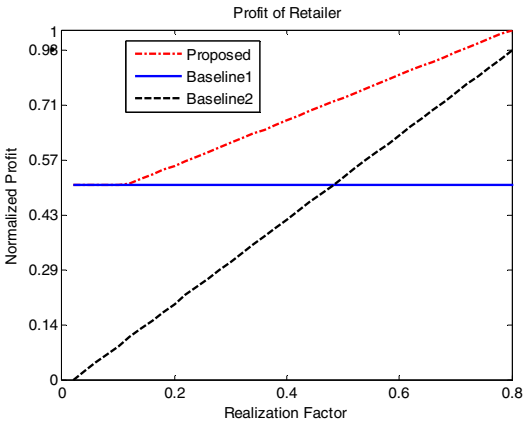

Fig. 2. Experiment results of retailer's profit.

In Figure 2, we compare our optimization results with two baseline results. For better comparison, we use normalized profit instead of its absolute value and we take the experimental result of our proposed algorithm at $P_R = 0.8$ as the normalization constant. For baseline 1, we assume that retailer acquire all the electricity from traditional power source. For baseline 2, we assume that retailer only buy electricity from renewable power sources. As we can see from the figure, when realization factor P_R becomes higher, retailer will get a better payoff if it acquires more electricity from renewable sources which is in low in unit price. Therefore, experiment results is a lot better than baseline1 when $P_R > 0.3$. Compared with baseline 2, the retailer's payoff will be less if there is too much electricity turn out to be not realizable. Obviously, when $P_R < 0.3$, our experimental result gets a higher payoff than that of baseline 2. Because the baseline 2 has reliability issues when the renewable energy becomes less reliable.

V. CONCLUSION

In this paper, we consider the interaction among energy sources, electricity retailer, and various consumers. The retailer procures electricity from both traditional and renewable energy sources, and sells it to its consumers using real time pricing policy. The consumers include residential users that can only consume power, and PEVs that can either consume power or supply power stored in its battery to the grid. We propose a novel four-stage nested game-based framework to model these interactions. The objective of the retailer is to maximize its overall profit as well as perform frequency regulation, whereas the goal of each consumer is to maximize a predefined utility function. In the game theoretic framework, the retailer should decide the amounts of electricity purchased from the renewable and traditional energy sources, respectively, and the real-time pricing scheme for its consumers. The consumers will react to the pricing mechanism and maximize their utility functions by adjusting the electricity demand. We derive the optimal solution of the nested game through finding the SPE of all the consumers and optimizing the retailer's action using the backward induction method.

ACKNOWLEDGEMENT

This work is supported in part by the Software and Hardware Foundations program of the NSF's Directorate for Computer & Information Science & Engineering.

REFERENCES

[1] M. Hashmi, S. Hannien, and K. Maki, "Survey of Smart Grid Concepts, Architectures, and Technological Demonstrations Worldwide," *IEEE PES Conference on Innovative Smart Grid Technologies* (ISGT Latin America), 2011.

[2] X. Fang, S. Misra and G. Xue, "Smart Grid - The New and Improved Power Grid: A Survey," *IEEE Communications Surveys & Tutorials*, 2012.

[3] P. Samadi, R. Schober and V. Wong, "Optimal Energy Consumption Scheduling Using Mechanism Design for the Future Smart Grid," *IEEE SmartGridComm*, 2011.

[4] M. Shinwari, A. Youssef and W. Hamouda, "A Water-Filling Based Scheduling Algorithm for the Smart Grid," *IEEE Transactions on Smart Grid*, 2012.

[5] T. Cui, Y. Wang, S. Yue, S. Nazarian, and M. Pedram, "An incentive-based price determination algorithm for utility companies in smart grid under game theoretic models," in *IEEE PES Innovative Smart Grid Technologies Conference* (ISGT), 2013.

[6] C. Wu, H. Mohsenian-Rad, J. Huang, "Vehicle-to-Aggregator Interaction Game," *IEEE Transactions on Smart Grid*, vol. 3, No. 1, March 2012.

[7] W. Shi and V. Wong, "Real-Time Vehicle-to-Grid Control Algorithm under Price Uncertainty," *IEEE SmartGridComm*, 2011.

[8] S. Han, S. H. Han and K. Sezaki, "Design of An Optimal Aggregator for Vehicle-to-Grid Regulation Service," *IEEE PES Innovative Smart Grid Technologies* (ISGT), 2010.

[9] W. Saad, Z. Han and T. Basar, "Game-Theoretic Methods for the Smart Grid: An Overview of Microgrid Systems, Demand-Side Management, and Smart Grid Communications," *IEEE Signal Processing Magazine*, vol. 29, no. 5, pp. 86-105, Sept. 2012.

[10] P. Yang, G. Tang and A. Nehorai, "A Game-Theoretic Approach for Optimal Time-of-Use Electricity Pricing," *IEEE Transactions on Power Systems*, 2012.

[11] C. Wu, H. Mohsenian-Rad and J. Huang, "Wind Power Integration via Aggregator-Consumer Coordination: A Game Theoretic Approach," *IEEE PES Innovative Smart Grid Technologies Conference* (ISGT), Jan. 2012.

[12] S. Bu, F. R. Yu and P. X. Liu, "A Game-Theoretical Decision-Making Scheme for Electricity Retailers in the Smart Grid with Demand-Side Management," *IEEE SmartGridComm*, 2011.

[13] K. Leyton-Brown and Y. Shoham, *Essentials of Game Theory: A Concise, Multidisciplinary Introduction*, Morgan & Claypool Publishers, 2008.

[14] J. B. Rosen, "Existence and uniqueness of equilibrium points for concave *n*-person games," *Econometrica*, vol. 33, pp. 347-351, 1965.

[15] S. Boyd and L. Vandenberghe, *Convex Optimization*, Cambridge University Press, 2004.

Resource Oriented and Energy Efficient Routing Protocol for IPv6 Wireless Sensor Networks

Antimo Barbato
Department of Information Technology and Mathematical Methods University of Bergamo, Italy
Email: antimo.barbato@unibg.it

Marica Barrano, Antonio Capone and Nicolò Figiani
Dipartimento di Elettronica, Informazione e Bioingegneria
Politecnico di Milano, Italy
Email: {marica.barrano, antonio.capone, nicolo.figiani}@polimi.it

***Abstract*—In the near future, the IPv6 protocol is expected to provide internet connectivity to any object embedding a communication device, by creating the so-called *Internet of Things* (IoT). In this scenario, IPv6 Wireless Sensor Networks (WSNs) have a key role since they can be used to collect several environment information, hence becoming the eyes, ears and nose of the IoT. Since wireless sensors are limited in power, it is essential to design energy efficient WSNs protocols. To this purpose, in this paper, we propose a Resource Oriented and Energy Efficient (ROEE) routing protocol based on the Routing Protocol for Low power and Lossy networks (RPL). ROEE RPL is intended as the very first building block to achieve the so called IoT. Simulation results show that our protocol has better performance than the basic RPL in terms of energy efficiency without compromising the network throughput.**

***Index Terms*—Sensor Networks, Energy Efficiency, Routing Protocol, RPL.**

I. Introduction

The growth and evolution of WSNs experienced during the last decade has made possible to develop and deploy inexpensive and self-adaptive monitoring systems composed of multifunctional and distributed wireless sensors [1]. WSNs have significant advantages over traditional communication technologies such as rapid development, low cost, flexibility and aggregate intelligence through parallel processing. The IETF has proposed different standards as methods to interconnect sensor nodes and the Internet by bringing the Internet Protocol version 6 (IPv6) into WSNs [2]. With this solution, in fact, sensors can be natively addressed and connected through the Internet Protocol with several advantages such as plug-and-play installation, simplified development of applications and compatibility with existing architectures. The vision of attaching tiny devices to every single object is known as the *Internet of Things* (IoT) [3]. In the IoT vision, everyday physical objects cab be connected to the Internet and are able to autonomously communicate with other devices. In such a scenario, IPv6 wireless sensors play a key role since they can be used to collect several environment information, hence becoming the eyes, ears and nose of the *Internet of Things*.

The field of IoT, due to the powerful implications it could bring, is a research area of widespread interest. In particular, WSNs have received great attention since they have some limitations that may prevent their diffusion in IoT frameworks. One of the the most crucial constraints in the design and development of sensor networks is represented by their energy consumption: energy is a very critical resource of sensors since WSN nodes are often battery powered and it is usually very difficult to recharge or change batteries. For this reason, because of the limited energy availability, it is of fundamental importance to develop WSNs protocols that optimize sensors energy consumption. Moreover, in the IoT scenario, WSNs can be deployed over large area, therefore also the issue of multi-hop routing must be properly addressed. For these reasons, in this paper, we propose an energy aware version of the the Routing Protocol for Low power and Lossy networks (RPL) [4], one of the most widespread multi-hop routing protocols for WSNs. RPL, defined by the IETF community through the ROLL working group, is a well-known routing protocol for constrained devices, and it has been implemented in the most common operating systems for embedded networked sensors (e.g. Contiki[5] and TinyOS[6]).

The default metric used by the basic implemented version of RPL to build up routing tables is called Expected Transmission count (ETX). It is a link metric that estimates the number of re-transmissions required to successfully send a data packet between two nodes and is a measure of the quality of the channel. In this paper, we extend the RPL protocol by defining a new metric that aims to be resource oriented and more energy efficient with respect to the basic version of RPL. In several IoT scenarios in which WSNs are used, applications (e.g. smart city environment, security, traffic, light monitoring services) can request a certain WSN to monitor a specific resource (e.g. temperature, light and, more in general, environmental and physical parameters). This request is transmitted to sensors by the network sink node that is directly connected to the application data collection center. WSN nodes, in a cooperative way, reply back by providing the requested measurements to the sink node. These data can be monitored both periodically and on-demand, depending on the application and context. Moreover, several resources can be monitored at the same time. As a matter of fact, in heterogeneous WSNs and in reference to each resource request by an IoT application, only a subset of nodes can provide the requested measurements. For this reason, it can be convenient to define multiple routing topologies (as provided in RPL specifications) in the case of multiple resource requests and to assign different roles to nodes in the routes creation phase depending on their

978-1-4799-0354-2/13/$31.00 ©2013 IEEE

monitoring features (i.e. resource availability). In particular, in defining paths towards the root in reference to a specific request, a key routing role must be assigned to nodes that can monitor the requested resource. In our work, we address this aspect, hence defining a resource oriented routing protocol. Moreover, we also focus our attention on defining energy aware routing node-metrics, based on the residual energy and power vulnerability of nodes, so as to reduce the energy consumption of the whole network. By considering these two crucial aspects, we propose a new, energy aware and resource oriented optimized version of RPL, which is called Resource Oriented and Energy Efficient (ROEE) RPL.

The remainder of this paper is organized as follows. In Section II we review the RPL protocol. In Section III we describe the basic characteristics of the routing protocol that we propose to optimize the energy consumption of WSNs in IoT scenarios. Section IV reports some numerical results, obtained through simulations, to evaluate the impact of our optimized routing protocol in terms of network performances with respect to the basic RPL protocol. Finally, in Section V, the paper is concluded and further developments are discussed.

II. Routing Protocol for Low power and Lossy networks

A Low power and Lossy network (LLN) consists of a multitude of constrained nodes, with limited processing power and memory, short range wireless communication channels and low data rate, interconnected by lossy links that are usually unstable. The traffic patterns of such networks are mainly Point-to-Multipoint (P2M) or Multipoint-to-Point (M2P). Based on these features, the scientific community has produced big efforts to offer a routing solution suitable for this type of networks. In particular, the IETF ROLL working group has defined, over the years, specific requirements for a LLN routing protocol, giving rise to RPL. RPL routes are optimized for traffic to, or from, one or more roots that act as the sink of the routing topology. Specifically, in order to define routing paths, this protocol creates Destination Oriented Directed Acyclic Graphs (DODAGs), each one associated with a specific sink node and characterized by a proper routing Objective Function (OF). The OF identifies a routing performance objectives (e.g. low delay, high throughput, energy efficiency) as well as the specific routing metrics to use to determine link costs.

RPL uses several identifiers to build and maintain the routing topologies:

- *RPLInstanceID*: it is a unique identifier within a network, that identifies a set of one or more DODAGs, and is characterized by a specific objective function. The set of DODAGs, identified by the same RPLInstanceID, is called RPL instance.
- *DODAGID*: it is the identifier of a DODAG root and it's unique within a RPL instance.
- *Rank*: it is a scalar number which represents the link (or node) cost. The exact way how the rank is computed depends on the OF and it is often application-dependent.

Upward routes

RPL provisions routes towards DODAGs roots, by defining acyclic graphs that are optimized according to a given objective function. Each OF defines how RPL nodes have to choose their parents and how they select and optimize routes within a RPL instance. As a result, the main role of an OF is to define the mechanism used to translate metrics and constraints into rank values. Nodes construct and maintain the topologies through particular signalling packets named DODAG Information Object (DIO) messages. These packets carry information that allows a node to discover a RPL instance and its parameters, join a DODAG and maintain the network topology.

Upward routes, supporting multipoint-to-point traffic, are identified by means of defining DODAGs. The macro-steps involved in the definition of a DODAG by a root node are the following:

1) DODAG formation is started by the root node by sending DIOs messages. These messages contain the rank of the sender of the DIO;
2) When a node receives a DIO, it computes its own rank based on the OF and on the rank of the DIO sender. Moreover, it updates the rank field of the message and forwards the DIO to other sensors. In this way, DIOs are propagated through the network;
3) Each node identifies the parent set by selecting neighbours from which a DIO has been received and characterised by lower ranks. Within the parent set, a preferred parent is identified (based on routing metrics) to be the preferred next hop in upstream routes (i.e. from the nodes towards the root), hence identifying the DODAG.

After a DODAG has been defined, it is updated and maintained mainly by means of DIO massages. In particular, RPL supports mechanisms which can be used for local repair and loop detection within DODAGs.

Downward routes

The RPL routing algorithm uses another type of signalling packets, called Destination Advertisement Object (DAO) messages, to propagate destination information upwards along the graph in order to establish downward routes (i.e. from the root towards the other nodes). Downward routes support point-to-multipoint data flows, from the DODAG root to the lowest-ranked nodes and also Point-to-Point (P2P) flows where messages firstly reach the sink through an upward route and then the proper destination through a downward route.

In the downstream routes definition, each node sends a DAO to the preferred parent(s). In turn, the parent(s) forwards the DAO to its preferred parent(s), and so on until it eventually reaches the root. In this way, the downward routes are created. In RPL, two modes are available to store and manage downward routes. In the first mode, called *storing*, all nodes must store downward routing information for their DODAG in a local table. On the other hand, in the second mode, called *non-storing*, nodes do not store downward routing tables and the DODAG root is the only one in charge of storing downstream routing table entries.

Routing Metrics

A routing metric is a quantitative value that is used to evaluate the path cost, therefore the best path is the one that satisfies all the supplied constraints (if any) and that has the lowest cost with respect to some specified metrics. Metrics and constraints are advertised in the DIO packets and the set of routing parameters, used by the RPL instance, is signalled along the DAG, which is built according to the particular OF. In the RPL implementations available in the literature (TinyRPL for the operating system TinyOS and ContikiRPL for Contiki), two OFs [7], [8] are defined and implemented based on two routing metrics:

- Expected transmission count (ETX): it represents the number of transmissions (eventually including retransmissions) a node expects to make in order to successfully deliver a packet to its destination. This metric is used as a cumulative link metric, therefore its value is the sum of the same metric computed on all the link previously used. The expected transmission count takes into account two parameters:
  - P_f: represents the probability that a data packet is successfully delivered to the receiver;
  - P_r: is the measured probability that the acknowledgement packet is successfully received;

  and, since each transmission attempt can be considered as a Bernoulli trial, it is generally computed according to the specific formula:

$$ETX = \frac{1}{P_f \cdot P_r} \tag{1}$$

  In this case, in defining DODAG graphs, each node selects as parent the sensor with the minimum value of the expected transmission count.
- Hop Count (HP): it represents the number of traversed nodes along the path. In this case, the definition of the optimal path is made by taking into account the number of hops required to reach the destination. Specifically, in constructing DODAG graphs, each sensor selects as its parent the node with the minimum hop count and no energy optimization mechanism is considered to route packets.

These metrics, used by the default RPL version, are not able to save energy of nodes, although in conditions of an ideal transmission channel, they allow identifying optimal paths.

III. ROEE RPL PROTOCOL

In the current implementation of RPL, the most relevant objective function is based on the ETX metric as link cost, whereas the other proposed OF uses the hop-count and is not very useful to deploy efficient WSNs. Since an energy-aware RPL implementation is missing, in this paper we propose and implement it to extend the available features of this routing protocol for low power and lossy networks.

In order to define this energy-aware OF, it is required to use a node metric that takes into account nodes energy consumption and usage. To this end, we have combined two metrics discussed in the literature: Energy consumption (E_c) and Battery Index (BI).
The energy consumption [9] represents the amount of energy used by a certain node and can be expressed as:

$$E_c = \frac{B_{cap} - B_l}{B_{cap}} \tag{2}$$

where B_{cap} represents the battery capacity of the sensor and B_l is the current battery charge level. This metric can be used to try and set up routes involving nodes with the highest residual energy, so as to increase the life of the whole network. The advantage of this metric is that it is easy to compute and low CPU resources are required. However, the values of this parameter have little meanings unless they are compared with each other. For this reason, in optimizing routing graphs, the global knowledge of all node information is required. Moreover, nodes have to periodically monitor and report to the sink their energy consumption, therefore the signalling frequency can be quite high.

The other metric that we have used in defining our protocol is the battery index [10] [11] that represents how much prone a node is to consume energy, depending on its position within the network and other factors. It can be computed based on the power used by the node in each of the following four states in which a node can operate: Transmission (TX), Reception (RX), idle and sleep (actually other states are involved in the life-cycle of nodes, but almost all the energy consumed by nodes is associated with those four states). Let T_{state} and ω_{state} be, respectively, the amount of time a node has spent in that particular state and the corresponding energy consumed in that state per unit of time. The battery index can be computed, for each node, with the following formula:

$$BI = K' \cdot \frac{\omega_{TX} \cdot T_{TX} + \omega_{RX} \cdot T_{RX} + \omega_{idle} \cdot T_{idle}}{T_{sleep}(t) \cdot D_c} \tag{3}$$

where K' is a normalization factor and D_c is the duty cycle, that is the ratio between the Active Time (ACT) and the sum of the active and the inactive (i.e. Low Power Mode (LPM)) time of a node:

$$D_c = \frac{T_{ACT}}{T_{ACT} + T_{LPM}} \tag{4}$$

In using this metric, we have simplified the equation (3) so as to reduce the sensors CPU usage. In particular, since radio communication is the main energy consumer of a sensor battery, $w_{idle} \cdot T_{idle}$ can be ignored. Moreover, in this paper we have used sensors Tmote Sky using a CC2420 chip whose transmission and reception consumptions are almost the same [12]. For this reason, w_{TX} and w_{RX} can be considered equal and equation (3) can be modified as follows:

$$BI = K \cdot \frac{T_{TX} + T_{RX}}{T_{sleep} \cdot D_c} \tag{5}$$

where K is a new normalization factor that incorporates ω_{TX} and ω_{RX}. The battery index can be used to detect the nodes

that are prone to run out of energy. In particular, vulnerable nodes are those having significantly high BI values, since the larger the BI, the more vulnerable to energy consumption the node tends to be. The main disadvantage of this metric is that it requires more CPU resources than the energy consumption case. However, the BI metric is more stable in time so that a lower signalling frequency is required.

In addition to the energy consumption and battery index metrics, we have also used the resource availability information to define the rank of each node. In fact, our routing protocol intends to be resource oriented which means that in defining the DODAG paths associated with a certain data request by an IoT application, network nodes must play different roles in the routing topology depending on their features. In particular, a key routing role has to be assigned to nodes that can monitor the requested resource by means of decreasing their ranks so to have more chances to become parents of other nodes. To this end, for each node, we define the binary Resource Availability (RA) parameter as follows:

$$RA = \begin{cases} 1 & \text{if the node can retrieve the requested resource} \\ 0 & \text{otherwise} \end{cases} \tag{6}$$

By combining the energy consumption and battery index metrics with the resource availability information, we have defined a new version of the RPL protocol, called Resource Oriented and Energy Efficient (ROEE) RPL, whose goal is to define the routing RPL topology by assigning a more important role to motes that can reply positively to requests made by the application and by improving the energy efficiency of the network by means of using energy-aware metrics. In this new version of the RPL protocol, the rank of each node, R, is computed as follows:

$$R = \frac{E_c \cdot BI}{N} - RA \tag{7}$$

where N is a normalization factor defined based on experimental tests. The battery index is computed according to the equation (5), using shift operators whenever possible to reduce the sensors CPU usage. This value is then multiplied by the estimated energy consumption, so that each node uses as energy-aware metric the consumed energy weighted for the battery index. Finally, the RA binary parameter is subtracted from the result of the previous computation. The normalization parameter, N, is introduced to make parameters $E_c \cdot BI$ and RA comparable to each other. At the end of the DIOs propagation described in Section II, each node selects as parent the sensor with the lowest rank among neighbour nodes. As a consequence, sensors with low energy consumption, low BI value and that are able to measure the requested resource are the most preferable nodes in the selection of RPL DODAG parents.

IV. Numerical Results

To evaluate the performance of the ROEE RPL protocol, a simulation campaign has been carried out. In our tests, in fact, we have relied on simulations mainly to test the proposed solution in several testing scenarios and evaluate several parameters. The purpose of simulations was to evaluate the performance of the proposed routing protocol with respect to the basic version of RPL both in terms of energy consumption and network performance.

In our tests, we have used the Contiki operating system, a widely used open source, portable and multi-tasking operating system designed for memory-efficient networked-embedded systems and wireless sensor networks [13]. Contiki, in particular, contains μIPv6, a full IPv6 stack including a comprehensive Application Programming Interface (API) for programming protocols using User Datagram Protocol (UDP), Transmission Control Protocol (TCP) or Internet Control Message Protocol version 6 (ICMPv6). In our tests, a specific version of Contiki OS has been used, called ContikiRPL, containing a RPL implementation. The main goal of ContikiRPL is to provide a versatile and simple programming interface that can be used to study objective functions. In order to test the above stated ROEE protocol, we have implemented a new version of ContikiRPL, called ContikiROEE-RPL, implementing the proposed routing protocol.

In order to simulate the sensors network, we have used Cooja, a flexible Java-based simulator designed for WSNs running the Contiki operating system [14]. Cooja, in particular, simulates networks of sensor nodes where each node can be of a different type in terms of software and hardware.

In our tests, we have simulated a 31 node WSN (node 0 is the sink sensor), randomly placed in an area of $200m^2$. Even if Cooja can be used to simulate networks composed of different types of sensors, we have decided to use the same simulated platform for all sensors, the Tmote Sky, also named Telos B, a ultra low power IEEE 802.15.4 compliant wireless sensor module based on a TI MSP430 and Chipcon CC2420 radio. For this reason, in the simulated network, the MAC and PHY layers are compliant with the IEEE 802.15.4 specifications, while the IPv6 RPL/ROEE RPL is used to implement the Network layer. Moreover, every sensor but the sink, has a UDP application agent used to periodically send (i.e. every 10 seconds) a UDP data packet to the sink node. For this reason, the sink sensor, is both a RPL router and a UDP server. The channel model used in our simulation is the Unit Disk Graph Medium (UDGM) distance loss model in which the transmission range is modelled as a disk. All nodes behind that disk do not receive packets while the nodes within the transmission distance receive all the packets. The disk radius depends on the transmission power and, in our tests, is the same for all sensors (i.e. 30 meters). The UDGM-distance loss model also considers the interferences even if in a very simple manner: if packets interfere they are lost. As a consequence, all communications running at the same time are unsuccessful. Simulation time for each test case was set to 72 minutes and repetitive simulations for each scenario were performed to verify the reliability of our results. Specifically, two different scenarios have been simulated:

- *100% Resource availability*: all 30 sensors periodically

transmit best effort UDP packets, containing the requested information, to the root node;

- *50% Resource availability*: only 15 sensors are able to monitor the requested resource, hence periodically transmitting best effort UDP packets, containing the measures, to the root node.

Test results in terms of network lifetime are represented in Figure 1 and Figure 2. In Figure 1, in particular, we represent the results obtained with RPL and ROEE RPL in terms of number of nodes alive as a function of the simulation time in the *100% Resource availability* scenario. Figure 1 shows that after about 2800 seconds all the sensor nodes of the basic ContikiRPL network have already run out of energy and only the sink mote, which is not battery powered, is still alive. On the other hand, in the ROEE RPL implementation proposed in this paper, 14 motes (including the root node) are still alive at the end of the simulation which lasted nearly 4300 seconds (about 72 minutes). Therefore, by employing our version of the protocol, the life of the network can be substantially increased. The same consideration can be done for the *50% Resource availability* scenario, whose results are represented in Figure 2. Specifically, in the RPL case, there is almost no difference between the average lifetime of resource (i.e. nodes with $RA = 1$) and non-resource nodes (i.e. nodes with $RA = 0$). On the other hand, in the ROEE RPL implementation, at the end of the simulation there are 4 alive resource nodes and 8 non-resource motes. This different behaviour is due to the fact nodes with $RA = 1$, have lower ranks, so they are more involved in the network routing operations.

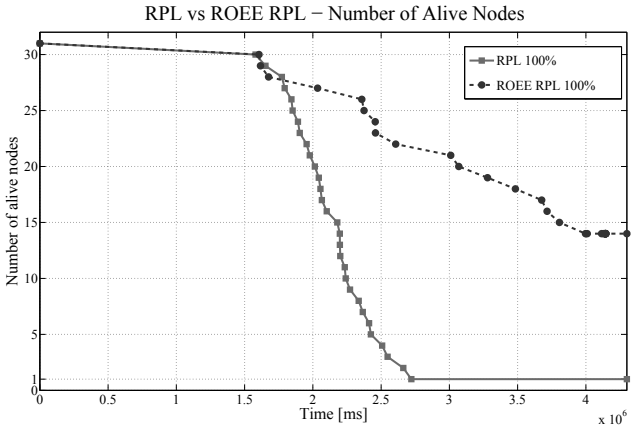

Figure 1: Number of alive nodes with RPL and ROEE RPL in the *100% Resource availability* scenario.

In Figure 3 we show the numerical results obtained with RPL and ROEE RPL in terms of cumulative energy consumption of the network as a function of the simulation time, both in the *100% Resource availability* an *50% Resource availability* scenario. Results show that the ETX based RPL is the most energy intensive RPL routing protocol. Specifically, for the two standard versions of ContikiRPL, the energy consumption rapidly increases, reaches its maximum value and then it gets stabilized since all motes but the sink run out of energy. On

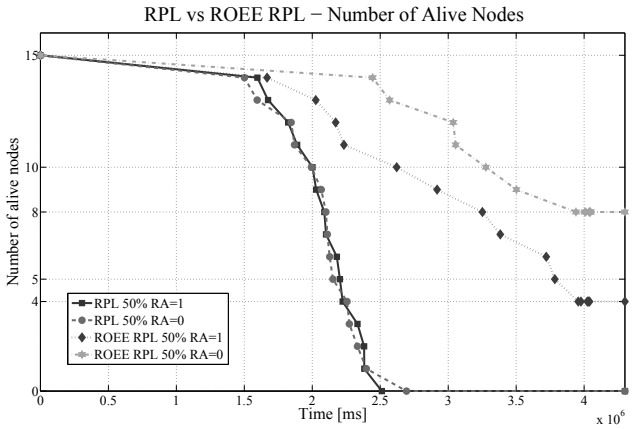

Figure 2: Number of alive nodes with RPL and ROEE RPL in the *50% Resource availability* scenario for resource and non-resource nodes.

the other hand, the energy consumption of the two ROEE RPL versions grows very smoothly, almost linearly and, at the end of the simulation, it reaches a smaller value of total power consumption than in the corresponding RPL case so that the entire network can last longer.

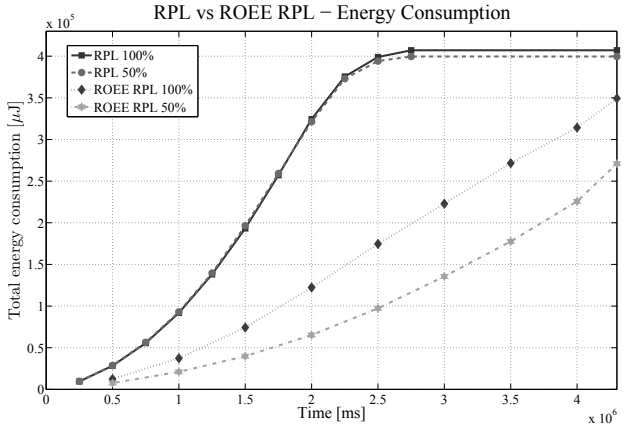

Figure 3: Cumulative energy consumption with RPL and ROEE RPL in the *100% Resource availability* and *50% Resource availability* scenarios.

Results in terms of sensors energy consumption are also represented in Table I in which the mean values and the standard deviation of the sensors energy consumption are computed for each considered test scenario. Numerical data show that in the *100% Resource availability* scenario, the proposed protocol allows saving around 31% of the WSN consumption with respect to the corresponding RPL basic network. This saving is even higher (i.e. 48%) in the *50% Resource availability* case because of the resource-oriented feature of the ROEE RPL routing metric.

Finally, in Figure 4, we show the results obtained in terms of throughput as a function of the simulation time. Results

Table I: Sensors energy consumption mean value and standard deviation with RPL and ROEE RPL in the 100% Resource availability and 50% Resource availability scenarios.

Scenario	Mean value [μJ]	Standard deviation
RPL 100%	1167	283.5
ROEE RPL 100%	802.7 (-31%)	310.8
RPL 50%	1180	310.9
ROEE RPL 50%	604 (-48%)	226.3

show that there's no significant variation of this parameter between the basic RPL version and the one proposed in this paper. Although the new protocol requires more processing at the application layer, the network throughput is just slightly affected. Consequently, in the ROEE RPL cases, very few packets must be retransmitted and a very small amount of energy consumption has to be used to this end.

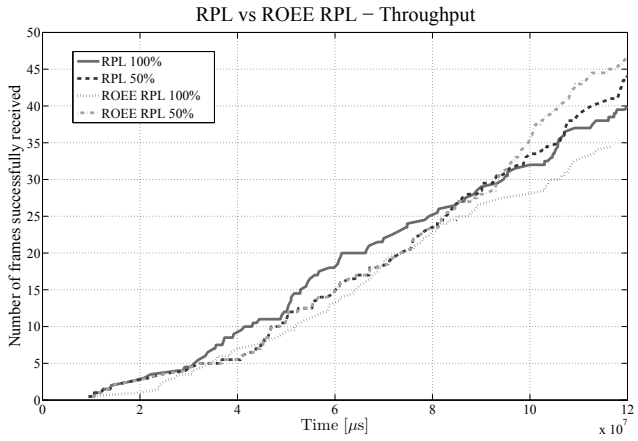

Figure 4: WSN throughput with RPL and ROEE RPL in the *100% Resource availability* and *50% Resource availability* scenarios.

V. Conclusions

In this paper, we have focused on the RPL routing protocol, a solution designed to match the requirements of networks characterized by low power supplies and by deployment in lossy environments. Specifically, we have presented a new, energy aware and resource oriented optimized version of RPL, called Resource Oriented and Energy Efficient (ROEE) RPL, in which energy aware routing metrics and information on resources availability of sensors are used to improve the energy efficiency of RPL. In our protocol, we have combined two energy-aware routing metrics, Energy Consumption and Battery Index, which represent, respectively, the energy consumed by each sensor and the vulnerability of each node in consuming power. The resulting new metric has been further extended to take into account the resource availability of each node with respect to data requests of IoT applications. As a result, ROEE RPL uses an energy aware routing metric which takes advantage of the capability of motes to retrieve a given resource requested by the application.

To evaluate the performance of the proposed routing protocol, we have implemented a prototype version of the proposed architecture in Contiki OS. Specifically, the WSNs using the basic RPL protocol and the proposed one have been simulated in Cooja, a flexible Java-based simulator designed for WSNs running the Contiki operating system. Numerical results have shown that the proposed ROEE RPL has better performance than the basic RPL in terms of energy usage and network lifetime without compromising the network throughput.

Although having discussed the efficiency of the proposed enhanced version of the RPL protocol, this study represents just one first cut analysis and further investigation is required. Firstly, additional tests can be performed to verify the efficiency of the proposed solution through experimental testbeds deployed in realistic IoT use-case scenarios. Moreover, ROEE RPL can be further improved by designing a mechanism in which the algorithm itself can weight the resource availability metric and the energy aware metrics depending on the context and application, in a self-adaptive way.

Acknowledgment

This work was partially supported by Italian MIUR in the framework of the PRIN Gatecom project.

References

[1] Waltenegus Dargie and Christian Poellabauer. *Fundamentals of wireless sensor networks: theory and practice*. Wiley, 2010.

[2] Jonathan W Hui and David E Culler. Ip is dead, long live ip for wireless sensor networks. In *Proceedings of the 6th ACM conference on Embedded network sensor systems*, pages 15–28. ACM, 2008.

[3] Luigi Atzori, Antonio Iera, and Giacomo Morabito. The internet of things: A survey. *Computer Networks*, 54(15):2787–2805, 2010.

[4] Tim Winter. Rpl: Ipv6 routing protocol for low-power and lossy networks. 2012.

[5] Contiki OS web site. http://www.contiki-os.org, 2013.

[6] TinyOS web site. http://www.tinyos.net, 2013.

[7] Pascal Thubert. Objective function zero for the routing protocol for low-power and lossy networks (rpl). 2012.

[8] Omprakash Gnawali. The minimum rank with hysteresis objective function. 2012.

[9] V. Shnayder, M. Hempstead, B. Chen, G.W. Allen, and M. Welsh. Simulating the power consumption of large-scale sensor network applications. In *Proceedings of the 2nd international conference on Embedded networked sensor systems*, pages 188–200. ACM, 2004.

[10] F. Kerasiotis, A. Prayati, C. Antonopoulos, C. Koulamas, and G. Papadopoulos. Battery lifetime prediction model for a wsn platform. In *Sensor Technologies and Applications (SENSORCOMM), 2010 Fourth International Conference on*, pages 525–530. IEEE, 2010.

[11] Joan Cortés, Qi Wang, and John Dunlop. Novel metric for identifying energy-vulnerable nodes and corresponding proactive schemes in wireless sensor network. In *Wireless Communications and Networking Conference, 2009. WCNC 2009. IEEE*, pages 1–6. IEEE, 2009.

[12] L. Paradis and Q. Han. A survey of fault management in wireless sensor networks. *Journal of Network and Systems Management*, 15(2):171–190, 2007.

[13] M. Dohler, D. Barthel, T. Watteyne, and T. Winter. Routing requirements for urban low-power and lossy networks. 2009.

[14] A. Dunkels, B. Gronvall, and T. Voigt. Contiki-a lightweight and flexible operating system for tiny networked sensors. In *Local Computer Networks, 2004. 29th Annual IEEE International Conference on*, pages 455–462. IEEE, 2004.

A Greener MAC Layer Protocol for Smart Home Wireless Sensor Networks

Sajjadul Latif, Xavier Fernando
Department of Electrical and Computer Engineering
Ryerson University
Toronto, Ontario M5B 2K3
Email: sajjadul.latif@ryerson.ca, fernando@ee.ryerson.ca

Alan Fung, Farrokh Janabi-Sharifi
Department of Mechanical and Industrial Engineering
Ryerson University
Toronto, Ontario M5B 2K3
Email: alanfung@ryerson.ca, fsharifi@ryerson.ca

***Abstract*—The wireless sensor network (WSN) is an important element on many advanced, energy efficient data acquisition (DAQ), and control systems. Sleep/wake-up scheduling and network overhead are some of the major burdens to achieve energy efficient WSNs. In this paper, an energy efficient communication algorithm is proposed for smart home sensor networks. The proposed approach targets the wasted energy during the idle listening, collision, and overhearing processes. A three-tier Medium Access Control (MAC) protocol has been developed to minimize the total energy consumption of the network. The new protocol reduces the total energy requirement by each node, facilitates confirmed communication for steady traffic, and gives adaptive control during varying traffic load. Overall, the proposed MAC protocol shows better performance than conventional WSN protocols.**

I. Introduction

There are many different sources of energy wastage in a WSN. *Idle listening, collision, overhearing* and *control packet overhead* are the major sources of energy loss. During idle listening, the nodes are actively listening to receive packets but there is no data intended for that specific node. It is observed that often most of the nodes in the system are idly listening even if there is no activity in the network [1]. Previous research shows during idle listening, nodes may consume up to 50-100% of the energy required for actually receiving a packet. Typically the idle:receive:send power ratios are 1:1.05:1.4 [2].

Generally, packets are discarded when there is a collision in the network which will require re-transmission of the packet and therefore waste energy. A node may also pickup packets intended for other nodes. This is called overhearing problem and wastes as much energy as receiving a packet [1]. Energy is needed to transmit and receive control packets as well. If the network is really complex, the control packets might consume significant amount of energy. Minimizing all these energy wastage is essential for achieving a high efficiency energy management system.

In recent years, many developments in smart home automation systems have been reported [3]. Most of these studies did not clearly focus on the energy requirements of the communication network itself. Although many researchers worked to make the WSN energy efficient in various scenarios, only few of those researches were related to smart home environment. Thus, the aim of this study was to develop an energy efficient MAC protocol for smart home communication network.

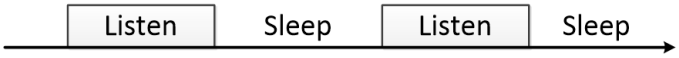

Fig. 1: SMAC protocol

A distributed, quasi-planned scheduling algorithm has been described in this paper, which can be used in a smart home environment as well as any other similar network conditions. The proposed Greener MAC algorithm was a combination of Quorum-MAC (QMAC), Pattern-MAC (PMAC) and back-off-sleep algorithm with some improvements [4,5,6].

II. Previous Research Works

One very basic and effective mechanism is sensor MAC (SMAC) protocol [1]. In SMAC, the communication nodes go to periodic sleep mode as shows in Fig. 1 to conserve energy. This will save energy proportional to the sleeping duration. However, this protocol is still not very energy efficient due to periodic wake up of sensor nodes despite the presence of data. There is no control over scheduling for variable traffic load. In order to improve this further, many other MAC protocols, namely DMAC, BMAC, TMAC, and TaMAC were also introduced [7,8].

A. Quorum MAC

In a Quorum-MAC system, the network nodes are assumed to be uniformly distributed in a circular area centered at the sink node. Then based on the distance between the nodes and the sink, the area is divided into several clusters known as *coronas* [4]. Each corona can only accommodate certain number of nodes based on their corona (cluster) number. Center cluster is corona 1 and the sequence increases outwards. In order to minimize unnecessary wake-up and idle times, the nodes are allowed to communicate to each other using a *quorum* based system as described in [4]. The use of quorum ensures that only the specified nodes will wake up and communicate with each other at a particular time slot. In a grid based quorum, a node picks one row and one column of time matrix as shown in Fig 2 [4]. Any sensor node with a $g \times g$ grid will wake up for $\frac{(2g-1)}{g^2}$ of the frame time. The grid size depends on traffic load of the nodes. The traffic load, in turn depends on the next hop corona and the area covered. In [4] the relationship was formulated as:

978-1-4799-0354-2/13/$31.00 ©2013 IEEE

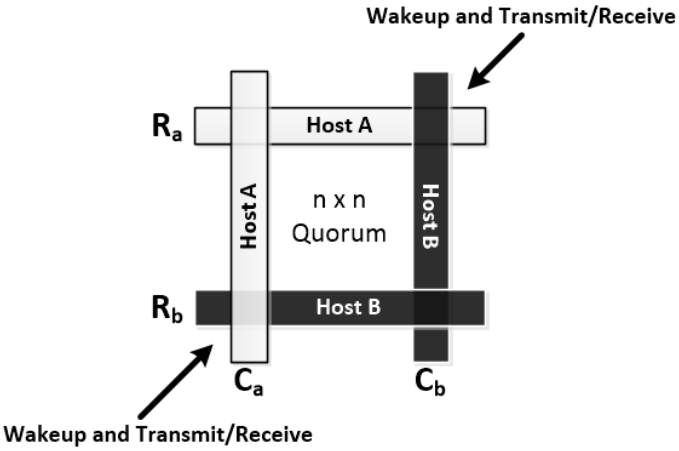

Fig. 2: Grid based Quorum System

$$TL_{c_i} = 1 + \frac{c_i+1}{c_i} \times TL_{c_{i+1}}$$

In order to solve the latency issue a technique called QMAC_LR was introduced in [4]. In QMAC_LR multiple sensor nodes from inner coronas are capable of data transfer to/from a node of outer corona. These nodes together are called 'next hop group'. They are selected during the network initialization. In a smart home WSN system, most nodes have only one way traffic towards center corona. The QMAC_LR seems to perform well under steady traffic but, does not have much control on energy in a variable traffic load.

B. Pattern MAC

A pattern based adaptive scheme described in [5] creates wake-up event schedules of a node based on the traffic load of the network. Pattern-MAC (PMAC) is a time slotted protocol like SMAC [1]. In this protocol, the generated pattern is a binary string of 1's and 0's. Here 1 means plan to wake up and 0 means plan to sleep. These patterns are not confirmed schedule but tentative sleep-wake plans for the nodes. These plans are called pattern repeat time frame (PRTF). The sensors adjust the sleep-wake schedule according to neighbor's PRTF and transmit as pattern exchange time frame (PETF). The time period is divided into multiple super time frames (STF) [5].

The pattern generation model P^j was analytically shown in [5] by considering a predefined threshold value δ. Total number of time slots in a pattern can be maximized up to N or equal to the time period. When a pattern P^j has a length less than N, the same pattern gets repeated for the remaining duration of the period. By changing the δ value, any application can change the sleep-wake ratio of the system. For high value of δ, the system will sleep more and consume less energy. In case of large data traffic, the network manager can decrease the value of δ to allow more network up time [5].

The effect of pattern in the wake-up time of a node can be shown by the steady state probability of awake node [5]. If p is the steady state probability, P_0 is the probability of no zero bit in the pattern and δ = period (N) = 2^M. Using Markov chain model and the probability of *(i+1)* zero bits in the pattern the equation for average sleep was deduced in [5] as: $E(0) = \sum_{i=0}^{M}(2^i P_2^i)$.

The PMAC system performs very well in variable traffic load. However, in a steady traffic load, this system may not save as much energy as QMAC [4].

C. Back-off-Sleep MAC

A back-off-sleep based data transfer protocol was derived in [6]. This protocol claims to save up to 80% receiving energy during data transfer under 50% traffic load. Most of the regular WSN protocols use RTS/CTS packets to solve collision and overhearing problems. However, these protocols are not compatible for low-rate wireless personal area network (LR-WPAN). RTS/CTS packets bring out a lot of overhead compared to traffic load. The back-off-sleep method gets rid of RTS/CTS packet and uses a back-off algorithm for data transfer. The back-off mechanism used in the technique is derived in [9]. The energy model of system was formulated in [6] as:

$$E_{save}^{tr} = \sum_{i=0}^{m}\left(\sum_{j=0}^{W_i-1} x_{B,i,j}(\omega P_r + (1-\omega)P_i)\right) - \sum_{i=0}^{m}\left(\sum_{j=0}^{k-1} x_{B,i,j}(\omega P_r + (1-\omega)P_i) + \sum_{j=k}^{W_i-1} x_{B,i,j}P_s\right)$$

The back-off-sleep algorithm proved to be very effective in energy saving during data transfer. But the system does not perform very well in a variable traffic load or in a distributed network with large number of networking nodes. The sensors do not have any information about when a neighboring node will be available. The protocol may suffer greatly if there is heavy traffic load.

All these algorithms try to reduce the energy consumption by sensors. However, a good algorithm needs to be optimized to suit a particular environment and the traffic pattern. One solution may not fit all. Hence, there is a need to introduce a MAC protocol specifically for the unique smart home WSN environment.

III. New MAC Layer Protocol Design

The proposed design for MAC layer is based on the specific network requirements of a smart home [3]. QMAC, PMAC and back-off-sleep algorithms described in previous section perform well in their own intended environments. But, their performance is not as efficient as it should be in other network scenarios. All these algorithms somehow try to reduce the energy consumption by WSN. However, a good algorithm needs to be optimized to suit a particular environment and the traffic pattern. One solution may not fit all. Hence, there is a need to introduce a MAC protocol specifically for the unique smart home WSN environment. In such environment the system needs to deal with both steady and variable traffic loads depending on the sensor's assigned role. The protocol should better meet the specific requirements of the smart home sensing and communication scenario. In this paper, above three protocols were combined together to develop a versatile and 'Greener' MAC algorithm for smart home environment. Overall network algorithm from network initialization to transmission can be illustrated by Fig 3. The

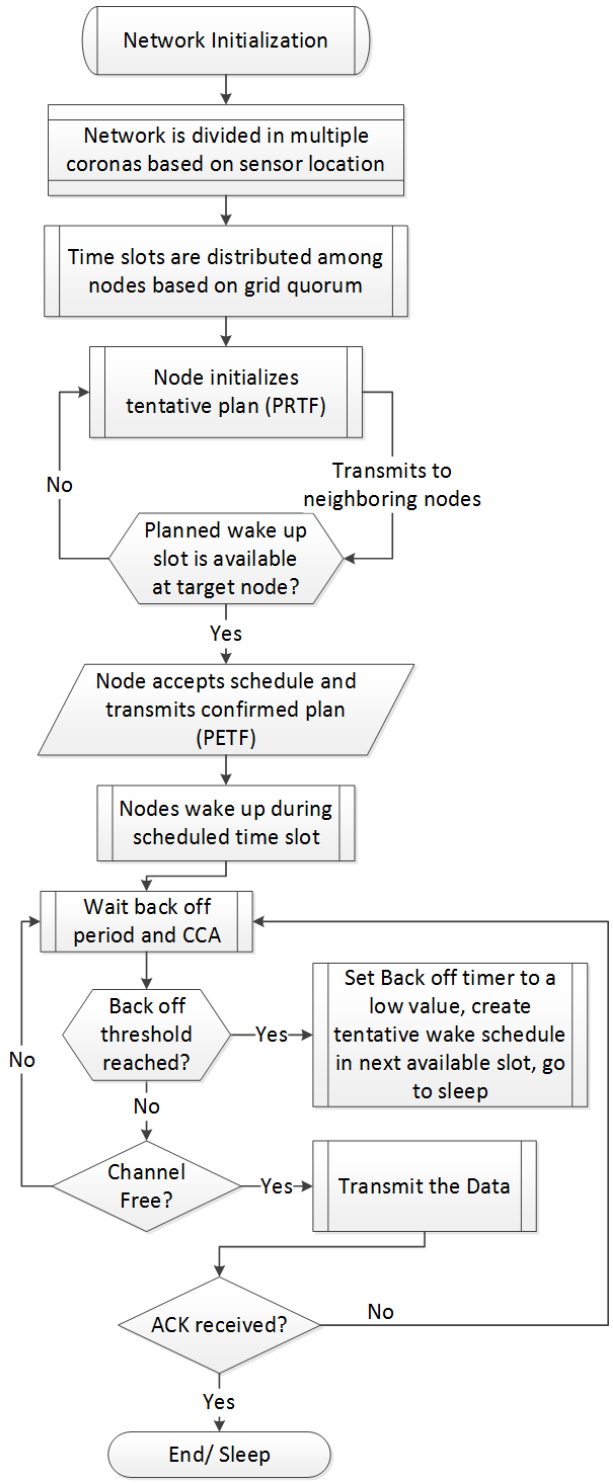

Fig. 3: MAC Algorithm

design of MAC protocol follows a three tier development. These are:

1) Planned Distribution
2) Planned Scheduling
3) Energy Efficient Transmission

A. Planned Distribution

The network nodes in a smart home environment are mostly stationary and the mobility is not an issue. The intelligent communication network has a network manager or sink node. Typically, all other nodes send information to this sink and receive control data from the sink. Therefore, the network model has 'many to one' communication architecture. In such a model, the nodes that are close to the sink deplete energy faster to accommodate the heavy flow of traffic, whereas the nodes far from the Network Manager barely use their energy. This issue is known as the *energy-hole* problem. In order to solve this problem, a planned node distribution scheme can be used in the MAC Layer. A quorum based MAC protocol described in previous section can easily solve this problem. A QMAC protocol with latency reduction (QMAC_LR) is adopted in this new protocol [4]. The network was first divided into several coronas depending on hop count and number of nodes. Then a grid based quorum system was assumed to create slotted time matrix. The sensor nodes would create small next hop groups with few nodes in the next corona during network initialization. So, after planned distribution with quorum, the sensors know when their neighboring nodes may wake up. For any node of an outer corona, the probability of finding a next hop awake node to transmit data was calculated in [4] as:

$$P_i = 1 - (\frac{n_g - 1}{n_g})^{2 \times n_h}$$

Here, n_g is the grid size for C_i and $n_g \geq 2$. n_h is the next hop group and $n_h \geq 1$. C_i is next hop corona.

This planned distribution solves the *energy-hole* problem and improves sleep-wake pattern compared to SMAC. However, in a smart home communication system, some DAQ sensors (e.g., temperature sensors) do not need to send data as often as Safe-Plug^{TM} sensors [10]. So, the network will encounter variable traffic loads for some sensors and steady traffic load for others. The quorum protocol does not have any control mechanism for variable traffic load. The Greener MAC algorithm in this paper combines the advantages of patterns with the quorum for adaptive control. The nodes need to be trained only to wake-up when they have any data to send or receive which will be described in the following section.

B. Planned Scheduling

A pattern based adaptive scheme has been adopted from PMAC protocol [5]. The nodes will train themselves using the neighbor's load and previous traffic history. Fig 4 captures the pattern generation method adopted in this protocol. The sensor will generate a tentative sleep-wake plan for the node and broadcast as PRTF packet. The nodes already know when their next hop neighbors are available according to the grid distribution. So, PRTF will be generated based on next hop neighbor's availability. When the sensor receives similar PRTFs from next hop neighbors, it adjusts the sleep-wake schedule accordingly and transmits as PETF. The neighbors will save the final wake-up schedule of this node as PETF. The sleep-wake pattern generation algorithm used in this protocol was derived in [5].

This PRTF and PETF mechanism may pose a problem when combined with quorum. Multiple nodes may generate same patterns in some cases. For example, host 'B' and host

'C' are from two different corona levels. They both want to communicate to host 'A' during a single time slot. Host 'A' needs to generate own pattern based on B and C's pattern. But, it cannot give the same time slots to two different nodes. The new protocol derives a CCA (clear channel assessment) technique to address this issue. If any host sees it has 'n' number of incoming plans for a single time slot, it will generate a PETF to wake up 'n' time slots when it can communicate to those nodes. The sink node will wake up during the extra time slots that it created. Source nodes will wake up based on the schedule they created for themselves. All the sensors will wait a random back-off period to sense the channel using CCA. The first one to send the packet will get the channel and others will go to sleep after the back-off period. The failed node will attempt to transmit again during the next immediate wake schedule known from PETF of sink. Also, the central sink node can control the aggressiveness of energy saving by changing the δ value and broadcasting it to all the sensor nodes [5].

Some synchronization is needed for this kind of time slotted protocol. But in this case only large time scales (in order of hundred milliseconds) were involved [5]. In such a way, the system does not need to have a complex synchronization method for the sensors. The system can perform very well with the synchronization method derived in SMAC [1]. This reduces the complexity and control overhead of the network.

The saved energy for this algorithm can be calculated using sleep time. For any time slot T_R in the period, the length of time interval is $(1-waketime) \times T_R$. For the new system the nodes will be sleeping through the entire time length when there is no data to send or receive. If T is the frame duration for SMAC protocol and d is duty cycle, then the time interval for SMAC protocol becomes:

$$t = \frac{E(0)T_R}{T} \times d.$$

So, the additional energy saving by each node in the new system can be given by:

$$E_{save} = \frac{E(0) \times T_R \times d \times P_{idle} \times [(\frac{n_g - 1}{n_g})^{2 \times n_h}]}{T}$$

Here P_{idle} is the idle power consumption for any node (i.e., when the node is awake but not sending or receiving any data). For a total n number of nodes in the network that are not transmitting or receiving any data, the total energy saving is:

$$E_{save} = n \times \frac{E(0) \times T_R \times d \times P_{idle} \times [(\frac{n_g - 1}{n_g})^{2 \times n_h}]}{T}$$

The PMAC's ability to control energy saving adaptively by changing δ gives more flexibility without increasing network

PRTF →	Host – A →	0	0	0	0	0	0	0	1	0	0	0	0	0
PRTF →	Host – B →	0	0	0	0	0	0	0	0	0	0	1	0	0
PETF →	Host – A →	0	0	0	0	0	0	0	1	0	0	1	0	0
PETF →	Host – B →	0	0	0	0	0	0	0	1	0	0	1	0	0

Fig. 4: Planned scheduling using pattern

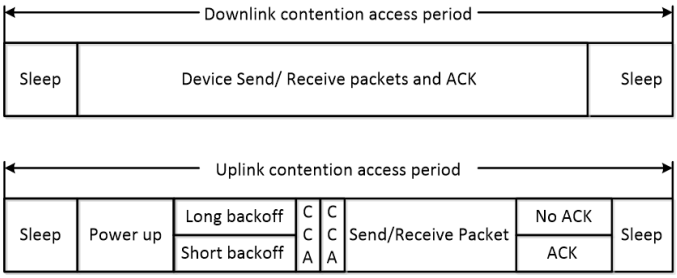

Fig. 5: Energy Saving Transmission and Reception

complexity. The synchronization method that was used in this protocol is simple and slight deviation in time will not pose any serious issues. The sensors were trained to wake up only when they can transmit or receive from next hop member. The nodes were aware about their next hop neighbor's availability from grid distribution and tentative pattern.

C. Energy Efficient Transmission

The communication network in a smart home has been developed using LR-WPAN. Although the new distributed and planned system above showed good performance, there are still energy losses during data transfer by RTS and CTS packets [10]. These RTS/CTS packets are also not compatible with LR-WPAN network. The above system controls which nodes are active during a certain time slot. So, errorless transmission can be achieved without the use of RTS and CTS packets. A back-off-sleep based data transfer protocol was considered to save more energy during data transfer as described in previous section.

Fig 5 shows the downlink and uplink mechanisms used in this new protocol. The algorithm is same as the one shown in *section II-(C)*. Combining this technique with the planned distribution and scheduling will result in more energy saving. The saved energy can be calculated as:

$$E_{save}^{total} = n \times \frac{E(0) \times T_R \times d \times P_{idle} \times [(\frac{n_g - 1}{n_g})^{2 \times n_h}]}{T} + \sum_{i=0}^{m} \left(\sum_{j=0}^{W_i - 1} x_{B,i,j} (\omega P_r + (1-\omega) P_i) \right) - \sum_{i=0}^{m} \left(\sum_{j=0}^{k-1} x_{B,i,j} (\omega P_r + (1-\omega) P_i) + \sum_{j=k}^{W_i - 1} x_{B,i,j} P_s \right)$$

The MAC layer protocol in proposed system uses the back-off-sleep transmission mechanism with the combination of planned distribution and scheduling to save even more energy during sensor's lifetime.

IV. Relevancy to the Smart Homes

A net-zero (NZ) (or net positive) smart home is a house that consumes less than or equal to the energy it produces [3]. The net-zero status is achieved by locally generating energy from renewable sources and by minimizing the energy requirement. Typically a NZ smart house is equipped with many wireless communication nodes (IEEE 802.15.4) to get

information from hundreds of temperature, humidity, airflow, and occupancy sensors [11, 12]. These sensors make up the Data Acquisition (DAQ) system of the house. This data is used to automatically optimize the control algorithm for Energy Demand Management (EDM) system. These smart homes will also periodically communicate with the Smart Grid to optimize various parameters.

Since the NZ smart home supposed to minimize the energy consumption in all possible ways, power reduction in the wireless sensor network (WSN) is also very important. Low power consuming WSN will also prolong the battery life, to reduce maintenance cost and increase the networks reliability by reducing number of faulty nodes.

A well connected smart house needs about 600-700 DAQ and control sensors within about 150 m range. All these sensors need to be connected to the central controller in a wireless manner. The wireless sensors will need typically 150 mW - 600 mW energy in a multi-hop network [5], depending on the number of nodes and the distance among them. Well-connected, energy efficient wireless networks are essential for net zero smart home realization. The first step is probably to reduce the energy wastage by the wireless sensor network.

The archetype sustainable model homes at Kortright Centre for Conservation, Vaughan, Ontario, Canada built by Toronto Regional Conservation Authority (TRCA) is used to develop a preliminary understanding on various sensing and communication requirements for this algorithm. The TRCA smart home uses around 300+ temperature, airflow, humidity and occupancy sensors. Currently these sensors are wired and the objective was to replace them with distributed WSN. A conceptual WSN network diagram is illustrated in Fig 6. The communication sensors will also connect the smart and regular appliances in the house to EDM system. The central control server can communicate to any sensor in the house for DAQ or control purpose.

We can categorize the wireless nodes in the smart home into two categories:

Sensing Only Nodes

These sensors communicate the sensed information only in one direction. They do not take part into any control mechanisms. Examples are the temperature sensors. The central controller decides whether to adjust the temperature in the Heat, Ventilation and Air Conditioning (HVAC) system [2].

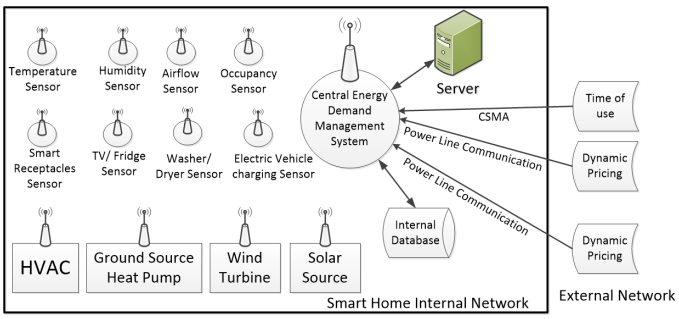

Fig. 6: Network Design

TABLE I: Simulation Parameters

Parameters	Value
Transmission power	0.69 Watts
Receiving power	0.36 Watts
Sleep power	0.03 Watts
Idle power	0.24 Watts

Sensing and Controlling Nodes

Here the sensors, such as the Safe- Plug^{TM} modules have the sensing as well as controlling capability to turn off certain appliances or put them in energy saving mode when required. Here the communication is duplex (bi-directional).

In the TRCA smart house, older appliances are controlled by proprietary Safe-Plug^{TM} modules. The Safe-Plug^{TM} works as a regular receptacle but has built-in ZigBee sensors. Each appliance has a unique RFID tag [7]. The receptacles are equipped with RFID readers to identify the appliance. The central controller will decide to turn on or off an appliance based on the optimization requirements. The lights, temperature and security system are also controlled using IEEE 802.15.4 compliance ZigBee sensors [12]. The energy management system gets information about the status of three local energy sources (i.e., geothermal, wind and, solar) on the availability of local energy.

V. Simulation Results

A simulation model was developed in MATLAB to validate the performance of the new protocol. Table I shows the parameters used in the simulation. A distribute network was created using the grid-quorum system [4]. The scheduling pattern was generated according to the pattern generation algorithm in [5]. The simulation results in Fig 7 showed the energy performance of the new Greener MAC algorithm during a time frame. It was observed that the nodes in higher level

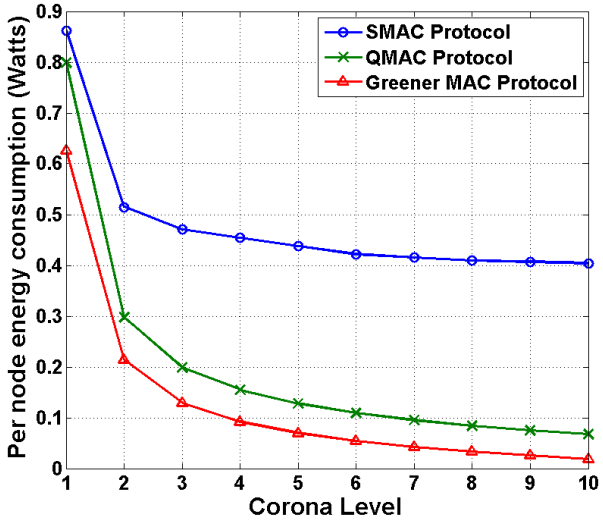

Fig. 7: Energy performance of the new protocol

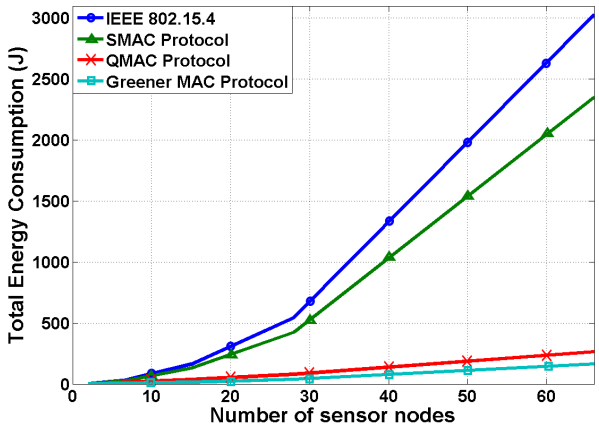

Fig. 8: Energy usage vs number of nodes

coronas were using less energy than the nodes closer to center. This can be explained using the grid-quorum algorithm. The number of nodes in outer corona is higher than inner coronas. As the total time frame distributed between all the nodes in the grid, nodes in outer corona can sleep during more time slots. The improvements in energy performance over SMAC and QMAC are very clear from results [1,4]. The new protocol in this paper has distributed nodes with planned scheduling. So, theoretically the new system should perform well in both static and variable traffic load situation. The new Greener MAC protocol saves energy in 3 different levels and each of them are more efficient than any basic MAC protocols like SMAC or TMAC [8]. The protocol is also capable of handling large number of nodes efficiently. Fig 8 illustrates the energy usage of the network with large number of sensors. As the number of nodes increased the energy consumption by the new protocol decreased as compared to SMAC or QMAC protocol. Fig 9 shows that overall awake duration of a node was decreased for new protocol in each corona level as compared to others.

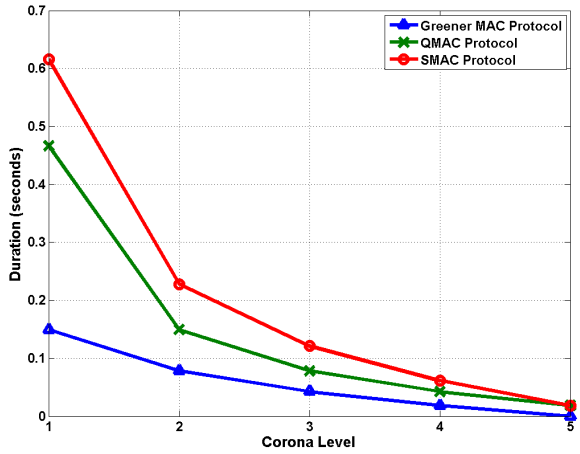

Fig. 9: Awake duration of a node during a time period

VI. Conclusion

An energy efficient communication algorithm was proposed for NZ smart home sensor networks. The total energy requirement by each node was reduced by the new MAC layer protocol. The planned distribution of nodes facilitates confirmed communication for steady traffic. The planned scheduling gives adaptive control during varying traffic load. The back-off algorithm reduces more energy consumption during data transfer. The new Greener MAC protocol shows better performance than SMAC, TMAC, QMAC, and many other WSN protocols. It increases the energy efficiency and lifetime of the smart home network. Although the system is built for residential environment, it can be applicable to other structures and environments where a planned network deployment is possible.

Acknowledgment

The authors would like to thank Center for Urban Energy (CUE) Ryerson, Toronto and Region Conservation Authority (TRCA), and Toronto Hydro for their support in this project.

References

[1] W. Ye, J. Heidemann and D. Estrin, "An Energy-Efficient MAC Protocol for Wireless Sensor Networks," *Proceedings of IEEE INFOCOM*, New York, NY, pp. 1567-1576, June 2002.

[2] M. Stemm and R. H Katz, "Measuring and reducing energy consumption of network interfaces in hand-held devices," *IEICE Transactions on Communications*, vol. E80-B, no. 8, pp. 11251131, Aug. 1997.

[3] M. Jahn, M. Jentsch, C. R. Prause, F. Pramudianto, A. Al-Akkad and R. Reiners, "The Energy Aware Smart Home," *Future Information Technology (FutureTech), 2010 5^{th} International Conference on*, vol. 1, no. 8, pp. 21-23, May 2010.

[4] C. M. Chao and Y. W. Lee, "A Quorum-Based Energy saving MAC Protocol for Wireless Sensor Network," *IEEE Trans. on Vehicular Technology*, vol. 59, No. 2, pp. 813-822, Feb 2010.

[5] T. Zheng, S. Radhakrishnan and V. Sarangan, "PMAC: And Adaptive Energy-efficient MAC Protocol for Wireless Sensor Networks," *Proceedings of the 19^{th} IEEE International Parallal and Distributed PRocessing Symposium*,Denver, USA, IEEE Press, pp. 237-244, 2005.

[6] Q. Xu, L. Rong, S. Fang and Y. Du, "Energy-Efficient Scheme for IEEE 802.15.4 Compliant Device," *Progress in Electromagnetics Research Symposiam*, pp. 353-356, March 2009.

[7] S. Hayat, N. Javaid, Z. A. Khan, A. Shareef, A. Mahmood and S. Bouk, "Energy Efficient MAC Protocols in Wireless Body Area Sensor Networks", *14^{th} IEEE International Conference on High Performance Computing and Communications (HPCC-2012)*, Liverpool, UK, pp. 1185-1192, June 2012.

[8] T. V. Dam and K. Langendoen, "An adaptive energy-efficient MAC protocol for wireless sensor networks", *In Proceedings of the 1^{st} international conference on Embedded networked sensor systems (SenSys '03)*, ACM, New York, NY, USA, pp. 171-180, 2003.

[9] S. Pollin, M. Ergen, B. Bougard, L. V. der Perre, F. Cathoor, I. Moerman, A. Bahat and P. Varaiya, "Performance Analysis of Slotted IEEE 802.15.4 Medium Access Layer," *Tech. Rep.*, DAWN Project, 2005.

[10] F. Peng, B. Peng and V. C. M. Leung, "An Application Oriented Power Saving MAC Protocol for Wireless Sensor Networks," *Wireless Personal Communication*, Springer, August 2011.

[11] H. Chen, P. Chou, S. Duri, L. Hui, and J. Reason, "The Design and Implementation of a Smart Building Control System," *IEEE International Conference on e-Business Engineering (ICEBE '09)*, pp.255,262, October 2009.

[12] S. Fang, R. Lu, Q. Xu and Y. Du, "Performance Analysis of Unsaturated Slotted IEEE 802.15.4 Medium Access Layer," *Progress in Electromagnetic Research Symposium Proceedings*, Hangzhou, March 2008.

A QoS Aware Message Scheduling Algorithm in Internet of Things Environment

Saima Abdullah
School of Computer Science & Electronic Engineering
University of Essex Colchester CO4 3SQ, UK
Email: sabdulf@essex.ac.uk

Kun Yang
School of Computer Science & Electronic Engineering
University of Essex Colchester CO4 3SQ, UK
Email: kunyang@essex.ac.uk

***Abstract*—Internet of Things (IoT) is a novel approach of connecting things/objects and thus transmitting information from the physical world to control centres (or vice versa) where this information can be interpreted. Where majority of the research focuses on sensor technologies (including energy harvesting), communications and routing, this paper positions itself on a higher layer, i.e., message scheduling, which is more targeted towards service provisioning. In particular messages are classified into high priority (HP) and best effort (BE) and the corresponding Quality of Service (QoS) scheduling algorithm is proposed. Doing so will enable the IoT network to differ emergency messages from non-mission critical messages. In addition, network-layer routing algorithms are also taken into consideration in message scheduling, aiming to provide a more optimal solution by applying certain degree of cross-layer design methodology.**

Here sensor nodes are divided in IoT subgroups. Each subgroup has a broker delivering for all nodes and maintaining two queues for HP and BE messages respectively. QoS awareness is introduced in IoT subgroups by assigning traffic priorities and scheduling them with proposed algorithm making them energy efficient as well .Simulation results have shown the efficiency of the proposed algorithm.

keywords: Internet of Things (IoT), Message Scheduling, Service Oriented Architecture (SOA), QoS awareness.

I. Introduction

Internet of things (IoT) is the new wave in the era of computing and networking. This term was used by K. Ashton in 1999 in the context of supply chain management. Many objects that are around us will be on the internet using Radio Frequency Identification (RFID), Wireless sensor Networks (WSN) communication technologies and by any underlying communication protocol. Smart intelligent objects would work for humans and machines in the every walk of life. An IoT model will consist of services that are commodities and would be delivered in a manner similar to traditional commodities [1].

Service-oriented Architecture (SOA) provides standard way of representation and communication for these services.These services call and talk with other services [2]. To ensure a reliable interaction between these SOA services, new protocols, networking technologies and devices are being researched and implemented. That enable these enormous physical world objects to communicate and interact with surrounding environment with enhanced computation powers [3].

The same idea of SOA was applied to interconnect these small embedded objects and the underlying infrastructure can be used to select, find and utilize real world services in dynamic way. Here functional part of these smart objects i.e. sensing is considered as a service. The services, based on heterogeneous objects, are directly related to real world by sensing the information from real world environment. SOA can be used for the management of IoT and provisioning of these services [4]. Real-time and critical applications shall have high priority (HP) than non-real time and non-emergency applications which are regarded as best effort (BE) services.

Future IoT systems require cross layer optimization to achieve all the pre-requisite like low latency, high throughput. While considering messaging network, properly designed scheduling is significant to achieve already mentioned goals and making them highly efficient.

QoS requirement is one of the dominant and challenging factors that need be addressed in order to achieve effective communication in the design of WSNs [5].

With a numerous number of objects and to keep them talking to each other, for IoT one challenge is to deal this scalability in an efficient way. Two-tier architecture does not support scalability with loose coupling of these objects. Because of these limitations we are considering an IoT brokered system architecture based on a 3-tier system architecture as in Figure 1. Sensor nodes/objects are grouped and connected to one server called broker. Broker provides buffering for incoming request and works as a transfer centre for forwarding responses from all the member of that group.

Hence message scheduling at sensor nodes is significantly important for prioritizing applications and it is required for intermediate nodes/brokers to change the delivery order of data in their ready queue based on priorities to ensure delivering critical data first.

Our purpose is to deal with optimized QoS scheduling and routing with the energy efficiency problem with respect to IoT and how to make them efficient in terms of end-to-end delay and sensors energy consumption as per our previous findings [11]. Much of the related work is seen according to the enabling technologies for IoT i.e., WSNs and Wireless multimedia sensor networks (WMSNs).

I.Almalkawi et al. gave the idea of cross layer communication architecture for WMSNs between the routing and MAC

978-1-4799-0354-2/13/$31.00 ©2013 IEEE

layer. Scheduling protocol was considered from the energy aware and QoS point of view using multipath cluster based approach [6].

K. Wongthavarawat et al. discussed a scheduling algorithm with QoS support in term of bandwidth and delay bounds for traffic classes defined by IEEE 802.16 standard [7].

D. Vinayagamet et al. proposed a cross layer based two way scheduling algorithm for two type of services as we are considering. This algorithm worked well for throughput, packet loss ratio, delay and QoS requirements using Proportional Fair (PF), Modified Long Weighted Delay First (MLWDF) and Exponential Proportional Fair (EXP/PF) schedulers when compared with their selected benchmarks [8].

A. Ghiasian et al. analyzed the end to end delay for two randomized algorithms for link scheduling in wireless sensor networks. They also checked the same by assigning traffic priorities [9].

R.uthra et al. given a survey on based on QoS routing in WSNs by the parametric comparison, mainly concentrating on the network congestions point of view [10].

We are working with cross-layer unified architecture with QoS aware application layer scheduling and also interacting with network-layer routing algorithm extending our previous work in [11]. The aim is to design QoS aware energy-efficient message scheduling algorithm for IoT systems.

For more intricate processing by brokers in our IoT subgroups, it is important to follow a right order of messages while sending them to the ultimate receiver sink. The end to end delay or waiting time affects the battery life of the large number of tiny nodes equipped with processor, memory and short range wireless communication. For these kinds of systems who support wide range of IoT applications it is a strong requirement to reduce end-to-end delay and losses during message transmissions.

The improvement of messaging order in term of delay time for two classes of priority experimented in term of energy and prolonged lifetime of the network can be seen in the evaluation results of the implemented system.

The proposed algorithm adapts well to the dynamic requirements of IoT applications and schedules real-time tasks with the highest priority ensuring a minimum end-to-end data transmission delay. It also schedules BE second priority tasks with fairness to avoid starvation in delivery of messages for a longer period of time.

We discuss proposed QoS aware IoT Messaging Service Architecture and Problem Statement in Section II. Section III describes the proposed QoS aware message scheduling algorithm. Section IV is based on performance evaluation and discussion related to simulation results. In section V a summary of contribution is given with further work ideas and possible future enhancement.

II. Proposed IoT Messaging Service Architecture and Problem Statement

A. Proposed IoT Message System Architecture

Our system architecture comprises of IoT brokered system as shown in the figure 1. The environment where there is a single server serving multiple clients, there will be more and more direct links to it, that put certain limitation on number of clients that can be attached. To solve this problem, the idea is to divide the system into small units or subsystems called IoT subgroups. We follow a clustering based approach. Here set of objects/sensor nodes makes one IoT subgroup, where every node can get the role of broker each time. The node which becomes the broker takes the responsibility of collecting and fusing the data from its member nodes and sends them to the base station on their behalf reducing their energy wastage [11].

In networking, routing means selection of an optimal and an appropriate path to transmit the data over it. The followed routing technique in our previous work was derived from the Low Energy Adaptive Clustering Hierarchy (LEACH) [12], now the improvement in this energy efficient message scheduling algorithm is done with multihop LEACH [13] by the introduction of QoS in it.

In each IoT subgroup messages are heterogeneous in nature sent by the different sensor nodes to the central authority i.e broker. Messages are carrying different properties of them for example size, requesting time period, priority etc. Unlike the previous work this time broker gets the message and send those to the sink according to its importance level i.e. priority.

We are considering two types of prioritising applications providing two classes of services. The one class would be services for high priority (HP) which are real time and critical while second class best effort (BE) is for all other kinds of services that are not critical and non emergency data. HP messages can preempt the data at the other queue. The system is working for multi-hop clustered systems [13].

After dividing the incoming messages into two queues HP and BE where all messages are being served on FCFS basis. The relationship of both queues with the energy efficiency is shown in the evaluation results. These nodes are energy constrained and lot of work has been done that how to make them long lived. When they receive, process and send the data that takes more of their energies. Poor transmission efficiency reduces the battery life of node and the delay a node faces after sending the message also affects them.

We worked with the proposed system as in [11] from the two integrated aspects: network layer routing and application-layer message scheduling making them together in one unified system architecture. This architecture cosiders routing with QoS aware message scheduling at the top.

B. Problem Statement

We investigate QoS-aware service provisioning in IoT environment. We consider a combined architecture of network level routing and application level QoS aware message scheduling. Our aim is to enhance our previous work [11]

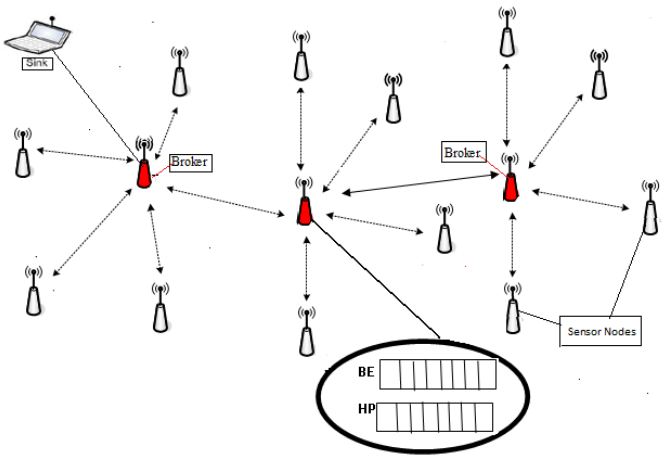

Fig. 1. Proposed IoT QoS Aware Messaging System and Network Architecture

by introducing the concept of service differentiation in IoT system and check its effect in relation to energy conservations of nodes.

Energy aware system for WSNs has not considered this aspect of QoS aware service provisioning and affect of delay/waiting time on the battery life time of nodes. We use clustered WSNs approach following multihop-LEACH [13].

III. Proposed Energy-aware Message Scheduling Algorithm

A. Energy Consumption Model

We consider a network consisting of N randomly distributed sensor nodes where these nodes are organized/grouped into IoT subgroup. In each IoT subgroup nodes send messages to their respective broker. All nodes perform at the same level of working for example sensing, processing and transmitting messages. We use First order radio energy consumption model as in [12]. Different assumption may affect the performance of different protocols so our assumptions of the system at the start are:

1) Ultimate receiver or sink is fixed and located far away from sensors.
2) All sensor nodes are homogeneous and energy-constrained. We are not assuming that there is a "high-energy" node which can be assigned the duty to work as broker for global communication. Such communication indicates that any node can be connected to the farther base station at any time during simulation.
3) This routing protocol also got a way to perform data fusion to reduce the amount of information send to the sink.

The capacity to perform data fusion makes it suitable in term of scalability and flexible for dynamic network environment. However this data compression really affected by the amount of IoT subgroups we are making if we are making them very less that data compression would lead to larger loss of energy as each broker has to do for larger no of nodes. While very larger percentage of IoT subgroup would also result in larger depleted energy which is necessary to transmit many global messages to base station. An optimal percentage is 5 of all nodes [12]. E_{elec}: Varaible to represent energy dissipation to run the transmitter or receiver circuitry. E_{amp}: Variable to represent energy dissipation in transmission amplifier in order to amplify the signal enough to reach the destination. For every single message r, E_{T_r} and E_{R_r} are energy calculations to transmit and receive a message respectively.

$$E_{T_r} = E_{elec} * K + E_{amp} * K * d^2 \tag{1}$$

$$E_{R_r} = E_{elec} * K \tag{2}$$

K=number of bits per message. d= distance between end points in eq (1) and eq (2) as in [11]. These two points could be sensors, brokers and sink/receiver [12].

In this paper we are following multihop technique where brokers are also communicating with each other. Nodes send messages to the nearby brokers finding the closest path to the sink. Long connection consume less power when using multihop routing [13]. Weightiest load is put on the node working as a broker closest to the sink as it has to perform communication on behalf of the other brokers. Weightiest load indicates the global connection between any node/broker and the sink in the network.

However more load means more energy dissipation and ultimately death of that closest node with sink. For next, then another closest broker take this responsibility and so on. A significant total of power saving has been observed if there is a closer cluster-head to these non-cluster-head nodes and it extends the network lifetime longer than others which is the main reason to have multihop system of communication.

B. Mathematical Analysis using M/M/1 Queuing Model

To model the arrivals and service rates of all messages coming from IoT subgroups to the broker we use an M/M/1 queue. Every IoT subgroup has its local broker which is working on behalf of all the IoT sensors devices within this subgroup. Then this broker finds the optimal path to reach to the closest broker to sink. The QoS aware scheduler is running at each broker level. Every broker has two queues which is maintained for two types of incoming messages. The arrival rate and service rate for r_{th} message for r=$\{1, 2, \ldots, n\}$ are represented by λ_r and $\mu_r$respectively. We can have the total traffic intensity as given in eq 3.

To analyse the system effectiveness we are interested to get the waiting times/end to end delay of each message in their respective class of priority. We can get the traffic intensity of each class as given in the eq (3) and eq (4) by using results in [14] and can get the waiting times of queue 1 and queue 2 as in eq (5) and eq (6):

$$\rho_r = \frac{\lambda_r}{\mu_r} = \frac{T_{trans_r}}{T_{request_r}} \tag{3}$$

here k is for the no of priorties, as we are dealing with two priority classes so k=2.

$$\sigma_k = \sum_{i=1}^{k} \rho_i, \rho < 1 \tag{4}$$

$$W_{Queue_1} = \frac{\sum_{k=1}^{2} \frac{\rho_k}{\mu_k}}{1 - \sigma_1} \tag{5}$$

$$W_{Queue_2} = \frac{\sum_{k=1}^{2} \frac{\rho_k}{\mu_k}}{(1 - \sigma_1)(1 - \sigma_2)} = \frac{W_{Queue_1}}{(1 - \sigma_2)} > W_{Queue_1} \tag{6}$$

So from the deduction of (5) and (6) we can have

$$W_{Queue_1} < W_{Queue_2} \tag{7}$$

We get that waiting time for the high priority queue is less than the waiting time for lower priority queue. It means that a lower priority causes a longer waiting time in the queue [14]. In our case, we represent HP and BE as high and low priority queues.

For every message there is a service request period time and successful transmission time. Service time define the successful transmission time by the broker to the nearby broker in multihop way. While the request period time is the rate at which the messages are coming into the broker queue. Now in this work for service differentiation each message has a randomly assigned prioritiy.

As heterogeneous types of messages are coming to be served in the borker queue. The queue is prioritised with two classes, HP and BE and then we check the traffic intensity of each class. In proposed algorithm for every message, delay or waiting times will be calculated and checked by analyzing the traffic intensity of their respective classes.

C. QoS Aware Message Scheduling Algorithm

Following the assumption stated before, firstly the priority of the incoming message is checked and according to the service type, it is sent into their respective queue. By having results in [14], we compare two queue model with priority. We get that $\mu_1 > \mu_2$ for a two-class model. The higher will be the priority the faster would be the service rate. The higher priority queue leads to less overall waiting time.

We have n types of messages coming from sensor nodes to the broker. For every r_{th} type of message *r={1, 2, …, n}* successful transmission time of the request is denoted as T_{trans_r} , and request time period is denoted as $T_{request_r}$, while the priority of each message is defined by P_r . Each message can be represented as $Mess_r(T_{request_r}, T_{trans_r}, P_r)$. The arrival rate and the service rate of the r_{th} message are represented as $\lambda_r = \frac{1}{T_{request_r}}$ and $\mu_r = \frac{1}{T_{trans_r}}$, respectively as in [11]. Next check is the overall system traffic ρ, by adding traffic intesity of each of r_{th} message ρ_r in all IoT subgroups.

Every message that is coming from the sensor objects are having information regarding environment, such as temperature, humidity, etc. The changes in these informations are sometime negligible, so the idea is to ignore some of the non-important and emergency data. The long waiting queues of messages can be avoided by ignoring the messages that are non critical, and improvement of the overall performance of the message transmission can be done by following the messages with important emergency information [12]. In the

Algorithm 1 Proposed QoS Aware Message scheduling Algorithm in Each IoT Subgroup

1: **for** r_{th} periodic message:$Mess_r(T_{request_r}, T_{trans_r}, P_r)$ **do**
2: **if** P_r=1 **then**
3: put $Mess_r$ in pr_1 queue
4: **else if** P_r= 2 **then**
5: put $Mess_r$ in pr_2 queue
6: **end if**
7: **while** $currtime > SimTime$ **do**
8: **if** $Mess_r$ in pr_1 queue $T_{request_r} <= currtime$ **then**
9: goto step12 for pr_1 queue
10: **else if** $Mess_r$ is in pr_2 queue $T_{request_r} <= currtime$ **then**
11: goto step 12 for pr_2 queue
12: **for** r_{th} traffic intensity ρ_r **do**
13: $\rho_r = \frac{T_{trans_r}}{T_{request_r}}$, for r={1, 2, …, n}
14: sort $Mess_r$ in a $T_{request_r}$ descendent order. for all r={1, 2, …, n}
15: $\rho = \sum_{r=1}^{n} \frac{T_{trans_r}}{T_{request_r}}$
16: **end for**
17: **end if**
18: increment currtime by timeslot
19: **end while**
20: Request $Mess_r$ in a descendant $\mu_r = \frac{1}{T_{trans_r}}$ order.
21: **end for**

proposed algorithm messages are received at the broker and then according to the priority of the message it is assigned to the respective queues,Pr_1 and Pr_2.

We have set the simulation time which is incrementing according to the assumed timeslot. If in that slot of time we receive some message, we would check its request period time if it is less than the current time, we may start processing the message, while keeping in view that Pr_1 would be served first than Pr_2 . We calculate the traffic intensities of two classes and can compute the waiting times of two priority classes as above mentioned. Using these waiting times we made a graph against number of messages as shown in the figure 2. Waiting times of 400 messages are shown here in the graph, for HP messages the curve starts from 0 to 6 microseconds while for BE messages the waiting times starts from 1.5 to 16 microsecond of time.

The next section describes how end to end delay faced by a message moving through different IoT subgroups affects the battery life of IoT sensor network under considered routing protocol. For sending message from sensor or device to the broker energy dissipated by the batteries of the nodes. When these messages are given to broker for further processing these nodes have to wait for the response from the broker. This

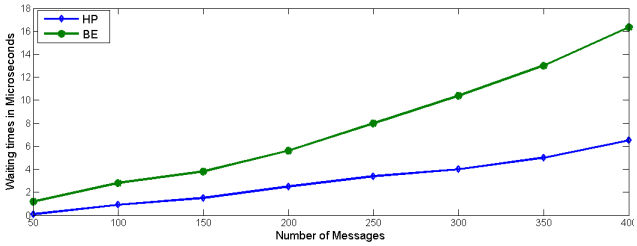

Fig. 2. Graph showing waiting times of 400 messages for HP and BE priorities

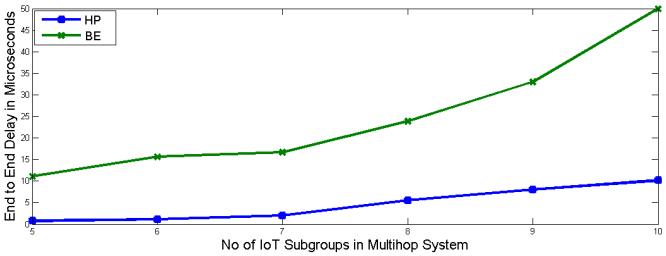

Fig. 3. Graph showing waiting times of two priority queues while moving through different numbers of IoT subgroups

waiting time definitely affects the battery life of the sensor or device as they remain running/active during this time. In our system we are using multihop approach the delay depends on the number of brokers in the way to get to the sink node. On every broker level there is a queue where the message has to face certain delay. As the message passes through different level of brokers, this delay added up at each level of subgroups. The delay time of the system is large and ultimately a sensor/node has to wait for longer time. Every node spends the battery life with every tick of the clock. This delay time is less experienced by the high priority messages than Best effort ones.

So in our proposed system we have introduced QoS aware scheduling algorithm in our previous work [11] and also checked its affect on ultimate goal of the work i.e., energy/network life of the system.

IV. Performance Evaluation and Discussion

A. Simulation Setup

For our experiments we use Matlab version 7.8. We modelled our messaging system within each IoT subgroup using M/M/1 priority queue model. For every r_{th} periodic message $Mess_r$, their request period time, transmission time and priorities are represented by variables/notations $T_{request_r}$,T_{trans_r} , P_r respectively. Energy consumption model is used as in [12]. For every node transmitting energy dissipation is represented as E_{T_r} and computed as in eq (1) and receiving energy is represented by E_{R_r} and computed by eq (2).

We assume all the sensor nodes are same as per their energy levels at the beginning and then with running the simulation their energies are computed and reduced as per their roles Broker or ordinary node. Waiting times faced by the nodes according to priorities also become the reason of energy reduction when they send the messages. The node that plays the role of broker is selected on random basis in each round of the simulation. The objective is the introduction of the service differentiation in the proposed system comprises of IoT subgroups while considering its affect on energy efficiency as well.

B. IoT Subgroups with Service Differentiation

We checked our proposed system by experimenting with different numbers of IoT subgroups in the system. Different number of IoT subgroups are defined and controlled by percentages of brokers defined in initialization. If for example this percentage is 3 , it means out of 100 nodes 3 nodes would be working as broker and there will be 3 IoT subgroups. So the percentage of brokers in the multihop routing system varied against the waiting times faced by the messages after the nodes send them.

According to our findings, when there was larger number of subgroups, a message has to wait more than when there were less subgroups. Within these subgroups, as message passes through every broker and moving toward the sink, every time the message has to wait in broker queue and then its moved down in multihop way.

As shown by the graph in Figure 3, for BE messages the delay is higher up to 50 microseconds when there are 10 subgroups and then it moves untill 5 subgroups(we limit the minimum number of broker as optimal percentage of brokers defined in [12]) where the end to end delay is minimum i.e., 10 microseconds. While the delay experienced by the HP messages are less and starting from 10 microseconds even for 10 subgroups and move to almost 0 when the IoT subgroups are 5. With less number of brokers, the messages move quickly towards the ultimate receiver i.e., sink and experience less delay. We keep the least percentage of brokers as 5 because after that there will very few brokers to receive and process the messages from large number of sensors nodes.

C. Energy efficiency with Service differentiation

We consider clustering approach in which node that acts as broker is randomly selected in each iteration of simulation and we also define the percentage of nodes that would be brokers. However this percentage among the whole number of sensor nodes in a network affects the total amount of energy consumption and accuracy of data transmission. For example, if we keep this percentage very small, there would be few brokers to compress data for large number of nodes. This may leads to large loss in the energy. Secondly, some nodes may suffer for being located at a large distance from broker as there are few brokers, so this distance results in consumption of their energies. On the other hand, large percentage of brokers would also result in high consumption of energies. So to keep energy efficiency and data accuracy side by side an optimal level must be found.

We consider the system from the point of view of energy dissipation when service differentiation through our proposed

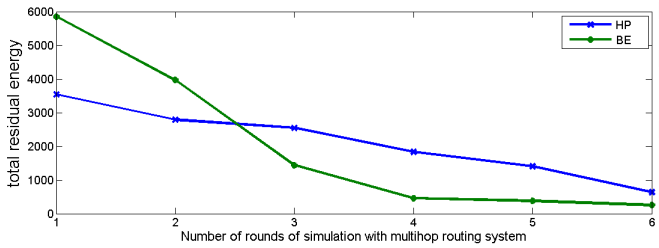

Fig. 4. Graph showing total residual energy for HP and BE queues in multihop system for six rounds of simulation

QoS aware scheduling is applied with multihop routing protocol.

We computed the waiting times or end to end delays faced by two different types of messages according to their priorities. Energy calculation for every node is done as per their roles i.e., broker or ordinary node. If they are ordinary nodes then the waiting time also affects their battery life/energies after sending the message is considered. We calculated the total energy used by every node and got the sum as shown by graph in figure 4. Total residual energy is drawn against the number of rounds in the simulation. The total residual energy by the nodes for the BE messages is high in first round at the level of 6000J and going down towards to 20J-30J at 6th round of simulation. We keep the same optimal percentage of broker here. While HP messages results in conservation of more energy of the batteries of the nodes and in 1st round it starts from the 350J and moves to 90J almost.

V. Conclusion and Future work

We proposed a QoS message scheduling algorithm, which is more targeted towards service provisioning with the idea of service differentiation as well continuing our previous work [11]. Messages are classified into high priority (HP) and best effort (BE) carrying all other non- critical kind of data. While extending our previous work the idea is to enable the IoT network to differentiate emergency messages from the non-mission critical messages finding optimal balance by the cross-layer design methodology with network-layer routing and application layer QoS aware message scheduling. Simulation results are shown in term of waiting time and energy using proposed algorithm.

The immediate future work is to apply the same service differentiation with three classes of priorities and have different kinds of scheduling strategies within these classes of services.

Acknowledgment

The work of the paper was partly supported by UK EPSRC Project DANCER (EP/K002643/1) and EU FP7 Project CLIMBER (GA-2012-318939).

References

[1] J.Gubbi, R. Buyya, S. Marusic, and M. Palaniswami. "Internet of Things (IoT): A vision, architectural elements, and future directions." Future Generation Computer Systems, 2013.

[2] S.Mokhtar, "Delivery of Service Oriented Architecture with Web Services." 2012.

[3] S. De, P. Barnaghi, M. Bauer , and S. Meissner, "Service modelling for the Internet of Things." In Computer Science and Information Systems (FedCSIS), 2011 Federated Conference on, IEEE, 2011, pp: 949-955.

[4] H.Xu, W. Liu, C. Wang, H. Chen, "Service-Oriented Management for Internet of Things." International Journal of Information and Network Security (IJINS) Vol 2.1, 2012, pp: 54-59.

[5] P. Nayak, G. Ramamurthy "A Novel Approach to an Energy Aware Routing Protocol for Mobile WSN: QoS Provision." 2012 International Conference on Advances in Computing and Communications (ICACC), IEEE, August 2012, pp: 38-41.

[6] T. I. Almalkawi, G. Z. Manel, N. A. Jamal "A Cross-Layer-Based Clustered Multipath Routing with QoS-Aware Scheduling for Wireless Multimedia Sensor Networks." International Journal of Distributed Sensor Networks 2012.

[7] K. Wongthavarawat, A. Ganz, "Packet scheduling for QoS support in IEEE 802.16 broadband wireless access systems". International Journal of Communication System, vol:16(1), 2003 pp: 8196..

[8] D. Vinayagam, R. Kurinjimalar, D. Srinivasan. "Performance evaluation of cross layer QoS scheduling for Long Term Evolution Network." International Journal of Advanced Computer Research, vol 2(3) 2012.

[9] A. Ghiasian, S. Saidi, M. Behdadfar. "Delay analysis of randomised algorithms for link scheduling in wireless networks." International Journal of Ad Hoc and Ubiquitous Computing, vol 13(1) 2013 pp: 59-72.

[10] R. A. Uthra, S. V. Raja. "QoS routing in wireless sensor networksa survey." ACM Computing Surveys (CSUR) vol: 45(1)9. 2012.

[11] S. Abdullah , K. Yang An Energy-efficient Message Scheduling Algorithm in Internet of Things Environment. 9th International Wireless Communications and Mobile Computing Conference (IWCMC), 2013 , pp: 311-316.

[12] W. R. Heinzelman, A. Chandrakasan, H. Balakrishnan, "Energy efficient communication protocol for wireless microsensor networks". Proceedings of the 33rd Annual Hawaii International Conference on System Sciences, January 2000, pp: 10-pp.

[13] F. Xiangning, S. Yulin, "Improvement on LEACH protocol of wireless sensor network", In IEEE International Conference on Sensor Technologies and Applications SensorComm., October 2007, pp: 260-264.

[14] D. Gross, J.F. Shortle, J.M. Thompson, C. M. Harris, "Fundamentals of queuing theory", Wiley. com, 2013.

Energy-Efficient Cascaded Bit-Interleaving Protocol for Integrated Optical Access/In-Building Networks

Tolga Ayhan, Ahmad R. Dhaini, Leonid G. Kazovsky
Photonics and Networking Research Laboratory
Stanford University
Stanford, CA, USA

Dusan Suvakovic, Hungkei K. Chow
Alcatel-Lucent Bell Labs
NJ, USA

Abstract— **This paper proposes and experimentally evaluates the Cascaded Bit-interleaving architecture and protocol, an energy-efficient solution that aims to reduce the power consumption of integrated optical access/in-building networks, while offering high-speed Internet service to end-users. In the new architecture, optical-electrical-optical (OEO) regeneration is employed at the interface between the access and in-building networks, and downstream frames are generated at the central office using the two-stage bit-interleaving scheme. The users' network nodes only process the data destined for them without any buffering at a lower clock rate than the aggregate PON rate, thereby significantly reducing their energy consumption. Simulation and experimental results demonstrate the proof of concept and show that the power consumption of the access/in-building network can be significantly reduced when the proposed cascaded bit-interleaving protocol is employed.**

Keywords—Optical Networks, Energy Efficiency, PONs, Protocols

I. INTRODUCTION

Energy efficiency in communication networks has become a very important subject due to the explosive growth in the number of users and the demand for higher data rates per user. It is predicted in [1] that by year 2018, communication networks will consume about an order of magnitude more power than today unless disruptive improvements in the energy efficiency are achieved. Therefore, it is essential to reduce the power consumption of communication networks while at the same time providing high data rates to end-users. Specifically, decreasing the power consumption of access networks in general and of optical access and in-building networks in particular has become an urgent need, as these networks constitute the largest part of the Internet and connect a very big amount of active devices.

Passive optical network (PON) has been considered an attractive technology for broadband access networks [2]. It comprises an Optical Line Terminal (OLT) that resides in a Central Office (CO) and connects a set of associated Optical Network Terminals (ONTs) through a single fiber after being fed via a remote node (RN) in which a passive power splitter is employed. Time division multiple access (TDMA)- based PONs, such as Ethernet PON (EPON) and Gigabit PON (GPON), have been standardized, and they employ one wavelength in the upstream (i.e., from ONTs to OLT) and another wavelength in the downstream (i.e., from OLT to ONTs). Existing PON protocols are not optimized in terms of energy-efficiency. Therefore, it is important to design the protocol with the goal of achieving energy-efficiency while at the same time satisfying the data rate and quality-of-service (QoS) requirements. Various solutions have been proposed in the literature aiming at reducing the power consumption of PONs. One promising technique is to enable the *sleep* mode operation at the ONT, and perform dynamic power management [3, 4]. However, the amount of reduced power has not been as great as desired.

In TDM-PON, downstream frames are formed at the OLT and are broadcast to all ONTs. Thus the ONT processes all downstream frames at the line rate of the PON, and subsequently if the destination address does not match the ONT's address, it drops the frame. This mechanism significantly impacts the power consumption of PON [4], since it forces the ONT to perform unnecessary frame processing for the biggest part of the incoming traffic.

Consequently, bit-interleaving was proposed as an effective solution for mitigating this problem [5]. In bit-interleaving passive optical network (Bi-PON), the downstream frame's payload is interleaved at the OLT and broadcast in the downstream direction, and each ONT processes its designated payload bits at a low rate, and thus it drops all other payload bits without processing them. This reduces the average power consumption for protocol processing in the ONT by more than an order of magnitude. Taking into account the consumption of other components like the optical transceiver and home gateway processing, the total power consumption of the ONT can be reduced by about 67% in a 10 Gbps PON [6].

Today, Internet service providers such as Verizon FiOS terminate the PON at the ONT and employ a Multimedia-Over-Coax (MOCA) in the building [7]. A straightforward approach to make the network more energy-efficient could be to replace the MOCA in home with an in-building PON. However, this approach would not be good since the ONT in this case has to behave as both an ONT terminating the WAN PON and an OLT serving the LAN PON. That would raise complexity and cost issues and increase the power consumption of the ONT. Therefore in this paper, we propose a protocol that allows for a very simple ONT architecture (which we refer to as *Repeater*), which helps reduce the power

978-1-4799-0354-2/13/$31.00 ©2013 IEEE

consumption. It is also known that the power consumption of in-building networks is a significant contributor to the overall power consumption of communications networks, especially with the increase in demand for very high-speed services. Therefore, we envision an integrated access/in-building network with centralized processing at the central office, which reduces the processing overhead of the customer premise equipment (CPE) and decrease the total energy consumption in the network.

In this paper, we propose a cascaded bit-interleaving architecture and protocol for the integrated optical access/in-building network. The proposed architecture replaces the ONT with the *Repeater* and extends the optical distribution network to penetrate the in-building network, which terminates at an end-ONT residing inside the building. The new architecture implements the bit-interleaving technique to reduce the energy consumption of the ONT. It also centralizes the routing function at the OLT to further decrease the end-ONT power consumption. Furthermore, the clock rate is decreased at the interface in the CPE to make the overall network even more energy efficient.

The rest of this paper is organized as follows. In Section II, we describe the proposed Cascaded Bit-Interleaving architecture and protocol. This includes a detailed description on the structure of the repeater and end-ONT, as well as how the downstream frame is generated at the OLT. In Section III, we discuss the energy savings achieved using our proposed architecture. In Section IV, we present our simulation and experimental results, which highlight the merits of the proposed solution. Section V concludes the paper.

II. CASCADED BIT-INTERLEAVING PROTOCOL

In this section, the proposed integrated access/in-building network is presented. The network nodes and their building blocks are also detailed. The proposed downstream transmission protocol is explained, and the frame generation strategy at the OLT is described. The upstream control protocol is the same as the legacy PON upstream protocol, and is supported in the proposed scheme via embedding the upstream control information in the downstream frame header.

A. Network Architecture

The proposed integrated access/in-building network architecture is illustrated in Fig. 1. We employ passive optical networks in both access and in-building networks, such that there is optical-electrical-optical (OEO) regeneration at the repeater. We consider the downstream data rate to be 10 Gbps for the access network and 1 Gbps (peak) for the in-building network. We design the cascaded bit-interleaving protocol for the combined access/in-building network. The repeater provides the interface between the access and in-building networks. The end-ONT can be considered as a network interface unit connected to the end-user's terminal.

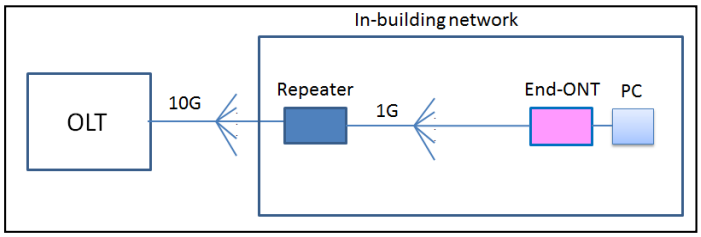

Fig. 1: Proposed network architecture

B. General Downstream Frame Structure

The downstream frame in the proposed architecture is generated at the OLT and broadcast to all repeaters. The frame consists of a header section and a payload section. The header section consists of a constant synchronization bit pattern, ONT IDs, and downstream and upstream bandwidth map. The downstream bandwidth map contains the flag, decimation rate and offset information so that when a network unit starts getting its payload bits, it can locate its designated bits from the already interleaved payload block. The general architecture of a downstream frame is illustrated in Fig.2. A specific lane, which is associated with an ONT-ID, is described by the horizontal bar in the header in Fig. 2, and the corresponding payload bits are represented by the small rectangles in the payload section. It should be noted that the payload bits of a node are defined by the rate and offset information extracted from the downstream bandwidth map associated with the node's ONT-ID number. The frame structure shown in Fig.2 is based on a fixed number of ONT-IDs.

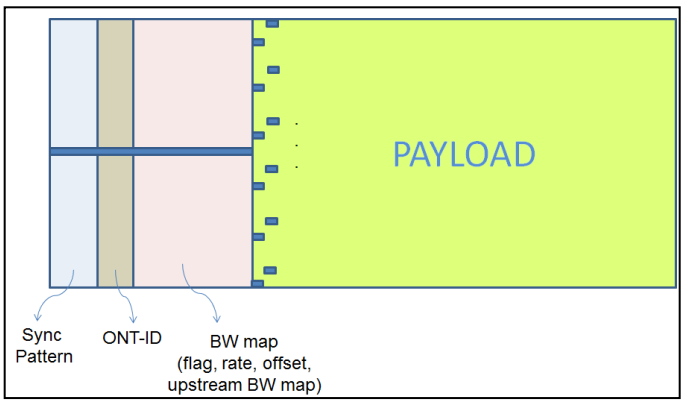

Fig. 2: Downstream frame structure

C. Repeater and End-ONT Structures

The building blocks of the repeater are provided in Fig.3. The receiving procedure at the repeater can be described as follows: First, the repeater recovers the line rate clock from the access network. Next, it decimates received bit stream at the rate of 1/N, where N is the number of repeaters in the network. The repeater searches for a synchronization pattern from the decimated stream. If it synchronizes successfully, it locks to its own lane (i.e. finds the lane with the associated ONT-ID). Next, the bandwidth map field is descrambled and parsed. Then, the downstream payload flag associated with its ONT ID is extracted from the bandwidth map (BW map) parser, which indicates whether there is any downstream

payload for this repeater from the header. If there is payload data, it fetches the corresponding bits from the payload section of the frame using the rate and offset information that were extracted from the header using the BW map parser. This is done by sending the rate and offset parameters to the decimator. The repeater then forwards the decimated bits to the descrambler. However, if there is no payload data for the corresponding repeater in the current frame, it does not fetch any payload bits and waits for the next frame. The descrambled bits are sent to the Forward Error Correction (FEC) decoder, and then broadcast to the in-building network.

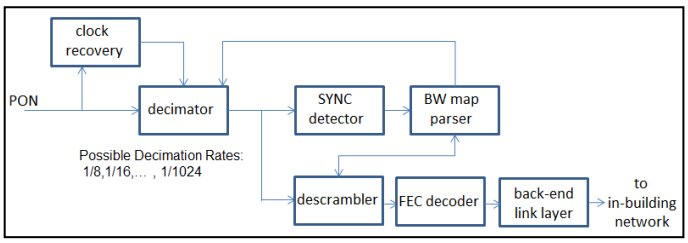

Fig. 3: Building blocks of the repeater

A detailed illustration of the decimator block in the repeater is provided in Fig. 4. To fetch 4 bits from the 32-bit register, the 32:4 multiplexer (MUX) is used at each clock cycle, and similarly to fetch 2 bits from register, the 32:2 MUX is used at each clock cycle. If the decimation rate is between 1/32 and 1/1024, the 32:1 MUX is used at every appropriate number of clock cycles to achieve these decimation rates.

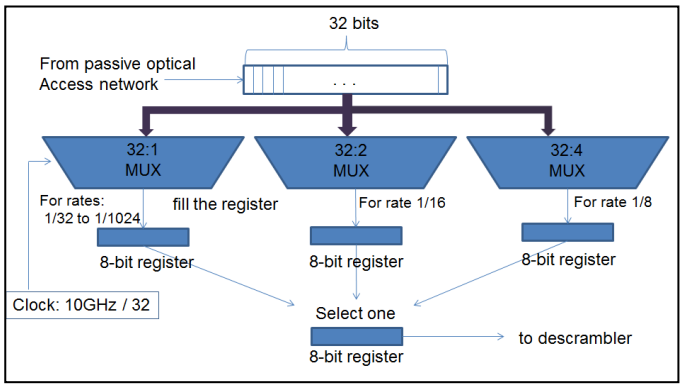

Fig. 4: Decimator block in the repeater

The building blocks of the end-ONT are provided in Fig. 5. Same as the repeater, the end-ONT processes only the necessary parts of the frame's payload block if it has any downstream data to receive. In addition to the decimator block, a descrambler, and a payload decryption block that are rate adaptive are employed in both the repeater and end-ONT. It should be noted that the bits are descrambled after the decimation, so we need to consider the decimation rate and take it as a parameter to correctly perform the necessary operations for the descrambler and other subsequent blocks. FEC is not applied to the in-building frames due to the short distance between the repeater and end-ONTs. The optical power of the 1Gbps SFP at the repeater (for downstream transmission) can be slightly increased to compensate for that.

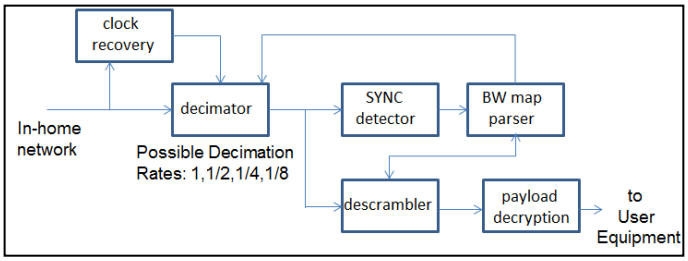

Fig. 5: Building blocks of the end-ONT

Fig. 6 gives the internal structure of the decimator block in the end-ONT. For each distinct possible data rate, there is a separate register. The possible decimation rates range from full rate (i.e., rate = 1) to 1/8. When the register (that is at the bottom in Fig. 6) is full, the content is sent to the descrambler block.

D. Frame Generation at the OLT

In the proposed protocol, the OLT performs the following three steps to generate the proper downstream frame for each end-ONT. First, it forms and interleaves the payload blocks for each in-building network, using the decimation rate and offset information of the end-ONTs. These frames consist of a synchronization block, end-ONT id block, downstream bandwidth map that contains the decimation rate and offset, upstream bandwidth map, and the interleaved payload as shown in Fig. 7a. After forming all small frames in step 1, the payload and bandwidth map sections are scrambled and FEC encoder is applied to the scrambled sections as illustrated in Figure 7b in step 2. Then, after all small frames are ready; the OLT interleaves all small frame bits and places them into the payload section of a large frame (i.e., the frame that is sent in the downstream direction of the access network), before scrambling all the parts except for the synchronization and ONT-ID blocks as shown in Fig. 7c. Subsequently, the FEC encoding is performed on the scrambled parts of the frame as the final step.

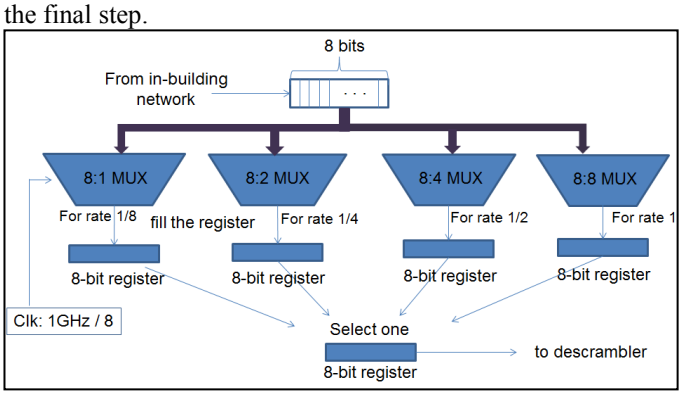

Fig. 6: Decimator block in the end-ONT

The OLT assigns time slots for all end-ONTs and repeaters in the network for upstream transmission and inserts this information in the upstream bandwidth map in the header section.

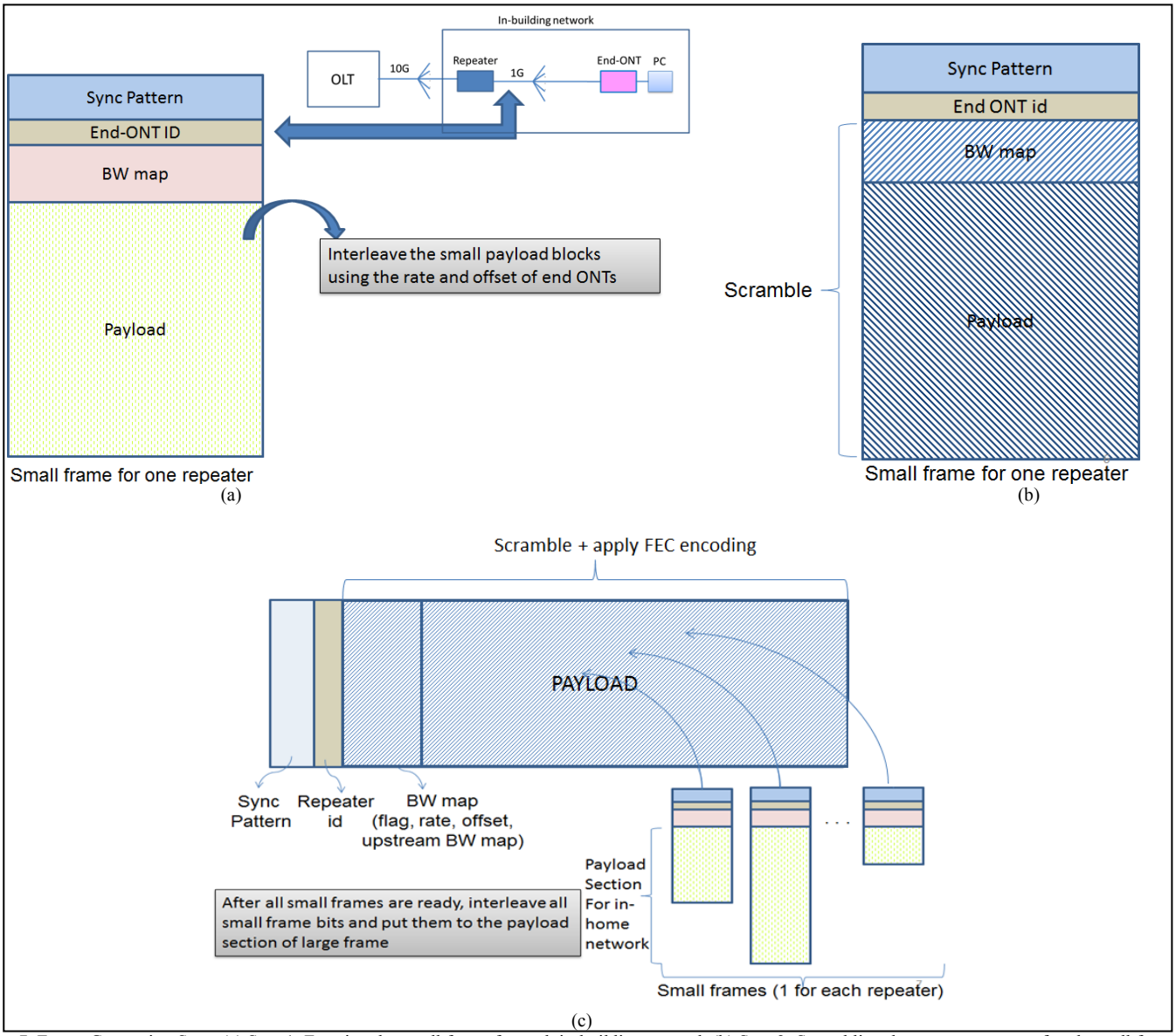

Fig. 7. Frame Generation Steps (a) Step 1: Forming the small frame for each in-building network (b) Step 2: Scrambling the necessary parts of each small frame (c) Step 3: Forming the final frame to be sent in the downstream direction

III. ENERGY SAVINGS IN THE PROPOSED ARCHITECTURE

When the cascaded bit-interleaving protocol is used in the integrated access/in-building network, each end-ONT receives only its own payload data, and is able to process at a low clock rate due to the decimation steps at the repeater and end-ONT. Hence, the amount of digital signal processing at the end-ONT is reduced, which contributes to power savings. In addition, the PON interfaces (i.e. SFP, oscillators, PLLs, transimpedance amplifier and limiting amplifier) consume less power in each end-ONT since the data rate is reduced and the distance to the repeater is short (typically less than 100 meters). When there is no data rate reduction at the repeater, the PON interfaces at the end-ONT consumes more power than the case when the decimation is performed at the repeater, due to the fact that when the repeater performs decimation, the line rate at the in-building PON is lower than the access network, hence the end ONTs can have low-clock rate PON interface modules. This makes the proposed network architecture more energy-efficient than one-stage Bi-PON, in which the PON interface has to operate at 10 Gbps.

It should be noted that the repeater is shared among all the end-ONTs in the in-building network, and the complexity of the repeater is reduced since the routing functionality is centralized in the OLT. Centralizing the repeater functionalities at the OLT reduces the repeater power consumption and increases the OLT power consumption; however when the routing functionality is centralized and shared, the total static power consumption and cooling power consumption can be significantly reduced per-user. Also, one OLT replaces the routing functionality in multiple repeaters, thus the power overhead of all repeaters, including interleaving and power supply losses, leakage etc. is eliminated.

IV. PERFORMANCE EVALUATION

In order to test the protocol, the functions of repeater and end-ONT are implemented in VHDL to program FPGAs. The VHDL code is simulated using Modelsim. For different decimation rates, the frame is constructed and taken as an input to the repeater. The output of the repeater is given to the end ONT as input and the output of end ONT is observed for different decimation rates. The transmission is verified using different in-home data rates in the simulation environment.

We use PowerPlay Power Analyzer Tool in Quartus II software using the project files for the repeater and end-ONT separately. The repeater and end-ONT functions are implemented using Altera Stratix IV Field Programmable Gate Array (FPGA). The power consumption values of the FPGA boards are obtained using gate-level simulations in Quartus II. The dynamic power consumption (including the I/O power consumption) estimations of repeater and end-ONT under the proposed Cascaded Bit- interleaving protocol in the integrated access/in-building network are provided in Table I and Table II, respectively. The I/O power consumption is the power consumed by external load capacitors connected to the output pins plus power consumption of the output driver circuits. In the results shown in Table I and Table II, the FEC decoding at the repeater and the payload decryption at the end-ONT are not included. Also, the transceiver interface modules (i.e. the modules that provide the interface between the FPGA fabric and the SFP) are not included in the gate-level simulation results. It should be noted that the access network data rate is 10 Gbps.

TABLE I. THE DYNAMIC POWER CONSUMPTION OF REPEATER FPGA BOARD AS A FUNCTION OF DECIMATION RATE (I/O POWER CONSUMPTION INCLUDED)

Decimation Rate *(Access Network Data Rate = 10 Gbps)*	**Dynamic Power Consumption (mW)**
1/8	118.48
1/128	81.63
1/1024	78.45

TABLE II. THE DYNAMIC POWER CONSUMPTION OF END-ONT FPGA BOARD AS A FUNCTION OF DECIMATION RATE (I/O POWER CONSUMPTION INCLUDED)

Decimation Rate *(In-Building Data Rate = 1 Gbps)*	**Dynamic Power Consumption (mW)**
1	90.09
1/2	74.84

Despite the fact that FPGAs are not designed for achieving energy efficiency but rather for providing flexibility and ease of implementing a digital design, the results suggest that we can reduce the power consumption significantly when we use the proposed Cascaded Bit-interleaving protocol as compared to the legacy access/in-building networks. In [5], it is shown that when legacy XGPON protocol is implemented in the access network, the dynamic power consumption of the ONT (which is used instead of a repeater) is 3.6 Watts alone when the in-building rate is 1 Gbps. It can also be observed that the dynamic power consumption of repeater and end-ONT scales well with the decimation rate. In addition to the power savings at the ONT (repeater in the proposed architecture), the proposed Cascaded Bit-interleaving protocol can make the in-building end user equipment energy efficient with the use of proposed end-ONT, thereby providing a low power network interface function to the user's equipment. It should be noted that the repeater is shared between 8 end-ONTs, so the repeater power penalty per user is (118.48 mW)/8 when the decimation rate at the repeater is 1/8 and the access network data rate is 10 Gbps.

V. CONCLUSIONS

In this paper, we have described the architecture and operation of an integrated access/in-building network based on the Cascaded Bit-interleaving protocol, which aims to reduce the power consumption of integrated optical access/in-building networks. Additionally, we have experimentally demonstrated the energy-efficiency of the proposed scheme. In the proposed architecture, the repeater performs the OEO regeneration and provides the interconnection between the access and in-building networks. The end-ONTs provide network interface to the end user equipment, which can also be a wireless access point. The main advantages of our proposed protocol can be summarized as follows: First, the repeater/end-ONT processes only the data that is destined for it, and not all the data in a passive optical network environment, which is one of the factors making the protocol energy efficient. Furthermore, the repeater/end-ONT processes the payload data at a lower rate than the aggregate rate of the PON (the exact rate depends on the decimation rate), which is another step for achieving high energy-efficiency. Finally, since there is no buffering in repeater or end ONT, the repeater/end ONT consumes less power. We envision the proposed network architecture and protocol to be a promising candidate for future green access/in-building networks.

ACKNOWLEDGMENT

The authors from Stanford University acknowledge Alcatel-Lucent Bell Labs, NJ, USA and NSERC for their support.

REFERENCES

[1] R. Tucker, R. Ayre, K. Hinton, "Charting a Path to Sustainable and Scalable ICT Networks," GreenTouch June Open Forum, 2012.

[2] N. Yoshimoto, "Operator Perspective on Next-Generation Optical Access for High-Speed Mobile Backhaul," in *Optical Fiber Communication Conference/National Fiber Optic Engineers Conference 2013*, OSA Technical Digest (online) (Optical Society of America, 2013), paper OTu2E.1.

[3] A. R. Dhaini , P. H. Ho and G. Shen, "Toward green next-generation passive optical networks", *IEEE Commun. Mag.*, vol. 49, no. 11, pp.94 - 101 2011.

[4] J. Kani, "Power Saving Techniques and Mechanisms for Optical Access Networks Systems", *Lightwave Technology, Journal of,* page(s): 563 - 570 Volume: 31, Issue: 4, Feb.15, 2013.

[5] D. Suvakovic, H. Chow, D. V. Veen, J. Galaro, B. Farah, N. P. Anthapadmanabhan, P. Vetter, A. Dupas, R. Boislaigue, "Low Energy Bit-Interleaving Downstream Protocol for Passive Optical Newtorks, " IEEE Online GreenComm 2012.

[6] L. G. Kazovsky, T. Ayhan, A. S. Gowda, A. R. Dhaini, A. Ng'oma, and P. Vetter, "Green In-Building Networks: the Future Convergence Green Optical and Wireless Technologies", International Conference on Transparent Optical Networks (ICTON) 2013, Cartagena, Spain, June 2013.

[7] Verizon FiOS. Available online: http://www22.verizon.com/home/aboutfios/